

Copyright
by
Sergio Francisco Breña
2000

STRENGTHENING REINFORCED CONCRETE BRIDGES
USING CARBON FIBER REINFORCED POLYMER COMPOSITES

by

Sergio Francisco Breña, B.S, M.S.

Dissertation

Presented to the Faculty of the Graduate School of

the University of Texas at Austin

in Partial Fulfillment

of the Requirements

for the Degree of

Doctor of Philosophy

The University of Texas at Austin

December 2000

**STRENGTHENING REINFORCED CONCRETE BRIDGES
USING CARBON FIBER REINFORCED POLYMER COMPOSITES**

**Approved by
Dissertation Committee:**

Sharon L. Wood

Michael E. Kreger

James O. Jirsa

Timothy J. Fowler

Eric B. Becker

Dedication

To Susana, Mariana, and Fernanda, the loves of my life

To the memory of my Father

To my Mother

Acknowledgements

The research presented in this dissertation was sponsored by the Texas Department of Transportation (TxDOT) under Project No. 0-1776. The involvement of Mark Steves and Richard Wilkison from TxDOT were extremely important for the the succesful completion of the research project. Their fruitful suggestions were incorporated into the research project to guarantee the applicability of the results from the experimental program to actual field situations.

Many students participated at different times during the duration of this project. Regan Bramblett presented the results of the first phase of the investigation as her Masters Thesis. Her active participation throughout the duration of the project and her friendship are very much appreciated. Michaël Benouaich participated in the construction, testing, and data reduction of the beams subjected to repeated loads as part of the long-term testing program. These tests were performed in a relatively short period of time due to the extraordinary effort he put into the project. Nicole García, Sarah Orton, and Janna Renfro participated during the fabrication and testing of specimens during different phases of the project. Testing would have taken much longer without their assistance.

The laboratory technicians at the Ferguson Structural Engineering Laboratory (FSEL) were always willing to lend a hand to make our lifes easier and safer. Their help throughout the fabrication and testing phases is much appreciated. In particular, Blake Stasney for his constant suggestions and extraordinary knowledge on the laboratory operation, Mike Bell for his more than often help with crane operation, Wayne Fontenot for his skills with machining and tool operation, and Ray Madonna for his experience with electronics. I would also like to extend my appreciation to the administrative staff at FSEL for their help with general administrative issues

(Ruth Goodson), production of documents (Regina Forward), and material procurement (Laurie Golding and Dijaira Smith).

The composites that were used to strengthen the laboratory specimens were graciously donated by the manufacturers of the composite systems. The support from the representatives of the different organizations that participated in this research project is recognized. The assistance of Bill Light, Sika Corporation; Howard Kliger and Bob Snider, Master Builders Technology; Paul Gugenheim, Delta Structural Technology, Inc. (Fyfe Co.), and Ali Ganjehlou, Mitsubishi/Sumitomo Corp. is very much appreciated.

The research presented in this dissertation was conducted under the supervision of Professors Sharon Wood and Mike Kreger. I would like to thank both of them for the insightful suggestions and direction throughout the duration of the research project. I would personally like to thank Professor Sharon Wood for the advice and continuous support in the difficult moments during these four years. Working with her was a very enlightening and enjoyable experience. I would also like to thank Professors Jim Jirsa, Tim Fowler and Eric Becker for their useful suggestions and their participation in my dissertation committee. Finally, I would like to acknowledge CONACYT for the partial support I received that allowed me to pursue my Ph.D. Degree.

STRENGTHENING REINFORCED CONCRETE BRIDGES
USING CARBON FIBER REINFORCED POLYMER COMPOSITES

Publication No. _____

Sergio Francisco Breña, Ph.D.

The University of Texas at Austin, 2000

Supervisor: Sharon L. Wood

The need to develop economic strengthening techniques for the aging infrastructure has received considerable attention in recent years. In Texas, a significant percentage of bridges in off-system roads were constructed in the 1950s and require strengthening to upgrade them to the current load used for design. Therefore, the Texas Department of Transportation (TxDOT) was interested in examining the use of carbon fiber reinforced polymer (CFRP) composites to strengthen existing bridges and avoid replacement.

Four full-scale specimens representative of bridge construction during the 1950s in Texas were constructed, strengthened, and tested in the laboratory to assess the effectiveness of CFRP composites for flexural strengthening. The response of the laboratory specimens is compared with calculations based on an analytical model that was developed to reproduce the measured response and to design future strengthening schemes.

Results from the laboratory tests indicate that composite materials may be used successfully to strengthen existing elements. The maximum strength in the specimens was controlled by debonding of the CFRP composites from the surface of the concrete. The analytical model was able to reproduce the general response of the specimens accurately, but did not replicate the mode of failure experienced in the tests. Therefore, the model can be used with a modification to incorporate the failure mode observed during the tests for the future design of strengthening schemes. Finally, recommendations for the design of strengthening procedures of similar bridges in the field are presented.

Table of Contents

| | |
|--|-------------|
| LIST OF TABLES | xvii |
| LIST OF FIGURES | xix |
| CHAPTER 1: INTRODUCTION | 1 |
| 1.1 Background | 1 |
| 1.2 Identification of Candidate Bridges | 3 |
| 1.3 Objectives and Scope of Research | 3 |
| 1.3.1 Summary of Results from Phase 1 | 4 |
| 1.3.2 Summary of Results from Phase 2 | 12 |
| 1.3.3 Description of Phase 3 and Organization of Dissertation | 14 |
| CHAPTER 2: LITERATURE REVIEW | 17 |
| 2.1 Introduction | 17 |
| 2.2 Historical Background | 17 |
| 2.3 Previous Experimental Studies | 19 |
| 2.3.1 Flexural Tests on Small-Scale Specimens | 21 |
| 2.3.2 Flexural Tests on Large-Scale Specimens | 30 |
| 2.3.3 Tests to Characterize the Concrete-Composite Interface | 31 |
| 2.4 Summary | 37 |
| CHAPTER 3: MODEL TO CALCULATE THE RESPONSE OF REINFORCED CONCRETE ELEMENTS STRENGTHENED USING CFRP COMPOSITES | 39 |
| 3.1 Introduction | 39 |
| 3.2 Moment-Curvature Analysis of Strengthened Sections | 40 |
| 3.2.1 Assumptions Used in the Sectional Analysis Model | 40 |
| 3.2.2 Stress-Strain Material Models Used for Sectional Analysis | 41 |
| 3.2.3 Internal Equilibrium of Strengthened Cross Section | 48 |
| 3.3 Load-Deflection Response | 53 |
| 3.4 Validation of Model | 57 |

| | | |
|-------------------|--|------------|
| 3.4.1 | Tests by Spadea, Bencardino, and Swamy | 58 |
| 3.4.2 | Tests by GangaRao and Vijay | 63 |
| 3.4.3 | Tests by Arduini, Di Tommaso, and Nanni | 66 |
| 3.4.4 | Tests by Nakamura, Sakai, Yagi, and Tanaka | 69 |
| 3.4.5 | Summary of Published Data | 70 |
| 3.5 | Refinement of Analytical Model..... | 72 |
| 3.5.1 | Limiting Debonding Strain of CFRP Composites | 72 |
| 3.5.2 | Initial Strains Caused by Dead Loads | 73 |
| 3.6 | Summary | 75 |
| CHAPTER 4: | DESCRIPTION OF PAN-JOIST SPECIMENS | 76 |
| 4.1 | Introduction | 76 |
| 4.2 | Prototype Bridge..... | 78 |
| 4.2.1 | Physical Characteristics of Prototype Bridge..... | 79 |
| 4.2.2 | Calculated Capacity of Prototype Bridge..... | 80 |
| 4.2.3 | Load Rating for Prototype Bridge..... | 84 |
| 4.3 | Design and Construction of Laboratory Specimens..... | 91 |
| 4.4 | Design and Construction of Strengthening Schemes for Laboratory Specimens | 96 |
| 4.4.1 | Strengthening Scheme for Specimen J-1 | 101 |
| 4.4.2 | Strengthening Scheme for Specimen J-2 | 106 |
| 4.5 | Load Levels for Prototype Bridge..... | 109 |
| 4.6 | Summary | 111 |
| CHAPTER 5: | MEASURED RESPONSE OF PAN-JOIST SPECIMENS..... | 113 |
| 5.1 | Introduction | 113 |
| 5.2 | Test Setup and Instrumentation..... | 113 |
| 5.2.1 | Description of Experimental Setup | 113 |
| 5.2.2 | Loading Sequence | 115 |
| 5.2.3 | Instrumentation | 118 |
| 5.3 | Observed Behavior During Tests | 123 |
| 5.3.1 | Description of Failure Sequence and Cracking Distribution | 123 |

| | |
|--|------------|
| 5.4 Measured Response | 134 |
| 5.4.1 Deflection Measurements..... | 134 |
| 5.4.2 Strain Gage Measurements | 148 |
| 5.5 Summary | 155 |
| | |
| CHAPTER 6: VERIFICATION OF THE ANALYTICAL MODEL USING THE MEASURED RESPONSE OF THE PAN-JOIST SPECIMENS..... | 156 |
| 6.1 Introduction | 156 |
| 6.2 Evaluation of Strain Response | 156 |
| 6.2.1 Strains due to Dead Loads | 157 |
| 6.2.2 Measured Strain Profiles due to Live Loads | 159 |
| 6.2.3 Comparison of Measured and Calculated Strains due to Live Loads..... | 163 |
| 6.2.4 Measured Strains at which the CFRP Composites Debonded from the Surface of the Concrete..... | 172 |
| 6.3 Evaluation of Moment-Curvature Response | 177 |
| 6.3.1 Calculating Internal Forces from Measured Strains for Specimen J-1 | 177 |
| 6.3.2 Calculating Internal Forces from Measured Strains for Specimen J-2 | 184 |
| 6.3.3 Moment-Curvature Response | 190 |
| 6.3.4 Comparison of Internal and External Moments | 194 |
| 6.4 Evaluation of Load-Deflection Response..... | 196 |
| 6.5 Summary | 199 |
| | |
| CHAPTER 7: DESCRIPTION OF FLAT-SLAB SPECIMENS..... | 200 |
| 7.1 Introduction | 200 |
| 7.2 Prototype Bridge..... | 201 |
| 7.2.1 Physical Characteristics of Prototype Bridge..... | 201 |
| 7.2.2 Calculated Capacity of Prototype Bridge..... | 203 |
| 7.2.3 Prototype Bridge Load Rating | 206 |
| 7.3 Design and Construction of Laboratory Specimens..... | 215 |

| | |
|---|------------|
| 7.4 Design and Construction of Strengthening Schemes for Laboratory Specimens | 219 |
| 7.4.1 Strengthening Scheme for Specimen FS-1 | 224 |
| 7.4.2 Strengthening Scheme for Specimen FS-2 | 228 |
| 7.5 Summary | 231 |
| | |
| CHAPTER 8: MEASURED RESPONSE OF FLAT-SLAB SPECIMENS | 233 |
| 8.1 Introduction | 233 |
| 8.2 Test Setup and Instrumentation | 233 |
| 8.2.1 Description of Experimental Setup | 233 |
| 8.2.2 Loading Sequence | 234 |
| 8.2.3 Instrumentation | 237 |
| 8.3 Observed Behavior During Tests | 242 |
| 8.3.1 Description of Failure Sequence and Cracking Distribution | 242 |
| 8.4 Measured Response | 253 |
| 8.4.1 Deflection Measurements | 253 |
| 8.4.2 Strain Gage Measurements | 264 |
| 8.5 Summary | 271 |
| | |
| CHAPTER 9: VERIFICATION OF THE ANALYTICAL MODEL USING THE MEASURED RESPONSE OF THE FLAT-SLAB SPECIMENS | 272 |
| 9.1 Introduction | 272 |
| 9.2 Evaluation of Strain Response | 272 |
| 9.2.1 Strains due to Dead Loads | 273 |
| 9.2.2 Measured Strain Profiles due to Live Loads | 274 |
| 9.2.3 Comparison of Measured and Calculated Strains due to Live Loads | 275 |
| 9.2.4 Measured Strains at which the CFRP Composites Debonded from the Surface of the Concrete | 286 |
| 9.3 Evaluation of Moment-Curvature Response | 290 |
| 9.3.1 Internal Forces Calculated from Measured Strains for Specimen FS-1 | 291 |
| 9.3.2 Internal Forces Calculated from Measured Strains for Specimen FS-2 | 295 |

| | | | |
|--------------------|--|------------|--|
| 9.3.3 | Moment-Curvature Response | 300 | |
| 9.3.4 | Comparison of Internal and External Moments | 301 | |
| 9.4 | Evaluation of Load-Deflection Response..... | 306 | |
| 9.5 | Summary | 309 | |
| CHAPTER 10: | DESIGN RECOMMENDATIONS..... | 310 | |
| 10.1 | Introduction | 310 | |
| 10.2 | Calculation of Nominal Flexural Capacity of Strengthened Sections | 311 | |
| 10.2.1 | Strain Distribution within Strengthened Sections | 312 | |
| 10.2.2 | Preliminary Estimate of the Area of CFRP Composite | 315 | |
| 10.2.3 | Maximum Recommended Area of CFRP Composite..... | 319 | |
| 10.3 | Recommended Strength Reduction Factor for Use in the Basic Design Equation..... | 322 | |
| 10.4 | Serviceability Considerations | 324 | |
| 10.5 | Detailing Recommendations | 324 | |
| 10.5.1 | Anchoring Straps..... | 324 | |
| 10.5.2 | Length of CFRP Composites | 326 | |
| 10.6 | Summary | 328 | |
| CHAPTER 11: | SUMMARY AND CONCLUSIONS..... | 329 | |
| 11.1 | Summary | 329 | |
| 11.2 | Conclusions | 331 | |
| 11.3 | Areas for Future Research | 334 | |
| APPENDIX A: | MEASURED MATERIAL PROPERTIES..... | 336 | |
| A.1 | Concrete..... | 336 | |
| A.1.1 | Pan-Joist Specimens..... | 337 | |
| A.1.2 | Flat Slab Specimens | 340 | |
| A.2 | Reinforcing Steel..... | 343 | |
| A.2.1 | Pan-Joist Specimens..... | 344 | |
| A.2.2 | Flat-Slab Specimens..... | 350 | |
| A.3 | CFRP Plates and Sheets..... | 353 | |
| APPENDIX B: | BRIDGE LOAD RATING PROCEDURE | 357 | |

| | |
|---|------------|
| B.1 Introduction | 357 |
| B.2 Description of Design Trucks used for Load Rating..... | 358 |
| B.3 Distribution of Moments on Flat-Slab Bridges..... | 359 |
| B.4 Bridge Load Rating | 362 |
| | |
| APPENDIX C: APPLICATION OF CFRP COMPOSITE SYSTEMS TO EXISTING REINFORCED CONCRETE ELEMENTS | 368 |
| C.1 Introduction | 368 |
| C.2 Pultruded CFRP System..... | 368 |
| C.2.1 Description of Composite System..... | 368 |
| C.2.2 Application to Reinforced Concrete Element | 370 |
| C.3 Wet-Layup CFRP System..... | 374 |
| C.3.1 Description of Composite System..... | 374 |
| C.3.2 Application to Reinforced Concrete Element | 374 |
| | |
| APPENDIX D: MEASURED STRAINS..... | 377 |
| | |
| REFERENCES | 429 |
| | |
| VITA | 436 |

List of Tables

| | | |
|-----------|---|-----|
| Table 1.1 | Summary of Test Results from Beams in Phase 1 [adapted from Bramblett, 2000] | 11 |
| Table 2.1 | Qualitative Comparison of Different Fibers used in Composites [Meier and Winistörfer, 1995]..... | 21 |
| Table 2.2 | Summary of Previous Investigations on Flexural Tests..... | 24 |
| Table 2.3 | Summary of Flexural Tests by Previous Investigators | 26 |
| Table 2.4 | Geometry and Reinforcement of Flexural Specimens from Previous Investigators | 27 |
| Table 2.5 | Observed Failure Modes and Main Conclusions from Previous Flexural Tests | 29 |
| Table 3.1 | Dimensions and Reinforcement of Specimens Reported by Other Researchers | 60 |
| Table 3.2 | Material Properties and Dimensions of CFRP Composites of Specimens Reported by Other Researchers | 61 |
| Table 3.3 | Summary of Results from Published Data and Analytical Model | 64 |
| Table 4.1 | Calculated Flexural and Shear Capacities of a Single Joist in the Prototype Bridge | 83 |
| Table 4.2 | Maximum Live Load Moments and Shears Per Joist for the Prototype Bridge | 86 |
| Table 4.3 | Unfactored Load Effects Per Joist Used to Rate Prototype Bridge .. | 89 |
| Table 4.4 | Load Rating Results for Prototype Pan-Joist Bridge Originally Designed for an H- 10 Truck Loading..... | 90 |
| Table 4.5 | Average Measured Material Strengths for Joist Specimens | 93 |
| Table 4.6 | Nominal Flexural and Shear Capacities of Pan-Joist Specimens | 96 |
| Table 4.7 | Parameters Used to Design the Strengthening Schemes..... | 99 |
| Table 4.8 | Moments Associated to Different Design Levels for One Joist in Prototype Bridge | 110 |
| Table 5.1 | Required Moments and Loads During Testing Corresponding to Design Levels in the Prototype Bridge | 117 |
| Table 5.2 | Displacement Limits of Linear Potentiometers..... | 119 |
| Table 5.3 | Characteristics of Strain Gages | 120 |
| Table 5.4 | Maximum Response Measured During Testing of Specimen J-1 ... | 144 |
| Table 5.5 | Maximum Response Measured During Testing of Specimen J-2... | 145 |
| Table 5.6 | Measured Deflections during Service Load Stages | 147 |
| Table 5.7 | Comparison of Displacement Ductility..... | 147 |
| Table 6.1 | Calculated Dead-Load Strains..... | 159 |
| Table 6.2 | Measured and Calculated Live-Load Strains for Specimen J-1 | 170 |
| Table 6.3 | Measured and Calculated Live-Load Strains for Specimen J-2..... | 171 |
| Table 7.1 | Design Flexural Strength of Slab (per ft) and Curbs for Prototype Bridge | 207 |
| Table 7.2 | Unfactored Load Effects Used in Prototype Bridge Rating..... | 210 |
| Table 7.3 | Load Rating Results for Flat-Slab Prototype Bridge | 211 |
| Table 7.4 | Unfactored Load Effects Used to Rate the Slab in the Prototype Bridge | 213 |
| Table 7.5 | Prototype Bride Load Rating after Curb Removal..... | 213 |

| | | |
|-----------|--|-----|
| Table 7.6 | Average Measured Material Strengths for Flat-Slab Specimens | 218 |
| Table 7.7 | Flexural Capacity of Flat-Slab Specimens (per unit width of slab) | 219 |
| Table 7.8 | Flexural Strength Parameters and Calculated Capacity of a 6-ft Section of Strengthened Slab in the Prototype Bridge | 222 |
| Table 8.1 | Applied Moments and Loads During Testing..... | 236 |
| Table 8.2 | Displacement Limits of Linear Potentiometers..... | 238 |
| Table 8.3 | Characteristics of Strain Gages | 238 |
| Table 8.4 | Maximum Response Measured During Testing of Specimen FS-1 | 262 |
| Table 8.5 | Maximum Response Measured During Testing of Specimen FS-2 | 263 |
| Table 9.1 | Calculated Dead Load Strains..... | 274 |
| Table 9.2 | Measured and Calculated Live-Load Strains for Specimen FS-1 ... | 285 |
| Table 9.3 | Measured and Calculated Live-Load Strains for Specimen FS-2... | 285 |
| Table A.1 | Concrete Compression Tests and Parameters Used for Material Models | 343 |
| Table A.2 | Tensile Strength of Concrete Determined from Split Cylinder Tests | 343 |
| Table A.3 | Measured Yield and Ultimate Stresses for Reinforcing Bars | 352 |
| Table A.4 | Properties of CFRP Composite Systems Used for Specimen Strengthening Published by Manufacturers [Master Builders, 1998; Sika, 1997]. | 354 |
| Table A.5 | Mechanical Properties of Resin used for Mbrace TM System (Mbrace TM Saturant) [Master Builders, 1998] | 355 |
| Table A.6 | Mechanical Properties of Epoxy Paste (SikaDur [→] 30) Used to Bond Pultruded Plates [Sika, 1997] | 356 |
| Table A.7 | Mechanical Properties of Impregnating Resin (SikaDur [→] Hex 300/306) for SikaWrap [→] Hex 103 C Woven Fabric [Sika, 1999] | 356 |
| Table B.1 | Load Rating of Pan-Joist Prototype Bridge | 365 |
| Table B.2 | Load Rating of Flat-Slab Prototype Bridge Including the Contribution of Structural Curbs | 366 |
| Table B.3 | Load Rating of Flat-Slab Bridge Without the Contribution of Structural Curbs | 367 |
| Table D.1 | Characteristics of Strain Gages | 378 |

List of Figures

| | | |
|-------------|--|----|
| Figure 1.1 | Prying Action Observed on CFRP Composite Attached to the Bottom Surface of the Beams | 6 |
| Figure 1.2 | Summary of CFRP Configurations Used in Phase 1 | 8 |
| Figure 1.3 | Summary of Results from Phase 2 | 13 |
| Figure 2.1 | Observed Failure Modes of Strengthened Members Using CFRP Composites | 22 |
| Figure 2.2 | Techniques used by Previous Researchers to Anchor Longitudinal CFRP Composites | 23 |
| Figure 2.3 | Strengthening of Tee-Beams using CFRP composite sheets [Shahawy and Beitelman, 1996] | 31 |
| Figure 2.4 | Direct Shear Test Apparatus | 32 |
| Figure 2.5 | Bar-Pullout Bond Test Apparatus | 33 |
| Figure 2.6 | Variation of Interface Shear Stress with Distance [Brosens and VanGemert, 1997] | 35 |
| Figure 2.7 | Regions in Strengthened Beam where Different Peeling Modes Initiate [Blaschko et al., 1998] | 36 |
| Figure 3.1 | Idealized Stress-Strain Relationship for Concrete | 43 |
| Figure 3.2 | Idealized Stress-Strain Relationships for Steel | 47 |
| Figure 3.3 | Idealized Stress-Strain Relationship for CFRP Composites | 48 |
| Figure 3.4 | Schematic Representation of Sectional Response Illustrating the Procedure Used in the Calculations | 52 |
| Figure 3.5 | Procedure to Calculate Deflections of an Element with a Nonlinear Moment-Curvature Relationship | 55 |
| Figure 3.6 | Comparison of Load-Deflection Curves of Specimens A.3 and A3.3 Reported by Spadea et al. (1998) | 62 |
| Figure 3.7 | Comparison of Load-Deflection Curves for Specimens 1A ₂ -R and 3B ₂ -C Reported by GangaRao and Vijay (1998) | 65 |
| Figure 3.8 | Comparison of Load-Deflection Curves for Specimens B1, B2, and B4 Reported by Arduini et al. (1997) | 68 |
| Figure 3.9 | Comparison of Load-Deflection Curves for Specimens BL, E24-1P, and E24-2P Reported by Nakamura et al. (1997) | 71 |
| Figure 3.10 | Effect of Initial Dead Load Strains on Calculation of Moment-Curvature Response | 74 |
| Figure 4.1 | View of Metal Pan-Forms inside the Laboratory | 77 |
| Figure 4.2 | Photograph of Pan-Joist Bridge in Buda, Texas Indicating Uneven Surfaces on Bottom of Joists | 78 |
| Figure 4.3 | Reinforcement Details for Prototype Bridge | 81 |
| Figure 4.4 | H-10 Truck Positions Corresponding to Critical Moments and Shears | 87 |
| Figure 4.5 | HS-10 Truck Positions Corresponding to Critical Moments and Shears | 88 |
| Figure 4.6 | Specimen Reinforcement and Formwork | 94 |
| Figure 4.7 | Joist Specimen Geometry and Reinforcement | 95 |

| | | |
|-------------|--|-----|
| Figure 4.8 | Calculated Moment-Curvature Response of Two Joists of Prototype Bridge Strengthened Using Different Composite Systems | 100 |
| Figure 4.9 | CFRP Strengthening Details for Specimen J-1 | 103 |
| Figure 4.10 | Required CFRP Plate Length for HS-20 Truck Loading on 28 ft Clear Span for the Design of Specimen J-1 (2-Joists) | 104 |
| Figure 4.11 | Calculated Moment-Curvature Response of Specimen J-1 Using Measured Material Properties | 105 |
| Figure 4.12 | Partial Wrapping of Joists in Specimen J-2 to Avoid Concrete Surface Irregularities | 107 |
| Figure 4.13 | CFRP Strengthening Details for Specimen J-2 | 108 |
| Figure 4.14 | Calculated Moment-Curvature Response of Specimen J-2 Using Measured Material Properties | 109 |
| Figure 5.1 | Side View of Pan-Joist Specimen in Laboratory Test Setup | 114 |
| Figure 5.2 | Overhead View of Pan-Joist Specimen Showing the Location of Loading Points | 115 |
| Figure 5.3 | Location of Instrumented Sections Showing Position of Potentiometers and Strain Gages in Specimen J-1 | 121 |
| Figure 5.4 | Location of Instrumented Sections Showing Position of Potentiometers and Strain Gages in Specimen J-2 | 122 |
| Figure 5.5 | Typical Cracking Patterns for Specimen J-1 (West Joist) | 125 |
| Figure 5.6 | Observed Initial Debonding of CFRP Plate on East Joist | 126 |
| Figure 5.7 | Transverse Strap Debonding at Ultimate Design Load | 126 |
| Figure 5.8 | East Joist of Specimen J-1 Before CFRP Debonding | 127 |
| Figure 5.9 | East Joist of Specimen J-1 at Failure | 128 |
| Figure 5.10 | Typical Cracking Patterns for Specimen J-2 (West Joist) | 131 |
| Figure 5.11 | Initiation of Debonding Along CFRP Sheet | 132 |
| Figure 5.12 | Cracking Propagation Behind Strap Originated Debonding | 132 |
| Figure 5.13 | View of West Joist in Specimen J-2 at Failure | 133 |
| Figure 5.14 | Bottom Surface Condition of West Joist after CFRP Debonding | 133 |
| Figure 5.15 | Measured Displacements at Supports in Specimen J-1 | 137 |
| Figure 5.16 | Measured Deflections at Sections N1 and S1 in Specimen J-1 | 138 |
| Figure 5.17 | Measured Deflections at Mid-Span in Specimen J-1 | 139 |
| Figure 5.18 | Measured Displacements at Supports in Specimen J-2 | 140 |
| Figure 5.19 | Measured Deflections at Sections N1 and S1 in Specimen J-2 | 141 |
| Figure 5.20 | Measured Mid-Span Deflections in Specimen J-2 | 142 |
| Figure 5.21 | Load-Deflection Behavior Characterized by Change in Global Stiffness | 143 |
| Figure 5.22 | Typical Stiffness Increase after CFRP Strengthening (Specimen J-1) | 143 |
| Figure 5.23 | Average Strains Measured at Section N1 (Specimen J-1) | 151 |
| Figure 5.24 | Average Strains Measured at Section N2 (Specimen J-1) | 152 |
| Figure 5.25 | Average Strains Measured at Section N1 (Specimen J-2) | 153 |
| Figure 5.26 | Average Strains Measured at Section N2 (Specimen J-2) | 154 |

| | | |
|-------------|---|-----|
| Figure 6.1 | Measured Live-Load Strain Profiles in Sections N1 and S1 for Specimen J-1 | 161 |
| Figure 6.2 | Measured Live-Load Strain Profiles in Sections N1 and S1 for Specimen J-2 | 162 |
| Figure 6.3 | Comparison of Measured and Calculated Live-Load Strains at Section N1 (Specimen J-1)..... | 166 |
| Figure 6.4 | Comparison of Measured and Calculated Live-Load Strains at Section S1 (Specimen J-1) | 167 |
| Figure 6.5 | Comparison of Measured and Calculated Live-Load Strains at Section N1 (Specimen J-2)..... | 168 |
| Figure 6.6 | Comparison of Measured and Calculated Live-Load Strains at Section S1 (Specimen J-2) | 169 |
| Figure 6.7 | Comparison of Measured and Calculated CFRP Strains for Specimen J-1 | 175 |
| Figure 6.8 | Comparison of Measured and Calculated CFRP Strains for Specimen J-2 | 176 |
| Figure 6.9 | Typical Strain Profile for Specimen J-1 | 178 |
| Figure 6.10 | Internal Force Resultants for Specimen J-1 | 179 |
| Figure 6.11 | Possible Strain Distribution Corresponding to Equilibrium of Internal Forces | 181 |
| Figure 6.12 | Comparison of Revised and Measured Peak Compressive Strains for Specimen J-1 | 182 |
| Figure 6.13 | Comparison of Neutral Axis Depth from Revised and Measured Strain Profiles | 183 |
| Figure 6.14 | Variation of Tensile Force Components at Section N1 for Specimen J-1 | 184 |
| Figure 6.15 | Distribution of Live-Load Strains on CFRP Sheets..... | 186 |
| Figure 6.16 | Internal Force Resultants for Specimen J-2 | 187 |
| Figure 6.17 | Comparison of Revised and Measured Peak Compressive Strains for Specimen J-2 | 188 |
| Figure 6.18 | Comparison of Neutral Axis Depth from Revised and Measured Strain Profiles | 189 |
| Figure 6.19 | Contribution of the CFRP Sheets to the Total Internal Moment at Section N1 for Specimen J-2 | 190 |
| Figure 6.20 | Comparison of Measured and Calculated Moment-Curvature Response for Specimen J-1 | 192 |
| Figure 6.21 | Comparison of Measured and Calculated Moment-Curvature Response for Specimen J-2 | 193 |
| Figure 6.22 | Comparison of Internal and External Moments | 195 |
| Figure 6.23 | Measured Load-Deflection Response of Pan-Joist Specimens..... | 197 |
| Figure 6.24 | Comparison of Measured and Calculated Load-Deflection Response of Specimen J-1 | 198 |
| Figure 6.25 | Comparison of Measured and Calculated Load-Deflection Response of Specimen J-2 | 198 |
| Figure 7.1 | Reinforcement Details for FS-Slab Prototype Bridge..... | 204 |

| | | |
|-------------|---|-----|
| Figure 7.2 | Geometric Properties of the Curbs to Compute Flexural Strength | 206 |
| Figure 7.3 | Picture Showing Reinforcement in a Typical Flat-Slab Specimen before Casting | 216 |
| Figure 7.4 | Geometry and Reinforcement Details of Flat-Slab Specimens FS-1 and FS-2 | 217 |
| Figure 7.5 | Calculated Moment-Curvature Response of a Strengthened and Unstrengthened 6-ft Wide Section of the Slab in the Prototype Bridge | 223 |
| Figure 7.6 | Required CFRP Plate Length on Specimen FS-1 Based on Moments Generated During Laboratory Testing | 225 |
| Figure 7.7 | Strengthening Details for Specimen FS-1 | 226 |
| Figure 7.8 | Picture of the Bottom Surface of Specimen FS-1 after Strengthening with the CFRP Pultruded System | 227 |
| Figure 7.9 | Calculated Moment-Curvature Response of Specimen FS-1 Using the Measured Material Properties | 228 |
| Figure 7.10 | Strengthening Details for Specimen FS-2 | 229 |
| Figure 7.11 | Picture of the Bottom Surface of Specimen FS-2 after Strengthening with the CFRP Wet-Layup System | 230 |
| Figure 7.12 | Calculated Moment-Curvature Response of Specimen FS-2 Using the Measured Material Properties | 231 |
| Figure 8.1 | Picture Showing the Experimental Setup Used for the Laboratory Tests of the Flat-Slab Specimens | 234 |
| Figure 8.2 | Position of Linear Potentiometers on East and West Sides and Location of Instrumented Sections in Flat-Slab Specimens | 239 |
| Figure 8.3 | Position of Strain Gages on the Reinforcement and Concrete Surface in Specimens FS-1 and FS-2 | 240 |
| Figure 8.4 | Position of Strain Gages Bonded to the CFRP Composite Systems in Specimens FS-1 and FS-2 | 241 |
| Figure 8.5 | Typical Cracking Distribution after Load Cycles to 7 kip on Specimen FS-1 before CFRP Strengthening | 242 |
| Figure 8.6 | Cracking Pattern of Specimen FS-1 at Load Stage 2 (34 kip) | 245 |
| Figure 8.7 | Bottom View Toward North End of Specimen FS-1 after CFRP-Plate Debonding | 246 |
| Figure 8.8 | South End of the CFRP Plates Still Attached After Failure of Specimen FS-1 | 246 |
| Figure 8.9 | Evidence of Plate Delamination of the East CFRP Plate at the North End of Specimen FS-1 | 247 |
| Figure 8.10 | Extent of Debonding of CFRP Plates on Specimen FS-1 | 247 |
| Figure 8.11 | Cracking Pattern of Specimen FS-2 at Load Stage 2 (34 kip) | 249 |
| Figure 8.12 | Initiation of Debonding Along CFRP Sheet | 250 |
| Figure 8.13 | View of West CFRP Sheet after Debonding from Specimen FS-2 | 251 |
| Figure 8.14 | Deformation and Splitting of Transverse Sheet Caused by Movement of the Longitudinal Sheet | 251 |

| | | |
|-------------|---|-----|
| Figure 8.15 | Bottom View of Specimen FS-2 Indicating the Extent of Debonding of CFRP Sheets | 252 |
| Figure 8.16 | West Side View of Specimen FS-2 at Ultimate Deformation Corresponding to Initiation of Concrete Crushing..... | 252 |
| Figure 8.17 | Measured Displacements at Supports in Specimen FS-1..... | 256 |
| Figure 8.18 | Measured Deflections at Sections N1 and S1 in Specimen FS-1 | 257 |
| Figure 8.19 | Measured Deflections at Mid-Span in Specimen FS-1 | 258 |
| Figure 8.20 | Measured Displacements at Supports in Specimen FS-2..... | 259 |
| Figure 8.21 | Measured Deflections at Sections N1 and S1 in Specimen FS-2 | 260 |
| Figure 8.22 | Measured Deflections at Mid-Span in Specimen FS-2..... | 261 |
| Figure 8.23 | Average Strains Measured at Section N1 (Specimen FS-1)..... | 267 |
| Figure 8.24 | Average Strains Measured at Section N2 (Specimen FS-1)..... | 268 |
| Figure 8.25 | Average Strains Measured at Section N1 (Specimen FS-2)..... | 269 |
| Figure 8.26 | Average Strains Measured at Section N2 (Specimen FS-2)..... | 270 |
| Figure 9.1 | Measured Live-Load Strain Profiles in Sections N1 and S1 for Specimen FS-1 | 276 |
| Figure 9.2 | Measured Live-Load Strain Profiles in Sections N1 and S1 for Specimen FS-2 | 277 |
| Figure 9.3 | Comparison of Measured and Calculated Live-Load Strains at Section N1 (Specimen FS-1)..... | 281 |
| Figure 9.4 | Comparison of Measured and Calculated Live-Load Strains at Section S1 (Specimen FS-1) | 282 |
| Figure 9.5 | Comparison of Measured and Calculated Live-Load Strains at Section N1 (Specimen FS-2)..... | 283 |
| Figure 9.6 | Comparison of Measured and Calculated Live-Load Strains at Section S1 (Specimen FS-2) | 284 |
| Figure 9.7 | Comparison of Measured and Calculated CFRP Strains for Specimen FS-1 | 288 |
| Figure 9.8 | Comparison of Measured and Calculated CFRP Strains for Specimen FS-2 | 289 |
| Figure 9.9 | Internal Force Resultants for Specimen FS-1 | 292 |
| Figure 9.10 | Comparison of Revised and Measured Peak Compressive Strains for Specimen FS-1 | 293 |
| Figure 9.11 | Comparison of Neutral Axis Depth from Revised and Measured Strain Profiles | 294 |
| Figure 9.12 | Variation of Tensile Force Components at Section N1 for Specimen FS-1 | 295 |
| Figure 9.13 | Internal Force Resultants for Specimen FS-2 | 296 |
| Figure 9.14 | Comparison of Revised and Measured Peak Compressive Strains for Specimen FS-2 | 298 |

| | | | |
|-------------|--|-----|-----|
| Figure 9.15 | Comparison of Neutral Axis Depth from Revised and Measured Strain Profiles | 299 | |
| Figure 9.16 | Contribution of the CFRP Sheets to the Total Internal Moment at Section N1 for Specimen FS-2 | 300 | |
| Figure 9.17 | Comparison of Measured and Calculated Moment-Curvature Response for Specimen FS-1 | 303 | |
| Figure 9.18 | Comparison of Measured and Calculated Moment-Curvature Response for Specimen FS-2 | 304 | |
| Figure 9.19 | Comparison of Internal and External Moments | 305 | |
| Figure 9.20 | Measured Load-Deflection Response of Flat-Slab Specimens | 307 | |
| Figure 9.21 | Comparison of Measured and Calculated Load-Deflection Response of Specimen FS-1 | 308 | |
| Figure 9.22 | Comparison of Measured and Calculated Load-Deflection Response of Specimen FS-2 | 308 | |
| | | | |
| Figure 10.1 | Calculation of Strains Caused by Dead-Load Moments | 313 | |
| Figure 10.2 | Increment of Strains on Strengthened Reinforced Concrete Section | 314 | |
| Figure 10.3 | Internal Stress Distribution for a Strengthened Rectangular Section at Capacity..... | 318 | |
| Figure 10.4 | Strain Profile for Maximum Recommended Area of CFRP Composite | | 320 |
| Figure 10.5 | CFRP Composite Length Determined Based on Ultimate Moment Diagram | 327 | |
| Figure A.1 | Variation of Concrete Compressive Strength with Time for Specimen J-1 | 338 | |
| Figure A.2 | Variation of Concrete Compressive Strength with Time for Specimen J-2 | 338 | |
| Figure A.3 | Concrete Stress-Strain Curve for Specimen J-1 | 339 | |
| Figure A.4 | Concrete Stress-Strain Curve for Specimen J-2..... | 339 | |
| Figure A.5 | Variation of Concrete Compressive Strength with Time for Specimen FS-1 | 341 | |
| Figure A.6 | Variation of Concrete Compressive Strength with Time for Specimen FS-2 | 341 | |
| Figure A.7 | Concrete Stress-Strain Curve for Specimen FS-1 | 342 | |
| Figure A.8 | Concrete Stress-Strain Curve for Specimen FS-2..... | 342 | |
| Figure A.9 | Stress-Strain Curves for #8 Bars in Joist Specimens | 346 | |
| Figure A.10 | Stress-Strain Curves for #3 Bars in Joist Specimens | 347 | |
| Figure A.11 | Stress-Strain Curves for #4 Bars in Joist Specimens | 348 | |
| Figure A.12 | Stress-Strain Curves for #5 Bars in Joist Specimens | 349 | |
| Figure A.13 | Stress-Strain Curves for #6 Bars in Flat-Slab Specimens..... | 350 | |
| Figure A.14 | Stress-Strain Curves for #4 Bars in Flat-Slab Specimens..... | 351 | |
| Figure A.15 | Stress-Strain Curves for #3 Bars in Flat-Slab Specimens..... | 351 | |
| Figure B.1 | Design Trucks used for Bridge Load Rating..... | 358 | |
| Figure C.1 | Schematic Representation of the Fabrication of a Fiber Reinforced Polymer Plate using the Pultrusion Process [Mallick, 1993] | | 369 |

| | | |
|-------------|--|-----|
| Figure C.2 | Application of CFRP Pultruded Plates to Reinforced Concrete Beam..... | 372 |
| Figure C.3 | Application of Woven Straps Around CFRP Pultruded Plates..... | 373 |
| Figure C.4 | Application of CFRP Wet-Layup System to Reinforced Concrete Element..... | 376 |
| Figure D.1 | Position of Instrumented Sections for Pan-Joist Specimens..... | 378 |
| Figure D.2 | Position of Instrumented Sections for Flat-Slab Specimens..... | 378 |
| Figure D.3 | Measured #8 Reinforcing Bar Strains in Specimen J-1 (Section N1)..... | 381 |
| Figure D.4 | Measured #8 Reinforcing Bar Strains in Specimen J-1 (Section S1)..... | 382 |
| Figure D.5 | Measured #8 Reinforcing Bar Strains in Specimen J-1 (Section N2)..... | 383 |
| Figure D.6 | Measured #8 Reinforcing Bar Strains in Specimen J-1 (Section S2)..... | 384 |
| Figure D.7 | Measured CFRP Strains in Specimen J-1 (Section N1)..... | 385 |
| Figure D.8 | Measured CFRP Strains in Specimen J-1 (Section S1)..... | 386 |
| Figure D.9 | Measured CFRP Strains in Specimen J-1 (Section N2)..... | 387 |
| Figure D.10 | Measured CFRP Strains in Specimen J-1 (Section S2)..... | 388 |
| Figure D.11 | Measured Strains on Concrete Slab in Specimen J-1 (Section N1)..... | 389 |
| Figure D.12 | Measured Strains on Concrete Slab in Specimen J-1 (Section S1)..... | 390 |
| Figure D.13 | Measured Strains on Concrete Slab in Specimen J-1 (Section N2)..... | 391 |
| Figure D.14 | Measured Strains on Concrete Slab in Specimen J-1 (Section S2)..... | 392 |
| Figure D.15 | Measured #8 Reinforcing Bar Strains in Specimen J-2 (Section N1)..... | 393 |
| Figure D.16 | Measured #8 Reinforcing Bar Strains in Specimen J-2 (Section S1)..... | 394 |
| Figure D.17 | Measured #8 Reinforcing Bar Strains in Specimen J-2 (Section N2)..... | 395 |
| Figure D.18 | Measured #8 Reinforcing Bar Strains in Specimen J-2 (Section S2)..... | 396 |
| Figure D.19 | Measured CFRP Strains in Specimen J-2 (Section N1)..... | 397 |
| Figure D.20 | Measured CFRP Strains in Specimen J-2 (Section S1)..... | 398 |
| Figure D.21 | Measured CFRP Strains in Specimen J-2 (Section N2)..... | 399 |
| Figure D.22 | Measured CFRP Strains in Specimen J-2 (Section S2)..... | 400 |
| Figure D.23 | Measured Strains on Concrete Slab in Specimen J-2 (Section N1)..... | 401 |
| Figure D.24 | Measured Strains on Concrete Slab in Specimen J-2 (Section S1)..... | 402 |
| Figure D.25 | Measured Strains on Concrete Slab in Specimen J-2 (Section N2)..... | 403 |

| | | |
|-------------|---|-----|
| Figure D.26 | Measured Strains on Concrete Slab in Specimen J-2 (Section S2)..... | 404 |
| Figure D.27 | Measured Reinforcing Bar (#6) Strains on Specimen FS-1 (Section N1)..... | 405 |
| Figure D.28 | Measured Reinforcing Bar (#6) Strains on Specimen FS-1 (Section S1)..... | 406 |
| Figure D.29 | Measured Reinforcing Bar (#6) Strains on Specimen FS-1 (Section N2)..... | 407 |
| Figure D.30 | Measured Reinforcing Bar (#6) Strains in Specimen FS-1 (Section S2)..... | 408 |
| Figure D.31 | Measured Strains on Concrete Slab in Specimen FS-1 (Section N1)..... | 409 |
| Figure D.32 | Measured Strains on Concrete Slab in Specimen FS-1 (Section S1)..... | 410 |
| Figure D.33 | Measured Strains on Concrete Slab in Specimen FS-1 (Section N2)..... | 411 |
| Figure D.34 | Measured Strains on Concrete Slab in Specimen FS-1 (Section S2)..... | 412 |
| Figure D.35 | Measured Strains on CFRP Plates in Specimen FS-1 (Section N1)..... | 413 |
| Figure D.36 | Measured Strains on CFRP Plates in Specimen FS-1 (Section S1)..... | 414 |
| Figure D.37 | Measured Strains on CFRP Plates in Specimen FS-1 (Section N2)..... | 415 |
| Figure D.38 | Measured Strains on CFRP Plates in Specimen FS-1 (Section S2)..... | 416 |
| Figure D.39 | Measured Reinforcing Bar (#6) Strains in Specimen FS-2 (Section N1)..... | 417 |
| Figure D.40 | Measured Reinforcing Bar (#6) Strains in Specimen FS-2 (Section S1)..... | 418 |
| Figure D.41 | Measured Reinforcing Bar (#6) Strains in Specimen FS-2 (Section N2)..... | 419 |
| Figure D.42 | Measured Reinforcing Bar (#6) Strains in Specimen FS-2 (Section S2)..... | 420 |
| Figure D.43 | Measured Strains on Concrete Slab in Specimen FS-2 (Section N1)..... | 421 |
| Figure D.44 | Measured Strains on Concrete Slab in Specimen FS-2 (Section S1)..... | 422 |
| Figure D.45 | Measured Strains on Concrete Slab in Specimen FS-2 (Section N2)..... | 423 |
| Figure D.46 | Measured Strains on Concrete Slab in Specimen FS-2 (Section S2)..... | 424 |
| Figure D.47 | Measured Strains on CFRP Sheets in Specimen FS-2 (Section N1)..... | 425 |
| Figure D.48 | Measured Strains on CFRP Sheets in Specimen FS-2 (Section S1)..... | 426 |

| | |
|--|-----|
| Figure D.49 Measured Strains on CFRP Sheets in Specimen FS-2 (Section N2) | 427 |
| Figure D.50 Measured Strains on CFRP Sheets in Specimen FS-2 (Section S2) | |

Chapter 1: Introduction

1.1 BACKGROUND

The need to develop economic and efficient methods to upgrade, repair, or strengthen existing reinforced concrete bridges has received considerable attention recently. The motivation to strengthen an existing reinforced concrete bridge typically comes from two sources: a desire to increase the strength of the bridge to keep pace with increases in the weight of the design vehicle, and a desire to repair deterioration that has taken place over the years of operation.

According to the National Bridge Inventory (NBI) there are approximately 47,000 bridges in Texas. Of these, only 15,300 form part of the National Highway System (NHS). Therefore, approximately 70% of the total number of bridges are part of the off-system roadways [FHWA, 1999].

Many of the reinforced concrete bridges in off-system roads were constructed over 50 years ago. The trucks crossing these bridges often correspond to overload conditions because legal truck loads have increased considerably during this time. The Texas Department of Transportation (TxDOT) has an ongoing bridge rating and inspection program to insure that these bridges can remain in operation and to mitigate the potential risk of structural failure. Bridges need to be inspected either on a one-year or two-year frequency depending on the load rating

of the bridge. Current practice is to inspect bridges that do not meet an HS-20 inventory rating on a yearly basis. Therefore, the Department of Transportation can incur significant savings if the number of bridges that currently have a low load rating are upgraded.

Additionally, off-system roadways often require widening to accommodate a larger vehicular traffic volume due to an increase in the market activity of an area. Internal TxDOT policies require that bridges that do not meet the current design-truck standard (HS-20) can not qualify for widening and therefore need to be replaced when the road is widened. The economic impact of bridge replacement is represented by, not only the direct costs associated to demolition and construction of a new bridge, but also by the indirect costs associated to the loss of roadway use and traffic disruption. The latter are often difficult to quantify and foresee.

An alternative to bridge replacement is strengthening using well-established methods. Casting additional elements, increasing cross-section size, and bonding steel plates are techniques that have been used in the past to widen an existing bridge. These solutions can be expensive and difficult to implement, especially for low-river crossings. Therefore, TxDOT was interested in developing economic and efficient methods to strengthen existing reinforced concrete bridges and increase their live-load capacity as an alternative to bridge replacement.

The use of carbon fiber reinforced polymer (CFRP) composites to increase the flexural capacity of elements in the bridge superstructure was identified as a possible alternative to other strengthening methods. This alternative was considered particularly attractive to increase the live-load capacity of the bridges because the increase in dead loads is insignificant with these materials. Therefore, the increase in capacity after strengthening is used entirely to resist the increase in live loads.

1.2 IDENTIFICATION OF CANDIDATE BRIDGES

A large percentage of the total number of bridges in Texas is part of off-system roadways. Pan-joist and flat-slab bridges are commonly found along these roads. Approximately 30% of the total number of pan-joist bridges and 20% of the total number of flat-slab bridges were not designed using the current design truck (HS-20). Therefore, many of these bridges are load posted and do not meet the TxDOT criteria for roadway widening discussed in Section 1.1. Because of the large number of these types of bridges, pan-joist and flat-slab bridges were selected as candidates for the application of the strengthening methods investigated in this research project.

1.3 OBJECTIVES AND SCOPE OF RESEARCH

The objectives of this research project were to investigate the effectiveness of composite materials to strengthen reinforced concrete bridges, and to develop

design guidelines for the safe implementation of these materials in existing bridges. The use of the guidelines presented in this dissertation are limited to bridges that do not show signs of damage or deterioration. The bridges considered in this investigation were inspected recently and there were no indications that the original capacity has been compromised.

To meet the goals of this project, a comprehensive research program was developed in coordination with TxDOT engineers. The overall research project was divided into three phases. A summary of the most important results from phase 1 and 2 are presented in Sections 1.3.1 and 1.3.2, respectively. Only the results from phase 3 are presented in detail in this dissertation, but results from the other phases are referenced throughout.

1.3.1 Summary of Results from Phase 1

Twenty-two rectangular beams were tested in the first phase of the research project to investigate the effect of CFRP composites on the flexural strength of reinforced concrete elements. Composites supplied by four different manufacturers were used in this part of the project. The main objective of this phase of the research project was to develop strengthening schemes using CFRP composites that would produced reliable and repeatable response of the strengthened elements. The effects of placement of the composite on the reinforced concrete element, external anchorage using transverse composites straps, and long-term wetting and drying

cycles were among the variables included in these tests. Bramblett [2000] gives a detailed discussion of the results obtained from the beams tested in phase 1. Therefore, only a summary of the most important research findings are presented here.

The laboratory tests were initially designed to determine the bond length required to develop the rupture stress of the composite before the CFRP composites debonded from the surface of the concrete. The CFRP was bonded to the tension face to maximize the contribution to the flexural capacity of the beams. All beams were simply supported and were subjected to four-point loading. The bond length was measured from a critical section, where a crack was pre-formed in the beams, to the end of the composite. The critical section also corresponded to the position of one of the applied loads on the beams (Figure 1.2b). However, the results from these tests indicated that debonding of the CFRP composites from the surface of the concrete was the controlling mode of failure for all specimens, even when the composites were bonded along the entire span.

The tests with composites applied to the bottom face of the specimens revealed that debonding predominantly initiated from the flexural crack closest to the critical section on the shear span of the beams. The combination of shear and moment caused the crack to open and simultaneously generate a vertical offset on the surface of the concrete. This phenomenon triggered local debonding of the composite in the vicinity of the crack due to prying action (Figure 1.1c). Therefore,

ways to control the detrimental effects of local debonding due to vertical offset of the surface of the beam were investigated.

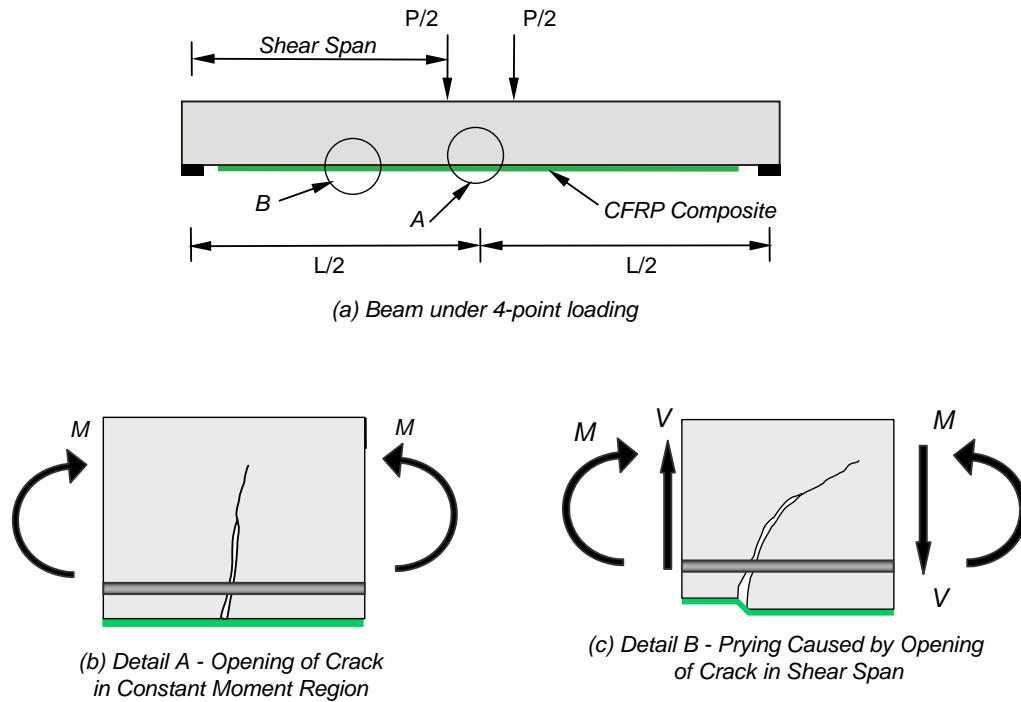
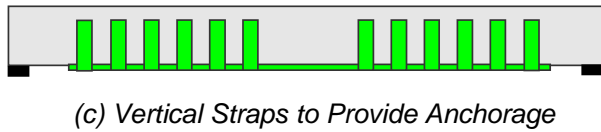
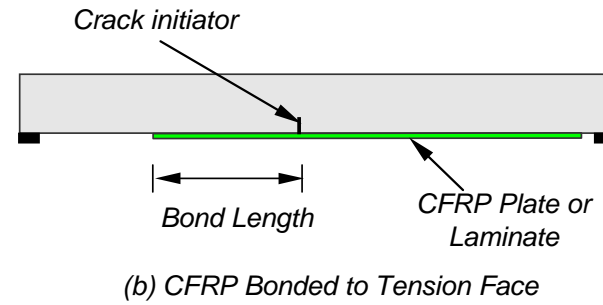
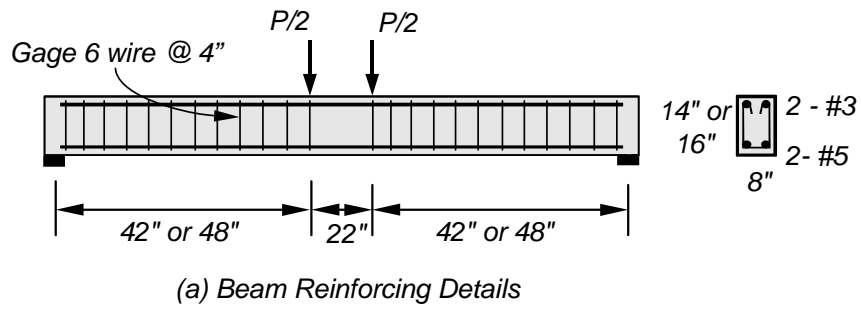


Figure 1.1 Prying Action Observed on CFRP Composite Attached to the Bottom Surface of the Beams

The addition of transverse composite straps along the bonded length of the laminate arrested the debonding crack and prevented it from spreading along the entire length. This technique was initially implemented on beams with composites attached to the bottom face (Figure 1.2c).

Another strengthening configuration was investigated to delay local debonding caused by the vertical offset at flexural cracks. In this scheme the CFRP composites were attached to the side faces of the beams to eliminate the prying action that caused local debonding (Figure 1.2d). Also, a combination of the schemes presented in Figure 1.2 (c) and (d) was tested in some beams. Transverse CFRP woven fabric was wrapped around the CFRP pultruded plates that were attached to the sides of the beams (Figure 1.2e).

The test results indicated that debonding was delayed by the addition of transverse straps along the span of the specimens. In most cases, however, failure of the beams was still controlled by debonding of the CFRP composites. The measured strains on the composites in beams with transverse straps were larger than the strains on the composites developed in beams with the composites bonded to the bottom surface. In some specimens, although debonding had initiated at several locations, failure was controlled by CFRP rupture. This event indicated that the maximum composite strain was reached before total debonding from the surface of the concrete occurred. This technique was only used for beams strengthened using wet-layup composite systems.



∞

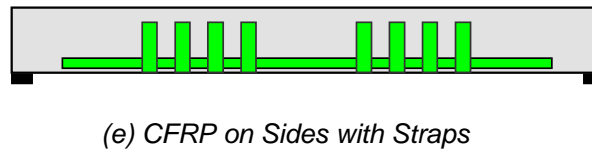


Figure 1.2 Summary of CFRP Configurations Used in Phase 1

Attaching the composites to the sides of the beams was also effective in delaying total debonding. One beam was strengthened using a CFRP wet-layup system and two beams were strengthened using a CFRP pultruded system using this technique. The beam strengthened with the wet-layup system failed by rupture of the CFRP laminate at the critical section. Both beams strengthened using the pultruded system failed by debonding of the composite from the surface of the concrete. However, these beams failed after significant deformations had occurred and local debonding was observable at several locations along the CFRP plates.

The largest measured CFRP strains corresponded to beams where one of the techniques devised to delay debonding was used. A summary of the maximum measured CFRP strains on the beams tested in phase 1 is presented in Table 1.1. The beams where debonding was delayed by one of the methods described in this section achieved a more ductile and repeatable response.

Two beams were tested statically to failure after being exposed to cycles of wet and dry conditions. These beams were strengthened using an identical strengthening scheme as used for beam B4. A sustained load equal to 20% of the yield load was also applied in one of the beams. The results of these tests indicate that the bond between the composite and the surface of the concrete was not affected by exposure to moisture or sustained load. Both beams failed by CFRP rupture and the maximum measured CFRP strains were comparable to beam B4.

Results from this phase indicate that all four of the commercially available CFRP systems could be used to strengthen undamaged reinforced concrete beams. Two were selected for study in phase 3 because they are representative of the different composite systems that were used in phase 1. Therefore these techniques were used in the strengthening schemes for the large scale specimens. A conservative value of the maximum measured CFRP strains in the beams where these schemes were implemented was obtained from the tests in phase 1 and used for design of the strengthening schemes in phase 3. The maximum strain that could be reliably developed in the CFRP composites was assumed to be 0.007.

Table 1.1 Summary of Test Results from Beams in Phase 1 [adapted from Bramblett, 2000]

| Specimen | CFRP Strengthening Scheme | Failure Mode | Maximum Measured CFRP Strain |
|-----------------|----------------------------------|---------------------|-------------------------------------|
| Control A & B | None | Crushing | NA |
| A1 | Bottom | Debonding | 0.0079 |
| A2 | Bottom | Debonding | 0.0061 |
| A3 | Bottom | Debonding | 0.0120 |
| A4 | Bottom | Debonding | 0.0078 |
| B1 | Bottom | Debonding | 0.0072 |
| B2 | Bottom w/Straps | CFRP Rupture | 0.0113 |
| B3 | Sides | CFRP Rupture | 0.0107 |
| B4 | Bottom w/Straps | CFRP Rupture | 0.0119 |
| B5 | Bottom w/Straps | CFRP Rupture | 0.0132 |
| Control C & D | None | Crushing | NA |
| C1 | Bottom | Debonding | 0.0076 |
| C2 | Bottom | Debonding | 0.0070 |
| C3 | Bottom w/Straps | CFRP Rupture | 0.0075 |
| C4 | Sides | Debonding | Unavailable |
| D1 | Bottom | Debonding | 0.0035 |
| D2 | Bottom | Debonding | 0.0048 |
| D3 | Sides | Debonding | 0.0044 |
| D4 | Sides w/Straps | Debonding | 0.0065 |
| D5 | Sides w/Straps | Debonding | 0.0062 |
| E1 (exposure) | Bottom w/Straps | CFRP Rupture | 0.0111 |
| E2 (exposure) | Bottom w/Straps | CFRP Rupture | 0.0118 |

1.3.2 Summary of Results from Phase 2

Bridge elements are subjected to live loads that are applied repeatedly throughout their design life. Therefore, it was considered important to investigate the effects of repeated loads on the behavior of the reinforced concrete beams strengthened using CFRP composites.

Eight rectangular beams strengthened using two different composite systems were subjected to load cycles using different load amplitudes to investigate the effect of cycling on the response of the beams in phase 2. The beams were divided in two groups; four beams were strengthened using an identical strengthening scheme as beam B4 and four were strengthened using a strengthening scheme identical to beam D5. Therefore, it was possible to directly compare the beam response after load cycling to the companion specimens tested during phase 1. The experimental setup was identical to the one used for phase 1 but the load was controlled using a closed-loop system in this case. The load was applied cyclically from a load approximately equal to zero to the load that generated the desired stress in the steel reinforcement.

The load amplitude was selected initially to represent service-load conditions in an existing bridge. Therefore, the beams were subjected to repeated loads that generated stresses equal to 30% or 50% of the yield stress on the longitudinal steel reinforcement. These beams were subjected to either 10,000 or 1,000,000 cycles of load and then tested statically to failure. Results from these

tests indicated that the bond between the composites and the surface of the concrete did not deteriorate with service-level loading cycles because all the beams failed at approximately the same load as the companion beams tested in phase 1 (Figure 1.3).

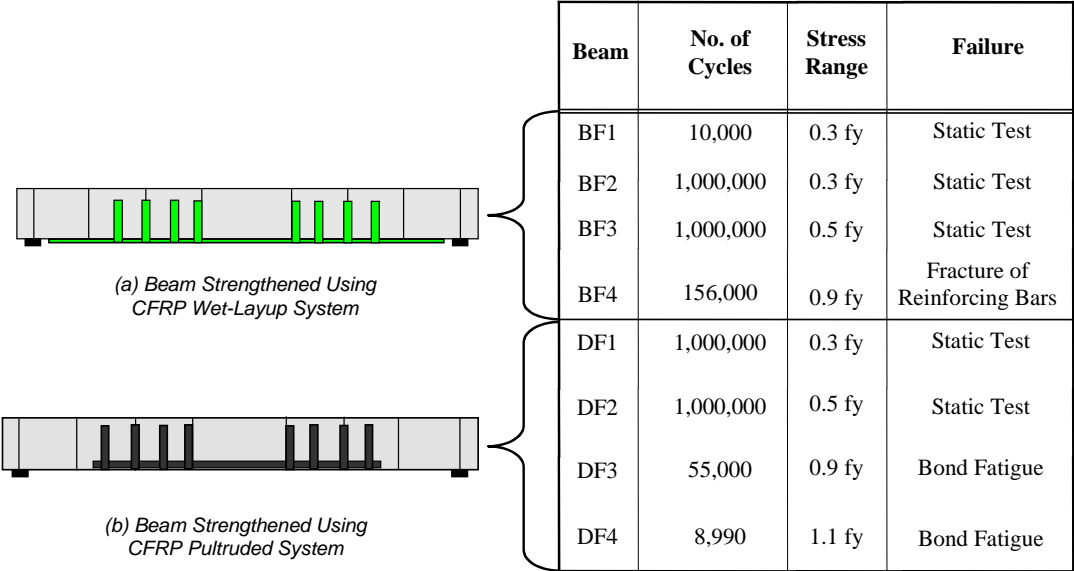


Figure 1.3 Summary of Results from Phase 2

Subsequently, the remaining beams were subjected to higher stress ranges to cause either fatigue failure either between the composite and surface of the concrete or on the reinforcing steel. One beam strengthened using a wet-layup composite system failed by fatigue of the steel reinforcement after the application of 156,000 load cycles at a reinforcing bar stress amplitude equal to 90% of the yield stress (Figure 1.3a). Two beams strengthened with a pultruded composite

system failed by fatigue of the bond between the composite and the surface of the concrete at stress ranges equal to 90% and 110% of the yield stress (Figure 1.3b).

The results from these tests indicate that cycling under stresses representative of service-load conditions does not deteriorate the bond between the composite and the surface of the concrete. Beams subjected to service-load level stress ranges failed at approximately the same load as the companion specimens tested in phase 1. Fatigue failures were only generated after cycling to very high stress ranges. A detailed discussion of the results of the repeated load tests conducted during this phase of the research program is presented by Benouaich [2000].

1.3.3 Description of Phase 3 and Organization of Dissertation

Four full-scale laboratory specimens representative of reinforced concrete bridges in Texas were constructed and tested in phase 3. For this phase of the research project, candidate bridges were first identified in conjunction with TxDOT engineers. The behavior of strengthened reinforced concrete bridge elements using CFRP composites was investigated in the laboratory. A detailed presentation of the design, construction and laboratory tests for phase 3 is included in this dissertation.

The use of CFRP composites to strengthen existing reinforced concrete elements has been investigated in the past by other researchers. The conclusions and observations from these programs, as they relate to this research project, are

summarized in Chapter 2. Areas where additional information is required or conclusions need verification are also identified. To meet the objectives of this investigation, it was considered essential to be able to calculate the capacity and reproduce the behavior of the laboratory specimens representing the strengthened bridge elements that were selected for this project. The analytical model presented in Chapter 3 was able to reproduce the behavior of the strengthened elements and was used as the basis for the design procedure presented in Chapter 10.

Pan-joist bridges were one of the two types selected for detailed investigation in this project. The prototype bridge selected for this study is presented in Chapter 4. The design of the laboratory specimens is also discussed in this chapter. The measured response of two pan-joist specimens is presented in Chapter 5, and the analytical model is verified using measured response of the pan-joist specimens in Chapter 6.

Flat-slab bridges were also selected for investigation in the research project. The prototype bridge that was selected to represent this type of construction is presented in Chapter 7. Particular aspects of this form of construction and the criteria adopted to design the strengthening schemes are also discussed. The measured response and observed behavior of the two flat-slab specimens are discussed in Chapter 8. The analytical model is verified using the measured response of the flat-slab specimens in Chapter 9.

The primary goal of the research project was to develop design guidelines that would produce safe designs of strengthening schemes for the reinforced concrete bridges studied throughout the project. The design recommendations presented in Chapter 10 are based on the experience gained from the laboratory tests of the strengthened specimens. Finally, the conclusions that can be drawn from the results of this investigation are summarized in Chapter 11. Areas requiring further research are also identified.

| | |
|---|----------|
| CHAPTER 1: INTRODUCTION | 1 |
| 1.1 Background..... | 1 |
| 1.2 Identification of Candidate Bridges | 3 |
| 1.3 Objectives and Scope of Research | 3 |
| 1.3.1 Summary of Results from Phase 1 | 4 |
| 1.3.2 Summary of Results from Phase 2 | 12 |
| 1.3.3 Description of Phase 3 and Organization of Dissertation..... | 14 |
| | |
| Figure 1.1 Prying Action Observed on CFRP Composite Attached to the Bottom Surface of the Beams..... | 6 |
| Figure 1.2 Summary of CFRP Configurations Used in Phase 1 | 8 |
| Figure 1.3 Summary of Results from Phase 2..... | 13 |
| | |
| Table 1.1 Summary of Test Results from Beams in Phase 1 [adapted from Bramblett, 2000]..... | 11 |

Chapter 2: Literature Review

2.1 INTRODUCTION

A review of previous investigations on the strengthening of reinforced concrete elements using CFRP composites is presented in this chapter. A brief overview of the evolution of the use of composites in civil engineering is presented in Section 2.2. The main failure modes observed during previous testing and the conclusions drawn from these programs are presented in Section 2.3. A review of the literature revealed that although CFRP composites are already being used to repair and strengthen existing structural concrete bridges, the technology is still in its developmental stage.

2.2 HISTORICAL BACKGROUND

The earliest applications of structural plastics for civil engineering structures date back to the late 1950s. A house designed entirely with structural plastics was presented by Whittier [1957] as part of a demonstration project built in an amusement park in Anaheim, California. Two years later, structural plastics were used for the construction of the U.S. Pavillion as part of the American Exhibition in Moscow [Modern Plastics, 1959]. However, the use of fiber reinforced plastics for civil engineering applications has been limited due to the lack of comprehensive design guidelines [ASCE, 1984].

Fiber reinforced composites have been consistently used in other fields of engineering since the late 1960s. Their use had been restricted mainly to the aerospace and automotive industries, where the use of high strength, lightweight materials results in significant fuel savings and the possibility of increasing the payload. Airplane and automobile parts that were traditionally fabricated using aluminum are being replaced with composites [Mallick, 1993]. Other fields such as the boating industry and sporting goods industry have also benefitted from the used of fiber reinforced composites. For pressure vessels and piping applications, where corrosion protection is a primary concern, fiber reinforced plastics have also been used extensively [ASME, 1992 and 1998].

In civil engineering, the use of composites is only beginning to gain acceptance because composite materials have not been economically competitive with traditional building materials such as steel or concrete. The use of these materials for the repair and strengthening of the aging infrastructure provides an interesting alternative to traditional methods, because of their high strength-to-weight ratio, corrosion resistance, and excellent fatigue performance. Although the technology of the use of composites in the aerospace industry has advanced significantly over the last 30 years, many methods for their application to strengthen existing structures are still under investigation.

To assess the applicability of composite materials for the bridge infrastructure in the United States, the Federal Highway Administration conducted a scanning tour of Europe (UK, Switzerland, Germany) and Japan, where composites had already been used to strengthen existing bridges [FHWA, 1997]. During this survey, applications that did not require modification for use in the United States were identified. In addition, areas where further research was needed before the technology could be implemented in field applications were highlighted. In the case of strengthening of existing bridges using CFRP composites, areas that need further research included the development of design guidelines consistent with U.S. practice and the development of adequate details to insure the full participation of the concrete substrate. The full-scale tests documented in this dissertation provide information about these two topics.

2.3 PREVIOUS EXPERIMENTAL STUDIES

Research on strengthening existing structures using fiber reinforced composites (FRP) was motivated by the need to eliminate some of the problems associated with the traditional method of strengthening by bonding steel plates to the surface of the concrete. By using FRP composite plates, the corrosion potential of the plates was eliminated and the use of heavy equipment to handle the plates during construction was minimized.

Investigations on the use of fiber reinforced composites to strengthen bridge structures began in the late 1980s. These investigations examined the behavior of strengthening reinforced concrete beams using glass fiber reinforced polymers (GFRP). Relatively thick GFRP plates (more than ¼ in.) had to be used to achieve from 40% to 100% increase in strength, if anchorage was provided at the ends of the plates [Saadatmanesh and Ehsani, 1991]. The predominant failure mode that was observed in these tests was similar to that observed during tests on beams strengthened using steel plates. The composite material debonded from the surface of the concrete at failure and debonding of the plates initiated at the ends due to the presence of large normal and shear stresses. Therefore, measures were taken to prevent this type of failure by anchoring the ends of the GFRP plates to the concrete.

One of the earliest research programs that investigated the use of CFRP composites to strengthen reinforced concrete elements was conducted at the Swiss Federal Institute of Technology [Meier et al., 1992] in the late 1980s. Bridges that had been strengthened using steel plates were showing signs of corrosion after only a few years in service and carbon fiber composites were selected as an alternative. A qualitative comparison of the performance of carbon, glass, and aramid composites is presented in Table 2.1 [Meier and Winistörfer, 1995].

Table 2.1 Qualitative Comparison of Different Fibers used in Composites [Meier and Winistörfer, 1995]

| Criterion | Type of Fiber used in Composite | | |
|----------------------|---------------------------------|--------------|---------------|
| | Carbon Fibers | Glass Fibers | Aramid Fibers |
| Tensile strength | Very good | Very good | Very good |
| Compressive strength | Very good | Inadequate | Good |
| Young's modulus | Very good | Good | Adequate |
| Long-term behavior | Very good | Good | Adequate |
| Fatigue behavior | Excellent | Good | Adequate |
| Bulk density | Good | Excellent | Adequate |
| Alkaline resistance | Very good | Good | Inadequate |
| Price | Adequate | Adequate | Very good |

2.3.1 Flexural Tests on Small-Scale Specimens

During the early and mid 1990s, a significant number of studies were conducted in several parts of the world to investigate the use of CFRP composites to increase the flexural strength of existing beams. The majority of the laboratory tests were conducted on small-scale rectangular beams tested under four-point bending. The main modes of failure for these specimens are identified in Figure 2.1, where the critical crack is indicated using a thick line:

- a) Tensile rupture of the CFRP composites (sheets).
- b) Failure by crushing of the concrete in compression.
- c) Diagonal tension failure at end of CFRP composites (plates).
- d) Debonding (peeling) of the CFRP composites.

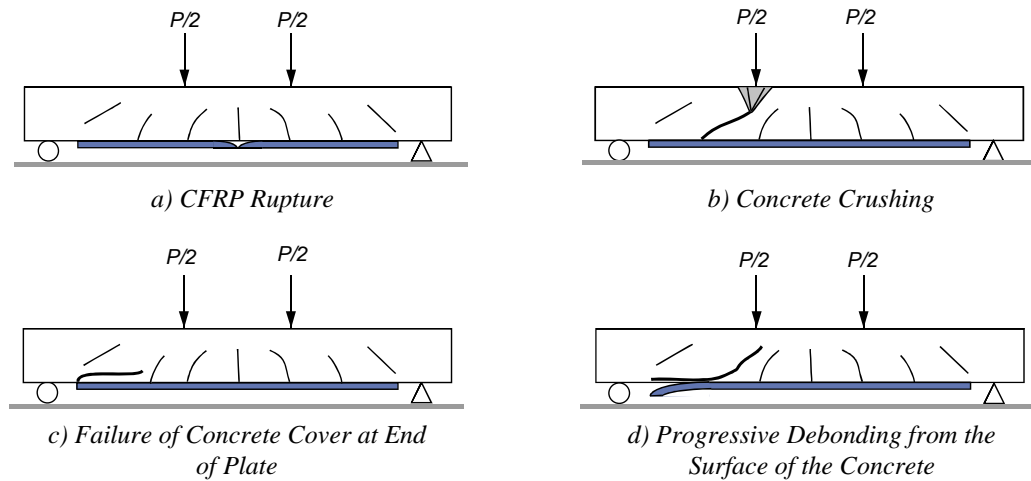


Figure 2.1 Observed Failure Modes of Strengthened Members Using CFRP Composites

A list of the research programs that were included in this investigation and the experimental parameters are summarized in Table 2.2. These studies were selected to give an overview of the most important parameters that affect the performance of strengthened beams. The specimen characteristics tested in these research programs are summarized in Tables 2.3 and 2.4. The predominant modes of failure and main conclusions are summarized in Table 2.5.

A common observation in these research programs was that failure of the beams was often controlled by CFRP debonding from the surface of the concrete (Table 2.5). Therefore, several researchers investigated the use of different

techniques to delay or eliminate debonding as a failure mode. Some of the techniques that were investigated are illustrated in Figure 2.2.

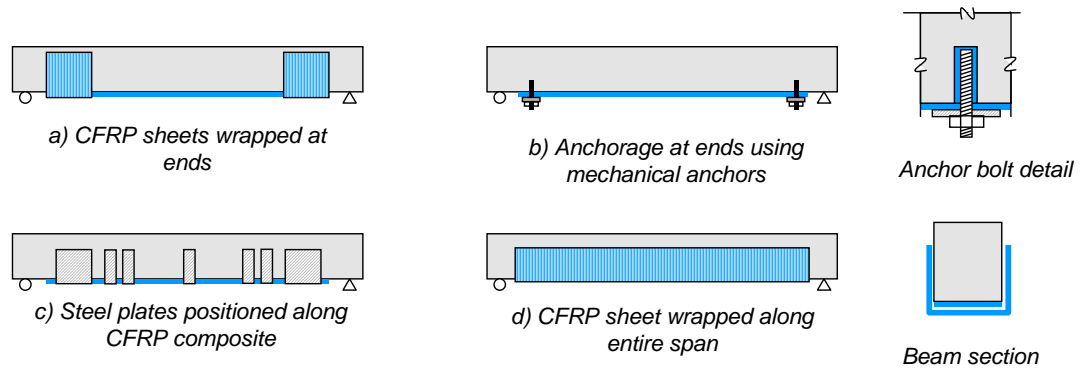


Figure 2.2 *Techniques used by Previous Researchers to Anchor Longitudinal CFRP Composites*

Table 2.2 Summary of Previous Investigations on Flexural Tests

| Test Series | Research Group | Experimental Parameters |
|--------------------|--|--|
| 1 | Ritchie, Thomas, Lu, and Connelly (1991) | <ul style="list-style-type: none"> • Composite type. • Anchorage at end of plate. |
| 2 | Arduini and Nanni (1997) | <ul style="list-style-type: none"> • Composite type. • Shear span/depth ratio. • Effect of precracking. • Surface preparation. |
| 3 | Norris, Saadatmanesh, and Ehsani (1997) | <ul style="list-style-type: none"> • Configuration of CFRP system. • Fiber orientation. |
| 4 | Arduini, DiTommaso, and Nanni (1997) | <ul style="list-style-type: none"> • Number of composite plates. • Anchorage at end of plates. |
| 5 | He, Pilakoutas, and Waldron (1997) | <ul style="list-style-type: none"> • Anchorage technique at ends of plates. |
| 6 | David, Djelal, and Buyle-Bodin (1997) | <ul style="list-style-type: none"> • Composite type. • Thickness and/or number of plies. |
| 7 | GangaRao and Vijay (1998) | <ul style="list-style-type: none"> • Number of plies. • Effect of precracking. • Anchorage by wrapping with CFRP sheets. |
| 8 | Spadea, Bencardino, and Swamy (1998) | <ul style="list-style-type: none"> • External anchorage for CFRP plates (to control slip). |
| 9 | Garden and Hollaway (1998) | <ul style="list-style-type: none"> • Shear span to depth ratio. • Plate end anchorage. |
| 10 | Ross, Jerome, Tedesco, and Hughes (1999) | <ul style="list-style-type: none"> • Existing reinforcement ratio. • Effect of composite area to steel ratio. |
| 11 | Grace, Sayed, Soliman, and Saleh (1999) | <ul style="list-style-type: none"> • Placement of CFRP system. • Anchorage with vertical sheets. |

The ends of the composites received particular attention due to the normal stresses that are generated at the ends of the plates. To anchor the composite ends, the use of steel bolts or composite wraps were investigated (Figure 2.2 a and b). However, these methods were only partially effective in delaying debonding and anchoring at other locations was required (Figure 2.2 c). To develop the maximum strength of the composite in tension, composites wrapped along the entire beam length were used to anchor the longitudinal laminates [GangaRao and Vijay, 1998]. However, this technique can be extremely expensive because a large amount of material is required to strengthen a full-scale structure (Figure 2.2 d).

Numerous anchoring techniques have been investigated without achieving uniform results. The locations where the CFRP composites require anchorage have been determined based on the characteristics of the particular specimens used in each research program. Additionally, the effectiveness of these anchoring techniques has not been evaluated in large-scale elements. Therefore, a uniform criterion is required for the design of the strengthening schemes using composites for its application to actual bridges.

Table 2.3 Summary of Flexural Tests by Previous Investigators

| Group No. | No. of Beams | Strengthening Method | | | | |
|-----------|--------------|----------------------|------|------|------|-------|
| | | Control | CFRP | GFRP | AFRP | Steel |
| 1 | 16 | 2 | 2 | 9 | 1 | 2 |
| 2 | 18 | 2 | 16 | - | - | - |
| 3 | 13 | 1 | 12 | - | - | - |
| 4 | 6 | 2 | 4 | - | - | - |
| 5 | 10 | 5 | 3 | - | - | 2 |
| 6 | 10 | 1 | 4 | 5 | - | - |
| 7 | 24 | 4 | 17 | - | - | 3 |
| 8 | 4 | 1 | 3 | - | - | - |
| 9 | 18 | 2 | 16 | - | - | - |
| 10 | 24 | 6 | 18 | - | - | - |
| 11 | 14 | 1 | 6 | 7 | - | - |

CFRP – Carbon FRP composite.

GFRP – Glass FRP composite.

AFRP – Aramid FRP composite.

Steel – Steel plates bonded to bottom.

Table 2.4 Geometry and Reinforcement of Flexural Specimens from Previous Investigators

| Research No. | Section Properties | | | | | | Span Geometry | | |
|--------------|--------------------|----------------|----------------|-----------------|---|--|-----------------|----------------|----------------|
| | b, in. (mm) | h, in. (mm) | d, in. (mm) | d', in. (mm) | A _s , in. ² (mm ²) | A' _s , in. ² (mm ²) | L, in. (mm) | a, in. (mm) | x, in. (mm) |
| 1 | 6 (152) | 12 (305) | - | - | 0.4 (258) | - | 96 (2,440) | 36 (915) | 24 (610) |
| 2a* | 12.5 (320) | 6.3 (160) | 4.3 (110) | 2 (50) | 0.4 (258) | 0.4 (258) | 43.3 (1,100) | 16.5 (420) | 10.2 (260) |
| 2b* | 6.3 (160) | 12.6 (320) | 10.6 (270) | 2 (50) | 0.62 (400) | 0.62 (400) | 82.7 (2,100) | 37.4 (950) | 7.9 (200) |
| 3 | 5 (127) | 8 (203) | - | - | 0.22 (142) | 0.22 (142) | 90 (2,286) | 22.5 (572) | 45 (1,145) |
| 4 | 8 (200) | 8 (200) | 6.4 (163) | 1.5 (37) | 0.48 (308) | 0.48 (308) | 78.7 (2,000) | 27.6 (700) | 23.6 (600) |
| 5 | 6 (150) | 10 (250) | 8.5 (215) | 1.4 (35) | 0.97 (628) | 0.1 (56) | 90 (2,300) | 30 (767) | 30 (766) |
| 6 | 6 (150) | 12 (300) | - | - | 0.48 (308) | - | 110 (2,800) | 35 (900) | 40 (1,000) |
| 7 | 6 (150) | 12 (300) | 10.6 (270) | 1.2 (30) | 0.88 (568) | 0.22 (142) | 107 (2,730) | 35.8 (910) | 35.8 (910) |

Note: Values not indicated in table were not reported in the literature.

* Beams from same investigation with different cross section and span.

Table 2.4 (Continued) Geometry and Reinforcement of Flexural Specimens from Previous Investigators

| Research No. | Section Properties | | | | | | Span Geometry | | |
|------------------|--------------------|----------------|----------------|-----------------|---|--|----------------|----------------|----------------|
| | b, in. (mm) | h, in. (mm) | d, in. (mm) | d', in. (mm) | A _s , in. ² (mm ²) | A' _s , in. ² (mm ²) | L, in. (mm) | a, in. (mm) | x, in. (mm) |
| 8 | 5.5 (140) | 12 (300) | 10.8 (275) | 1 (25) | 0.62 (400) | 0.62 (400) | 189 (4,800) | 71 (1,800) | 47 (1,200) |
| 9a | 4 (100) | 4 (100) | 3.3 (84) | 3.3 (16) | 0.13 (85) | 0.09 (57) | 40 (1,000) | Variable | 32 (400) |
| 9b ⁺ | 4 (100) | 4 (100) | 3.3 (84) | 0.6 (16) | 0.13 (85) | 0.09 (57) | 40 (1,000) | Variable | - |
| 10 | 8 (200) | 8 (200) | 6 (152) | 2 (48) | Variable | 0.22 (142) | 108 (2,742) | 36 (914) | 36 (914) |
| 11 ⁺⁺ | 6 (152) | 11.5 (292) | - | - | 0.62 (400) | 0.62 (400) | 108 (2,742) | 54 (1,371) | 0 |

⁺ Cantilever beam.

⁺⁺ Beams tested with single concentrated load at midspan.

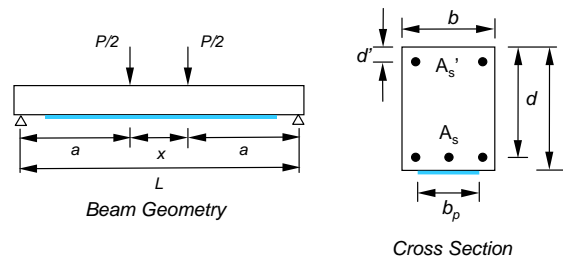


Table 2.5 Observed Failure Modes and Main Conclusions from Previous Flexural Tests

| Test Series | Observed Modes of Failure | Main Conclusions |
|--------------------|--|--|
| 1 | <ul style="list-style-type: none"> • Debonding after yielding of reinforcing steel. | <ul style="list-style-type: none"> • Stress concentration at end of plates needs more study. • Selection of bonding agent is critical. |
| 2 | <ul style="list-style-type: none"> • Debonding at adhesive-concrete interface. • Shear-peeling at ends of plates. | <ul style="list-style-type: none"> • Improve concrete-FRP adhesion. • Wrapping entire length effective as anchorage. |
| 3 | <ul style="list-style-type: none"> • Debonding of FRP composite. | <ul style="list-style-type: none"> • Fiber orientation has large effect on maximum strength. • Pre-cracking has negligible effect. |
| 4 | <ul style="list-style-type: none"> • Concrete crushing. • FRP composite debonding. • Shear at ends of plates. | <ul style="list-style-type: none"> • Brittle failure modes need to be considered in design. • Need to improve knowledge on adhesion performance. |
| 5 | <ul style="list-style-type: none"> • Peeling-off at end of plates. • Shear/peeling-off. | <ul style="list-style-type: none"> • Peeling-off related to thickness and stiffness of plates. • Unless anchored, plates peel off. |
| 6 | <ul style="list-style-type: none"> • Peeling-off along concrete cover. | <ul style="list-style-type: none"> • Use anchoring system to avoid brittle mode of failure. |

Table 2.5 (Continued) Observed Failure Modes and Main Conclusions from Previous Flexural Tests

| Test Series | Failure Modes | Main Conclusions |
|--------------------|--|--|
| 7 | <ul style="list-style-type: none"> • Debonding. • Crushing (fully wrapped beams). • Debonding along concrete cover. | <ul style="list-style-type: none"> • Full wrap required to achieve maximum strength without debonding. |
| 8 | <ul style="list-style-type: none"> • Debonding if not anchored. • Gradual slip if anchored. | <ul style="list-style-type: none"> • Anchorage required for adequate performance. |
| 9 | <ul style="list-style-type: none"> • Shear/Peeling along concrete cover. • Debonding. | <ul style="list-style-type: none"> • Failure mode depends on shear span/depth ratio. • Anchorage required at ends especially for low a/d ratios. |
| 10 | <ul style="list-style-type: none"> • Concrete crushing (high ρ). • FRP debonding (low ρ). | <ul style="list-style-type: none"> • Unable to develop full FRP strength without anchorage. |
| 11 | <ul style="list-style-type: none"> • FRP rupture if transverse sheets are used along entire length. • Debonding when plates are placed on bottom of beams. | <ul style="list-style-type: none"> • Wrapping along full length of CFRP increases maximum load. • Bonding plates on bottom and sides improves performance. |

2.3.2 Flexural Tests on Large-Scale Specimens

Very few tests have been conducted on large-scale flexural strengthened specimens that do not have a rectangular cross section. A testing program was conducted on strengthened half-scale beams by the Florida DOT [Shahawy and

Beitelman, 1996]. A total of eight tee-beams representative of a type of bridge construction in Florida were tested, both under static and fatigue loads. They were strengthened using three different types of CFRP laminates wrapping the entire length of the specimens. The results reported indicate that strengthening existing elements using CFRP composites is a viable option. However, it is evident that the configuration that was used would demand a significant amount of material.

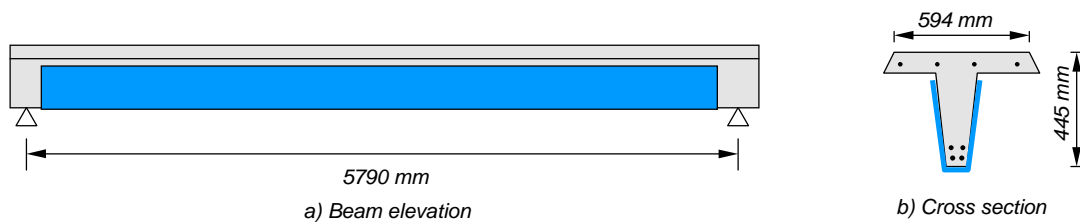


Figure 2.3 Strengthening of Tee-Beams using CFRP composite sheets [Shahawy and Beitelman, 1996]

2.3.3 Tests to Characterize the Concrete-Composite Interface

A common observation in the research projects reported in Section 2.3.1 was that the behavior of the interface between the concrete and the composite needed further study to be able to calculate the capacity of the strengthened members accurately. Therefore, several investigators designed laboratory specimens to obtain more information about the behavior of the composites. However, the mechanisms that are involved in the debonding phenomenon are difficult to replicate with a simple testing apparatus.

Chajes et al. [1996] studied the effects of surface preparation, concrete strength, and adhesive type on the bond strength of single lap joints between composite plates and a concrete block (Figure 2.4). In these tests, the length of the joint was kept constant to identify the set of parameters that gave the highest strength. The ideal parameters were then used to investigate the force transfer between the composites and the surface of the concrete by attaching strain gages to the composites along the length of the connection. The test results indicated that the maximum measured load did not increase when the bonded length was more than 4 in.

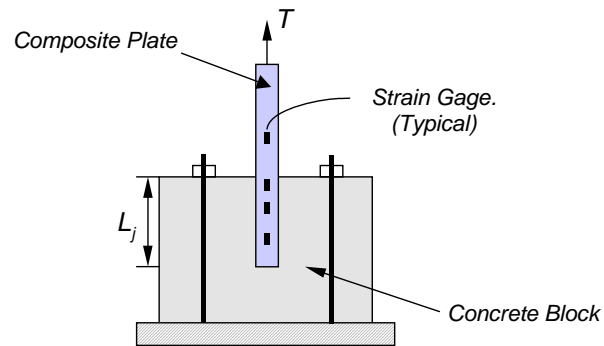


Figure 2.4 Direct Shear Test Apparatus

Bizindavyi and Neale [1999] conducted similar tests of carbon and glass fiber composite laminates bonded to concrete. The effects of multiple plies on the bond transfer characteristics were investigated. Their findings indicate that the maximum strengths of 1-ply and 2-ply 25-mm CFRP laminates can be developed using bonded lengths equal to 80 and 220 mm, respectively.

Other researchers have investigated the effect of cracking in the distribution of bond stresses along the composite-concrete interface. Iketani and Jinno [1997] used the test specimen illustrated in Figure 2.5 to study the transfer of shear stresses between the surface of the concrete and CFRP composite sheets. This figure illustrates a pair of concrete blocks that are held together through the use of CFRP sheets bonded on both sides. Tension loads were applied through a steel bar that was cast in each concrete block. The CFRP sheets were instrumented using strain gages to quantify the distribution of strain with distance from the concrete discontinuity. The variables investigated included the influence of concrete strength and number of plies on the maximum load that could be applied to the bar pullout specimens.

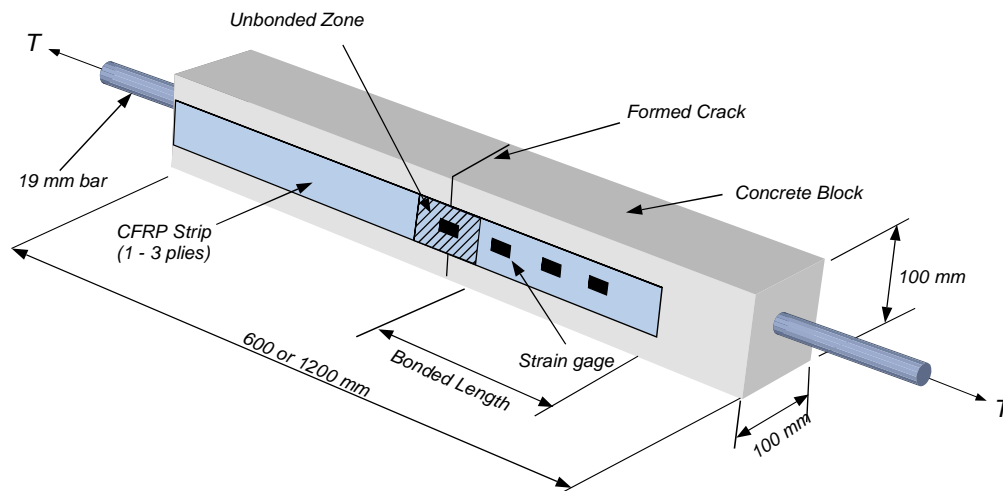


Figure 2.5 Bar-Pullout Bond Test Apparatus

The main conclusions from this study were:

- There is little effect of concrete strength on maximum applied load.
- Number of layers of CFRP sheets increases stiffness of composite and causes shear stresses to be distributed more uniformly along the bonded length.
- Bond lengths of more than 100 mm do not result in an increase in the maximum measured load.
- Debonding started from the position of the concrete discontinuity and proceeded toward the end of the composites.

From these tests, the variation of shear stress at the interface between the composite and the surface of the concrete with distance from the free edge has been identified. The distribution of shear stresses along the composite-concrete interface is illustrated schematically in Figure 2.6. The distance where the interface shear stresses can be considered negligible changed among different investigators, but it typically ranged between 100 and 275 mm.

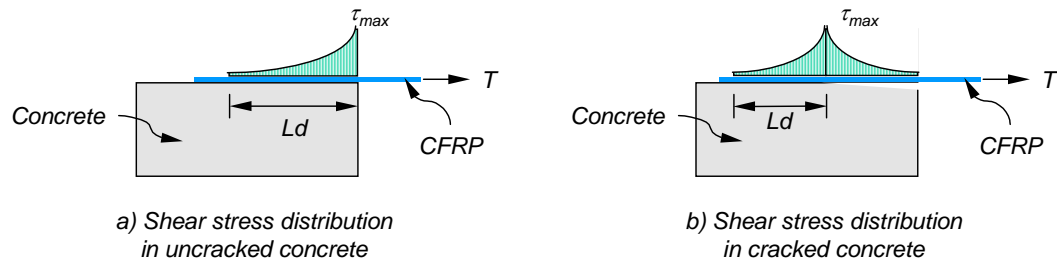


Figure 2.6 Variation of Interface Shear Stress with Distance [Brosens and VanGemert, 1997]

All the previous research presented in this section focused on the determination of stresses caused by an applied force parallel to the concrete surface. However, the mechanisms involved in an actual strengthened element subjected to bending are diverse and can be caused by several factors. The different phenomena that can initiate peeling along the interface between the composite and the surface of the strengthened element were summarized by Blaschko et al. [1998]. They identified five different modes of peeling that can originate in a strengthened flexural member (Figure 2.7):

- FRP peeling-off at the outermost flexural crack in the uncracked anchorage zone (Mode 1).
- FRP peeling-off at flexural cracks in the area of maximum moment (Mode 2).

- FRP peeling-off at flexural cracks between the outermost crack and the area of maximum moment (Mode 3).
- FRP peeling-off caused by shear cracks (Mode 4).
- FRP peeling-off caused by unevenness of the concrete surface (Mode 5).

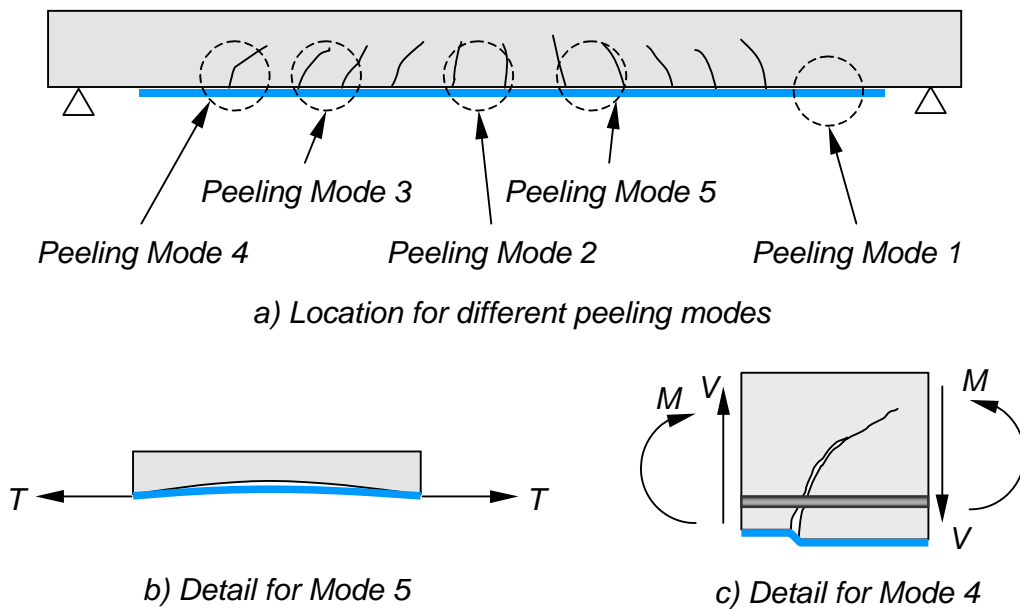


Figure 2.7 Regions in Strengthened Beam where Different Peeling Modes Initiate [Blaschko et al., 1998]

As can be noted from the previous discussion, different failure modes associated with local conditions between the composite and the surface of the concrete can occur in a strengthened element. An efficient way to eliminate the occurrence of these failure modes has not yet been developed; therefore, current

efforts should be focused towards delaying debonding of CFRP composites and not preventing it entirely.

2.4 SUMMARY

The conclusions from previous investigations on the behavior of strengthened reinforced concrete elements using CFRP composites was presented in this chapter. From this review, it is evident that, although the benefits that can be obtained from strengthening flexural members are well identified, there are still areas where further research is required. In particular, most of the previous research was conducted on small-scale specimens where local effects can have a large impact on the global response.

The need to understand the bond behavior between the composite and the surface of the concrete was a consistent conclusion from previous investigations. A summary of previous efforts in this area was also presented. It was found that this phenomenon is highly dependent on local surface and damage conditions and is consequently very difficult to quantify.

Given the degree of information available from previous research in the area of strengthening existing members with composites, testing full-scale specimens representative of actual bridges was considered a priority for this research project. Instead of approaching the debonding problem at the local

concrete-composite interface level, the approach that was taken in this project was to delay total failure of the strengthened element by using techniques that would control total debonding of the composite in an economic manner.

| | |
|---|-----------|
| CHAPTER 2: LITERATURE REVIEW | 17 |
| 2.1 Introduction..... | 17 |
| 2.2 Historical Background..... | 17 |
| 2.3 Previous Experimental Studies | 19 |
| 2.3.1 Flexural Tests on Small-Scale Specimens | 21 |
| 2.3.2 Flexural Tests on Large-Scale Specimens | 30 |
| 2.3.3 Tests to Characterize the Concrete-Composite Interface | 31 |
| 2.4 Summary..... | 37 |
| | |
| Figure 2.1 Observed Failure Modes of Strengthened Members Using CFRP Composites | 22 |
| Figure 2.2 Techniques used by Previous Researchers to Anchor Longitudinal CFRP Composites | 23 |
| Figure 2.3 Strengthening of Tee-Beams using CFRP composite sheets [Shahawy and Beitelman, 1996]..... | 31 |
| Figure 2.4 Direct Shear Test Apparatus | 32 |
| Figure 2.5 Bar-Pullout Bond Test Apparatus | 33 |
| Figure 2.6 Variation of Interface Shear Stress with Distance [Brosens and VanGemert, 1997] | 35 |
| Figure 2.7 Regions in Strengthened Beam where Different Peeling Modes Initiate [Blaschko et al., 1998]..... | 36 |
| | |
| Table 2.1 Qualitative Comparison of Different Fibers used in Composites [Meier and Winistörfer, 1995]..... | 21 |
| Table 2.2 Summary of Previous Investigations on Flexural Tests | 24 |
| Table 2.3 Summary of Flexural Tests by Previous Investigators..... | 26 |
| Table 2.4 Geometry and Reinforcement of Flexural Specimens from Previous Investigators | 27 |
| Table 2.5 Observed Failure Modes and Main Conclusions from Previous Flexural Tests..... | 29 |

Chapter 3: Model to Calculate the Response of Reinforced Concrete Elements Strengthened Using CFRP Composites

3.1 INTRODUCTION

This chapter describes an analytical procedure that was developed to calculate the moment-curvature and load-deflection response of reinforced concrete members strengthened using CFRP composites. The procedure uses the nonlinear material properties of concrete, steel, and CFRP composites to calculate the internal forces corresponding to equilibrium for a strengthened section. Moment and curvature are then calculated from the internal forces, and deflections along the span are calculated from the moment-curvature relationship.

Procedures used to calculate the moment-curvature response of a strengthened section are described in Section 3.2, and procedures used to calculate deflections are described in Section 3.3. The model is validated in Section 3.4 using published data for reinforced concrete elements strengthened with CFRP composites, and is refined in Section 3.5 to include debonding of the CFRP composites from the surface of the concrete.

3.2 MOMENT-CURVATURE ANALYSIS OF STRENGTHENED SECTIONS

The analytical procedure described in this chapter is based on a sectional model. Moment-curvature relationships for reinforced concrete sections strengthened with carbon fiber reinforced composites were calculated using nonlinear material properties. Basic assumptions are presented in Section 3.2.1 and the idealized stress-strain curves for the materials are presented in Section 3.2.2.

3.2.1 Assumptions Used in the Sectional Analysis Model

Similar to most analytical methods used to calculate the flexural response of reinforced concrete elements, the cross section was divided into horizontal slices. The total response of the cross section is obtained by adding the contribution of each slice. Separate slices were used for the different materials; therefore, the idealized behavior of each slice is controlled by the stress-strain relationship for a given material. However, multiple slices may be located at the same position along the depth of the cross section.

The following assumptions, which are consistent with current design practice of reinforced concrete sections, were used in the model:

- Strains increase proportionally with distance from the neutral axis.
- No slip occurs between the steel reinforcement and concrete surrounding it.
- Perfect bond exists between the carbon fiber reinforced composite material and concrete surface.

- Failure is reached when the extreme fiber in compression reaches the maximum usable strain in the concrete (ϵ_{cu}).

The third assumption was later refined because the CFRP material was observed to slip relative to the concrete surface during the experimental phase of this project. Modifications to the analytical model to include debonding of the CFRP and concrete are discussed in Section 3.5.

3.2.2 Stress-Strain Material Models Used for Sectional Analysis

Three material models were used to calculate the response of the strengthened reinforced concrete sections. The models represent the uniaxial stress-strain behavior of the materials in the cross-section. The parameters that are needed to define each material model were based on the measured material properties for concrete and steel, and data obtained from the manufacturers' data for the CFRP composites (Appendix A).

(a) Concrete

The uniaxial stress-strain behavior of concrete in compression was modeled using the curve proposed by Hognestad [1950]. In this model, the ascending branch of the compressive stress-strain curve is modeled with a parabolic relationship. The maximum concrete stress is defined as f'_c , and the strain corresponding to the maximum stress is called ϵ_{co} . The peak compressive stress

was calculated as the product of a constant k_3 , which was set equal to 0.9, by the compressive stress determined from concrete cylinder tests in compression, f'_c . The constant k_3 is defined as the ratio of the compressive stress as determined from compression tests on concrete cylinders to the maximum compressive stress reached in the concrete in the actual member [Hognestad et al., 1955; Rüsçh, 1960]. After this point, stresses decrease linearly with increasing strain until the maximum usable strain in the concrete is reached (ϵ_{cu}). The stress corresponding to the maximum concrete strain is assumed to be equal to 85 percent of the peak stress. The equations that describe the behavior of concrete in compression for the different regions of the stress-strain diagram are presented in Figure 3.1.

Concrete in tension was assumed to behave linearly up to the stress corresponding to its tensile capacity (f_t). After this point, the tensile strength of concrete was assumed to be equal to zero. The slope used for the concrete stress-strain relationship in tension was assumed to be equal to the initial tangent modulus of elasticity in compression (E_c).

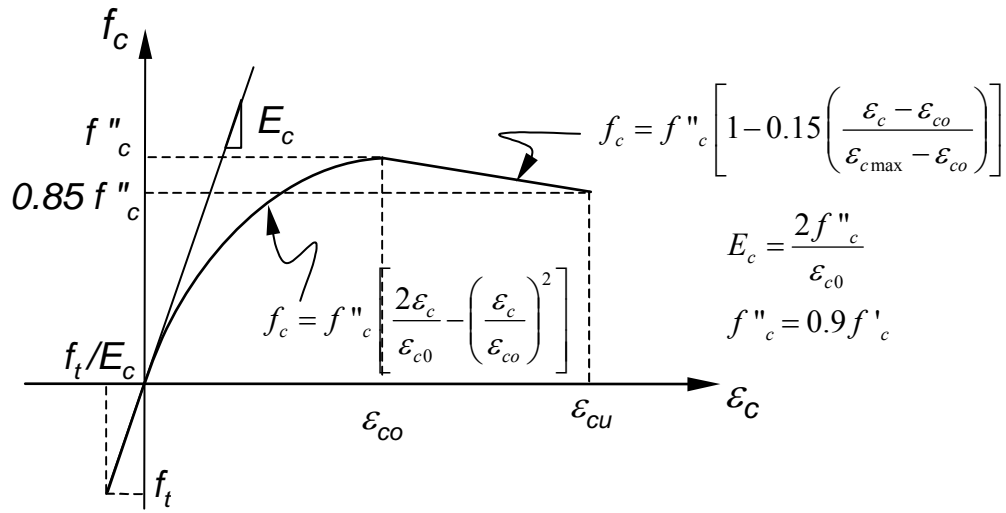


Figure 3.1 Idealized Stress-Strain Relationship for Concrete

Compressive tests of cylinders and split-cylinder tests were used to define the parameters in the concrete model. The concrete cylinders were fabricated using the same concrete mix that was used for the construction of the specimens. The concrete stress-strain parameters determined for the laboratory specimens are listed in Appendix A. When actual material tests were not available, f'_c was assumed to be the specified compressive strength of concrete used for design, f_t was assumed to be equal to $0.1 f'_c$, and ϵ_{c0} was assumed equal to 0.002. The maximum usable strain of concrete, ϵ_{cu} , was considered equal to 0.004.

(b) Reinforcing Steel

The stress-strain relationship for steel reinforcement with a well-defined yield point was idealized using three linear segments. The elastic modulus for the initial slope in the stress-strain curve (E_s) was assumed to be 29,000 ksi. After reaching the yield strain (ϵ_y), the slope of the stress-strain curve was assumed equal to zero until the strain corresponding to initiation of strain hardening (ϵ_{sh}) was reached. The strain-hardening behavior of the reinforcement was modeled using a line with a positive slope beginning at ϵ_{sh} . Details of the material stress-strain model are shown schematically in Figure 3.2 (a).

Reinforcing steel that did not exhibit a well-defined yield point was approximated using the model proposed by Menegotto and Pinto [1973]. In this model the stress-strain relationship of steel is described by an equation that represents a curved transition between initial and final asymptotes to the measured stress-strain curve (Figure 3.2 (b)). The nonlinear stress-strain response of steel can be approximated using the following equation:

$$\frac{f}{f_0} = b \frac{\epsilon}{\epsilon_0} + \frac{(1-b) \frac{\epsilon}{\epsilon_0}}{\left[1 + \left(\frac{\epsilon}{\epsilon_0} \right)^n \right]^{\frac{1}{n}}} \quad (3.1)$$

where:

- f_0 = Stress at intersection of initial and final asymptotes to the stress-strain curve.
- ε_0 = Strain at intersection of initial and final asymptotes to the stress-strain curve.
- b = Ratio of the slopes of the final to initial asymptotes to the stress-strain curve, $b = \frac{E_\infty}{E_0}$.
- n = Parameter that defines the curvature of the transition from the initial asymptotic line to the final asymptotic line.

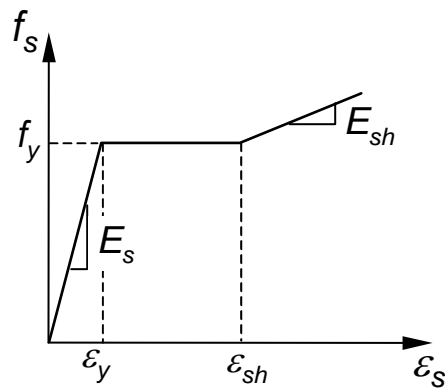
The parameters in the Menegotto-Pinto model can be determined using the following steps [Stanton and McNiven, 1979]:

- Obtain initial and final asymptotic lines to the stress-strain curve.
- Compute the ratio of initial to final asymptotic lines, b . Find coordinates at the intersection of asymptotes (f_0 and ε_0).
- Normalize stress-strain curve by f_0 and ε_0 .
- Compute d^* , where $d^* = \frac{f}{f_0} - b$ at $\frac{\varepsilon}{\varepsilon_0} = 1$.
- Calculate $n = \frac{\log 2}{\log(1-b) - \log d^*}$.

After calculating the Menegotto-Pinto parameters using this procedure, the exponential factor n was modified to better fit the measured stress-strain relationship.

Steel coupons were tested in tension for the different bar sizes used in the fabrication of the specimens. Using these tests, the values that define the stress-strain parameters for the bars were determined. The slope of the line corresponding to the strain-hardening region, E_{sh} , was calculated as the slope of a line going from the stress at ϵ_{sh} to the stress at a strain equal to 0.015. If steel with unknown properties was used in the calculations, the E_{sh} was assumed to be equal to 5% of the initial elastic modulus.

a) Steel with well-defined yield point



b) Steel without well-defined yield point

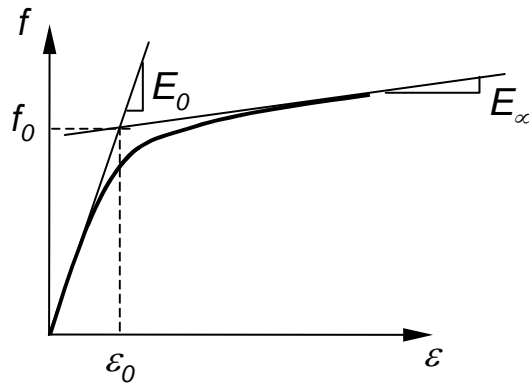


Figure 3.2 Idealized Stress-Strain Relationships for Steel

(c) Fiber Reinforced Polymer Composites

The uniaxial behavior of the carbon fiber reinforced polymer composites (FRP) used in this study was assumed to be linear up to failure (Figure 3.3). Failure in these materials was reached when the strain (ϵ_{pu}) corresponding to the rupture stress (f_{pu}) was reached.

The properties published by the manufacturers were used to define the material models for the different carbon fiber reinforced polymer materials. The values for these parameters are summarized in Appendix A for the composites used in the research project.

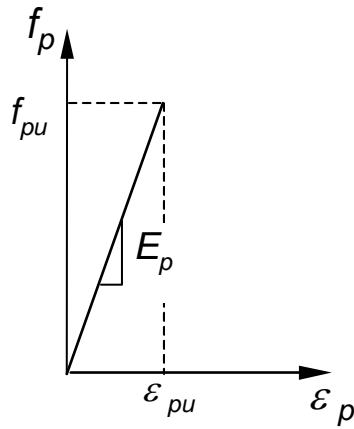


Figure 3.3 Idealized Stress-Strain Relationship for CFRP Composites

3.2.3 Internal Equilibrium of Strengthened Cross Section

The moment-curvature response of a reinforced concrete section strengthened with CFRP composites was calculated dividing the section into horizontal slices and assigning specific material properties to each slice. The procedures used to calculate the stress and strain in each slice and to calculate the corresponding moment and curvature are described in this section.

Internal force equilibrium was established for a series of maximum concrete compressive strains. Moment and curvature were calculated at each point corresponding to the maximum concrete strain assigned to the extreme fiber under compression.

The procedure used to calculate moment and curvature of a strengthened section is described in the following steps:

- Set the maximum compression strain in the concrete (ϵ_{cmax}) to a value between zero and the maximum usable concrete strain (ϵ_{cu}).
- Estimate an initial neutral axis position. The initial neutral axis position was assumed to be $h/2$ in this study.
- Calculate the strain profile based on the extreme compression fiber strain and the position of the neutral axis and then compute the corresponding internal stress components using the material models discussed in Section 3.2.2.
- Check equilibrium in the horizontal direction using the internal stresses computed in step 3 and the known area of each slice.
- Adjust the neutral axis depth, c , until force equilibrium is achieved (repeat steps 1 through 4). A tolerance of 0.05 kip was used in this study.
- Calculate the internal moment and curvature.
- Increase ϵ_{cmax} and repeat steps 1 through 6 for another point in the moment-curvature response.

The internal stress within each slice was calculated at mid-thickness and was assumed to be constant throughout the slice. The stress distribution was approximated by a series of rectangles having a depth equal to the slice thickness

and height equal to the compressive stress calculated from the stress-strain equations. The force contribution from each slice was computed using the width of the cross-section at the slice mid-plane (b_i) and the slice thickness (t_{slice}). This is illustrated for sections that have a non-rectangular cross-section in Figure 3.4 (b).

The internal force components were multiplied by their distance to the neutral axis, z_i , to calculate the internal moment (Figure 3.4). Curvature was calculated by dividing the extreme compressive strain by the neutral axis depth:

$$M = \sum_i F_i z_i$$

$$\phi = \frac{\epsilon_{c \text{ max}}}{c} \quad (3.2)$$

where,

M = Internal moment, kip-in.

ϕ = Curvature, 1/in.

F_i = Internal tensile or compressive force component, kip.

z_i = Distance from neutral axis to internal force component, F_i , in.

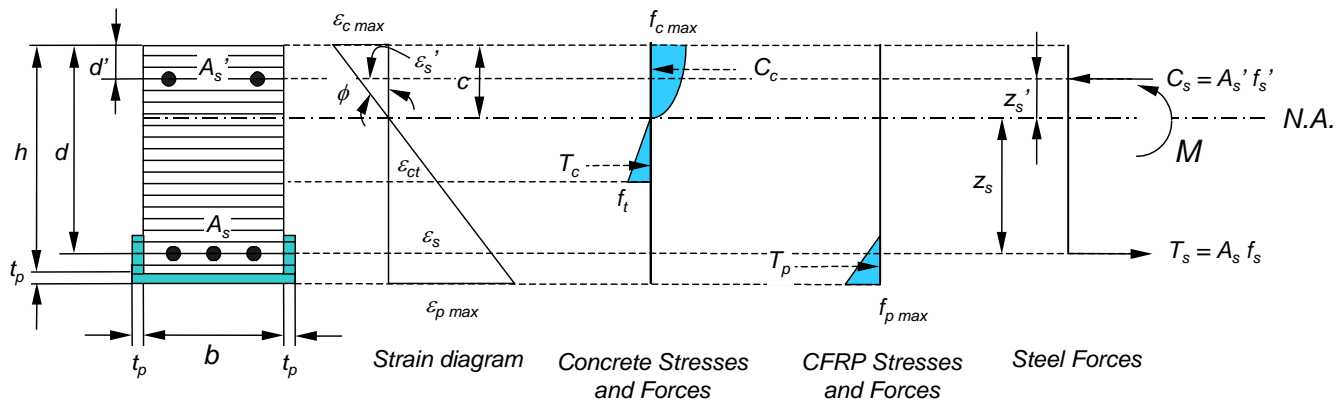
$\epsilon_{c \text{ max}}$ = Strain at the extreme compression fiber.

c = Neutral axis position, in.

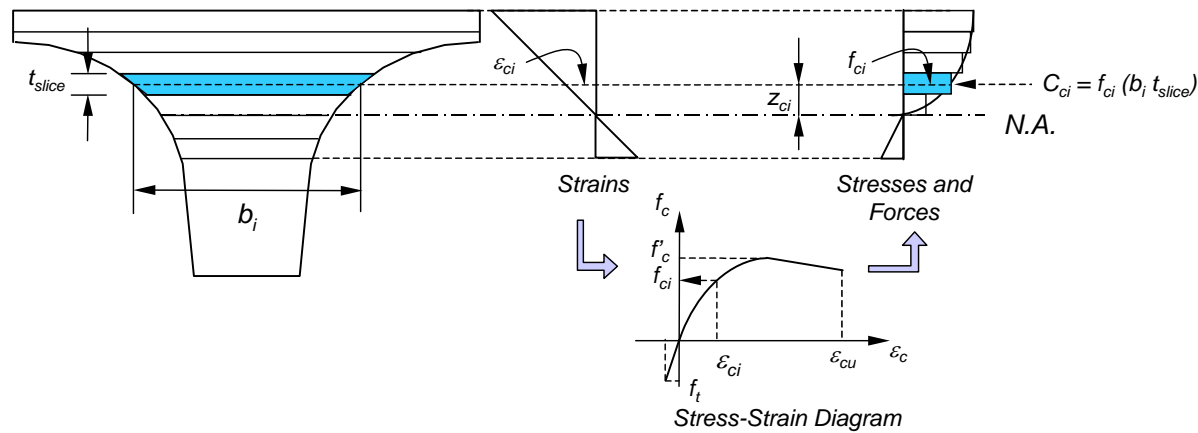
The procedure described above was repeated for other points in the moment-curvature diagram of the section until the maximum usable concrete strain was reached in the extreme compression fiber.

The model initially assumed that the CFRP composites remained attached to the concrete surface. Using this assumption, the maximum stress that can be developed in the CFRP is equal to the rupture stress, f_{pu} . The contribution of the CFRP composite to the total tensile force became zero once the rupture stress was reached. However, experimental testing showed that debonding usually occurred before reaching the CFRP rupture stress and the model was subsequently modified to account for this failure mode (Section 3.5.1).

The procedure described above to calculate moments and their associated curvatures assumes that the CFRP composites are attached to the reinforced concrete section before any load is applied. However, dead loads are always on a structure before strengthening and this needs to be considered particularly for field applications. A modification to the procedure presented in this section is described in Section 3.5.2 to account for the presence of dead loads on the section before bonding the CFRP composites.



(a) Internal Stresses and Forces in Strengthened Section



(b) Calculation of Compressive Stresses

Figure 3.4 Schematic Representation of Sectional Response Illustrating the Procedure Used in the Calculations

3.3 LOAD-DEFLECTION RESPONSE

The calculated moment-curvature relationships for the strengthened members were used to determine deflections. Deflections were calculated using the moment-area method because this method is applicable to members that have a non-linear moment-curvature relationship.

The moment-area method is summarized in this section (Figure 3.5). First, the moment diagram was calculated for a specific span length and configuration of loading. Then, the curvature at every point along the span was determined using the moment-curvature relationship calculated previously for the cross section.

After determining the curvature diagram along the span, rotations and deflections at any point may be calculated using the moment-area theorems. Numerical integration of the curvature diagram was used to determine the rotations and deflections of tangents to the deflected shape. The change in rotation of the tangents to the deflected shape at two points is determined by computing the area under the curvature diagram between the two points. The vertical distance between two tangents to the deflected curve at a point along the span is determined by calculating the first moment of area of the curvature diagram about the point of interest. Deflections are then determined from geometric considerations.

The procedure used to compute the deflection at point j , δ_j , of an element with a nonlinear moment-curvature relationship using the moment-area theorems is

illustrated in Figure 3.5. This procedure can be summarized in the following steps for a simply supported beam:

- Determine the moment and curvature diagrams along the span. Curvatures associated with the moment at each location are obtained from the moment-curvature relationship of the cross section.
- Divide the curvature diagram into sufficient segments (twenty segments were used for this study). The curvature diagram is assumed to be linear within each segment. The curvatures defining an arbitrary segment, ϕ_i and ϕ_{i+1} are shown in Figure 3.5 (b).
- Calculate the area and centroid of each segment using the trapezoidal rule:

$$\begin{aligned}
 A_i &= (\phi_i + \phi_{i+1}) \frac{\Delta x_i}{2} \\
 \bar{x}_i &= \left(\frac{\phi_i + 2\phi_{i+1}}{\phi_i + \phi_{i+1}} \right) \frac{\Delta x_i}{3}
 \end{aligned}
 \tag{3.3}$$

- Compute the first moment of area of each segment about point j . where the distance between tangents needs to be determined.
- Calculate the deflection at a point from geometric considerations using the tangents to the deflected shape.

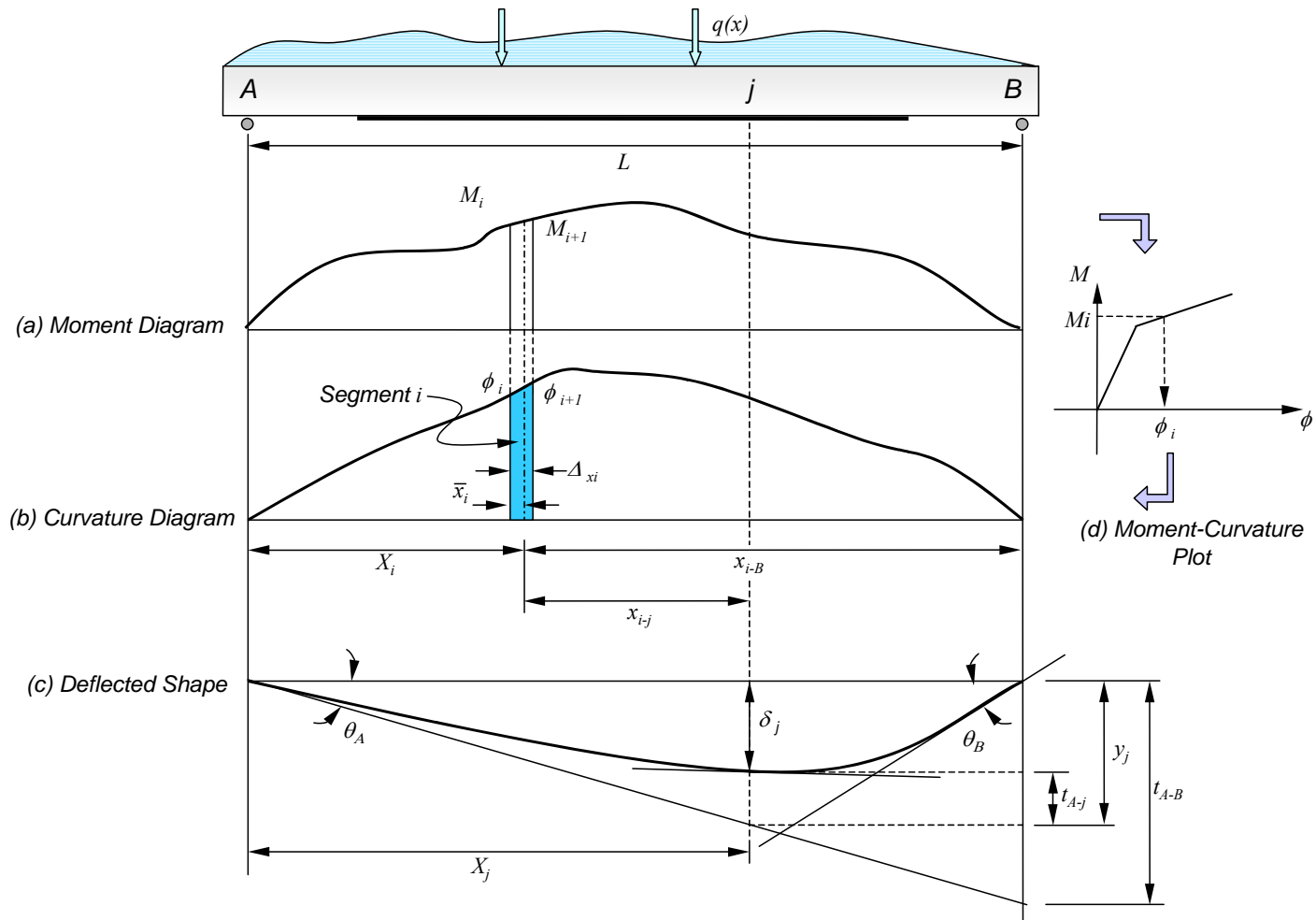


Figure 3.5 Procedure to Calculate Deflections of an Element with a Nonlinear Moment-Curvature Relationship

The distance between two tangents to the deflected shape of the element is determined by taking moments of each segment about the desired point. For example, the distance between the tangents at points A and B is equal to the sum of the product of the area of each segment from the curvature diagram times the distance from point B to the centroid of each segment (Figure 3.5). The distance between two tangents at points A and j can be calculated similarly by computing the moment of the area of each segment on the curvature diagram about point j . The deflection at point j is calculated using Equation (3.4) after determining the distance y_j from similar triangles (Equation 3.5):

$$\delta_j = y_j - t_{A-j} \quad (3.4)$$

where:

$$y_j = \frac{t_{A-B}}{l} X_j \quad (3.5)$$

and:

$$\begin{aligned} t_{A-B} &= \sum x_{i-B} A_i \\ t_{A-j} &= \sum x_{i-j} A_i \end{aligned} \quad (3.6)$$

The nomenclature used in Equations 3.4 to 3.6 and in Figure 3.5 is listed below:

- δ_j = Vertical deflection at point j .
- X_j = Horizontal distance from point A to point j .

y_j = Vertical distance from tangent at A to undeformed position at point j .

x_{i-B} = Horizontal distance from centroid of segment i to point B .

x_{i-j} = Horizontal distance from centroid of segment i to point j .

Ai = Area under the curvature diagram of segment i .

t_{A-B} = Vertical distance from tangent at point A to tangent at point B .

t_{A-j} = Vertical distance from tangent at point A to tangent at point j .

3.4 VALIDATION OF MODEL

The analytical model presented in Sections 3.2 and 3.3 was evaluated using available experimental results. The use of CFRP composites to strengthen reinforced concrete beams has been investigated in the past. Data from some of the previous experimental investigations were used to validate the analytical model. Four experimental studies were selected for this purpose. All specimens in these studies were strengthened using CFRP systems similar to those used in this research project. Only a brief description and comparisons between the measured and calculated displacement response of these specimens are presented in this section.

Table 3.1 summarizes the dimensions and reinforcement for the specimens that were selected for the comparisons. The measured and assumed material properties are presented in Table 3.2. The CFRP composite was bonded to the tension face of the beams considered.

Debonding of the CFRP composites from the surface of the concrete was not considered as a possible failure mode in this part of the investigation. However, after review of the available data and results from this experimental program, it is clear that this mode of failure often controls the behavior of strengthened reinforced concrete members. A procedure for including debonding of the CFRP composites from the concrete surface is introduced in Section 3.5.

3.4.1 Tests by Spadea, Bencardino, and Swamy

Spadea et al. (1998) investigated the effect of using steel plates to prevent debonding of the CFRP from the bottom concrete surface. The response of two specimens from their program was compared with the calculations from the analytical model developed in this study: Specimens A3 and A3.3. Specimen A3 was the control beam and Specimen A3.3 was strengthened using a CFRP pultruded plate. The CFRP plate in the strengthened specimen was anchored using steel plates at several locations along the span length. Although the measured strains in the CFRP composite in Specimen A3.3 were the highest in the test series, failure was still controlled by debonding of the CFRP from the concrete surface.

The responses of Specimens A3 and A3.3 are compared with the calculated responses in Figure 3.6. The vertical axis for the calculated response was truncated at 100 kN in order to facilitate comparisons with the measured results.

The maximum measured loads are compared with the calculated capacities in Table 3.3. The calculations were based on assumed stress-strain relationships for the steel because these data were not available. A well-defined yield point was assumed. Strain hardening was assumed to begin at a tensile strain of 0.015, and the assumed slope of the stress-strain curve after the onset of strain-hardening portion was 5,100 MPa (2.5% E_s). The same material properties were used for both specimens. The ratio of the measured to the calculated capacity was 0.94 for Specimen A3. This 6% difference was believed to be acceptable given the limited available information about the material properties.

The calculated capacity of Specimen A3.3 was higher than the maximum measured load. Failure of this specimen was caused by CFRP debonding from the concrete surface. Therefore, it should be expected that the analytical model would calculate a higher load because it assumes perfect bond between the composite and concrete until the composite reaches its rupture stress f_{pu} . In this case, the capacity ratio (P_{test}/P_{calc}) was 0.86.

The calculated strain in the CFRP plate at the maximum measured load in the tests is reported in Table 3.3. The ratio of ϵ_{calc} , the calculated strain at the measured capacity of the beam, to ϵ_{rupt} , the rupture strain of the material, gives an indication of the fraction of stress that was developed during the tests compared with the CFRP rupture stress. In this case, the CFRP achieved a stress of 75% of the rupture stress before the specimen failed by debonding.

Table 3.1 Dimensions and Reinforcement of Specimens Reported by Other Researchers

| Specimen | b, mm | h, mm | d, mm | d', mm | L, mm | x, mm | a, mm | A _s | A _s ' |
|---|-------|-------|-------|--------|-------|-------|-------|----------------|------------------|
| Spadea et al. (1998) | | | | | | | | | |
| A3, A3.3 | 140 | 300 | 275 | 25 | 4,800 | 1,200 | 1,800 | 2-16 mm | 2-16mm |
| GangaRao et al. (1998) | | | | | | | | | |
| 1A ₂ -R, 3B ₂ -C | 150 | 300 | 270 | 30 | 2,740 | 610 | 1,065 | 2-19 mm | 2-10mm |
| Arduini et al. (1997) | | | | | | | | | |
| B1, B2, B4 | 300 | 400 | 350 | 50 | 2,500 | 300 | 1,100 | 3-13mm | 2-13mm |
| Nakamura et al. (1996) | | | | | | | | | |
| BL, E24-1P, E24-2P | 150 | 150 | 120 | 30 | 1,200 | 400 | 400 | 2-13mm | 2-13mm |

69

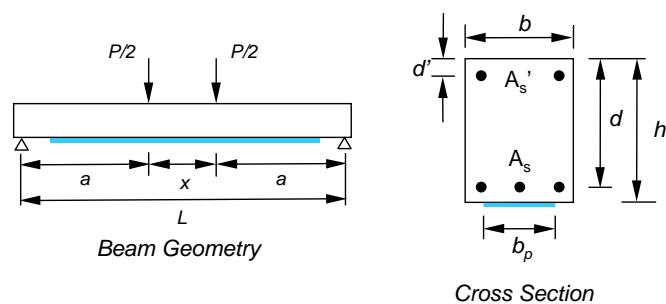


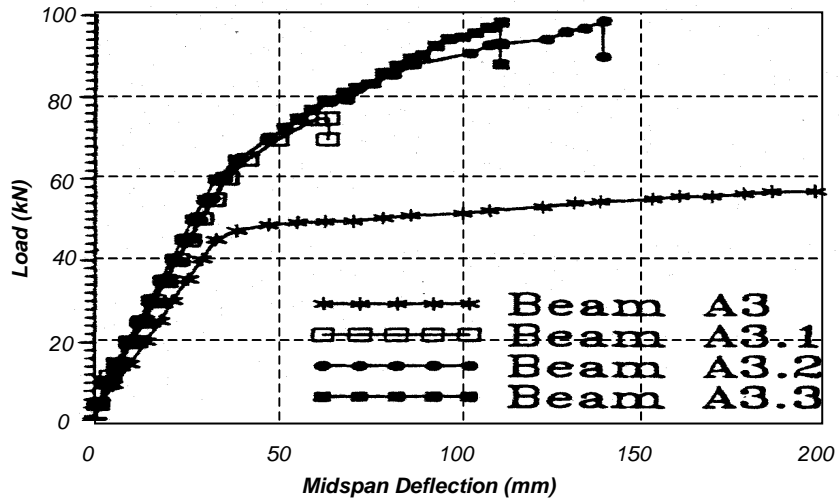
Table 3.2 Material Properties and Dimensions of CFRP Composites of Specimens Reported by Other Researchers

| Specimen | f' _c , MPa | f _y , MPa | CFRP Composite | | | | |
|------------------------|-----------------------|----------------------|---------------------|---------------------|-----------------------|----------------------|------------------|
| | | | t _p , mm | b _p , mm | f _{pu} , MPa | E _p , GPa | Type |
| Spadea et al. (1998) | | | | | | | |
| A3 | 29.5 | 435 | - | - | - | - | - |
| A3.3 | 30.5 | 435 | 1.2 | 80 | 2,300 | 152 | Pultruded Plates |
| GangaRao et al. (1998) | | | | | | | |
| 1A ₂ -R | 50.2 | 415 | - | - | - | - | - |
| 3B ₂ -C | 50.2 | 415 | 0.33 | 150 | 3,100 | 240 | Sheets (3 Plies) |
| Arduini et al. (1997) | | | | | | | |
| B1 | 26 | 340 | - | - | - | - | - |
| B2 | 26 | 340 | 0.17 | 300 | 3,000 | 400 | Sheets (1 Ply) |
| B4 | 26 | 340 | 0.51 | 300 | 3,000 | 400 | Sheets (3 Plies) |
| Nakamura et al. (1996) | | | | | | | |
| BL | 23.5 | 410 | - | - | - | - | - |
| E24-1P | 23.5 | 410 | 0.098 | 150 | 3,430 | 235 | Sheets (1 Ply) |
| E24-2P | 23.5 | 410 | 0.196 | 150 | 3,430 | 235 | Sheets (2 Plies) |

Moduli of elasticity for concrete and steel were not reported. The values used in the calculations were:

$$E_c = 2 f'_c / 0.002, E_s = 200,000 \text{ MPa}$$

a) Measured Response



b) Calculated Response

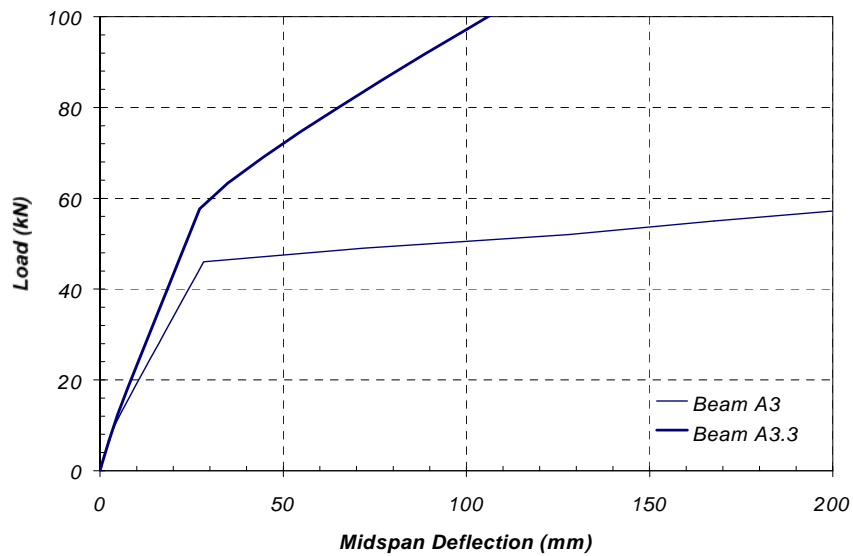


Figure 3.6 Comparison of Load-Deflection Curves of Specimens A.3 and A3.3 Reported by Spadea et al. (1998)

3.4.2 Tests by GangaRao and Vijay

Two beams from the experimental program reported by GangaRao and Vijay (1988) were used for the comparison with the analytical model: Specimens 1A₂-R and 3B₂-C. Specimen 1A₂-R was the control beam companion to Specimen 3B₂-C. The geometry and material properties for these specimens are included in [Tables 3.1 and 3.2](#) respectively.

Specimen 3B₂-C was strengthened after first cracking the concrete using a CFRP composite fabricated by a wet-layup procedure (Appendix C). This specimen was strengthened using 3 layers (plies) of CFRP sheets bonded to the tension face of the reinforced concrete beam. The sheets were made of unidirectional carbon fibers that were oriented longitudinally along the axis of the beam. An additional CFRP sheet was wrapped around the beam on top of the 3-ply, longitudinal sheets along the entire length to control slip of the CFRP composite.

A comparison of the load-deflection response of the two specimens is presented in Figure 3.7. Failure of both specimens was controlled by concrete crushing in the compression zone. The ratios of maximum measured to calculated loads are included in Table 3.3. The excellent correlation to the model in this case is a result of the failure mode experienced by Specimen 3B₂-C (concrete crushing). No debonding of the CFRP composite was detected during the test, indicating that

wrapping a sheet of CFRP along the entire length of the beam is an effective method of anchoring the sheets.

The ratio of calculated strain at maximum load (ϵ_{calc}) to CFRP rupture strain (ϵ_{rupt}) is presented in Table 3.3. This ratio is very close to 1.0 because the failure mode was controlled by crushing of the concrete and not debonding of the CFRP sheets.

Table 3.3 Summary of Results from Published Data and Analytical Model

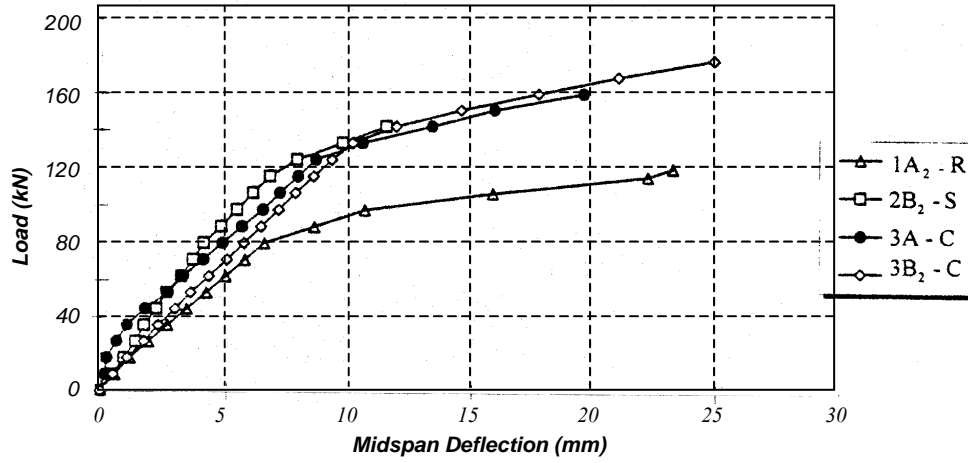
| Test Series | Specimen | P_{test} , kN | P_{calc} , kN | P_{test}/P_{calc} | ϵ_{calc} ¹ | ϵ_{rupt} ² | $\epsilon_{calc}/\epsilon_{rupt}$ |
|--------------------|--------------------|--------------------|--------------------|---------------------|--------------------------------|--------------------------------|-----------------------------------|
| Spadea et al. | A3 | 57.2 | 61.0 | 0.94 | - | - | - |
| | A3.3 | 98.3 | 114.3 | 0.86 | 0.0112 | 0.015 | 0.75 |
| GangaRao et al. | 1A ₁ -R | 115.7 | 111.3 | 1.04 | - | - | - |
| | 3B ₂ -C | 191.4 | 185.2 | 1.03 | 0.0128 | 0.013 | 0.98 |
| Arduini et al. | B1 | 90 * | 85.6 | 1.05 | - | - | - |
| | B2 | 170 * | 182.7 | 0.93 | 0.0066 | 0.0075 | 0.88 |
| | B4 | 270 * | 371.8 | 0.73 | 0.0048 | 0.0075 | 0.60 |
| Nakamura et al. | BL | 51.9 | 54.1 | 0.96 | - | - | - |
| | E24-1P | 73.0 | 83.4 | 0.88 | 0.0093 | 0.015 | 0.62 |
| | E24-2P | 89.2 | 102.8 | 0.87 | 0.0088 | 0.015 | 0.59 |

* Values estimated from published load-deflection curves.

¹ Calculated CFRP strain at maximum measured load, P_{test} .

² Strain corresponding to CFRP rupture, $\epsilon_{rupt} = \frac{f_{pu}}{E_p}$.

a) Measured Response



b) Calculated Response

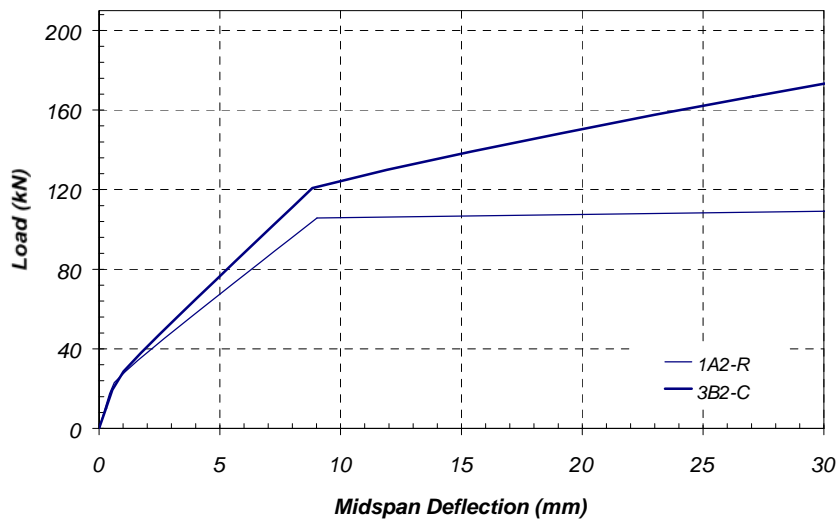


Figure 3.7 Comparison of Load-Deflection Curves for Specimens 1A₂-R and 3B₂-C Reported by GangaRao and Vijay (1998)

3.4.3 Tests by Arduini, Di Tommaso, and Nanni

Arduini et al. (1997) tested square reinforced concrete beams strengthened using CFRP pultruded plates (Series A). They also reported the results of tests performed at Penn State University in 1995 of four rectangular beams strengthened using CFRP flexible sheets (Series B). Three beams from series B: Specimens B1, B2, and B4 were used for comparison to the analytical model in this chapter.

Beam B1 was the control specimen. Beams B2 and B4 were strengthened using 1 and 3 layers of CFRP sheets, respectively, bonded to the tension side of the specimens. These sheets were made with unidirectional carbon fibers and they were oriented longitudinally along the beams. An additional carbon fiber sheet was wrapped around the bottom and sides of Specimen B4 throughout the strengthened portion of the beam to avoid debonding of the longitudinal sheets. Details of the specimen geometry and reinforcement are summarized in Table 3.1. The reported material properties and the characteristics of the CFRP sheets are contained in Table 3.2.

Failure of Specimen B2 was controlled by CFRP rupture at midspan. Specimen B4 failed by concrete crushing at one of the loading points after local debonding of the transverse CFRP sheet was observed at several places.

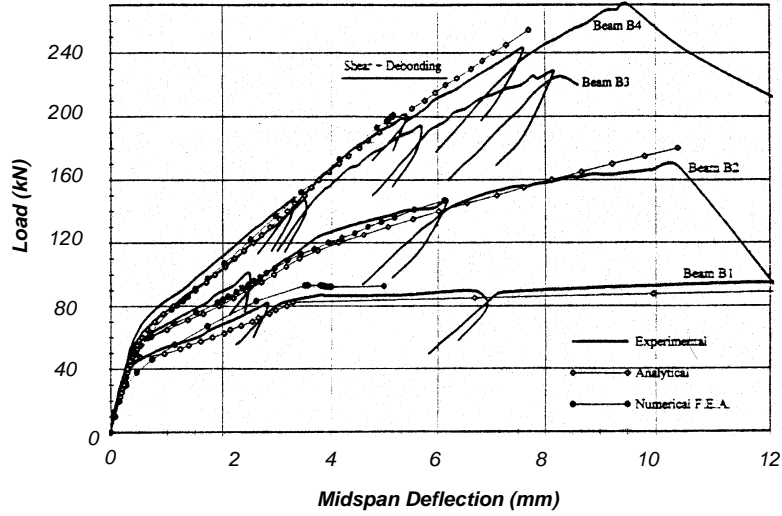
Measured and calculated responses are compared in Figure 3.8. The plot reported by Arduini et al. (1998) was truncated at a displacement of 12 mm

although it is apparent that Specimen B1 experienced larger displacements before failure. The calculated results are plotted to the same scale to facilitate comparisons.

The calculated response of Specimens B1 and B2 show excellent agreement with the measured data. Measured loads corresponding to cracking, yielding, and ultimate capacity are reproduced closely with the sectional model for both specimens. The ratio between the measured and calculated capacities for Specimen B2 was 0.93 (Table 3.3). In this case the model estimated the capacity closely because this specimen failed by rupture of the CFRP sheet, rather than debonding.

The calculated and measured responses of Specimen B4 are also shown in Figure 3.8 and Table 3.3. The calculated curve was truncated at a load of 280 kN to facilitate comparison with the measured response, although the calculated capacity was over 370 kN (Table 3.3). The poor correlation with the measured response is due to the failure mode experienced by the specimen (crushing after localized debonding of the transverse sheet).

a) Measured Response



b) Calculated Response

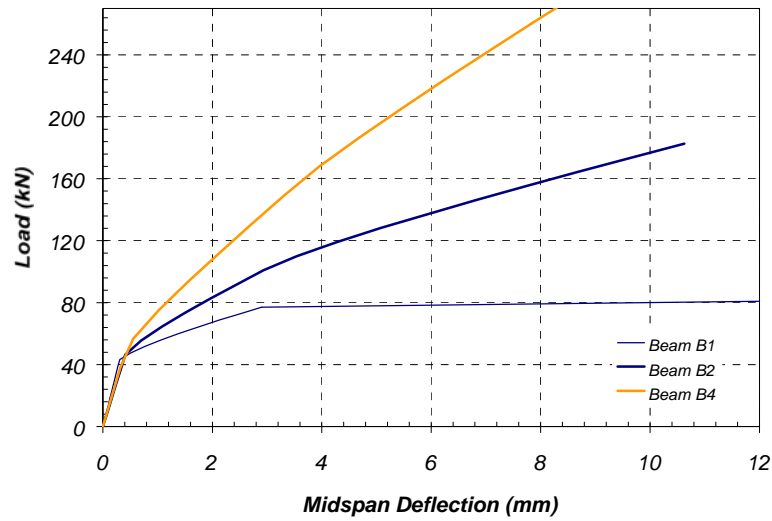


Figure 3.8 Comparison of Load-Deflection Curves for Specimens B1, B2, and B4 Reported by Arduini et al. (1997)

3.4.4 Tests by Nakamura, Sakai, Yagi, and Tanaka

Nakamura et al. (1996) conducted tests on square reinforced concrete beams strengthened with two types of CFRP systems applied using a wet-layup procedure (Appendix C). The two systems had different elastic moduli and strengths (E24 and E64 Series). Only beams from the E24 Series and the control specimens were used for the comparison with the analytical model.

Beams in the E24 Series were strengthened by bonding either 1 or 2 layers of CFRP sheets to the bottom face of the specimens (Specimens E24-1P and E24-2P, respectively). The entire bottom face of the beams was covered with the CFRP sheets. Specimen BL was the control specimen for this series and was constructed with the same materials as the other specimens in this group. The geometry of the specimens and the loading configuration are summarized in Table 3.1. The properties of the materials used in the specimen fabrication and the characteristics of the CFRP system used in the E24 Series are contained in Table 3.2.

The plots showing the measured and calculated load-deflection response are shown in Figure 3.9. Both strengthened specimens (E24-1P and E24-2P) failed when the CFRP sheets debonded from the concrete surface. Therefore, the analytical model calculated higher loads than those reached during the tests. The measured to calculated ratios are 0.88 and 0.87 for Specimens E24-1P and E24-2P,

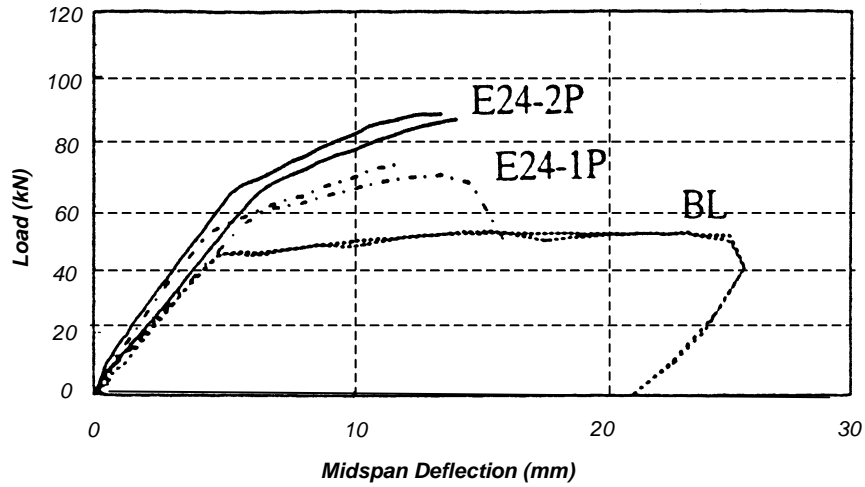
respectively (Table 3.3). The difference in loads is again due to the assumption of perfect bond between the concrete surface and CFRP composite.

The ratio of calculated to rupture strain indicates that the maximum stress developed in CFRP sheets was about 60% of the maximum rupture stress. No attempt was made to prevent debonding of the CFRP sheets from the beams in these tests.

3.4.5 Summary of Published Data

The analytical model presented in this chapter can reliably reproduce the general behavior of strengthened reinforced concrete specimens using CFRP composites. The shapes of the calculated load-deflection curves follow very closely the measured response reported by other researchers. The agreement between measured and calculated capacity clearly depends on the mode of failure observed during the individual tests. If the composites debond from the concrete surface before reaching their tensile strength, the analytical model will overestimate the capacity of these specimens.

a) Measured Response



b) Calculated Response

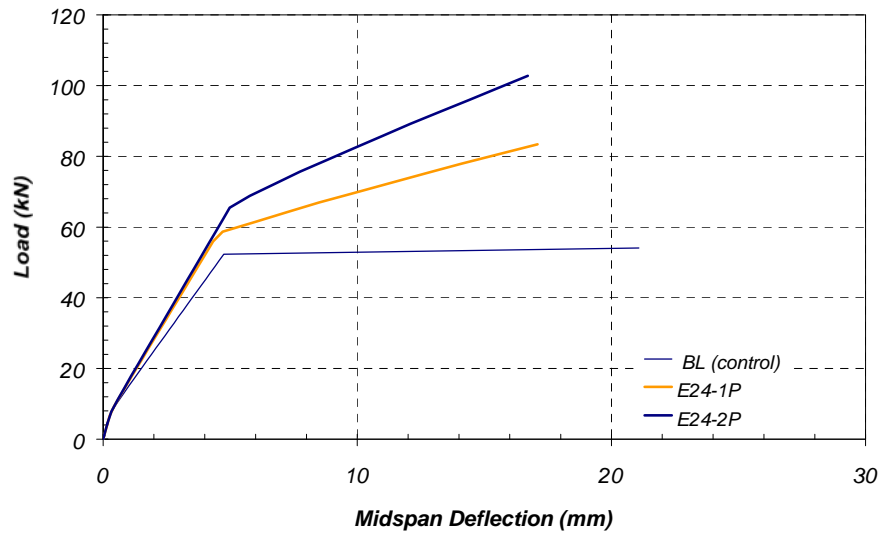


Figure 3.9 Comparison of Load-Deflection Curves for Specimens BL, E24-1P, and E24-2P Reported by Nakamura et al. (1997)

3.5 REFINEMENT OF ANALYTICAL MODEL

3.5.1 Limiting Debonding Strain of CFRP Composites

The analytical model was modified based on the results presented in Section 3.4 and the laboratory tests presented in Chapters 4 and 7. Evaluation of previous experimental research indicated that the maximum measured strains developed in the CFRP composites varied significantly (Table 3.3). This strain clearly depends on the ability of the CFRP to deform without debonding from the surface of the concrete.

Anchoring the CFRP composites is required to develop the maximum rupture strain reliably. Otherwise, the bond properties between the composite and the concrete surface are highly dependent on the concrete surface conditions at the time of strengthening. In many cases, however, anchoring is not sufficient to develop the rupture strain of the CFRP material but a more stable response can be achieved.

The model was therefore modified to permit debonding before rupture of the CFRP. This was accomplished by limiting the maximum strain that can be developed in the CFRP. A unique value for the limiting strain could not be defined at this stage in the research project because of the sparse test data. For the design of the large-scale test specimens; however, a limiting strain was selected based on the tests of rectangular beams that comprised an earlier phase of this research

project [Bramblett, 2000]. In some of these tests, transverse composite straps were provided to control debonding of the longitudinal CFRP composites that were designed to increase the flexural strength. The CFRP systems used in these tests were similar to those selected for strengthening the large-scale tests in this phase of the research program.

Maximum CFRP strains were measured on two types of carbon composites: a pultruded CFRP system and a wet-layup CFRP system. The average maximum measured strains in the CFRP systems attached to the rectangular beams that also contained transverse straps were 0.0065 and 0.011 for the pultruded and the wet-layup systems, respectively. The average strains were calculated based on two beams for the pultruded system and four beams for the wet-layup system. A limiting CFRP strain value within this range was selected for the design of the large-scale specimens ($\epsilon_{\text{CFRP}} = 0.007$). The maximum measured strains will be compared with the value assumed for design in Chapter 6 for the pan-joint specimens and Chapter 9 for the flat-slab specimens.

3.5.2 Initial Strains Caused by Dead Loads

The analytical model was initially developed based on the assumption that the CFRP composites were attached to the surface of the concrete when the reinforced concrete element was in an undeformed state. This assumption may be valid for elements tested in the laboratory where the CFRP composites are bonded

to the concrete before the beam is subjected to dead loads. However, existing bridges and the full-scale specimens tested in this part of the experimental program, must continue to carry dead load while the CFRP composites are being applied. Therefore, the reinforcing bars and concrete must carry the total strains induced by the combined live and dead load, but the CFRP composites carry only the strains induced by the live load.

The analytical model was modified to accommodate an initial strain profile. The computational procedure followed the same steps as those described in Section 3.2.3, except that the dead load strains in the concrete and steel were calculated first. These strains were added to the live-load strains at each step in the analysis, and the internal stresses and forces in the materials were calculated using the total strains (Figure 3.10). Only the live load strains contributed to the response of the CFRP composites.

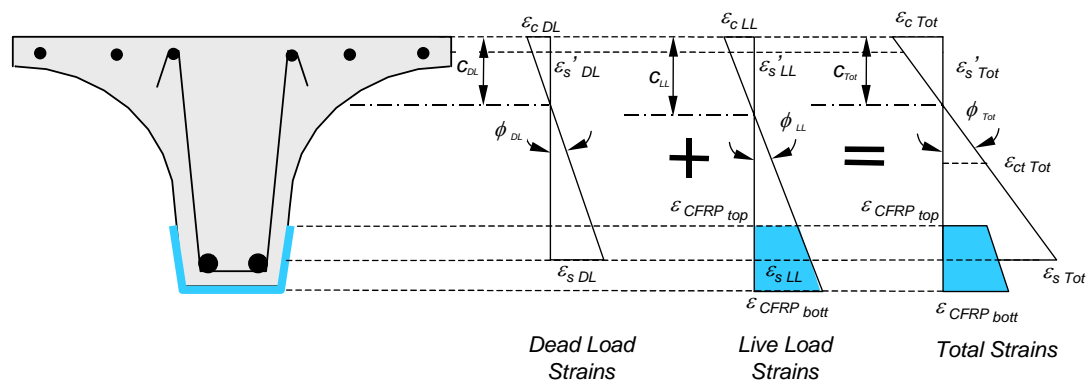


Figure 3.10 *Effect of Initial Dead Load Strains on Calculation of Moment-Curvature Response*

The live-load strains were assumed to vary linearly with depth, as discussed in Section 3.2.3. However, a discontinuity existed in the total strain profile due to the dead-load strains.

3.6 SUMMARY

An analytical model for calculating the moment-curvature and load-deflection response of reinforced concrete sections strengthened using CFRP composites was presented in this chapter. This model was validated using existing experimental data from reinforced concrete beams using CFRP composites. The model provides an accurate estimate of the observed capacity if the beam fails after rupture of the CFRP composite or crushing of the concrete. However, most beams failed after the CFRP composite debonded from the surface of the concrete, and the original model was not capable of reproducing this mode of failure. The model was later refined by adding a limiting composite strain before debonding.

The analytical method presented in this chapter was used to design the composite systems to strengthen the large-scale specimens for this experimental program. The measured response of these specimens is compared with the calculated response in Chapters 6 and 9.

CHAPTER 3:MODEL TO CALCULATE THE RESPONSE OF REINFORCED CONCRETE ELEMENTS STRENGTHENED USING CFRP COMPOSITES 39

| | |
|--|-----------|
| 3.1 Introduction | 39 |
| 3.2 Moment-Curvature Analysis of Strengthened Sections | 40 |
| 3.2.1 Assumptions Used in the Sectional Analysis Model..... | 40 |
| 3.2.2 Stress-Strain Material Models Used for Sectional Analysis..... | 41 |
| 3.2.3 Internal Equilibrium of Strengthened Cross Section | 48 |
| 3.3 Load-Deflection Response | 53 |
| 3.4 Validation of Model | 57 |
| 3.4.1 Tests by Spadea, Bencardino, and Swamy | 58 |
| 3.4.2 Tests by GangaRao and Vijay | 63 |
| 3.4.3 Tests by Arduini, Di Tommaso, and Nanni..... | 66 |
| 3.4.4 Tests by Nakamura, Sakai, Yagi, and Tanaka..... | 69 |
| 3.4.5 Summary of Published Data | 70 |
| 3.5 Refinement of Analytical Model | 72 |
| 3.5.1 Limiting Debonding Strain of CFRP Composites | 72 |
| 3.5.2 Initial Strains Caused by Dead Loads..... | 73 |
| 3.6 Summary | 75 |

| | |
|--|----|
| Figure 3.1 Idealized Stress-Strain Relationship for Concrete | 43 |
| Figure 3.2 Idealized Stress-Strain Relationships for Steel | 47 |
| Figure 3.3 Idealized Stress-Strain Relationship for CFRP Composites | 48 |
| Figure 3.4 Schematic Representation of Sectional Response Illustrating the Procedure Used in the Calculations..... | 52 |
| Figure 3.5 Procedure to Calculate Deflections of an Element with a Non-linear Moment-Curvature Relationship..... | 55 |
| Figure 3.6 Comparison of Load-Deflection Curves of Specimens A.3 and A3.3 Reported by Spadea et al. (1998) | 62 |
| Figure 3.7 Comparison of Load-Deflection Curves for Specimens 1A ₂ -R and 3B ₂ -C Reported by GangaRao and Vijay (1998)..... | 65 |
| Figure 3.8 Comparison of Load-Deflection Curves for Specimens B1, B2, and B4 Reported by Arduini et al. (1997)..... | 68 |

| | |
|---|----|
| Figure 3.9 Comparison of Load-Deflection Curves for Specimens BL, E24-1P, and E24-2P Reported by Nakamura et al. (1997) | 71 |
| Figure 3.10 Effect of Initial Dead Load Strains on Calculation of Moment-Curvature Response..... | 74 |
| Table 3.1 Dimensions and Reinforcement of Specimens Reported by Other Researchers..... | 60 |
| Table 3.2 Material Properties and Dimensions of CFRP Composites of Specimens Reported by Other Researchers | 61 |
| Table 3.3 Summary of Results from Published Data and Analytical Model | 64 |

Chapter 4: Description of Pan-Joist Specimens

4.1 INTRODUCTION

Pan-joist construction was a very popular type of construction in Texas in the 1950s for reinforced concrete bridges spanning 30 to 40 feet. Even today, some bridges in off-system roadways with spans up to 40 feet are built using this form of construction. The name given to this type of bridge comes from the formwork used to construct them. Pan-joist bridges are cast using self-supporting metal forms that span from one bent-cap to the next. The forms have a cross-section consisting of an upper semi-circular portion with straight ends at the bottom on each side (Figure 4.1). Two pans are placed next to each other to form one concrete web. Adjoining pans are connected using bolts that pass through holes on the sides of the forms.

Because the pans are not perfectly straight, concrete can flow through gaps between adjacent forms during the casting operation leaving an irregular bottom surface on the bridge webs (Figure 4.2). Although this surface irregularity does not affect the bridge capacity, it does influence the placement of composites used to strengthen the bridges. The composites that were used to strengthen this type of bridge could not be placed along the middle of the web soffit without significant surface preparation. This constraint was considered when designing the

strengthening method for pan-joist bridges in order to minimize the labor involved in preparing the concrete surface.



Figure 4.1 View of Metal Pan-Forms inside the Laboratory

The prototype bridge that was selected to examine the effectiveness of the composite strengthening procedures is described in this chapter. The inventory rating for the prototype bridge was calculated to estimate the percentage increase in capacity that would be required to upgrade it to a higher design load. Calculated capacities of both prototype and laboratory specimens are compared.

Two strengthening schemes used to meet the desired increase in capacity are presented in this chapter. The physical characteristics of the two different

composite systems are highlighted. Finally, the calculated capacities of the strengthened specimens are compared with the flexural strength required to increase the load rating of the prototype bridge to an HS-20 design standard.



Figure 4.2 Photograph of Pan-Joist Bridge in Buda, Texas Indicating Uneven Surfaces on Bottom of Joists

4.2 PROTOTYPE BRIDGE

Most pan-joist bridges constructed in Texas during the 1950s were designed to carry two H-10 or two H-15 design vehicles. Modern bridges are designed to carry two HS-20 design vehicles.

Drawings were obtained from TxDOT for a standard, two-lane, pan-joist bridge designed in 1951 for two H-10 trucks. This bridge was used as the

prototype for the laboratory tests and was considered to represent the worst case scenario for existing bridges.

4.2.1 Physical Characteristics of Prototype Bridge

The prototype bridge was designed for a 30-ft span. The drawings included options for roadway widths ranging from 14'-4½" to 23'-4½". The narrowest bridge had eight joists and the widest had eleven. The bridge cross section and reinforcement details are shown in Figure 4.3. The total depth of the bridge is 24 in. and girder webs are 8¼ in. wide. The slab has a minimum thickness of 3½ in. There are structural curbs on each side of the bridge that extend 1'-6" above the bridge deck.

The longitudinal reinforcement consists of 2 - # 11 bars, and the shear reinforcement consists of #3 stirrups spaced at 15 in. throughout the span. Slab reinforcement consists of #4 bars at 12 in. longitudinally, and #5 bars at 10 in. transversely.

The joists in the prototype bridge are supported directly on bent caps. One layer of roofing felt is placed between the end diaphragms and the bent cap. Although these types of bridges were designed as simply-supported spans, measured response during diagnostic load tests of an existing pan-joist bridge

indicates that significant end-restraint is provided by adjacent bridge spans [Velázquez, 1998].

4.2.2 Calculated Capacity of Prototype Bridge

Nominal flexural and shear capacities of the prototype bridge were calculated in accordance with the current AASHTO *Design Specifications* [AASHTO, 1996]. Because the actual material strengths were unknown and the nominal design values were not reported on the structural drawings, values recommended in the *AASHTO Manual for Condition Evaluation of Bridges* [AASHTO, 1994] for concrete and reinforcing bar strengths were used. Concrete was assumed to have a compressive strength of 3,000 psi, and reinforcing steel was assumed to have a yield stress of 33,000 psi.

Although the selected prototype bridge was designed with integral structural curbs on each side of the road, the curbs must be removed to widen the bridge. In addition, many pan-joist bridges in Texas were constructed without the concrete curbs, so the joists must carry all the bridge loads longitudinally into the bent caps. For these two reasons, the contribution of the curbs to the flexural capacity of the bridge was neglected in this analysis.

Design flexural strength for each joist was computed using standard design procedures [AASHTO, 1996]:

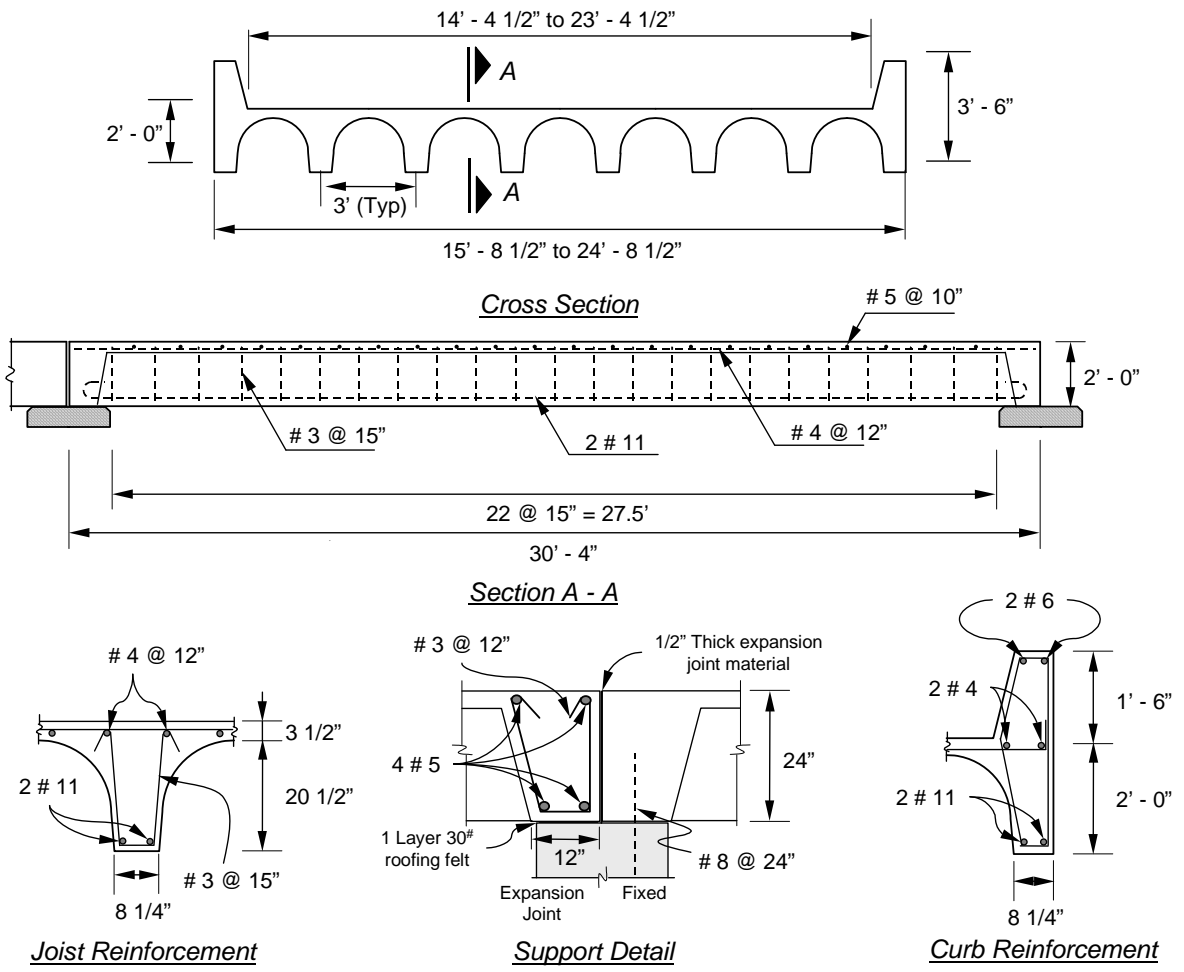


Figure 4.3 Reinforcement Details for Prototype Bridge

$$\phi M_n = A_s f_y \left(d - \frac{a}{2} \right) \quad (4.1)$$

with $a = \frac{A_s f_y}{b(0.85 f'_c)}$

Similarly, the design shear strength was calculated as [AASHTO, 1996]:

$$\phi V_n = \phi (V_c + V_s) \quad (4.2)$$

where

M_n = Nominal flexural strength, lb-in.

V_n = Nominal shear strength of member, lb.

$V_c = 2\sqrt{f'_c} b_w d$ = concrete contribution to shear strength of member, lb.

$V_s = \frac{A_v f_y d}{s}$ = steel shear reinforcement contribution to nominal shear strength of member, lb.

ϕ = Strength reduction factor, equal to 0.9 for flexural effects and 0.85 for shear effects.

A_s = Area of flexural reinforcement, in².

A_v = Area of shear reinforcement within a distance s , in².

d = Distance from extreme compression fiber to centroid of flexural reinforcement, in.

b = Width of compression face of member, in.

b_w = Web width used to compute V_c , in.

s = Spacing of shear reinforcement, in.

f_y = Yield strength of flexural or shear reinforcement, psi.

f'_c = Concrete compressive strength, psi.

The concrete contribution to the shear strength was calculated using the web width increase allowed for members with tapered sections [AASHTO, 1996]. Therefore, the web width for concrete shear strength, b_w , was calculated as 1.2 times the minimum joist width. The calculated nominal flexural and shear capacities for a single joist in the prototype bridge are listed in Table 4.1 along with the parameters used in the calculations.

Table 4.1 Calculated Flexural and Shear Capacities of a Single Joist in the Prototype Bridge

| Parameter | Value |
|--------------------------|--------|
| f'_c , psi | 3,000 |
| f_y , psi | 33,000 |
| A_s , in. ² | 3.12 |
| b , in. | 36 |
| b_w^* , in. | 9.9 |
| A_v , in. ² | 0.22 |
| d , in. | 21.625 |
| $\phi_{flexure}$ | 0.9 |
| ϕ_{shear} | 0.85 |
| ϕM_n , kip-ft | 162.6 |
| V_c , kip | 23.5 |
| V_s , kip | 10.5 |
| ϕV_n , kip | 28.9 |

* $b_w = 1.2 b_{min} = 1.2(8.25) = 9.9$ in. [AASHTO, 1996]

4.2.3 Load Rating for Prototype Bridge

The load factor method given in the AASHTO *Manual for Condition Evaluation of Bridges* [AASHTO, 1994] was used to rate the prototype bridge. Details of the load rating procedure are given in Appendix B. Two load-rating levels are described in the AASHTO *Manual* [AASHTO, 1994]: inventory rating and operating rating. The difference between the two is the load factors used for live load effects in the rating equation (see Appendix B).

A 28-ft clear span was used in all calculations. Live load effects were calculated following the procedures outlined in the *AASHTO Design Specifications*. Maximum moments and shears were determined using the tables contained in Appendix A of the *AASHTO Specifications*. The values reported in these tables are the same as the maximum values that would be calculated for moving loads representing a single H-20 or HS-20 truck (two wheel loads in the transverse direction). Therefore, these values were divided by two to get effects for H-10 or HS-10 trucks, and divided by two again to get effects due to a single wheel loading. Finally, to calculate the live load design effects for a single joist, the moments and shears were distributed transversely using a lateral distribution factor equal to $S/6.0$ [AASHTO, 1996], where S is the joist spacing in feet. The moments and shears obtained using this procedure are listed in Table 4.2, where each step in the calculations is presented in a separate row.

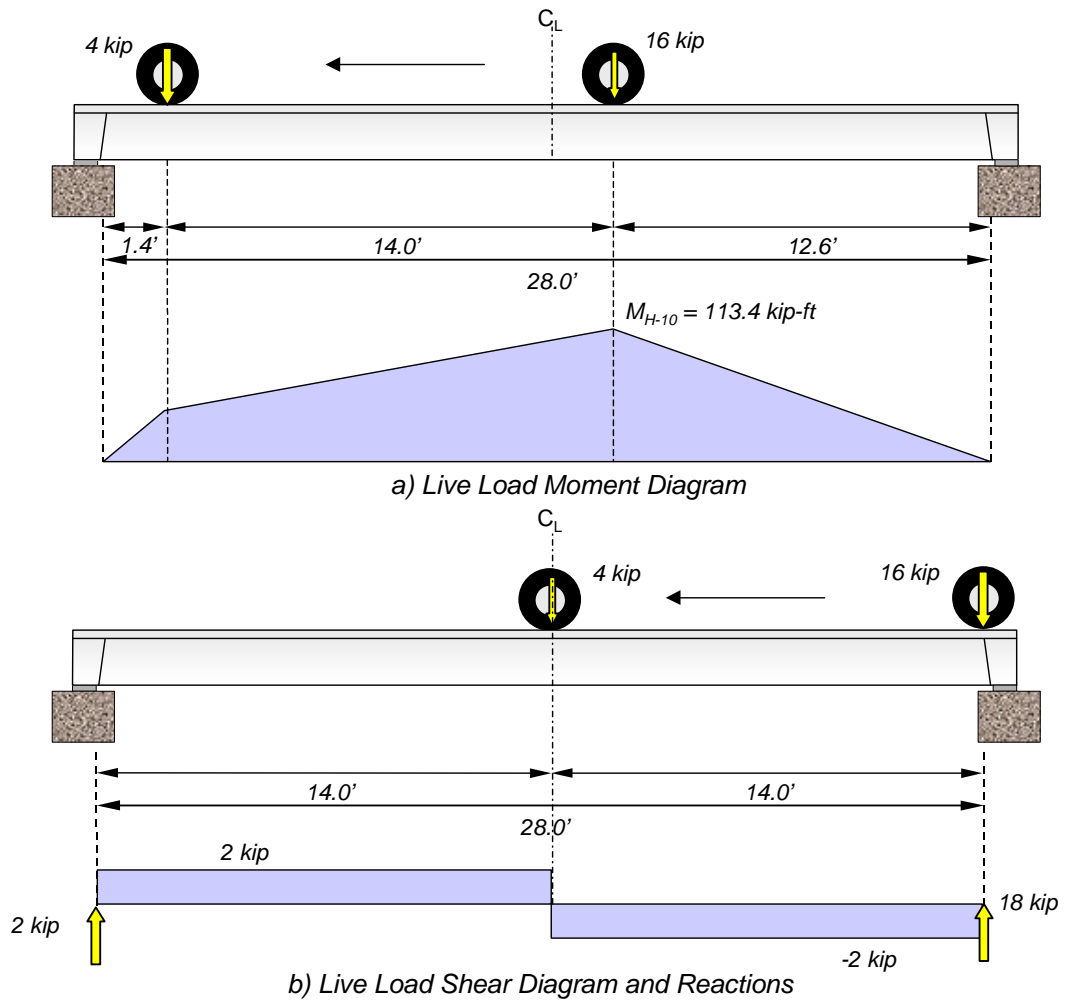
The controlling shear and moment diagrams that produced the maximum live load effects are shown in Figure 4.4 for H-10 loading and in Figure 4.5 for HS-10 loading. The diagrams shown in these figures correspond to one loading lane. For flexure, the critical sections depended on the design truck. The critical sections for an H-truck and an HS-truck were located at 12.6 ft and at 10.5 ft, respectively, from the face of the end diaphragms. The critical section for shear effects was taken at the face of the end diaphragms.

Maximum moments and shears for dead and live load forces for the prototype bridge are listed in Table 4.3. The corresponding load-rating results for H and HS-truck loadings are given in Table 4.4 for both flexure and shear. Although the HS-10 loading vehicle is not included in the AASHTO Design Specifications [AASHTO, 1996], this idealized truck was used to facilitate comparison between the two types of truck loading. The HS-10 truck effects were determined using the magnitudes of the axle loads from the H-10 truck but distributed according to an HS-design vehicle.

Table 4.2 Maximum Live Load Moments and Shears Per Joist for the Prototype Bridge

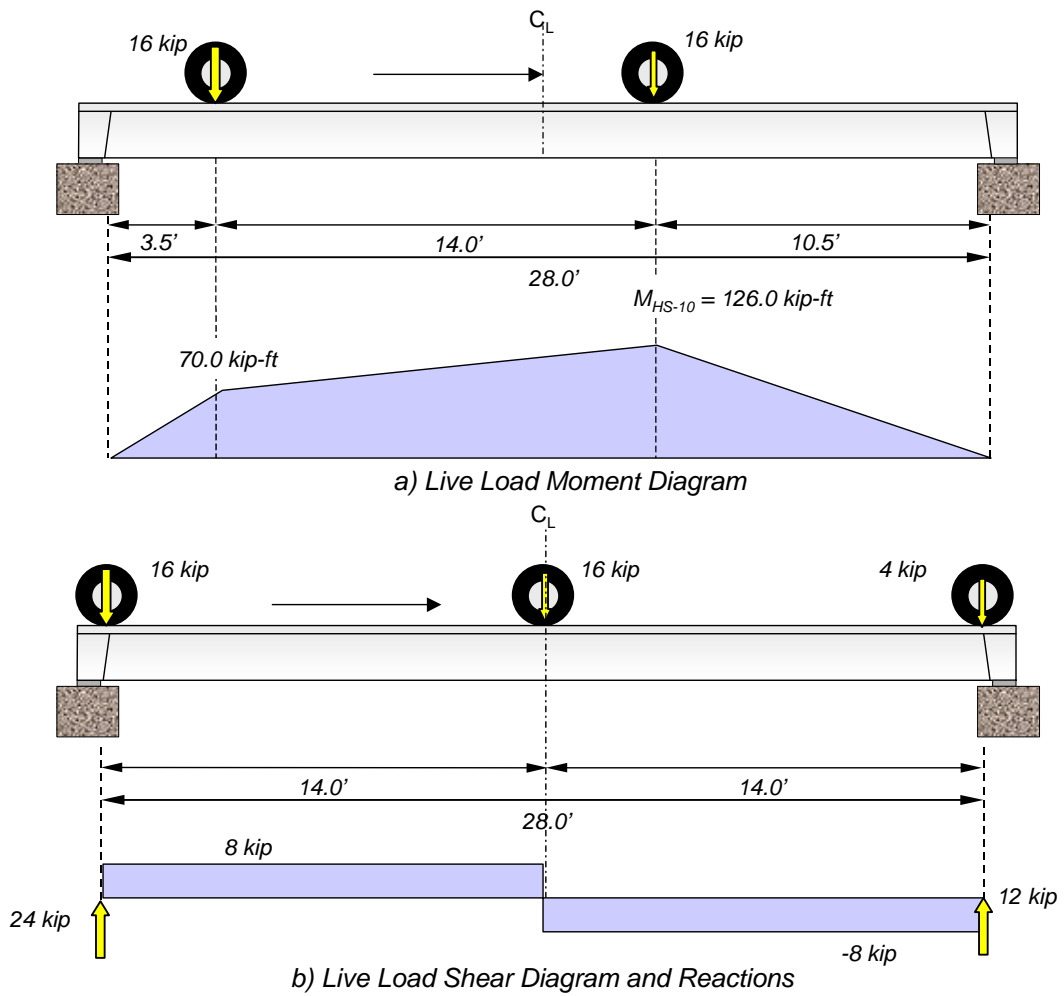
| H-truck loading | | HS-truck loading | | Notes |
|-----------------|-------------|------------------|-------------|--|
| Moment, kip-ft | Shear, kips | Moment, kip-ft | Shear, kips | |
| 226.8 | 36.0 | 252.0 | 48.0 | Maxima for one lane of H-20 or HS-20 loading |
| 113.4 | 18.0 | 126.0 | 24.0 | Maxima for one lane of H-10 or HS-10 loading |
| 56.7 | 9.0 | 63.0 | 12.0 | Maxima for H-10 or HS-10 wheel loads |
| 28.4 | 4.5 | 31.5 | 6.0 | Maxima for one joist of prototype bridge |
| 36.9 | 5.9 | 40.9 | 7.8 | Maxima per joist including impact factor |

Note: Span is 28.0 ft.



Note: Moment and shear diagrams correspond to a single lane loading

Figure 4.4 H-10 Truck Positions Corresponding to Critical Moments and Shears



Note: Moment and shear diagrams correspond to a single lane loading

Figure 4.5 HS-10 Truck Positions Corresponding to Critical Moments and Shears

Table 4.3 Unfactored Load Effects Per Joist Used to Rate Prototype Bridge

| Unfactored Load Effect | Value |
|-------------------------------|---|
| H – 10 truck axle loads, kips | 4, front; 16, rear (14 ft from front) |
| M_{DL} , kip-ft | 41.7 |
| $(1 + I) M_{LL}$, kip-ft | 36.9 |
| V_{DL} , kip | 6.0 |
| $(1 + I) V_{LL}$, kip | 5.9 |
| HS – 10 truck axle loads, kip | 4, front; 16, middle (14 ft from front); 16, rear (14 ft from middle) |
| M_{DL} , kip-ft | 41.7 |
| $(1 + I) M_{LL}$, kip-ft | 40.9 |
| V_{DL} , kip | 6.0 |
| $(1 + I) V_{LL}$, kip | 7.8 |

Notes: Live load effects include a 0.3 impact factor (I).
The weight of a ½” overlay is included in dead load.

Table 4.4 Load Rating Results for Prototype Pan-Joist Bridge Originally Designed for an H-10 Truck Loading

| Load Effect | Rating Level | Design truck | |
|-------------|--------------|-------------------|--------------------|
| | | H – truck loading | HS – truck loading |
| Flexure | Inventory | H – 13.6 | HS – 12.2 |
| | Operating | H – 22.6 | HS – 20.4 |
| Shear | Inventory | H – 16.5 | HS – 12.5 |
| | Operating | H – 27.5 | HS – 20.8 |

The rating for the prototype bridge was higher than the design H-10 truck loading (Table 4.4). Also, the flexural rating results for the H-truck are very close to those for the HS-truck because one of the truck axles must be located close to midspan to produce maximum live load moments in short span bridges. Therefore, the rear axle lies close to the support for the HS vehicle, and has little influence on the moment (10% difference). On the other hand, there is about a 32% difference in ratings based on shear for the two standard vehicles. If an HS-truck is used, the two 16-kip axles contribute to the maximum live-load shear, while the 4-kip and 16- kip axles contribute to the maximum shear if rating is based on an H-truck.

To comply with current TxDOT requirements, bridges need to have an inventory rating of at least HS-20 to be able to qualify for widening and also to

qualify for the two-year inspection frequency. If the operating rating is at least HS-20, load posting is not required. Therefore, the prototype bridge requires strengthening to meet the inventory-rating criteria.

4.3 DESIGN AND CONSTRUCTION OF LABORATORY SPECIMENS

The laboratory specimens were selected to reproduce key features of the expected behavior of a portion of the prototype bridge. An interior section of the prototype bridge was chosen for the test specimens because the structural curbs are not present in all bridges and will be removed before an existing bridge is widened. Two identical joist specimens were constructed and tested. Different types of composite materials were used to strengthen the two specimens. The response of each specimen is summarized in Chapter 5 and compared to the calculated response in Chapter 6.

Each test specimen consisted of two interior joists. The specimens were constructed at full scale to avoid scaling effects on the behavior. Concrete diaphragms were cast at both ends of the specimen to replicate field conditions.

The end diaphragms were supported on elastomeric pads to simulate a simply supported span. The amount of end restraint provided in actual bridges is difficult to predict and can vary from span-to-span as demonstrated in previous research [Velázquez, 1998]. Therefore, simply-supported boundary conditions

were chosen in order to evaluate specimen behavior without the influence of end restraint. Also, the most critical condition that could be encountered in the field was replicated by choosing a simply-supported span, because positive moments at midspan are the largest in this case.

Specimens were cast using the same metal forms that are used for pan-joint bridge construction in the field. Therefore, the joist cross sections represent actual field conditions. Wood forms were assembled in the lab to cast the diaphragms at each end of the specimen integrally with the joists. A picture illustrating the reinforcement and formwork prior to casting one of the specimens is shown in Figure 4.6.

Specimen dimensions and reinforcement details are shown in Figure 4.7. The specified yield stress for all reinforcing steel used for the fabrication of the specimens was 60,000 psi. The design 28-day concrete compressive strength was 3,500 psi. Table 4.5 shows average measured material properties for pan-joint specimens J-1 and J-2. Details of the material tests for each of the specimens are given in Appendix A.

Table 4.5 Average Measured Material Strengths for Joist Specimens

| Specimen | Concrete | | | Reinforcing Bars | | | |
|----------|-----------|--------------|-------------|------------------|-------------|-------------|-------------|
| | | | | (#8) | | (#3) | |
| | Age, days | f'_c , psi | f_t , psi | f_y , ksi | f_u , ksi | f_y , ksi | f_u , ksi |
| J-1 | 79 | 3,900 | 410 | 71.7 | 114 | 65.4 | 106.4 |
| J-2 | 62 | 3,500 | 370 | | | | |

The main longitudinal reinforcement in the specimens consisted of 2 - #8 bars. The area of the main flexural reinforcement was adjusted for the difference in the nominal yield stresses in the prototype and specimen. Only grade 60 steel was available to construct the test specimens, while it was assumed that 33-ksi steel was used in the prototype bridge. The area was adjusted by multiplying the reinforcement area in the prototype bridge by the ratio of reinforcement yield stress in the prototype to nominal yield stress of the reinforcement in the specimens.

Slab reinforcement consisted of #4 bars at 12" in the transverse direction and #4 bars at 11" in the longitudinal direction. The area of the longitudinal slab reinforcement in the specimens was not adjusted by the ratio of the yield stresses because the additional negative moment strength was required to lift the specimens in the laboratory.

Joist stirrups were #3 bars at 15” spacing throughout the entire span. The stirrup area was not adjusted by the ratio of the yield stresses either. It was considered that using the same bar size in the laboratory specimens as in the prototype bridge replicates field conditions more closely. Also, to have the same number of stirrups crossing a potential diagonal crack, the stirrup spacing in the specimens was the same as in the prototype bridge.

Flexural and shear capacities of the test specimens were determined using Eq. (4.1) and (4.2) respectively [AASHTO, 1996]. The average measured material strengths listed in Table 4.5 were used in these calculations. The specimen capacities are listed in Table 4.6 and are compared with the capacities of two joists from the prototype bridge.



Figure 4.6 Specimen Reinforcement and Formwork

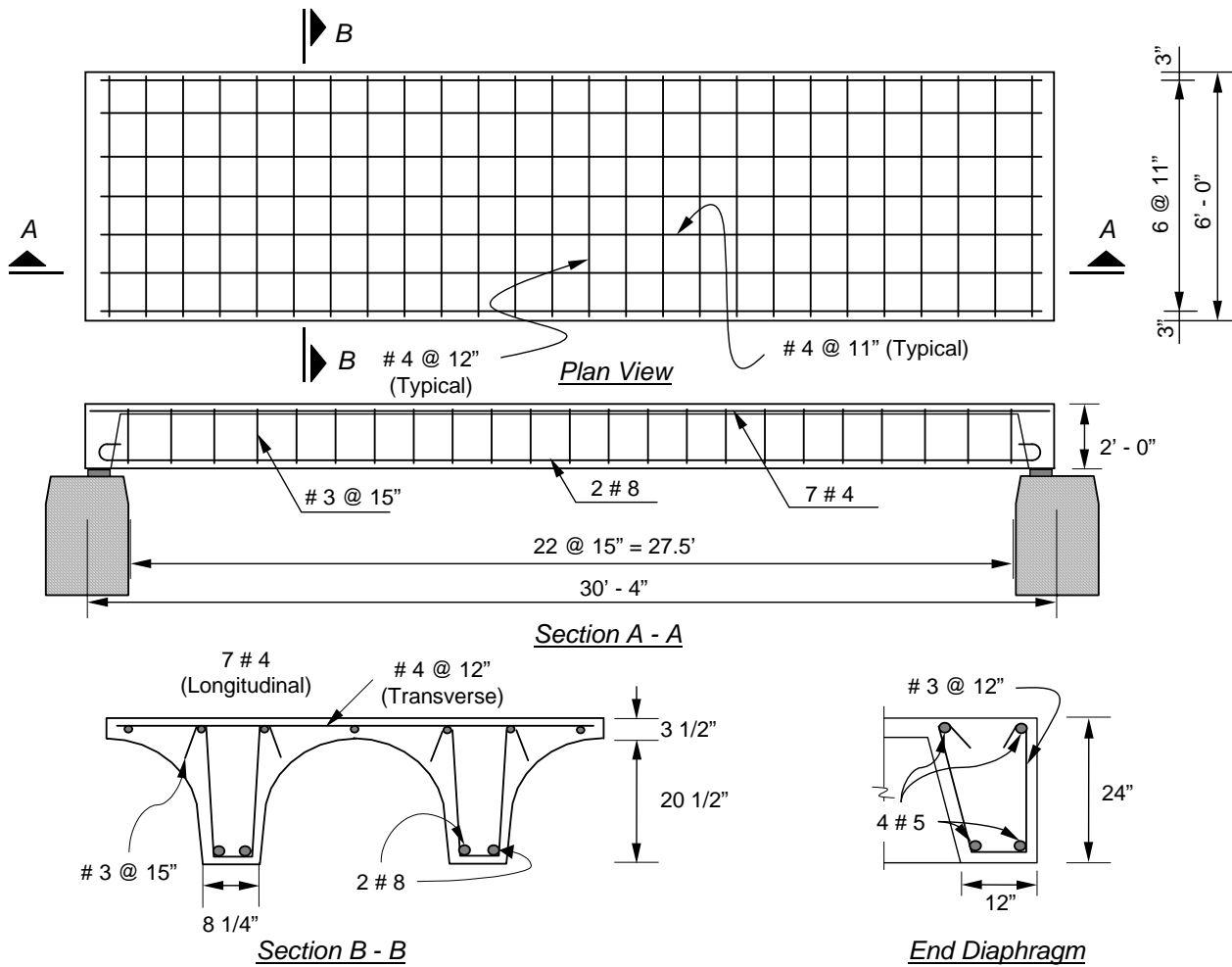


Figure 4.7 Joist Specimen Geometry and Reinforcement

Table 4.6 Nominal Flexural and Shear Capacities of Pan-Joist Specimens

| Capacity | Specimen J-1 | Specimen J-2 | Prototype Bridge |
|-------------------------|---------------------|---------------------|-------------------------|
| M_n , kip-ft | 399.4 | 398.4 | 361.4 |
| V_c , kip | 44.6 | 42.2 | 47.0 |
| V_s , kip | 41.4 | 41.4 | 21.0 |
| $V_n = V_c + V_s$, kip | 86.0 | 83.6 | 68.0 |

As seen in Table 4.6, the flexural strength for both specimens was approximately 10% higher than the calculated flexural capacity of the two joists from the prototype bridge. Shear strengths were approximately 25% higher in the laboratory specimens compared with the prototype. The percentages are higher in this case because the area of shear reinforcement was the same in the test specimens and the prototype, but the yield stress of the reinforcement was higher in the test specimens.

4.4 DESIGN AND CONSTRUCTION OF STRENGTHENING SCHEMES FOR LABORATORY SPECIMENS

The design of the strengthening schemes for each specimen was based on the load-rating procedure described in Section 4.2.3. The required flexural increase

in capacity for the prototype bridge to achieve an inventory rating of an HS-20 truck was determined using the rating equation, cast in terms of the capacity, C (Appendix B):

$$C = RF [A_2 L (1 + I)] + A_1 D \quad (4.3)$$

where L is the live load effect, D is the dead load effect, I is the impact factor equal to 0.3, $A_1 = 1.3$, $A_2 = 2.17$, and $RF = 2.0$ to reach an HS-20 inventory rating. The load effects used in Eq. (4.3) were those listed in Table 4.3 for flexure.

Equation (4.3) gives a required nominal flexural capacity, $C = \phi M_n$, of 232 kip-ft per joist in the prototype. As shown in Table 4.1, the original flexural strength per joist in the prototype is 163 kip-ft. Therefore, the nominal flexural capacity must be increased by 42% to raise the inventory rating of the prototype bridge from HS-12.2 to HS-20.

Both joist specimens were strengthened using CFRP composite systems to increase their flexural capacity. The required nominal strength of the specimens was obtained by multiplying the required capacity of one joist in the prototype, C , by two and dividing by the strength reduction factor, ϕ . The strength reduction factor was assumed to be 0.85. This factor was chosen because, failure of the specimens was expected to occur suddenly when the composite systems debonded

from the surface of the concrete. This assumption is evaluated based on the observed response of the test specimens in Chapter 10.

Two commercially available CFRP systems were chosen to strengthen the laboratory specimens: a pultruded system and a wet-layup system. The pultruded system consisted of CFRP plates that were fabricated in a manufacturing facility through the process of pultrusion and subsequently attached to the concrete surface using an epoxy paste. The wet-layup system consisted of dry unidirectional carbon fibers that were formed into a composite by impregnation using an epoxy resin. Details of the application procedure for each system are described in Appendix C.

The required area of composite material to reach the target flexural strength was determined using the analysis procedure described in Chapter 3. As discussed in Section 3.4, the expected strength of the strengthened member depends on the strain in the CFRP at which debonding occurs. For design of the test specimens, this strain was determined using results of previous testing on rectangular concrete beams strengthened using similar CFRP systems [Bramblett, 2000]. In those tests, the strains were measured on the surface of the CFRP composites. For design of the strengthening schemes, a strain of 0.007 was assumed to be the strain at debonding. This value represents an average from six tests with similar composite systems. The debonding strains were approximately the same for the two types of CFRP composites in those tests [Bramblett, 2000].

The parameters used for the design of the strengthening schemes are summarized in Table 4.7. The factored design moments in Table 4.3 were multiplied by two, because each test specimen comprised two joists.

Table 4.7 Parameters Used to Design the Strengthening Schemes

| Parameter | Value | Notes |
|----------------------------|--------------|--|
| $A_1 M_D$, kip-ft | 108 | Factored dead load moment |
| $A_2 M_L (1 + I)$, kip-ft | 355 | Factored live load moment + impact |
| M_u , kip-ft | 463 | Required ultimate strength (2-joists) |
| ϕ | 0.85 | Strength reduction factor |
| $M_n = M_u/\phi$, kip-ft | 545 | Required nominal capacity (2-joists) |
| ϵ_{CFRP} | 0.007 | Max. attainable CFRP strain for design |

Notes: Moments calculated using HS-20 loading on 2 joists of prototype bridge

A_1 and A_2 = Load factors for dead and live load effects equal to 1.3 and 2.17, respectively, for inventory rating

I = Impact factor for live load effects equal to 0.3

Using the analysis procedures described in Chapter 3, an iterative approach was used to determine the area and placement of the CFRP plates and sheets. The areas of CFRP plates or sheets were adjusted using commercially available dimensions until the desired capacity of the strengthened specimens was achieved

within a reasonable tolerance. The calculated moment-curvature curves for two strengthened sections are shown in Figure 4.8. For comparison, the calculated moment-curvature response of the unstrengthened prototype is also shown. The nominal material properties were used in these calculations.

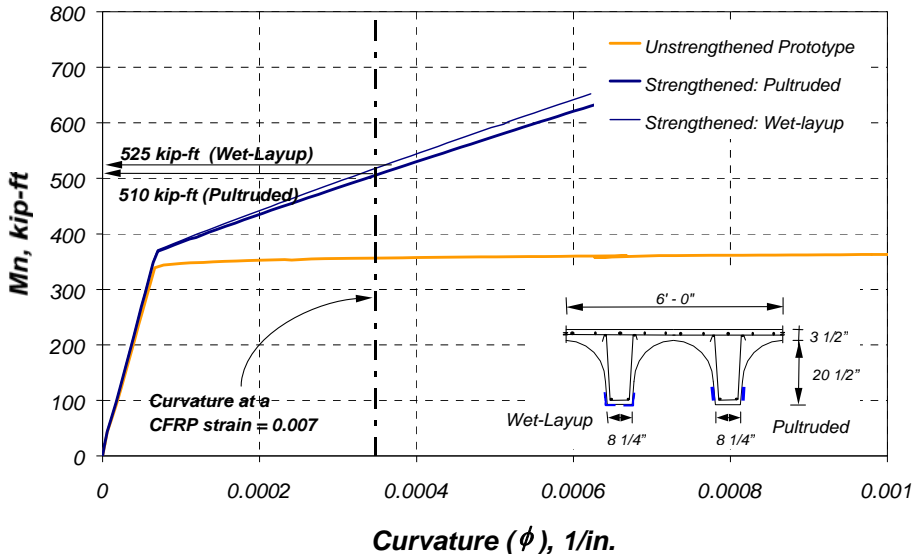


Figure 4.8 Calculated Moment-Curvature Response of Two Joists of Prototype Bridge Strengthened Using Different Composite Systems

The required specimen flexural strength was 545 kip-ft (Table 4.7) in order to achieve an inventory rating of HS-20. The calculated flexural capacity of the strengthened prototype consisting of two joists was slightly lower than the target strength because commercially available CFRP systems were used.

The strengthened prototype bridge was first designed using the CFRP pultruded system because only specific plate widths are available commercially. Then the wet-layup system was designed to develop the same strength as the pultruded system design in order to facilitate comparisons of the performance during the laboratory tests.

Details of the final CFRP configuration for each of the specimens are presented in Sections 4.4.1 and 4.4.2 for Specimens J-1 and J-2 respectively. All calculations were based on the measured material properties for concrete and steel and the material properties provided by the manufacturers for the CFRP systems.

4.4.1 Strengthening Scheme for Specimen J-1

Specimen J-1 was strengthened using pultruded carbon fiber reinforced polymer (CFRP) plates bonded to the sides of each joist. The composite plates were bonded to the concrete specimen following the procedures specified by the manufacturer. Details of this procedure are presented in Appendix C.

Previous tests on strengthened rectangular beams showed that bonding these types of composite plates to the sides of flexural members instead of adhering them to the tension face delayed debonding and increased the deformation capacity of the members [Bramblett, 2000]. Therefore, the composite plates were bonded to the side of the joists. An epoxy-based adhesive paste supplied by the plate

manufacturer was used to bond the pultruded plates to the concrete surface. The procedures recommended by the manufacturers were followed to prepare the concrete surface before bonding the composites (Appendix C).

The CFRP plates used for this specimen were fabricated with continuous unidirectional carbon fibers (fiber roving) using the pultrusion process (see Appendix C). The volumetric content of carbon fibers in the plates is 68% and the cross sectional dimensions are 3 1/8 in. wide by 0.047 in. thick. Mechanical properties of the CFRP plates and epoxy paste are listed in Appendix A.

CFRP composite straps were placed at 12-in. spacing around the pultruded plates throughout the shear span of the specimen using a wet lay-up procedure. A unidirectional carbon fiber woven fabric supplied by the same manufacturer as the pultruded plates was used to form these straps. The composite straps were intended to delay debonding of the pultruded plates from the concrete surface as demonstrated in previous research [Bramblett, 2000]. Straps were fabricated using a 3-in. wide ply of carbon fiber fabric. The straps extended 11 in. above the bottom of the specimen. The length of the straps was selected so that they would end before the curved portion of the joist cross section. No attempt was made to determine the strap length based on calculations. However, longer straps are advised in the future based on results from the experimental testing.

Epoxy paste was built up next to the pultruded plates where CFRP straps intersected the plates to avoid wrapping the straps around sharp bends at the edges of the pultruded plates. Both the epoxy paste used to bond the pultruded plates, and the composite straps were allowed to cure at ambient temperature for 7 days before testing. The locations of CFRP pultruded plates and anchoring straps on Specimen J-1 are shown in Figure 4.9.

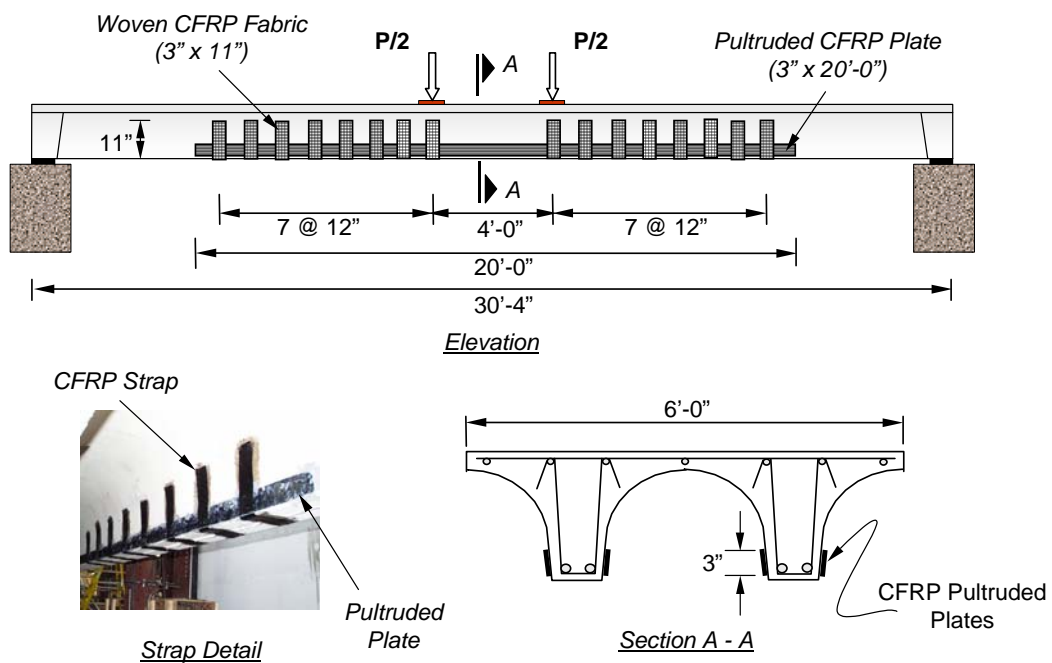


Figure 4.9 CFRP Strengthening Details for Specimen J-1

The required length of the plates was determined using the loading configuration and the maximum moment expected to be applied during the test.

The plates were extended beyond the theoretical cut-off points to prevent premature debonding.

The procedure used to determine the plate length is illustrated graphically in Figure 4.10. The maximum moment indicated in the figure was calculated by subtracting the service dead load moment from the required nominal capacity listed in Table 4.7. Dead load moments were acting on the specimen before the composite system was bonded. The theoretical cut-off points were situated where a moment equal to the prototype nominal capacity minus the service dead load moment intersects the applied moment diagram.

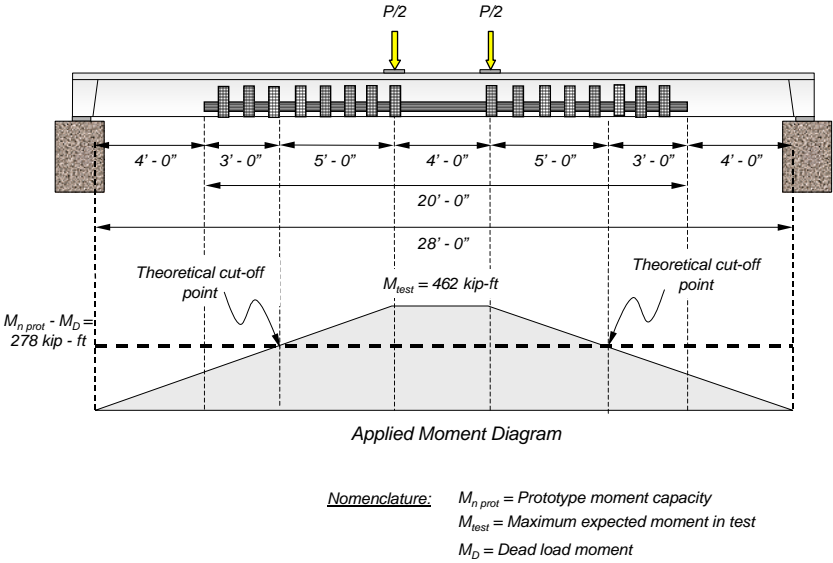


Figure 4.10 Required CFRP Plate Length for HS-20 Truck Loading on 28 ft Clear Span for the Design of Specimen J-1 (2-Joists)

The calculated flexural capacity of Specimen J-1 with the CFRP plates was determined using a maximum strain in the CFRP plates of 0.007 and the measured material properties for steel and concrete. The calculated moment-curvature response is shown in Figure 4.11. Also shown is the calculated response of the bare, reinforced concrete specimen. The difference in the calculated capacity of the strengthened joists from the prototype bridge, 510 kip-ft, and the calculated capacity of the laboratory specimen, 570 kip-ft, may be attributed to two factors: (a) Strain hardening of the reinforcement was considered for Specimen J-1, but was ignored for the prototype and (b) the measured yield stress in the longitudinal reinforcement exceeded the nominal yield stress.

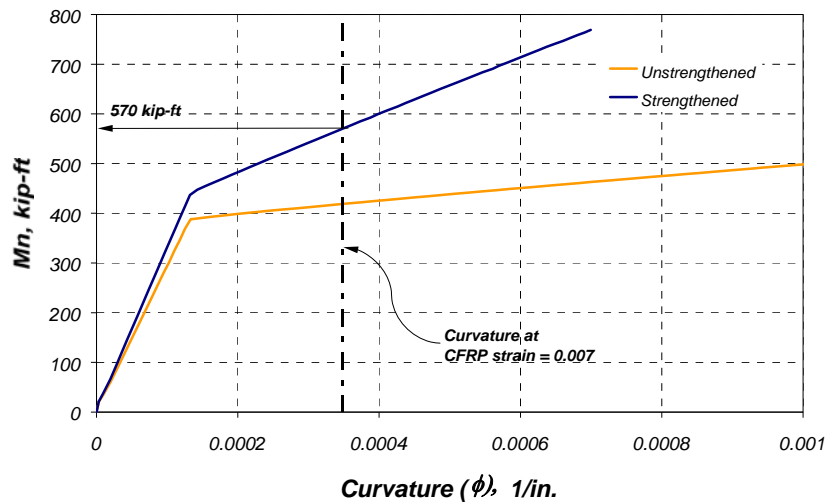


Figure 4.11 *Calculated Moment-Curvature Response of Specimen J-1 Using Measured Material Properties*

4.4.2 Strengthening Scheme for Specimen J-2

Specimen J-2 was strengthened using CFRP sheets that were applied using a wet lay-up procedure (see Appendix C). These sheets were fabricated with continuous unidirectional carbon fibers. A two-component epoxy resin was used to impregnate the carbon fibers to form and bond the composite to the concrete surface. A detailed description of the fabrication procedure for this type of system is presented in Appendix C.

Two layers of carbon fiber sheets (plies) were formed on Specimen J-2 to be able to reach the required target strength. The carbon fiber sheets were cut to 8-in. widths and placed around the bottom corners of each joist, leaving 3 in. on the bottom and 5 in. on the sides. Partially wrapping the bottom surface was necessary to avoid the concrete surface irregularity that was generated during casting (Figure 4.12). The length of these sheets was determined as for Specimen J-1 (see Section 4.4.1). Details showing the location and geometry of the CFRP composite on Specimen J-2 are shown in Figure 4.13.



Figure 4.12 Partial Wrapping of Joists in Specimen J-2 to Avoid Concrete Surface Irregularities

Straps were placed to anchor the longitudinal composites at 1-ft spaces along the shear span. The straps were fabricated using one ply of 3-in. wide strips with the same carbon fiber sheets used for the longitudinal direction. In this case, the straps extended into the curved part of the cross section (16-in. from the bottom). The composite fabrication was done on the same day and left to cure for 7 days at ambient temperature before testing.

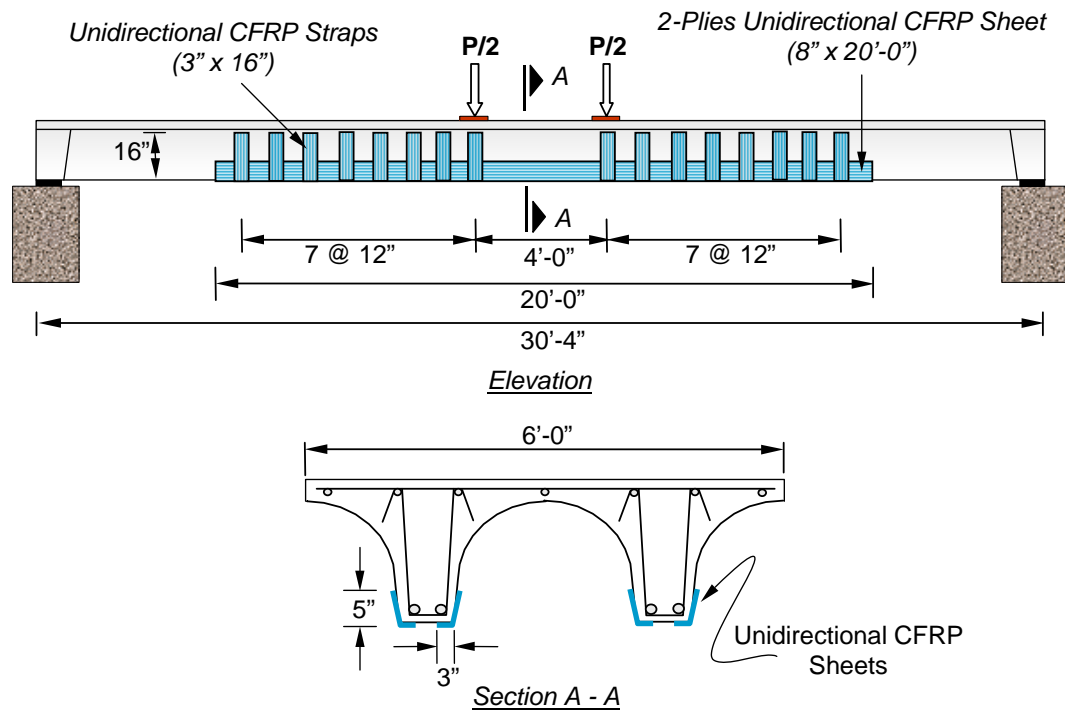


Figure 4.13 CFRP Strengthening Details for Specimen J-2

The calculated moment-curvature response of Specimen J-2 is shown in Figure 4.14. The measured strengths of steel and concrete were used in the calculations. The flexural capacity of the specimen was estimated at a curvature corresponding to an expected maximum CFRP composite strain equal to 0.007.

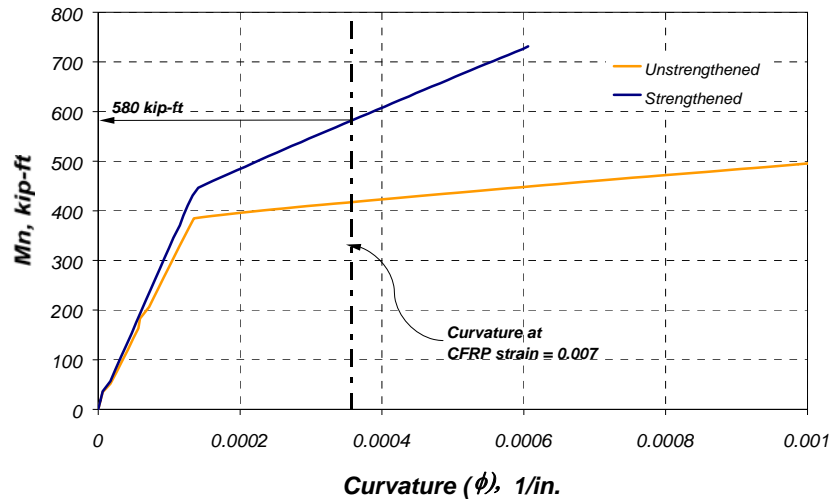


Figure 4.14 *Calculated Moment-Curvature Response of Specimen J-2 Using Measured Material Properties*

As shown in Figure 4.14, the calculated specimen capacity, 580 kip-ft, exceeds the required flexural capacity, 510 kip-ft, determined during design of the strengthening scheme. The same explanation can be given for the difference in calculated prototype capacity and calculated capacity of the laboratory specimen as for Specimen J-1.

4.5 LOAD LEVELS FOR PROTOTYPE BRIDGE

As discussed in Section 4.2, the prototype bridge must be strengthened to meet the inventory rating criteria for widening and reduced inspection frequency. The strengthening scheme for the prototype bridge was designed such that the strengthened bridge would have an inventory rating of at least HS-20. Maximum moments and shears corresponding to service and design levels for the original and strengthened bridge are summarized in Table 4.8.

The service-level moments due to dead and live load in a single joist in the as-built prototype bridge are 41.7 and 36.9 kip-ft, respectively (Table 4.8). If the design vehicle is changed from an H-10 truck to an HS-20 truck, the service-level live load moment increases to 81.8 kip-ft. Design-level moments due to dead and live loads increase to 54.2 kip-ft and 177.5 kip-ft, respectively. Moments corresponding to the four load levels listed in Table 4.8 were used to define the stages of loading used during the experimental tests.

Table 4.8 Moments Associated to Different Design Levels for One Joist in Prototype Bridge

| Design Truck | Load Level | Design Condition | M_{DL} , kip-ft | $M_{LL(1+I)}$, kip-ft | Load Factor | |
|--------------|------------|---|----------------------|---------------------------|-------------|-------------|
| | | | | | D | L |
| H-10 | 1 | Service loads (Unstrengthened) | 41.7 | 36.9 | D L | 1.0 1.0 |
| HS-20 | 2 | Service loads (Strengthened) | 41.7 | 81.8 | D L | 1.0 1.0 |
| HS-20 | 3 | Service dead load + Factored live load | 41.7 | 177.5 | D L | 1.0 2.17 |
| HS-20 | 4 | (Factored dead load + Factored live load)/ ϕ | 63.8 | 208.8 | D L | 1.3 2.17 |

Notes: Impact factor, $I = 0.3$.

Load levels were used during laboratory tests to evaluate performance of strengthened joists.

4.6 SUMMARY

Typical pan-joist bridge construction in Texas was presented in this chapter. This form of construction was common 50 years ago, and many existing bridges were designed for lower loads than are now required, typically H-10 or H-15 truck loading. Therefore, a two-lane prototype bridge, which was designed for an H-10 truck loading, was selected to represent the case where maximum strengthening is required.

The calculated inventory load ratings for the prototype bridge were H-13.6 and HS-12.2 for the different types of design trucks used currently. Because TxDOT requires that a bridge have an inventory rating of at least HS-20 to qualify for widening, an increase in flexural capacity of the prototype bridge was required. A 42% increase in flexural capacity is required to meet this design objective.

The design, construction, and strengthening procedures used in two full-scale laboratory specimens were presented in this chapter. These specimens represent a 6-ft wide section of the prototype bridge consisting of two joists. The design of these specimens in the laboratory was aimed at capturing the general behavior of the prototype bridge after strengthening.

The procedures used for design and construction of two strengthening schemes that are appropriate for joist specimens were presented. Two different composite systems were used to increase the capacity of the prototype bridge from

an HS-12.2 inventory rating to an HS-20 rating. These systems were constructed and applied to the laboratory specimens. The measured response of the laboratory tests of the pan-joint specimens is presented in [Chapter 5](#).

| | |
|---|------------|
| CHAPTER 4: DESCRIPTION OF PAN-JOIST SPECIMENS..... | 76 |
| 4.1 Introduction | 76 |
| 4.2 Prototype Bridge | 78 |
| 4.2.1 Physical Characteristics of Prototype Bridge | 79 |
| 4.2.2 Calculated Capacity of Prototype Bridge | 80 |
| 4.2.3 Load Rating for Prototype Bridge | 84 |
| 4.3 Design and Construction of Laboratory Specimens | 91 |
| 4.4 Design and Construction of Strengthening Schemes for Laboratory Specimens..... | 96 |
| 4.4.1 Strengthening Scheme for Specimen J-1 | 101 |
| 4.4.2 Strengthening Scheme for Specimen J-2..... | 106 |
| 4.5 Load Levels for Prototype Bridge | 109 |
| 4.6 Summary | 111 |

| | |
|---|-----|
| Figure 4.1 View of Metal Pan-Forms inside the Laboratory | 77 |
| Figure 4.2 Photograph of Pan-Joist Bridge in Buda, Texas Indicating Uneven Surfaces on Bottom of Joists | 78 |
| Figure 4.3 Reinforcement Details for Prototype Bridge | 81 |
| Figure 4.4 H-10 Truck Positions Corresponding to Critical Moments and Shears | 87 |
| Figure 4.5 HS-10 Truck Positions Corresponding to Critical Moments and Shears | 88 |
| Figure 4.6 Specimen Reinforcement and Formwork | 94 |
| Figure 4.7 Joist Specimen Geometry and Reinforcement | 95 |
| Figure 4.8 Calculated Moment-Curvature Response of Two Joists of Prototype Bridge Strengthened Using Different Composite Systems | 100 |
| Figure 4.9 CFRP Strengthening Details for Specimen J-1 | 103 |
| Figure 4.10 Required CFRP Plate Length for HS-20 Truck Loading on 28 ft Clear Span for the Design of Specimen J-1 (2-Joists) | 104 |
| Figure 4.11 Calculated Moment-Curvature Response of Specimen J-1 Using Measured Material Properties | 105 |

| | |
|---|-----|
| Figure 4.12 Partial Wrapping of Joists in Specimen J-2 to Avoid Concrete Surface Irregularities | 107 |
| Figure 4.13 CFRP Strengthening Details for Specimen J-2 | 108 |
| Figure 4.14 Calculated Moment-Curvature Response of Specimen J-2 Using Measured Material Properties | 109 |
| | |
| Table 4.1 Calculated Flexural and Shear Capacities of a Single Joist in the Prototype Bridge..... | 83 |
| Table 4.2 Maximum Live Load Moments and Shears Per Joist for the Prototype Bridge | 86 |
| Table 4.3 Unfactored Load Effects Per Joist Used to Rate Prototype Bridge..... | 89 |
| Table 4.4 Load Rating Results for Prototype Pan-Joist Bridge Originally Designed for an H-10 Truck Loading..... | 90 |
| Table 4.5 Average Measured Material Strengths for Joist Specimens..... | 93 |
| Table 4.6 Nominal Flexural and Shear Capacities of Pan-Joist Specimens..... | 96 |
| Table 4.7 Parameters Used to Design the Strengthening Schemes | 99 |
| Table 4.8 Moments Associated to Different Design Levels for One Joist in Prototype Bridge..... | 110 |

Chapter 5: Measured Response of Pan-Joist Specimens

5.1 INTRODUCTION

The measured response of Specimens J-1 and J-2 is presented in this chapter. The experimental setup, loading history, and specimen instrumentation are also described. The instrumentation was designed to provide information about the internal forces at specified sections, as well as global response of the specimens. Recorded outputs from the instruments are presented and discussed.

5.2 TEST SETUP AND INSTRUMENTATION

5.2.1 Description of Experimental Setup

The strengthened joist specimens (J-1 and J-2) were subjected to static loads to evaluate their behavior under service and ultimate loads. The test specimens were idealized as being simply supported. Each end diaphragm rested on two steel-rubber elastomeric pads on top of concrete blocks.

Loads were applied statically using a 200-kip hydraulic ram reacting against a steel frame that was anchored to the laboratory strong floor. The total load was distributed to 4 points on the slab to simulate wheel loads. The loading points were located symmetrically about the specimen centerline with a 4-ft spacing in the longitudinal direction and a 3-ft spacing in the transverse direction. Loading point

spacing in the transverse direction was selected to load each joist directly. In the longitudinal direction, the load spacing was selected to simulate the tandem rear axle of a typical truck. AASHTO design vehicles have a longer axle spacing, but real trucks have an axle spacing that resembles the tandem configuration more closely.

Elastomeric pads were used under each load point to avoid crushing of the concrete due to stress concentrations. Details of the test setup are shown in [Figures 5.1 and 5.2](#).



Figure 5.1 Side View of Pan-Joist Specimen in Laboratory Test Setup



Figure 5.2 Overhead View of Pan-Joist Specimen Showing the Location of Loading Points

5.2.2 Loading Sequence

The loading sequence was selected to evaluate the behavior of the joists under moments equivalent to service and factored load conditions in the prototype bridge. Before bonding the CFRP composites to the reinforced concrete joists, the specimens were subjected to the load corresponding to service load moments for

the original design (78.6 kip-ft). The objective of this step was to induce cracking in the test specimens before the CFRP systems were applied. Flexural cracking has been observed in existing pan-joint bridges [Velázquez, 1998]. The specimens were subjected to 2 cycles at this load level after which they were unloaded and strengthened using the composite systems described in Chapter 4.

The second stage of loading began after the composite systems had undergone a 7-day curing period at ambient temperature. During this stage, the specimens were subjected to moments corresponding to different design levels: service live load before strengthening, service live load after strengthening, factored live load, and required ultimate load. After reaching each of the predetermined load levels, the specimens were unloaded and then reloaded to the same load. This repeated loading scheme was adopted to evaluate changes in specimen stiffness, and to observe deterioration of the composite-concrete interface.

The different load levels and the number of cycles at each load that were imposed on both pan-joint specimens are listed in Table 5.1. These loads correspond to service and design loads for the prototype bridge (Table 4.8). Because the specimens were constructed at full scale, it was assumed that the service-level dead loads were acting at the time of the test. Therefore, the applied

load level was selected such that the total moment at midspan of the test specimen matched the total moment in the prototype bridge for two joists.

Table 5.1 Required Moments and Loads During Testing Corresponding to Design Levels in the Prototype Bridge

| Load Level | Moments in Prototype Bridge | | Moments in Test Specimen | | Total Applied Load, kip | # of Cycles |
|------------|-----------------------------|-------------------|--------------------------|----------------------|-------------------------|-------------|
| | Dead Load, kip-ft | Live Load, kip-ft | Dead Load, kip-ft | Applied Load, kip-ft | | |
| 1 | 83.4 | 73.8 | 83.4 | 73.8 | 12.3 | 2 |
| 2 | 83.4 | 163.6 | 83.4 | 163.6 | 27.3 | 2 |
| 3 | 83.4 | 355.0 | 83.4 | 355.0 | 59.2 | 2 |
| 4 | 127.5 | 417.6 | 83.4 | 461.7 | 77.0 | 1 |

Note: Total moments in two joists are tabulated.

Load Level 1: $1.0D + 1.0L$ (Original Live Load).

Load Level 2: $1.0D + 1.0L$ (Increased Live Load).

Load Level 3: $1.0D + 2.17L$ (Increased Live Load).

Load Level 4: $(1.3D + 2.17L)/0.85$ (Increased Live Load).

After the last design-level load was applied, the specimens were unloaded and reloaded until the composite systems debonded from the concrete surface. Failure of the composite system was defined when there was a sudden reduction in the strength of the specimen.

After debonding of the CFRP composites, the reinforced concrete elements were still able to carry load, although at a reduced level. Therefore, the loading

was continued until the onset of concrete crushing to determine the capacity of the bare reinforced concrete joists.

5.2.3 Instrumentation

Three types of instruments were used in the tests: linear potentiometers, strain gages, and load cells. Linear potentiometers were used to monitor global specimen response. A total of 10 potentiometers were attached to Specimen J-1 and 12 were attached to Specimen J-2. Four sections in each specimen were instrumented with strain gages bonded to the reinforcement, CFRP composites, and concrete slab. A total of 13 gages were attached in each section for Specimen J-1 and 11 were attached in each section for Specimen J-2. A 200-kip load cell was used to monitor load throughout the tests. The voltage output from the instruments was collected every 4 seconds using a Hewlett Packard-75000 scanner and recorded in a computer.

Linear potentiometers were positioned on the east and west sides of the specimens at midspan and at the points of load application. Because the specimens were supported on flexible bearing pads, the ends were also instrumented with potentiometers to determine the deformation of the supports. The support movement was subtracted from the displacement measured along the span to determine the deformation of the specimen relative to its ends. Potentiometers with a 6-in. stroke were used at midspan and with a 2-in. stroke for the rest of the

locations. The location of the linear potentiometers for Specimens J-1 and J-2 are summarized in Table 5.2.

Strain gages were used to calculate internal forces and the neutral axis depth at four sections along the span. The moment-curvature response at the instrumented sections was calculated from these values.

Table 5.2 Displacement Limits of Linear Potentiometers

| Test Specimen | Joist | North Load Point | Mid-span | South Load Point | End Diaphragms * |
|---------------|-------|------------------|----------|------------------|------------------|
| J-1 | East | 2 in. | 6 in. | 2 in. | 2 in. |
| | West | 2 in. | 6 in. | 2 in. | 2 in. |
| J-2 | East | 2 in. | 6 in. | 2 in. | 2 in. |
| | West | 2 in. | 6 in. | 2 in. | 2 in. |

*See Figures 5.3 and 5.4 for the location of potentiometers at the end diaphragms

Each instrumented section had strain gages placed on the bottom longitudinal reinforcement in both joists, on the concrete slab, and on the CFRP composite bonded to each joist. Characteristics of the strain gages are listed in Table 5.3.

Table 5.3 Characteristics of Strain Gages

| Material | Strain Gage Type | Gage Length, mm |
|----------|------------------|-----------------|
| Steel | Foil | 6 |
| CFRP | Foil | 6 |
| Concrete | Wire | 60 |

The locations of the strain gages are shown in Figure 5.3 for Specimen J-1 and Figure 5.4 for Specimen J-2. These sections were selected to be able to determine the moment-curvature response at the maximum moment section in the specimen and at a section within the shear span.

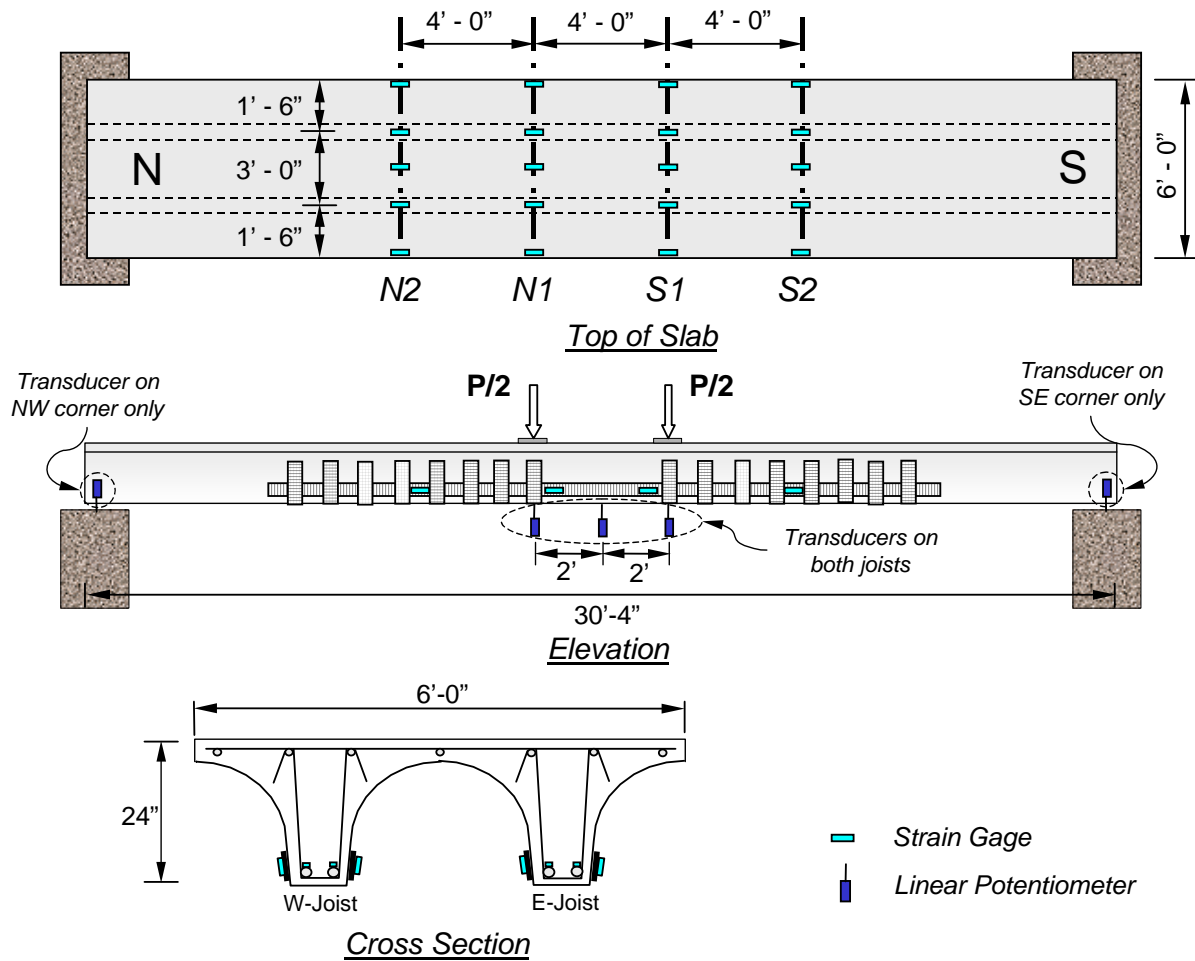


Figure 5.3 Location of Instrumented Sections Showing Position of Potentiometers and Strain Gages in Specimen J-1

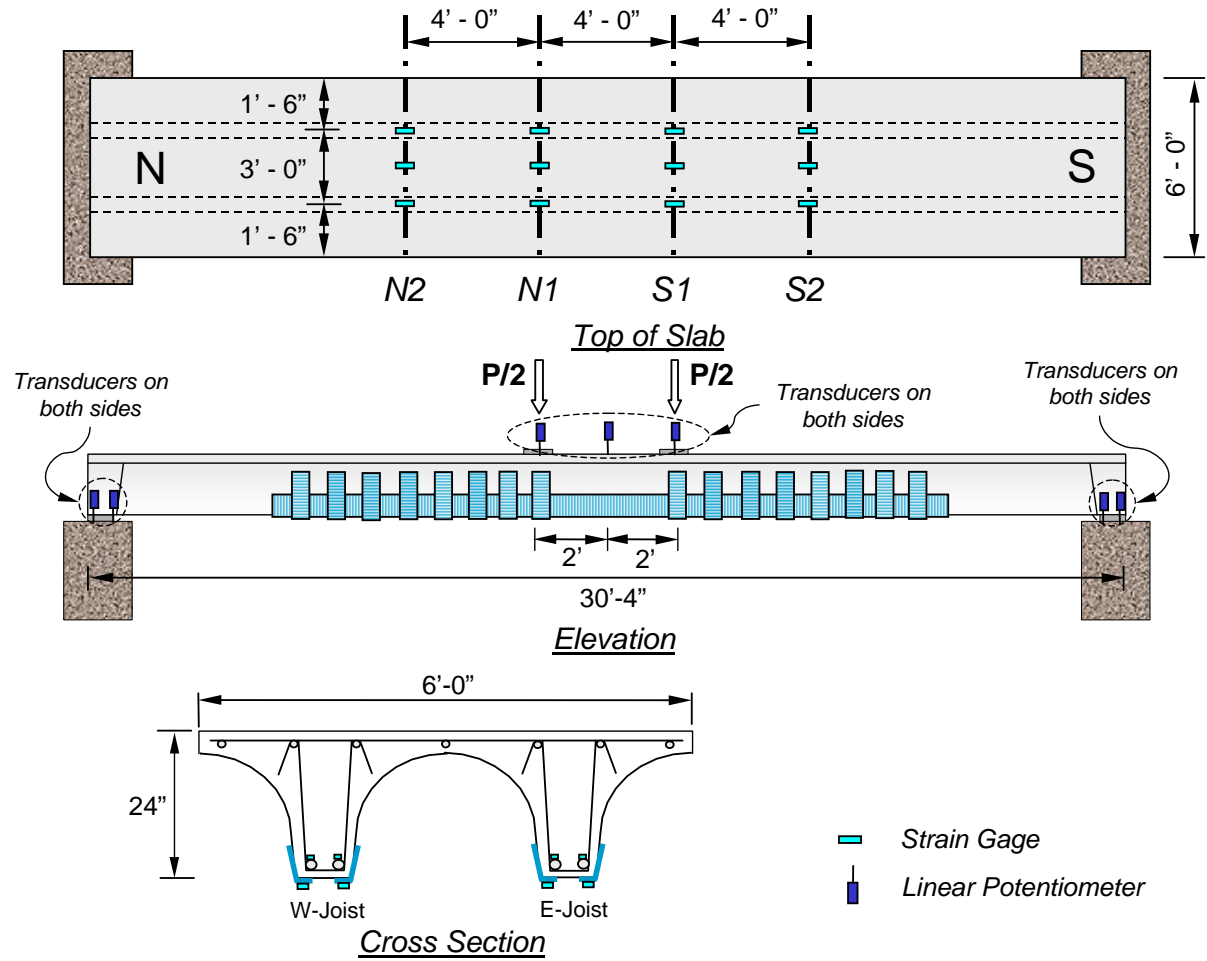


Figure 5.4 Location of Instrumented Sections Showing Position of Potentiometers and Strain Gages in Specimen J-2

5.3 OBSERVED BEHAVIOR DURING TESTS

The observed behavior of the specimens during the tests is described in this section. Visible damage in the concrete-CFRP composite interface due to debonding is summarized in Section 5.3.1. Cracking patterns that were observed at two of the design levels are also presented. Representative measured response from the instruments is discussed in Section 5.4.

5.3.1 Description of Failure Sequence and Cracking Distribution

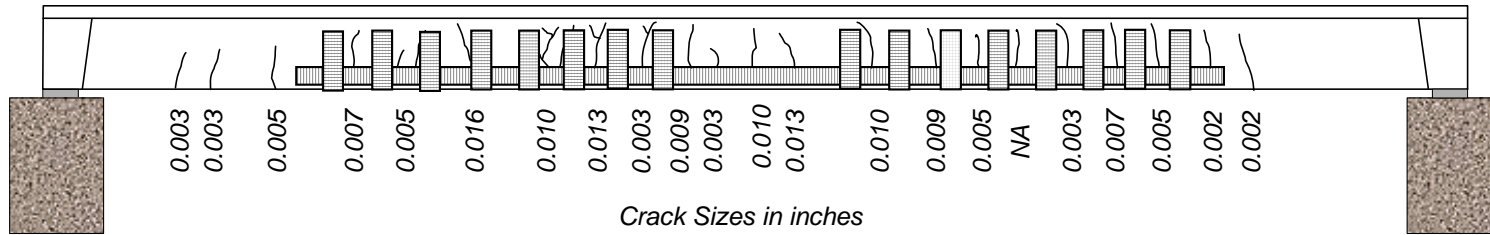
(a) Specimen J-1

The bare reinforced concrete specimen was subjected to two cycles at the original service load level. Cracks formed uniformly at about 12-in. spacing. The last observed crack was located at approximately 4 ft from the face of the end diaphragms. All the cracks that formed within the shear span were less than 0.002 in. wide. The maximum crack width inside the constant moment region was 0.007 in. The specimen was strengthened without repairing the cracks that formed after these loading cycles.

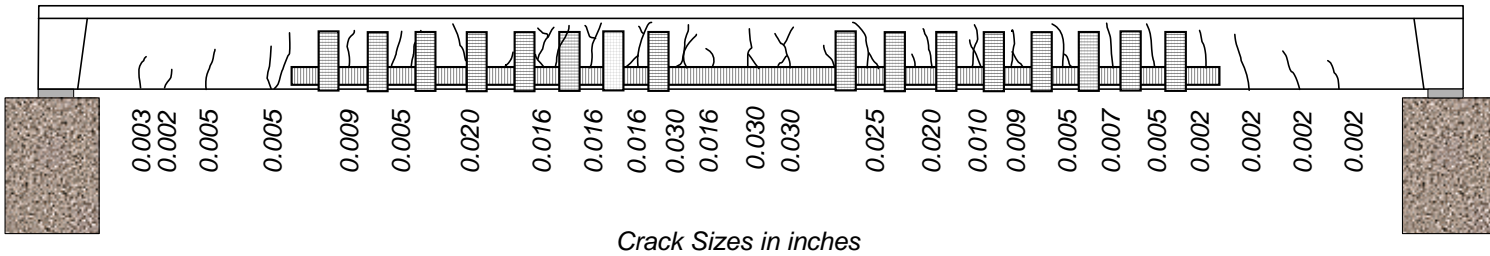
After strengthening, Specimen J-1 did not show signs of distress during the first load cycle to the original service loads. Cracks were documented at load levels 2 and 3. The longitudinal reinforcement was observed to yield at load level 3. Cracking patterns on the west joist are shown in Figure 5.5 for both of these

loading stages. Diagonal cracks propagated from existing flexural cracks as the specimen was loaded to 60 kip. This behavior gave an indication of stresses being transferred into the CFRP plates after the longitudinal reinforcement yielded. Also, crack widths increased considerably, especially inside the constant moment region.

Initial debonding of the CFRP plate was observed on the east joist after the first excursion to yield. Debonding initiated at midspan and was only observed on the top of the plate (see Figure 5.6). However, no other signs of bond deterioration were seen along other plates or transverse straps. The specimen was then unloaded and reloaded past the observed yield point. The first transverse strap debonding occurred at an applied load of approximately 77 kip (load level 4). Strap debonding was characterized by a sudden release from the concrete surface (Figure 5.7). Debonding of straps took place after a flexural crack propagated behind the strap leaving only the upper portion of the strap bonded to the concrete surface.



Load Level 2 (Applied Load = 27 kip)



Load Level 3 (Applied Load = 60 kip)

Figure 5.5 Typical Cracking Patterns for Specimen J-1 (West Joist)



Figure 5.6 Observed Initial Debonding of CFRP Plate on East Joist



Figure 5.7 Transverse Strap Debonding at Ultimate Design Load

As the load was increased, the ends of the CFRP plates detached from both joists. Also, cracks propagated horizontally along the top of the CFRP plates, mainly at strap locations. Finally, the CFRP plate debonded from the east joist at an applied load of 97.3 kip. As the CFRP plates pulled-off from the concrete surface, they sheared the anchoring straps and pulled off a significant amount of surface concrete. The debonding sequence is illustrated in [Figures 5.8 and 5.9](#).



Figure 5.8 East Joist of Specimen J-1 Before CFRP Debonding



Figure 5.9 East Joist of Specimen J-1 at Failure

Immediately after debonding, the specimen was unloaded to insert steel shims between the actuator and the loading beams in order to accommodate the permanent deformation of the specimen and permit further testing. Upon reloading to 78.5 kip, the plates on the west joist debonded from the surface and the load dropped to 61.8 kip. Finally, the specimen was unloaded and reloaded until concrete crushing was observed on the top surface of the slab at an applied load of approximately 70 kip.

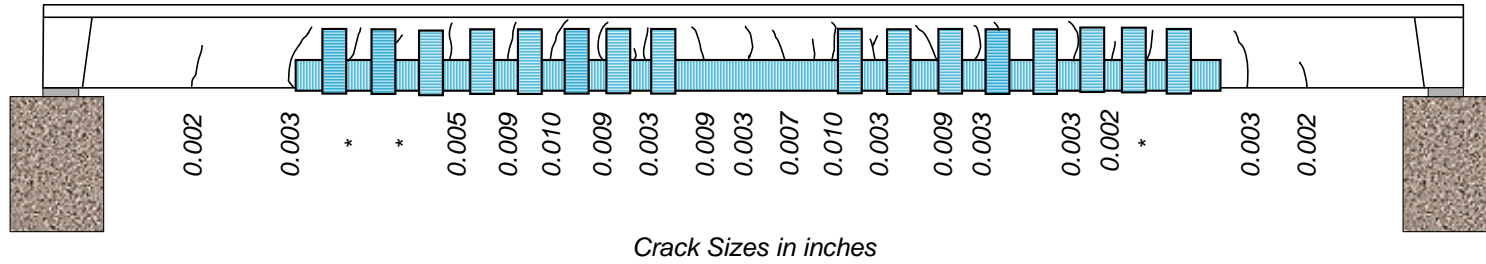
(b) Specimen J-2

The bare reinforced concrete specimen was subjected to the original design service loads. Cracking distribution and widths were similar to those observed for Specimen J-1 at this load stage. Crack spacing was fairly uniform (12 in. approximately) throughout the 20-ft center portion of the specimen. The maximum observed crack width after this load stage was 0.007 in. within the constant moment region. Cracks that formed in the shear span had a maximum width of 0.002 in. The composite system was applied without repairing the cracks that formed after subjecting the bare specimen to this load level.

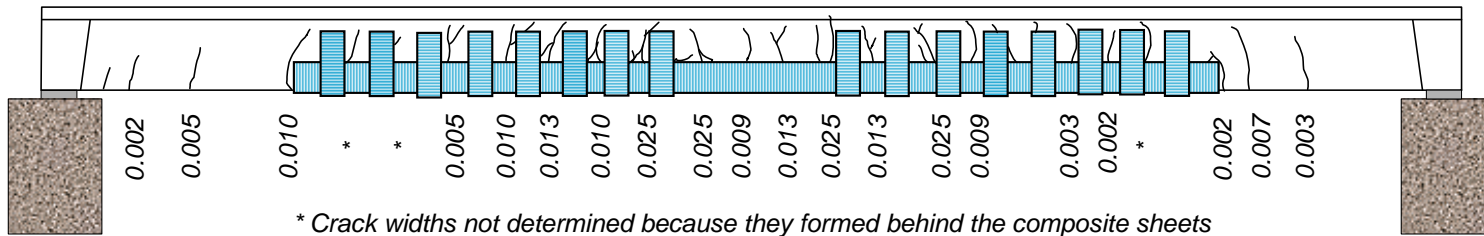
The global behavior of Specimen J-2 after strengthening was similar to that of Specimen J-1. Typical cracking patterns at load levels 2 and 3 are shown in Figure 5.10. Cracking along the top of the CFRP sheet was observed during the load hold at yield on some areas between strap locations and gave an indication of initiation of debonding (Figure 5.11). Debonding of the CFRP sheet at midspan was observed at a load of 78 kip (load level 4). At this stage, flexural cracks started crossing the top portion of some of the anchoring straps located on the south shear span of the specimen (east joist). It is important to note, however, that strap debonding was delayed because the straps on Specimen J-2 were extended farther toward the top of the specimen (Figure 5.12).

As loads were increased, debonding of the longitudinal CFRP sheets propagated towards the ends of the specimen. The portion of CFRP sheet bonded to the bottom of the joists experienced localized fiber rupture at approximately 83 kip within the maximum moment region. However, only a minor drop in load was observed and the specimen was able to carry higher loads. Failure of Specimen J-2 occurred at a load of 95.4 kip when the CFRP sheets debonded completely. The north end of the east joist debonded first, followed by the south end of the west joist (Figure 5.13).

The concrete surface condition after CFRP debonding is shown in Figure 5.14. This surface appearance was typical of the bottom surface of the joists. A significant amount of concrete was pulled off after the sheets debonded from the surface.



Load Level 2 (Applied Load = 27 kip)



Crack Sizes in inches

Load Level 3 (Applied Load = 60 kip)

Figure 5.10 Typical Cracking Patterns for Specimen J-2 (West Joist)



Figure 5.11 Initiation of Debonding Along CFRP Sheet



Figure 5.12 Crack Propagation Behind Strap Caused Debonding



Figure 5.13 View of West Joist in Specimen J-2 at Failure



Figure 5.14 Bottom Surface Condition of West Joist after CFRP Debonding

5.4 MEASURED RESPONSE

The measured displacement and strain response are presented in this section. The instrument readings are plotted against the applied load to verify that the instruments were operating properly throughout the tests. Calculations using the instrument readings to compare measured response parameters with calculated specimen response are presented in [Chapter 6](#). Summaries of the measured response parameters corresponding to different load levels are presented in [Tables 5.4 and 5.5](#) for Specimens J-1 and J-2, respectively.

5.4.1 Deflection Measurements

Linear potentiometers were used to monitor deflections at midspan, at Sections N1 and S1, and at the supports. The instruments at Sections N1 and S1 were removed before failure. Their stroke capacity was exceeded and it was considered too dangerous for research staff to reposition them. They were removed from Specimen J-1 at load level 3 and from Specimen J-2 at load level 4. Midspan potentiometers were repositioned at load level 3 and left in place until failure of both specimens. More potentiometers were used to monitor movement of the supports for Specimen J-2 than for Specimen J-1, because significant rotation occurred at the supports during testing of Specimen J-1.

Recorded deflections along the span and at the supports are shown in [Figures 5.15 to 5.17](#) for Specimen J-1 and in [Figures 5.18 to 5.20](#) for Specimen J-2.

The deflection readings of instruments at midspan, and Sections N1 and S1 were corrected by subtracting the average support deflections shown in [Figures 5.15 and 5.18](#) for Specimens J-1 and J-2, respectively.

The plots show readings taken on the east and west sides of the specimens. The similarity in these plots indicates that the specimens did not twist during the tests. Therefore, the average deflection was used in the comparison to the calculated response presented in [Chapter 6](#).

The load-deflection plots for both specimens exhibit similar characteristics. The slope in the load-deflection diagrams is indicative of the specimen stiffness at different stages of loading. The response of the specimens was characterized by three different regions ([Figure 5.21](#)). The initial two regions in the load-deflection diagrams correspond to uncracked and cracked specimen response, respectively. These two regions are typical of the behavior of reinforced concrete members. The third region corresponds to member response after yielding of the longitudinal reinforcement. The post-yield stiffness was larger than would be expected for ordinary reinforced concrete. This difference is the result of the contribution of the CFRP composites to the member stiffness.

Although the specimens were initially cracked, the CFRP composites increased the specimen stiffness at low load levels after strengthening. This can be observed in [Figure 5.22](#). The figure compares the unstrengthened and strengthened

load-deflection cycles up to the first two load stages for Specimen J-1. After strengthening, the slope in the load-deflection diagram increased to approximately the slope before cracking the unstrengthened specimen. Points A and B in the figure indicate where the apparent stiffness reduction took place (approximately 5 and 18 kip, respectively). Point A corresponds to specimen cracking before strengthening and point B corresponds to the initial stiffness reduction after strengthening. It can be seen that stiffness reduction takes place at a higher load after the specimen was strengthened although the specimen had already been cracked before strengthening. The broken line in the figure shows that the apparent stiffness after cracking is approximately equal to the strengthened specimen stiffness after point B. Similar behavior to the one described above was also observed in Specimen J-2.

Tables 5.4 and 5.5 give a summary of the measured specimen response at different loading stages for Specimens J-1 and J-2, respectively. The measured midspan deflection in these tables has been corrected by subtracting the support displacements.

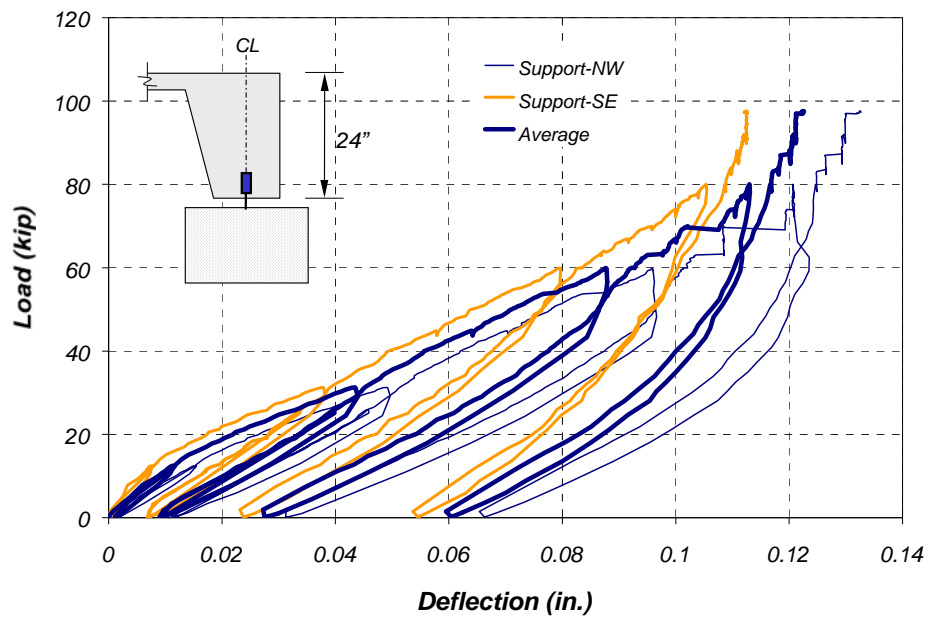


Figure 5.15 Measured Displacements at Supports in Specimen J-1

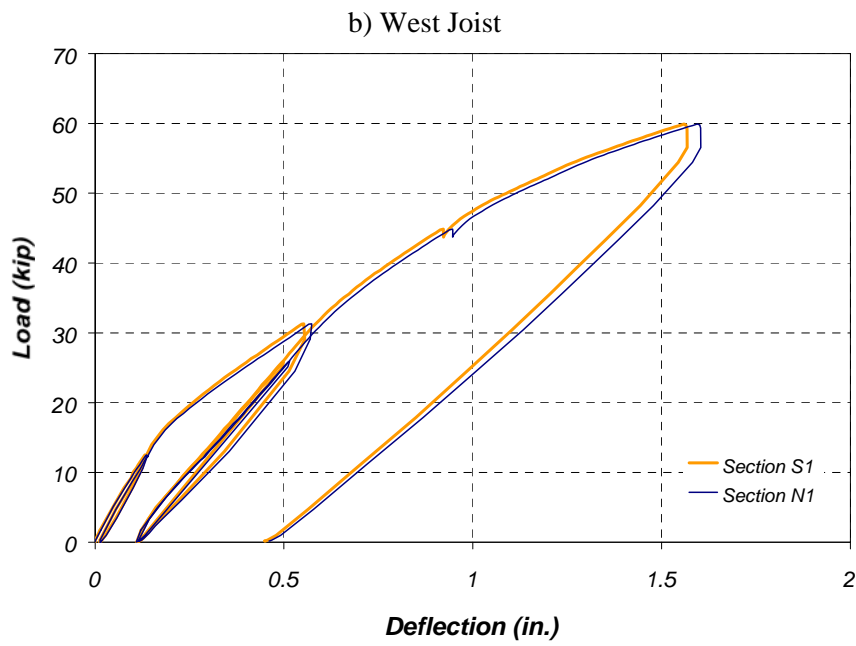
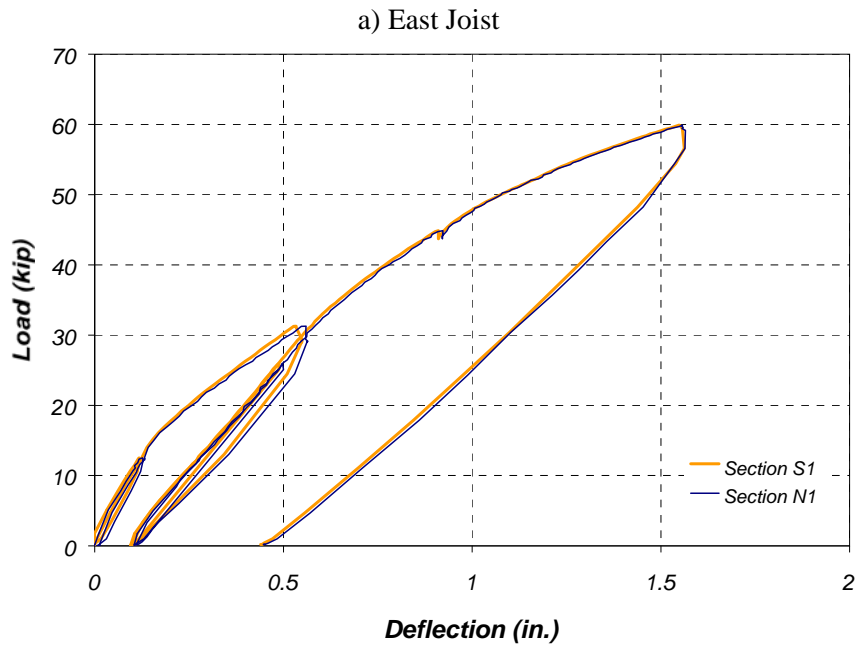


Figure 5.16 Measured Deflections at Sections N1 and S1 in Specimen J-1

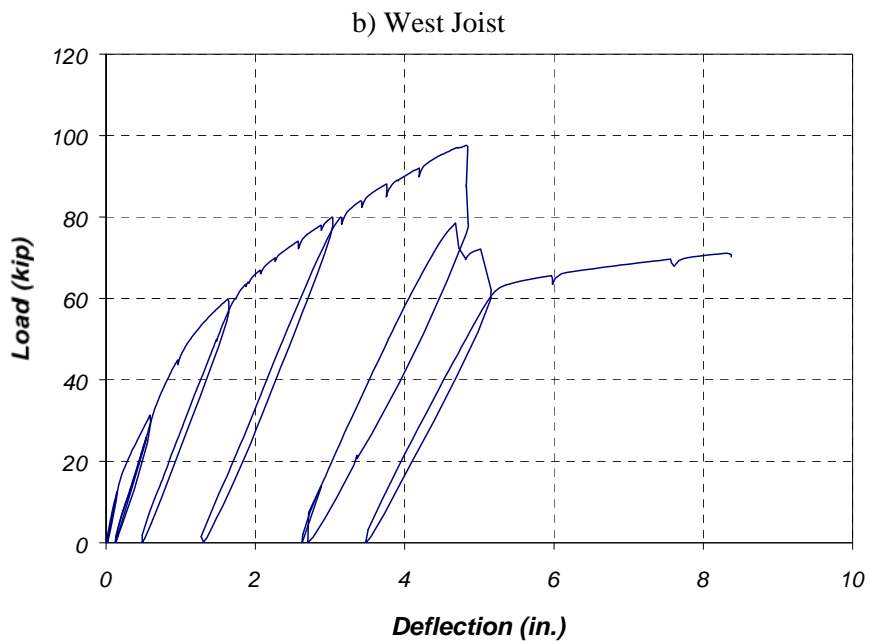
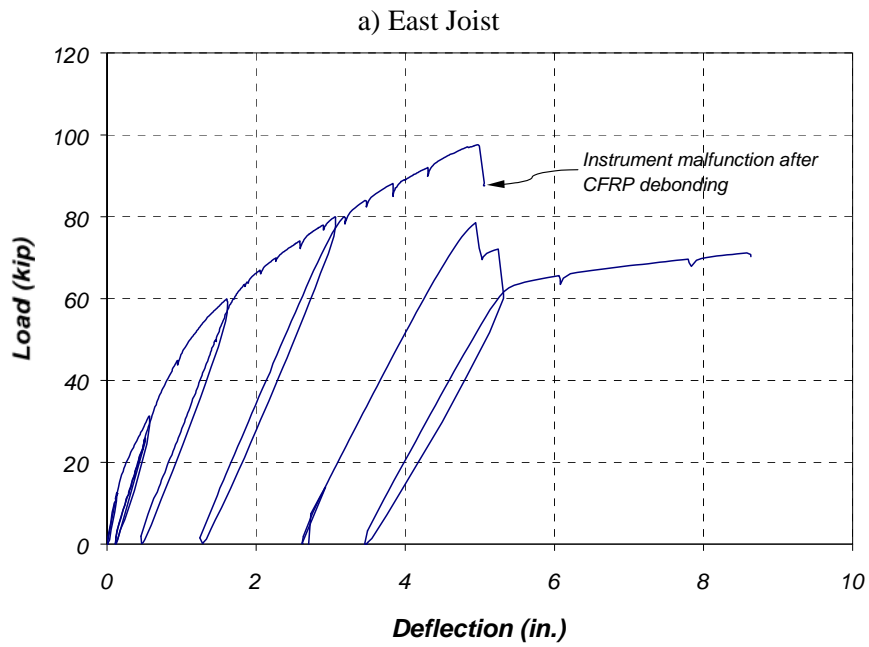


Figure 5.17 Measured Deflections at Mid-Span in Specimen J-1

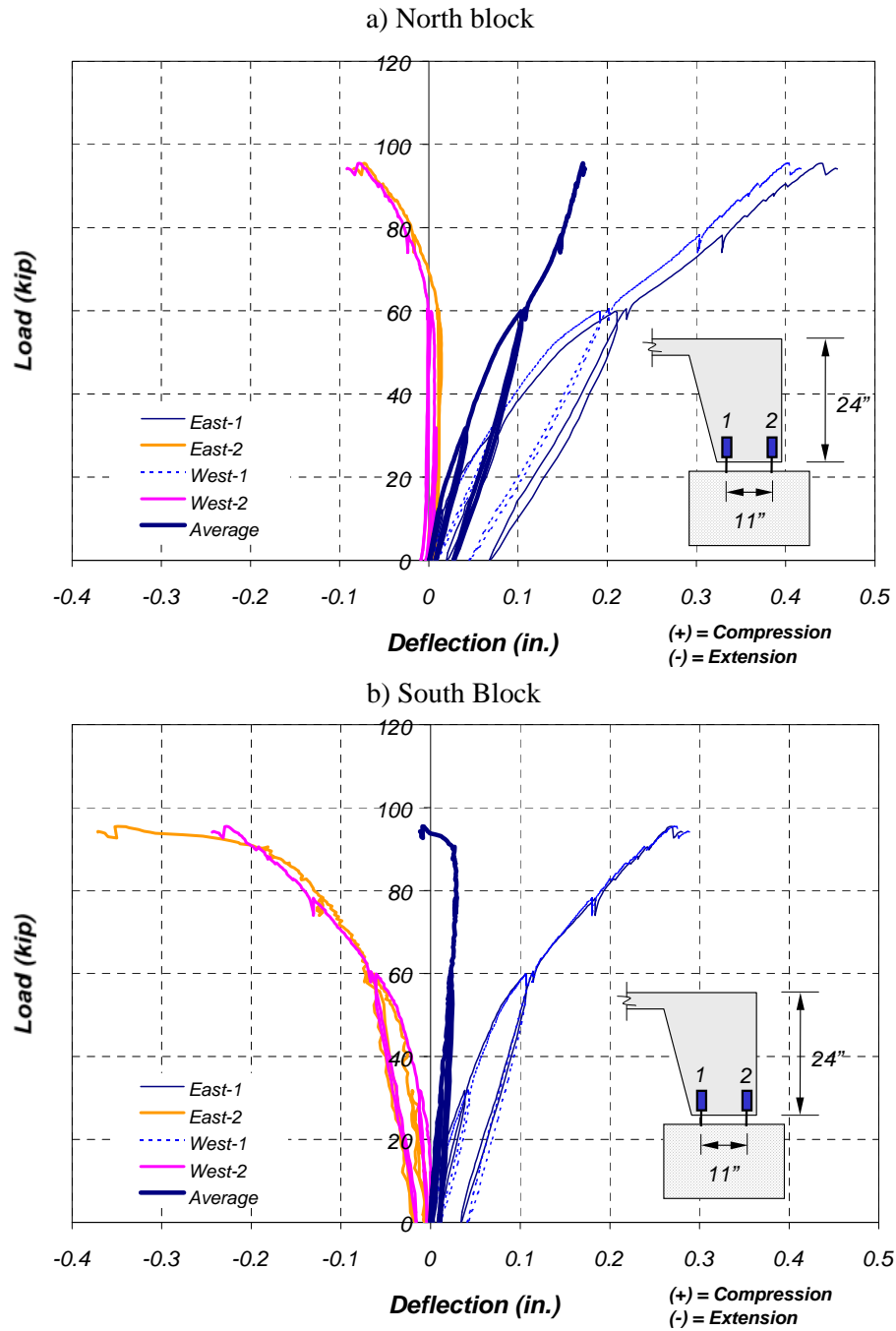


Figure 5.18 Measured Displacements at Supports in Specimen J-2

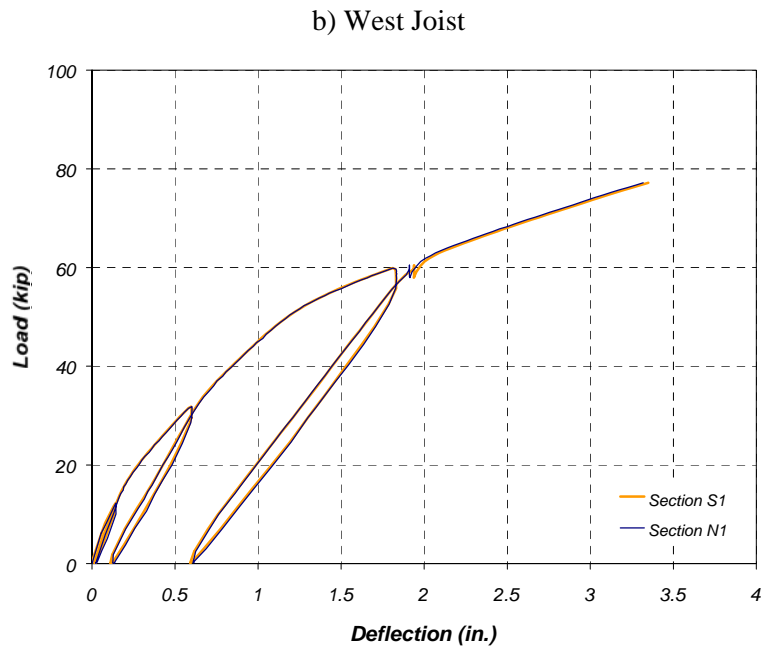
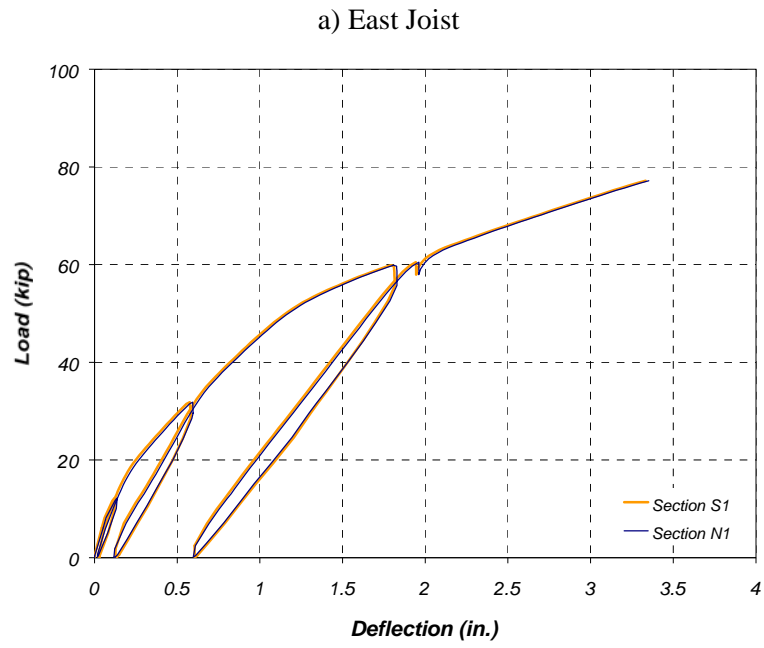
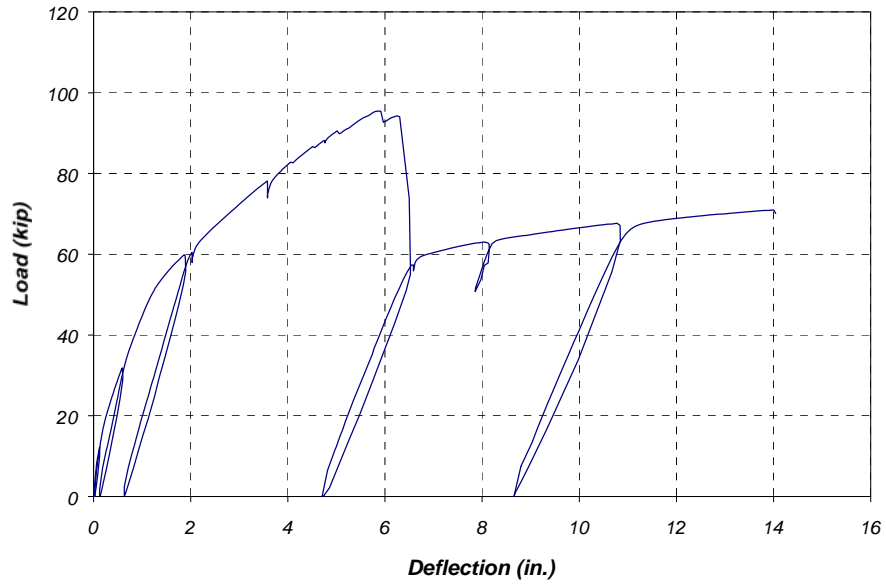


Figure 5.19 Measured Deflections at Sections N1 and S1 in Specimen J-2

a) East Joist



b) West Joist

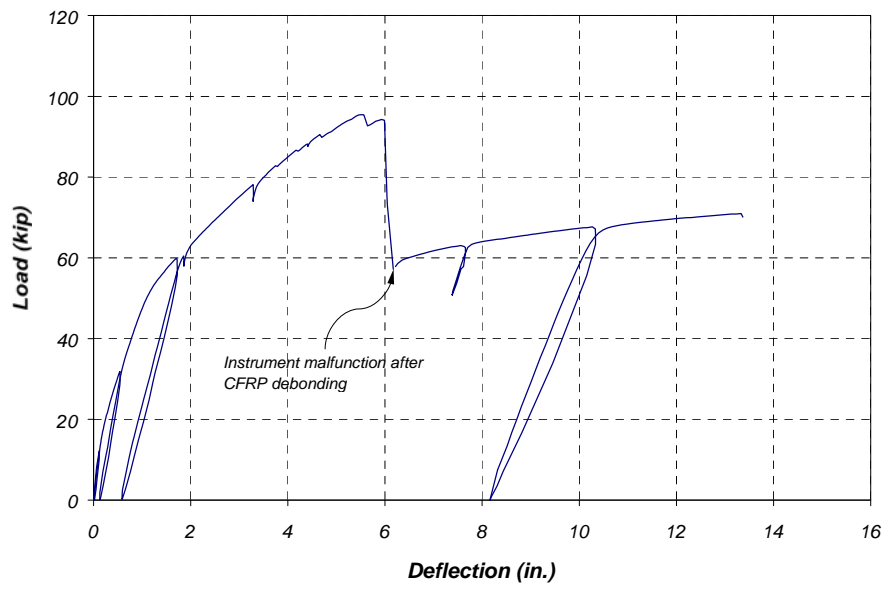


Figure 5.20 Measured Mid-Span Deflections in Specimen J-2

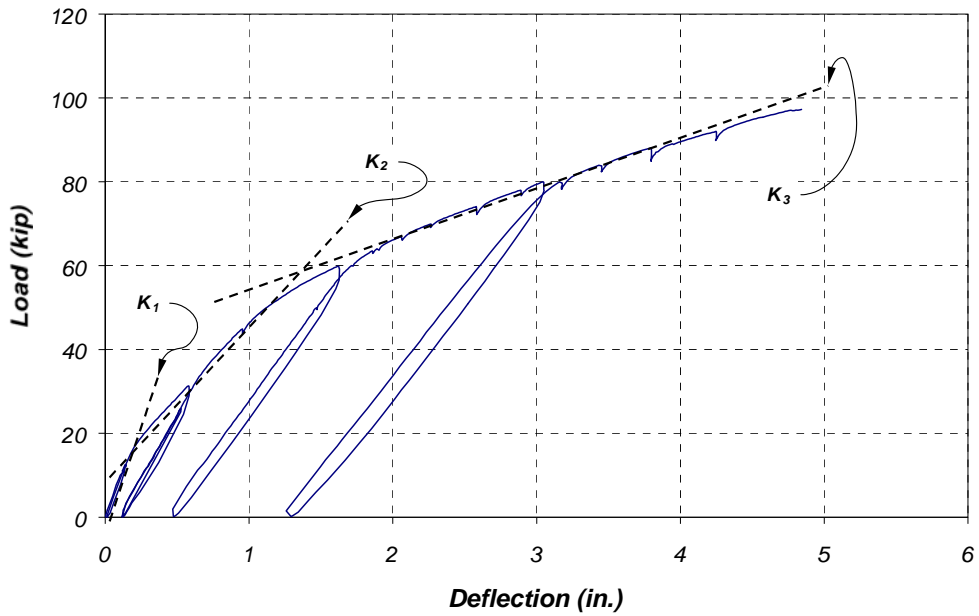


Figure 5.21 Load-Deflection Behavior Characterized by Change in Global Stiffness

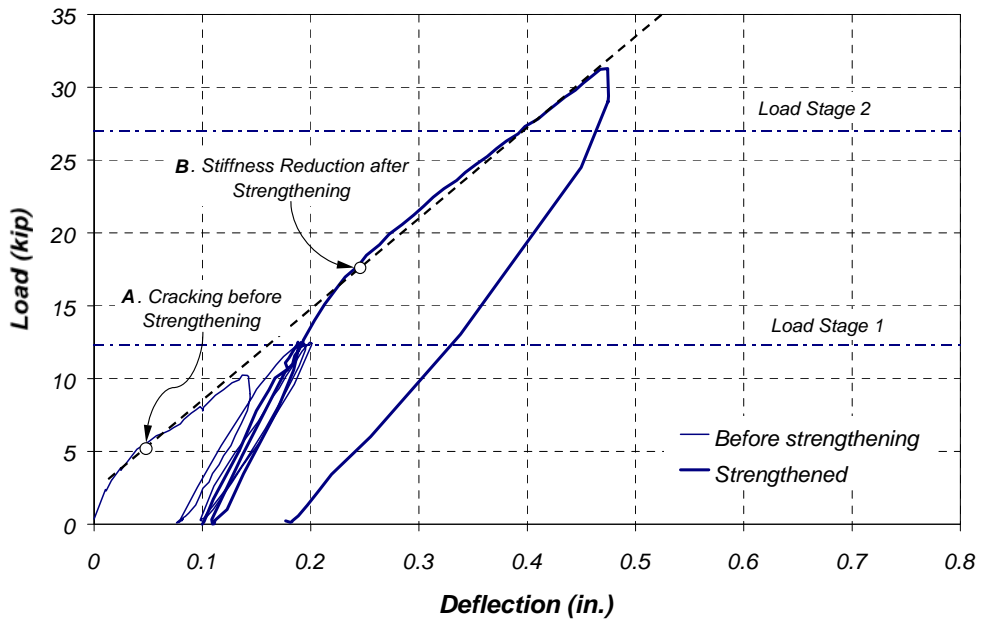


Figure 5.22 Typical Stiffness Increase after CFRP Strengthening (Specimen J-1)

Table 5.4 Maximum Response Measured During Testing of Specimen J-1

| Load Stage | Maximum Measured Parameters | | | Maximum Average Strain (Microstrain) | | | Notes |
|------------|-----------------------------|----------------|-----------------|--------------------------------------|----------|-------------|---|
| | Load, kip | Moment, kip-ft | Deflection, in. | Reinforcement | Concrete | CFRP Plates | |
| 1A | 12.3 | 74 | 0.20 | 453 | 110 | - | Reinforced concrete specimen before application of CFRP |
| 1B | 12.3 | 74 | 0.14 | 200 | 61 | 137 | Reinforced concrete joists with CFRP plates |
| 2 | 27.3 | 164 | 0.54 | 737 | 178 | 836 | Reinforced concrete joists with CFRP plates |
| 3 | 59.2 | 355 | 1.68 | 2,778 | 534 | 2,845 | Observed yielding of longitudinal reinforcement |
| 4 | 75 | 450 | 2.66 | 4,920 | 878 | 5,038 | Target design load |
| 5 | 97.3 | 584 | 4.92 | 8,993 | 1,615 | 8,441 | Debonding of CFRP plate on east joist |
| 6 | 78.5 | 471 | 4.91 | * | 1,548 | * | Debonding of CFRP plate on east joist |
| 7 | 71 | 426 | 8.60 | * | 2,590 | * | Capacity of bare reinforced concrete specimen |

* Readings were unavailable because gages were damaged after CFRP debonding

Table 5.5 Maximum Response Measured During Testing of Specimen J-2

| Load Stage | Maximum Measured Parameters | | | Maximum Average Strain (Microstrain) | | | Notes |
|------------|-----------------------------|----------------|-----------------|---|----------|-------------|---|
| | Load, kip | Moment, kip-ft | Deflection, in. | Reinforcement | Concrete | CFRP Sheets | |
| 1A | 12.3 | 74 | 0.20 | 495 | 125 | - | Reinforced concrete specimen before application of CFRP |
| 1B | 12.3 | 74 | 0.12 | 204 | 76 | 68 | Reinforced concrete joists with CFRP sheets |
| 2 | 27.3 | 164 | 0.41 | 602 | 199 | 368 | Reinforced concrete joists with CFRP sheets |
| 3 | 59.2 | 355 | 1.66 | 2,726 | 718 | 3059 | Observed yield of longitudinal reinforcement |
| 4 | 75 | 450 | 3.05 | 5,122 | 1,285 | 4751 | Target design load |
| 5 | 95.4 | 572 | 5.66 | 8,514 | 2,311 | 8717 | Local rupture of CFRP sheet on east joist |
| 6 | 73.8 | 443 | 6.19 | 7,828 | 2,496 | * | Debonding of CFRP sheet on east and west joists |
| 7 | 70 | 420 | 13.88 | * | 4,316 | * | Capacity of bare reinforced concrete specimen |

* Readings were unavailable because gages were damaged after CFRP debonding

The measured deflections for load stages 1 to 3, corresponding to service load levels, are summarized in Table 5.6. These deflection values were normalized by the span length. It is interesting to note that the deflections measured after the specimens were strengthened were smaller than those measured for the bare reinforced concrete joists. This indicates that the application of the CFRP composites stiffened the specimens at low load levels.

The global response of the specimens was evaluated also by comparing the displacement ductility (μ_{Δ}) of the strengthened specimens with the displacement ductility of the bare reinforced concrete section. Displacement ductility was defined as the ratio of maximum displacement measured at failure to the displacement measured at yield. Even though the specimens did not exhibit a well-defined yield point, the measured deflection at the start of load stage 3 was assumed to be the yield deflection. The yield displacement for the bare reinforced concrete section was assumed to be the same as the yield displacement for the strengthened specimens.

Table 5.6 Measured Deflections during Service Load Stages

| Load Stage | Specimen J-1 | | Specimen J-2 | |
|------------|----------------|--------------------------|----------------|--------------------------|
| | Δ , in. | Δ/L_{test} | Δ , in. | Δ/L_{test} |
| 1A | 0.195 | 1/1,720 | 0.197 | 1/1,710 |
| 1B | 0.143 | 1/2,350 | 0.120 | 1/2,800 |
| 2 | 0.490 | 1/690 | 0.467 | 1/720 |
| 3 | 1.858 | 1/180 | 1.876 | 1/180 |

Displacement ductility of the strengthened specimens is compared with the displacement ductility of the bare reinforced concrete specimens in Table 5.7. The displacement ductility of the strengthened specimens was lower than the ductility of the unstrengthened specimen. However, considerable deformation capacity was observed after yielding before failure of the specimens.

Table 5.7 Comparison of Displacement Ductility

| Specimen | Strengthened | | | Unstrengthened | | |
|----------|------------------|-----------------------------|--|------------------|-----------------------------|--|
| | Δ_y , in. | Δ_{max} , in. | μ_{Δ} ($\Delta_{\text{max}}/\Delta_y$) | Δ_y , in. | Δ_{max} , in. | μ_{Δ} ($\Delta_{\text{max}}/\Delta_y$) |
| J-1 | 1.66 | 4.92 | 3.0 | 1.66 | 8.60 | 5.2 |
| J-2 | 1.74 | 5.66 | 3.3 | 1.74 | 13.84 | 8.0 |

5.4.2 Strain Gage Measurements

Strain gage readings were used to compute internal stresses and forces and to determine the location of the neutral axis at various stages of loading. The calculated moment-curvature response using the strain gage readings is presented in Chapter 6. Load vs. average strain plots for Sections N1 and N2 are presented in this section. The characteristics of these plots were the same for the mirror sections (S1 and S2) on the south side of the specimens. The recorded output from all the instruments can be found in Appendix D. Further discussion on the measured strain response is presented in Chapter 6.

(a) Strain gage readings in Specimen J-1

Measured strains for instrumented sections N1 and N2 in Specimen J-1 are presented in [Figures 5.23 and 5.24](#). These figures show the average strain readings taken on gages bonded to the main flexural reinforcement (#8 bars), CFRP pultruded plates, and concrete slab surface. The average strain readings were used to determine internal stresses in the reinforcement to calculate the moment-curvature response of the specimen.

Whenever the output from an instrument was considered unreliable, it was eliminated from the average calculations. After this point, only the readings from gages that were still functioning were used to calculate the average readings. Gage readings were considered unreliable whenever there was a sudden change in

voltage output caused by gage debonding or wire damage during the test. The curves for the individual gages included in Appendix D indicate whenever readings were considered unreliable.

Curves for instruments located in Section N1 show very distinct regions that are bounded by loads corresponding to the loss in specimen stiffness due to cracking (15 – 20 kip) and yielding of the steel reinforcement (55 – 60 kip). These sections are located at the points of load application and correspond to the start of the constant moment region in the specimen (Figure 5.23).

The load-strain curves for instruments located in Section N2 also show distinct regions defined by different slopes. However, as expected, the loads that define the change in general slope in the plots for Section N2 are higher than for Section N1. At a specific load stage, the moment in Section N2 was lower than the moment in Section N1. The readings of the concrete gages on Section N2 exhibit a fairly linear response after the change in slope corresponding to cracking.

(b) Strain gage readings in Specimen J-2

Strain vs. load plots for Sections N1 and N2 in Specimen J-2 are presented in [Figures 5.25 and 5.26](#), respectively. The location of these instrumented sections was shown in Figure 5.4. These figures show readings taken with gages bonded to

the main flexural reinforcement (#8 bars), CFRP pultruded plates, and concrete slab surface.

In this specimen, only three strain gages were bonded to the top concrete slab at each section instead of the five that were used for Specimen J-1. This was decided after observing that the readings across a section in Specimen J-1 were very similar so the gages at the slab edge were eliminated (see Appendix D).

The same general trends that were observed for the gages in Specimen J-1 can be observed in these figures. Therefore, similar conclusions can be reached about the observed strain response for this specimen.

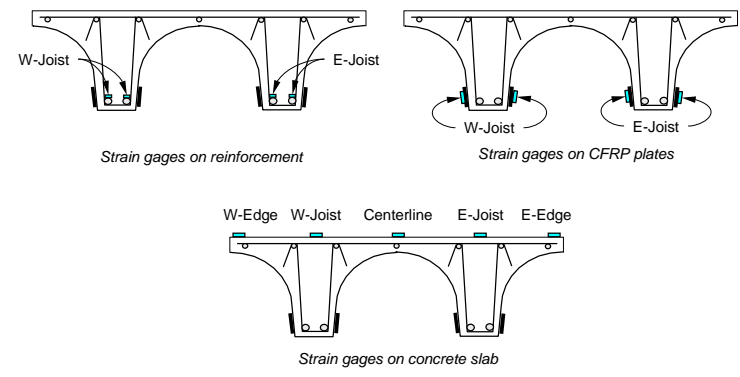
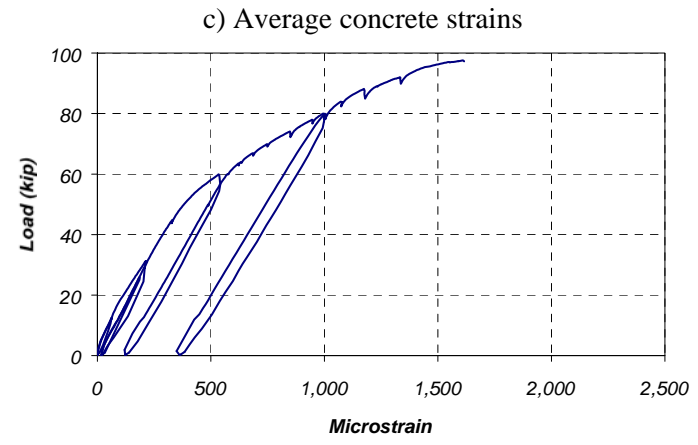
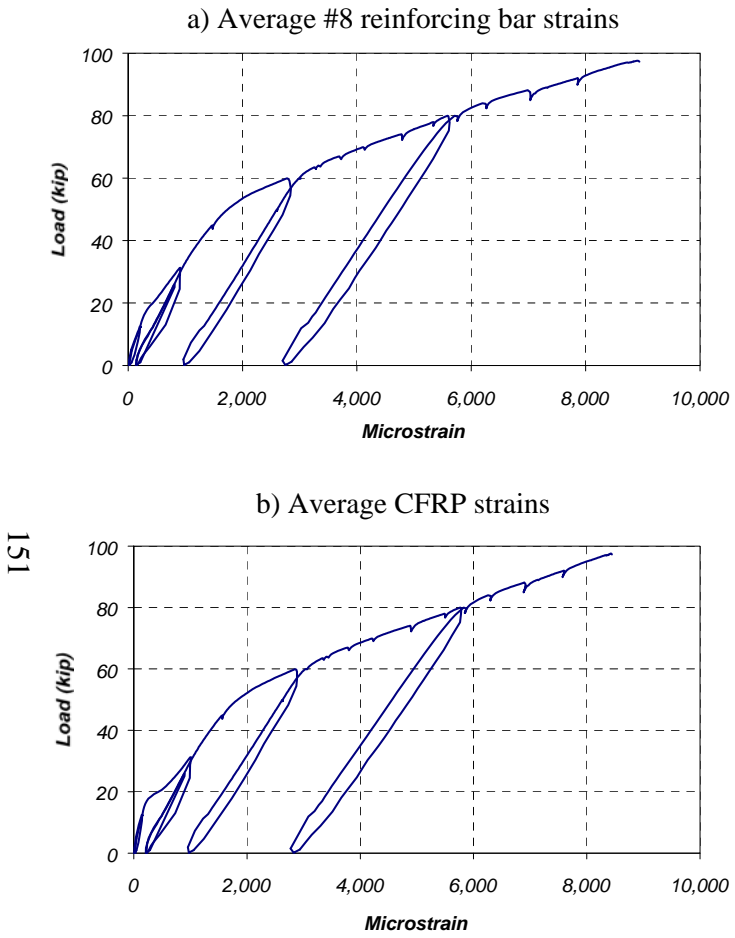


Figure 5.23 Average Strains Measured at Section N1 (Specimen J-1)

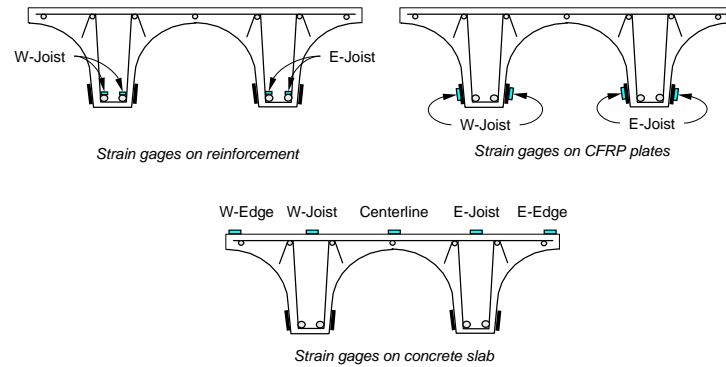
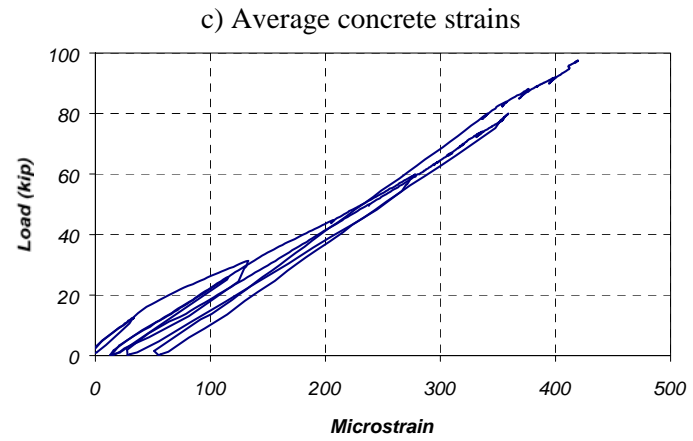
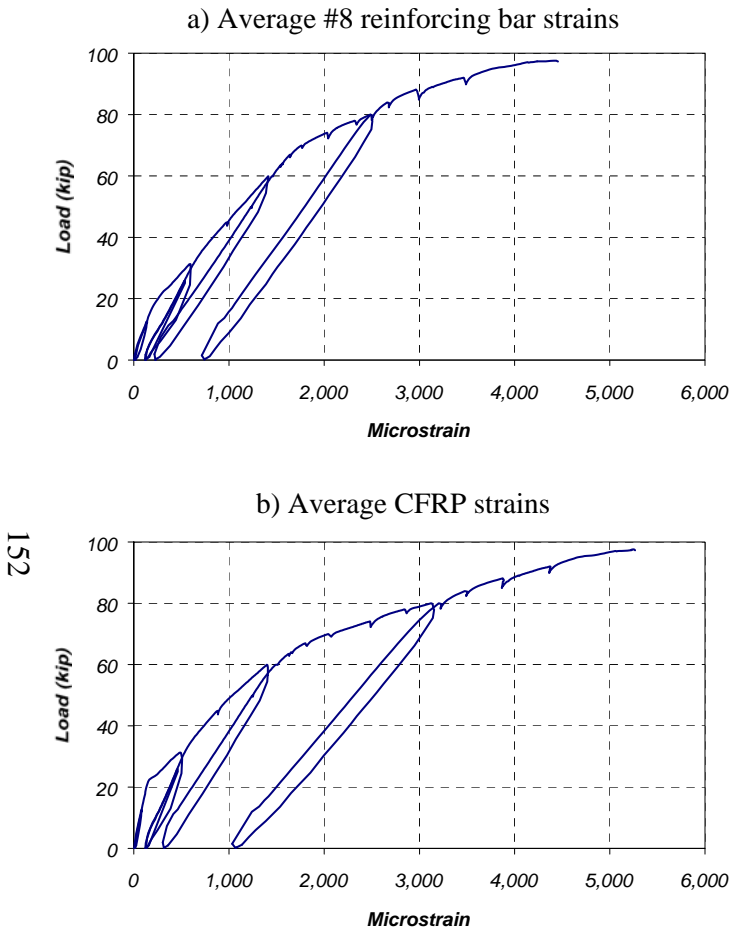


Figure 5.24 Average Strains Measured at Section N2 (Specimen J-1)

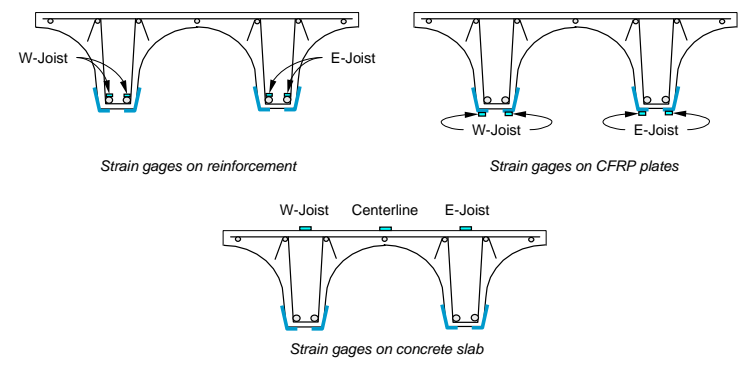
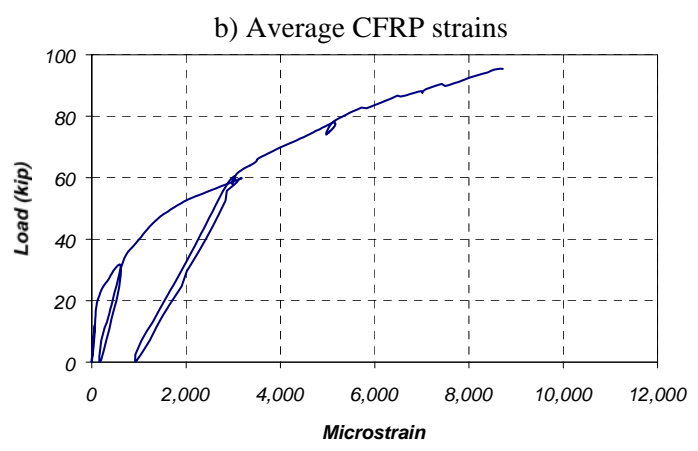
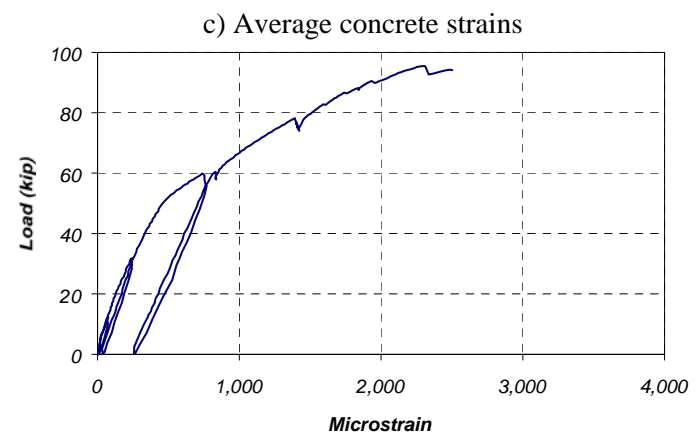
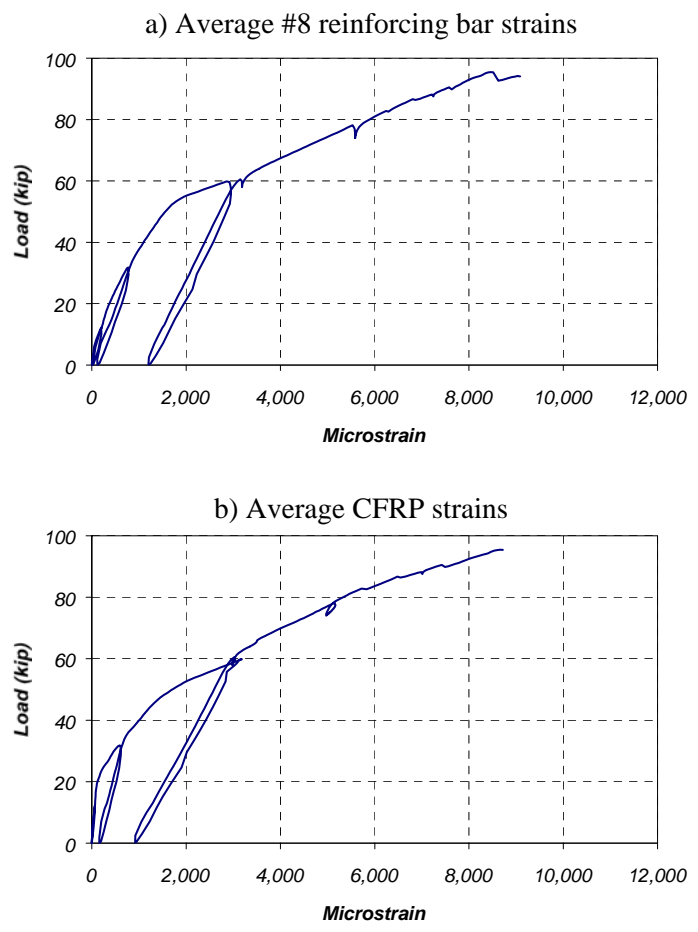


Figure 5.25 Average Strains Measured at Section N1 (Specimen J-2)

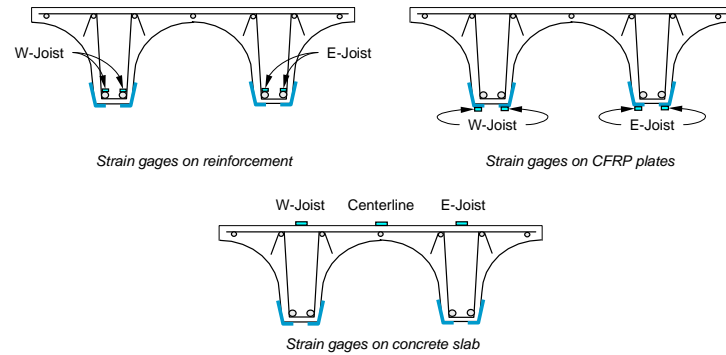
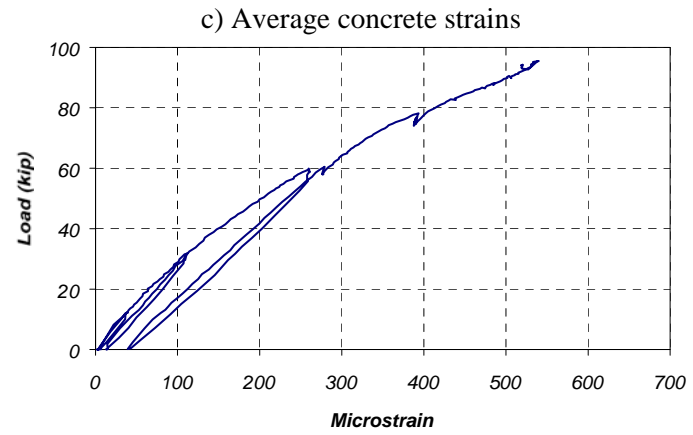
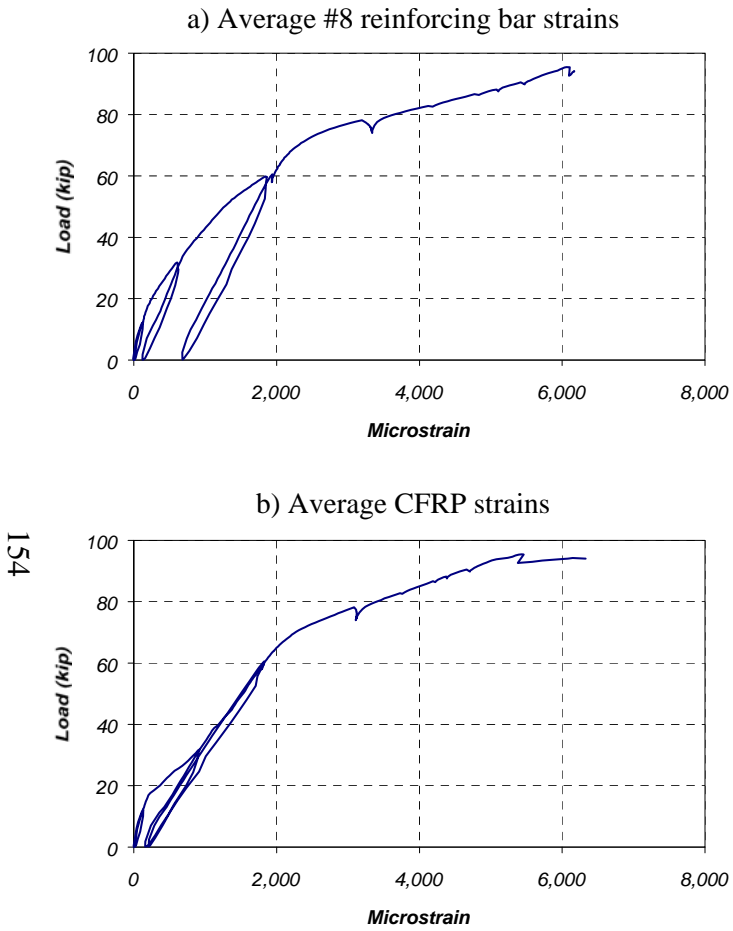


Figure 5.26 Average Strains Measured at Section N2 (Specimen J-2)

5.5 SUMMARY

The laboratory tests of the two pan-joist specimens are described in this chapter. The loading sequence, testing apparatus, and instrumentation were also presented.

Selected results of recorded instrument readings during the tests were shown as load-deflection or load-strain plots. The average strain readings from two sections in each specimen were shown to illustrate the general behavior observed during the tests. These figures illustrate the general characteristics of the observed response and are representative of the behavior at the other sections symmetrically located about midspan. The average strains were used to compute the specimen moment-curvature response presented in [Chapter 6](#).

CHAPTER 5: MEASURED RESPONSE OF PAN-JOIST SPECIMENS .. 113

5.1 Introduction 113

5.2 Test Setup and Instrumentation 113

5.2.1 Description of Experimental Setup 113

5.2.2 Loading Sequence 115

5.2.3 Instrumentation..... 118

5.3 Observed Behavior During Tests..... 123

5.3.1 Description of Failure Sequence and Cracking Distribution... 123

5.4 Measured Response..... 134

5.4.1 Deflection Measurements 134

5.4.2 Strain Gage Measurements..... 148

5.5 Summary..... 155

Figure 5.1 Side View of Pan-Joist Specimen in Laboratory Test Setup 114

Figure 5.2 Overhead View of Pan-Joist Specimen Showing the Location of Loading Points..... 115

Figure 5.3 Location of Instrumented Sections Showing Position of Potentiometers and Strain Gages in Specimen J-1 121

Figure 5.4 Location of Instrumented Sections Showing Position of Potentiometers and Strain Gages in Specimen J-2 122

Figure 5.5 Typical Cracking Patterns for Specimen J-1 (West Joist) 125

Figure 5.6 Observed Initial Debonding of CFRP Plate on East Joist..... 126

Figure 5.7 Transverse Strap Debonding at Ultimate Design Load 126

Figure 5.8 East Joist of Specimen J-1 Before CFRP Debonding 127

Figure 5.9 East Joist of Specimen J-1 at Failure 128

Figure 5.10 Typical Cracking Patterns for Specimen J-2 (West Joist) 131

Figure 5.11 Initiation of Debonding Along CFRP Sheet 132

Figure 5.12 Cracking Propagation Behind Strap Originated Debonding..... 132

Figure 5.13 View of West Joist in Specimen J-2 at Failure 133

Figure 5.14 Bottom Surface Condition of West Joist after CFRP Debonding..... 133

Figure 5.15 Measured Displacements at Supports in Specimen J-1 137

Figure 5.16 Measured Deflections at Sections N1 and S1 in Specimen J-1 138

Figure 5.17 Measured Deflections at Mid-Span in Specimen J-1 139

| | |
|---|-----|
| Figure 5.18 Measured Displacements at Supports in Specimen J-2 | 140 |
| Figure 5.19 Measured Deflections at Sections N1 and S1 in Specimen J-2 | 141 |
| Figure 5.20 Measured Mid-Span Deflections in Specimen J-2..... | 142 |
| Figure 5.21 Load-Deflection Behavior Characterized by Change in Global Stiffness | 143 |
| Figure 5.22 Typical Stiffness Increase after CFRP Strengthening (Specimen J-1) | 143 |
| Figure 5.23 Average Strains Measured at Section N1 (Specimen J-1) | 151 |
| Figure 5.24 Average Strains Measured at Section N2 (Specimen J-1) | 152 |
| Figure 5.25 Average Strains Measured at Section N1 (Specimen J-2) | 153 |
| Figure 5.26 Average Strains Measured at Section N2 (Specimen J-2) | 154 |
| | |
| Table 5.1 Required Moments and Loads During Testing Corresponding to Design Levels in the Prototype Bridge | 117 |
| Table 5.2 Displacement Limits of Linear Potentiometers..... | 119 |
| Table 5.3 Characteristics of Strain Gages | 120 |
| Table 5.4 Maximum Response Measured During Testing of Specimen J-1 | 144 |
| Table 5.5 Maximum Response Measured During Testing of Specimen J-2..... | 145 |
| Table 5.6 Measured Deflections during Service Load Stages..... | 147 |
| Table 5.7 Comparison of Displacement Ductility | 147 |

Chapter 6: Verification of the Analytical Model Using the Measured Response of the Pan-Joist Specimens

6.1 INTRODUCTION

The analytical model developed in Chapter 3 is verified in this chapter by comparing the strains, curvatures, and displacements with the measured response of Specimens J-1 and J-2. Strains are discussed in Section 6.2, and moment-curvature response is presented in Section 6.3. Data from both these sections may be used to evaluate the strain at which the CFRP composites debond from the surface of the concrete. This information is needed to calculate the capacity of reinforced concrete members strengthened using CFRP composites. Displacement response is evaluated in Section 6.3.4. In general, the analytical models are able to represent the measured global response quite well; however, some of the local behavior was not well represented.

6.2 EVALUATION OF STRAIN RESPONSE

The analytical procedures developed in Chapter 3 were based on a number of assumptions about the distribution of strain within the cross section. Therefore, the first step in evaluating the applicability of the computational models must be a detailed comparison of the calculated and measured strains. If the measured strains follow the same trends that form the basis of the analytical model, then it is likely

that the analytical model will be successful in representing the response of the specimens. However, if the measured strains differ significantly from these assumptions, then the analytical model will be of limited use for understanding the response of reinforced concrete elements strengthened using CFRP composites.

Strains were measured on the reinforcing bars, on the top surface of the concrete, and on the surface of the CFRP composites during testing of Specimens J-1 and J-2. Measured data were presented in Chapter 5 and Appendix C, and those data are compared with the calculated response of the test specimens in this section. Strains due to dead loads are evaluated in Section 6.2.1, the variations of strain with distance from the neutral axis are discussed in Section 6.2.2. Calculated and measured strains in each of the three materials are compared in Section 6.2.3, and the strains at which the CFRP composites debonded from the surface of the concrete are evaluated in Section 6.2.4.

6.2.1 *Strains due to Dead Loads*

Strains due to dead loads are typically ignored in laboratory tests of reinforced concrete members because test specimens are often constructed at a reduced scale, and the resulting strains are small. However, Specimens J-1 and J-2 were the same size as the prototype bridge, and the dead loads in the laboratory were nearly the same as the dead loads in the field. Therefore, the strains due to

dead loads could not be ignored when evaluating the response of the test specimens.

The construction process precluded direct measurement of dead-load strains. Although the strain gages were attached to the reinforcing bars before the concrete was cast, the gages were not connected to the data acquisition system until the beam was positioned on the support blocks. The strain gages were attached to the top surface of the concrete after the test specimens were in their final position in order to avoid damaging the gages as the specimens were moved. The CFRP composites were bonded to the surface of the concrete while the full dead load was acting on the system. Therefore, the measured strains in the CFRP during the tests corresponded to the strains induced by the applied loads.

The strains in the reinforcing steel and concrete under dead load were estimated using the analytical procedure discussed in Chapter 3 for the bare cross section. The dead-load moment was calculated by assuming a unit weight of concrete equal to 150 pcf and a span of 28 ft. The measured material properties (Appendix A) were used in these calculations. Calculated dead-load strains for sections N1 and S1 are reported in Table 6.1.

Table 6.1 Calculated Dead-Load Strains

| M_{DL}, kip-ft | Strains, Microstrain | | Curvature, 1/in. | NA Depth, in. |
|-----------------------------------|---------------------------------|--------------|-----------------------------|------------------------------|
| | Concrete | Steel | | |
| Specimen J-1 | | | | |
| 81.6 | 116 | 514 | 2.9×10^{-5} | 4.00 |
| Specimen J-2 | | | | |
| 81.6 | 117 | 528 | 3.0×10^{-5} | 3.92 |

6.2.2 Measured Strain Profiles due to Live Loads

During the development of the analytical model, perfect bond was assumed between the CFRP laminates and the surface of the concrete. If this assumption is true, then the measured live-load strains would vary linearly with depth within the cross section at all levels of applied load.

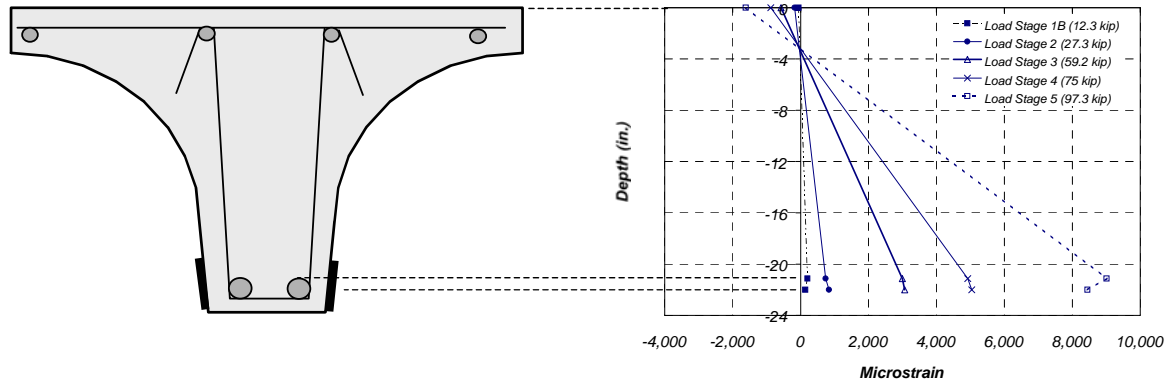
Measured strain profiles at sections N1 and S1 are shown in Figure 6.1 for Specimen J-1. Similar data are shown in Figure 6.2 for Specimen J-2. The average strain in each material at each stage of loading is plotted as a function of the distance from the top of the specimen to the gage.

The strains in the two specimens were similar at the load points. The strain profiles were approximately linear up to yielding of the reinforcement (load stage

3). At the higher load levels, the strains in the CFRP composites tended to be lower than those expected using a linear distribution of strain. Debonding of the CFRP composites from the surface of the concrete would tend to reduce the measured strains, because the CFRP composite deformations are distributed over a longer length. Therefore, the measured response is not surprising.

It is clear from the measured strain profiles that debonding of the CFRP composites and cracking of the concrete has a significant influence on the distribution of strain within the cross section. The strains in the CFRP composites were typically lower than those expected using a linear variation of strain with depth.

a) Section N1



b) Section S1

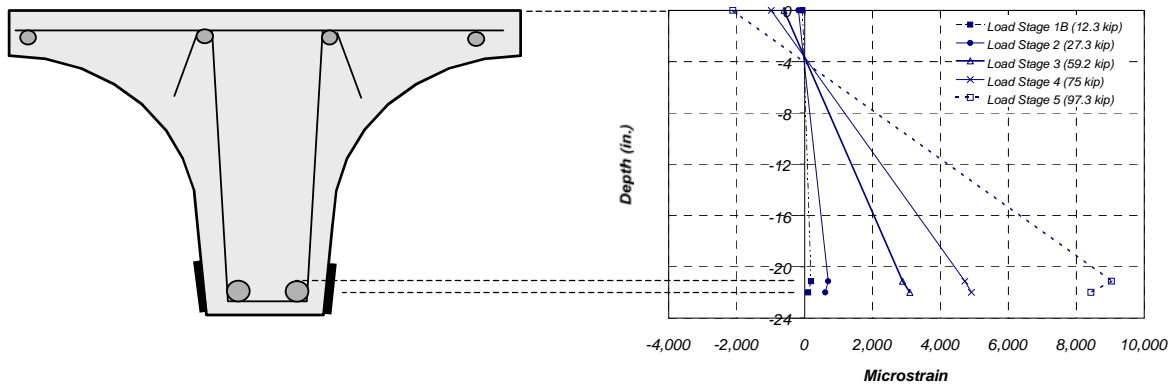
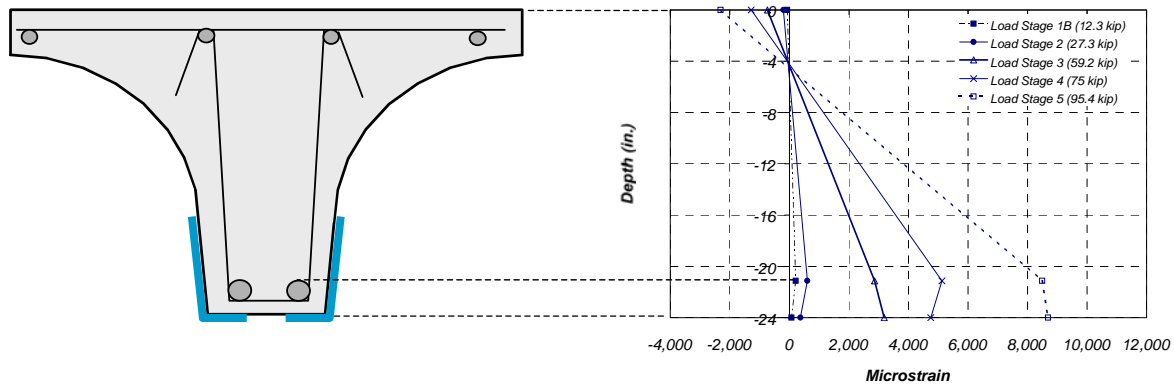


Figure 6.1 Measured Live-Load Strain Profiles in Sections N1 and S1 for Specimen J-1

a) Section N1



b) Section S1

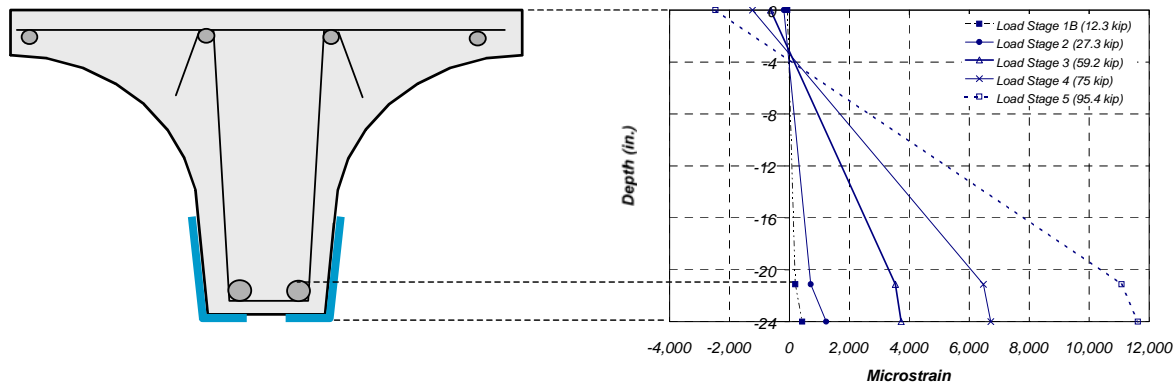


Figure 6.2 Measured Live-Load Strain Profiles in Sections N1 and S1 for Specimen J-2

6.2.3 Comparison of Measured and Calculated Strains due to Live Loads

The live-load strains in each of the materials were calculated to provide a direct comparison with the measured strain response. The analytical procedures in Chapter 3 were used to relate the calculated total strains in the materials to the internal moment in the cross section using the measured material properties (Appendix A). The internal moment was then related to the applied load using the clear span of the beam, 28 ft, and the dead loads described in Section 6.2.1. The calculated strains corresponding to dead loads were then subtracted from the calculated total strains in the reinforcement and concrete. No attempt was made to model debonding of the CFRP laminates from the surface of the concrete in this phase of the analysis. Therefore, the failure condition for all calculations corresponds to rupture of the CFRP composites or crushing of the concrete.

Calculated and measured live-load strains are compared in Figure 6.3 through Figure 6.6 for locations under the loading points (Sections N1 and S1). The measured steel and CFRP strains represent the average of readings from four gages, while the measured concrete strains represent the average of readings from five gages for Specimen J-1 and the average of readings from three gages for Specimen J-2.

The calculated strain curves approximate the measured response very closely. The primary difference between the measured and calculated strain

response is the magnitude of the strain at failure. Because the CFRP composites debonded from the concrete during the tests, the measured failure strains were less than the calculated failure strains in the reinforcement and CFRP composites. The strains corresponding to debonding of the CFRP are quantified later in this section; therefore, discussion of failure conditions is deferred until later.

Above the yield load (approximately 60 kip), the calculated strains in the reinforcing bars and the CFRP were nearly the same as the measured strains. The calculated strains were approximately 1,000 microstrain less than the measured strains at Section S1 in Specimen J-2, but the calculated strains were within 100 microstrain at the other three sections. The cause of this difference is likely due to the location of cracks near Section S1 in Specimen J-2. In contrast, the calculated strains in the concrete were less than the measured strains at all four sections. At load levels above 80 kip, the differences exceeded 500 microstrain at three of the sections.

At applied loads below 60 kip, the calculated strains in all three materials tended to be greater than the measured strains. In most cases, these differences were less than 50 microstrain. It appears that bonding the CFRP laminates to the surface of the concrete stiffened the test specimens, even though the specimens had been cracked previously. No attempt was made to incorporate the influence of stiffening into the analytical model. A comparison of the strains measured at the

critical load stages with the calculated strains for Specimens J-1 and J-2 is presented in Table 6.2 and Table 6.3, respectively.

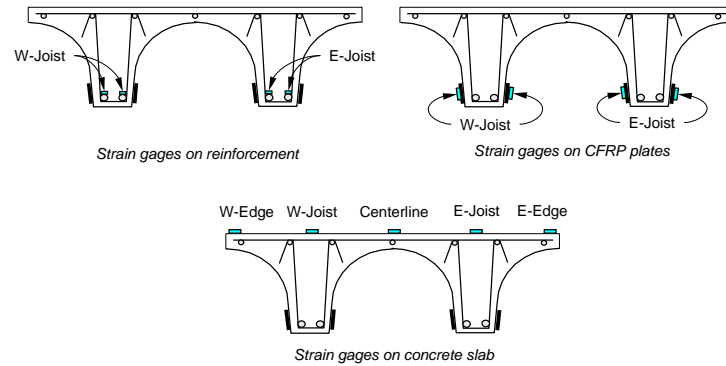
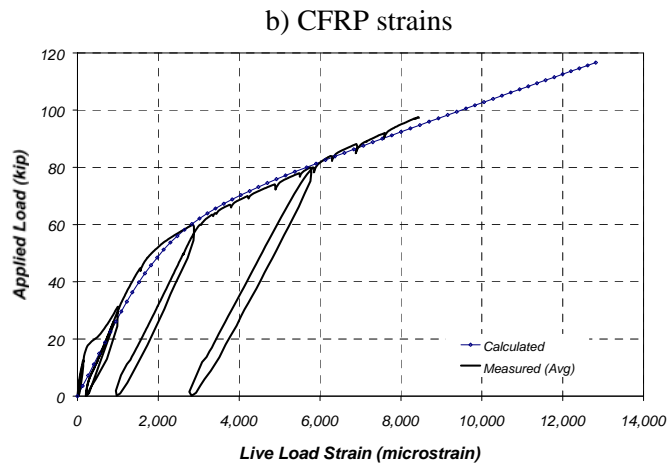
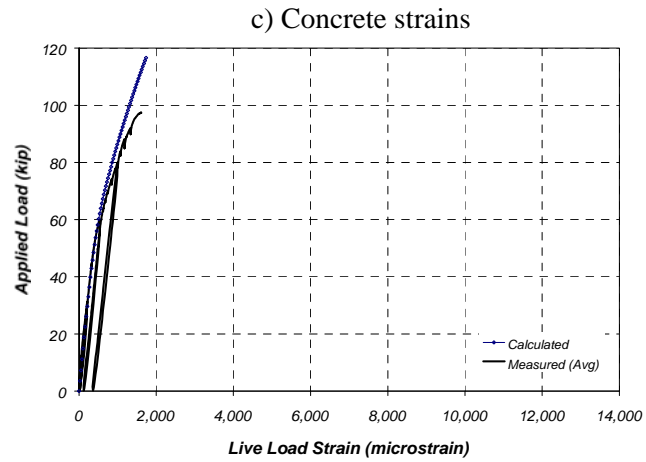
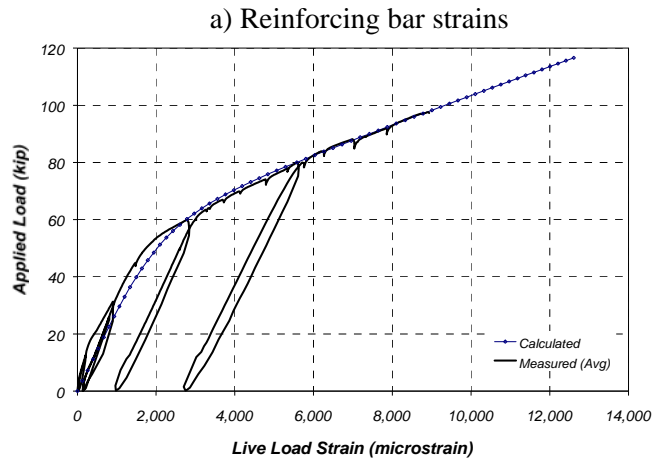


Figure 6.3 Comparison of Measured and Calculated Live-Load Strains at Section N1 (Specimen J-1)

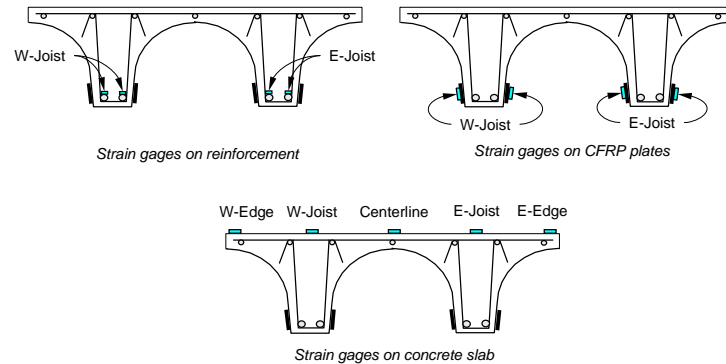
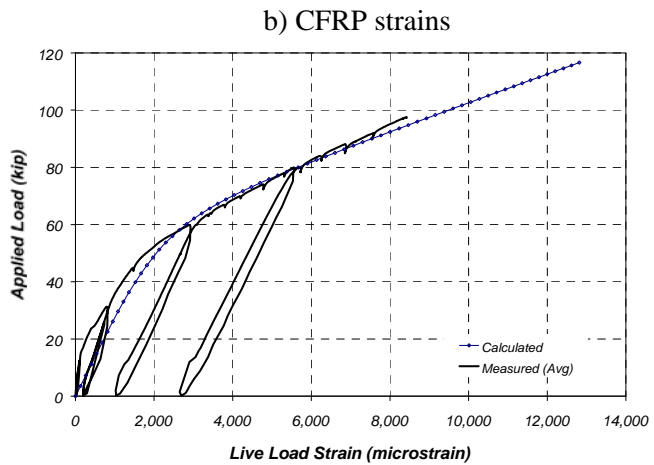
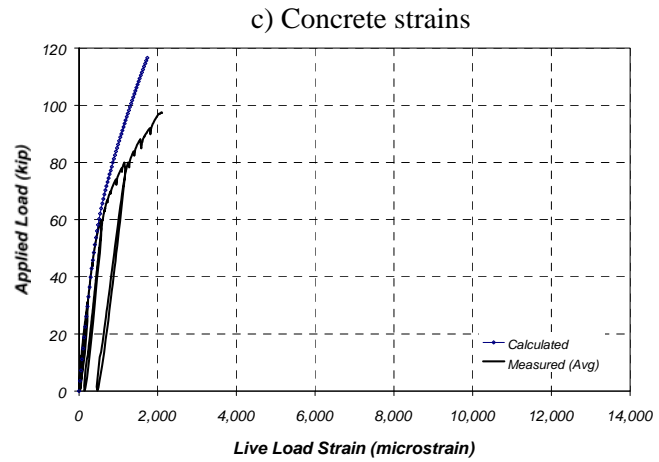
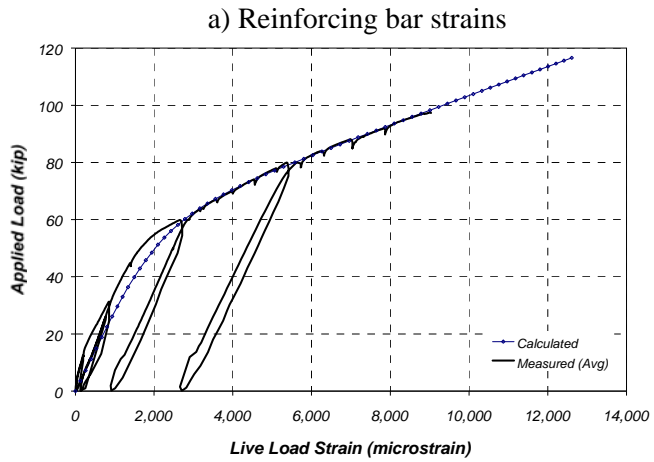


Figure 6.4 Comparison of Measured and Calculated Live-Load Strains at Section S1 (Specimen J-1)

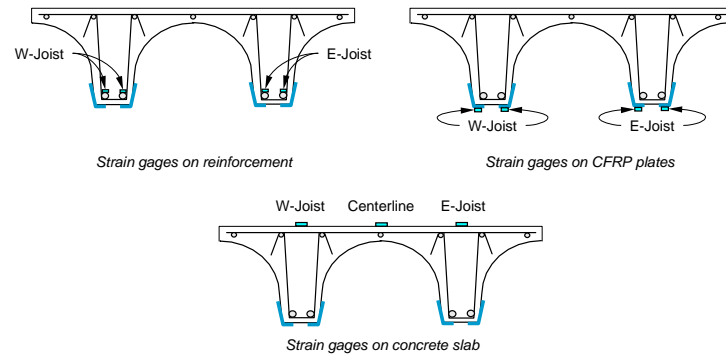
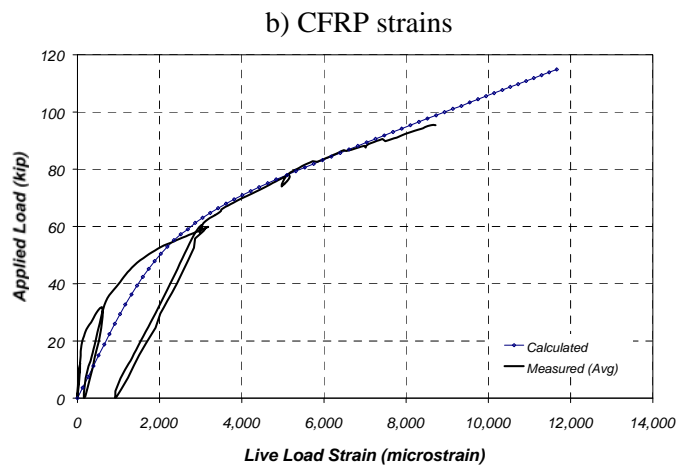
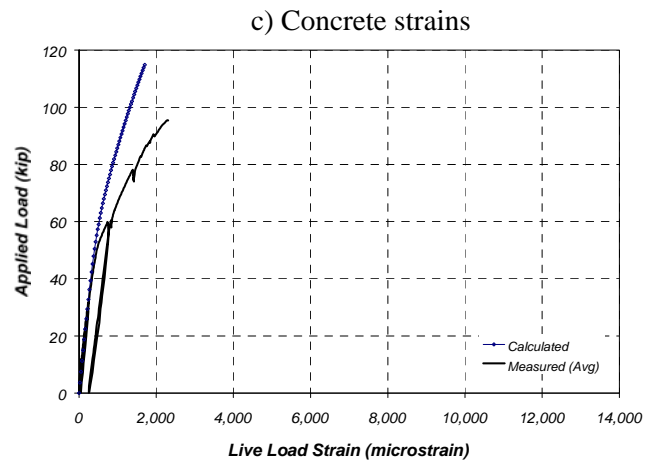
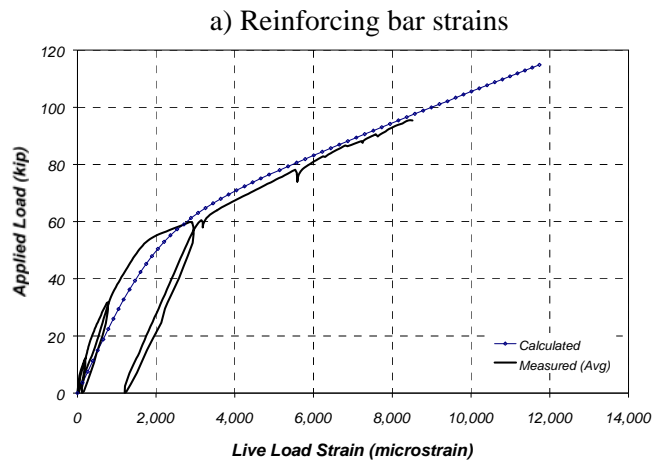


Figure 6.5 Comparison of Measured and Calculated Live-Load Strains at Section N1 (Specimen J-2)

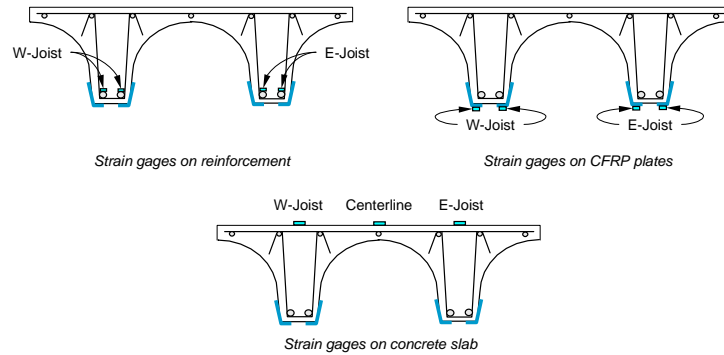
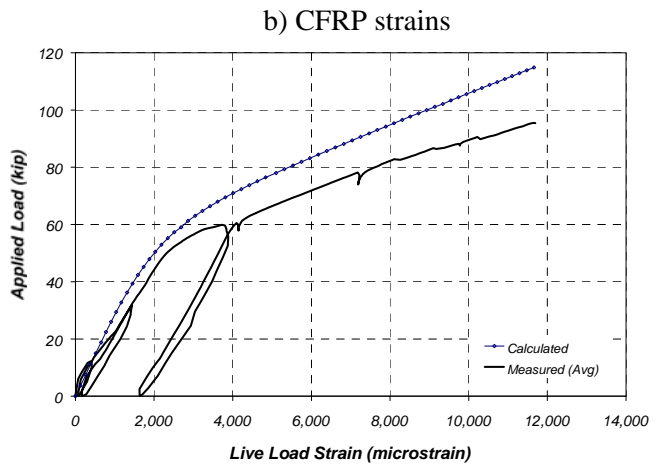
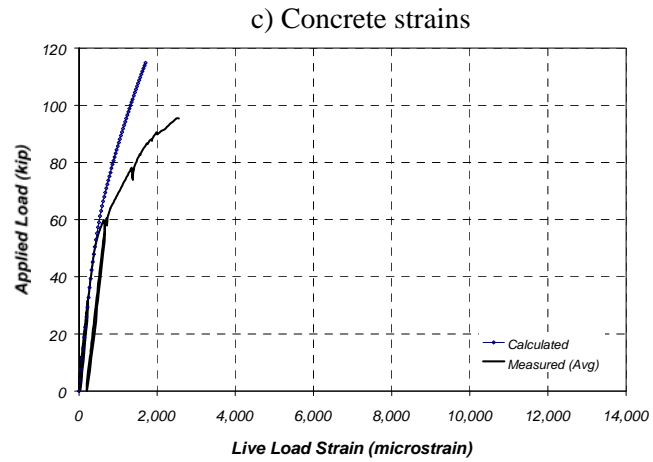
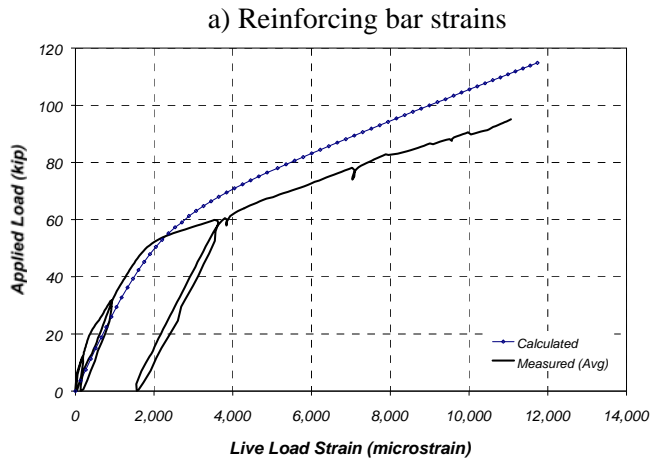


Figure 6.6 Comparison of Measured and Calculated Live-Load Strains at Section S1 (Specimen J-2)

Table 6.2 Measured and Calculated Live-Load Strains for Specimen J-1

| Load Stage | Load, kip | Steel Strain, microstrain | | | CFRP Strain, microstrain | | | Concrete Strain, microstrain | | |
|------------|-----------|---------------------------|-------|------------|--------------------------|-------|------------|------------------------------|-------|------------|
| | | Measured | | Calculated | Measured | | Calculated | Measured | | Calculated |
| | | N1 | S1 | | N1 | S1 | | N1 | S1 | |
| 1B | 12.3 | 200 | 189 | 399 | 137 | 102 | 406 | 61 | 64 | 75 |
| 2 | 27.3 | 737 | 692 | 934 | 836 | 607 | 951 | 178 | 182 | 186 |
| 3 | 59.2 | 2,693 | 2,558 | 2,783 | 2,766 | 2,817 | 2,831 | 522 | 543 | 511 |
| 4 | 75.0 | 4,920 | 4,683 | 4,839 | 5,038 | 4,909 | 4,921 | 878 | 983 | 778 |
| 5 | 97.3 | 8,938 | 9,035 | 8,781 | 8,442 | 8,428 | 8,927 | 1,615 | 2,110 | 1,239 |

Table 6.3 Measured and Calculated Live-Load Strains for Specimen J-2

| Load Stage | Load, kip | Steel Strain, microstrain | | | CFRP Strain, microstrain | | | Concrete Strain, microstrain | | |
|------------|-----------|---------------------------|--------|------------|--------------------------|--------|------------|------------------------------|-------|------------|
| | | Measured | | Calculated | Measured | | Calculated | Measured | | Calculated |
| | | N1 | S1 | | N1 | S1 | | N1 | S1 | |
| 1B | 12.3 | 204 | 188 | 391 | 68 | 386 | 388 | 76 | 70 | 78 |
| 2 | 27.3 | 602 | 711 | 914 | 368 | 1,226 | 908 | 199 | 185 | 189 |
| 3 | 59.2 | 2,726 | 3,367 | 2,706 | 3,059 | 3,524 | 2,688 | 718 | 613 | 512 |
| 4 | 75.0 | 5,122 | 6,470 | 4,660 | 4,751 | 6,621 | 4,629 | 1,285 | 1,233 | 777 |
| 5 | 95.4 | 8,514 | 11,068 | 8,155 | 8,717 | 11,697 | 8,101 | 2,312 | 2,558 | 1,209 |

6.2.4 Measured Strains at which the CFRP Composites Debonded from the Surface of the Concrete

As noted in the previous section, the failure strains in the materials were not well represented by the analytical model, because failure was defined in the analytical model as rupture of the CFRP composites. Both strengthened specimens failed after the CFRP composites debonded from the surface of the concrete, and crushing of the concrete was not observed until later stages of the test when the bare specimen was loaded to failure. The strain at which the composites debonded from the concrete was estimated by comparing the measured and calculated strains.

Figures 6.7 and 6.8 show a comparison between measured and calculated CFRP strains assuming no slip of the CFRP composites from the surface of the concrete. The calculated CFRP strains were determined using the measured concrete and steel strains and extrapolating the strain diagram to the centroid of the CFRP composites. In addition to the curves representing the measured and calculated live-load strains, the difference between the strains is also shown. For Specimen J-1, a sudden increase in the difference between the calculated and measured strains may be seen at an applied load of approximately 80 kip. As the applied load increased, the difference in strain increased, reaching a maximum of nearly 1,000 microstrain immediately before the composites debonded completely from the surface of the concrete. Local debonding was observed at a measured

strain of approximately 6,000 microstrain, and failure was observed at a measured strain of approximately 8,500 microstrain.

These limits agree with the observed behavior of Specimen J-1 during the test. Local debonding was observed along the top of the CFRP plate at midspan at a load of approximately 60 kip. At approximately 80 kip, the first transverse strap debonded, which indicated that larger regions of the CFRP plates were debonding from the surface of the concrete (Chapter 5).

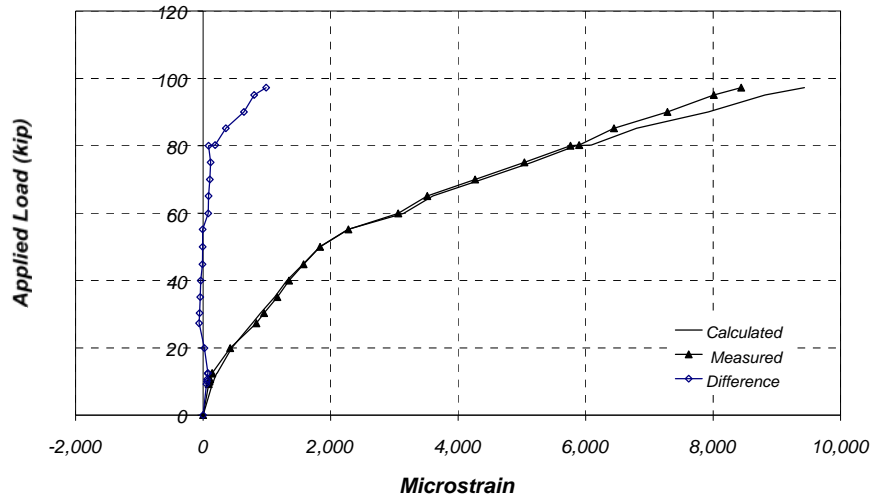
The trends were similar for Specimen J-2, although the calculated strains in the CFRP did not match the measured strains as well at the lower load levels. Local debonding was observed to occur at an applied load of approximately 60 kip, corresponding to a strain of less than 4,000 microstrain, and failure was observed at a strain between 8,500 and 11,500 microstrain. The CFRP laminates were observed to debond along the top edge at midspan at a load of approximately 80 kip. It can be assumed that laminates on the bottom surface began to debond at a lower load.

The maximum measured strains in the CFRP composites for both specimens were larger than the assumed value used to represent debonding (7,000 microstrain) for the design of the composite systems. At three locations, the average strain in the CFRP composites at debonding was approximately 8,500 microstrain. The failure strain exceeded 11,500 microstrain at location S1 in

Specimen J-2. This variation in the maximum measured strains in the CFRP composites can be attributed to the formation of cracks in the immediate vicinity of the strain gages. Higher failure strains were recorded at locations where the cracks crossed the instrumented section.

Because the measured strains in the CFRP were so sensitive to the distance between the strain gage and cracks in the concrete, it is recommended that more than one gage be used in future tests in order to evaluate the influence of local effects in more detail. In addition, positioning strain gages along the height of the composite will provide information about the distribution of strains in the CFRP.

a) Section N1



b) Section S1

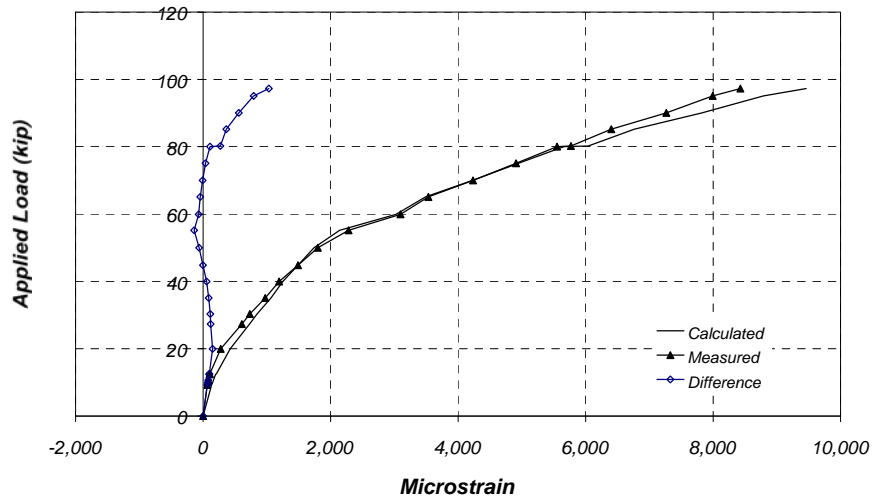
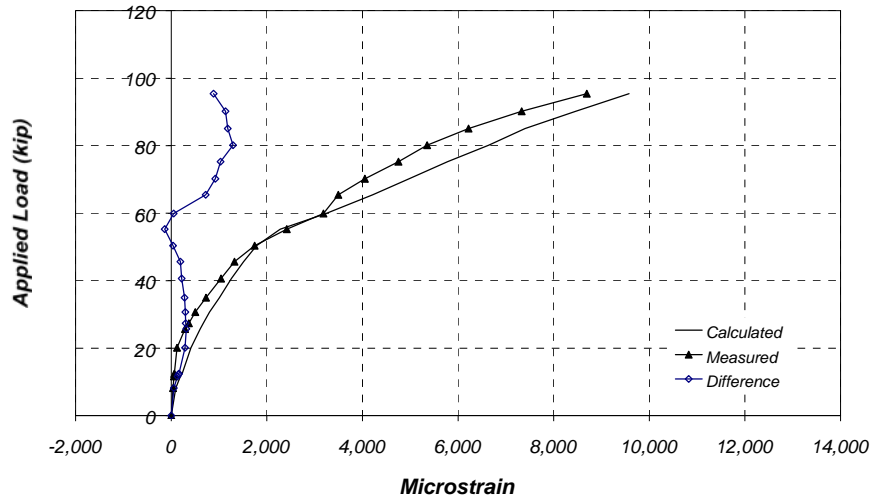


Figure 6.7 Comparison of Measured and Calculated CFRP Strains for Specimen J-1

a) Section N1



b) Section S1

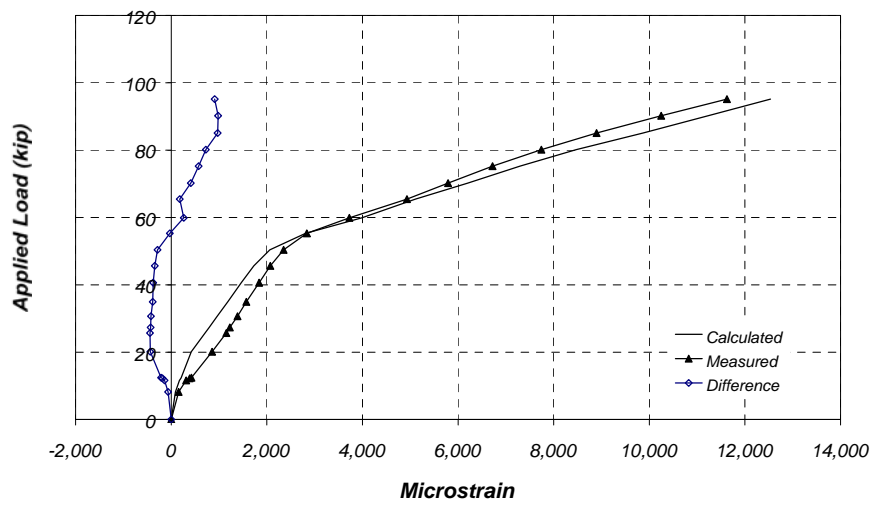


Figure 6.8 Comparison of Measured and Calculated CFRP Strains for Specimen J-2

6.3 EVALUATION OF MOMENT-CURVATURE RESPONSE

The measured strains were used to calculate the relationship between moment and curvature for the test specimens. Moment-curvature response derived from the measured strains is compared with the results of the analytical model in Section 6.3.3.

The procedures used to calculate internal forces and moments from the measured strains were similar to those used in the analytical model. The basic steps are outlined in Section 6.3.1 for Specimen J-1, where the strains were measured at the centroid of the CFRP plates. Modifications were required to calculate the internal forces in Specimen J-2, because strains were measured on the bottom surface of the specimen, and the CFRP sheets were wrapped around the bottom and side faces of the specimens. Therefore, the distribution of strains with depth within the CFRP sheets was assumed in the analysis. The procedures used to determine internal forces in Specimen J-2 are described in Section 6.3.2.

6.3.1 Calculating Internal Forces from Measured Strains for Specimen J-1

A typical profile of average live-load strains for Specimen J-1 is shown in Figure 6.9(a). The measured strain in the CFRP is less than the expected value corresponding to a linear variation of strain with depth in the cross section, as discussed in Section 6.2.2. The dead-load strains calculated in Section 6.2.1 were

added to the measured live-load strains in the concrete and tension steel to obtain the total strain, as shown in Figure 6.9(b).

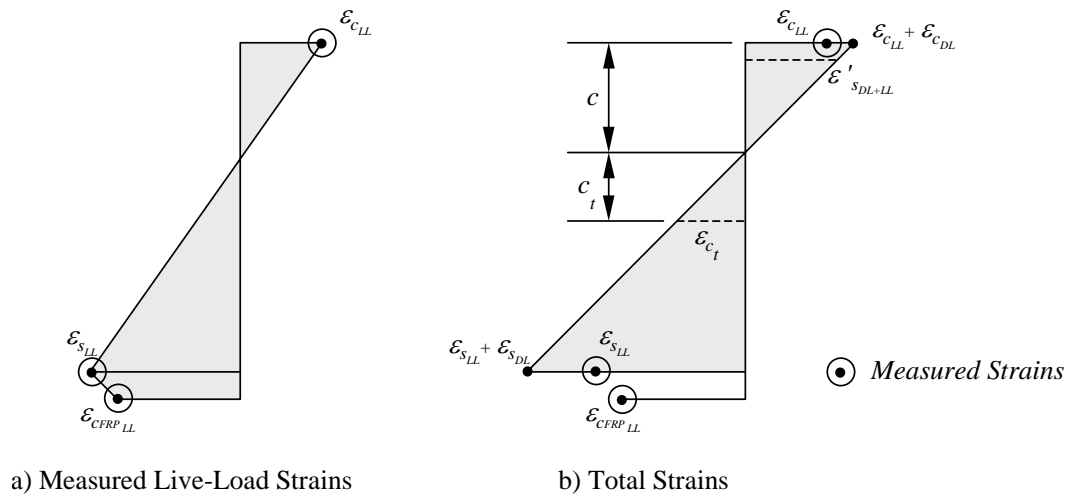


Figure 6.9 Typical Strain Profile for Specimen J-1

Total strains in the concrete and steel were assumed to vary linearly with depth between the maximum compressive strain in the concrete, $\epsilon_{c_{LL}} + \epsilon_{c_{DL}}$, and the maximum tensile strain in the steel, $\epsilon_{s_{LL}} + \epsilon_{s_{DL}}$. The neutral axis depth, c , and the strain in the compression steel, $\epsilon'_{s_{DL+LL}}$, were then determined from the assumed distribution of total strain. The depth of the concrete capable of resisting tension, c_t , was also determined using the tensile strain capacity of the concrete, which was estimated as the modulus of rupture divided by the initial tangent modulus of the concrete.

Stresses were calculated in each of the materials using the idealized stress-strain curves described in Chapter 3. Internal forces in the steel and CFRP were calculated by multiplying the stress at the centroid of the bar or plate by the cross-sectional area of the material. Internal forces in the concrete were calculated by dividing the tension and compression zones into ten segments, and multiplying the average stress in each segment by the cross-sectional area.

The sum of the measured internal forces in compression is plotted as a function of the sum of the measured internal forces in tension in Figure 6.10. These forces should be equal at all levels of applied load to satisfy equilibrium. However, the sum of the internal compressive forces consistently exceeded the sum of the internal tensile forces, and the differences between the force levels increased as the applied load increased.

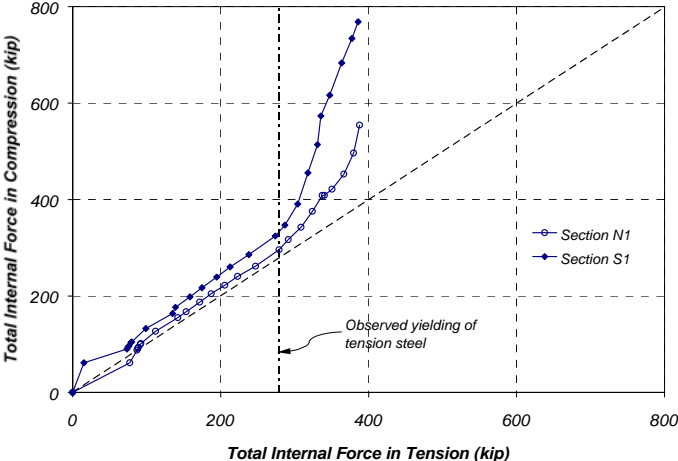


Figure 6.10 Internal Force Resultants for Specimen J-1

Several factors could have caused these differences in tensile and compressive forces. At low load levels, where the application of the theory of elasticity is still reasonable, a local perturbation of stress is generated at the sections of applied load. The tensile stresses can be expected to be lower than those calculated from a linear distribution of strain with depth [Timoshenko and Goodier, 1970]. After the concrete cracks, the strain readings on the reinforcement are largely dependent on the distance from the gage location to the section where the bar is crossed by a crack. If the gage happens to be offset from a crack, the strain readings on the reinforcement are lower than anticipated using a cracked section analysis because the concrete can still develop significant tensile stresses between cracks. At loads above yield, local bending of the reinforcing bars may also influence the measured strains.

It is impossible to identify the actual source of this discrepancy with the measured data. However, it is possible to use some of the measured data combined with the assumed linear distribution of strain to satisfy force equilibrium within the cross section, and then use the revised strain distribution to evaluate the moment-curvature response.

The revised strain distribution is shown in Figure 6.11 where the measured live-load strains in the reinforcement and CFRP plates are the same as those shown in Figure 6.9. However, the revised peak compressive strain in the concrete,

$\bar{\epsilon}_{c_{DL+LL}}$, was selected such that the cross section was in equilibrium. This revised peak compressive strain is plotted as a function of the measured peak compressive strain in Figure 6.12. The differences in strain tended to increase as the applied load increased, and were quite large near the failure load, especially at Section S1. However, the corresponding differences in the neutral axis depth were less than 10% for most of the testing sequence (Figure 6.13). Differences of more than 15% in the neutral axis depth were observed only at loads close to failure. These relatively modest changes in the neutral axis depth were considered to be reasonable, and the revised strains in the concrete and compression reinforcement were used in all subsequent calculations involving internal forces.

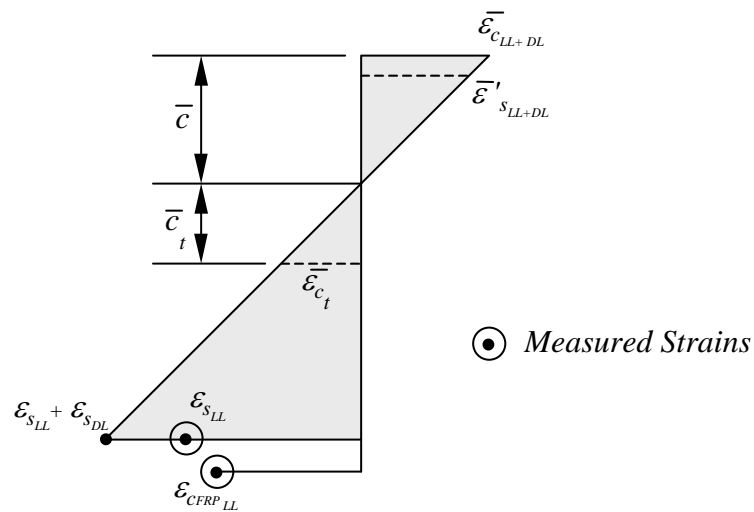


Figure 6.11 Possible Strain Distribution Corresponding to Equilibrium of Internal Forces

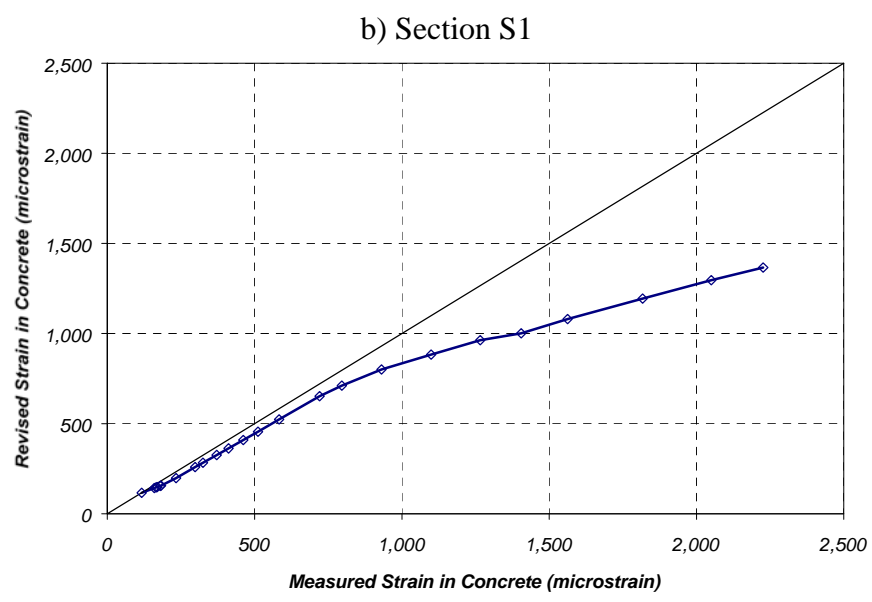
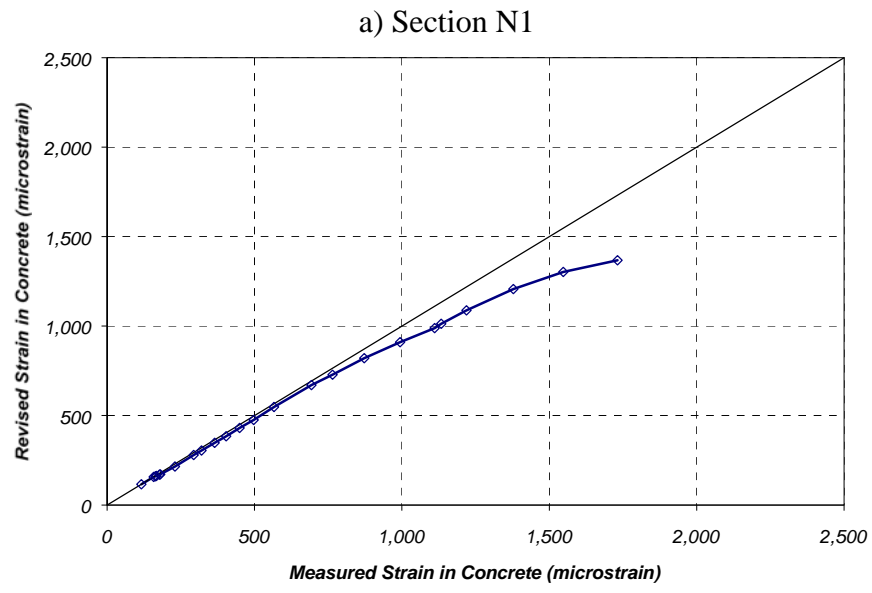


Figure 6.12 Comparison of Revised and Measured Peak Compressive Strains for Specimen J-1

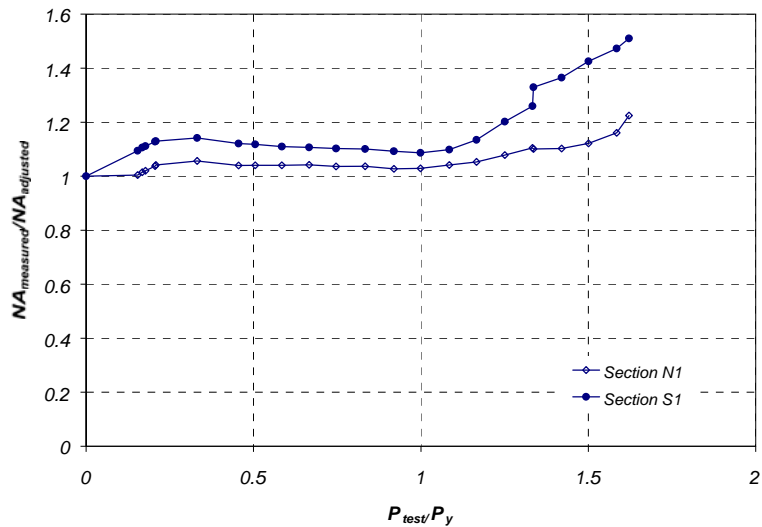


Figure 6.13 Comparison of Neutral Axis Depth from Revised and Measured Strain Profiles

It is interesting to note that the portion of the total internal tensile force carried by the CFRP plate increased as testing progressed. Each of the tensile force components (tensile force in the concrete, tensile force in the reinforcing bars, and tensile force in the CFRP plates) was normalized by the total tensile force. These data are plotted as a function of the ratio of applied load to yield load in Figure 6.14. The contribution of the tensile force in the concrete was approximately 40% of the total tensile force at low levels of load and decreased rapidly with applied load. The contribution of the reinforcing steel was close to 60% with only dead load acting on the specimen, increased to approximately 85% of the total tensile force near yield, and then decreased steadily to 70% at failure. As expected, the

tensile force in the CFRP plates was zero under dead load only and it increased to approximately 30% of the total tensile force at failure.

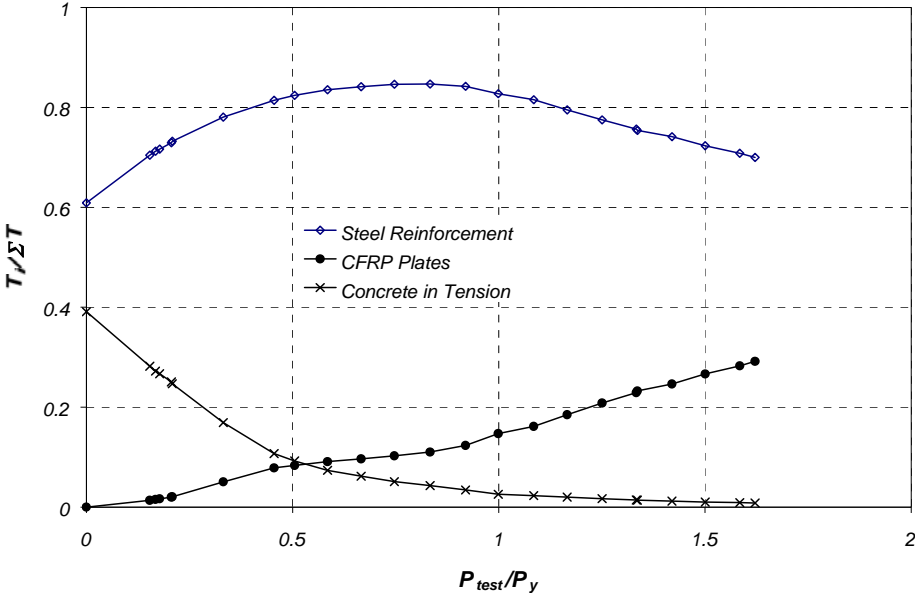


Figure 6.14 Variation of Tensile Force Components at Section N1 for Specimen J-1

6.3.2 Calculating Internal Forces from Measured Strains for Specimen J-2

The primary differences between Specimens J-1 and J-2 were the type and layout of the CFRP composites and the placement of the strain gages used to measure the strain in the CFRP. Pultruded plates were attached to the sides of the joists in Specimen J-1, and the strain gages were attached to the centroid of the plates. In contrast, CFRP sheets were wrapped around the bottom corners of the

joists in Specimen J-2, and the strain gages were attached to the bottom surface of the specimen.

The live-load strain distribution shown in Figure 6.15 was used to determine the tensile force in the CFRP laminates. The strain gradient in the CFRP composite was assumed to be the same as the live-load strain gradient in the reinforced concrete section. From this strain distribution, stresses were determined at the top and bottom of the CFRP sheets. The tensile force in the bottom portion of the sheets was calculated by multiplying the bottom stress by the area of the composite material attached to the bottom. The tensile force on the side portion of the sheets was determined by multiplying the average stress on the side by the corresponding area of CFRP sheet. The total tensile force in the CFRP sheet was the sum of the contributions from the bottom and sides. The internal force components from the concrete and reinforcement were calculated following the same procedure as described for Specimen J-1.

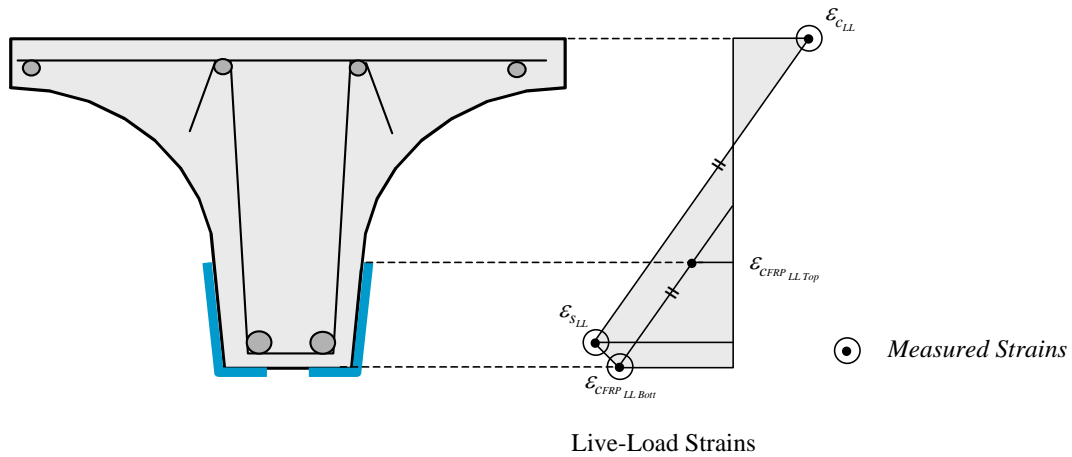


Figure 6.15 *Distribution of Live-Load Strains on CFRP Sheets*

A comparison of the total internal compressive force and the total tensile force for Specimen J-2 is shown in Figure 6.16. Similar to Specimen J-1, internal force equilibrium was not satisfied. Therefore, the peak compressive strain in the concrete was also adjusted using the procedure as for Specimen J-1 to satisfy internal force equilibrium.

Figure 6.17 shows the revised peak compressive strains as a function of measured peak compressive strain in the concrete. The same trend that was observed for Specimen J-1 is evident in this figure. The difference between the measured and revised strains increases with increasing applied load, particularly for load levels above the observed yield.

Although both sections shown in Figure 6.17 were subjected to the same external moment, the amount by which the neutral axis was shifted to satisfy equilibrium of internal forces was different for these two sections. For Section N1 a 20% adjustment of the neutral axis depth was required throughout most of the loading sequence, whereas the adjustment needed at Section S1 was typically less than 5% and only exceeded 20% during the final stages of loading (Figure 6.18). This variation is consistent with the assumption that the measured strains at a section are greatly influenced by the distance from gages to the nearest crack.

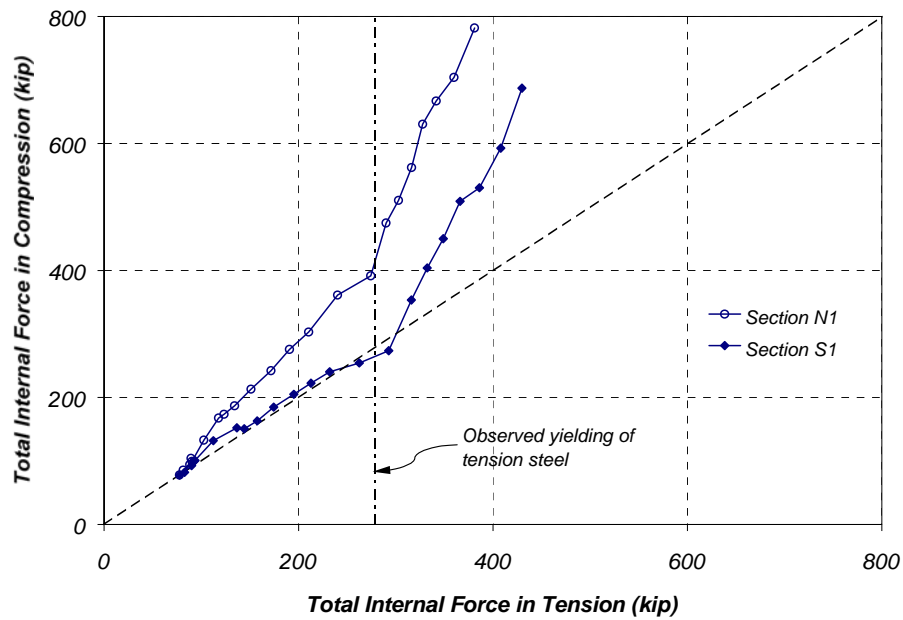


Figure 6.16 Internal Force Resultants for Specimen J-2

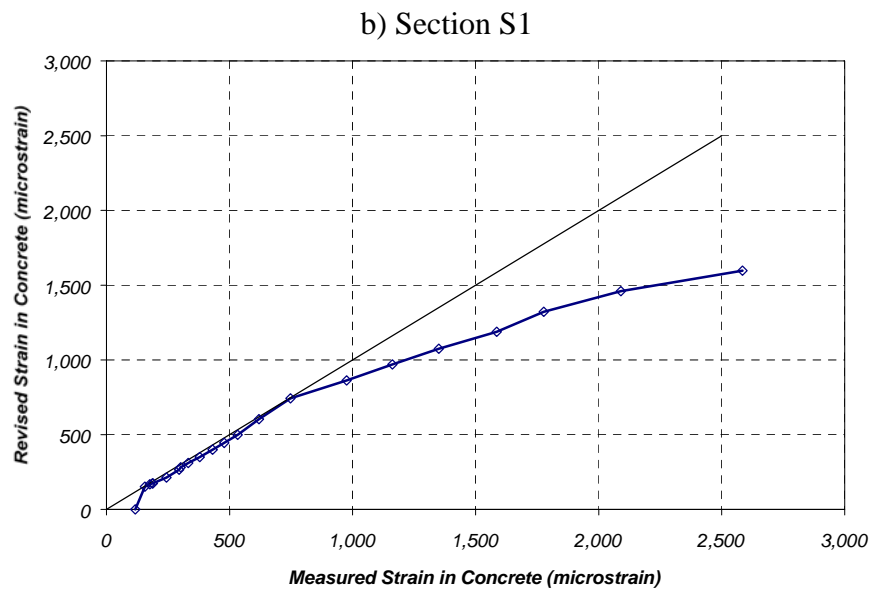
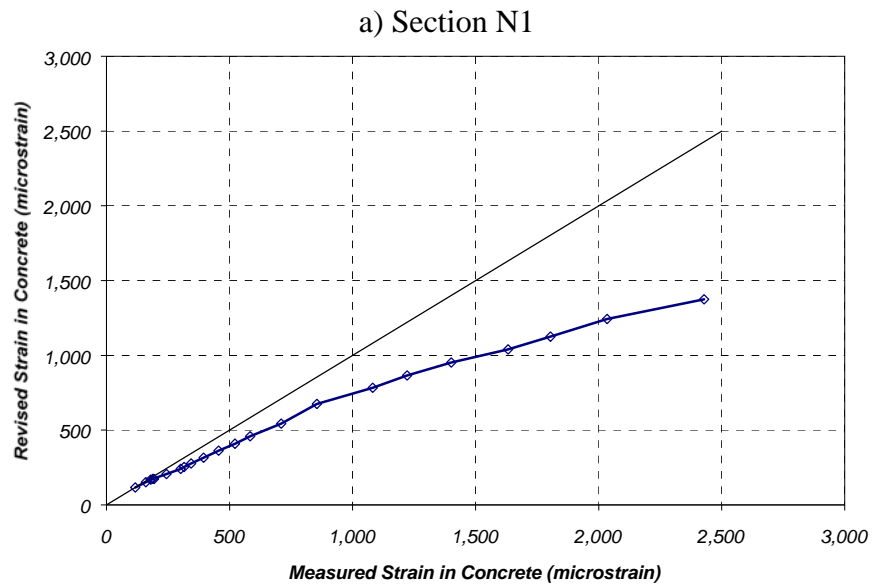


Figure 6.17 Comparison of Revised and Measured Peak Compressive Strains for Specimen J-2

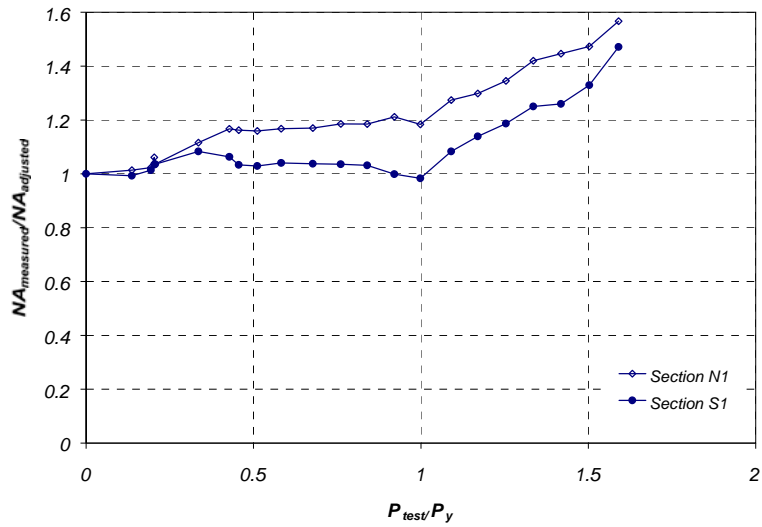


Figure 6.18 Comparison of Neutral Axis Depth from Revised and Measured Strain Profiles

The contribution of the individual tensile force components normalized by the total tensile force at a particular load level is plotted as a function of the applied load divided by the observed yield load in Figure 6.19. The relative contribution of each force component followed the same trends as those observed for Specimen J-1.

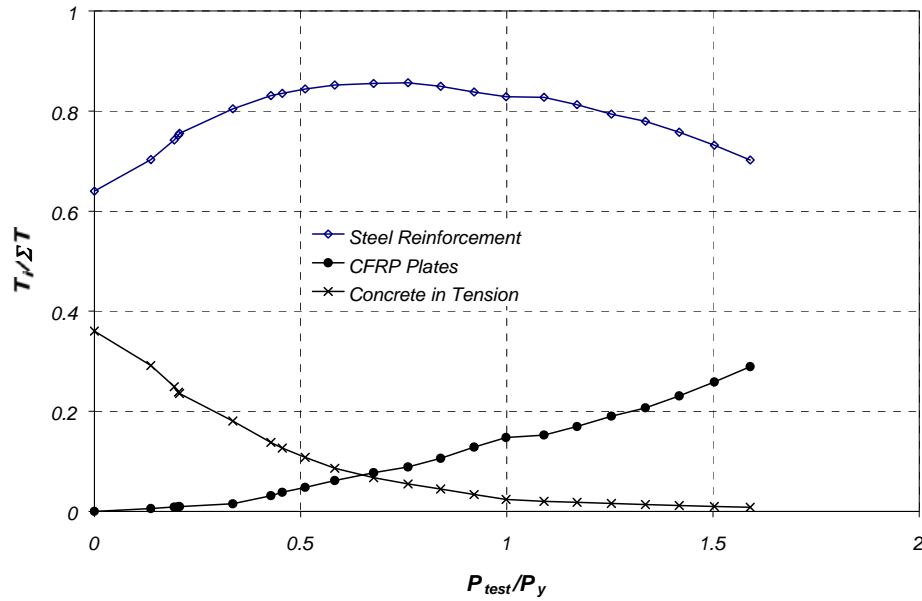


Figure 6.19 Contribution of the CFRP Sheets to the Total Internal Moment at Section NI for Specimen J-2

6.3.3 Moment-Curvature Response

Internal moments and curvature were calculated in both specimens using the internal forces that satisfied equilibrium. The moment and curvature corresponding to dead loads (Table 6.1) were then subtracted from each of the calculated values to obtain the relationship between moment and curvature for the applied loads. This response is compared with the results from the analytical model in Figure 6.20 and Figure 6.21 for Specimens J-1 and J-2, respectively. No attempt was made to include debonding of the CFRP in these calculations.

The moment-curvature response calculated from the measured strains is well represented by the results of the analytical model. At the same moment, the curvature inferred from the measured strains tended to be slightly less than the calculated curvature, but the differences were small. In most cases, the calculated curvature capacity exceeded the measured curvature at failure of the strengthened specimens.

Section S1 of Specimen J-2 was the only exception to these trends. The curvatures inferred from the measured strains exceeded the calculated curvatures above yield, and the curvature capacity was similar for the two curves. The CFRP ruptured near Section S1 during the test.

The CFRP composites debonded from the concrete at the other three locations; therefore, the actual curvatures at failure are expected to be less than the calculated curvatures at failure at these locations.

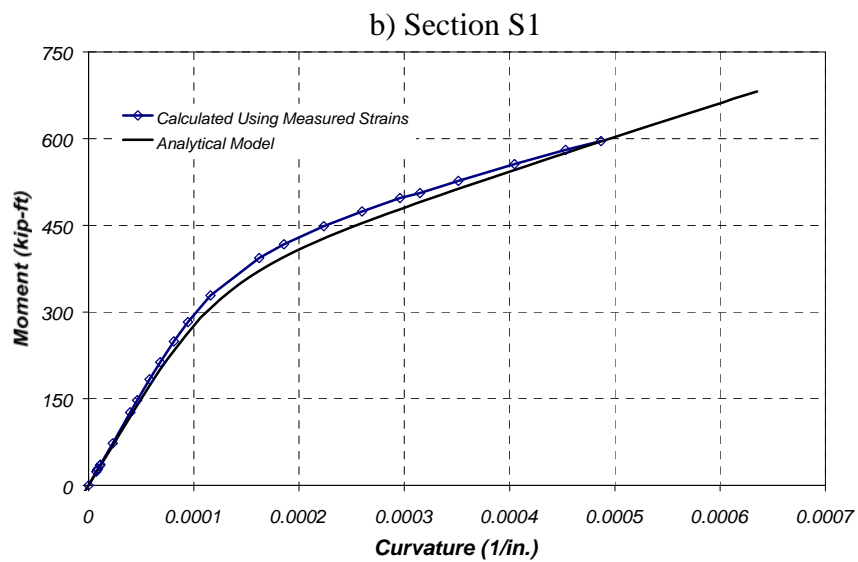
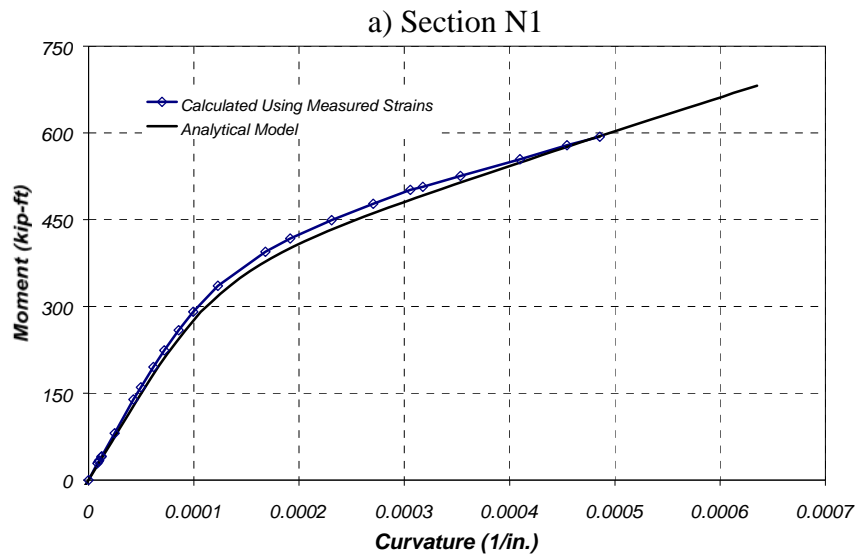


Figure 6.20 Comparison of Measured and Calculated Moment-Curvature Response for Specimen J-1

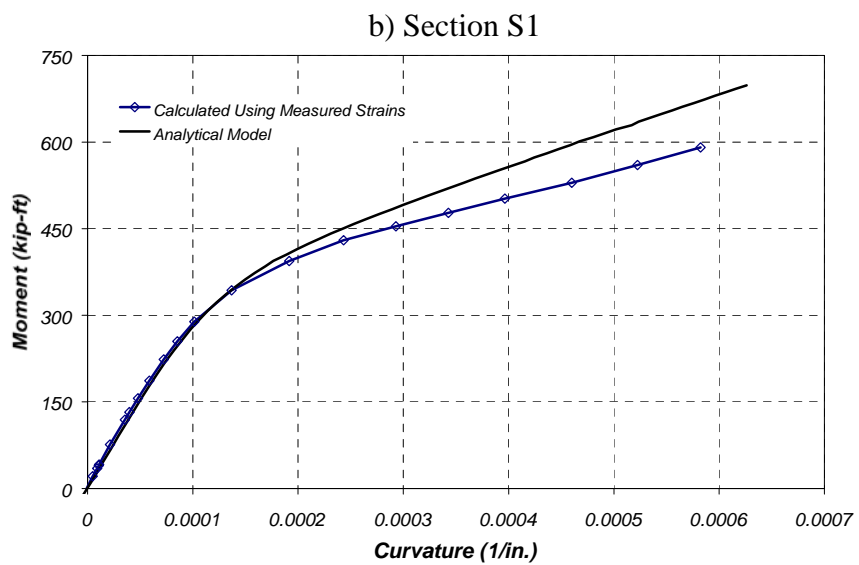
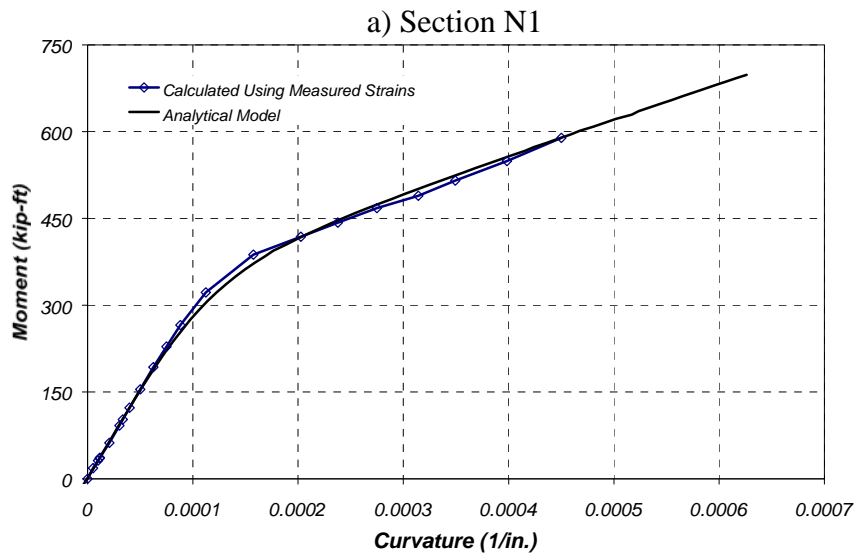


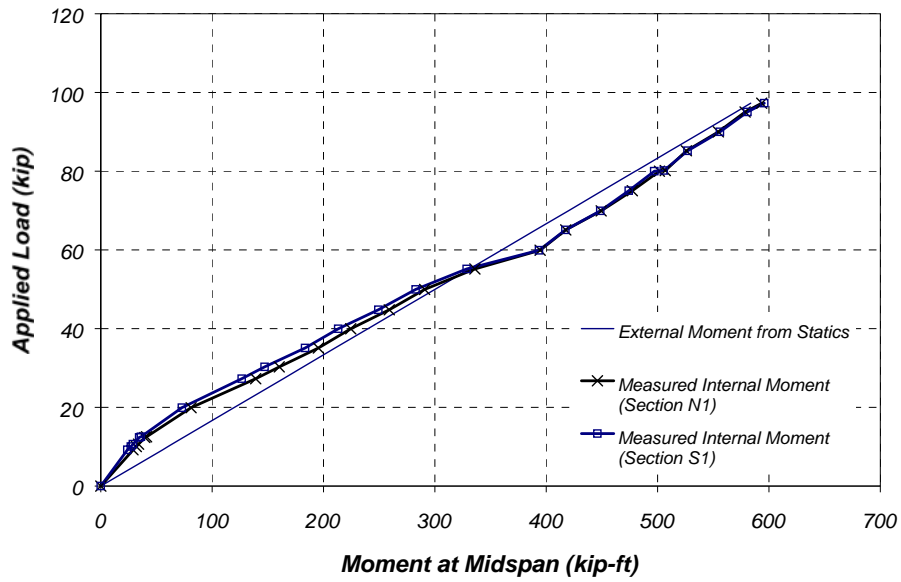
Figure 6.21 Comparison of Measured and Calculated Moment-Curvature Response for Specimen J-2

6.3.4 Comparison of Internal and External Moments

The applied load is plotted as a function of the maximum internal moment due to live load obtained from the measured strains in Figure 6.22. Also shown in the figure is the external midspan moment determined from statics using a span equal to 28 ft. Both specimens exhibited the same general response. At low levels of applied load, the internal moment was less than the external moment, and the internal moment was larger than the external moment at applied loads above the yield level (60 kip).

The response below the yield load is consistent with the assumption that the measured steel strains were less than the steel strains at the location of a crack due to concrete transmitting tensile stresses between cracks. Therefore, the internal moment was underestimated at low load levels. At load levels above yield, the span may have increased due to rotation of the bearings, leading to larger internal moments.

a) Specimen J-1



b) Specimen J-2

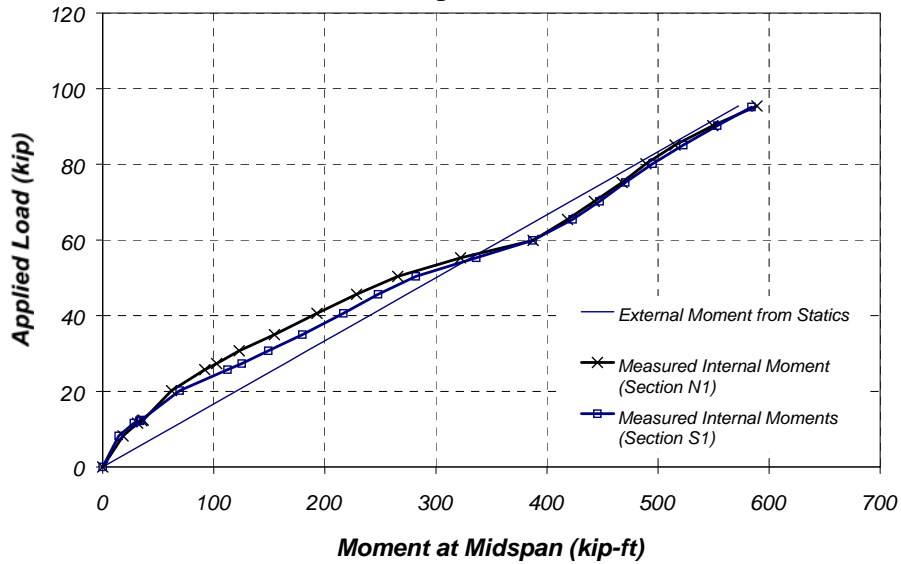


Figure 6.22 Comparison of Internal and External Moments

6.4 EVALUATION OF LOAD-DEFLECTION RESPONSE

The global response of the strengthened specimens was first evaluated by comparing their measured response. The response of each specimen was then compared with the calculated response obtained using the analytical procedure presented in Chapter 3. The displacement response of the strengthened specimens is compared with the bare reinforced concrete elements at the end of this section.

The average displacement response was obtained by averaging the displacement measurements from midspan of the east and west joists. The measurements were adjusted by subtracting the average vertical displacement at the supports. The load-deflection behavior of specimens J-1 and J-2 is shown in Figure 6.23. It can be seen that the overall behavior of both specimens was similar up to the yield point. After the yield point, Specimen J-1 was stiffer than Specimen J-2. Therefore, although both specimens were designed to reach approximately the same ultimate load, Specimen J-2 reached its failure load at a larger deflection than Specimen J-1. The post-yield stiffness was controlled by the stiffness of the two types of CFRP composites used to strengthen the specimens.

At failure, the load dropped suddenly and the residual load was carried by the bare reinforced concrete elements. The maximum deformation capacity of the bare specimens was also different. Specimen J-2 had a larger deformation capacity than Specimen J-1. The difference in deformation capacities can be attributed to

differences in the material properties of the concrete used to fabricate the specimens.

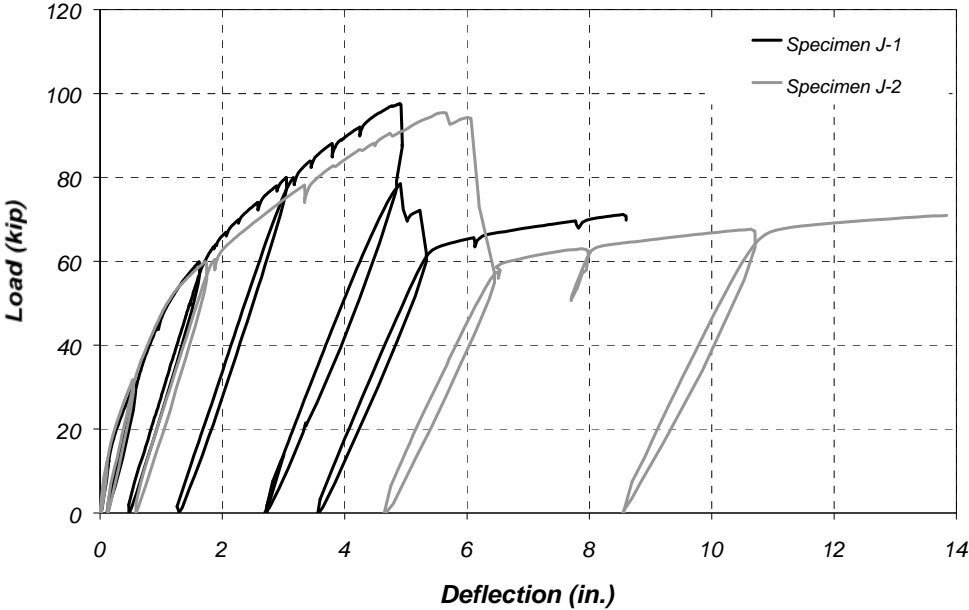


Figure 6.23 Measured Load-Deflection Response of Pan-Joist Specimens

The measured response of the test specimens is compared with the calculated load-deflection response in [Figures 6.24 and 6.25](#) for Specimens J-1 and J-2, respectively. The results presented show that the analytical model was able to reproduce the displacement response adequately for both specimens.

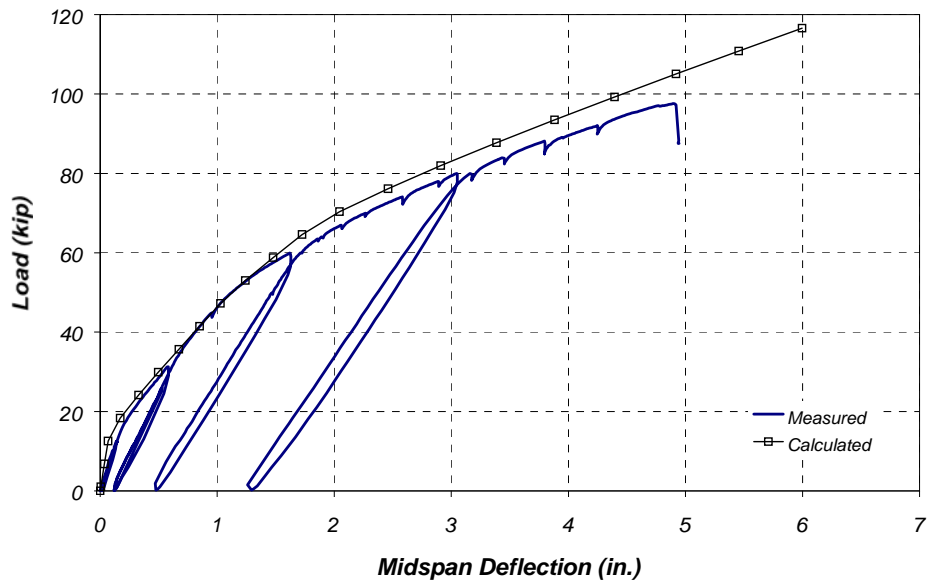


Figure 6.24 Comparison of Measured and Calculated Load-Deflection Response of Specimen J-1

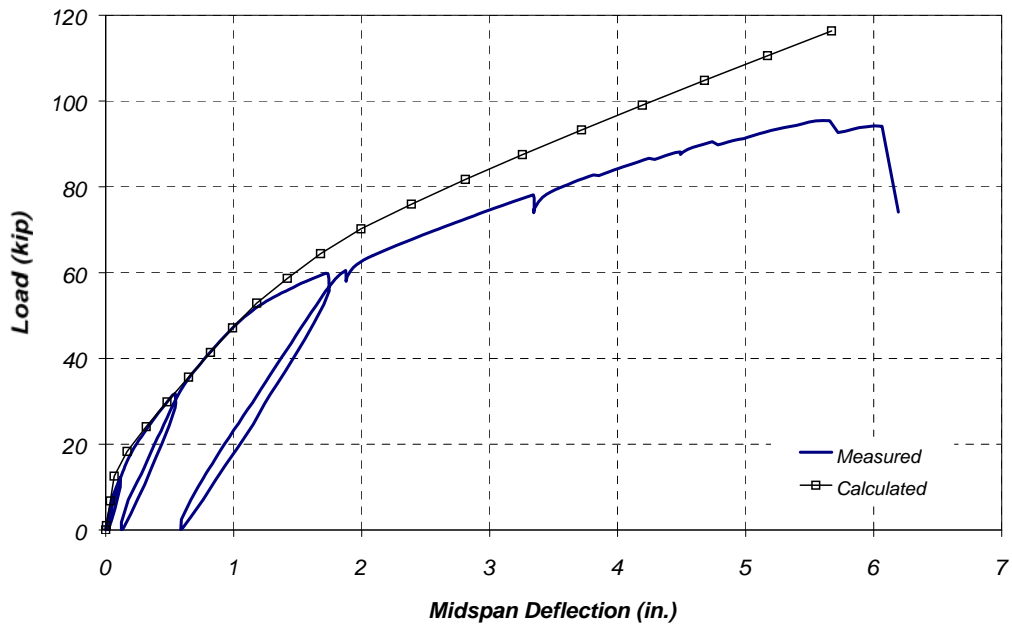


Figure 6.25 Comparison of Measured and Calculated Load-Deflection Response of Specimen J-2

6.5 SUMMARY

The measured response of Specimens J-1 and J-2 was compared to the response calculated using the analytical model presented in Chapter 3. The comparisons show that the model was able to reproduce the measured global response of the test specimens accurately at all levels of loading.

However, it was also clear that local effects such as cracking of the concrete and debonding of the CFRP composites controlled the measured response at a particular location. As expected, the analytical model was not able to reproduce aspects of the response controlled by local effects.

In order to obtain additional information about the local effects and the distribution of strain within the cross section, additional instruments must be used to monitor the response of the test specimens.

CHAPTER 6: VERIFICATION OF THE ANALYTICAL MODEL USING THE MEASURED RESPONSE OF THE PAN-JOIST SPECIMENS 156

6.1 Introduction 156

6.2 Evaluation of Strain Response 156

6.2.1 Strains due to Dead Loads 157

6.2.2 Measured Strain Profiles due to Live Loads..... 159

6.2.3 Comparison of Measured and Calculated Strains due to Live Loads..... 163

6.2.4 Measured Strains at which the CFRP Composites Debonded from the Surface of the Concrete..... 172

6.3 Evaluation of Moment-Curvature Response 177

6.3.1 Calculating Internal Forces from Measured Strains for Specimen J-1 177

6.3.2 Calculating Internal Forces from Measured Strains for Specimen J-2 184

6.3.3 Moment-Curvature Response 190

6.3.4 Comparison of Internal and External Moments..... 194

6.4 Evaluation of Load-Deflection Response 196

6.5 Summary 199

Figure 6.1 Measured Live-Load Strain Profiles in Sections N1 and S1 for Specimen J-1 161

Figure 6.2 Measured Live-Load Strain Profiles in Sections N1 and S1 for Specimen J-2 162

Figure 6.3 Comparison of Measured and Calculated Live-Load Strains at Section N1 (Specimen J-1)..... 166

Figure 6.4 Comparison of Measured and Calculated Live-Load Strains at Section S1 (Specimen J-1)..... 167

Figure 6.5 Comparison of Measured and Calculated Live-Load Strains at Section N1 (Specimen J-2)..... 168

Figure 6.6 Comparison of Measured and Calculated Live-Load Strains at Section S1 (Specimen J-2)..... 169

| | |
|--|-----|
| Figure 6.7 Comparison of Measured and Calculated CFRP Strains for Specimen J-1 | 175 |
| Figure 6.8 Comparison of Measured and Calculated CFRP Strains for Specimen J-2 | 176 |
| Figure 6.9 Typical Strain Profile for Specimen J-1 | 178 |
| Figure 6.10 Internal Force Resultants for Specimen J-1 | 179 |
| Figure 6.11 Possible Strain Distribution Corresponding to Equilibrium of Internal Forces | 181 |
| Figure 6.12 Comparison of Revised and Measured Peak Compressive Strains for Specimen J-1 | 182 |
| Figure 6.13 Comparison of Neutral Axis Depth from Revised and Measured Strain Profiles..... | 183 |
| Figure 6.14 Variation of Tensile Force Components at Section N1 for Specimen J-1 | 184 |
| Figure 6.15 Distribution of Live-Load Strains on CFRP Sheets..... | 186 |
| Figure 6.16 Internal Force Resultants for Specimen J-2 | 187 |
| Figure 6.17 Comparison of Revised and Measured Peak Compressive Strains for Specimen J-2 | 188 |
| Figure 6.18 Comparison of Neutral Axis Depth from Revised and Measured Strain Profiles..... | 189 |
| Figure 6.19 Contribution of the CFRP Sheets to the Total Internal Moment at Section N1 for Specimen J-2..... | 190 |
| Figure 6.20 Comparison of Measured and Calculated Moment-Curvature Response for Specimen J-1 | 192 |
| Figure 6.21 Comparison of Measured and Calculated Moment-Curvature Response for Specimen J-2..... | 193 |
| Figure 6.22 Comparison of Internal and External Moments | 195 |
| Figure 6.23 Measured Load-Deflection Response of Pan-Joist Specimens..... | 197 |
| Figure 6.24 Comparison of Measured and Calculated Load-Deflection Response of Specimen J-1 | 198 |
| Figure 6.25 Comparison of Measured and Calculated Load-Deflection Response of Specimen J-2 | 198 |
| | |
| Table 6.1 Calculated Dead-Load Strains..... | 159 |
| Table 6.2 Measured and Calculated Live-Load Strains for Specimen J-1 | 170 |
| Table 6.3 Measured and Calculated Live-Load Strains for Specimen J-2 | 171 |

Chapter 7: Description of Flat-Slab Specimens

7.1 INTRODUCTION

Flat-slab bridges were commonly used in off-system roads (Farm to Market Road System) in Texas in the 1940s and 1950s [Bussell, 1997]. Their design does not meet the current legal load requirement of HS-20 truck loading. The majority of the flat-slab bridges were designed using H-10 or H-15 design vehicles. These bridges were used for short spans (25 ft) with different roadway widths depending on the number of lanes to be carried (14 ft to 44 ft). However, bridges were typically designed for two lanes. In some cases structural curbs of the bridge were used on both sides to reduce the slab thickness. Bridges without edge curbs were named S-Slab bridges, and bridges with edge curbs were named FS-Slab bridges.

In FS-Slab bridges, most of the load is transferred to the curbs and into the supporting bent caps. When an FS-Slab bridge is widened, the curbs need to be removed and the load-carrying capacity of the bridge is reduced significantly. Therefore, temporary shoring needs to be placed under the bridge to avoid compromising the structural integrity of the bridge during the widening operation. This procedure can be very time-consuming and in some cases difficult to implement.

An alternative to bridge shoring is to strengthen the slab using carbon fiber reinforced polymer (CFRP) composites before the structural curbs are removed. The objective of this technique is to replace the capacity that was originally provided by the curbs, and to strengthen the existing slab once the bridge is widened to meet the current legal load (HS-20 vehicle). Two CFRP systems were used to strengthen laboratory specimens consisting of a section of a flat-slab bridge.

The description and load rating of a prototype FS-Slab bridge is presented in this chapter. The design of the laboratory specimens and key characteristics used to simulate the response of the prototype slab are also presented. The CFRP composite configurations that were used to meet the strengthening criterion described above are discussed.

7.2 PROTOTYPE BRIDGE

7.2.1 Physical Characteristics of Prototype Bridge

Drawings were obtained for an FS-Slab bridge designed in 1945 to carry two lanes of H-10 truck loading. The prototype bridge was designed for a 25-ft span and 20' – 0" roadway width. The bridge cross section and reinforcement details are shown in Figure 7.1.

The structural curbs on both sides of the prototype bridge have a trapezoidal cross section. The curbs extend 1'-6" above the bridge deck. The slab has a constant thickness of 11 in. across the prototype bridge.

The bottom reinforcement consists of # 7 bars spaced at 6 ½ in. longitudinally and #5 bars spaced at 7 ½ in. transversely throughout the bridge span. The concrete cover to the centroid of the main longitudinal reinforcement is 1 ¾ in. Top reinforcement consists of #4 bars placed longitudinally and transversely at 36 in. and 18-in. spaces, respectively. Curbs are reinforced with 2 - # 11 bars top and bottom longitudinally, and shear reinforcement consisting of #4 stirrups spaced at 12 in. throughout the span.

During construction, the flat-slab bridges are cast directly on top of 2-ft wide bent caps. At a typical expansion joint, one end of the slab is anchored to the supporting bent cap using dowels made from #6 bars spaced at 36 in. The bent caps are oiled with 60-grade oil and covered with powdered graphite to allow the slabs to expand and contract due to temperature effects. One layer of 30-lb felt is placed on top of the graphite layer before casting the slab on the bent cap (Figure 7.1). Even though this detail intended to avoid end restraint, the conditions encountered in the field show that there could be some rotational restraint provided by adjacent spans and by deterioration of the felt with time. Evaluation of the

results of the diagnostic testing of a flat-slab bridge supports this observation [Bussell, 1997].

7.2.2 *Calculated Capacity of Prototype Bridge*

The nominal flexural strength of the slab and curbs of the prototype bridge were calculated in accordance with the *AASHTO Design Specifications* [AASHTO, 1996]. Concrete was assumed to have a cylinder compressive strength of 3,000 psi, and reinforcing steel was assumed to have a specified yield stress of 40,000 psi. The capacity of prototype bridge components that contribute to the flexural strength was required for the prototype bridge load rating.

The nominal flexural strength, per ft of slab, was computed using,

$$M_n = A_s f_y \left(d - \frac{a}{2} \right) \quad (7.1)$$

with $a = \frac{A_s f_y}{b(0.85 f'_c)}$

and the nominal flexural strength of the curbs was calculated including the contribution of steel in the compression area using the following expression:

$$M_n = A_s' f_y (d - d') + C_{C1} \left(d - \frac{a}{2} \right) + C_{C2} \left(d - \frac{2a}{3} \right) \quad (7.2)$$

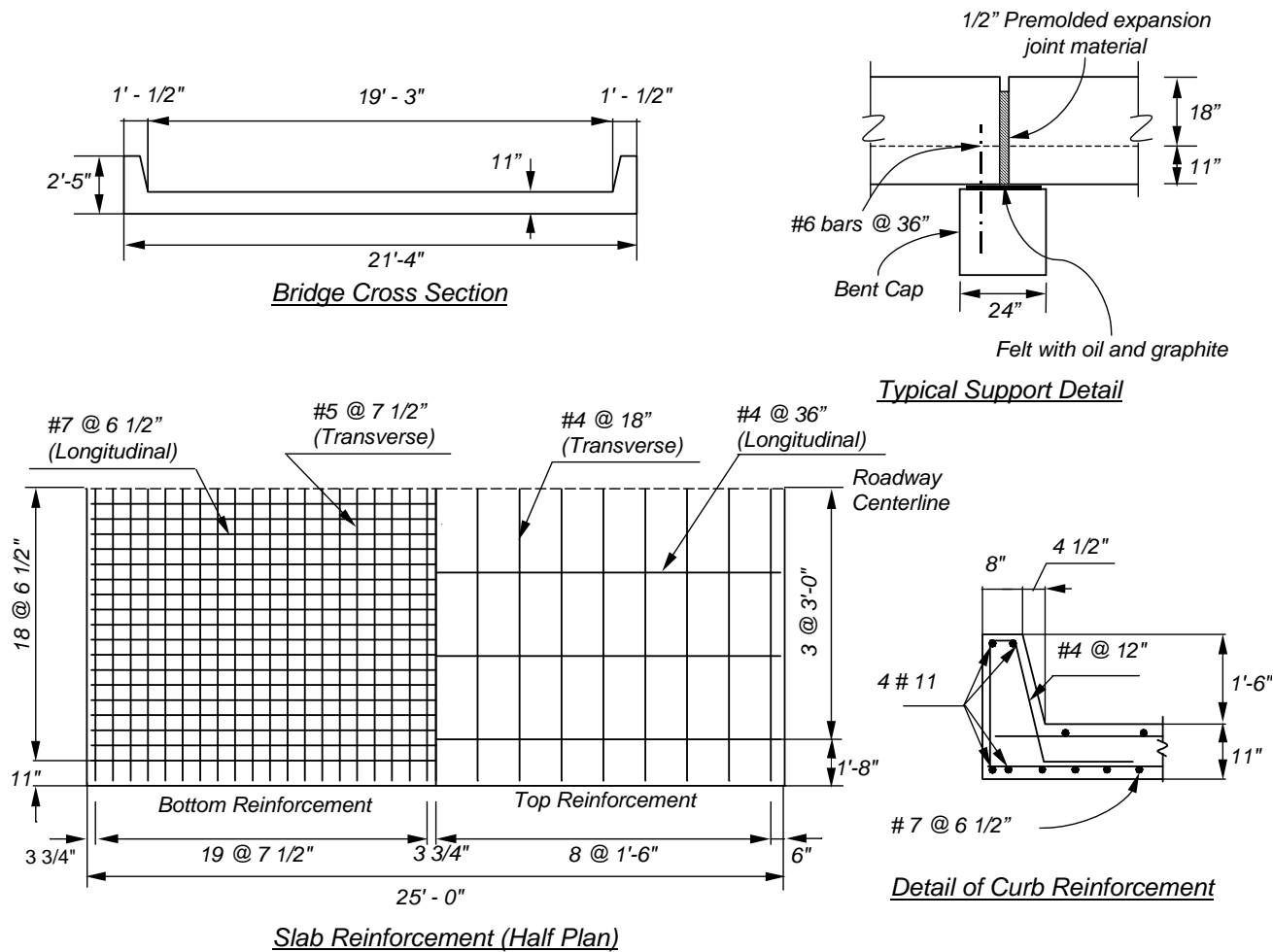


Figure 7.1 Reinforcement Details for FS-Slab Prototype Bridge

where a is the depth of the stress block and may be calculated as:

$$a^2 + 8b a = \frac{8 (A_s - A_s') f_y}{(0.85 f'_c)} \quad (7.3)$$

where

M_n = Nominal flexural strength, lb-in.

ϕ = Strength reduction factor equal to 0.9

A_s = Area of tensile reinforcement including portion of slab steel considered to be effective in the curb, in².

A_s' = Area of steel in the compression zone, in².

C_{C1} = Fraction of the total compressive force in the concrete calculated based on the rectangular portion of the compressed area, kips.

C_{C2} = Fraction of the total compressive force in the concrete calculated based on the triangular portion of the compressed area, kips.

d = Distance from extreme compression fiber to centroid of tensile reinforcement, in.

d' = Distance from extreme compression fiber to centroid of A_s' , in.

b = Width of the top face of member, in.

f_y = Yield strength of flexural or shear reinforcement, psi.

f'_c = Concrete compressive strength, psi.

The reinforcement within a 44-in. width of slab (4 times the slab thickness) was considered as part of the tensile reinforcement area for the curbs, Figure 7.2 [Jensen et al., 1943]. The calculated nominal flexural capacity of the slab and curbs in the prototype bridge are listed in Table 7.1 along with the parameters used in the calculations.

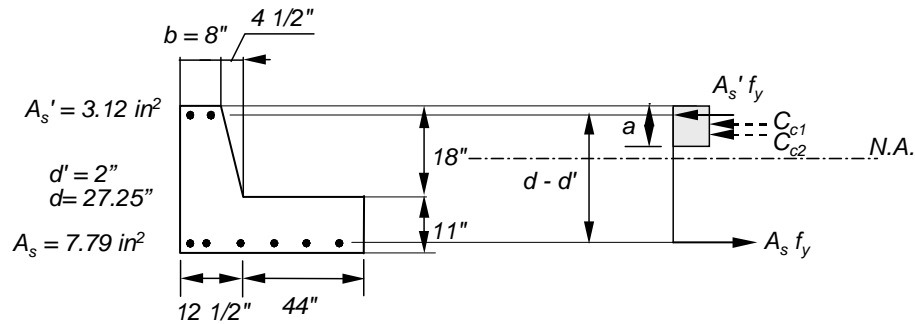


Figure 7.2 Geometric Properties of the Curbs to Compute Flexural Strength

7.2.3 Prototype Bridge Load Rating

The load factor method given in the AASHTO *Manual for Condition Evaluation of Bridges* [AASHTO, 1994] was used to rate the prototype bridge. In this procedure, moments are distributed to curbs and slab in accordance with *Bulletin 346* from the University of Illinois [Jensen et al., 1943]. A summary of the details of the load rating procedure are given in Appendix B and are described in greater detail elsewhere [Bussell, 1997]. The prototype bridge was first rated considering the contribution of the curbs to the flexural strength. The bridge was then rated considering only the contribution of the flat-slab to the strength to examine the effect of removing the curbs on the rating.

Table 7.1 Design Flexural Strength of Slab (per ft) and Curbs for Prototype Bridge

| Parameter | Value |
|---------------------------------------|--------------|
| f'_c , psi | 3,000 |
| f_y , psi | 40,000 |
| ϕ | 0.9 |
| Slab (per ft) | |
| d , in. | 9.25 |
| b , in. | 12 |
| A_s , in. ² | 1.11 |
| $M_{n \text{ slab}}$, kip-ft/ft | 31.54 |
| $\phi M_{n \text{ slab}}$, kip-ft/ft | 28.39 |
| One Curb (Figure 7.2) | |
| A_s' , in. ² | 3.12 |
| A_s , in. ² | 7.70 |
| b_{top} , in. | 8 |
| b_{bott} , in. | 44 |
| d' , in. | 2 |
| d , in. | 27.25 |
| h_{slab} , in. | 11 |
| $\phi M_{n \text{ curb}}$, kip-ft | 621.2 |
| $\phi M_{n \text{ curb}}$, kip-ft | 559.1 |

The two load-rating levels (inventory and operating) described in the AASHTO *Manual* [AASHTO, 1994] were used to rate the prototype bridge. In the case of FS-Slabs, the difference between the two rating levels depends, not only on

the load factors used for live load effects in the rating equation, but also on the way that the critical element is identified (Appendix B). For the inventory rating level, the element having the lowest rating factor controls the overall bridge rating. For the operating rating level, a weighted average of the ratings between slab and curbs is used to calculate the overall bridge rating. The weighting factor for each element is obtained using the ratio of its tributary width to the total bridge width. These factors are multiplied by the individual component rating to calculate the overall bridge rating.

The total moment across the bridge was distributed to the curbs and the slab using the empirical coefficients contained in *Bulletin 346* from the University of Illinois (Appendix B). The total moment included dead and live-load effects. Dead-load effects were generated by the slab and curbs self-weights. The live-load effects were calculated using the weight of the rear wheels of the design vehicles positioned at mid-span. The total live-load effect was obtained by multiplying the load from the individual wheels on the design truck by the number of wheels that can fit across the prototype bridge. A summary of this procedure is presented in Appendix B.

The dead and live load moments used in the prototype bridge rating are listed in Table 7.2 and the load-rating results for H-truck and HS-truck loading are presented in Table 7.3. The HS-truck effects were determined using the axle

weights from the H-10 truck but distributed according to an HS-design vehicle. A 24-ft span was used in all calculations after subtracting half the bearing length on each end of the prototype bridge.

The effective widths of the slab and curbs were determined to calculate the weighting factors for the operating rating of the prototype bridge. The same width of the slab that was considered to act compositely with the curbs for the flexural strength calculations was used in the effective width calculation (Figure 7.2). The effective widths of slab and curbs used for the operating rating level are also presented in Table 7.3.

Table 7.2 Unfactored Load Effects Used in Prototype Bridge Rating

| Unfactored Load Effect | Value |
|-------------------------------|---|
| H – 10 truck axle loads, kip | 4, front; 16, rear (14 ft from front) |
| Slab | |
| M_{DL} , kip-ft/ft | 5.2 |
| $(1 + I) M_{LL}$, kip-ft/ft | 8.0 |
| One Curb | |
| M_{DL} , kip-ft | 92.7 |
| $(1 + I) M_{LL}$, kip-ft | 93.2 |
| HS – 10 truck axle loads, kip | 4, front; 16, middle (14 ft from front); 16, rear (14 ft from middle) |
| Slab | |
| M_{DL} , kip-ft/ft | 5.2 |
| $(1 + I) M_{LL}$, kip-ft/ft | 8.0 |
| One Curb | |
| M_{DL} , kip-ft | 92.7 |
| $(1 + I) M_{LL}$, kip-ft | 93.5 |

Notes: Live load effects include a 0.3 impact factor (I).

The weight of a ½ in. overlay is included in dead load effects.

Slab effects determined for a 1-ft wide section.

Table 7.3 Load Rating Results for Flat-Slab Prototype Bridge

| Bridge Element | Effective Width, ft | Rating Level | Design truck | |
|---------------------------------|---------------------|--------------|--------------|------------|
| | | | H – truck | HS – truck |
| Individual Component Rating | | | | |
| Slab | 11.91 | Inventory | H – 12.5 | HS – 12.4 |
| | | Operating | H – 20.8 | HS – 20.8 |
| One Curb | 4.71 | Inventory | H – 21.7 | HS – 21.6 |
| | | Operating | H – 36.2 | HS – 36.1 |
| Overall Prototype Bridge Rating | | | | |
| Bridge | 21.33 | Inventory | H – 12.5 | HS – 12.4 |
| | | Operating | H – 27.6 | HS – 27.5 |

The prototype bridge had an inventory rating of H-12.5 (Table 7.3). Also, the rating results for the prototype bridge from H-truck loading are very close to those for HS-truck loading because the bridge has a total length of 25 ft. For the H-truck loading, the maximum positive total moment on the bridge is caused by positioning the rear axle at mid-span for this span. The rear axle of the HS-truck needs to be positioned at 3' – 6" from mid-span to generate the maximum positive

total moment on the bridge. However, the difference in maximum positive moments generated by each truck is less than 1% for this span.

As mentioned earlier, the curb strength represents a significant portion of the total bridge strength. Once the curbs are removed when the bridge undergoes widening, the bridge rating drops significantly. Therefore, the prototype bridge was also rated without considering the contribution of the curbs.

Results of the prototype bridge slab rating without the contribution of the curbs are presented in Table 7.5. The unfactored moments used for the slab rating are presented in Table 7.4. The dead and live-load effects listed in this table were calculated per unit width of slab. The live-load effects were determined by distributing the wheel loads from the design vehicles over a slab width equal to [AASHTO, 1996]:

$$E = 4 + 0.06 S \leq 7 \text{ ft} \quad (7.4)$$

where

E = Effective slab width over which wheel loads are distributed, ft.

S = Span length = Distance from center to center of supports, ft.

Table 7.4 Unfactored Load Effects Used to Rate the Slab in the Prototype Bridge

| Unfactored Load Effect | Value |
|-------------------------------|--|
| H – 10 truck axle loads, kip | 4, front;16, rear (14 ft from front) |
| Slab | |
| M_{DL} , kip-ft/ft | 10.3 |
| $(1 + I) M_{LL}$, kip-ft/ft | 11.5 |
| HS – 10 truck axle loads, kip | 4, front; 16, middle (14 ft from front); 16, rear (14 ft from middle) |
| Slab | |
| M_{DL} , kip-ft/ft | 10.3 |
| $(1+ I) M_{LL}$, kip-ft/ft | 11.5 |

Notes: Live load effects include a 0.3 impact factor (I).

The weight of a ½ in. overlay is included in dead load effects.

Span, $S = 24$ ft.

Effective slab width, $E = 5.44$ ft.

Slab effects were determined for a 1-ft wide section.

Table 7.5 Prototype Bridge Load Rating after Curb Removal

| Bridge Element | Rating Level | Design truck | |
|-----------------------|---------------------|--------------------------|---------------------------|
| | | H – truck loading | HS – truck loading |
| Slab | Inventory | H – 6.0 | HS – 6.0 |
| | Operating | H – 10.0 | HS – 10.0 |

It can be observed from comparing Table 7.2 with Table 7.4 that the dead load moment on the slab is higher after the curbs are removed from the bridge. This difference arises from the method that was used to rate the bridge. In this method, a portion of the total moment on the bridge (dead and live-load moment) is distributed to the curbs depending on the bridge width and the relative stiffness of the slab and curbs. Because dead and live-load effects have to be considered separately to rate the bridge, the total moment is then divided into the dead and live-load components using empirical coefficients obtained from analyses of elastic plate theory [Jensen et al., 1943]. Therefore, a portion of the dead load moment acting on the slab is effectively distributed to the curbs. Although it was recognized that some inconsistencies arose from using this method, it was selected to be coherent with the current practice used by TxDOT to rate slab-bridges.

Because the slab in the prototype bridge had an H-6.0 inventory rating after removing the curbs, strengthening of the slab was proposed as an alternative to the current construction practice of using temporary shoring during roadway widening. The criterion that was selected for the design of the strengthening schemes was to restore the bridge strength that was lost after curb removal. Therefore, the slab strength had to be increased to raise the inventory rating of the slab acting alone to the original design rating of H-10.

7.3 DESIGN AND CONSTRUCTION OF LABORATORY SPECIMENS

Two full-scale laboratory specimens (FS-1 and FS-2) were built and tested to compare the behavior of two different slab strengthening methods using CFRP composites. The specimens represent a 6-ft wide section of the slab in the prototype bridge. Only the slab was modeled in the laboratory to study the behavior of the strengthened specimens without the contribution from the structural curbs. This represents the condition of the prototype bridge after the curbs have been removed to widen the roadway.

The flat-slab specimens were assumed to be simply-supported. As has been demonstrated in previous research, the calculated moments during diagnostic testing of an actual FS-Slab bridge indicate that there is rotational restraint at the supports [Bussell, 1997]. The source of end restraint can vary considerably from span to span in a typical bridge and is therefore difficult to quantify. The moments generated during testing of the specimens using a simply-supported condition represent an upper bound of the positive moments that are developed at mid-span. This support condition was also chosen to facilitate the calculations to determine internal stresses and forces at the instrumented sections of the test specimens.

Reinforcement consisted of two mats of uniformly spaced reinforcement. The bottom reinforcement mat consisted of #6 bars at 8 ½ in. spacing in the longitudinal direction and #4 bars at 8 ½ in. in the transverse direction. The top

steel mat consisted of #3 bars at 18 in. spacing in both the longitudinal and transverse directions. The areas of steel reinforcement were adjusted to develop the same force as in the prototype bridge because Grade 60 steel was used in the specimens and Grade 40 steel was assumed for the prototype bridge construction. The total area of the top reinforcement in the longitudinal direction in the laboratory specimens does not represent the prototype design. The longitudinal top reinforcement was increased in the laboratory specimens to avoid failure during lifting. Figure 7.3 shows a picture of the reinforcement in one of the flat-slab specimens inside the formwork before concreting. Specimen dimensions and reinforcement details of the specimens are illustrated in Figure 7.4.



Figure 7.3 Picture Showing Reinforcement in a Typical Flat-Slab Specimen before Casting

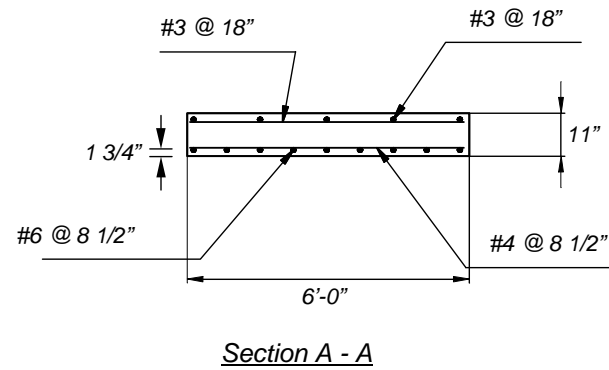
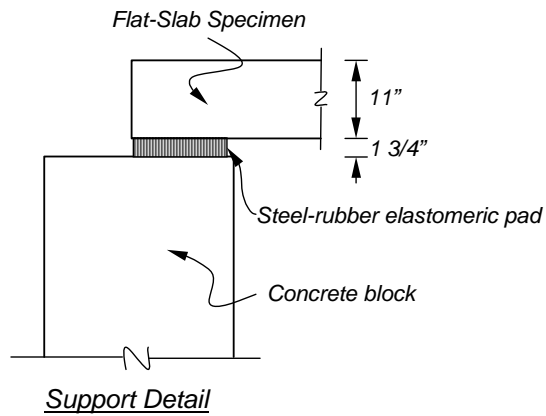
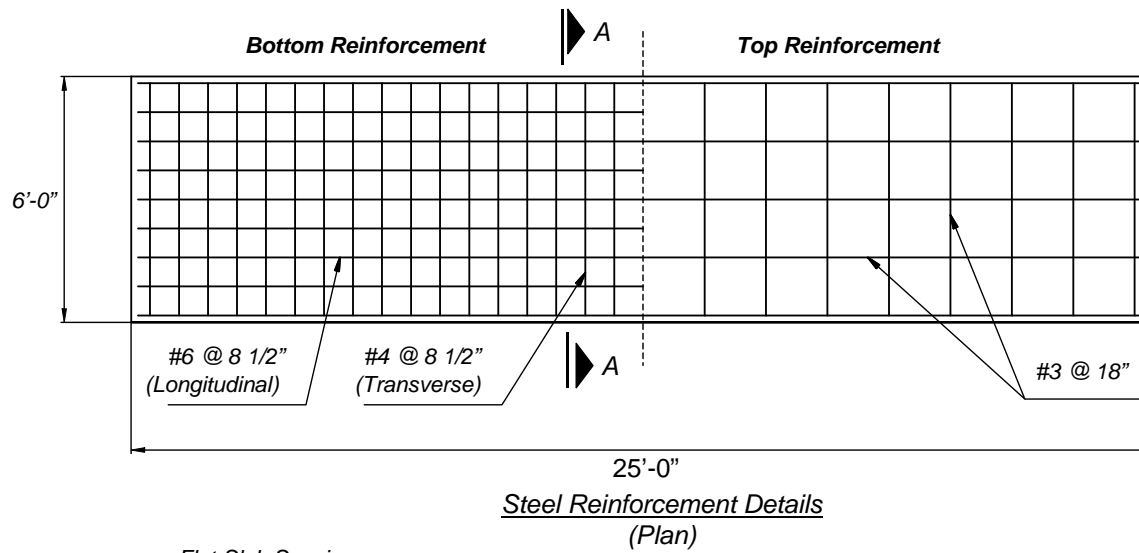


Figure 7.4 Geometry and Reinforcement Details of Flat-Slab Specimens FS-1 and FS-2

The specified yield stress for all reinforcing steel used for the fabrication of the specimens was 60,000 psi. The design 28-day concrete compressive strength was 4,000 psi. Table 7.6 lists the average measured material properties for the Flat-Slab Specimens at the time of testing. The values shown for the yield stress of the bottom bars correspond to the static yield measurements. Full details of the material tests for both specimens are presented in Appendix A.

Table 7.6 Average Measured Material Strengths for Flat-Slab Specimens

| Specimen | Concrete | | Longitudinal Bars (#6) | | Transverse Bars (#4) | | |
|----------|-----------|--------------|------------------------|-------------|----------------------|-------------|-------------|
| | Age, days | f'_c , psi | f_t , psi | f_y , ksi | f_u , ksi | f_y , ksi | f_u , ksi |
| FS-1 | 33 | 4,800 | 400 | 63.5 | 106.1 | 65.8 | 107.4 |
| FS-2 | 22 | 3,900 | 400 | | | | |

The nominal flexural capacity for each of the flat-slab specimens was calculated using the material strengths contained in Table 7.6. Equation 7.1 was used to compute the flexural strength per foot of slab of each specimen. The specimen capacities are listed and compared with the slab capacity of the prototype bridge in Table 7.7.

Table 7.7 Flexural Capacity of Flat-Slab Specimens (per unit width of slab)

| Specimen | M_n Prototype, kip-ft/ft | M_n Specimen, kip-ft/ft | M_{n spec}/M_{n prot} |
|-----------------|---|--|--|
| FS-1 | 31.5 | 29.0 | 0.92 |
| FS-2 | 31.5 | 28.7 | 0.91 |

The flexural strength for both specimens was lower than the calculated flexural capacity of the prototype bridge with a maximum difference between the specimens and prototype of approximately 10%.

7.4 DESIGN AND CONSTRUCTION OF STRENGTHENING SCHEMES FOR LABORATORY SPECIMENS

Two full-scale laboratory specimens were constructed to evaluate the behavior of the strengthened slab using different CFRP composite systems (Specimens FS-1 and FS-2). As discussed in Section 7.2.3, strengthening of the prototype bridge slab was required to raise the inventory rating. The slab capacity required to reach the target inventory rating of an H-10 design vehicle was determined using Eq. 7.5. The moments per unit width of slab generated by an H-10 design vehicle (Table 7.4) were used in this equation so the rating factor was set to 1.00. The bridge rating is obtained by multiplying the rating factor by the weight in tons of the two front axles of the design vehicle (Appendix B). Equation 7.5 yielded a required capacity, C , equal to 38.4 kip-ft/ft. The calculated flexural

strength of the slab in the prototype bridge was 28.4 kip-ft/ft (Table 7.1). The values that were used for the variables in Eq. 7.4 to determine the required slab moment strength increase are shown below.

$$C = \phi M_n = RF [A_2 L (1 + I)] + A_1 D$$

where:

$$\begin{aligned} RF &= 1.00 \\ A_1 &= 1.3 \\ D &= 10.3 \text{ kip - ft/ft} \\ A_2 &= 2.17 \\ L &= 8.8 \text{ kip - ft/ft} \\ I &= 0.3 \end{aligned} \tag{7.5}$$

The strength reduction factor (ϕ) used in the strengthening design was assumed equal to 0.85. Therefore, the target nominal flexural capacity for the strengthened slab was 45.2 kip-ft/ft ($M_n = 38.4/0.85$), which is more than 40% larger than the nominal capacity of the slab in the prototype bridge (Table 7.1).

The required area of composite material to develop the target flexural strength was determined by calculating the moment-curvature response of the slab in the prototype bridge strengthened using the two different types of CFRP composites (Chapter 3). An assumed limiting strain before debonding of the composite systems equal to 0.007 was used for design. This value was selected based on the results of previous tests of strengthened beams with rectangular section with similar composite systems [Bramblett, 2000]. The strain before

debonding was selected as the lower bound of the measured strains on composite plates and sheets from six beam tests.

The calculated moment-curvature response of a 6-ft section of the strengthened slab in the prototype bridge was determined and compared with the unstrengthened section capacity. Two different CFRP composite systems were used to increase the flexural capacity to the required strength of the prototype bridge slab. The area of CFRP composites was adjusted until the target strength was reached. The CFRP material properties published by each of the composite system manufacturers (Appendix A) and the nominal material strengths of the prototype bridge were used in these calculations. Table 7.8 lists the required flexural strength and the calculated capacities of the strengthened prototype based on a 6-ft slab section and using the two different CFRP composite systems.

Table 7.8 Flexural Strength Parameters and Calculated Capacity of a 6-ft Section of Strengthened Slab in the Prototype Bridge

| Parameter | Value | Notes |
|--------------------------|-------|--|
| $A_1 M_D$, kip-ft | 80.3 | Factored dead load moment |
| $A_2 M_L (1+I)$, kip-ft | 149 | Factored live load moment + impact |
| M_u , kip-ft | 229.3 | Required ultimate strength (6-ft slab) |
| ϕ | 0.85 | Strength reduction factor |
| $M_n = M_u/\phi$ | 270 | Required nominal capacity (6-ft slab) |
| M_n wet-layup | 282 | Calculated strength of laboratory specimen |
| M_n pultruded | 265 | Calculated strength of laboratory specimen |
| ϵ_{CFRP} | 0.007 | Maximum CFRP strain used for design |

Notes: A_1 and A_2 = Load factors for dead and live load effects equal to 1.3 and 2.17 respectively.

I = Impact factor for live load effects equal to 0.3.

Slab width equal to 6-ft.

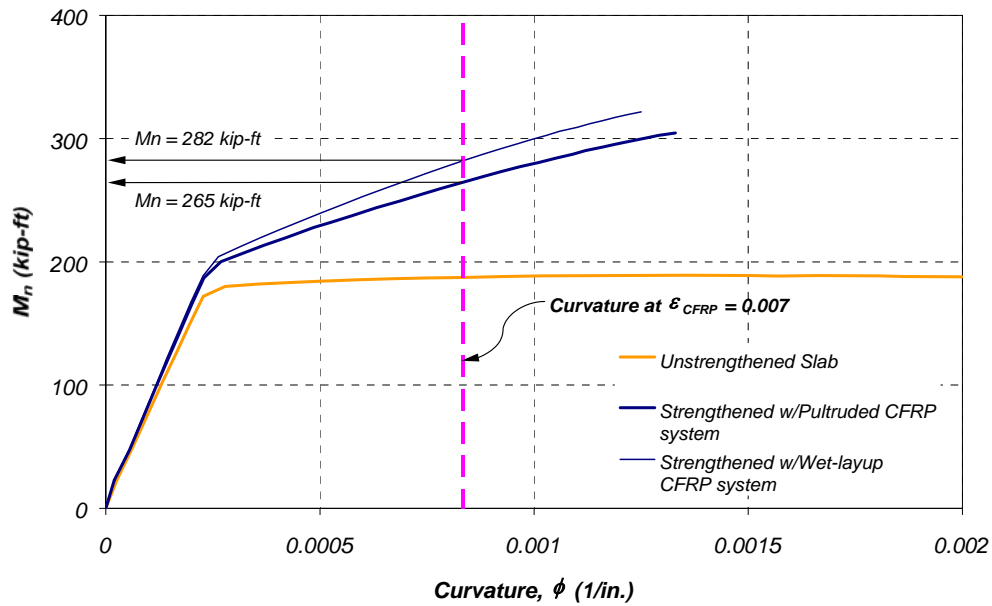


Figure 7.5 Calculated Moment-Curvature Response of a Strengthened and Unstrengthened 6-ft Wide Section of the Slab in the Prototype Bridge

The CFRP configuration that was used in the construction of the curves shown in Figure 7.5 for each system is presented in Sections 7.4.1 and 7.4.2 for Specimens FS-1 and FS-2, respectively. The calculated moment-curvature response of each specimen is also presented in each of these sections. The measured material properties for concrete and steel, and the properties contained in the manufacturers' literature for the CFRP systems were used in these calculations.

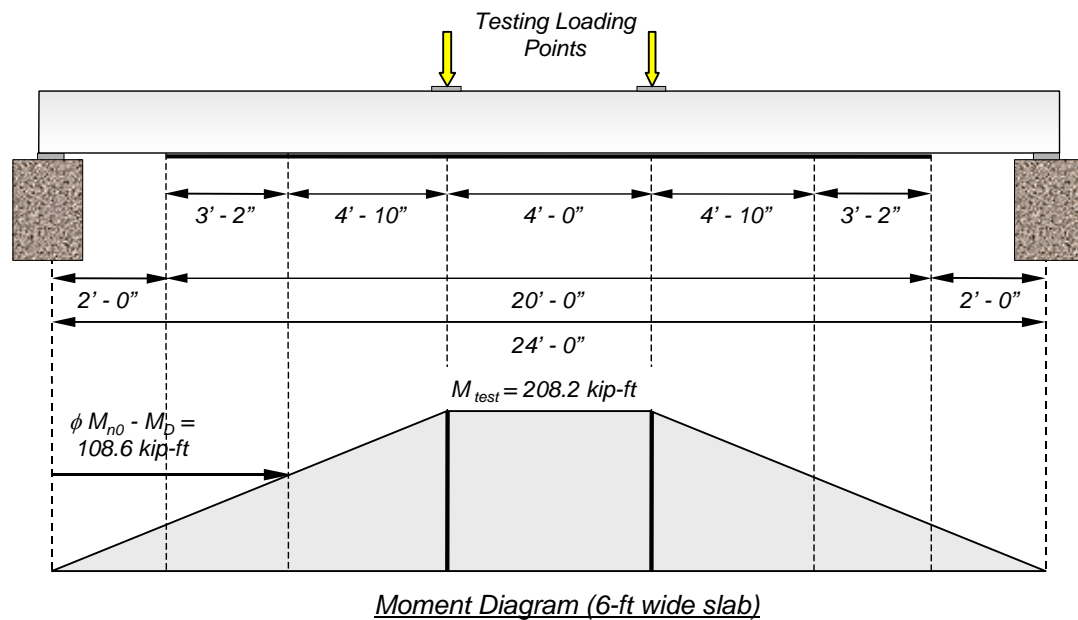
7.4.1 Strengthening Scheme for Specimen FS-1

Specimen FS-1 was strengthened using CFRP pultruded plates bonded to the slab bottom surface. The techniques used to bond this type of system to the test specimen are described in Appendix C. The plates were bonded to the concrete surface using an epoxy-based adhesive supplied by the plate manufacturer.

The CFRP plates had a 68% volumetric fiber content. The plate dimensions were 20 ft long by 3.17 in. wide and 0.047 in. thick. The cross sectional dimensions were obtained from the manufacturer's literature. Mechanical properties of the CFRP plates and the epoxy adhesive are listed in Appendix C. The plates were uniformly spaced at 18 in. across the bottom surface (Figure 7.7).

The longest practical CFRP plate length was used in the laboratory specimen. However, the shape of the moment diagram developed during testing was used to insure that the plate length would extend beyond the required theoretical cut-off point. The theoretical cut-off point was determined by superimposing the nominal prototype flexural strength on the test moment diagram. The unfactored moment caused by dead loads was subtracted from all calculations because the specimens were constructed at full-scale. The maximum moment applied during the test had to be equal to the required flexural strength of a 6-ft section of the slab in the prototype bridge minus the dead-load moment. In this

case, the plates extended 3'-2" beyond the theoretical cut-off points. This procedure is illustrated graphically in Figure 7.6.



Nomenclature: ϕM_{n0} = Original moment capacity = 170.4 kip-ft
 M_D = Service dead load moment = 61.8 kip-ft
 M_{test} = Applied moment = $M_U / \phi - M_D$

Figure 7.6 Required CFRP Plate Length on Specimen FS-1 Based on Moments Generated During Laboratory Testing

Six CFRP composite woven fabric sheets were placed transversely along the pultruded plates at 3 ft. on center. The sheets were 12-in. wide and were bonded using a two-component epoxy resin. Details of the bonding procedure are presented in Appendix C. The sheets were placed only on the bottom surface

without continuing them on the sides of the slab specimen because the specimen represents an interior section of the slab in the prototype bridge. Attaching these sheets transversely to the CFRP plates was expected to delay debonding of the pultruded plates from the concrete surface.

Both the epoxy adhesive used to bond the pultruded plates, and the composite straps were cured at ambient temperature for 7 days to develop their design strength. Details showing the location of CFRP pultruded plates and woven fabric sheets on Specimen FS-1 are shown in Figure 7.7. A picture showing the bottom surface of the slab specimen after strengthening can be seen in Figure 7.8.

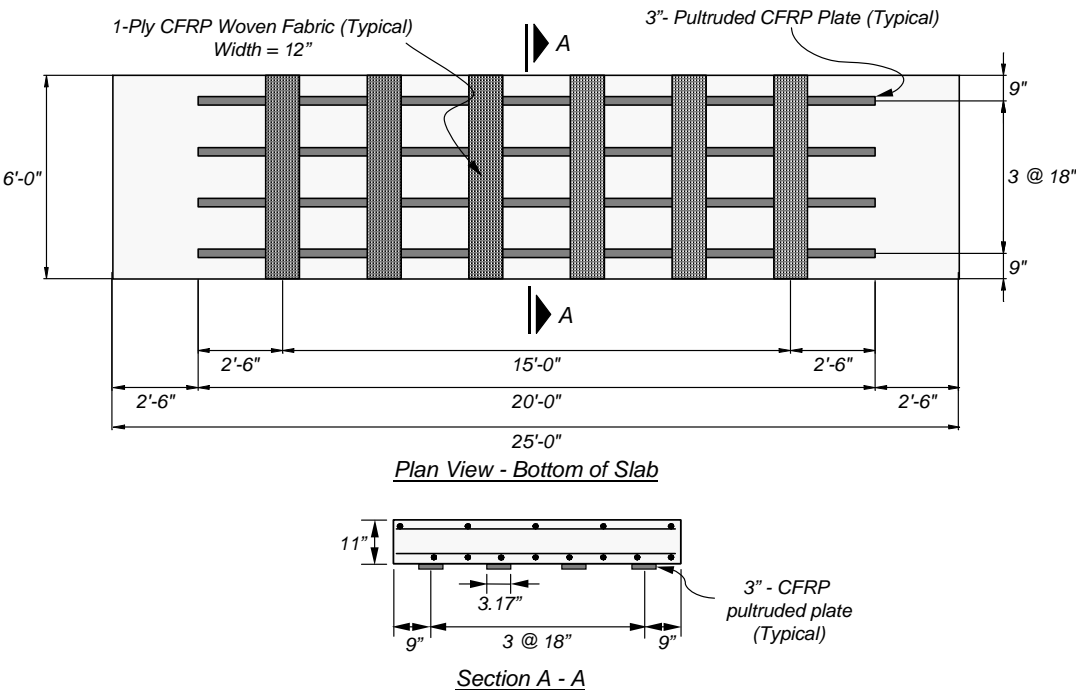


Figure 7.7 Strengthening Details for Specimen FS-1



Figure 7.8 Picture of the Bottom Surface of Specimen FS-1 after Strengthening with the CFRP Pultruded System

The calculated capacity of Specimen FS-1 was determined to compare it with the required capacity computed for the prototype bridge. The measured concrete compressive strength and steel yield stress were used in these calculations.

The calculated moment-curvature response of Specimen FS-1 is shown in Figure 7.9. The calculated response of the unstrengthened specimen is also shown for comparison. The calculated test specimen capacity was determined at a CFRP strain equal to 0.007 to compare with the prototype design strength. The difference in the calculated capacity of the strengthened prototype bridge (265 kip-ft) and the calculated capacity of the laboratory specimen (274 kip-ft) can be attributed to the

higher measured yield stress of the reinforcement and the higher concrete strength at the time of testing.

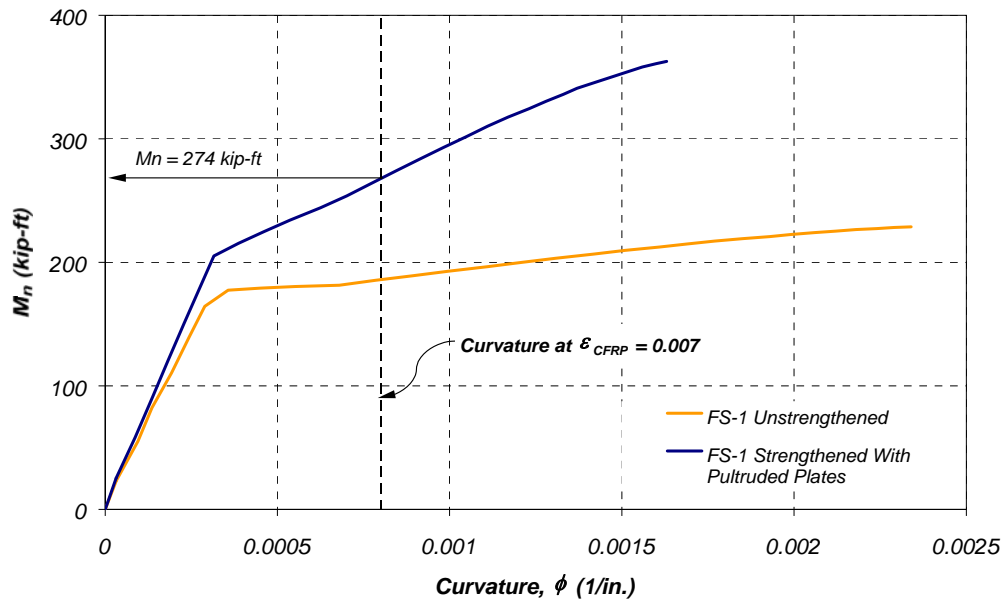


Figure 7.9 Calculated Moment-Curvature Response of Specimen FS-1 Using the Measured Material Properties

7.4.2 Strengthening Scheme for Specimen FS-2

Specimen FS-2 was strengthened using a CFRP composite system applied using a wet lay-up procedure (Appendix C). The system consisted of unidirectional carbon fiber sheets that had not been impregnated in epoxy prior to installation. A two-component epoxy resin was used to impregnate the carbon fibers and bond them to the concrete surface. A detailed description of the fabrication procedure for this type of system is presented in Appendix C.

Two 20-in.-wide layers (plies) of carbon fiber sheets were bonded to Specimen FS-2 at a spacing of 36 in. on centers. The length of the sheets was determined based on the moment generated during testing as for Specimen FS-1 (Figure 7.6). Details showing the location and geometry of the CFRP composite on Specimen FS-2 are illustrated in Figure 7.10.

CFRP sheets were also placed transversely at a 26-in. spacing along the total length of the longitudinal sheets. They were fabricated using one ply of 10-in. wide carbon fiber sheets. The objective of the transverse sheets was to increase the contact surface area and delay debonding of the longitudinal CFRP sheets that were used to increase the flexural capacity of the test specimen.

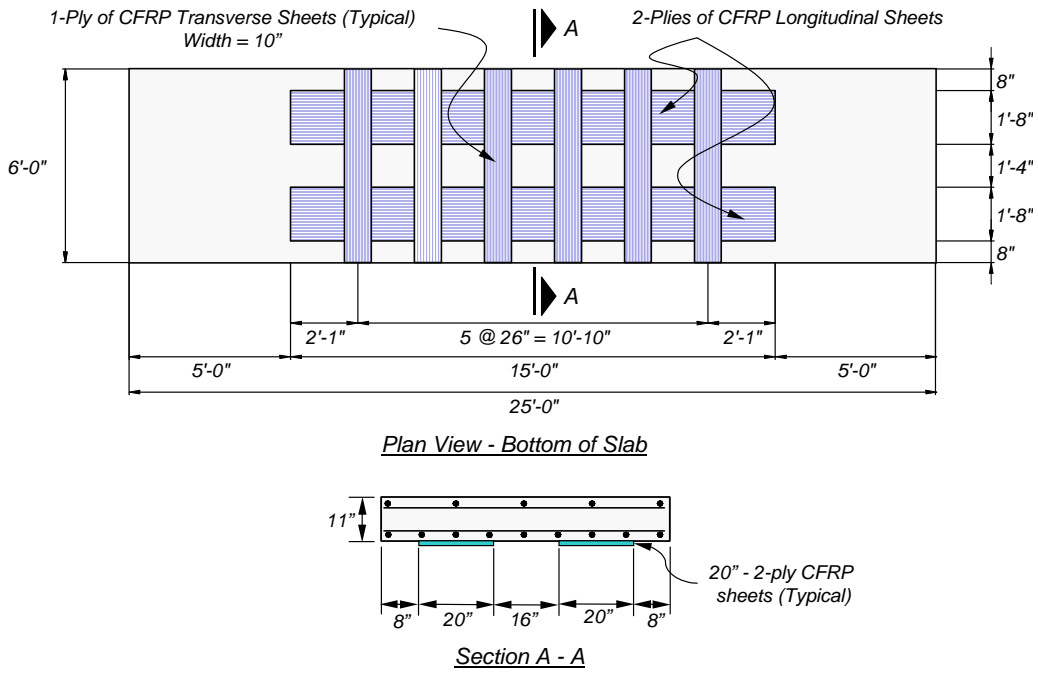


Figure 7.10 Strengthening Details for Specimen FS-2



Figure 7.11 Picture of the Bottom Surface of Specimen FS-2 after Strengthening with the CFRP Wet-Layup System

The calculated moment-curvature response of Specimen FS-2 is shown in Figure 7.12. The measured material properties of steel and concrete were used in the calculations. The flexural capacity of the specimen at CFRP debonding was estimated at a curvature corresponding to an expected maximum CFRP composite strain equal to 0.007.

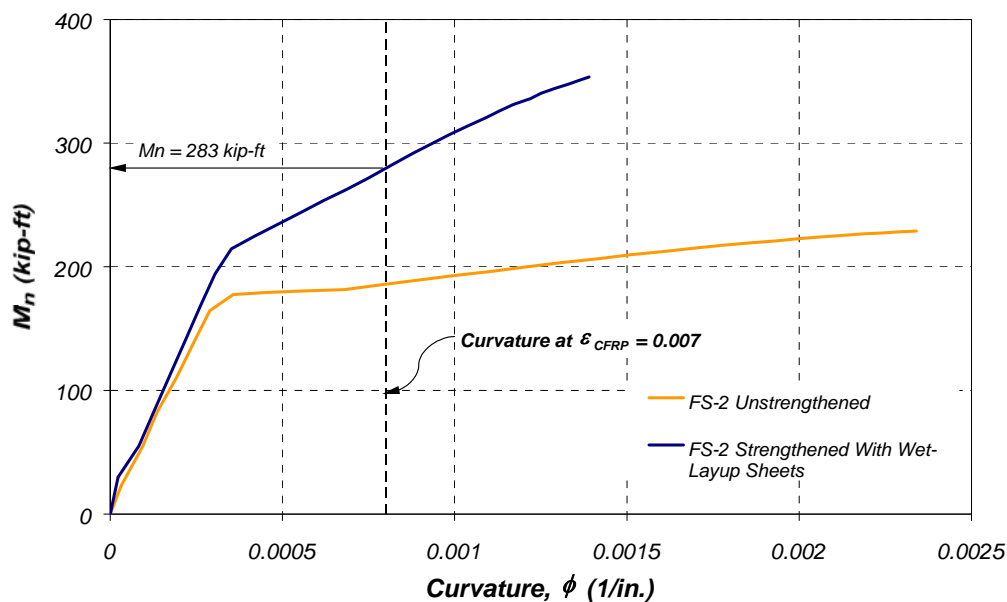


Figure 7.12 *Calculated Moment-Curvature Response of Specimen FS-2 Using the Measured Material Properties*

The calculated capacity of Specimen FS-2 exceeded the required flexural strength of 270 kip-ft. Therefore, the strengthened specimen was expected to meet the design goal. A comparison between the predicted and measured moment-curvature response of this specimen is presented in Chapter 10.

7.5 SUMMARY

A description of flat-slab bridge construction in Texas is presented in this chapter. Bridges in this category were designed using older load standards and therefore strengthening is required to meet current legal loads. The load rating deficiencies associated with this type of construction were discussed and the criterion used to justify strengthening this type of bridges was described.

The design, construction, and strengthening procedures used in two full-scale laboratory specimens were presented in this chapter. These specimens represent a 6-ft wide section of the slab in the prototype bridge. The laboratory specimens were designed to replicate the behavior of a strengthened slab after curbs have been removed from the bridge for widening purposes.

Two commercially available composite systems were used to restore the capacity of the bridge after the curbs are removed. The calculated moment-curvature response of the strengthened specimens was compared with the calculated response of the prototype bridge used in the design of the composite strengthening systems.

| | |
|--|------------|
| CHAPTER 7: DESCRIPTION OF FLAT-SLAB SPECIMENS | 200 |
| 7.1 Introduction | 200 |
| 7.2 Prototype Bridge | 201 |
| 7.2.1 Physical Characteristics of Prototype Bridge | 201 |
| 7.2.2 Calculated Capacity of Prototype Bridge | 203 |
| 7.2.3 Prototype Bridge Load Rating | 206 |
| 7.3 Design and Construction of Laboratory Specimens | 215 |
| 7.4 Design and Construction of Strengthening Schemes for Laboratory Specimens | 219 |
| 7.4.1 Strengthening Scheme for Specimen FS-1 | 224 |
| 7.4.2 Strengthening Scheme for Specimen FS-2 | 228 |
| 7.5 Summary | 231 |
| Figure 7.1 Reinforcement Details for FS-Slab Prototype Bridge..... | 204 |
| Figure 7.2 Geometric Properties of the Curbs to Compute Flexural Strength | 206 |
| Figure 7.3 Picture Showing Reinforcement in a Typical Flat-Slab Specimen before Casting..... | 216 |
| Figure 7.4 Geometry and Reinforcement Details of Flat-Slab Specimens FS-1 and FS-2 | 217 |
| Figure 7.5 Calculated Moment-Curvature Response of a Strengthened and Unstrengthened 6-ft Wide Section of the Slab in the Prototype Bridge..... | 223 |
| Figure 7.6 Required CFRP Plate Length on Specimen FS-1 Based on Moments Generated During Laboratory Testing..... | 225 |
| Figure 7.7 Strengthening Details for Specimen FS-1 | 226 |
| Figure 7.8 Picture of the Bottom Surface of Specimen FS-1 after Strengthening with the CFRP Pultruded System | 227 |
| Figure 7.9 Calculated Moment-Curvature Response of Specimen FS-1 Using the Measured Material Properties..... | 228 |
| Figure 7.10 Strengthening Details for Specimen FS-2..... | 229 |
| Figure 7.11 Picture of the Bottom Surface of Specimen FS-2 after Strengthening with the CFRP Wet-Layup System | 230 |
| Figure 7.12 Calculated Moment-Curvature Response of Specimen FS-2 Using the Measured Material Properties..... | 231 |
| Table 7.1 Design Flexural Strength of Slab (per ft) and Curbs for Prototype Bridge | 207 |

| | | |
|-----------|--|-----|
| Table 7.2 | Unfactored Load Effects Used in Prototype Bridge Rating | 210 |
| Table 7.3 | Load Rating Results for Flat-Slab Prototype Bridge..... | 211 |
| Table 7.4 | Unfactored Load Effects Used to Rate the Slab in the Prototype Bridge | 213 |
| Table 7.5 | Prototype Bridge Load Rating after Curb Removal..... | 213 |
| Table 7.6 | Average Measured Material Strengths for Flat-Slab Specimens | 218 |
| Table 7.7 | Flexural Capacity of Flat-Slab Specimens (per unit width of slab) | 219 |
| Table 7.8 | Flexural Strength Parameters and Calculated Capacity of a 6-ft Section of Strengthened Slab in the Prototype Bridge | 222 |

Chapter 8: Measured Response of Flat-Slab Specimens

8.1 INTRODUCTION

The measured response of Specimens FS-1 and FS-2 are presented in this chapter. The experimental setup, loading history, and specimen instrumentation are also described. Representative deflection and strain responses that were measured during the tests are presented and discussed.

8.2 TEST SETUP AND INSTRUMENTATION

8.2.1 Description of Experimental Setup

The flat-slab specimens were tested under loads that were applied statically. The test setup was the same as for the pan-joint specimens. The flat-slab specimens were supported on two steel-rubber elastomeric pads at each support simulating a simply-supported condition. The elastomeric pads rested on concrete blocks on both ends of the specimens.

Loads were applied using a 200-kip hydraulic ram reacting against a steel frame that was anchored to the laboratory strong floor. The total load was distributed to 4 points on the specimen slab surface using longitudinal and transverse spreader beams. The loads were applied symmetrically about the center of the specimen, spaced at 4 ft. longitudinally and 3 ft. transversely. The spreader

beams were supported on 10-in. by 5-in. steel-rubber elastomeric pads to avoid concrete crushing under the load points. A view of the experimental setup is shown in Figure 8.1.



Figure 8.1 Picture Showing the Experimental Setup Used for the Laboratory Tests of the Flat-Slab Specimens

8.2.2 Loading Sequence

The flat-slab specimens were initially loaded to form cracks before the CFRP composite systems were bonded. A load equal to 7 kip was applied to the specimens. This load approximated the service-load moments in the slab for the prototype bridge. Therefore, the strains in the reinforcing bars were assumed to be equal in the test specimens and the prototype bridge under service conditions. In

this way, cracks in the laboratory specimens were assumed to have approximately the same widths as cracks present in the prototype bridge

The composite systems were bonded to the specimens after the initial cracking test. The composite systems were cured for 7 days at ambient temperature. After curing, the flat-slab specimens were tested to failure.

The test to failure was conducted applying 2 cycles to predetermined load stages. The load that was used during the cracking test (7 kip) was initially applied to compare the strengthened specimen response (stiffness and reinforcement strains) with the unstrengthened behavior. The load was then increased until first yielding of the longitudinal reinforcement was observed. The load-level at yield was defined as the point on the load-deflection curve where an apparent reduction in stiffness was observed. This load was approximately equal to 34 kip in both specimens. Finally, the load was increased until failure of the specimens by CFRP composite debonding. Table 8.1 summarizes the load-levels and number of cycles used during testing of the Flat-Slab Specimens.

Table 8.1 Applied Moments and Loads During Testing

| Load Stage | Moments in Test Specimen | | Total Applied Load, kip | # of Cycles |
|------------|--------------------------|----------------------|-------------------------|-------------|
| | Dead Load, kip-ft | Applied Load, kip-ft | | |
| 1 | 59.4 | 35 | 7 | 2 |
| 2 | 59.4 | 170 | 34 | 2 |
| 3 (FS-1) | 59.4 | 270 | 54 | 1 |
| 3 (FS-2) | 59.4 | 285 | 57 | 1 |
| 4 (FS-1) | 59.4 | 201 | 40.2 | 1 |
| 4 (FS-2) | 59.4 | 184 | 36.7 | 1 |

Note: Load Stage 1: Service Live Load.

Load Stage 2: Yield Load.

Load Stage 3: Ultimate Load.

Load Stage 4: Maximum Load in Bare Specimen.

Failure of the flat-slab specimens was defined by debonding of the CFRP composite systems. After failure, both specimens retained the strength of the bare reinforced concrete slab because the maximum usable concrete strain, ϵ_{cu} , had not been reached. At this point, the specimens were unloaded to zero and reloaded

until initiation of concrete crushing on the slab top was observable to measure the strength of the bare reinforced concrete section.

8.2.3 Instrumentation

The flat-slab specimens were instrumented to measure deflections, strains on different materials and total load applied during the tests. The voltage outputs from all the instruments were collected and recorded every 4 seconds using a Hewlett Packard (HP-75,000) data acquisition unit.

The instrumentation used in the flat-slab specimen tests was similar to the one employed for the pan-joint specimens. The total load was measured using a 200-kip Interface load cell. Deflections were measured using either 2-in. or 6-in. linear potentiometers at different locations on the specimens. Strains were monitored at four instrumented sections on the steel reinforcement, concrete surface, and CFRP composites.

Linear potentiometers were attached at midspan and at sections under the points of load application on the east and west sides of the specimens. The ends of the specimens were also instrumented with potentiometers to determine the end rotation during the tests. All instruments had a resolution of 0.001 in. Table 8.2 summarizes the location of linear potentiometers on the Flat-Slab Specimens.

Table 8.2 Displacement Limits of Linear Potentiometers

| Test Specimen | Side | North Load Point | Mid-span | South Load Point | End Diaphragms |
|----------------------|-------------|-------------------------|-----------------|-------------------------|-----------------------|
| FS-1 and FS-2 | East | 2 in. | 6 in. | 2 in. | 2 in. |
| | West | 2 in. | 6 in. | 2 in. | 2 in. |

Four sections along the span were instrumented using electric resistance strain gages. Each instrumented section had strain gages attached to 3 bars on the bottom longitudinal reinforcement, to 3 points on the concrete slab, and to 4 points on the CFRP composite plates or sheets. Table 8.3 lists the characteristics of the strain gages used for the Flat-Slab Specimen tests. Additional technical specifications are contained in Appendix A.

Table 8.3 Characteristics of Strain Gages

| Material | Strain Gage Type | Gage Length, mm |
|-----------------|-------------------------|------------------------|
| Steel | Foil | 6 |
| CFRP | Foil | 6 |
| Concrete | Wire | 60 |

The position of linear potentiometers and the location of the sections instrumented with strain gages are presented in Figure 8.2. Figure 8.3 shows the

position of strain gages bonded to the steel reinforcement (#6 bars) and concrete surface for Specimens FS-1 and FS-2. The position of strain gages on the CFRP composite systems for each Flat-Slab Specimen is illustrated in Figure 8.4.

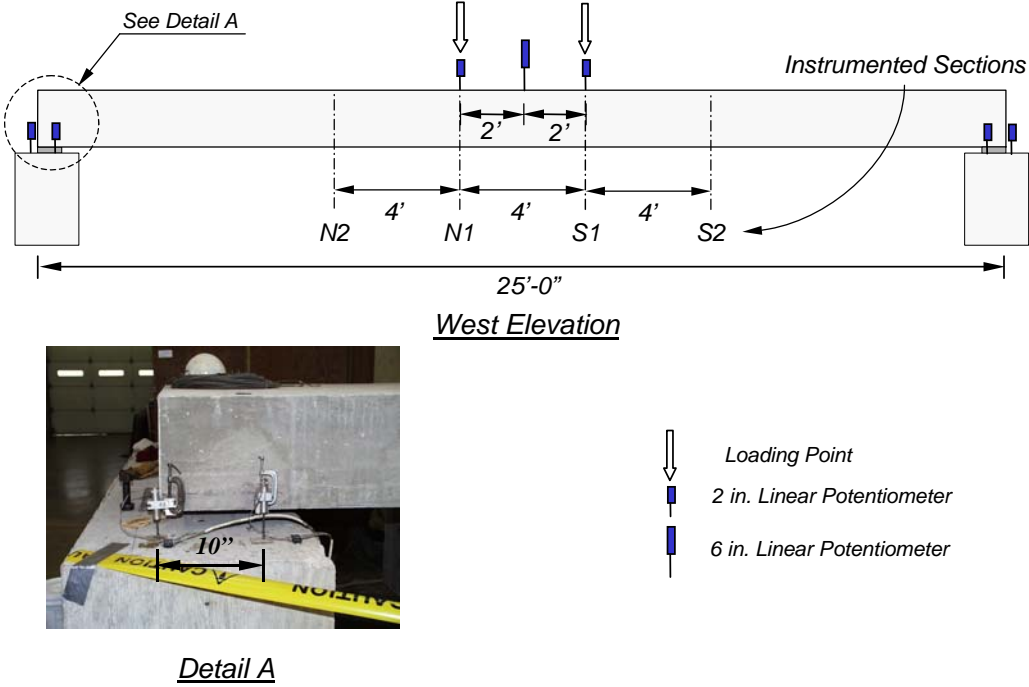
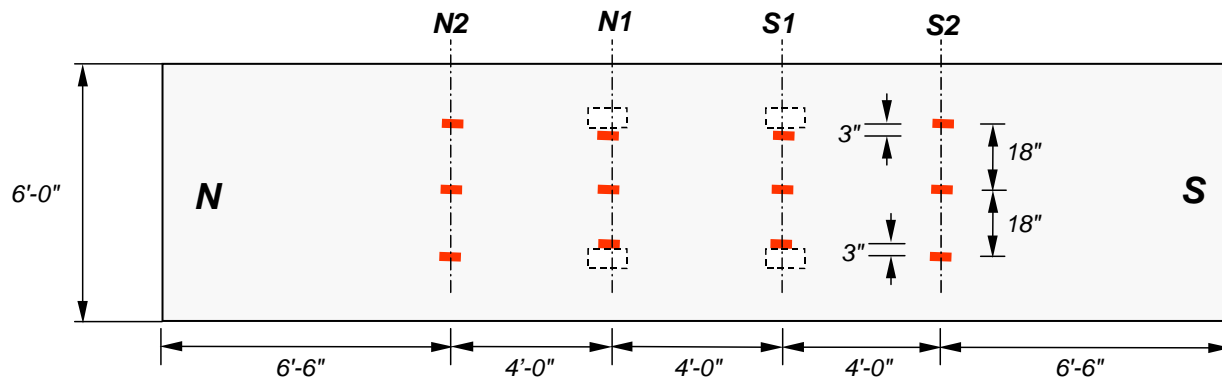
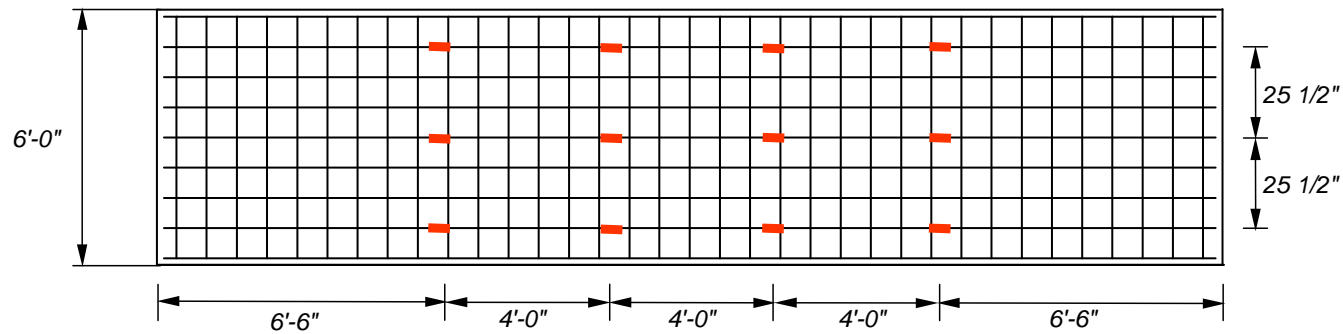


Figure 8.2 Position of Linear Potentiometers on East and West Sides and Location of Instrumented Sections in Flat-Slab Specimens



a) Position of Strain Gages on Concrete Slab (Plan)

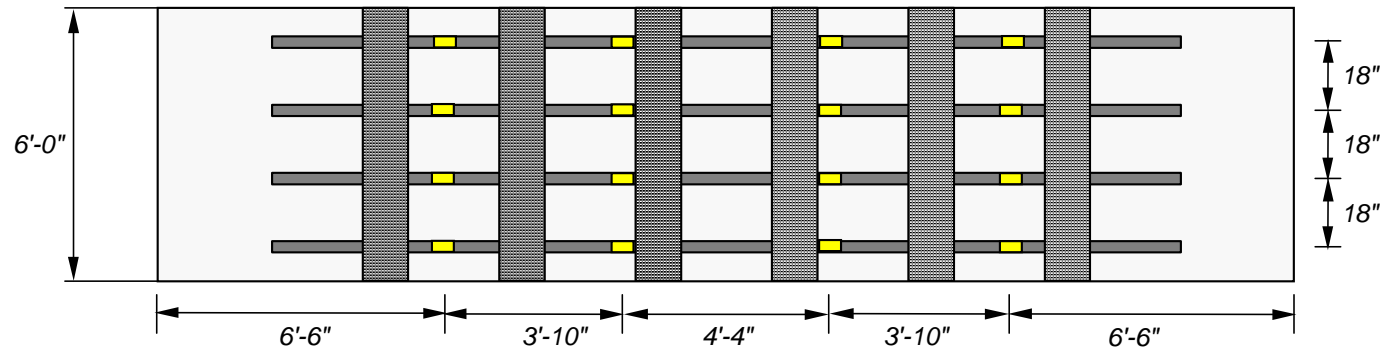


b) Position of Strain Gages on Bottom #6 Steel Reinforcement (Plan)

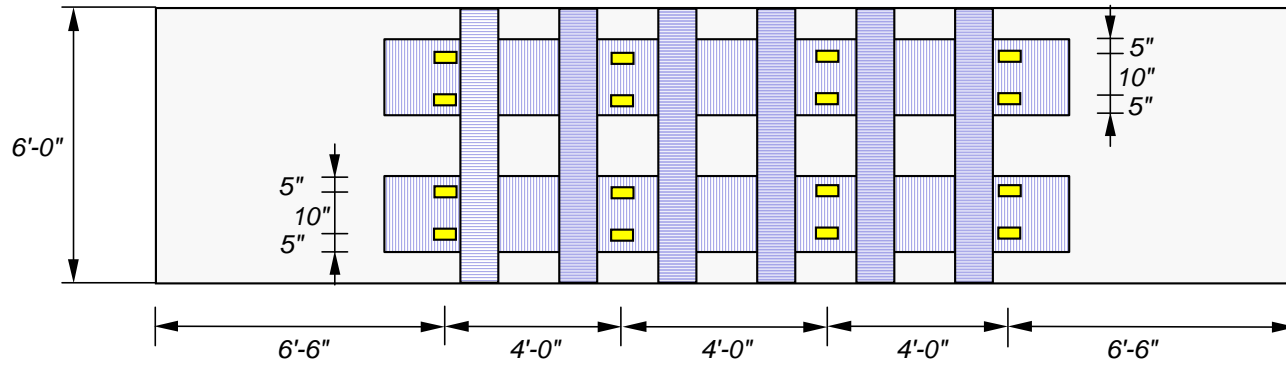
□ Position of Bearing Pads

■ Strain Gage

Figure 8.3 Position of Strain Gages on the Reinforcement and Concrete Surface in Specimens FS-1 and FS-2



a) Position of Strain Gages on CFRP Plates in Specimen FS-1 (Bottom View)



b) Position of Strain Gages on CFRP Sheets in Specimen FS-2 (Bottom View)

■ Strain Gage

Figure 8.4 Position of Strain Gages Bonded to the CFRP Composite Systems in Specimens FS-1 and FS-2

8.3 OBSERVED BEHAVIOR DURING TESTS

The observed behavior of the specimens during testing is described in this section. The concrete cracking that was observed on the side faces of the specimens at different load levels is presented. Representative outputs from the instruments are also discussed.

8.3.1 Description of Failure Sequence and Cracking Distribution

(a) Specimen FS-1

Cracks were marked and measured on the sides of the specimen after the application of 2 cycles to load-stage 1 (7 kip) on the unstrengthened specimen. The cracks formed across the bottom surface of the specimen and extended 6 in. towards the top surface on both sides. Cracking was visible on the sides in a region extending to sections N2 and S2. Cracks were spaced at approximately 6 to 8 in. throughout this region (Figure 8.5).

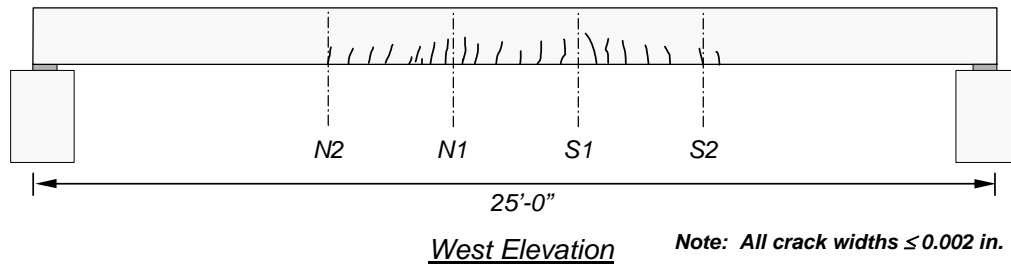


Figure 8.5 Typical Cracking Distribution after Load Cycles to 7 kip on Specimen FS-1 before CFRP Strengthening

After strengthening, cracks on Specimen FS-1 were marked and measured on the sides at load-stage 2 (34 kip). The cracking pattern on the west side is shown in Figure 8.6. CFRP debonding was not observed along the CFRP plates up to this load stage.

Initial debonding of the CFRP plate could not be determined by visual inspection because the plates were bonded to the bottom surface of the specimen. However, cracking sounds indicating initial debonding were heard at a load equal to 47 kip. Debonding initiated at midspan and proceeded toward the north end of the plates.

At a load of 54 kip, there was a sudden reduction of load to 53 kip accompanied by a cracking sound. The peak load was never reached again and debonding of the two east plates took place on the north end of the specimen. The load was maintained at approximately 44 kip for several minutes and finally the two west plates debonded from the bottom, at the north end of the specimen.

A picture illustrating the bottom view of the test specimen after CFRP debonding is shown in Figure 8.7. As the plates debonded, the woven CFRP-transverse sheets were pulled off the concrete surface along almost the entire width of the slab. Approximately two-thirds of the plates debonded longitudinally from the surface leaving only the plates attached on the south side of the specimen.

Some areas of the plates delaminated leaving pieces of carbon fibers attached to the concrete surface, particularly near the ends of the plates. A detail showing plate delamination and the concrete surface where the CFRP plate was bonded is presented in Figure 8.9. A drawing illustrating the areas on the slab bottom surface where the plates debonded is shown in Figure 8.10.

The load dropped to approximately 33 kip after CFRP debonding occurred. However, the specimen still retained its unstrengthened load-carrying capacity because the maximum usable concrete strain had not been reached. Loading was stopped when concrete crushing was observed at sections N1 and S1.

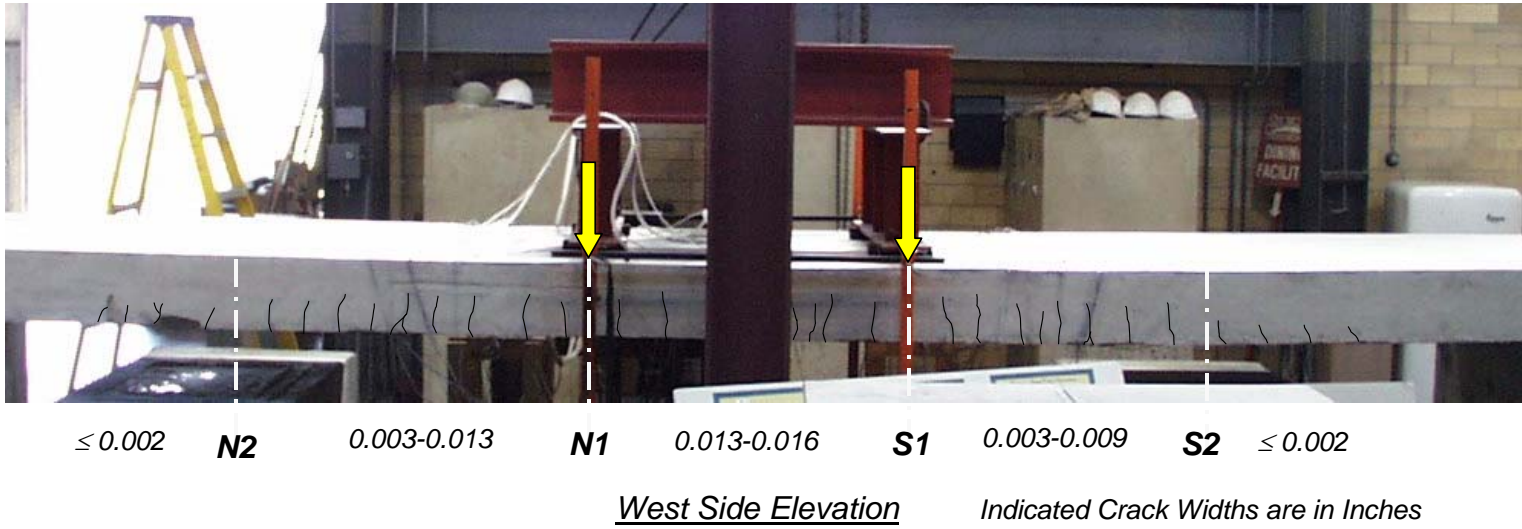


Figure 8.6 Cracking Pattern of Specimen FS-1 at Load Stage 2 (34 kip)



Figure 8.7 Bottom View Toward North End of Specimen FS-1 after CFRP-Plate Debonding



Figure 8.8 South End of the CFRP Plates Still Attached After Failure of Specimen FS-1



Figure 8.9 Evidence of Plate Delamination of the East CFRP Plate at the North End of Specimen FS-1

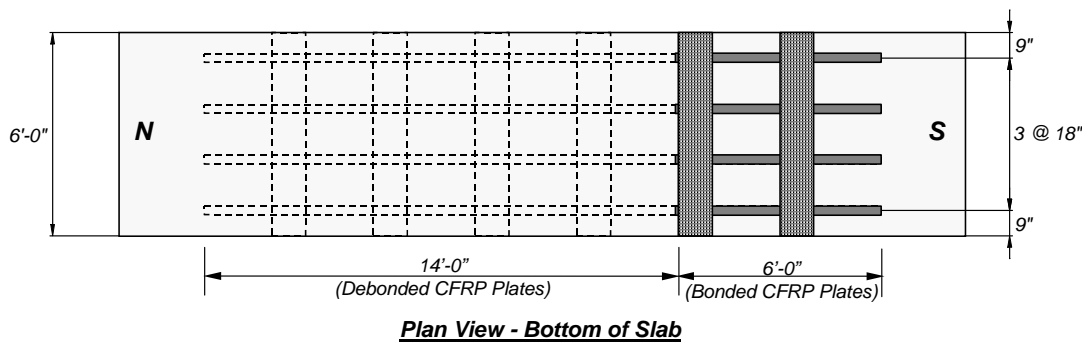


Figure 8.10 Extent of Debonding of CFRP Plates on Specimen FS-1

(b) Specimen FS-2

The response and cracking pattern of Specimen FS-2 during the initial cracking cycles was similar to Specimen FS-1 (Figure 8.5) except that cracks did not form at sections N2 and S2 in this specimen. After the load was increased to

the observed specimen yield, cracks were marked and measured. A picture illustrating the cracking pattern and widths is shown in Figure 8.11. The cracks in this figure have been remarked for clarity.

Initial debonding along the sides of the west CFRP sheet was observed at load stage 2 in a localized area near section N1 where the concrete surface had a small indentation (Figure 8.12). The formation of white lines along the carbon fiber direction in the sheets that were oriented transversely was also apparent at this load level. These lines gave an indication of epoxy cracking on the transverse sheets as the longitudinal laminates began to pull-off from the concrete surface.

As the applied load was increased to 57 kip, debonding of the CFRP sheet progressed toward the north end until the sheet detached completely from the concrete surface. A bottom view of the west CFRP sheet is seen in Figure 8.13. The deformation and splitting experienced by the transverse sheets after debonding can be observed in Figure 8.14. Similarly, the east sheet debonded toward the south end of Specimen FS-2. Only a portion on the north end of CFRP sheet remained attached to the concrete surface. The extent of CFRP sheet debonding at failure is indicated in Figure 8.15.

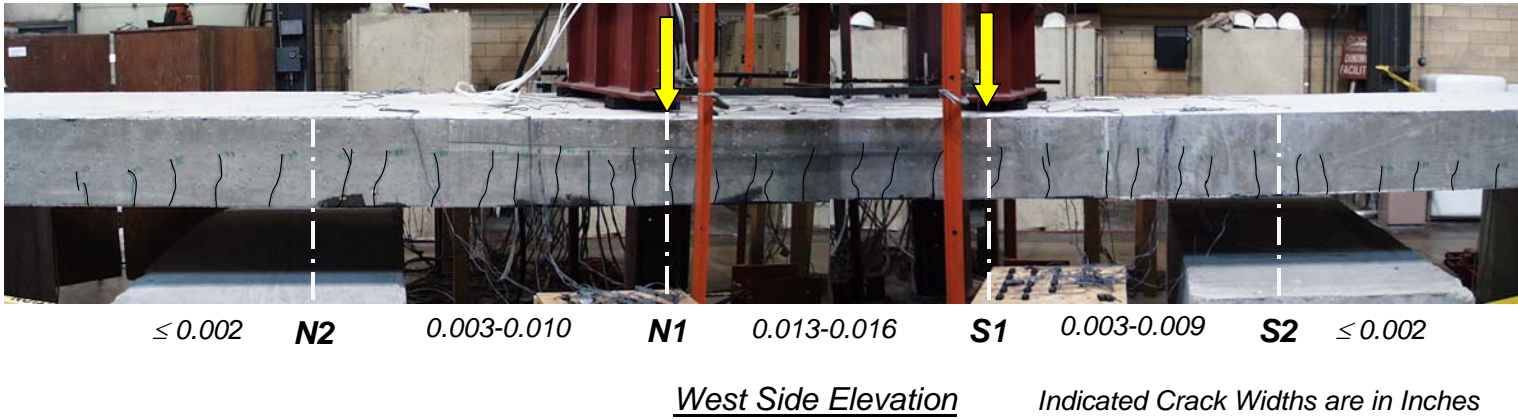


Figure 8.11 Cracking Pattern of Specimen FS-2 at Load Stage 2 (34 kip)

After debonding the load dropped to 32 kip. The specimen was unloaded and reloaded until concrete crushing initiated on top of the slab. Figure 8.16 illustrates the deformation typical of both Flat-Slab Specimens at initiation of concrete crushing.



Figure 8.12 Initiation of Debonding Along CFRP Sheet



Figure 8.13 View of West CFRP Sheet after Debonding from Specimen FS-2

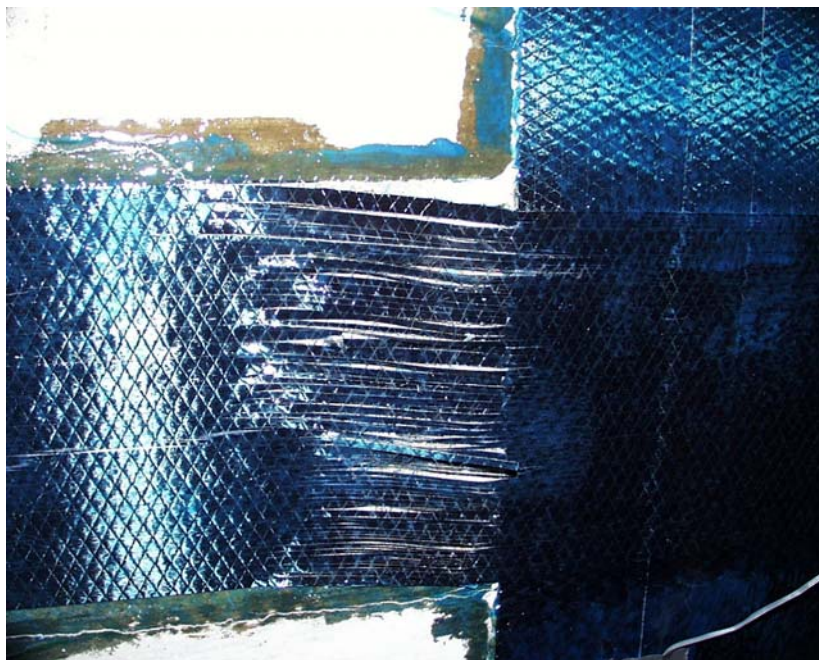


Figure 8.14 Deformation and Splitting of Transverse Sheet Caused by Movement of the Longitudinal Sheet

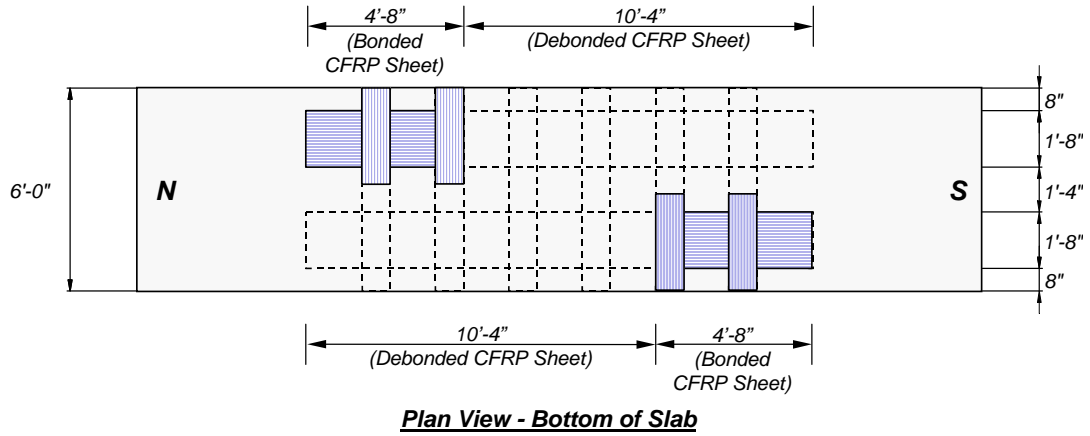


Figure 8.15 *Bottom View of Specimen FS-2 Indicating the Extent of Debonding of CFRP Sheets*



Figure 8.16 *West Side View of Specimen FS-2 at Ultimate Deformation Corresponding to Initiation of Concrete Crushing*

8.4 MEASURED RESPONSE

The recorded readings of representative instruments during the Flat-Slab Specimen tests are presented in this section. These readings were plotted against the applied load to verify that the instruments were operating properly throughout the tests.

8.4.1 Deflection Measurements

Plots showing the deflection response are illustrated in Figures 8.17 to 8.19 for Specimen FS-1 and in Figures 8.20 to 8.22 for Specimen FS-2. The instruments on sections N1 and S1 were removed at a load of approximately 47 kip. Their stroke capacity was exceeded and it was considered too dangerous for research staff to reposition them. Midspan potentiometers were repositioned at yield and left in place until failure.

The deformations at the supports are presented in Figure 8.17 for Specimen FS-1 and Figure 8.20 for Specimen FS-2. With these measurements the average bearing deformation was subtracted from the specimen deflections. The deflection readings of instruments at midspan, and sections N1 and S1 were corrected by subtracting the average support deflections for Specimens FS-1 and FS-2, respectively.

The plots show readings taken on the east and west sides of the specimens. The similarity in these plots indicates that the specimens did not twist during the

tests. Also, the deflection measurements taken at symmetric sections (sections N1 and S1) about the specimen centerlines are comparable (Figures 8.18 and 8.21). Therefore, the average deflection was used in the comparison with the calculated response presented in Chapter 9.

The measured deflection response of both specimens shows three distinct regions defined by the slope of lines tangent to the load-deflection curves. Although the specimens were previously cracked before running the test to failure, the curves show an initial steep slope. This is due to a stiffening effect from the CFRP composites. The global stiffness reduced to the fully cracked section stiffness at approximately 15 kip. The final change in slope observed in the load-deflection diagrams took place at load-stage 2, when the specimens reached yield of the main longitudinal reinforcement.

The post-yield slope observed in the load-deflection diagrams is steeper than expected for a conventionally reinforced concrete element. Instead of having an almost constant load after load-step 2, Specimens FS-1 and FS-2 exhibited a significant increase in load with increasing deflection. This behavior is attributable to the tensile stresses that were developed by the CFRP composites after yielding of the steel reinforcement.

Tables 8.4 and 8.5 show measured response parameters at different load stages for Specimens FS-1 and FS-2, respectively. The deflections listed in these

tables were measured at mid-span and were corrected by subtracting the average support displacements. The strains were calculated averaging the measured values at Sections N1 and S1 (maximum moment sections).

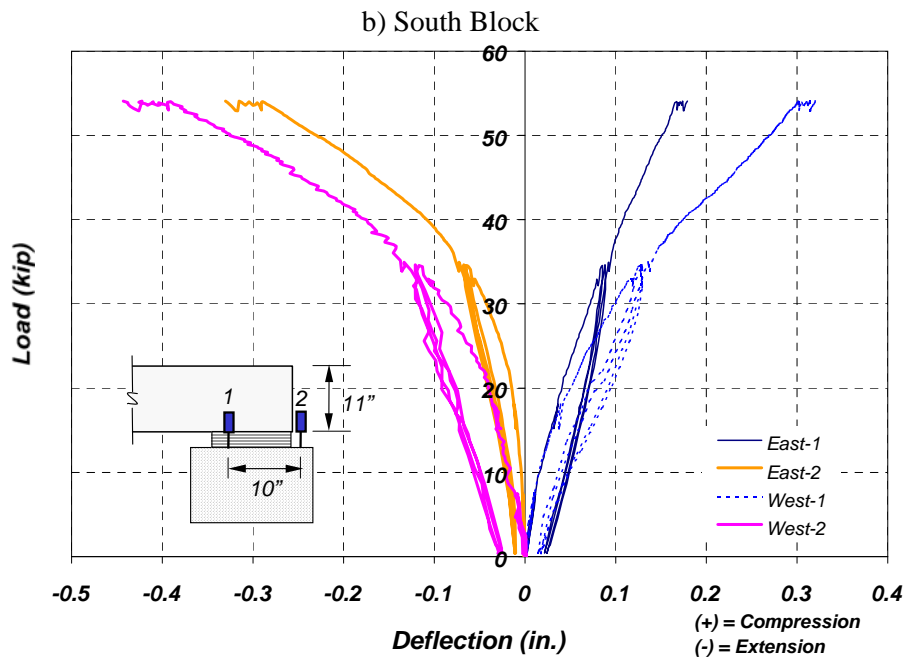
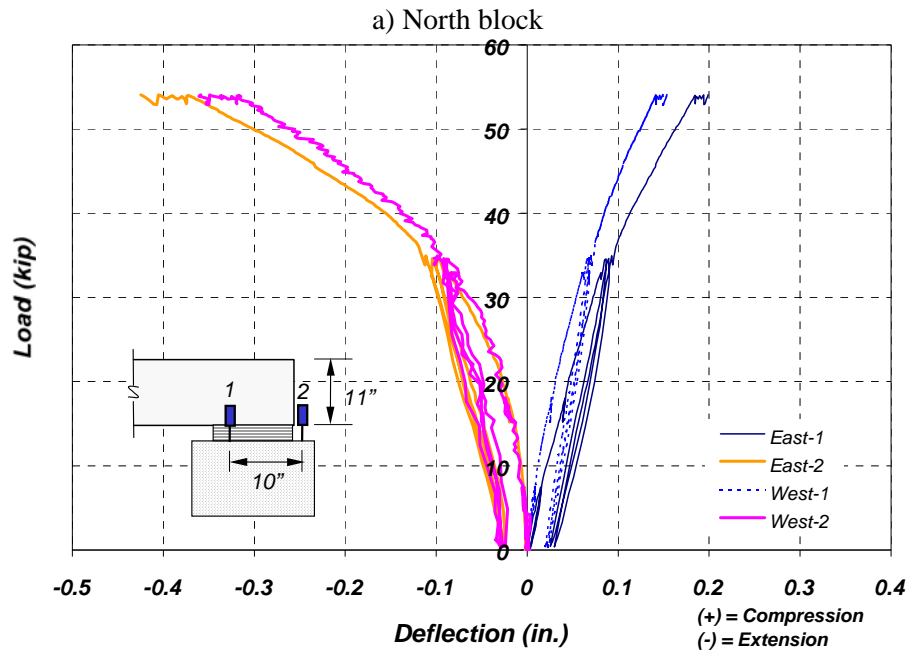


Figure 8.17 Measured Displacements at Supports in Specimen FS-1

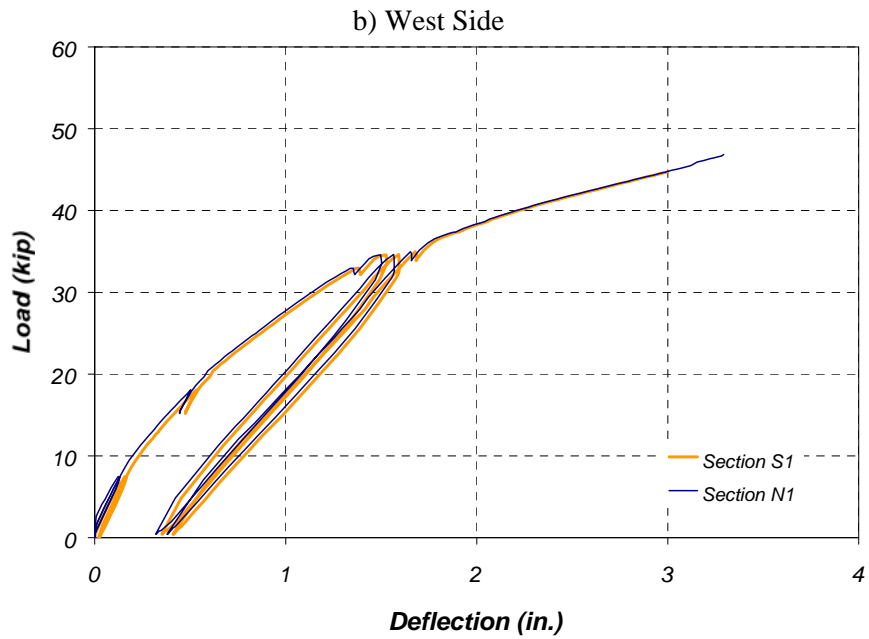
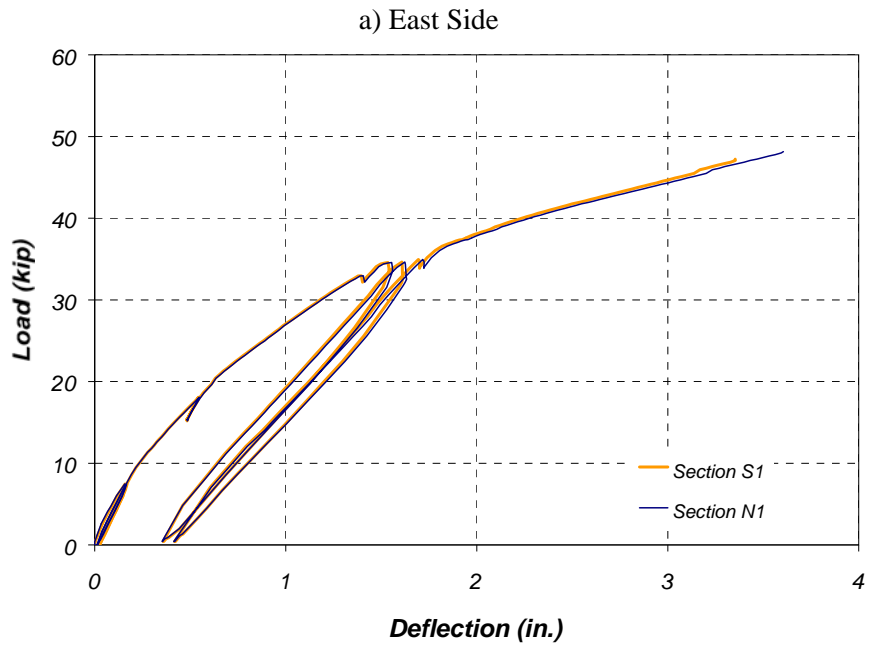


Figure 8.18 Measured Deflections at Sections N1 and S1 in Specimen FS-1

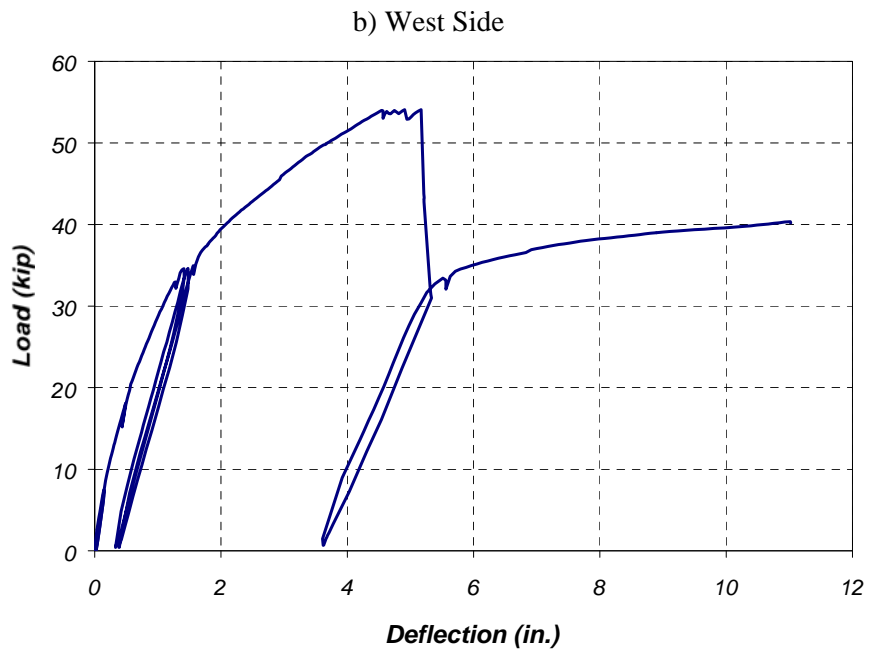
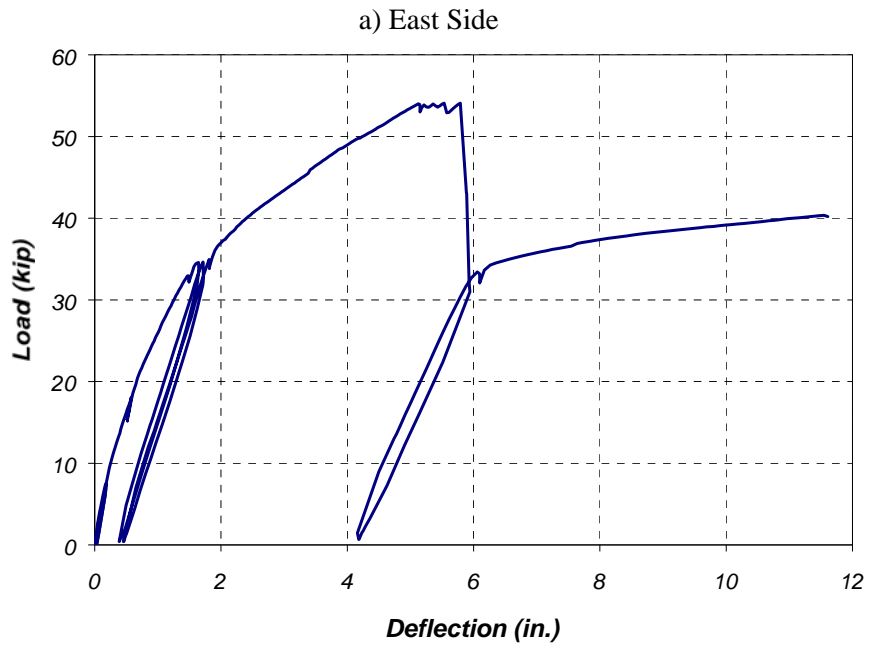


Figure 8.19 Measured Deflections at Mid-Span in Specimen FS-1

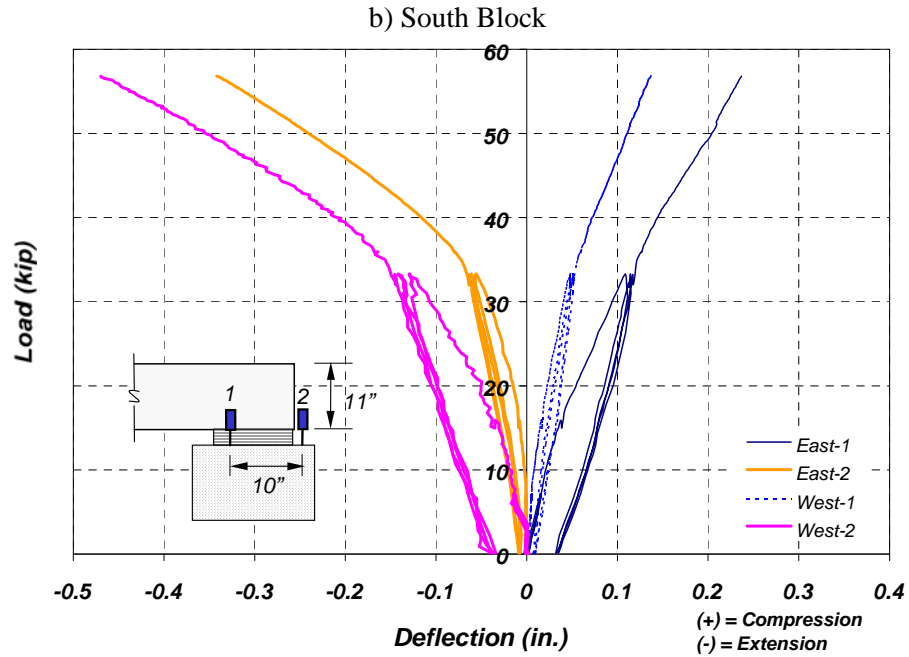
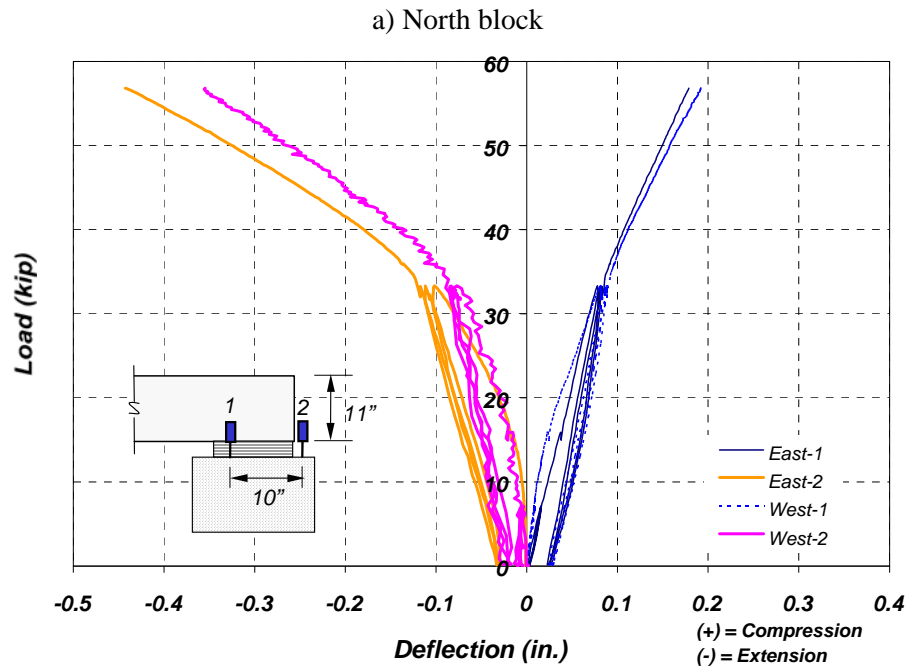


Figure 8.20 Measured Displacements at Supports in Specimen FS-2

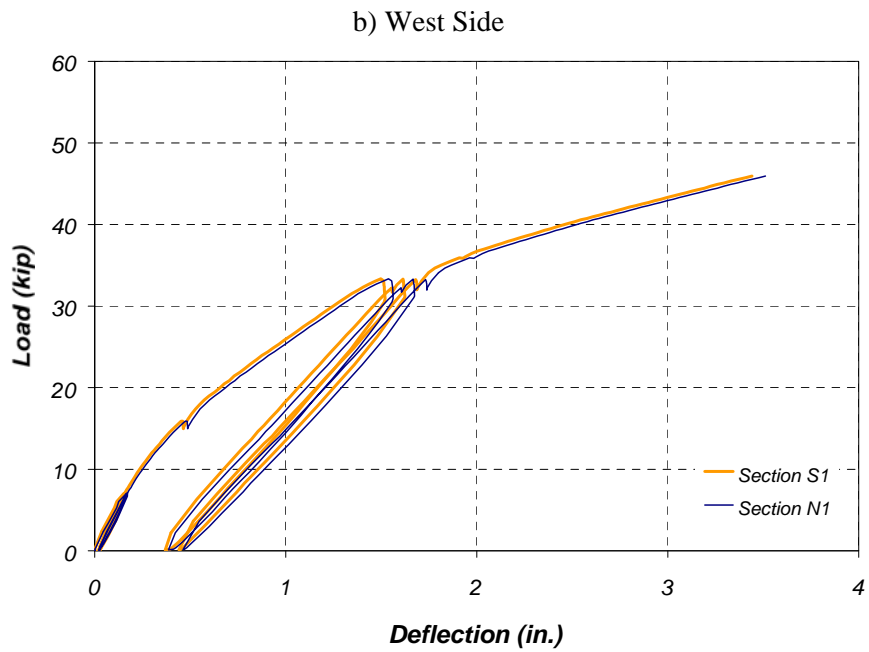
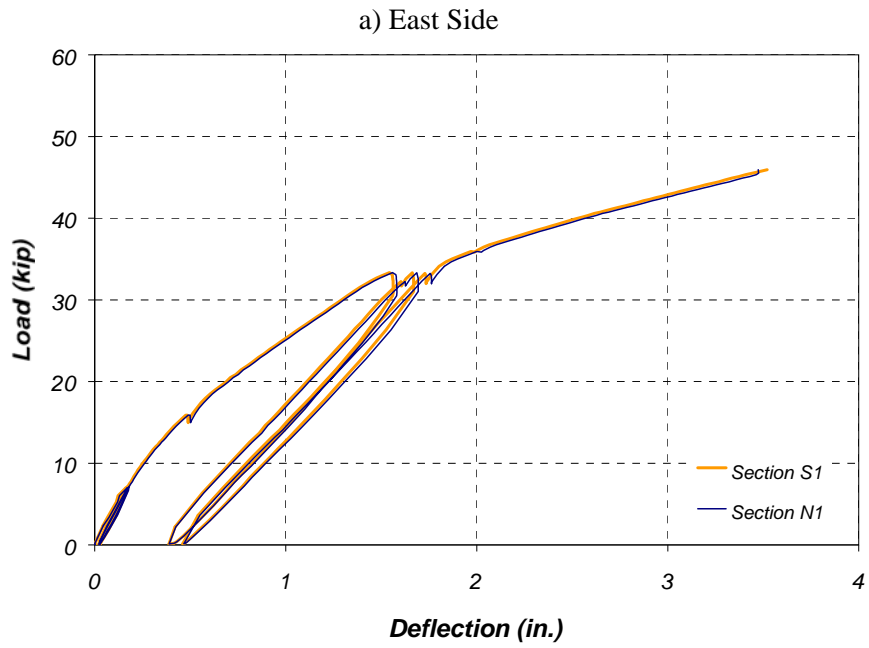


Figure 8.21 Measured Deflections at Sections N1 and S1 in Specimen FS-2

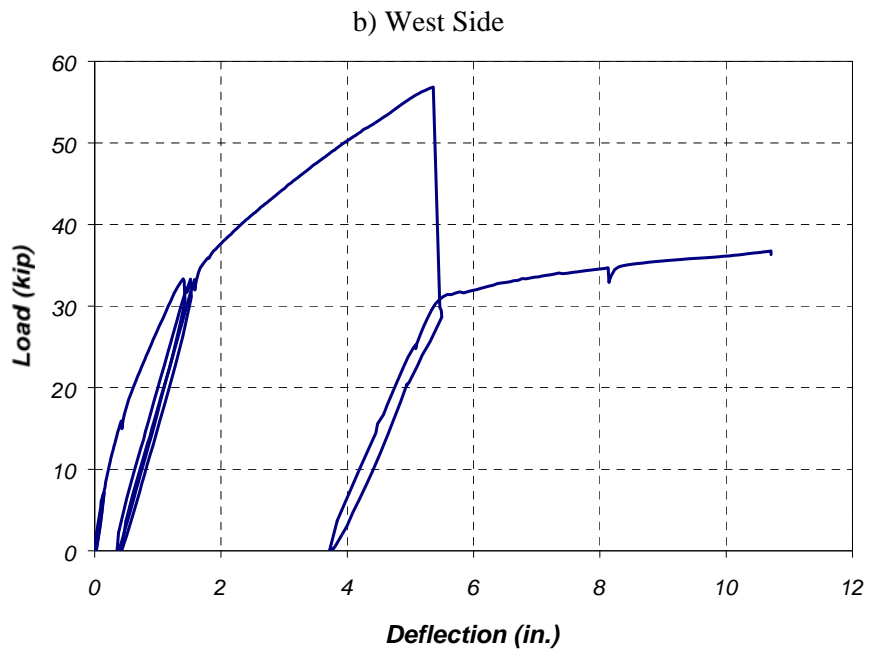
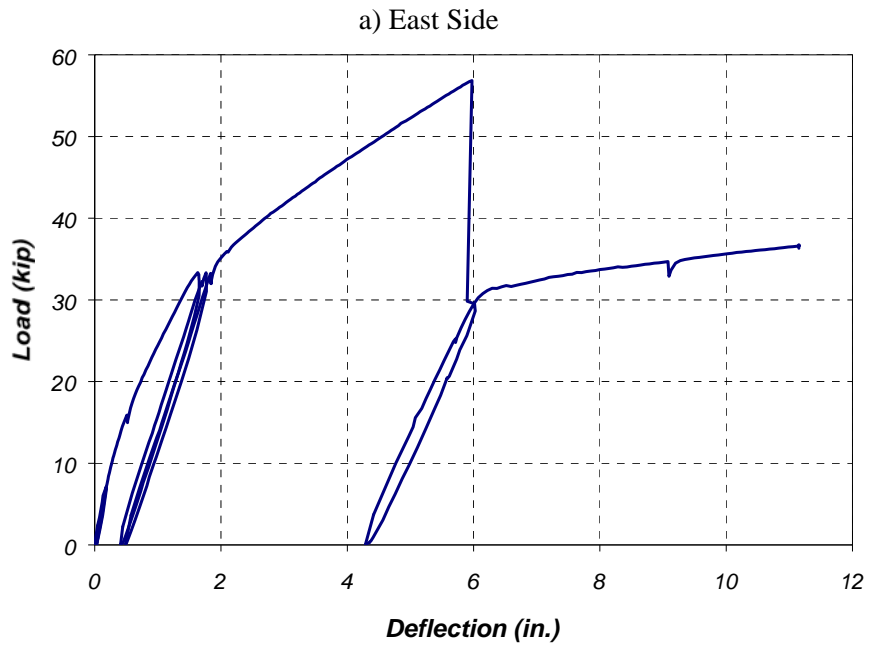


Figure 8.22 Measured Deflections at Mid-Span in Specimen FS-2

Table 8.4 Maximum Response Measured During Testing of Specimen FS-1

| Load Stage | Maximum Measured Parameters | | | Maximum Average Strain (Microstrain) | | | Notes |
|------------|-----------------------------|-------------------|--------------------|---|----------|----------------|---|
| | Load, kip | Moment, kip-ft | Deflection, in. | Reinforcement | Concrete | CFRP Plates | |
| 1A | 7 | 35 | 0.36 | 418 | 166 | - | Reinforced concrete specimen before application of CFRP |
| 1B | 7 | 35 | 0.16 | 155 | 80 | 233 | Reinforced concrete slab with CFRP plates |
| 2 | 34 | 170 | 1.53 | 2,062 | 640 | 2,152 | Observed yielding of longitudinal reinforcement |
| 3 | 54 | 270 | 5.48 | 5,390 | 2,055 | 6,392 | Debonding of CFRP plates |
| 4 | 40.2 | 200 | 11.31 | * | 3,204 | * | Capacity of bare reinforced concrete slab |

* Readings were unavailable because gages were damaged after CFRP debonding

Table 8.5 Maximum Response Measured During Testing of Specimen FS-2

| Load Stage | Maximum Measured Parameters | | | Maximum Average Strain (Microstrain) | | | Notes |
|------------|-----------------------------|-------------------|--------------------|---|----------|----------------|---|
| | Load, kip | Moment, kip-ft | Deflection, in. | Reinforcement | Concrete | CFRP Sheets | |
| 1A | 7 | 35 | 0.36 | 383 | 127 | - | Reinforced concrete specimen before application of CFRP |
| 1B | 7 | 35 | 0.16 | 184 | 87 | 254 | Reinforced concrete slab with CFRP sheets |
| 2 | 34 | 170 | 1.52 | 3,198 | 703 | 1,892 | Observed yield of longitudinal reinforcement |
| 3 | 57 | 285 | 5.67 | 8,154 | 2,222 | 7,473 | Debonding of CFRP sheets |
| 4 | 36.7 | 184 | 10.93 | 6,011 | 3,171 | * | Capacity of bare reinforced concrete specimen |

* Readings were unavailable because gages were damaged after CFRP debonding

8.4.2 Strain Gage Measurements

The strains measured on the steel reinforcement, CFRP composites and concrete surface were used to compute internal stresses and forces and to determine the location of the neutral axis at various load stages. The procedures to determine the moment-curvature response using the strain gage are presented in [Chapter 9](#). Load vs. average strain plots for sections N1 and N2 are presented in this section. The characteristics of these plots were the similar for the mirror sections (S1 and S2) on the south side of the specimens. The recorded output from all the instruments can be found in Appendix D. Further discussion on the measured strain response is presented in [Chapter 9](#).

The average measured strains were calculated using the readings from gages that were giving reliable outputs up to a specific load during the test. In some cases, the strain gages registered readings that were no longer reliable during the test so the outputs from these instruments were eliminated in the calculations. Strain gage debonding or wires being damaged during the test typically caused malfunction of strain gages.

(a) Strain Gage Readings in Specimen FS-1

Load vs. strain plots for sections N1 and N2 are presented in [Figures 8.23 and 8.24, respectively](#). These figures show the average measured strains on the reinforcing steel (#6 bars), on the CFRP pultruded plates, and on the concrete slab.

Figure 8.23(a) shows an increase in strain under constant load during cycling at load stage 2 (34 kip). This is due to the accumulation of plastic strains after reinforcement yielding. On the other hand, the average measured strains on the CFRP plates and concrete slab (parts (b) and (c)) remain approximately constant during cycling to 34 kip. Examination of Figure 8.24 indicates that the reinforcement did not yield at section N2. The measured strain on the reinforcement exhibits linear behavior until failure of the specimen.

The average measured strains on the CFRP plates are shown in part (b) of Figures 8.23 and 8.24 for sections N1 and N2, respectively. A comparison among the strains at sections N1 and N2 shows an interesting aspect of the behavior at the load corresponding to CFRP-plate debonding. It can be observed that as the plates began debonding at section N1 (Figure 8.23), the measured strains started to decrease. During CFRP-plate debonding, the measured strains decreased because deformations were distributed over a longer length of the plate. At the same time, measured strains in section N2 increased significantly without an increase in load as debonding approached this section. The average CFRP measured strains at both sections are similar just prior to total debonding of the composite plates.

The maximum average strain measured at section N1 on the concrete slab was approximately 0.0025 at debonding of the CFRP plates. This strain is below the value usually assumed as the maximum usable strain associated with concrete

crushing ($\epsilon_{cu} = 0.003$). Because of this, Specimen FS-1 was able to maintain its bare reinforced concrete strength after CFRP-plate debonding without collapsing.

(b) Strain Gage Readings in Specimen FS-2

The average measured strains on the reinforcing bars, CFRP sheets, and concrete surface are presented in [Figures 8.25 and 8.26](#) for sections N1 and N2, respectively. The measured strains on the reinforcement at Section N1 show a very large accumulation of plastic strains after cycling to 34 kip. This can be the consequence of a crack forming close to the instrument location. The reinforcing bar strains at section N2 remain fairly constant during cycling to 34 kip indicating that yielding did not reach this section (Figure 8.26).

Strains on the CFRP sheets are presented in part (b) of [Figures 8.25 and 8.26](#). The large reduction in slope at a load of approximately 25 kip at section N2 is attributable to specimen cracking. This change in slope is also observed in the reinforcing bar strain curve.

The maximum average strain measured on the concrete slab at section N1 before CFRP-sheet debonding was approximately 0.0024. As for Specimen FS-1, this strain is below the assumed maximum usable concrete strain of 0.003.

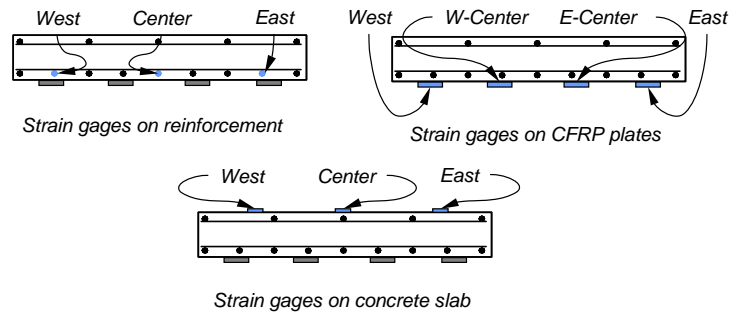
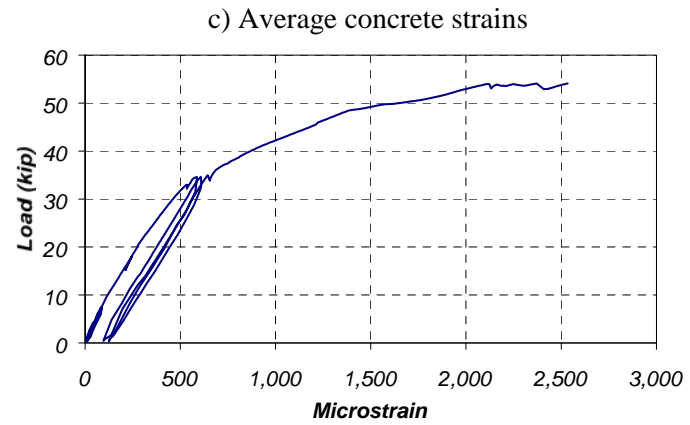
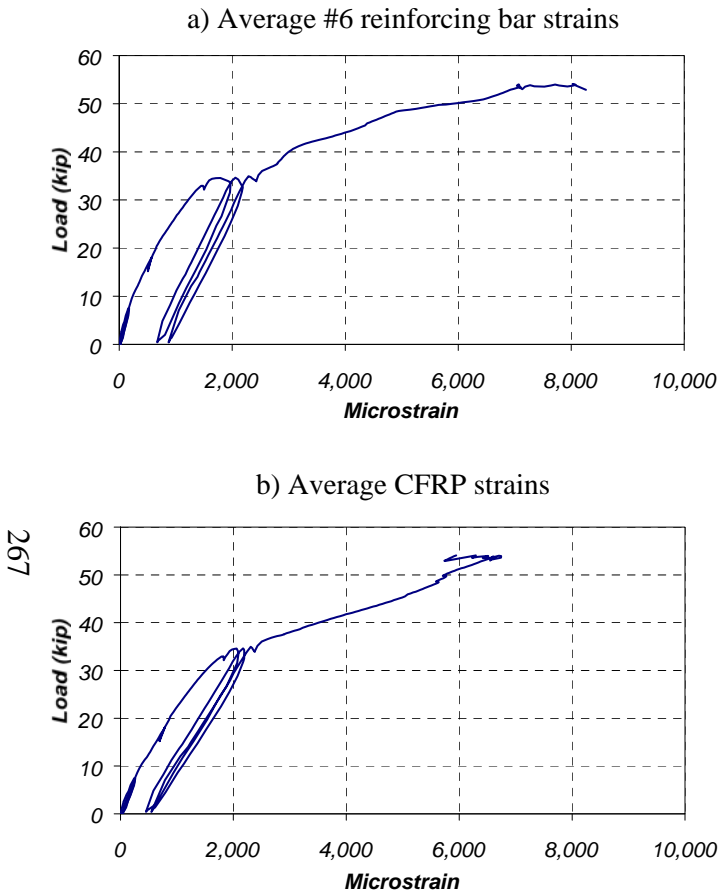


Figure 8.23 Average Strains Measured at Section N1 (Specimen FS-1)

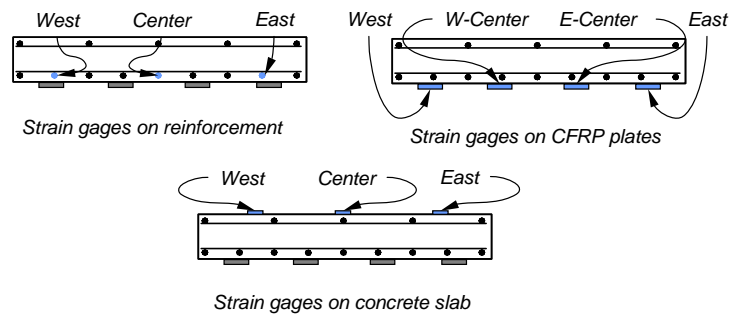
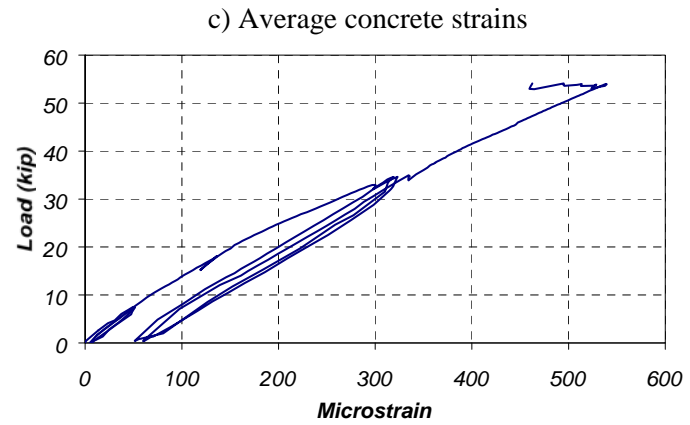
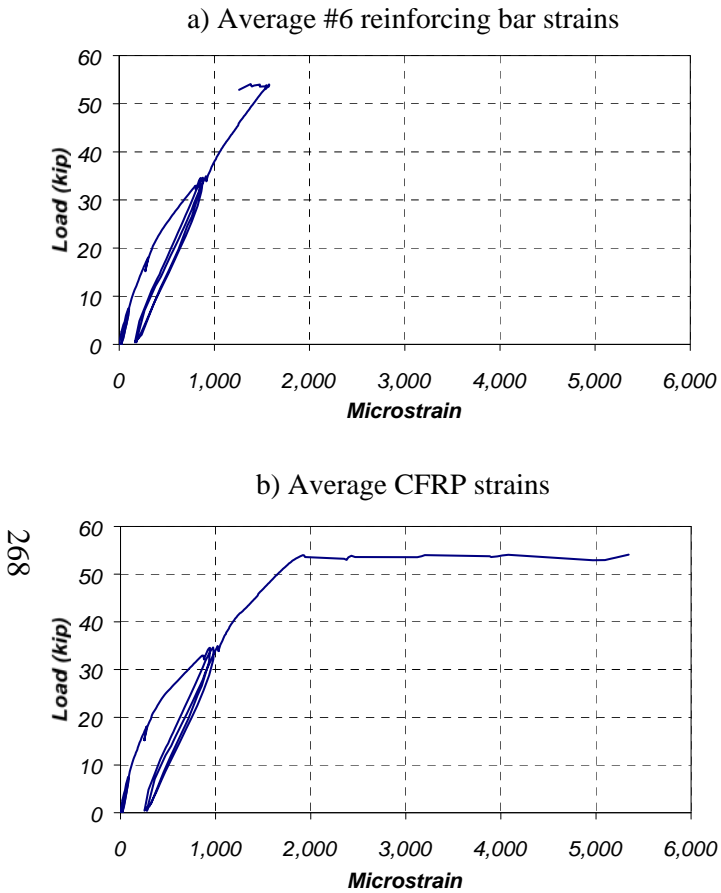


Figure 8.24 Average Strains Measured at Section N2 (Specimen FS-1)

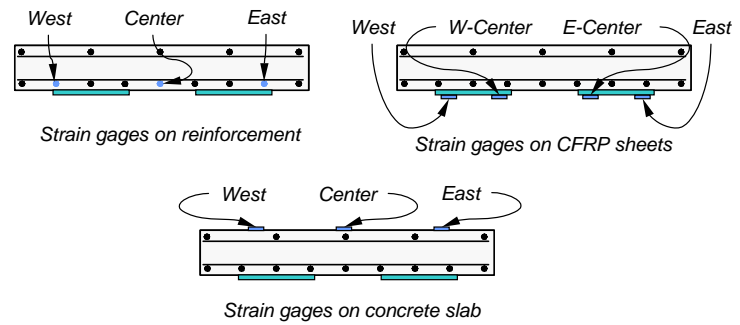
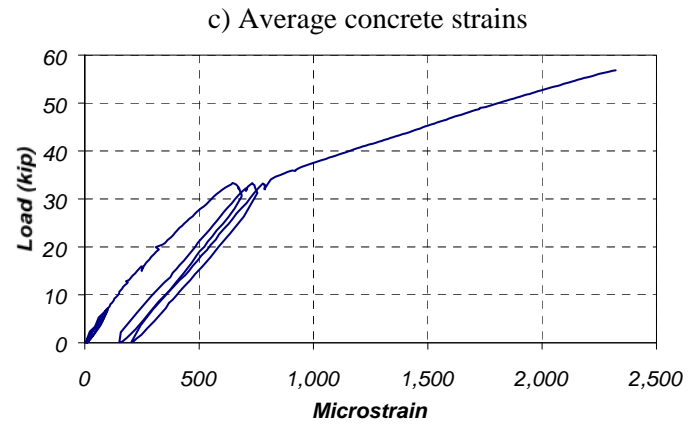
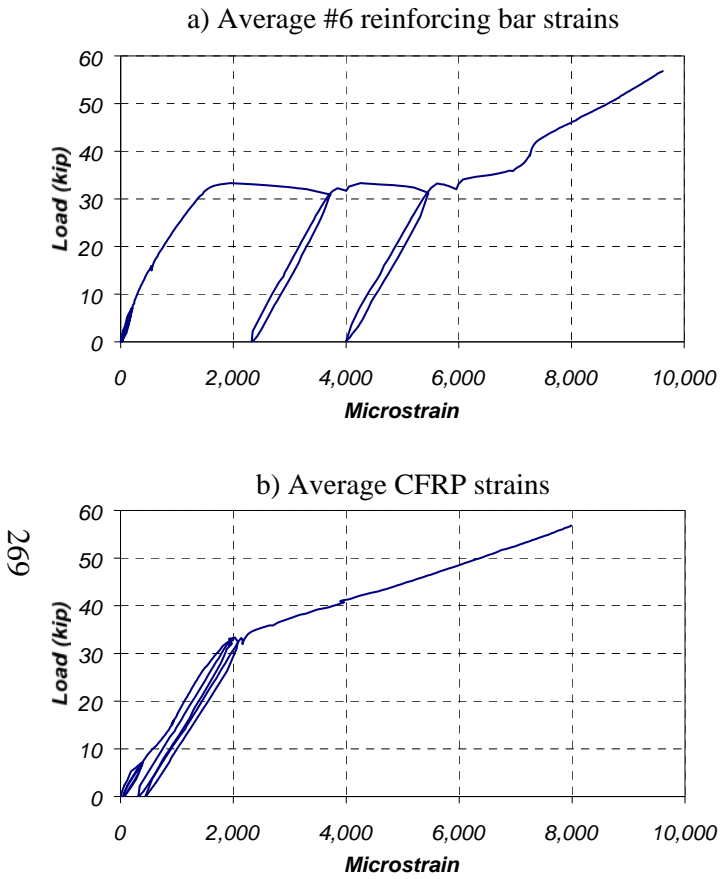


Figure 8.25 Average Strains Measured at Section N1 (Specimen FS-2)

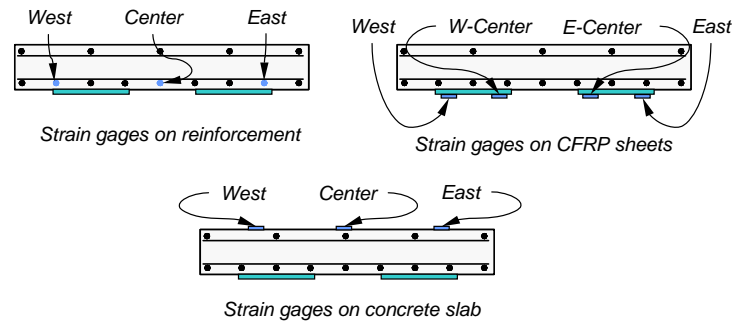
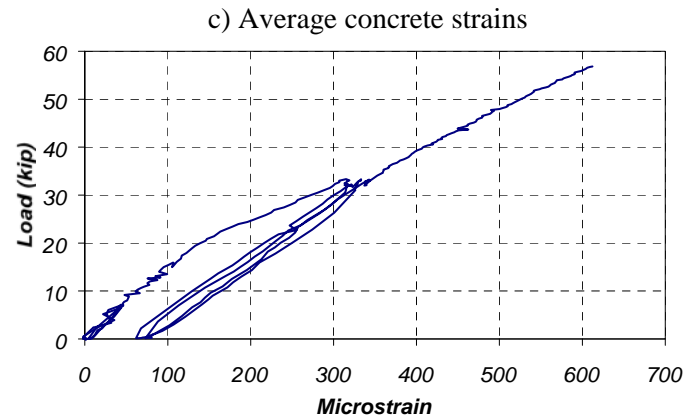
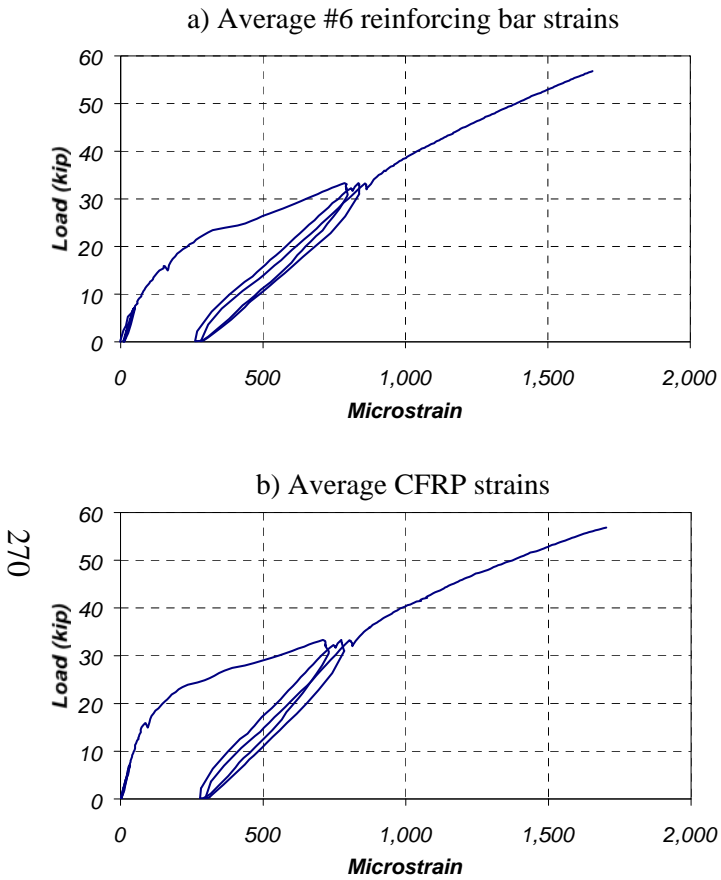


Figure 8.26 Average Strains Measured at Section N2 (Specimen FS-2)

8.5 SUMMARY

A description of the laboratory tests of two full-scale flat-slab specimens strengthened using different CFRP composite systems was presented in this chapter. The experimental setup, loading sequence, and test specimen instrumentation were also described. The specimen behavior and the failure sequence that were observed during the tests were discussed.

Representative outputs from instruments attached on the laboratory specimens were presented and discussed. These included the displacement and strain response of the specimens during testing. An evaluation of the measured response parameters of the flat-slab specimens is presented in [Chapter 9](#).

CHAPTER 8: MEASURED RESPONSE OF FLAT-SLAB SPECIMENS. 233

8.1 Introduction 233

8.2 Test Setup and Instrumentation 233

8.2.1 Description of Experimental Setup..... 233

8.2.2 Loading Sequence..... 234

8.2.3 Instrumentation 237

8.3 Observed Behavior During Tests..... 242

8.3.1 Description of Failure Sequence and Cracking Distribution 242

8.4 Measured Response..... 253

8.4.1 Deflection Measurements 253

8.4.2 Strain Gage Measurements 264

8.5 Summary 271

Figure 8.1 Picture Showing the Experimental Setup Used for the Laboratory Tests of the Flat-Slab Specimens 234

Figure 8.2 Position of Linear Potentiometers on East and West Sides and Location of Instrumented Sections in Flat-Slab Specimens 239

Figure 8.3 Position of Strain Gages on the Reinforcement and Concrete Surface in Specimens FS-1 and FS-2 240

Figure 8.4 Position of Strain Gages Bonded to the CFRP Composite Systems in Specimens FS-1 and FS-2 241

Figure 8.5 Typical Cracking Distribution after Load Cycles to 7 kip on Specimen FS-1 before CFRP Strengthening..... 242

Figure 8.6 Cracking Pattern of Specimen FS-1 at Load Stage 2 (34 kip) 245

Figure 8.7 Bottom View Toward North End of Specimen FS-1 after CFRP-Plate Debonding 246

Figure 8.8 South End of the CFRP Plates Still Attached After Failure of Specimen FS-1 246

Figure 8.9 Evidence of Plate Delamination of the East CFRP Plate at the North End of Specimen FS-1 247

Figure 8.10 Extent of Debonding of CFRP Plates on Specimen FS-1 247

Figure 8.11 Cracking Pattern of Specimen FS-2 at Load Stage 2 (34 kip) 249

Figure 8.12 Initiation of Debonding Along CFRP Sheet 250

Figure 8.13 View of West CFRP Sheet after Debonding from Specimen FS-2 251

| | |
|--|-----|
| Figure 8.14 Deformation and Splitting of Transverse Sheet Caused by Movement of the Longitudinal Sheet | 251 |
| Figure 8.15 Bottom View of Specimen FS-2 Indicating the Extent of Debonding of CFRP Sheets | 252 |
| Figure 8.16 West Side View of Specimen FS-2 at Ultimate Deformation Corresponding to Initiation of Concrete Crushing | 252 |
| Figure 8.17 Measured Displacements at Supports in Specimen FS-1 | 256 |
| Figure 8.18 Measured Deflections at Sections N1 and S1 in Specimen FS-1 | 257 |
| Figure 8.19 Measured Deflections at Mid-Span in Specimen FS-1 | 258 |
| Figure 8.20 Measured Displacements at Supports in Specimen FS-2 | 259 |
| Figure 8.21 Measured Deflections at Sections N1 and S1 in Specimen FS-2 | 260 |
| Figure 8.22 Measured Deflections at Mid-Span in Specimen FS-2 | 261 |
| Figure 8.23 Average Strains Measured at Section N1 (Specimen FS-1) | 267 |
| Figure 8.24 Average Strains Measured at Section N2 (Specimen FS-1) | 268 |
| Figure 8.25 Average Strains Measured at Section N1 (Specimen FS-2) | 269 |
| Figure 8.26 Average Strains Measured at Section N2 (Specimen FS-2) | 270 |
| | |
| Table 8.1 Applied Moments and Loads During Testing | 236 |
| Table 8.2 Displacement Limits of Linear Potentiometers | 238 |
| Table 8.3 Characteristics of Strain Gages | 238 |
| Table 8.4 Maximum Response Measured During Testing of Specimen FS-1 | 262 |
| Table 8.5 Maximum Response Measured During Testing of Specimen FS-2 | 263 |

Chapter 9: Verification of the Analytical Model Using the Measured Response of the Flat-Slab Specimens

9.1 INTRODUCTION

The analytical model developed in Chapter 3 is verified in this chapter by comparing the strains, curvatures, and displacements with the measured response of Specimens FS-1 and FS-2. Strains are discussed in Section 9.2, and moment-curvature response is presented in Section 9.3. Data from both these sections may be used to evaluate the strain at which the CFRP composites debond from the surface of the concrete. This information is needed to calculate the capacity of reinforced concrete members strengthened using CFRP composites. Displacement response is evaluated in Section 9.4. In general, the analytical models are able to represent the measured global response quite well; however, some of the local behavior was not well represented.

9.2 EVALUATION OF STRAIN RESPONSE

The same approach that was used for the pan-joist specimens was used for the flat-slab specimens to validate the analytical procedures developed in Chapter 3. Therefore, a detailed comparison of the calculated and measured strains was also conducted as a first step for these specimens.

Strains were measured on the reinforcing bars, on the top surface of the concrete, and on the surface of the CFRP composites during testing of Specimens FS-1 and FS-2. Measured data were presented in Chapter 8 and Appendix C, and those data are compared with the calculated response of the test specimens in this section. Strains due to dead loads are evaluated in Section 9.2.1, the variations of strain with distance from the neutral axis are discussed in Section 9.2.2. Calculated and measured strains in each of the three materials are compared in Section 9.2.3, and the strains at which the CFRP composites debonded from the surface of the concrete are evaluated in Section 9.2.4.

9.2.1 Strains due to Dead Loads

As for the pan-joint specimens, the strains caused by dead loads were calculated for the flat-slab specimens using the analytical model discussed in Chapter 3. Inclusion of dead-load strains was particularly important in this case because their effect was anticipated to have a greater impact on the response of these specimens due to the thinner cross section.

The dead-load moment was calculated by assuming a unit weight of concrete equal to 150 pcf and a span of 24 ft. The measured material properties (Appendix A) were used in these calculations. The calculated dead-load strains are reported in Table 9.1.

Table 9.1 Calculated Dead Load Strains

| M_{DL}, kip-ft | Strains, Microstrain | | Curvature, 1/in. | NA Depth, in. |
|-----------------------------------|---------------------------------|--------------|-----------------------------|------------------------------|
| | Concrete | Steel | | |
| Specimen FS-1 | | | | |
| 57.8 | 196 | 538 | 7.7×10^{-5} | 2.55 |
| Specimen FS-2 | | | | |
| 57.8 | 210 | 470 | 6.9×10^{-5} | 3.05 |

9.2.2 Measured Strain Profiles due to Live Loads

Measured strain profiles at sections N1 and S1 are shown in Figure 9.1 for Specimen FS-1. Similar plots are shown in Figure 9.2 for Specimen FS-2. The average strain in each material at each stage of loading is plotted as a function of the distance from the top of the specimen to the gage. Strain data for two additional load levels (20 and 50 kip) were also included to provide more information for applied load levels between the critical load stages.

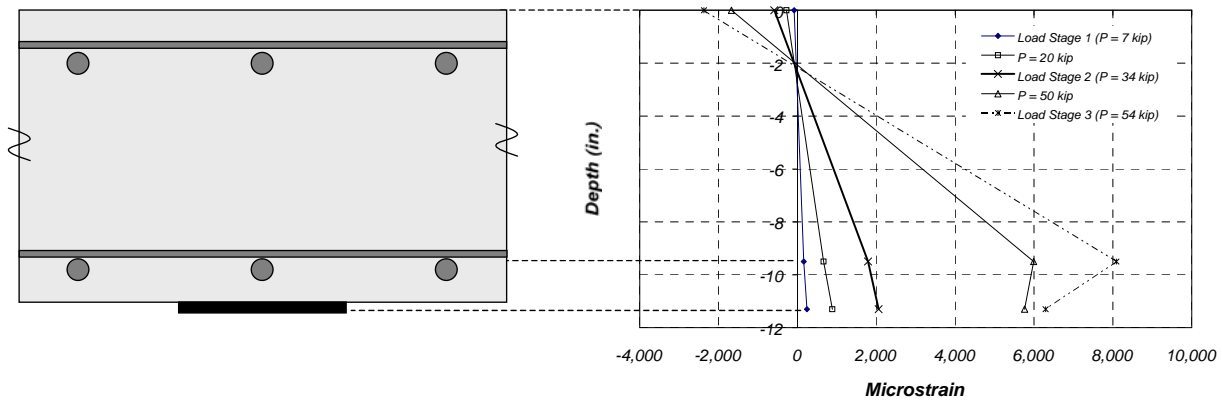
The strains in the two specimens were similar at these sections. The strain profiles were approximately linear up to yielding of the reinforcement (load stage 3). At the higher load levels, the strains in the CFRP composites tended to be lower than those expected using a linear distribution of strain. Debonding of the

CFRP composites from the surface of the concrete would tend to reduce the measured strains, because the CFRP composite deformations are distributed over a longer length. The measured response is similar to the response observed for the pan-joint specimens.

9.2.3 Comparison of Measured and Calculated Strains due to Live Loads

The live-load strains in each of the materials were calculated to provide a direct comparison with the measured strain response. These were calculated using the analytical procedures in Chapter 3. The same procedure that was used for the pan-joint specimens was used in the flat-slab specimens to calculate the internal moment from the calculated strains in each of the materials. The internal moment was related to the applied load using the clear span of the beam equal to 24 ft and the dead loads described in Section 9.2.1. The calculations were based on failure of the CFRP composite by rupture or crushing of the concrete and debonding was not incorporated into the calculations.

a) Section N1



b) Section S1

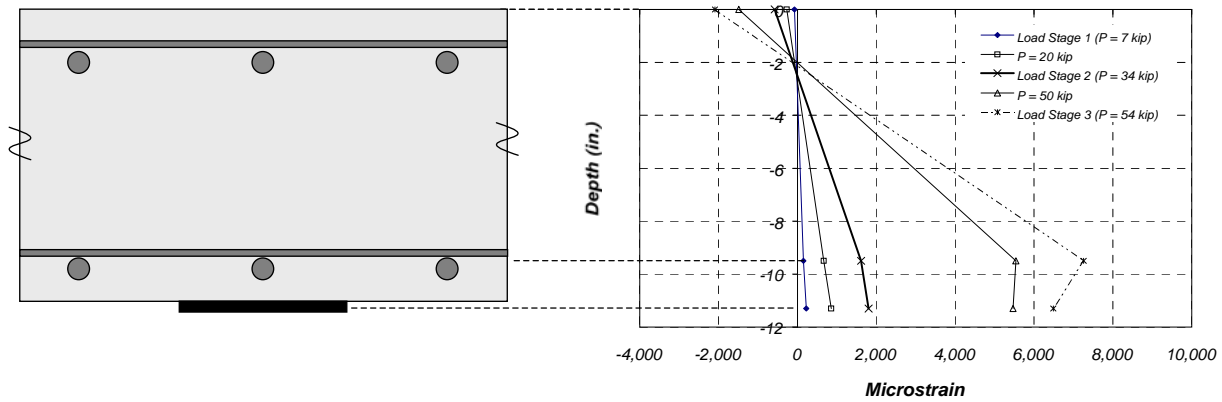
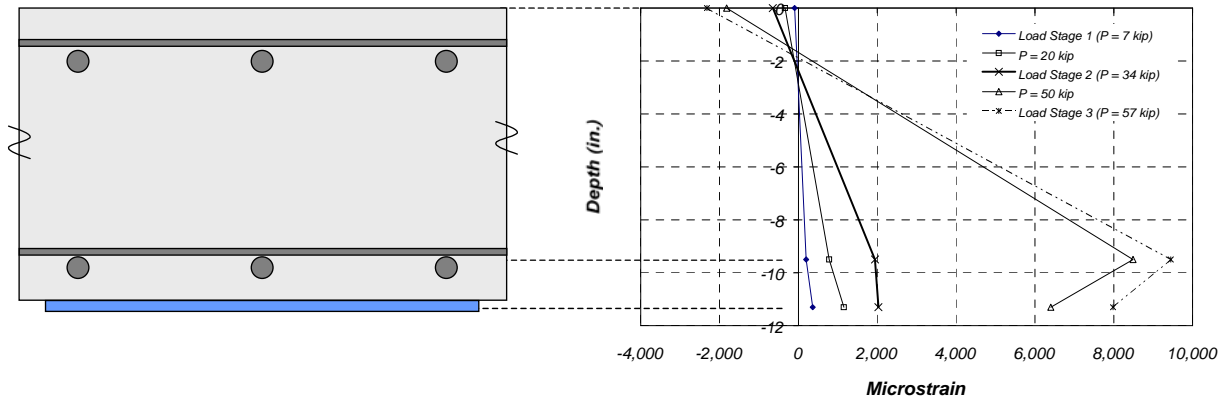


Figure 9.1 Measured Live-Load Strain Profiles in Sections N1 and S1 for Specimen FS-1

a) Section N1



b) Section S1

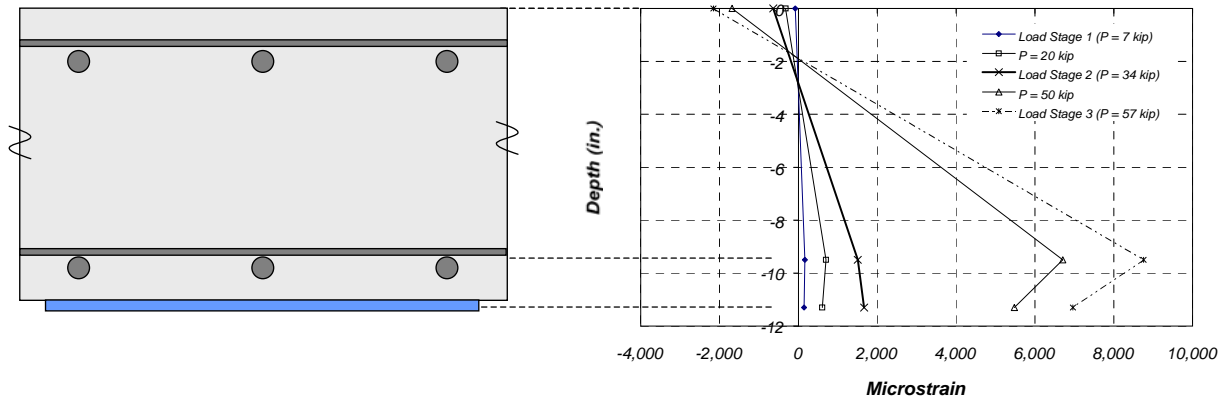


Figure 9.2 Measured Live-Load Strain Profiles in Sections N1 and S1 for Specimen FS-2

Calculated and measured live-load strains are compared in Figure 9.3 through Figure 9.6 for locations under the loading points (Sections N1 and S1). The measured steel strains represent the average from readings on three bars, the CFRP strains represent the average of readings from four gages, and the measured concrete strains represent the average of readings from three gages.

In general, the largest difference was in the magnitude of the calculated and measured strains at failure. While failure was caused by composite rupture in the calculated curves, it was always triggered by debonding of the CFRP materials in the laboratory tests. However, at specific load levels, the measured and calculated strains are relatively close for both specimens.

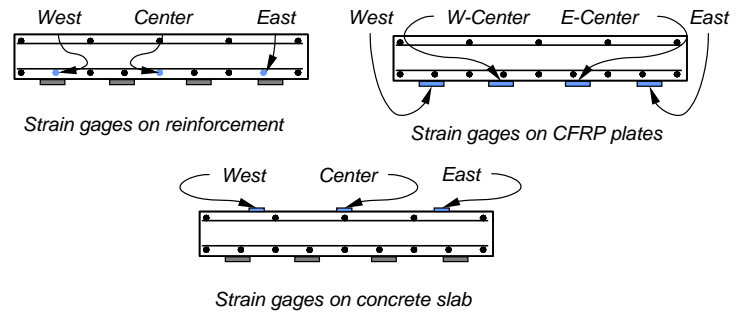
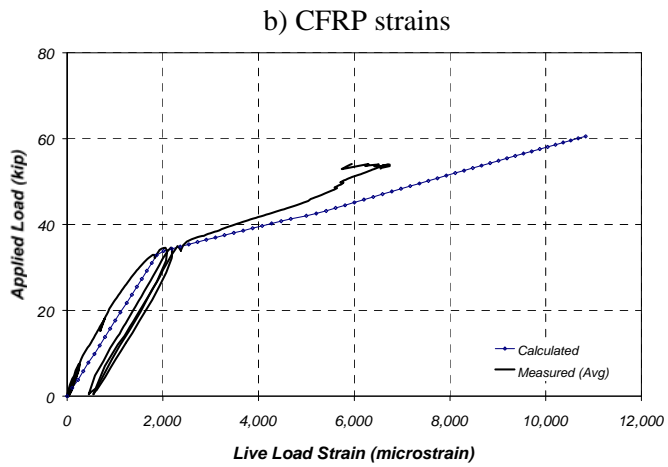
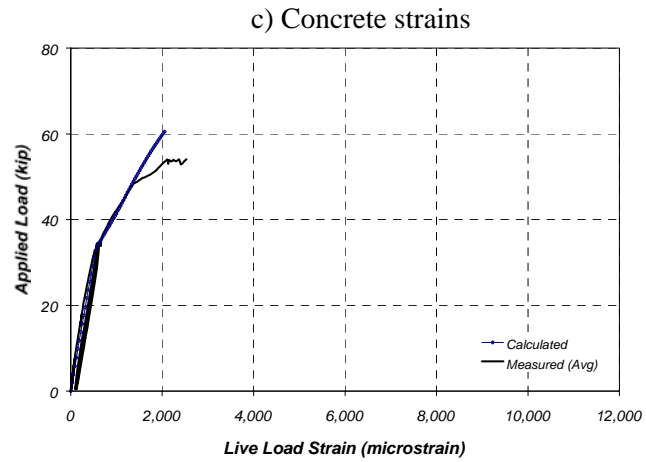
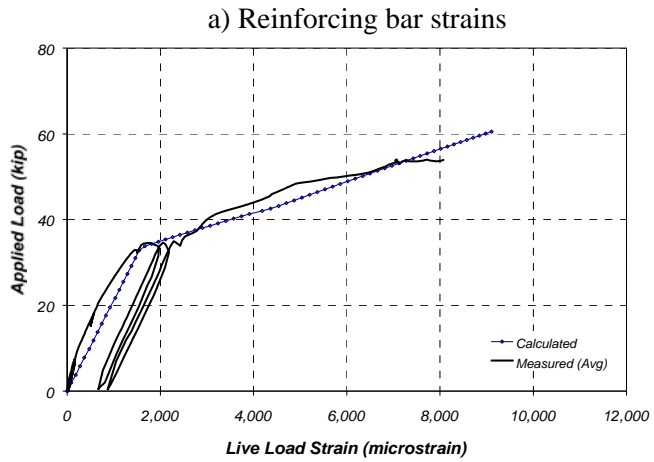
The trends observed in the comparisons of the calculated strain curves with the measured response are very similar for both sections for Specimen FS-1. The calculated and measured steel strains are very close, particularly for low load levels. The general trend of the calculated strains on the steel above the yield load (34 kip) is approximately the same as the measured curves. The irregular shape of the measured curves, especially section N1 in Specimen FS-2, is due to the formation of cracks at the location of the gage and concentrated yielding of the reinforcement. These local effects are not well represented by the analytical model, because it is based on a smeared distribution of cracks.

The calculated concrete strains are very close to the measured values for the majority of the response. At load levels above approximately 50 kip, the calculated concrete strains were 1,000 microstrain less than the measured values. At low load levels the difference is not noticeable in these curves but was less than 50 microstrain for most part of the loading sequence.

On the other hand, strains in the CFRP plates were adequately calculated with the analytical model at low load levels, but were overestimated at load levels above yield. The difference in the calculated and measured strains seemed to increase uniformly as loading progressed, reaching a maximum of approximately 1,500 microstrain at failure. Lower measured CFRP strains are consistent with debonding for load levels above yielding. The strains corresponding to debonding of the CFRP are quantified later in this section.

For Specimen FS-2, a significant difference is observed for the two sections. The measured CFRP and concrete strains had similar trends as the two sections for Specimen FS-1. However, the calculated steel strains are significantly different from the measured values above the yield load for Section N1. This difference is clearly due to the accumulation of plastic strains as the specimen was cycled to load stage 3 (yield load). The calculated strains obtained from the analytical model were not able to reproduce this effect because the model is based on a monotonic increase in load to failure. The maximum difference between the

measured and calculated strains in this case is about 3,000 microstrain at a load of approximately 40 kip. A comparison of the strains measured at the critical load stages with the calculated strains for Specimens FS-1 and FS-2 is presented in Table 9.2 and Table 9.3, respectively.



281

Figure 9.3 Comparison of Measured and Calculated Live-Load Strains at Section N1 (Specimen FS-1)

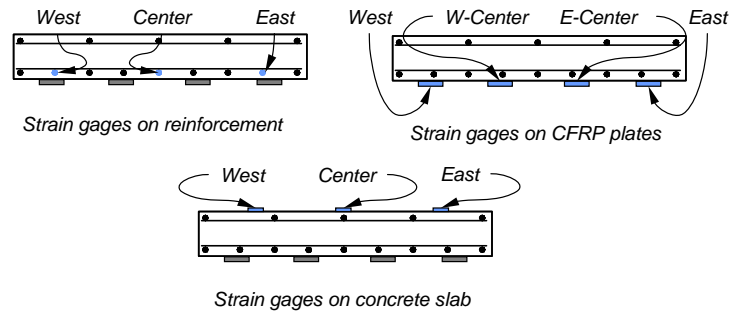
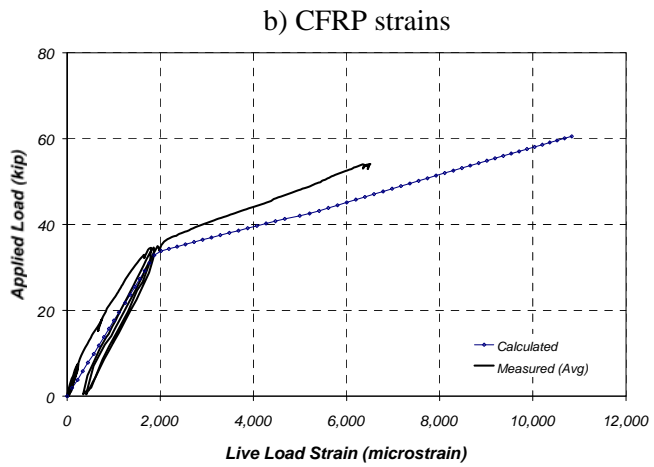
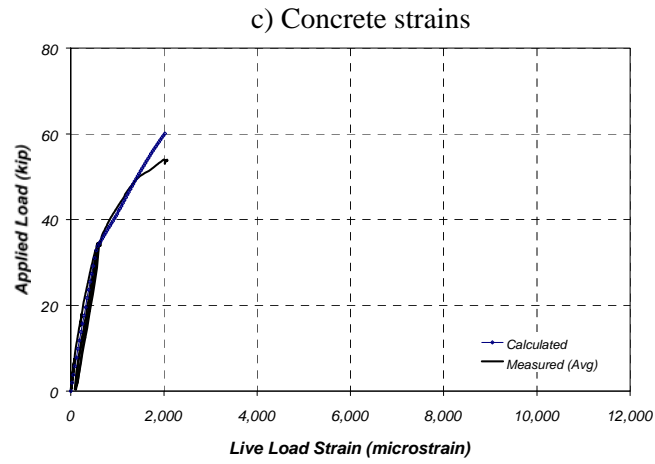
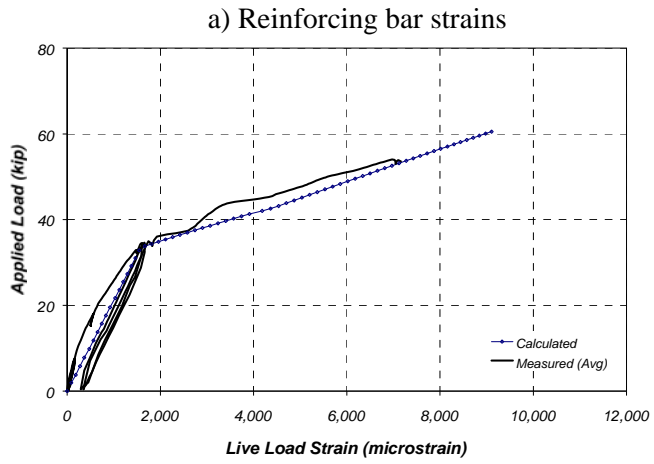


Figure 9.4 Comparison of Measured and Calculated Live-Load Strains at Section S1 (Specimen FS-1)

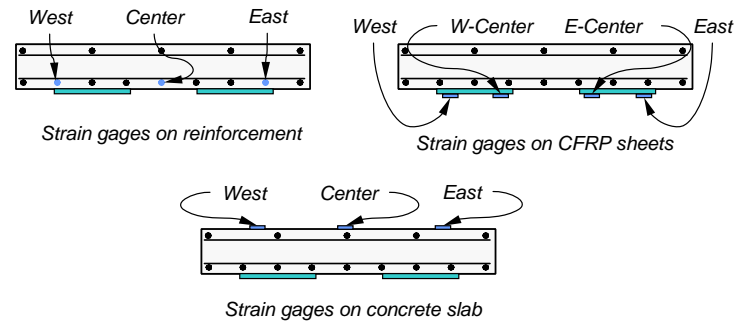
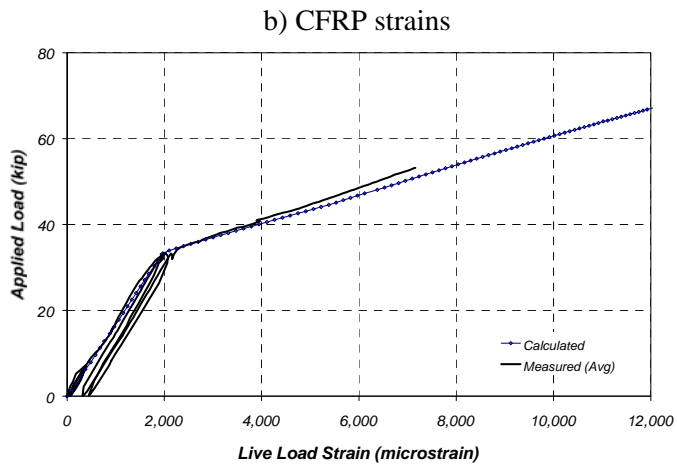
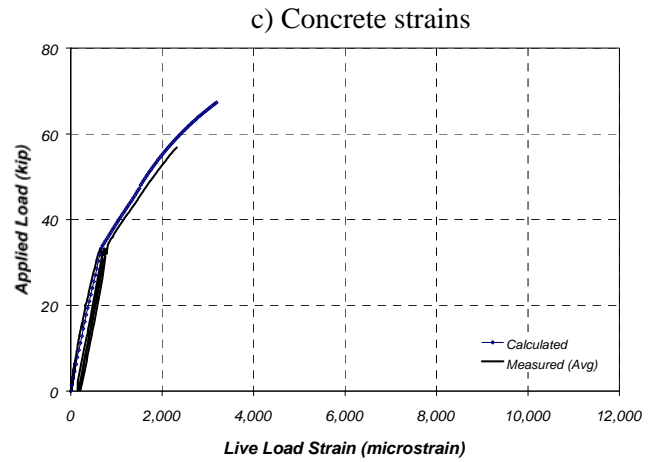
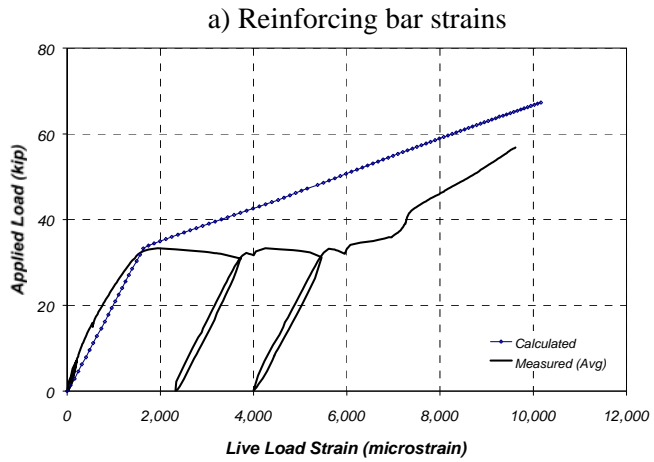


Figure 9.5 Comparison of Measured and Calculated Live-Load Strains at Section N1 (Specimen FS-2)

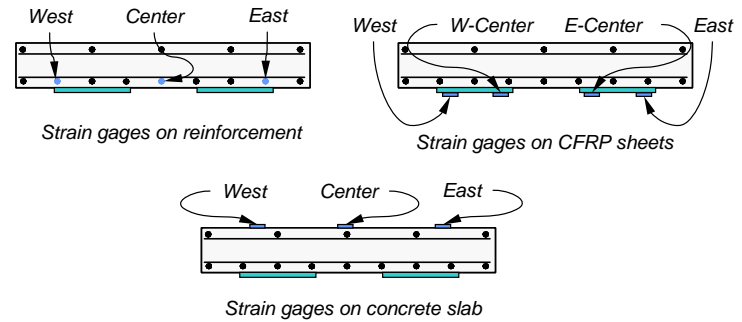
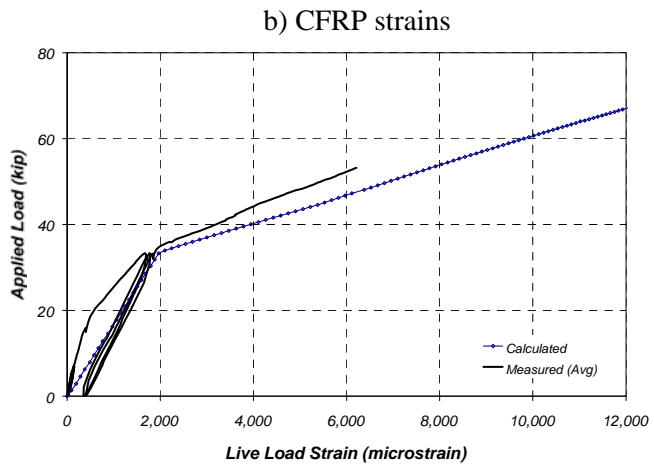
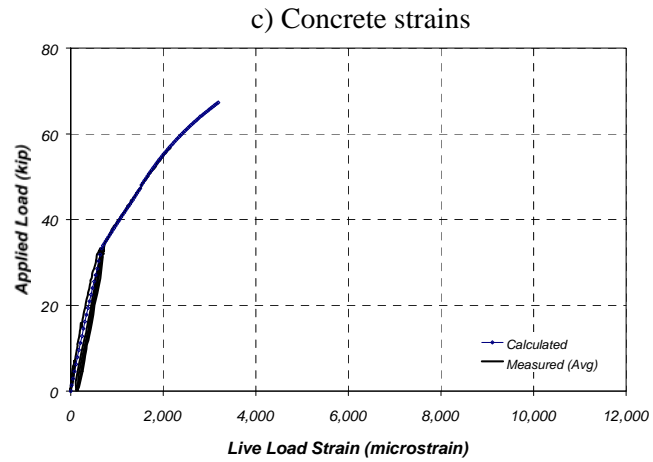
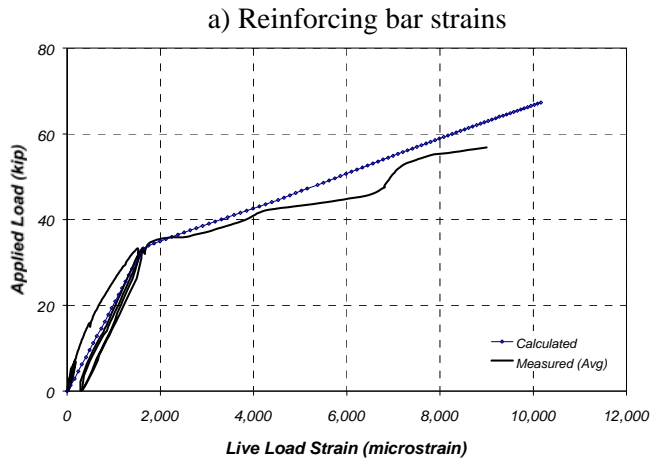


Figure 9.6 Comparison of Measured and Calculated Live-Load Strains at Section S1 (Specimen FS-2)

Table 9.2 Measured and Calculated Live-Load Strains for Specimen FS-1

| Load Stage | Load, kip | Steel Strain, microstrain | | | CFRP Strain, microstrain | | | Concrete Strain, microstrain | | |
|------------|-----------|---------------------------|-------|------------|--------------------------|-------|------------|------------------------------|-------|------------|
| | | Measured | | Calculated | Measured | | Calculated | Measured | | Calculated |
| | | N1 | S1 | | N1 | S1 | | N1 | S1 | |
| 1B | 7 | 160 | 152 | 368 | 243 | 224 | 444 | 84 | 77 | 125 |
| 2 | 34 | 1,788 | 1,613 | 1,960 | 2,059 | 1,804 | 2,363 | 587 | 579 | 636 |
| 3 | 54 | 4,508 | 7,433 | 7,427 | 5,948 | 6,510 | 8,837 | 2,534 | 2,117 | 1,664 |

Table 9.3 Measured and Calculated Live-Load Strains for Specimen FS-2

| Load Stage | Load, kip | Steel Strain, microstrain | | | CFRP Strain, microstrain | | | Concrete Strain, microstrain | | |
|------------|-----------|---------------------------|-------|------------|--------------------------|-------|------------|------------------------------|-------|------------|
| | | Measured | | Calculated | Measured | | Calculated | Measured | | Calculated |
| | | N1 | S1 | | N1 | S1 | | N1 | S1 | |
| 1B | 7 | 198 | 163 | 407 | 364 | 144 | 488 | 97 | 80 | 144 |
| 2 | 34 | 1,942 | 1,509 | 1,746 | 2,031 | 1,669 | 2,100 | 647 | 640 | 698 |
| 3 | 57 | 9,620 | 9,002 | 7,504 | 7,982 | 6,964 | 8,904 | 2,321 | 2,155 | 2,144 |

9.2.4 Measured Strains at which the CFRP Composites Debonded from the Surface of the Concrete

As noted in the previous section, the failure strains in the materials were not well represented by the analytical model, because failure was defined in the analytical model by rupture of the CFRP composites. Both strengthened specimens failed after the CFRP composites debonded from the surface of the concrete, and crushing of the concrete was not observed until later stages of the test when the bare specimens were loaded to failure. The strain at which the composites debonded from the concrete was estimated by comparing the measured strains on the CFRP composites and the strains extrapolated from the measured concrete and reinforcement strains, assuming a linear variation of strain with depth.

Measured envelopes of the CFRP strain curves are shown in **Figures 9.7 and 9.8** for Specimens FS-1 and FS-2, respectively. The calculated CFRP strain curves depicted in these figures were obtained from the measured concrete and steel strains and projected linearly to the position where the CFRP gages were attached. The difference between the measured and calculated CFRP strain envelopes is also plotted in **Figures 9.7 and 9.8**.

For Specimen FS-1, the difference in measured and calculated strains increases suddenly at a load of approximately 45 kip. The maximum difference between the measured and calculated CFRP strains was approximately 5,000

microstrain. For section S1, the difference in strains increased gradually for loads above the observed yield load (34 kip). The maximum difference at failure was approximately 3,000 microstrain. The difference between measured and calculated CFRP strains gives an indication when the composites began to debond from the surface of the concrete. A comparison between the strains in sections N1 and S1 for Specimen FS-1 indicates that debonding is largely dependent on local surface and cracking conditions. The difference in strains is larger in section N1 than section S1, consistent with the observed progression of debonding of the CFRP plates toward the north end (Chapter 8). The maximum measured CFRP strain at failure was approximately 7,000 microstrain in sections N1 and S1.

For Specimen FS-2, the behavior was dramatically different at sections N1 and S1. The effect of the accumulation of plastic strains in the reinforcing steel at section N1 on the calculated CFRP strains is observed in Figure 9.8 (a). This plot indicates that large plastic strains cause the composite to debond locally at the location of cracks. Once the reinforcing bar strains stabilize, the composite strains increase as the cross section deforms until failure. The calculated strains at section S1 also show the effect of reinforcing bar yielding but to a lesser extent. The maximum measured CFRP strain at failure was approximately 8,000 microstrain. Strains in the composites for both flat-slab specimens were approximately equal to the strain value assumed for design (7,000 microstrain).

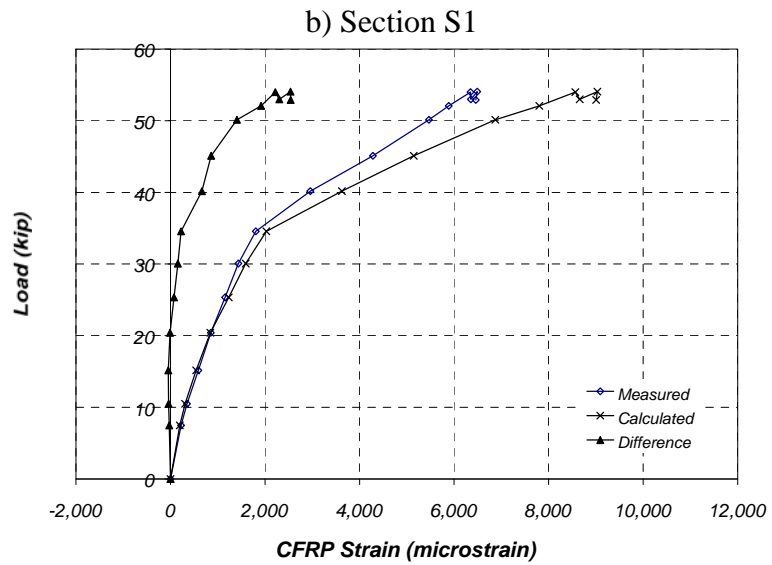
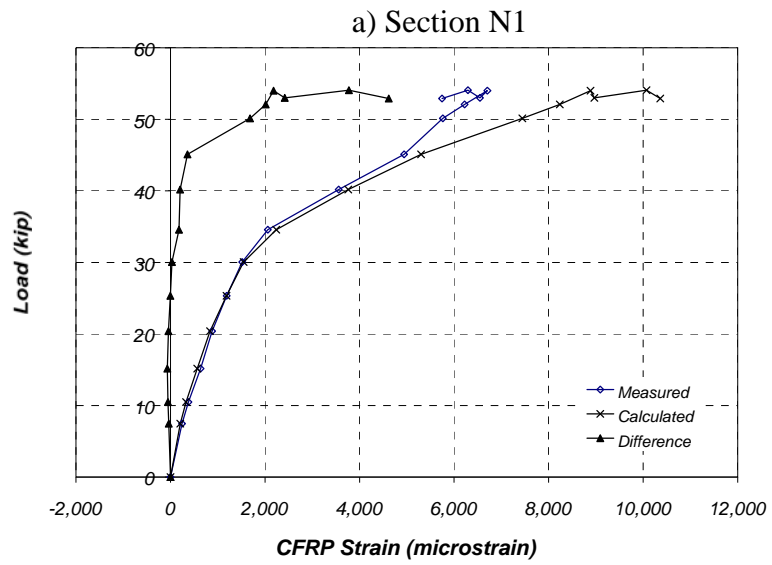


Figure 9.7 Comparison of Measured and Calculated CFRP Strains for Specimen FS-1

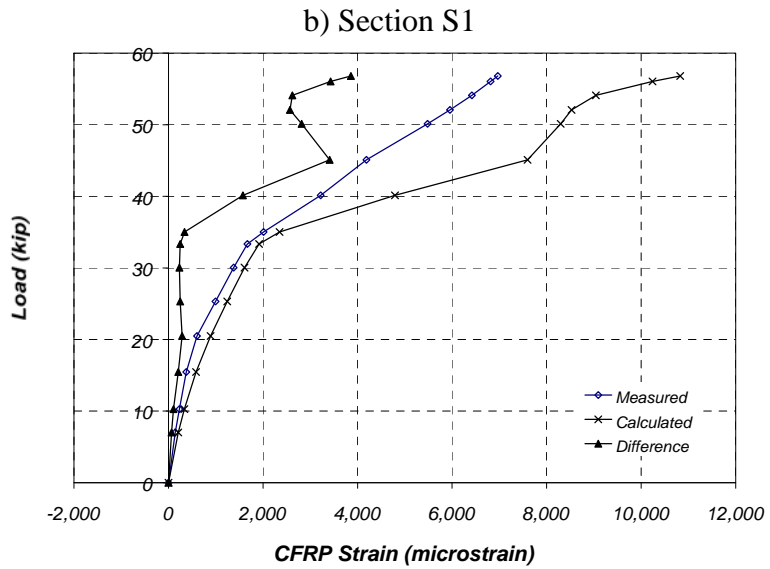
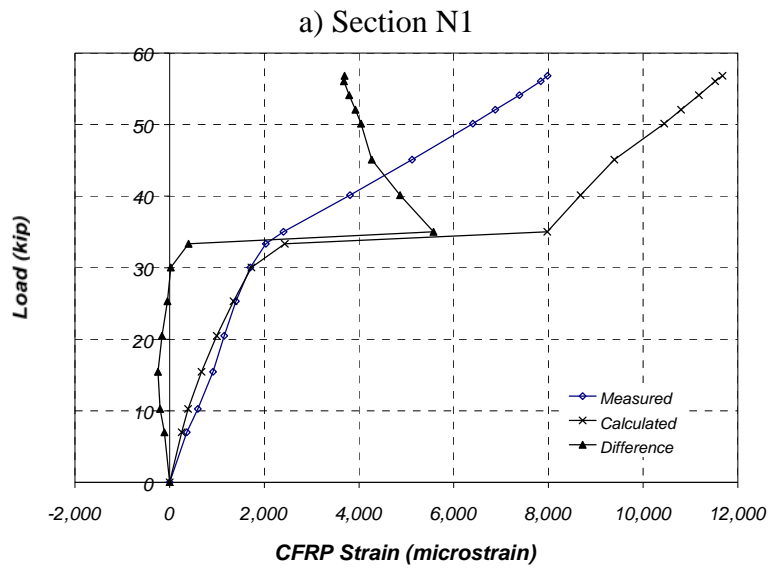


Figure 9.8 Comparison of Measured and Calculated CFRP Strains for Specimen FS-2

9.3 EVALUATION OF MOMENT-CURVATURE RESPONSE

The measured strains were used to calculate the relationship between moment and curvature for the test specimens. Moment-curvature response derived from the measured strains is compared with the results of the analytical model in Section 9.3.3.

The procedures used to calculate internal forces and moments from the measured strains were similar to those used in the analytical model. Internal forces were calculated following the same basic steps that were used for the pan-joint specimens (Chapter 6). In the case of the flat-slab specimens, the composites were bonded to the bottom surface of the concrete so the calculation of internal forces followed directly the procedure outlined for Specimen J-1 (Section 6.3.1). The only modification was the position of the composites on the cross section. Therefore, the methodology is not repeated in this chapter, and only the results from the calculations are presented.

The calculation of internal forces for Specimens FS-1 and FS-2 is presented in two separate sections because the measured strains were significantly different. The discussion of the results for the two specimens needs to be addressed separately because there was a large accumulation of plastic strains in the reinforcement for section N1 in Specimen FS-2.

9.3.1 Internal Forces Calculated from Measured Strains for Specimen FS-1

Internal force equilibrium was verified by comparing the total compressive force with the total tensile force at different load levels. The sum of the internal forces in compression is plotted as a function of the sum of the internal forces in tension in Figure 9.9. It can be observed that the sum of the internal compressive forces consistently exceeded the sum of the internal tensile forces, although the difference remained fairly constant below the observed yield load. Above yielding the differences between the compressive forces and tensile forces increased at a higher rate.

The factors that could have affected the readings used to obtain the tensile and compressive forces on the cross section were discussed in Section 6.3.1. Local perturbations at the sections of applied load, distance from the gage to cracks on the concrete surface, and bending of the reinforcement at large deformation levels could have affected the gage readings at different load levels.

To be consistent with the approach used for the pan-joist specimens, the neutral axis position was shifted to achieve equilibrium of internal forces. This procedure was based on revising the value of the concrete strains and using the measured strains in the reinforcement to define the neutral axis depth that satisfied equilibrium. The methodology is described in detail in Chapter 6.

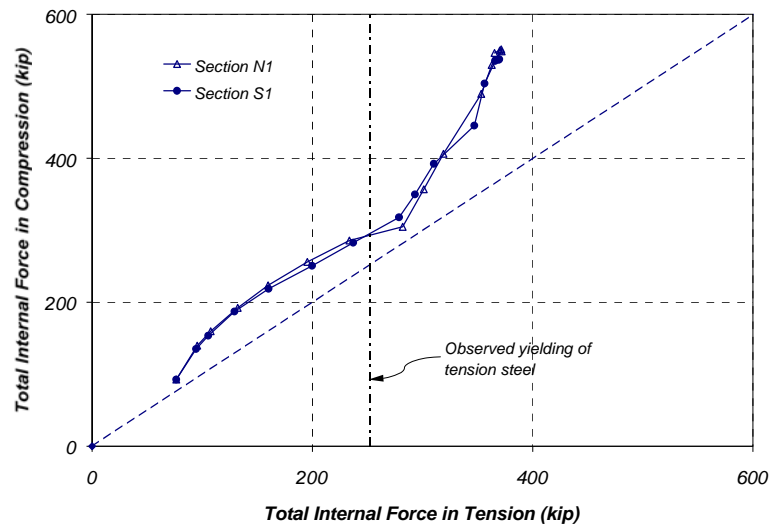


Figure 9.9 Internal Force Resultants for Specimen FS-1

The revised peak compressive strain is compared with the measured peak compressive strain in Figure 9.10. The differences in strain tended to increase as the applied load increased, and reached a maximum at failure. However, the revised neutral axis depth was modified less than 20% from the measured depth throughout the test to achieve equilibrium, except after the failure sequence initiated (Figure 9.11). The revised values of strain and neutral axis depth were used in the subsequent calculations.

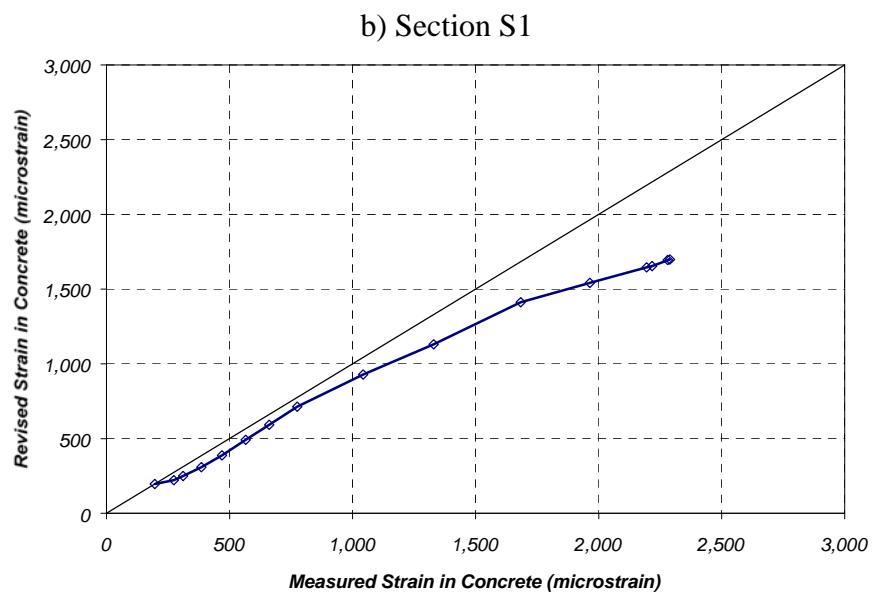
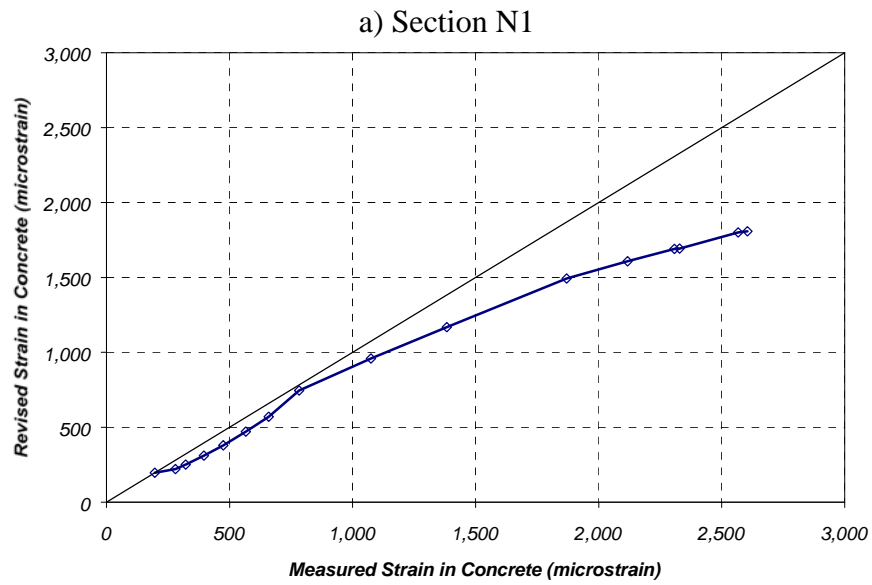


Figure 9.10 Comparison of Revised and Measured Peak Compressive Strains for Specimen FS-1

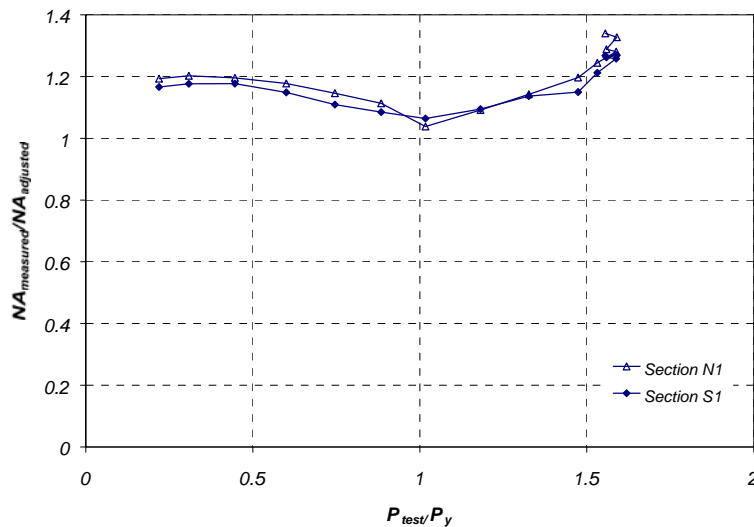


Figure 9.11 Comparison of Neutral Axis Depth from Revised and Measured Strain Profiles

The normalized tensile force components in the cross section are plotted as a function of the ratio of the applied load to the yield load in Figure 9.12. The contribution of the concrete to the total tensile force represented approximately 18% of the total tensile force and decreased constantly to almost zero at a load equal to the observed yield load. At the same time, the CFRP plates increased steadily up to the yield load and the reinforcing steel contribution remained fairly constant at about 85% up to this load level. After yielding, the portion of the total internal tensile force carried by the CFRP plate increased at a higher rate until failure. Prior to failure, the contribution of the reinforcing steel was close to 75% and the contribution of the CFRP composite was approximately 25%.

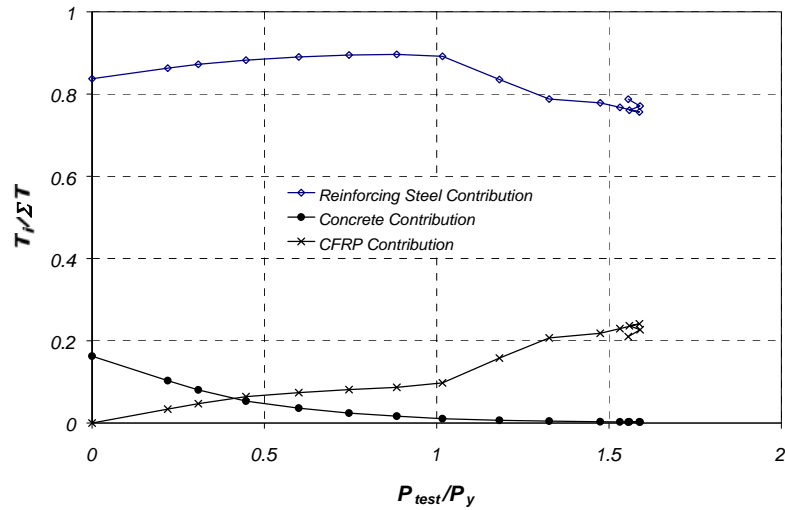


Figure 9.12 Variation of Tensile Force Components at Section N1 for Specimen FS-1

9.3.2 Internal Forces Calculated from Measured Strains for Specimen FS-2

Internal forces were calculated in Specimen FS-2 as described in Section 6.3.1. A comparison of the total internal compressive force and the total tensile force for Specimen FS-2 is shown in Figure 9.13. Below yielding of the reinforcing steel, the total internal compressive force exceeded total internal tensile force. However, unlike the distribution of internal forces of Specimen FS-1, tensile forces either exceeded or were nearly equal to the compressive forces at load levels. The large drop in the total compressive force is probably caused by the reduction of the neutral axis depth as plastic strains were accumulated during the cycles at yield load. This effect is more pronounced in section N1, consistent with the observation of accumulation of plastic strains shown in Figure 9.5(a). To be consistent,

however, the neutral axis depth was adjusted to satisfy force equilibrium using the same approach presented for Specimen FS-1 and the pan-joint specimens.

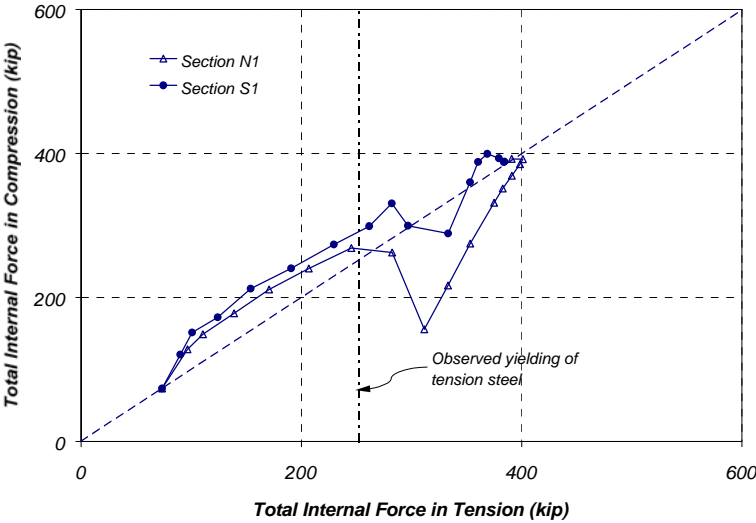


Figure 9.13 Internal Force Resultants for Specimen FS-2

Figure 9.14 shows the revised peak compressive strains as a function of measured peak compressive strains in the concrete. The largest difference between measured and revised strains is approximately 500 microstrain in section N1. Only minor adjustments were required in section S1 throughout the loading history. A comparison between sections N1 and S1 reveals that the change in magnitude of the concrete strains required to reach equilibrium was different at sections that were subjected to the same applied moment, supporting the observation that strain readings are largely influenced by local conditions occurring at each section.

The change in neutral axis position required to achieve internal force equilibrium is presented in Figure 9.15. The maximum change that was required was within 20% of the measured value calculated from the measured strain data, except at the observed yield load. Typically, the change in neutral axis depth was approximately 10% throughout the loading sequence.

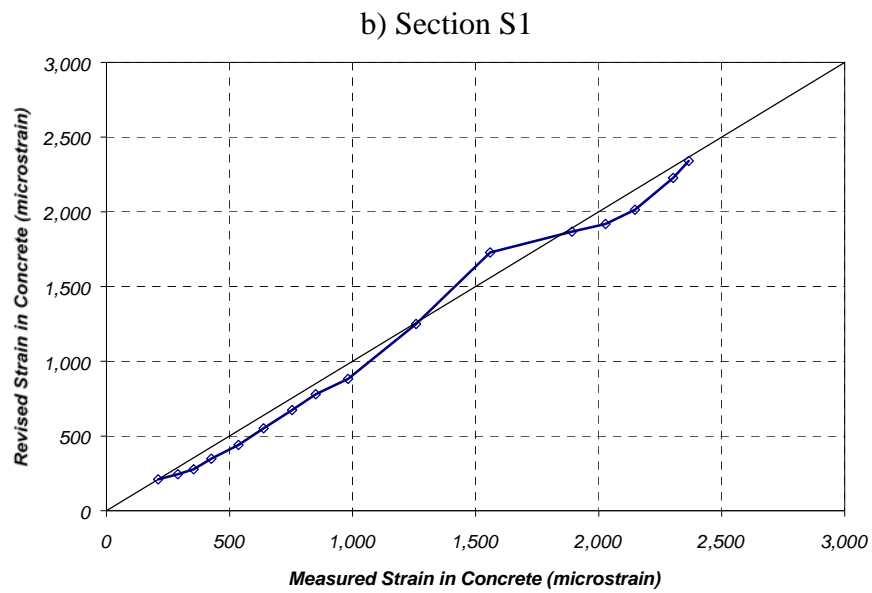
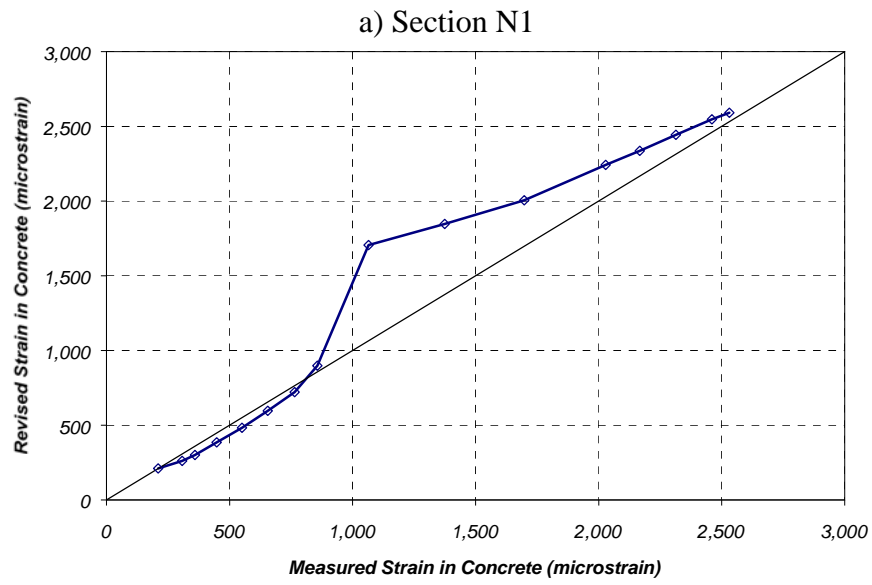


Figure 9.14 Comparison of Revised and Measured Peak Compressive Strains for Specimen FS-2

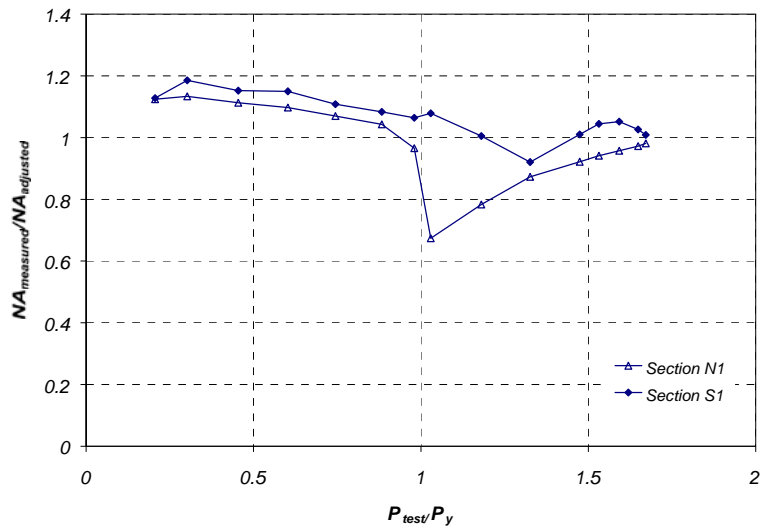


Figure 9.15 Comparison of Neutral Axis Depth from Revised and Measured Strain Profiles

The distribution of the total internal tensile force among the different force components at different load stages is illustrated in Figure 9.13. The trends are very similar to those observed in Specimen FS-1. Prior to failure, the CFRP composites contributed in approximately 30% to the total tensile force, while the reinforcing steel contributed approximately 70%. The contribution of concrete to the total tensile force was negligible at load levels above the yield load.

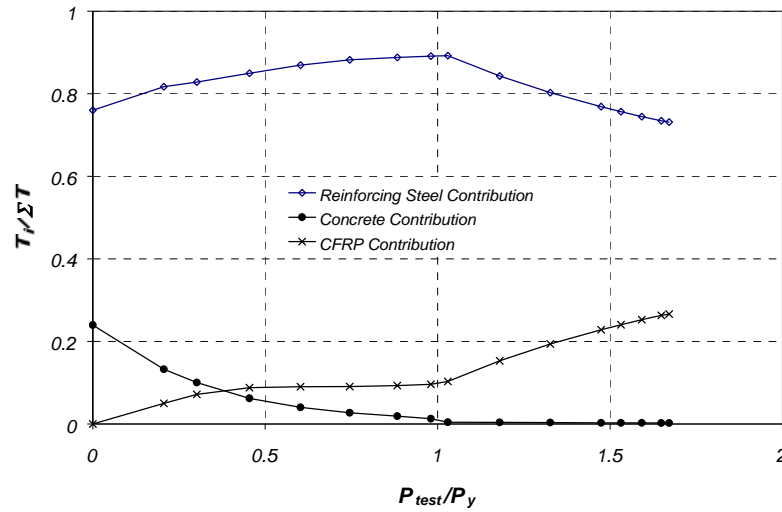


Figure 9.16 Contribution of the CFRP Sheets to the Total Internal Moment at Section N1 for Specimen FS-2

9.3.3 Moment-Curvature Response

Internal moments and curvature were calculated in both specimens using the internal forces that satisfied equilibrium. The moment and curvature corresponding to dead loads (Table 9.1) were then subtracted from each of the calculated values to obtain the relationship between moment and curvature for the applied loads. This response is compared with the results from the analytical model in Figure 9.17 and Figure 9.18 for Specimens FS-1 and FS-2, respectively. Debonding was not included in the analytical model at this point.

The moment-curvature response calculated from the measured strains is well represented by the results of the analytical model. The trends obtained from the analytical model and the measured data were similar for Specimen FS-1. At the

same moment, the curvature inferred from the measured strains tended to be slightly higher than the calculated curvature, but the differences were small. The calculated curvature capacity was larger than the curvature obtained from measured strains at both sections.

In contrast curvatures obtained from measured strains were much larger than the calculated values using the analytical model for Specimen FS-2, particularly at load levels above the yield load. This again was caused by the inability of the model to account for the accumulation of plastic strains in the reinforcement after cycling to yield. However, the prototype bridges are not expected to yield, much less experience cycles of large inelastic deformations during their service life. Therefore, the analytical model should be adequate to calculate the response in these cases.

9.3.4 Comparison of Internal and External Moments

The applied load is plotted as a function of the maximum internal moment due to live load obtained from the measured strains in Figure 9.19. Also shown in the figure is the external midspan moment determined from static equilibrium with a span equal to 24 ft. Both specimens exhibited the same general response. The internal moment at the two-instrumented sections was consistently smaller than the external moment at low load levels. The difference between internal and external moments decreased at load levels above yielding, but the internal moment was

never equal to the external moment in three out of the four sections. Only the internal moment at Section N1 in Specimen FS-2 was approximately equal to the external moment at applied loads above the yield level (34 kip).

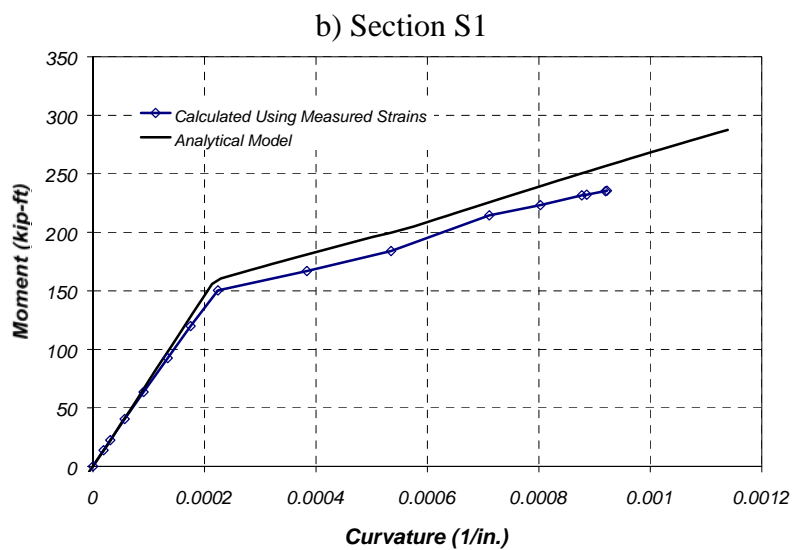
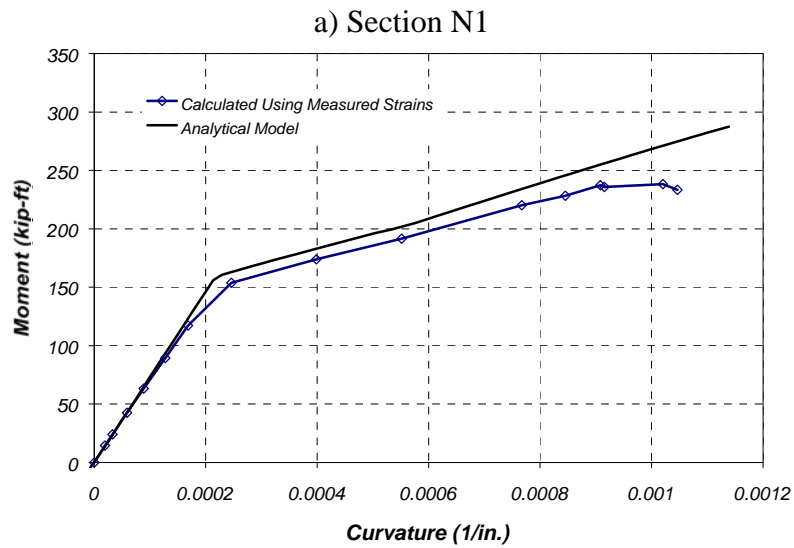


Figure 9.17 Comparison of Measured and Calculated Moment-Curvature Response for Specimen FS-1

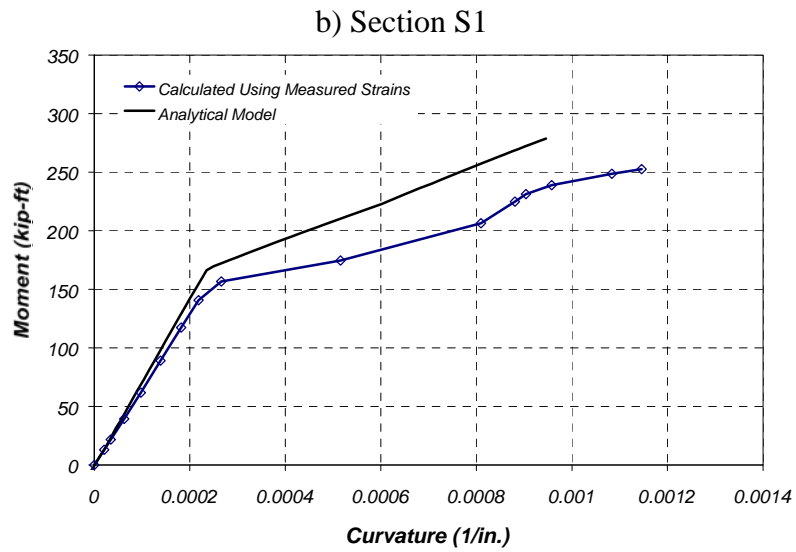
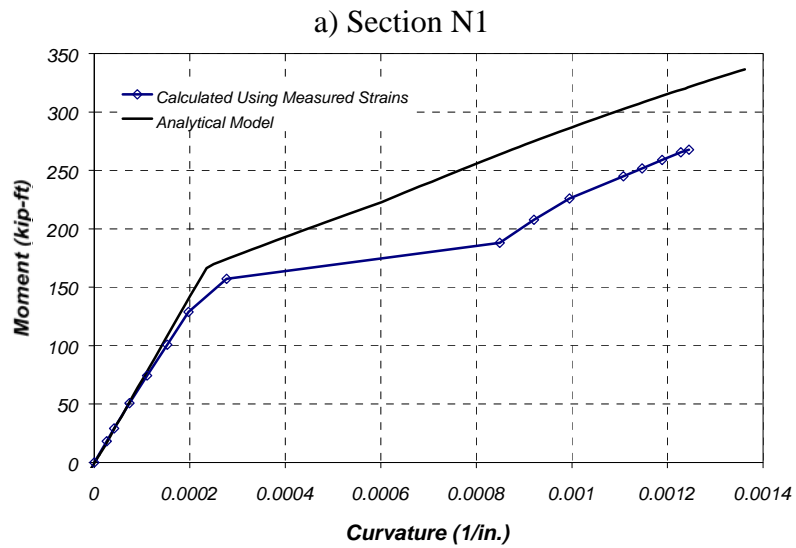
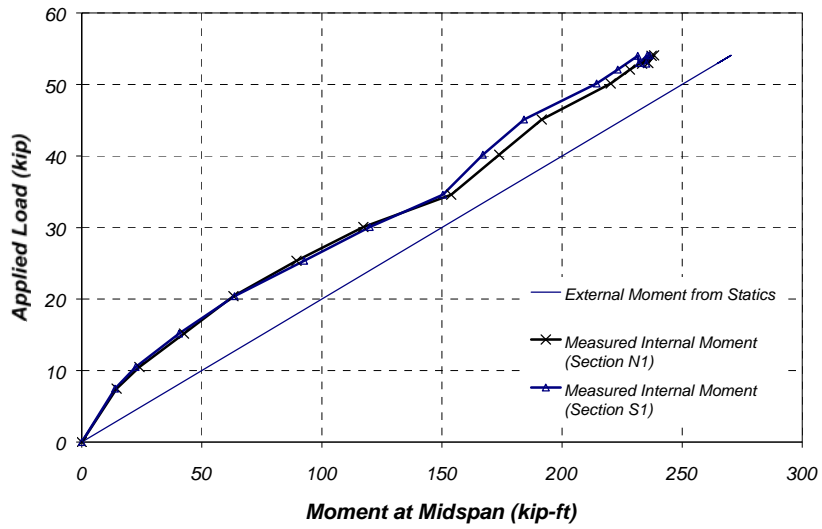


Figure 9.18 Comparison of Measured and Calculated Moment-Curvature Response for Specimen FS-2

a) Specimen FS-1



b) Specimen FS-2

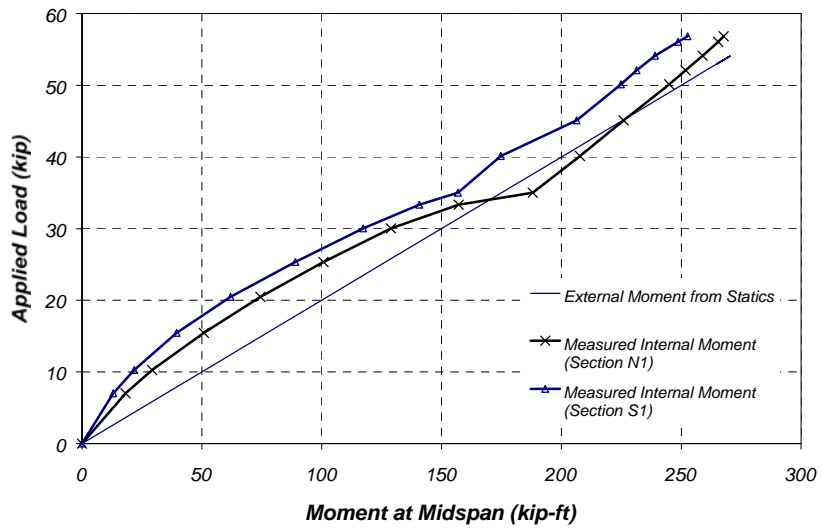


Figure 9.19 Comparison of Internal and External Moments

9.4 EVALUATION OF LOAD-DEFLECTION RESPONSE

The global response of the strengthened specimens is first evaluated by comparing the measured response of the two specimens. The response of each specimen was then compared with the calculated response obtained using the analytical procedure presented in Chapter 3. The displacement response of the strengthened specimens is compared with the bare reinforced concrete elements at the end of this section.

The displacement response was obtained by averaging the displacement measurements from midspan of the east and west sides of the slabs. The measurements were adjusted by subtracting the average vertical displacement at the supports. The load-deflection behavior of Specimens FS-1 and FS-2 is shown in Figure 9.20. It can be seen that the overall behavior of both specimens was similar throughout the loading history. The main difference between the response of Specimens FS-1 and FS-2 was observed at failure. While Specimen FS-1 exhibited an increase in displacement under almost constant load, Specimen FS-2 showed a uniform increase in load until failure. This behavior was caused by the progressive debonding of the CFRP plates in Specimen FS-1 at the peak load.

At failure, the load dropped suddenly and the residual load was carried by the bare reinforced concrete elements. The maximum deformation capacity of the bare specimens was approximately equal.

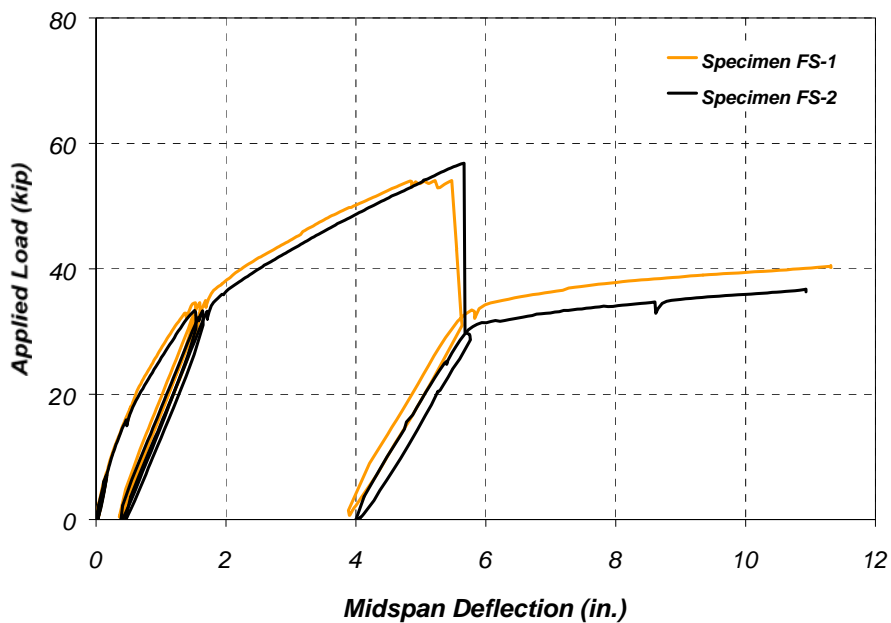


Figure 9.20 Measured Load-Deflection Response of Flat-Slab Specimens

The measured response of the test specimens is compared with the calculated load-deflection response in Figures 9.21 and 9.22 for Specimens FS-1 and FS-2, respectively. A 24-ft span was used for the calculated load-deflection response. The results presented show that the analytical model was able to reproduce the displacement response adequately for both specimens. However, the analytical model overestimated the peak load because debonding was not included in the calculations.

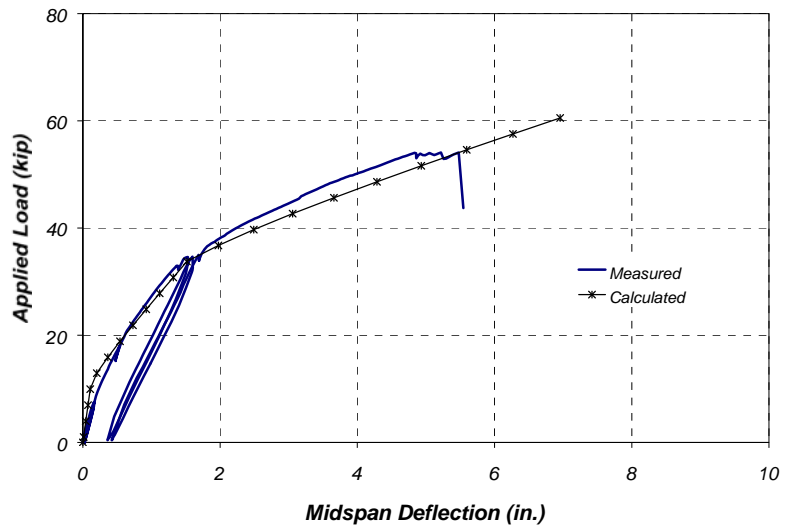


Figure 9.21 Comparison of Measured and Calculated Load-Deflection Response of Specimen FS-1

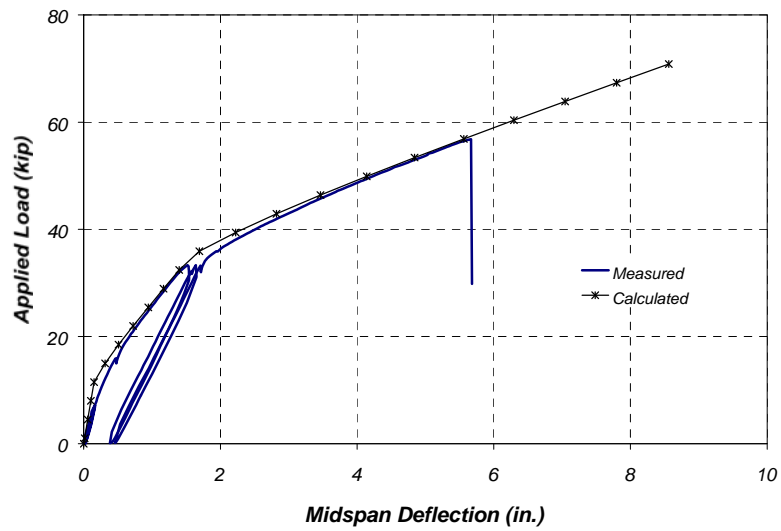


Figure 9.22 Comparison of Measured and Calculated Load-Deflection Response of Specimen FS-2

9.5 SUMMARY

The measured response of Specimens FS-1 and FS-2 was compared to the response calculated using the analytical model presented in Chapter 3. The comparisons show that the model was able to reproduce the measured global response of the test specimens accurately at all levels of loading.

As was the case for the pan-joint specimens, local effects such as cracking of the concrete, debonding of the CFRP composites, and accumulation of plastic strains in the reinforcement, were not adequately represented with the analytical model. Local effects controlled the response at a particular section and were highly variable at different sections subjected to the same moment level.

CHAPTER 9: VERIFICATION OF THE ANALYTICAL MODEL USING THE MEASURED RESPONSE OF THE FLAT-SLAB SPECIMENS..... 272

9.1 Introduction..... 272

9.2 Evaluation of Strain Response 272

9.2.1 Strains due to Dead Loads 273

9.2.2 Measured Strain Profiles due to Live Loads..... 274

9.2.3 Comparison of Measured and Calculated Strains due to Live Loads..... 275

9.2.4 Measured Strains at which the CFRP Composites Debonded from the Surface of the Concrete..... 286

9.3 Evaluation of Moment-Curvature Response..... 290

9.3.1 Internal Forces Calculated from Measured Strains for Specimen FS-1..... 291

9.3.2 Internal Forces Calculated from Measured Strains for Specimen FS-2..... 295

9.3.3 Moment-Curvature Response 300

9.3.4 Comparison of Internal and External Moments..... 301

9.4 Evaluation of Load-Deflection Response 306

9.5 Summary..... 309

Figure 9.1 Measured Live-Load Strain Profiles in Sections N1 and S1 for Specimen FS-1..... 276

Figure 9.2 Measured Live-Load Strain Profiles in Sections N1 and S1 for Specimen FS-2..... 277

Figure 9.3 Comparison of Measured and Calculated Live-Load Strains at Section N1 (Specimen FS-1)..... 281

Figure 9.4 Comparison of Measured and Calculated Live-Load Strains at Section S1 (Specimen FS-1)..... 282

Figure 9.5 Comparison of Measured and Calculated Live-Load Strains at Section N1 (Specimen FS-2)..... 283

| | |
|---|-----|
| Figure 9.6 Comparison of Measured and Calculated Live-Load Strains at Section S1 (Specimen FS-2)..... | 284 |
| Figure 9.7 Comparison of Measured and Calculated CFRP Strains for Specimen FS-1 | 288 |
| Figure 9.8 Comparison of Measured and Calculated CFRP Strains for Specimen FS-2 | 289 |
| Figure 9.9 Internal Force Resultants for Specimen FS-1 | 292 |
| Figure 9.10 Comparison of Revised and Measured Peak Compressive Strains for Specimen FS-1..... | 293 |
| Figure 9.11 Comparison of Neutral Axis Depth from Revised and Measured Strain Profiles..... | 294 |
| Figure 9.12 Variation of Tensile Force Components at Section N1 for Specimen FS-1 | 295 |
| Figure 9.13 Internal Force Resultants for Specimen FS-2 | 296 |
| Figure 9.14 Comparison of Revised and Measured Peak Compressive Strains for Specimen FS-2..... | 298 |
| Figure 9.15 Comparison of Neutral Axis Depth from Revised and Measured Strain Profiles..... | 299 |
| Figure 9.16 Contribution of the CFRP Sheets to the Total Internal Moment at Section N1 for Specimen FS-2..... | 300 |
| Figure 9.17 Comparison of Measured and Calculated Moment-Curvature Response for Specimen FS-1 | 303 |
| Figure 9.18 Comparison of Measured and Calculated Moment-Curvature Response for Specimen FS-2..... | 304 |
| Figure 9.19 Comparison of Internal and External Moments | 305 |
| Figure 9.20 Measured Load-Deflection Response of Flat-Slab Specimens..... | 307 |
| Figure 9.21 Comparison of Measured and Calculated Load-Deflection Response of Specimen FS-1..... | 308 |
| Figure 9.22 Comparison of Measured and Calculated Load-Deflection Response of Specimen FS-2..... | 308 |
| | |
| Table 9.1 Calculated Dead Load Strains | 274 |
| Table 9.2 Measured and Calculated Live-Load Strains for Specimen FS-1 | 285 |
| Table 9.3 Measured and Calculated Live-Load Strains for Specimen FS-2 | 285 |

Chapter 10: Design Recommendations

10.1 INTRODUCTION

The design recommendations presented in this chapter are based on ultimate strength theory for reinforced concrete structures for members subjected to flexure. This philosophy of design is consistent with the bridge load rating procedure currently used by TxDOT (Appendix B). These recommended procedures are based on the results of the laboratory tests of the strengthened full-scale bridge components discussed in Chapters 4 through 9. Therefore, it is intended that the response of elements strengthened using the recommended procedures outlined in this chapter will be similar to the observed response of the laboratory specimens.

The CFRP composites were bonded to laboratory specimens in which the condition of the concrete surface was not deteriorated. The performance of the strengthened elements may be significantly different from the response measured in the laboratory if the composite systems are attached to a deteriorated concrete surface. Therefore, the design provisions contained in this chapter should be used only for cases where the surface of the concrete is clean and sound.

The procedure to calculate the nominal capacity of a strengthened section is summarized in Section 10.2. The strength reduction factor is discussed in Section 10.3, and recommended details are presented in Section 10.5.

10.2 CALCULATION OF NOMINAL FLEXURAL CAPACITY OF STRENGTHENED SECTIONS

The procedures discussed in this section are based on the observed and calculated response of the laboratory specimens presented in Chapters 5 and 6 for the pan-joint specimens, and Chapters 8 and 9 for the flat-slab specimens. The objective is to present a set of design and analysis provisions for safe and reliable strengthening of reinforced concrete bridges using CFRP composites. The behavior of the strengthened bridge should be similar to the observed response of the laboratory specimens.

The assumptions used in the calculations for the flexural capacity of the strengthened sections are similar to current design practice for reinforced concrete members. The recommended design procedure is illustrated using a rectangular reinforced concrete element to facilitate the presentation. Nevertheless, the procedures can easily be modified to accommodate other shapes. However, the calculations can become quite involved so the use of a computer may be required.

Different modes of failure have been identified by other investigators for strengthened reinforced concrete elements using CFRP composites [Meier et al., 1992; Arduini and Nanni, 1997]. The failure mode depends primarily on the characteristics of the bare reinforced concrete section and the amount of CFRP composite used to strengthen the existing element. For the types of elements that were tested in this research project, failure was always governed by debonding of

the CFRP from the concrete surface. Debonding occurred after yielding of the reinforcing bars, before concrete crushing in the extreme compression fiber. Adequate deformation capacity and ample indications of impending failure were observed in the laboratory tests conducted in this research project. Therefore, this mode of failure was considered to be adequate, and the design recommendations were developed to duplicate this mode of failure.

10.2.1 Strain Distribution within Strengthened Sections

The distribution of strains across the depth of the cross section ultimately defines the internal forces within the strengthened reinforced concrete member. Strains in each material are related to the internal stresses through the stress-strain relationships. The same material relationships that were presented in Chapter 3 can be used for design; however, an elasto-plastic stress-strain relationship is considered adequate for the reinforcing steel.

As was discussed in Chapters 6 and 9, the bridge elements are subjected to dead-load moments before the CFRP composites are applied to the surface of the concrete. Therefore, the existing dead-load strain distribution on the existing reinforced concrete section needs to be determined before the capacity of the strengthened sections can be calculated. In some cases, the moments caused by dead loads do not exceed the cracking moment of the cross section. However, it is recommended that cracked section properties be used in the calculations because it

is likely that the section has been cracked due to the application of service live loads during the lifetime of the structure.

The calculation of the strains in the concrete and reinforcing bars caused by dead load moments is illustrated graphically for a cracked reinforced concrete beam with a rectangular cross section in Figure 10.1. In this figure, the transformed area concept is used to calculate the neutral axis depth required to achieve equilibrium with the external dead-load moment. The basic assumptions and methodology to calculate stresses and strains along the cross section using the transformed area concept is presented in detail by Ferguson [1958]. For these calculations, a linear relationship between stresses and strains for the concrete and reinforcing bars may be assumed. The figure only shows the contribution of the reinforcement in tension, but the effect of the compression reinforcement can be included if necessary.

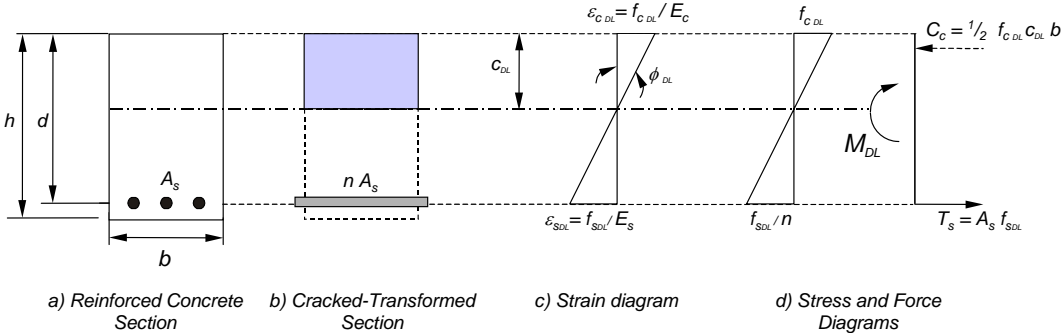


Figure 10.1 Calculation of Strains Caused by Dead-Load Moments

At capacity, the strengthened cross section is subjected to a strain increment corresponding to the factored dead and live-load condition. The strain distribution caused by service dead loads is added to the increase in strains on a strengthened rectangular cross section caused by factored loads in Figure 10.2. The figure illustrates a cross section strengthened with a CFRP plate attached to the bottom fiber, but the approach can be modified to accommodate composites bonded to the sides. The incremental strains in the concrete, reinforcement and CFRP composite are assumed to vary linearly with depth (Figure 10.2c). Therefore, an apparent incompatibility exists on the total strain profile between the CFRP composite and the original cross section because the composite was bonded while the reinforced concrete section was subjected to dead loads.

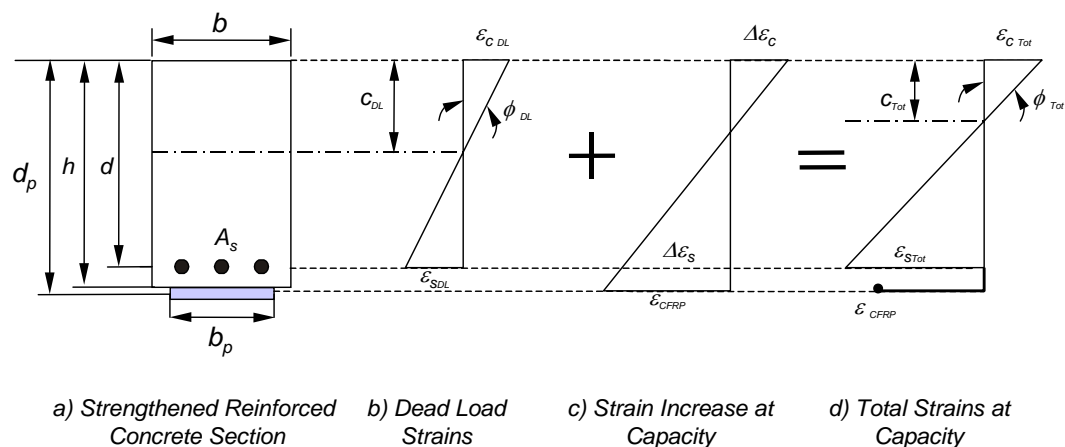


Figure 10.2 Increment of Strains on Strengthened Reinforced Concrete Section

10.2.2 Preliminary Estimate of the Area of CFRP Composite

A procedure to estimate a preliminary area of CFRP composite to reach the target strength is presented in this section. The procedure is based on an assumed distribution of compressive stresses in the concrete based on results of the experimental tests conducted in this project. Again, the procedure is demonstrated using a rectangular cross section. However, the general procedure may be applied to other cross sectional shapes.

The distribution of internal stresses on the cross section is calculated in Figure 10.3 based on the total strain distribution shown in Figure 10.2. The stress distribution shown in Figure 10.3(c) corresponds to the condition at nominal flexural capacity, defined as the capacity of the cross section when the CFRP composite debonds from the surface of the concrete.

The area of the CFRP can be calculated for preliminary design based on an assumed distribution of compressive stresses in the concrete. The material model for concrete presented in Chapter 3 is used in this discussion. The maximum measured concrete strain before debonding of the CFRP composite from the surface of the concrete during the laboratory tests was approximately 0.002. This value is equal to the commonly assumed value of strain corresponding to the peak compressive stress, ϵ_{co} . This value was chosen to provide an estimate of the compressive stress distribution in the concrete. At this strain value, the stress in the extreme compressive fiber in the concrete is equal to f'_c (Figure 10.3c). The

resultant of compressive stresses in the concrete, C_c , can then be calculated by integrating the assumed compressive stress distribution:

$$f_c = f''_c \left[\frac{2\varepsilon_c}{\varepsilon_{c0}} - \left(\frac{\varepsilon_c}{\varepsilon_{c0}} \right)^2 \right] \quad (10.1)$$

with

$$\begin{aligned} \varepsilon_c &= 0.002. \\ f''_c &= 0.9 f'_c. \\ f'_c &= \text{Concrete cylinder compressive strength.} \end{aligned}$$

For a rectangular cross section and the assumed value of ε_c equal to 0.002, the resultant compressive force and its position from the top surface can be calculated as:

$$C_c = \frac{2}{3} f''_c c_{Tot} b \quad (10.2)$$

and

$$z = \frac{3}{8} c_{Tot} \quad (10.3)$$

It should be emphasized that the use of the equivalent rectangular stress block that is commonly used for the design of reinforced concrete flexural members is not applicable in this case because the selected failure mode is by debonding of the composites from the surface of the concrete. The distribution of compressive stresses in the concrete depends on the total tensile force developed by the

reinforcing steel and CFRP composite when the failure condition is reached. However, the strain in the extreme compression fiber will not have reached the maximum usable strain in the concrete, ϵ_{cu} . The maximum recommended area of CFRP composite to guarantee this mode of failure is discussed in Section 10.2.3.

At the nominal strength condition, the reinforcing bars are assumed to have reached yield. The maximum strain in the CFRP composite is assumed to be equal to ϵ_{CFRP}^* , the strain corresponding to debonding from the surface of the concrete. As was discussed in Chapters 6 and 9, the maximum measured CFRP strain was highly dependent on the distance from the critical section to the nearest crack. Therefore, a conservative value of ϵ_{CFRP}^* equal to 0.007 is recommended for design. The tensile force from the individual components can be calculated with:

$$T_s = A_s f_y \quad (10.4)$$

$$T_p = A_p f_p = A_p \epsilon_{CFRP}^* E_p \quad (10.5)$$

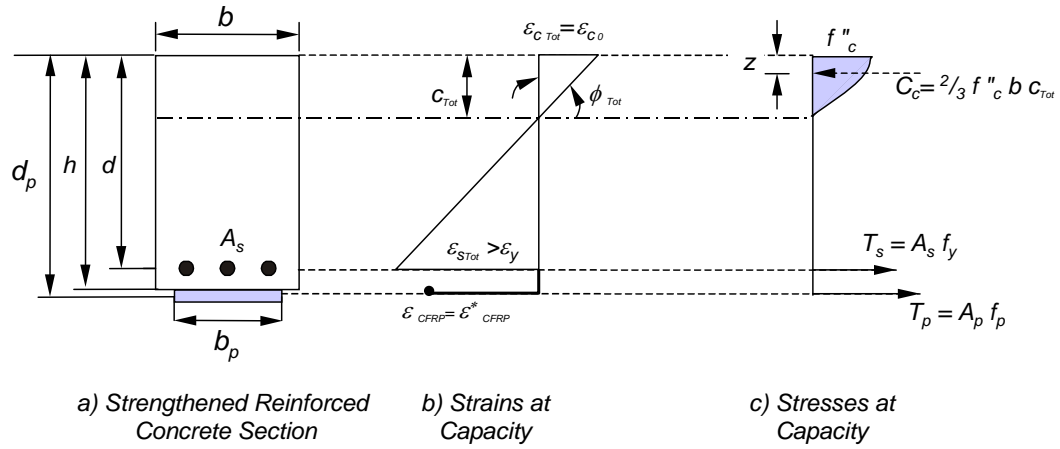


Figure 10.3 Internal Stress Distribution for a Strengthened Rectangular Section at Capacity

The initial estimate of required area of CFRP, A_p , can be calculated by solving the equations of equilibrium of horizontal forces and moments simultaneously:

$$A_s f_y + A_p \varepsilon^*_{CFRP} E_p = \frac{2}{3} f''_c c_{Tot} b \quad (10.6)$$

and

$$M_{n req} = A_s f_y \left(d - \frac{3}{8} c_{Tot} \right) + A_p \varepsilon^*_{CFRP} E_p \left(d_p - \frac{3}{8} c_{Tot} \right) \quad (10.7)$$

where

$M_{n req}$ = Required nominal capacity of the strengthened section, kip-in.

A_s = Existing area of reinforcing steel, in².

f_y = Specified yield stress of the reinforcing steel, ksi.

- c_{Tot} = Neutral axis depth due to total loads, in.
- A_p = Required area of CFRP composite, in².
- ε_{CFRP}^* = Strain in the CFRP composite before debonding from the concrete surface = 0.007.
- E_p = Tensile modulus of elasticity of the CFRP composite, ksi.
- d = Distance from extreme compression fiber to centroid of existing reinforcing steel, in.
- d_p = Distance from extreme compression fiber to centroid of CFRP composite, in.

With the initial estimate of the required area of CFRP composite, the procedures in Chapter 3 can be used to calculate the capacity of the strengthened section. A revised distribution of compressive stresses in the concrete is obtained and the area of CFRP can be adjusted to guarantee that the maximum strain in the composite does not exceed the recommended value.

10.2.3 Maximum Recommended Area of CFRP Composite

The procedure used to estimate the area of CFRP composite required to develop the required nominal flexural capacity was outlined in the previous section. However, no limitation was set on the maximum area that can be used in a section to prevent concrete crushing at the extreme compressive fiber. The criterion to calculate the maximum area of CFRP composite is similar to the limit set on the maximum area of reinforcing steel in current design of reinforced concrete members [ACI 318, 1999]. The procedure is illustrated for a rectangular concrete section in Figure 10.4, where the maximum usable concrete strain, ε_{cu} , is developed

at the extreme compressive fiber simultaneously as the strain in the CFRP composite, ϵ_{CFRP}^* , reaches the value equal to 0.007 assumed for debonding.

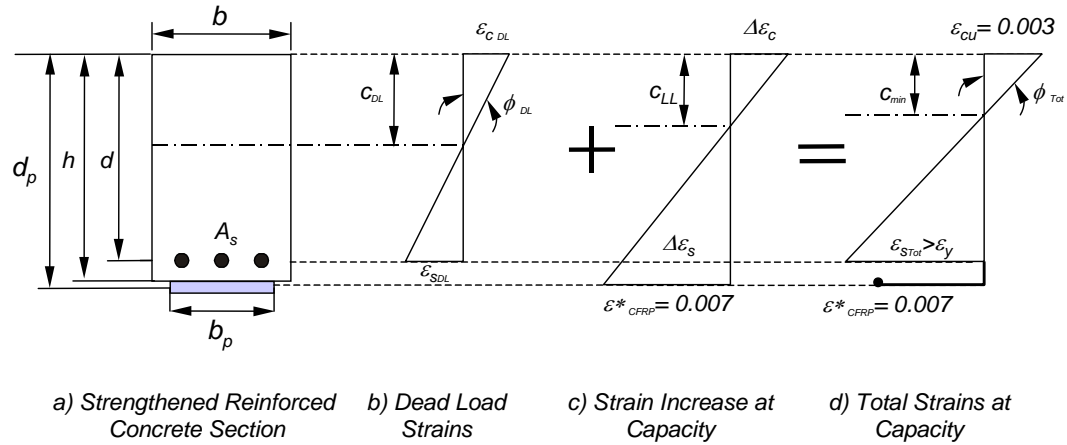


Figure 10.4 Strain Profile for Maximum Recommended Area of CFRP Composite

The maximum recommended area of CFRP composite can be calculated from horizontal force equilibrium, assuming that the distribution of compressive stresses can be represented by the commonly used rectangular stress block. In this calculation, the reinforcing steel is assumed to yielded. Horizontal force equilibrium yields:

$$A_{p\max} = \frac{0.85 f'_c b a_{\min} + A_s f_y}{\epsilon_{CFRP}^* E_p} \quad (10.8)$$

where

- a_{min} = Depth of the equivalent compressive stress block corresponding to concrete crushing at the same time the CFRP debonds from the surface of the concrete, in.
- $A_{p\ max}$ = Area of CFRP composite that generates concrete crushing and debonding at the same time, in².

and other variables were defined previously.

The depth of the rectangular stress block is assumed to be equal to β_1 times the neutral axis depth, c_{min} [ACI 318, 1999]. The neutral axis depth can be determined from compatibility of strains using:

$$c_{min} = \left(\frac{\varepsilon_{cu}}{\varepsilon_{cu} + \varepsilon_{sTot}} \right) d \quad (10.9)$$

where

$$\varepsilon_{sTot} = \frac{\varepsilon_{CFRP}^* d + \Delta\varepsilon_c d_p}{d_p(1 - \Delta\varepsilon_c)} + \varepsilon_{sDL} \quad (10.10)$$

The first term in Eq. (10.10) represents the increment in strains, $\Delta\varepsilon_s$, generated at capacity of the cross section. This value was calculated using the strain diagram presented in Figure 10.4. As discussed in Section 10.2.1, the existing strain condition caused by dead loads must be established for the calculation of the maximum area of CFRP composite.

The area of CFRP calculated with this procedure would cause the member to simultaneously fail by debonding and concrete crushing at the design capacity. The capacity of the strengthened member is reached after yielding of the reinforcement so adequate deformation capacity is expected. For design purposes, however, to insure debonding prior to concrete crushing, the maximum area of CFRP composite for a specific cross section is recommended to be limited to 90% of $A_{p \max}$.

10.3 RECOMMENDED STRENGTH REDUCTION FACTOR FOR USE IN THE BASIC DESIGN EQUATION

Current design practice for reinforced concrete design uses load and resistance factors in the basic design equation. The basic design equation contained in the *AASHTO Standard Specifications* [1996], expressed in terms of flexural actions can be written as:

$$M_u = \gamma_{DL}M_{DL} + \gamma_{LL}M_{LL}(1 + I) \leq \phi M_n \quad (10.11)$$

where

- M_{DL} = Maximum moment caused by dead loads, kip-in.
- M_{LL} = Maximum moment caused by live loads, kip-in.
- M_u = Maximum factored moment generated on the element, kip-in.
- M_n = Nominal flexural resistance, kip-in.
- I = Impact factor = 0.3.
- γ_{DL} = Load factor for dead load effects = 1.3.

- γ_{LL} = Load factor for live load effects = 2.17.
 ϕ = Strength reduction factor used for design.

Therefore, the required nominal moment capacity, $M_{n \text{ req}}$, to resist the design moment can be determined by writing Eq. 10.11 in terms of M_n :

$$M_{n \text{ req}} = \frac{M_u}{\phi} \quad (10.12)$$

The value that was used for the strength reduction factor, ϕ , in the design of the laboratory specimens was 0.85. The observed deflection response of the laboratory specimens was considered adequate and consistent with the current design philosophy implicit in the design of reinforced concrete flexural members. Therefore this value is recommended for the design of strengthening systems until more information is available to support the use of a higher value.

It is important to note that the use of this value was only evaluated for the failure mode that was observed in the laboratory. The failure sequence involved yielding of the reinforcing steel prior to debonding of the CFRP composites from the surface of the concrete. Therefore, this value for ϕ should only be used in designs similar to those presented for the laboratory specimens in this dissertation, where yielding of the steel reinforcement precedes debonding of the CFRP composites from the surface of the concrete.

10.4 SERVICEABILITY CONSIDERATIONS

The bridge sections that were studied in this research project exhibited adequate response under service-load conditions. No indications of distress along the composite-concrete interface were observed during the tests. Debonding always initiated at load levels that were above yielding.

Therefore, the yield capacity of the strengthened section should not be exceeded under the increased service loads to prevent damage to the composite-concrete interface. For the design conditions that were encountered in this research project, increased service loads on the bridge elements represented a maximum of approximately 70% of the yield capacity. The procedures described in Chapter 3 should be used to determine the yield capacity of the strengthened sections.

10.5 DETAILING RECOMMENDATIONS

The recommendations presented in this section were not supported by engineering calculations, but are based on experience gained from the laboratory tests of the strengthened specimens. These detailing practices are suggested based on the observation of adequate response of the strengthened test specimens.

10.5.1 Anchoring Straps

As discussed previously the observed failure of the strengthened elements was characterized by debonding of the CFRP composites from the surface of the

concrete. However, local debonding was observed before total debonding of the composite elements. Debonding was observed only after the longitudinal reinforcement yielded. The longitudinal CFRP composites were restrained from debonding by CFRP straps positioned at a space equal to $h/2$ along the length of the beam.

An analytical model to determine the required width, length, spacing, and position of the anchoring straps was not developed because debonding is a complicated phenomenon that is greatly influenced by the tensile strength of the concrete and the extent of cracking. These conditions vary greatly in the field and are essentially impossible to quantify in an existing reinforced concrete bridge. The straps were provided where debonding was expected to start, and this was always near the section of maximum moment. However, for a real structure, the section of maximum moment is generated under the axle of a moving truck and therefore, this section can vary depending on the span and loading configuration. Therefore, it is suggested that straps be provided along the entire length of the longitudinal composites used for flexural strengthening.

Strap spacing was based on the assumption that diagonal cracks would be oriented 45° from horizontal and that these cracks would trigger local debonding of the CFRP composite. Therefore, the strap spacing was selected such that at least one strap would cross a potential diagonal crack in the reinforced concrete bridge

element. A maximum spacing equal to the height of the cross section divided by two ($h/2$) was thus established.

The length of the straps can be determined by extending them beyond mid-depth to insure that the potential diagonal crack is crossed by a strap. The length of the extension should be determined so that the full tensile strength of the strap is developed at the crack location. Experimental studies conducted by other investigators [Bizindavyi and Neale, 1999] concluded that the maximum strength of 1-ply CFRP composites bonded to a concrete surface can typically be developed within a distance of approximately 3 to 4 in. measured from the free end. In these tests, the CFRP composites were attached to the concrete surface and subjected to direct shear by pulling with a force parallel to the bond surface at the free edge of the composite. Based on these results and the observations from this research project, it is recommended that the minimum strap length should extend at least 4 in. beyond the element mid-depth.

Finally, the width of the straps was selected based on the width of the longitudinal CFRP composites, bonded to either the bottom or side of the specimens. This dimension is recommended for use in design.

10.5.2 Length of CFRP Composites

The determination of the length for the composites that were used to strengthen the laboratory specimens was discussed in Chapters 5 and 8 for the pan-

joist and the flat-slab specimens, respectively. This length was based on the loading configuration that was used in the laboratory tests. The length of the CFRP composites required in an actual bridge, however, depends on the factored moment diagram acting on the bridge. This moment diagram is controlled by the live loads generated by the design vehicle. The procedure to determine the cut-off point on one side of the bridge is illustrated schematically in Figure 10.5. The CFRP composites should be extended at least a distance equal to the height of the member, h , from the theoretical cut-off point. However, this point will be located very close to the support in many cases for the bridges considered in this research study because of their short span length. In these cases, it is recommended that the CFRP composites be attached along the entire bridge span.

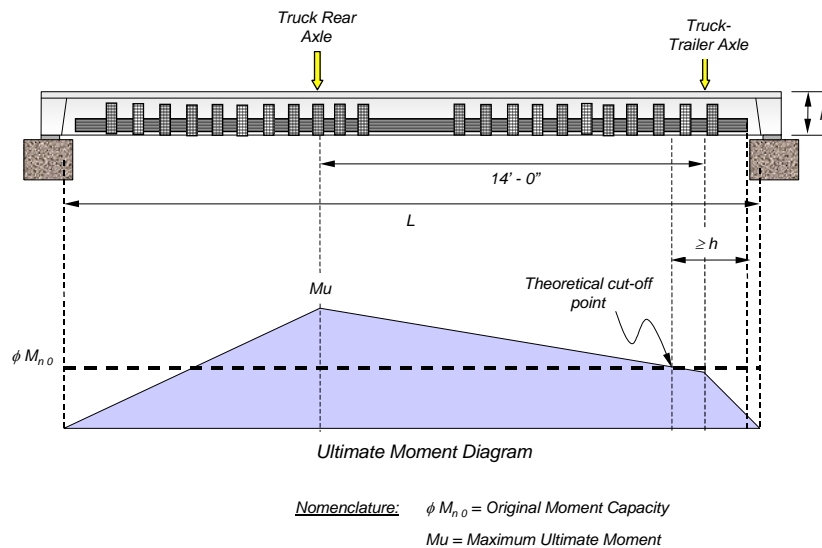


Figure 10.5 CFRP Composite Length Determined Based on Ultimate Moment Diagram

10.6 SUMMARY

Recommendations for the design of flexural strengthening techniques for reinforced concrete elements using CFRP composites were presented in this chapter. These recommendations were based on the results of the experimental portion of this research project and engineering judgement. Therefore, the procedures that are outlined in this chapter are only strictly applicable to similar situations encountered in the field.

| | |
|---|------------|
| CHAPTER 10: DESIGN RECOMMENDATIONS | 310 |
| 10.1 Introduction | 310 |
| 10.2 Calculation of Nominal Flexural Capacity of Strengthened Sections..... | 311 |
| 10.2.1 Strain Distribution within Strengthened Sections..... | 312 |
| 10.2.2 Preliminary Estimate of the Area of CFRP Composite | 315 |
| 10.2.3 Maximum Recommended Area of CFRP Composite | 319 |
| 10.3 Recommended Strength Reduction Factor for Use in the Basic Design Equation | 322 |
| 10.4 Serviceability Considerations..... | 324 |
| 10.5 Detailing Recommendations..... | 324 |
| 10.5.1 Anchoring Straps | 324 |
| 10.5.2 Length of CFRP Composites | 326 |
| 10.6 Summary | 328 |
| Figure 10.1 Calculation of Strains Caused by Dead-Load Moments | 313 |
| Figure 10.2 Increment of Strains on Strengthened Reinforced Concrete Section | 314 |
| Figure 10.3 Internal Stress Distribution for a Strengthened Rectangular Section at Capacity | 318 |
| Figure 10.4 Strain Profile for Maximum Recommended Area of CFRP Composite | 320 |
| Figure 10.5 CFRP Composite Length Determined Based on Ultimate Moment Diagram | 327 |

Chapter 11: Summary and Conclusions

11.1 SUMMARY

Laboratory tests were conducted on four full-scale reinforced concrete bridge specimens that were strengthened using carbon fiber reinforced polymer composites. The specimens represent two types of bridge construction that were very common in Texas approximately 50 years ago: pan-joint bridges and flat-slab bridges. The measured response of the laboratory specimens was compared with the calculated response using an analytical model that was developed to study the flexural behavior of reinforced concrete beams strengthened with CFRP composites.

The response of the strengthened specimens was excellent, and the design objectives were fully accomplished. The CFRP composites had little influence on the response of the specimens up to the yield load. A marginal increase in stiffness was observed after strengthening under low load levels; however, the yield load of the reinforced concrete element was not increased significantly.

However, the post-yield behavior of the specimens was drastically different from the response of a reinforced concrete element. The stiffness of the specimens after yielding was much higher than the stiffness expected of a bare reinforced

concrete element. Also, the measured strength exceeded the nominal capacity calculated during design of the test specimens.

Examination of the measured load-deflection response during the tests demonstrated that CFRP composites are effective in increasing the flexural strength of existing reinforced concrete elements. The maximum strength of the specimens was always controlled by CFRP debonding from the surface of the concrete. CFRP straps were attached transversely along the longitudinal composites to control the propagation of debonding and increase the deformation capacity of the specimens before failure. These straps also provided ample warning of impending failure due to debonding of the longitudinal composites.

An analytical model was developed to calculate the moment-curvature response for a strengthened cross section using the nonlinear properties of the materials. The global load-deflection response of the laboratory specimens was well represented with the analytical model. However, the calculated response at the section level sometimes departed from the measured response. This was mainly attributed to local effects such as the concentration of strains at a section caused by its proximity to cracks in the concrete. Local debonding of the CFRP composites from the surface of the concrete also affected the measured response. However, the analytical model was considered to be appropriate for reproducing the general

trends in the behavior of the strengthened elements, and was therefore recommended for use in design.

The controlling mode of failure in all four full-scale specimens was debonding of the composites from the concrete surface. The maximum strain that was developed in the CFRP composites prior to debonding was measured during the tests at discrete locations. This value was compared with the maximum expected strain assuming perfect bond to the surface of the concrete. The large variations in the difference between calculated and measured values indicated that strain measurements are largely influenced by local effects. Therefore, it is recommended to use a conservative estimate of the maximum strain that can be developed before debonding in design.

Design recommendations were developed based on the results of the laboratory tests and on the comparisons of the measured and calculated response. The design procedures are based on the assumption that the original reinforced concrete cross section is under-reinforced and that the steel will yield before the CFRP debonds in the strengthened cross section.

11.2 CONCLUSIONS

The results of earlier phases of this investigation [Bramblett, 2000; Benouaich, 2000] demonstrated that CFRP composites represent a viable means of

increasing the flexural strength of reinforced concrete beams. The four different CFRP systems that were investigated in these phases performed satisfactorily. Fatigue loading, sustained service-level loads, and exposure to wetting and drying cycles did not affect the behavior of the strengthened beams. Therefore, CFRP composites should be considered seriously for strengthening existing reinforced concrete bridges that were proportioned using lighter design vehicles, but do not exhibit any signs of deterioration after many years in service.

While most of the strengthened beams failed after the CFRP composites debonded from the surface of the concrete, this mode of failure was delayed by using transverse CFRP straps. In addition, placement of the longitudinal CFRP on the sides of the cross section, rather than on the bottom, reduced the tendency of the CFRP composites to pry off the surface of the concrete at locations where the laminates crossed existing cracks.

The prototype pan-joint and flat-slab bridges selected for study in phase 3 of this investigation were both designed to carry two, H-10 loading vehicles. The CFRP composites were selected for the pan-joint test specimens were selected to increase the inventory rating for the bridge to HS-20. When the curbs were removed from the prototype flat-slab bridge, the inventory rating for the slab alone was HS-6. In this case, the CFRP composites for the flat-slab specimens were designed to increase the inventory rating of the slab to HS-10.

The design procedures developed during this study were successful, and the strengthened specimens exceeded the desired capacities. All specimens exhibited significant inelastic behavior before the CFRP composites debonded from the surface of the concrete. The transverse straps began to exhibit distress after the longitudinal reinforcement in the specimens yielded, and provided ample warning of imminent failure.

In accordance with accepted flexural design procedures [ACI, 1999; AASHTO, 1996], the amount of longitudinal CFRP composites applied to a reinforced concrete beam should be limited such that the reinforcing steel yields before failure. For traditional reinforced concrete beams, failure is defined by crushing of the concrete, while failure is defined by debonding of the composites for the strengthened beams. In addition, transverse straps should be provided along the entire length of the reinforced concrete beam at a spacing not to exceed one-half the depth of the cross section in order to control debonding.

The two CFRP systems that were used to strengthen the laboratory specimens in this phase of the research project achieved similar performance. The strengthening techniques were designed for the same target strength. The laboratory tests revealed that any of the systems may be used to achieve similar response of the strengthened structures.

Application of CFRP composites to reinforced concrete beams that were cracked under service loads did not adversely influence the performance of the

strengthened beams. However, the concrete surface was sound for all beams tested, and the design procedures described in this dissertation should not be used for bridges with damaged or deteriorated concrete.

11.3 AREAS FOR FUTURE RESEARCH

Throughout this investigation, it was observed that, in order to be able to calculate the capacity of strengthened members, adequate strain limits at which the CFRP composites debonded from the surface of the concrete need to be determined. The strain limit recommended for use in design in Chapter 10 represents a conservative estimate that was established based on the particular conditions of the tested specimens in this project. Several factors are believed to affect the maximum strain that can be developed before debonding, such as conditions of the surface of the concrete at the time of bonding, stiffness of the CFRP composite, position of the CFRP composites on the element, supplemental anchorage of the composite to the concrete element, and the shear span of the element. Clarification on the influence of these factors on the maximum strain developed before debonding requires further investigation.

In this study, the CFRP composites were used to increase the flexural capacity of the reinforced concrete elements. Transverse CFRP straps were positioned along the longitudinal composites to prevent sudden failure of the strengthening system after initial debonding. However no attempt was made to

consider the effect of these straps in the shear capacity of the strengthened member. The loading configuration used in the laboratory precluded shear failure before reaching the flexural strength of the specimens and, therefore, the composites oriented transversely were not required for shear strength. It is believed, however, that composites can be used effectively to strengthen elements for shear. Further research is required to develop design guidelines for the use of composites in this area.

| | |
|--|------------|
| CHAPTER 11: SUMMARY AND CONCLUSIONS | 329 |
| 11.1 Summary | 329 |
| 11.2 Conclusions | 331 |
| 11.3 Areas for Future Research | 334 |

Appendix A: Measured Material Properties

This appendix is divided into three sections. Concrete material properties are summarized in Section A.1, reinforcement steel properties are summarized in Section A.2, and CFRP properties are summarized in Section A.3. Concrete cylinders and steel coupons were tested as part of this research program to determine the material properties. Material properties reported by the manufacturers are summarized for the composite material systems.

A.1 CONCRETE

Concrete cylinders (6 in. diameter by 12 in. in height) were fabricated using standard ASTM procedures as specified in ASTM C-40 (ASTM, 1996). Eighteen cylinders were cast for each specimen and cured under ambient conditions in the laboratory next to the specimens. Three cylinders were tested in compression 3, 7, 14, and 28 days after casting to evaluate the change in strength with time for the concrete used in each specimen. Also, compression tests and split cylinder tests were conducted within 24 hrs of testing each specimen to establish the concrete strength at the time of testing. Table A.1 and Table A.2 summarize the results of the compressive strength tests and split cylinder tests respectively for all specimens.

A.1.1 Pan-Joist Specimens

Concrete compressive strength vs. time curves for Specimens J-1 and J-2 are shown in Figure A.1 and Figure A.2, respectively. Stress-strain curves for Specimens J-1 and J-2 are shown in Figure A.3 and Figure A.4, respectively. Cylinder strains were measured using a compression meter with an 8-in. gage length. The cylinders were tested under force control using a 600-kip Forney testing machine at an average loading rate of 800 lb/sec.

The concrete model [Hognestad, 1950] used to calculate internal stresses for all specimens is superimposed in each of these figures. This model was adjusted using the individual material properties for each specimen (maximum compressive strength, f'_c , and strain at maximum strength, ϵ_{co}). The stress-strain parameters are summarized in Table A.1.

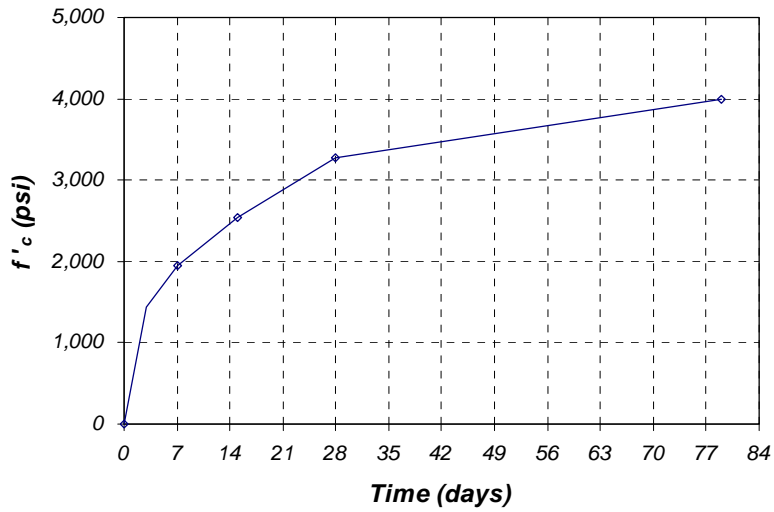


Figure A.1 Variation of Concrete Compressive Strength with Time for Specimen J-1

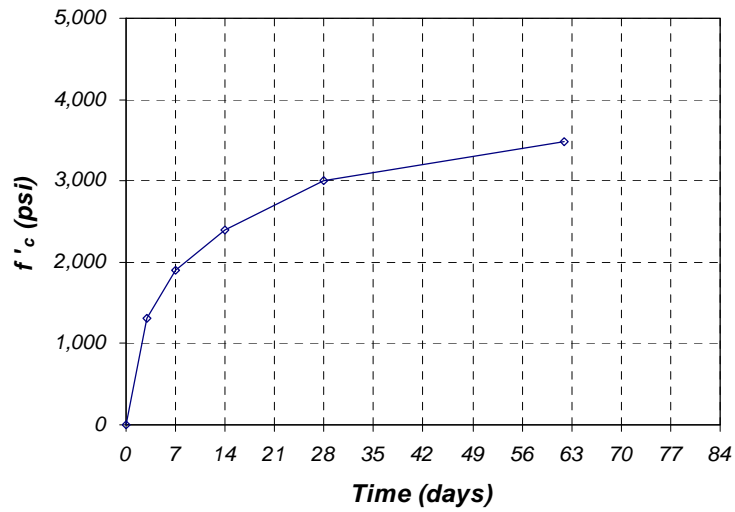


Figure A.2 Variation of Concrete Compressive Strength with Time for Specimen J-2

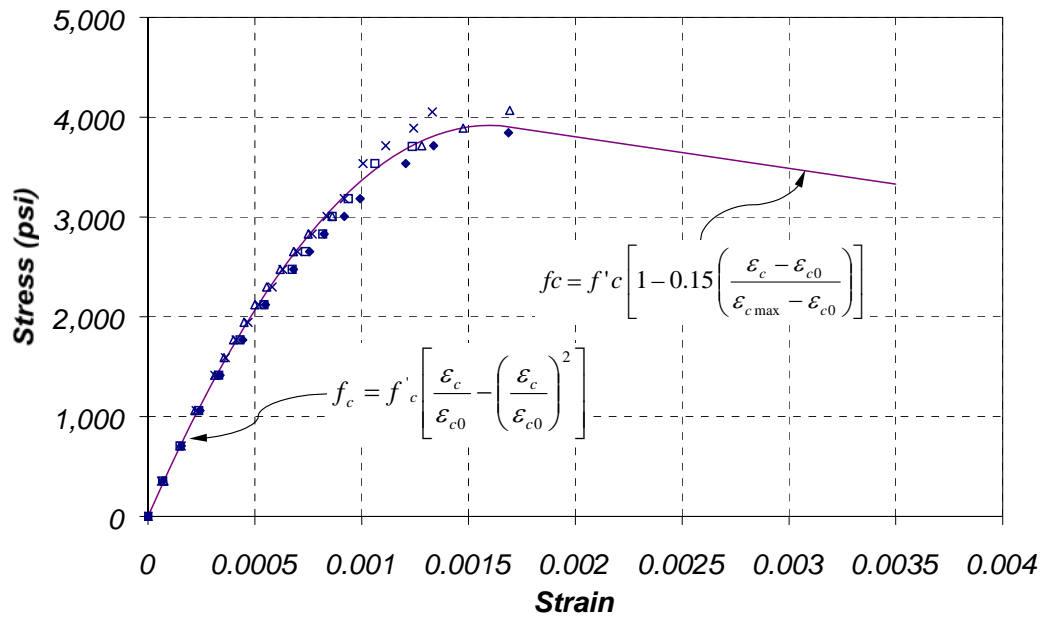


Figure A.3 Concrete Stress-Strain Curve for Specimen J-1

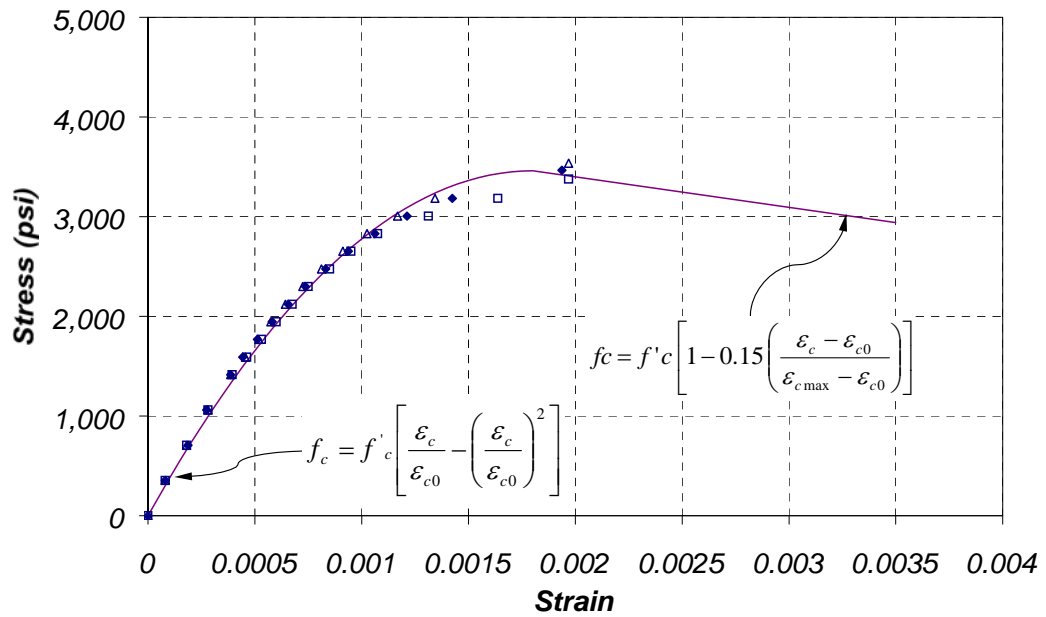


Figure A.4 Concrete Stress-Strain Curve for Specimen J-2

A.1.2 Flat Slab Specimens

Concrete compressive strength vs. time curves for Specimens FS-1 and FS-2 are shown in Figure A.5 and Figure A.6, respectively. In the case of Specimen FS-2, the specimen was tested before reaching its 28-day compression strength, so no cylinders were tested at this age. Concrete stress-strain curves for the flat slab specimens are shown in Figure A.7 and Figure A.8 respectively. These curves were obtained in the same manner as those for the joist specimens.

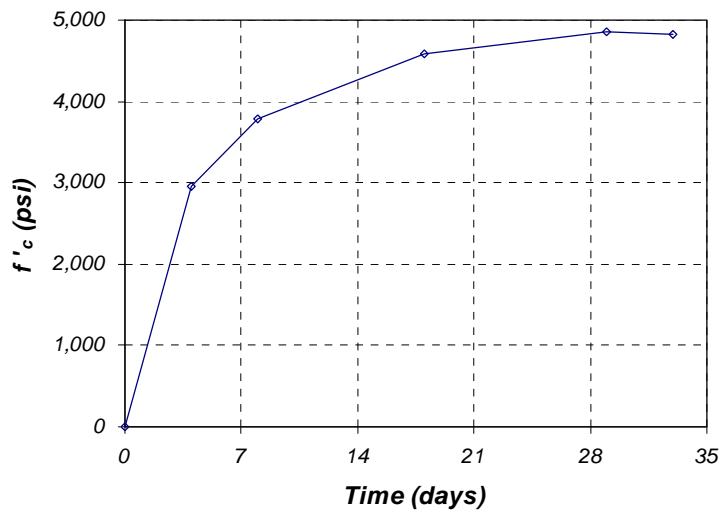


Figure A.5 Variation of Concrete Compressive Strength with Time for Specimen FS-1

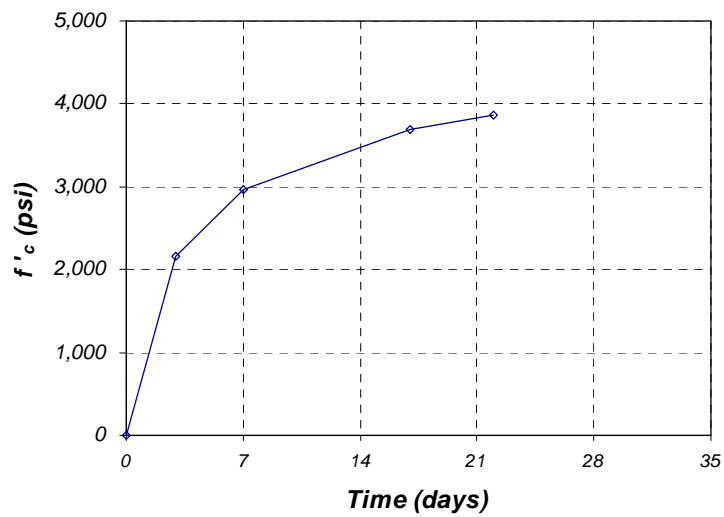


Figure A.6 Variation of Concrete Compressive Strength with Time for Specimen FS-2

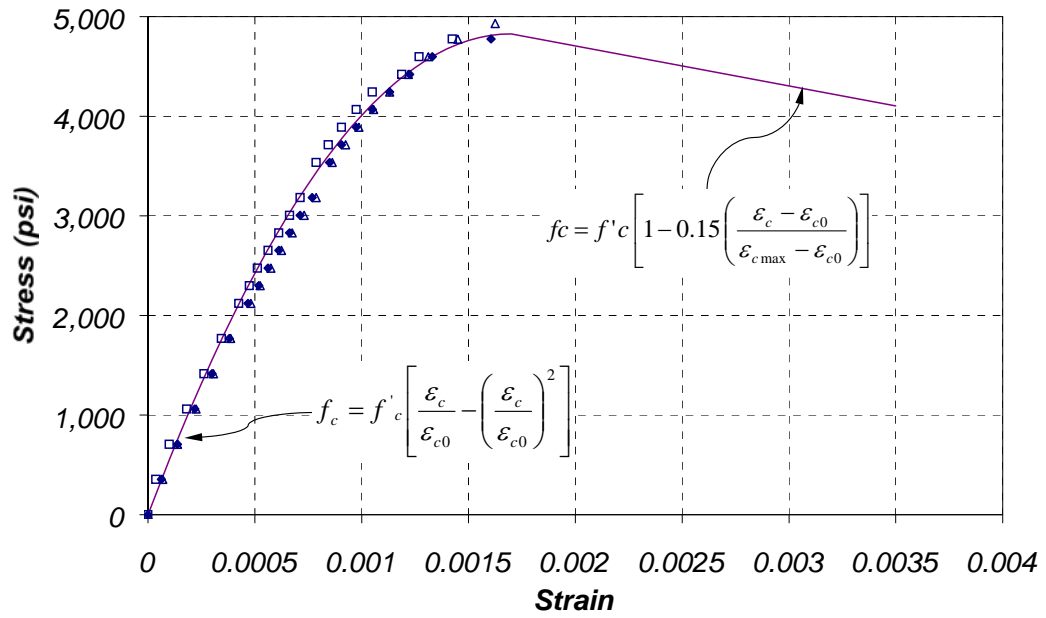


Figure A.7 Concrete Stress-Strain Curve for Specimen FS-1

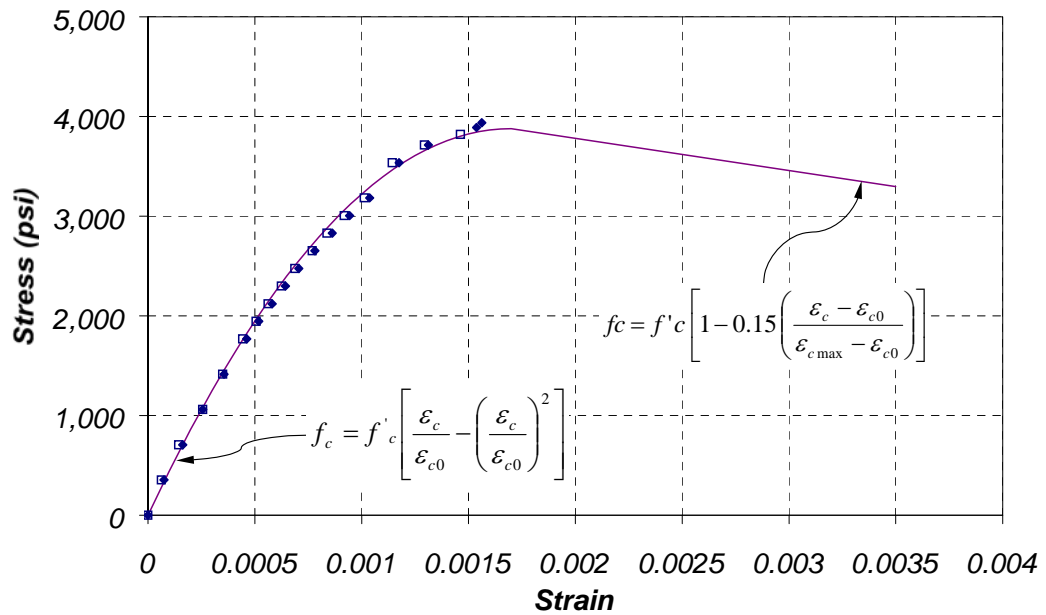


Figure A.8 Concrete Stress-Strain Curve for Specimen FS-2

Table A.1 Concrete Compression Tests and Parameters Used for Material Models

| Specimen | Age, days | Compressive Strength, psi | | | | Avg. f'_c , psi | Std. Dev., psi | ϵ_{co} |
|----------|-----------|---------------------------|--------|--------|--------|-------------------|----------------|-----------------|
| | | Test 1 | Test 2 | Test 3 | Test 4 | | | |
| J-1 | 79 | 3,850 | 3,710 | 4,070 | 4,050 | 3,920 | 170 | 0.0016 |
| J-2 | 62 | 3,470 | 3,540 | 3,380 | - | 3,460 | 80 | 0.0018 |
| FS-1 | 33 | 4,780 | 4,780 | 4,930 | - | 4,830 | 87 | 0.0017 |
| FS-2 | 22 | 3,820 | 3,940 | - | - | 3,880 | 85 | 0.0017 |

Table A.2 Tensile Strength of Concrete Determined from Split Cylinder Tests

| Specimen | Age, days | Tensile Strength, psi | | | Average f_t , psi | Standard Dev., psi |
|----------|-----------|-----------------------|--------|--------|---------------------|--------------------|
| | | Test 1 | Test 2 | Test 3 | | |
| J-1 | 79 | 450 | 380 | - | 415 | 50 |
| J-2 | 62 | 390 | 360 | - | 375 | 21 |
| FS-1 | 33 | 470 | 370 | 360 | 400 | 61 |
| FS-2 | 22 | 390 | 470 | 350 | 400 | 61 |

A.2 REINFORCING STEEL

Tension tests were done to determine the stress-strain curves for all sizes of reinforcing bars used to fabricate the specimens. Bar elongation was measured using a clip-on extensometer with an 8-in. gage length. The bars were tested in a 120-kip Tinius Olsen testing machine at a strain rate of 0.00125/min. The

extensometer was removed from the bars at a strain of approximately 0.04 to avoid damage.

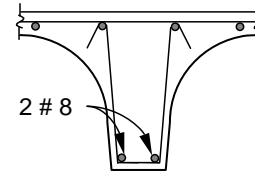
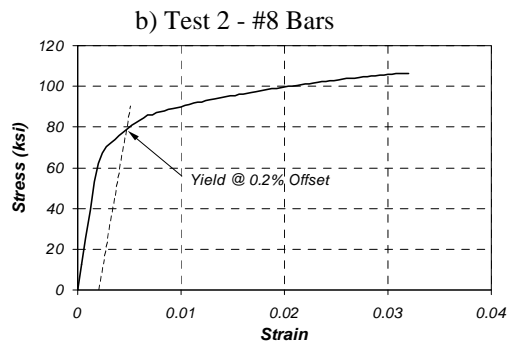
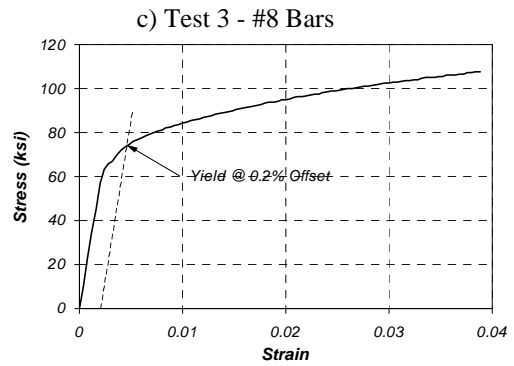
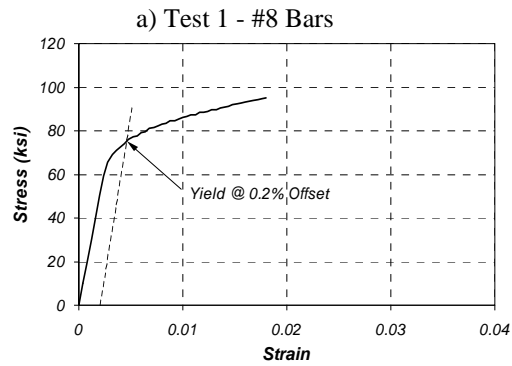
Both dynamic yield and static yield stresses were measured during these tests. . For bars with a well-defined yield plateau, the dynamic yield stress was defined as the stress measured with the testing running at the strain rate specified above. In bars that did not show a well-defined yield point, the yield stress was determined using the 0.2% offset method.

The static yield stress was determined by stopping the machine after the yield plateau was reached and holding the load during two minutes. After the two-minute hold had elapsed, the stress in the bar was determined and the machine was started and stopped again once the stress-strain plot leveled-off. This process was repeated three times. The static yield stress was defined as the average of the three readings after the load holds. Table A.3 summarizes the static and dynamic yield stresses measured during the tests and the average values used in the calculations.

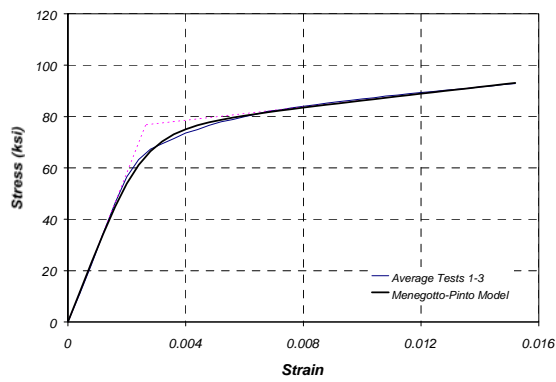
A.2.1 Pan-Joist Specimens

Four sizes of reinforcing bars were used to construct the Pan-Joist Specimens. Stress-strain curves for this reinforcement are shown in [Figures A.9 through A.12](#).

The measured stress-strain curves for the #8 bars are shown in Figure A.9. A mathematical model proposed by Menegotto and Pinto [Stanton and McNiven, 1979] was used to mimic the stress-strain behavior of these bars. The stress-strain response using this model is compared with the average measured stress-strain curves in part (d) of this figure along with the parameters for the mathematical expression that defines the model. Details of the material model are presented in Chapter 3.



d) Menegotto-Pinto Model



$$\frac{f}{f_0} = b \frac{\varepsilon}{\varepsilon_0} + \frac{(1-b) \frac{\varepsilon}{\varepsilon_0}}{\left[1 + \left(\frac{\varepsilon}{\varepsilon_0} \right)^n \right]^{\frac{1}{n}}}$$

$$b = 0.045$$

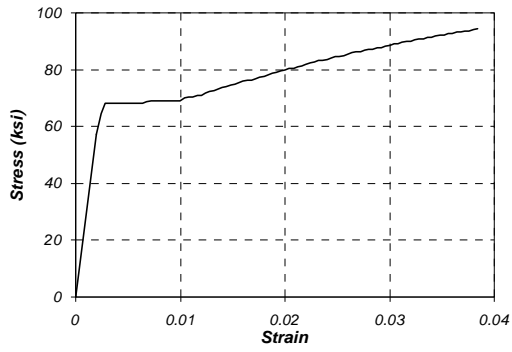
$$\varepsilon_0 = 0.0026$$

$$f_0 = 76.8 \text{ ksi}$$

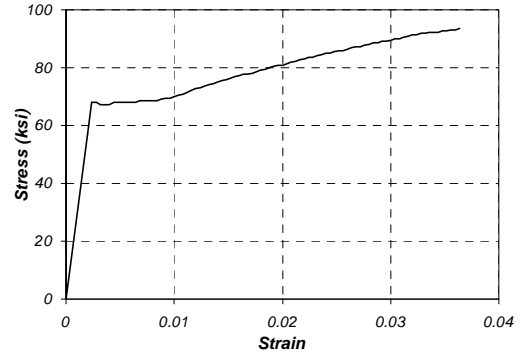
$$n = 3.83$$

Figure A.9 Stress-Strain Curves for #8 Bars in Joist Specimens

a) Test 1 - #3 Bars



c) Test 3 - #3 Bars



b) Test 2 - #3 Bars

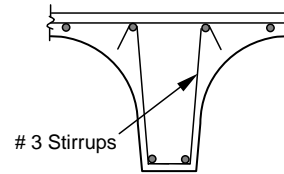
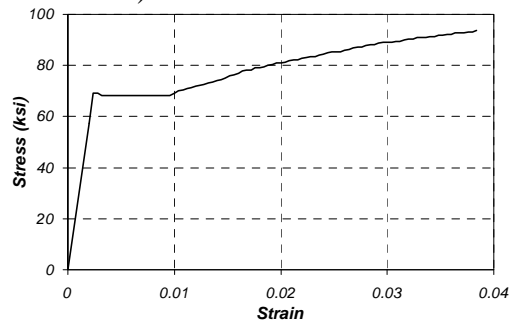


Figure A.10 Stress-Strain Curves for #3 Bars in Joist Specimens

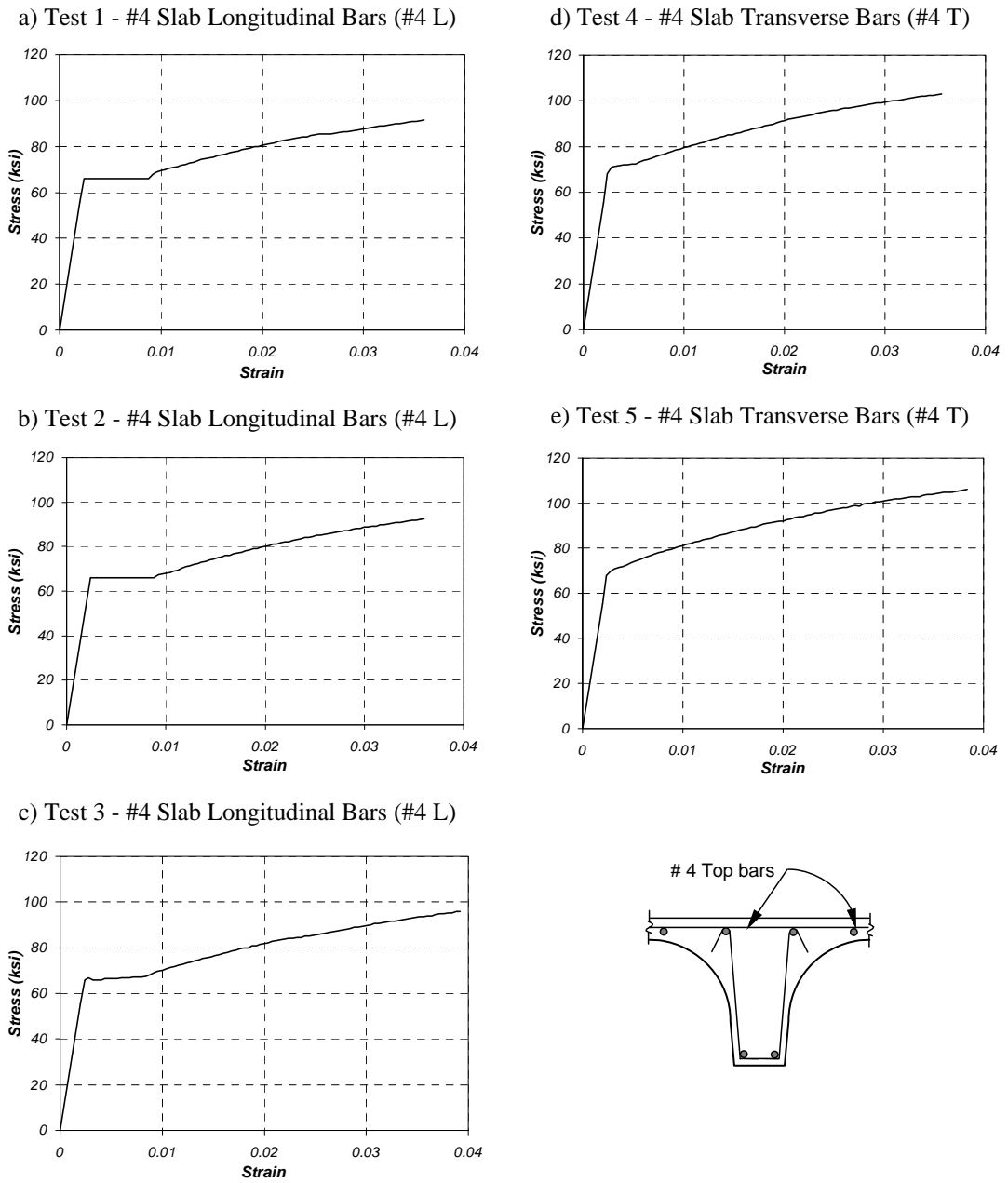


Figure A.11 Stress-Strain Curves for #4 Bars in Joist Specimens

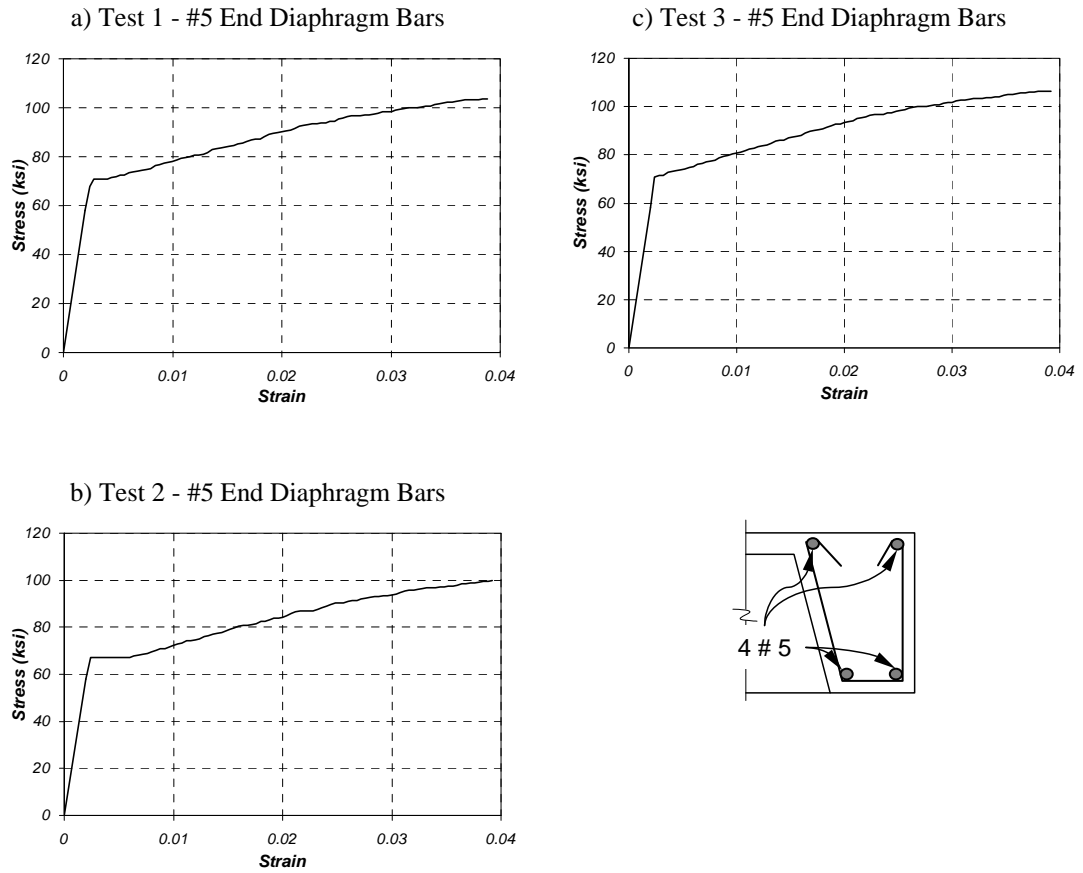


Figure A.12 Stress-Strain Curves for #5 Bars in Joist Specimens

A.2.2 Flat-Slab Specimens

Three sizes of reinforcing bars were used to construct the Flat-Slab Specimens. Strain-stress curves for this reinforcement are shown in [Figures A.13 through A.15](#).

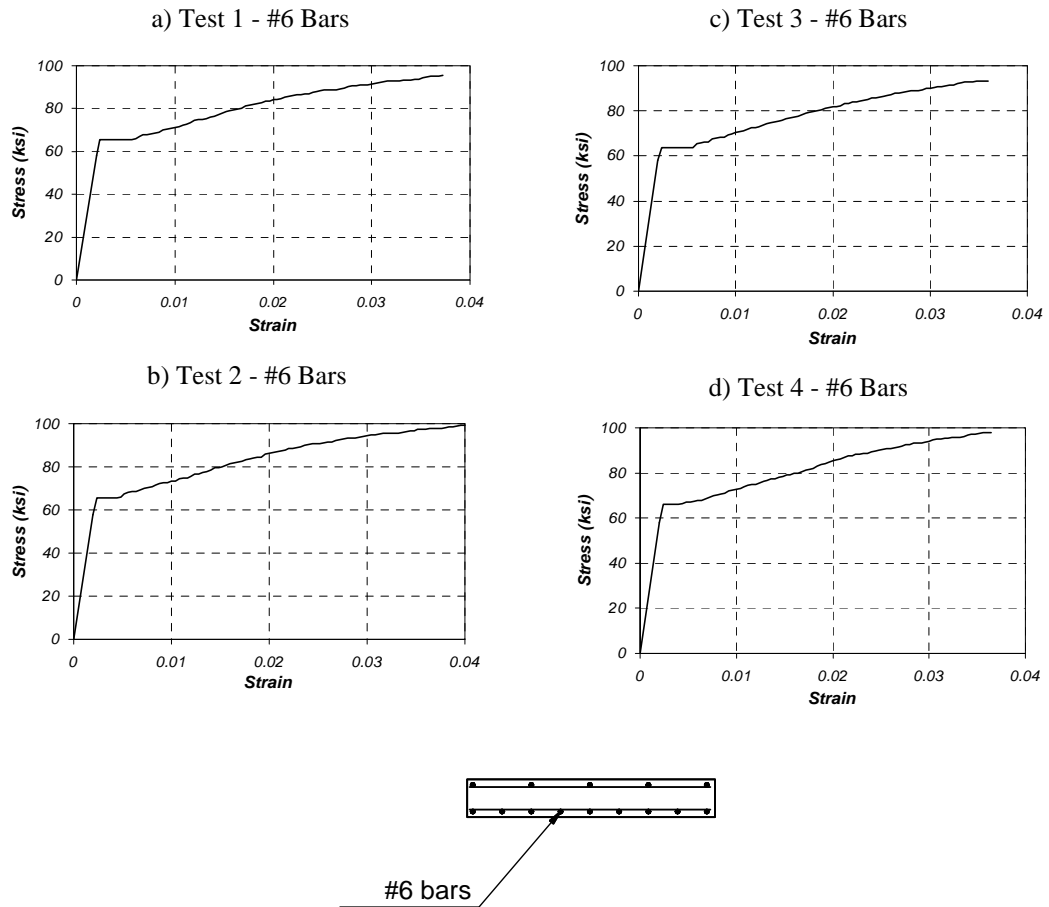
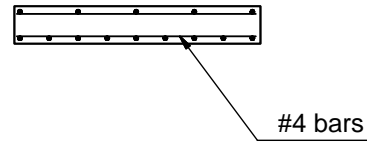
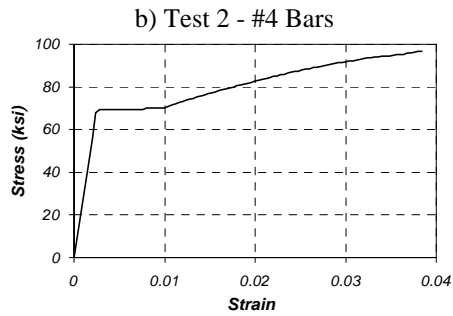
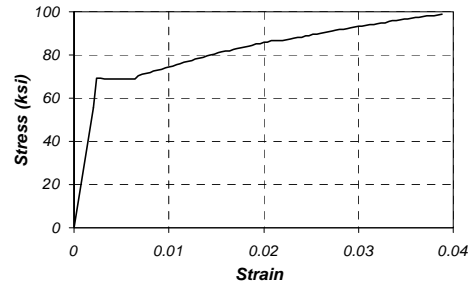
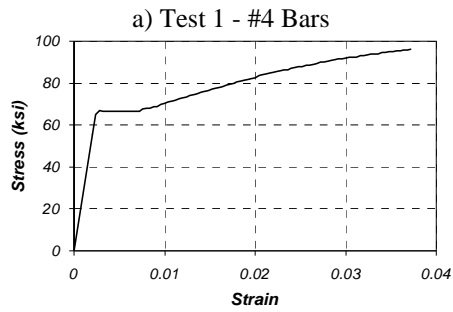


Figure A.13 Stress-Strain Curves for #6 Bars in Flat-Slab Specimens



c) Test 3 - #4 Bars

Figure A.14 Stress-Strain Curves for #4 Bars in Flat-Slab Specimens

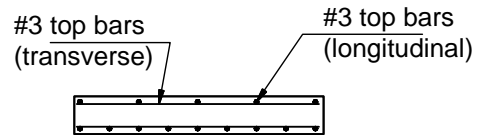
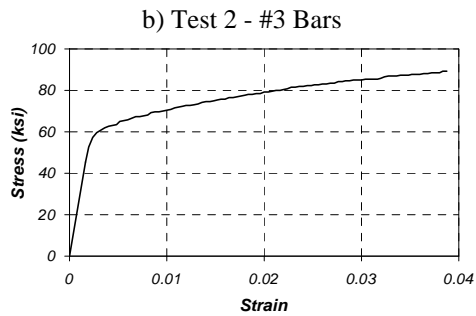
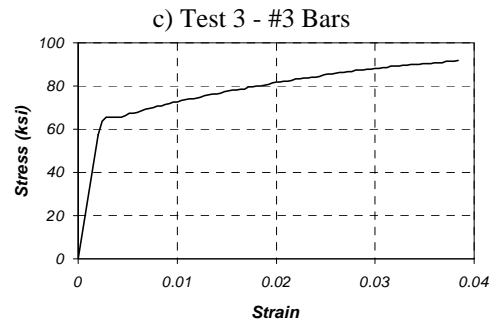
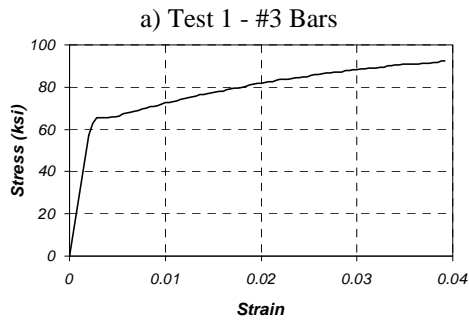


Figure A.15 Stress-Strain Curves for #3 Bars in Flat-Slab Specimens

Table A.3 Measured Yield and Ultimate Stresses for Reinforcing Bars

| Bar No. | f_y static, ksi | | | | f_y avg, ksi | Std Dev, ksi | f_y dynamic, ksi | | | | f_y avg, ksi | Std Dev, ksi | f_u avg, ksi | Std Dev, ksi |
|---------------------|-------------------|--------|--------|--------|----------------|--------------|--------------------|--------|--------|--------|----------------|--------------|----------------|--------------|
| | Test 1 | Test 2 | Test 3 | Test 4 | | | Test 1 | Test 2 | Test 3 | Test 4 | | | | |
| Pan-Joist Specimens | | | | | | | | | | | | | | |
| #8 | 75.3 | 70.0 | 72.8 | 68.5 | 71.7 | 3.0 | 77.7 | 72.2 | 74.6 | 70.3 | 73.7 | 3.2 | 114.0 | 1.9 |
| #3 | 66.3 | 64.8 | 65.1 | - | 65.4 | 0.8 | 69.0 | 68.8 | 68.2 | | 68.7 | 0.4 | 106.4 | 0.5 |
| #4L | 63.2 | 63.1 | 63.8 | - | 63.4 | 0.4 | 66.1 | 66.3 | 66.7 | | 66.4 | 0.3 | 105.1 | 0.8 |
| #4T | 69.6 | 68.7 | 69.3 | - | 69.2 | 0.5 | 72.1 | 71.1 | 71.6 | | 71.6 | 0.5 | 113.6 | 0.8 |
| #5 | 70.2 | 65.7 | 71.2 | - | 69.0 | 2.9 | 70.9 | 67.2 | 71.7 | | 69.9 | 2.4 | 112.7 | 2.7 |
| Flat-Slab Specimens | | | | | | | | | | | | | | |
| #6 | 63.1 | 64.2 | 62.4 | 64.4 | 63.5 | 0.9 | 65.0 | 65.8 | 64.4 | 66.3 | 65.4 | 0.8 | 106.1 | 1.5 |
| #4 | 63.8 | 67.1 | 66.6 | - | 65.8 | 1.8 | 67.0 | 69.7 | 69.5 | | 68.7 | 1.5 | 107.4 | 0.9 |
| #3 | 63.2 | 60.9 | 63.2 | - | 62.4 | 1.3 | 65.8 | 63.1 | 65.7 | - | 64.9 | 1.5 | 99.2 | 1.8 |

A.3 CFRP PLATES AND SHEETS

Properties for the CFRP systems were not determined in the laboratory. However, it is recommended that the CFRP systems be tested in future laboratory experiments. Coupons can be removed from the strengthened specimens after failure to determine the actual properties of the complete CFRP/epoxy system.

The values that were used in calculations are listed in Table A.4 and are the values reported in each of the manufacturers' literature. The systems used in this research project are proprietary so only the mechanical properties of the composites were available. For the composites formed using unidirectional carbon fibers, the manufacturer publishes the stress-strain parameters based on the dimensions of the fibers only and not on the thickness of the formed composite (see bottom row in Table A.4). This is the reason why the thickness of this system is smaller than the thickness of the other two types of composites listed in table.

The mechanical properties for the resins used to impregnate and bond the different composite systems to the surface of the concrete are listed in Tables A.5 through A.7. These data were also obtained from the literature published by the manufacturer of each proprietary system.

Table A.4 Properties of CFRP Composite Systems Used for Specimen Strengthening Published by Manufacturers [Master Builders, 1998; Sika, 1997]

| Composite Type | Manufacturer and System | t_p, in. | f_{pu}, ksi | E_p, ksi | ϵ_{max} (rupture) |
|-----------------------|---|------------------------------|---------------------------------|------------------------------|--|
| Pultruded | Sika, Corp. (Sika [→] Carbodur [→]) | 0.047 | 348 | 22,500 | 0.015 |
| Woven Fabric | Sika/Hexcel (SikaWrap [→] Hex 103 C) | 0.040 | 139 | 10,600 | 0.013 |
| Unidirectional Fiber | Master Builders (Mbrace TM CF 130) | 0.0065* | 505 | 33,000 | 0.015 |

* Thickness used for design calculations. Actual thickness after fabrication ranges from 0.03 to 0.06 in. per ply.

Table A.5 Mechanical Properties of Resin (Mbrace™ Saturant) used for Mbrace™ System [Master Builders, 1998]

| Property | Tension¹ | Flexure² | Compression³ |
|--------------------------|----------------------------|----------------------------|--------------------------------|
| Maximum Stress (psi) | 8,000 | 20,000 | 12,500 |
| Stress at Yield (psi) | 7,800 | 20,000 | 12,500 |
| Stress at Rupture (psi) | 7,900 | 18,000 | - |
| Strain at Maximum Stress | 0.030 | 0.042 | 0.050 |
| Strain at Yield | 0.025 | 0.038 | 0.050 |
| Strain at Rupture | 0.035 | 0.050 | - |
| Elastic Modulus (psi) | 440,000 | 540,000 | 380,000 |
| Poisson's Ratio | 0.40 | - | - |

Notes: Properties determined at 72° F and 40% relative humidity after curing for 7 days.

¹ASTM D-638 [ASTM, 2000a]

²ASTM D-790 [ASTM, 2000b]

³ASTM D-695 [ASTM, 1996]

Table A.6 Mechanical Properties of Epoxy Paste (SikaDur[→] 30) Used to Bond Pultruded Plates [Sika, 1997]

| Property | Tension¹ | Flexure² | Compression³ |
|--------------------------|----------------------------|----------------------------|--------------------------------|
| Maximum Stress (psi) | 3,600 | 6,800 | 8,600 |
| Strain at Maximum Stress | 0.010 | - | - |
| Elastic Modulus (psi) | 650,000 | 1,700,000 | 390,000 |

Notes: Properties determined at 73° F and 50% relative humidity after curing for 7 days.

¹ASTM D-638 [ASTM, 2000a]

²ASTM D-790 [ASTM, 2000b]

³ASTM D-695 [ASTM, 1996]

Table A.7 Mechanical Properties of Impregnating Resin (SikaDur[→] Hex 300/306) for SikaWrap[→] Hex 103 C Woven Fabric [Sika, 1999]

| Property | Tension¹ | Flexure² |
|--------------------------|----------------------------|----------------------------|
| Maximum Stress (psi) | 10,500 | 17,900 |
| Strain at Maximum Stress | 0.048 | - |
| Elastic Modulus (psi) | 459,000 | 452,000 |

Notes: Properties determined at 73° F and 50% relative humidity after curing for 7 days.

¹ASTM D-638 [ASTM, 2000a]

²ASTM D-790 [ASTM, 2000b]

³ASTM D-695 [ASTM, 1996]

| | |
|--|------------|
| APPENDIX A: MEASURED MATERIAL PROPERTIES..... | 336 |
| A.1 Concrete | 336 |
| A.1.1 Pan-Joist Specimens | 337 |
| A.1.2 Flat Slab Specimens..... | 340 |
| A.2 Reinforcing Steel | 343 |
| A.2.1 Pan-Joist Specimens | 344 |
| A.2.2 Flat-Slab Specimens | 350 |
| A.3 CFRP Plates and Sheets | 353 |
| Figure A.1 Variation of Concrete Compressive Strength with Time for Specimen J-1 | 338 |
| Figure A.2 Variation of Concrete Compressive Strength with Time for Specimen J-2 | 338 |
| Figure A.3 Concrete Stress-Strain Curve for Specimen J-1 | 339 |
| Figure A.4 Concrete Stress-Strain Curve for Specimen J-2..... | 339 |
| Figure A.5 Variation of Concrete Compressive Strength with Time for Specimen FS-1 | 341 |
| Figure A.6 Variation of Concrete Compressive Strength with Time for Specimen FS-2 | 341 |
| Figure A.7 Concrete Stress-Strain Curve for Specimen FS-1 | 342 |
| Figure A.8 Concrete Stress-Strain Curve for Specimen FS-2..... | 342 |
| Figure A.9 Stress-Strain Curves for #8 Bars in Joist Specimens | 346 |
| Figure A.10 Stress-Strain Curves for #3 Bars in Joist Specimens | 347 |
| Figure A.11 Stress-Strain Curves for #4 Bars in Joist Specimens | 348 |
| Figure A.12 Stress-Strain Curves for #5 Bars in Joist Specimens | 349 |
| Figure A.13 Stress-Strain Curves for #6 Bars in Flat-Slab Specimens..... | 350 |
| Figure A.14 Stress-Strain Curves for #4 Bars in Flat-Slab Specimens..... | 351 |
| Figure A.15 Stress-Strain Curves for #3 Bars in Flat-Slab Specimens..... | 351 |
| Table A.1 Concrete Compression Tests and Parameters Used for Material Models | 343 |
| Table A.2 Tensile Strength of Concrete Determined from Split Cylinder Tests . | 343 |
| Table A.3 Measured Yield and Ultimate Stresses for Reinforcing Bars..... | 352 |
| Table A.4 Properties of CFRP Composite Systems Used for Specimen Strengthening Published by Manufacturers [Master Builders, 1998; Sika, 1997]..... | 354 |

| | |
|--|-----|
| Table A.5 Mechanical Properties of Resin used for Mbrace™ System (Mbrace™ Saturant) [Master Builders, 1998] | 355 |
| Table A.6 Mechanical Properties of Epoxy Paste (SikaDur→ 30) Used to Bond Pultruded Plates [Sika, 1997] | 356 |
| Table A.7 Mechanical Properties of Impregnating Resin (SikaDur→ Hex 300/306) for SikaWrap→ Hex 103 C Woven Fabric [Sika, 1999] | 356 |

Appendix B: Bridge Load Rating Procedure

B.1 INTRODUCTION

The bridge load rating method contained in the AASHTO *Manual for Condition Evaluation of Bridges* [AASHTO, 1994] is summarized in this appendix. There are two rating methods as described in the AASHTO *Manual* [1994]: an allowable stress method and a load factor method. The method that was chosen for this research study is presented in Section B.4 and is based on the use of load factors.

The first step to determine the load rating of the prototype bridges used in this research project was to calculate the dead and live-load moments acting on the structural components. For the pan-joint prototype bridge, the dead-load moment was based on the self-weight of each joist and a weight provision for a ½ in. overlay. Live-load moments were calculated based on the distribution of wheel loads to individual joists depending on the joist spacing. The procedure is described in detail in Chapter 4.

For the flat-slab prototype bridge, the procedure to distribute the dead and live-load moments to the flat-slab and curbs was based on empirical coefficients developed from analytical studies conducted at the University of Illinois in the 1940s. Coefficients to distribute moments to the slab and curbs were obtained from

the analysis of edge-stiffened plates using elastic plate theory [Jensen et al., 1943].

This procedure is summarized in Section B.3.

B.2 DESCRIPTION OF DESIGN TRUCKS USED FOR LOAD RATING

Load rating is used as a measure of the load-carrying capacity of a bridge. Therefore, the load rating of a bridge is specified in terms of the same trucks that are used for design. Two different design trucks are used to specify the load rating of a bridge: H-truck and HS-truck. The characteristics of the design vehicles are illustrated in Figure B.1 [AASHTO, 1996].

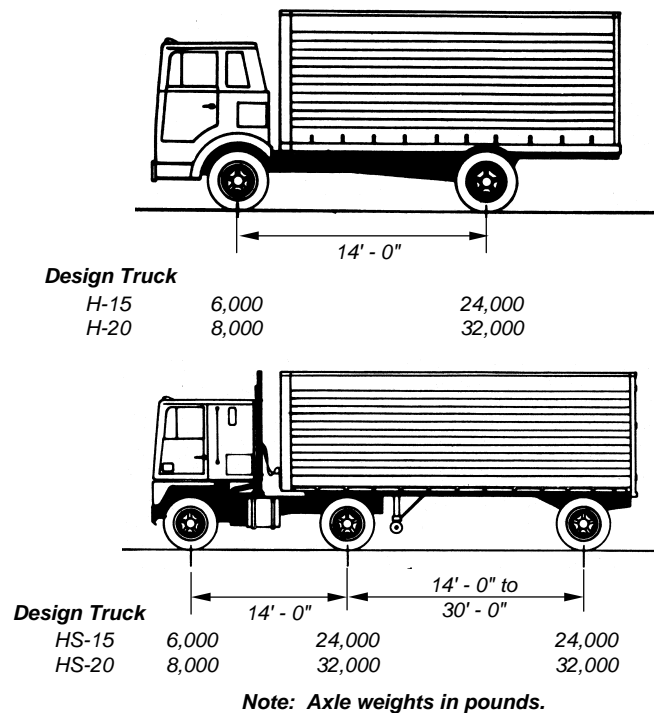


Figure B.1 Design Trucks used for Bridge Load Rating

B.3 DISTRIBUTION OF MOMENTS ON FLAT-SLAB BRIDGES

The total maximum moment at midspan on a short-span simply-supported bridge can be calculated using:

$$M_{total} = m \frac{Pl}{4} + \frac{pbl^2}{8} + \frac{2ql^2}{8} \quad (B.1)$$

where

- m = Number of wheel loads on bridge.
- P = Live load due to one rear wheel.
- l = Span length of the bridge from center to center of bearing areas.
- p = Dead load per unit area between inside faces of curbs.
- b = Width of the roadway between inside faces of curbs.
- q = Dead load per unit length along curb.

The first term in Eq. B.1 represents the moment due to live load from wheel loads at midspan, the second term represents the moment due to the dead load of the slab, and the third term represents the moment due to the dead load of the curbs. Equation B.1 assumes that the maximum live-load moment occurs when the rear axle of an H-design truck is located at mid-span. However, when multiple axles of the HS-truck configuration generate moments that are larger than the moments from the H-truck configuration at mid-span, the live-load moment at mid-span from a single axle is increased to the live-load moment caused by multiple axles on the bridge.

The total moment across the bridge is distributed to the curbs and slab using empirical coefficients. The moment distributed to the curbs can be calculated using:

$$M_{curb} = C_1 \frac{Pl}{4} + C_2 \frac{pbl^2}{8} + C_3 \frac{2ql^2}{8} \quad (B.2)$$

with the empirical coefficients, C_i , determined from:

$$C_1 = \left(\frac{12}{2.5 + G} \right) \frac{4 - (v/l)}{4 + 28(v/l)} \quad (B.3)$$

$$C_2 = \frac{0.5(l/b)}{0.47G + \sqrt[3]{1.15 + (l/b)^3}} \quad (B.4)$$

$$C_3 = \frac{\sqrt[3]{1.15 + (l/b)^3}}{0.47G + \sqrt[3]{1.15 + (l/b)^3}} \quad (B.5)$$

where

$$G = \text{Stiffness parameter} = \frac{lh^3}{12I}$$

h = Overall depth of slab.

I = Moment of inertia of the gross section of the curb outside the roadway width.

v = Axle width, center to center of truck tires.

The moment distributed to the slab is then calculated by subtracting the moment distributed to the curbs, M_{curb} , from the total static moment, M_{total} .

However, the moment calculated from Eq. B.2 is based on a wheel load located 2 ft from the curb to generate the maximum effect on the curb. Therefore, the term corresponding to live-load moment in Eq. B.2 is first reduced by 25% before subtracting the moment from the two curbs from the total moment across the bridge, M_{total} . This reduction reflects a truck location closer to the centerline of the roadway to generate maximum effects on the slab:

$$M_{es} = (m - 1.5C_1) \frac{Pl}{4} + (1 - 2C_2) \frac{pbl^2}{8} + (2 - 2C_3) \frac{ql^2}{8} \quad (\text{B.6})$$

Therefore, the average moment per unit width of slab can be calculated as:

$$M_{slab} = (m - 1.5C_1) \frac{Pl}{4b} + (1 - 2C_2) \frac{pbl^2}{8} + (1 - C_3) \frac{ql^2}{4b} \quad (\text{B.7})$$

The studies used to develop these provisions indicated that a portion of the slab adjacent to the curbs acted compositely and forming an L-shaped section on each side of the bridge. The recommended width acting compositely with the curbs was equal to 4 times the slab thickness. Therefore, the moment that needs to be resisted by the L-shaped curbs can be calculated as:

$$M_{L-curb} = M_{curb} + 4hM_{slab} \quad (\text{B.8})$$

Finally, for load rating, dead and live-load effects have to be considered separately on the individual components. The separate effects due to dead loads and live loads can be calculated from:

$$(M_{slab})_{DL} = (1 - 2C_2) \frac{pl^2}{8} + (1 - C_3) \frac{ql^2}{4b} \quad (\text{B.9})$$

$$(M_{slab})_{LL} = (m - 1.5C_1) \frac{Pl}{4b} \quad (\text{B.10})$$

$$(M_{L-curb})_{DL} = C_2 \frac{pbl^2}{8} + C_3 \frac{ql^2}{8} + 4h(M_{slab})_{DL} \quad (\text{B.11})$$

$$(M_{L-curb})_{LL} = C_1 \frac{Pl}{4} + 4h(M_{slab})_{LL} \quad (\text{B.12})$$

B.4 BRIDGE LOAD RATING

The moments distributed to the individual structural members according to [Section 4.2.3](#) for pan-joint bridges or Section B.3 for flat-slab bridges are used to calculate the overall bridge rating. The load rating procedure is based on calculating a rating factor for each of the structural elements. This procedure gives two rating levels depending on the load factors used to calculate the rating factor: operating and inventory rating. The inventory-rating level represents the load that a bridge can withstand, with an adequate margin of safety, under service conditions. The operating-rating level represents the load that can be supported under unusual bridge overloads. The rating levels are expressed in terms of an AASHTO design truck.

For the pan-joint bridge rating, the difference between the two rating levels is only due to the load factors that are used for the live load effects. The factors

used for live-load effects are equal to 2.17 and 1.30 for inventory-rating and operating-rating levels, respectively.

For the flat-slab bridge rating, the different rating levels depend, not only on the load factors used for live-load effects, but also on the manner in which the element that controls the rating is identified. For the inventory-rating level, the overall bridge rating is controlled by the element that has the lowest rating. For the operating level, the overall bridge rating is calculated using a weighted average of the individual element ratings. The weighting factors that are used are calculated based on the tributary width of each structural component on the bridge.

The rating factor equation is [AASHTO, 1994]:

$$RF = \frac{C - A_1 D}{A_2 L (1 + I)} \quad (B.13)$$

where

- RF = Rating factor for the live-load carrying capacity of the bridge.
- C = Strength reduction factor times nominal capacity of member.
- A_1 = Factor for dead load effects = 1.3 for inventory and operating rating.
- D = Dead-load effect on the member.
- A_2 = Factor for live-load effects = 2.17 for inventory rating and 1.3 for operating rating.
- L = Live-load effect on the member.
- I = Impact factor = 0.3

Once the rating factor is determined for all members that contribute to the structural capacity of the bridge, the rating of each member is determined with:

$$RT = (RF) W \quad (B.14)$$

where

RT = bridge member rating, tons.

W = weight of the first two axles of the design truck used in determining the live load effect, tons.

The load rating results for the pan-joint prototype bridge are shown in Table B.1 and those for the flat-slab prototype bridge are shown in Tables B.2 and B.3. These were obtained using a spreadsheet developed in TxDOT by their BRINSAP Division [TxDOT, 1999]. It should be noted, however, that these sheets only contain the rating results for flexural effects and shear effects for the pan-joint prototype bridge had to be considered separately. For the flat-slab prototype bridge, the rating was first calculated considering the structural curbs and then calculated based on the flat-slab acting alone to examine the effect of curb removal on the bridge rating.

Table B.1 Load Rating of Pan-Joist Prototype Bridge

Pan Girder Bridge Rating

To Print - Ctrl P

Note: Ratings should include any structural deterioration that affects the load capacity of the structure.

| <i>System Information</i> | |
|---------------------------|----------|
| Date | 05/28/00 |
| Engineer Initials | SFB |
| Program Version Number | 3.0 |

| <i>USER INPUT</i> | |
|--|-------|
| Overall Span (ft) | 30.00 |
| Beam+Slab Depth = 24 or 33 (in) | 24.00 |
| Misc Dead Load per Beam (k/ft) | |
| <i>Top Layer of Long. Steel</i> | |
| Total Area of Steel (in ²) | |
| Distance from bottom (in) | |
| <i>Bottom Layer of Long. Steel</i> | |
| Total Area of Steel (in ²) | 3.12 |
| Distance from bottom (in) | 2.375 |

| <i>SYSTEM DEFAULT INPUT</i> | |
|---------------------------------|-------|
| Span bearing length deduct (ft) | 2.00 |
| Fy (ksi) | 33.00 |
| f'c (ksi) | 3.00 |
| Overlay (in) | 0.50 |

| <i>Moments (kip-ft)</i> | |
|---------------------------|-------|
| Mdl | 41.7 |
| Cu | 162.7 |
| Undistributed MII (H-20) | 113.4 |
| Undistributed MII (HS-20) | 126.0 |

See formula 6-1a (Manual for Condition Evaluation of Bridges) for Rating Formula.

ADDITIONAL NOTES BELOW :

| <i>Bridge Information</i> | |
|---------------------------|------------------|
| District | District (#) |
| County | County (#) |
| Structure # | CCCC-SS-SSS |
| CSJ @ | CCCC-SS-JJJ |
| Year Built | 1951 |
| Location | PROTOTYPE BRIDGE |

@ Cont-Sec-Job used for this analysis

| <i>Recommended Material Properties</i> | | |
|--|------|---------------|
| Fy (ksi) | 33.0 | f'c (ksi) 2.5 |

| <i>HS RATING</i> | |
|-----------------------|----------|
| Inventory Rating | HS- 12.2 |
| Operating Rating | HS- 20.4 |
| Legal HS Equivalent § | HS- 24.2 |

§ Based on Span Length & Texas Legal Load

| <i>Recommendation</i> | |
|-----------------------|-----------|
| Posting | None |
| Inspection Frequency | 12 months |

| <i>H RATING</i> | |
|------------------|---------|
| Inventory Rating | H- 13.6 |
| Operating Rating | H- 22.6 |

| <i>Calculated Values</i> | |
|--------------------------|------|
| Distribution Factor | 0.50 |
| Impact Factor | 1.30 |
| a (in) * | 1.12 |

* Depth of concrete ultimate stress block

Table B.2 Load Rating of Flat-Slab Prototype Bridge Including the Contribution of Structural Curbs

| Slab Bridge Rating | |
|--|----------------------------|
| ***To Print - Ctrl P*** | |
| Note: Ratings should include any structural deterioration that affects the load capacity of the structure. | |
| System Information | |
| Date | 08/02/00 |
| Engineer Initials | SFB |
| Program Version Number | 3.0 |
| Bridge Information | |
| District | |
| County | |
| Structure # | |
| CSJ @ | |
| Year Built | 1945 |
| Location | Flat-Slab Prototype Bridge |
| © Cont-Sec-Job used for this analysis Structure # must be in format CCCC-SS-SSS | |
| Recommended Values | |
| Fy (ksi) | 33.0 |
| f'c (ksi) | 2.5 |
| Number of Live Load Lanes | 2 |
| HS RATING | |
| Inventory Rating | HS- 12.4 |
| Operating Rating | HS- 27.5 |
| Legal HS Equivalent § | HS- 26.5 |
| § Based on Span Length & Texas Legal Load | |
| Recommendation | |
| Posting | None |
| Inspection Frequency | 12 months |
| H RATING | |
| Inventory Rating | H- 12.5 |
| Operating Rating | H- 27.6 |
| Calculated Values | |
| Analysis Method | Illinois Bulletin 346 |
| Impact Factor | 1.30 |
| Effective Slab Width(in) | 44.00 |
| a-slab (in) | 1.45 |
| a-curb,left (in) | 8.13 |
| a-curb,right (in) | 8.13 |
| *a* = depth of concrete ultimate stress block Effective slab width is that portion acting integrally with curb or beam = 4 times slab thickness | |
| Additional CSJ's For This Structure | |
| Cont-Sec-Job | |
| Cont-Sec-Job | |
| Cont-Sec-Job | |
| ADDITIONAL NOTES BELOW : | |
| Moments | |
| Slab | |
| (M slab)DL (kft/ft) | 5.18 |
| (M slab)LL HS-20 (kft/ft) | 16.03 |
| (M slab)LL H-20 (kft/ft) | 15.97 |
| Cu slab (kft/ft) | 28.39 |
| Left Curb | |
| (M I-curb)DL (kft) | 92.73 |
| (M I-curb)LL HS-20 (kft) | 187.05 |
| (M I-curb)LL H-20 (kft) | 186.40 |
| Cu I-curb (kft) | 559.06 |
| Right Curb | |
| (M I-curb)DL (kft) | 92.73 |
| (M I-curb)LL HS-20 (kft) | 187.05 |
| USER INPUT | |
| Overall Span along Roadway (ft) | 25.00 |
| Overall Bridge Width (ft) | 21.33 |
| Skew (deg) | 0.00 |
| Slab Thickness (in) | 11.00 |
| Slab Steel Direction (P or N) | P |
| P = Parallel to rdwy, N = Normal to supports | |
| Area of Slab Tension Steel (in2/ft) | 1.110 |
| Distance from bottom of Slab (in) | 1.75 |
| Left (C)urb, (B)eam, or (N)one | |
| Curb Height above Slab (in) | 18.00 |
| Top of Curb Width (in) | 8.00 |
| Bottom of Curb Width (in) | 12.50 |
| Misc. Dead Load on Curb (k/ft) | 0.00 |
| Area of Curb Tension Steel (in2) | 3.720 |
| Distance from bottom of Slab (in) | 1.75 |
| Area of Curb Comp. Steel (in2) | 3.120 |
| Distance from top of Curb (in) | 2.00 |
| Right (C)urb, (B)eam, or (N)one | |
| Curb Height above Slab (in) | 18.00 |
| Top of Curb Width (in) | 8.00 |
| Bottom of Curb Width (in) | 12.50 |
| Misc. Dead Load on Curb (k/ft) | 0.00 |
| Area of Curb Tension Steel (in2) | 3.720 |
| Distance from bottom of Slab (in) | 1.75 |
| Area of Curb Comp. Steel (in2) | 3.120 |
| Distance from top of Curb (in) | 2.00 |
| SYSTEM DEFAULT INPUT | |
| Span bearing length deduct (ft) | 1.00 |
| Fy (ksi) | 40.00 |
| f'c (ksi) | 3.00 |
| Overlay (in) | 0.50 |
| Number of Live Load Lanes | 2 |

Table B.3 Load Rating of Flat-Slab Bridge Without the Contribution of Structural Curbs

Slab Bridge Rating

To Print - Ctrl P

Note: Ratings should include any structural deterioration that affects the load capacity of the structure.

| System Information | | Bridge Information | |
|--|----------|---|----------------------------|
| Date | 08/02/00 | District | |
| Engineer Initials | SFB | County | |
| Program Version Number | 3.0 | Structure # | |
| See below for input notes and assumptions. | | CSJ @ | |
| USER INPUT | | Year Built | 1945 |
| Overall Span along Roadway (ft) | 25.00 | Location | Flat-Slab Prototype Bridge |
| Overall Bridge Width (ft) | 21.33 | © Cont-Sec-Job used for this analysis | |
| Skew (deg) | 0.00 | Structure # must be in format CCCC-SS-SSS | |
| Slab Thickness (in) | 11.00 | Recommended Values | |
| Slab Steel Direction (P or N) | P | Fy (ksi) | 33.0 |
| P = Parallel to rdwy, N = Normal to supports | | f'c (ksi) | 2.5 |
| Area of Slab Tension Steel (in ² /ft) | 1.110 | Number of Live Load Lanes | |
| Distance from bottom of Slab (in) | 1.75 | 2 | |
| Left (C)urb, (B)eam, or (N)one | n | HS RATING | |
| | 18.00 | Inventory Rating | HS- 6.0 |
| | 8.00 | Operating Rating | HS- 10.0 |
| | 12.50 | Legal HS Equivalent § | HS- 26.5 |
| | 0.00 | § Based on Span Length & Texas Legal Load | |
| | 3.720 | Recommendation | |
| | 1.75 | Posting | Required |
| | 3.120 | Inspection Frequency | 24 months |
| | 2.00 | H RATING | |
| Right (C)urb, (B)eam, or (N)one | n | Inventory Rating | H- 6.0 |
| | 18.00 | Operating Rating | H- 10.0 |
| | 8.00 | Calculated Values | |
| | 12.50 | Analysis Method | AASHTO 3.24.3.2 |
| | 0.00 | Impact Factor | 1.30 |
| | 3.720 | a-slab (in) | 1.45 |
| | 1.75 | "a" = depth of concrete ultimate stress block | |
| | 3.120 | Additional CSJ's For This Structure | |
| | 2.00 | Cont-Sec-Job | |
| SYSTEM DEFAULT INPUT | | Cont-Sec-Job | |
| Span bearing length deduct (ft) | 1.00 | Cont-Sec-Job | |
| Fy (ksi) | 40.00 | MOMENTS | |
| f'c (ksi) | 3.00 | Slab | |
| Overlay (in) | 0.50 | (M slab)DL (kft/ft) | 10.33 |
| Number of Live Load Lanes | 2 | (M slab)LL HS-20 (kft/ft) | 23.02 |
| | | (M slab)LL H-20 (kft/ft) | 22.94 |
| | | Cu slab (kft/ft) | 28.39 |
| | | | |
| | | | |
| | | | |
| | | | |

ADDITIONAL NOTES BELOW :

| | |
|---|------------|
| APPENDIX B: BRIDGE LOAD RATING PROCEDURE..... | 357 |
| B.1 Introduction | 357 |
| B.2 Description of Design Trucks used for Load Rating | 358 |
| B.3 Distribution of Moments on Flat-Slab Bridges | 359 |
| B.4 Bridge Load Rating..... | 362 |
| Figure B.1 Design Trucks used for Bridge Load Rating..... | 358 |
| Table B.1 Load Rating of Pan-Joist Prototype Bridge | 365 |
| Table B.2 Load Rating of Flat-Slab Prototype Bridge Including the Contribution of Structural Curbs..... | 366 |
| Table B.3 Load Rating of Flat-Slab Bridge Without the Contribution of Structural Curbs..... | 367 |

Appendix C: Application of CFRP Composite Systems to Existing Reinforced Concrete Elements

C.1 INTRODUCTION

Two types of composite systems were used to strengthen the reinforced concrete specimens that were part of the experimental portion of this research project. These systems differ primarily in the method that is used for their fabrication and also on the procedure that is used to bond them to the concrete surface. A description of the procedures that were used to attach these systems to the laboratory specimens is presented in this appendix. These procedures were based on the recommendations provided by the manufacturer of each of the composite systems.

C.2 PULTRUDED CFRP SYSTEM

C.2.1 Description of Composite System

The CFRP pultruded system used in this research project consisted of plates that were fabricated using the putrusion process. In this process, continuous carbon fiber roving is impregnated in a resin bath and pulled through a forming die at an elevated temperature. The carbon fibers were oriented along the plate longitudinal axis (unidirectional carbon fibers). The resin bath is usually mixed with a curing agent so that curing initiates simultaneously as the fibers are pulled through the die.

The temperature, pulling speed, and length of the die are controlled to insure that the resin fully cures before the fiber-reinforced element exits the die [Mallick, 1993]. The member is cooled with air or water after exiting the forming die. The elements are then cut to the required length using a diamond saw at the end of the pultrusion line (Figure C.1).

A limitation of this fabrication process is that only elements that have a constant cross section can be manufactured economically. An advantage of using this procedure is that the elements are fabricated in a controlled environment and better quality control is achieved. Also, large volume contents of fibers can be used in the composites fabricated using this procedure.

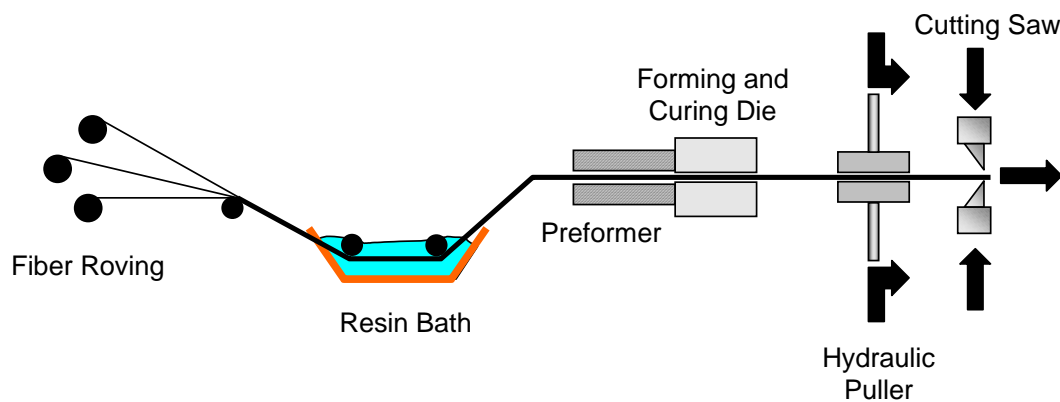


Figure C.1 Schematic Representation of the Fabrication of a Fiber Reinforced Polymer Plate using the Pultrusion Process [Mallick, 1993]

C.2.2 Application to Reinforced Concrete Element

The application of the pultruded CFRP system that was used to strengthen the reinforced concrete laboratory specimens can be summarized in the following steps and is illustrated in Figure C.2:

a) Preparation of concrete surface and CFRP plate

- Prepare concrete surface by grinding or light sandblasting to expose aggregates.
- Remove loose concrete particles generated during surface preparation using pressurized air.
- Clean concrete surface and CFRP pultruded plates with acetone until a white cloth remains white after wiping.

b) CFRP system application

- Mix epoxy paste and hardener for three minutes at approximately 400 to 600 RPM. The mixing proportions should follow the values recommended by the manufacturer.
- Apply a thin layer (approximately 1/16-in.) of mixed epoxy paste to the concrete surface, covering the area where the pultruded plates will be installed.
- Apply a layer of epoxy paste to the clean CFRP plate. The epoxy paste should have a triangular section after application on the plate

- Place CFRP plate on concrete surface and apply hand pressure to force epoxy paste out of the plate.
- Clean excess epoxy from sides of plates.

A woven carbon fiber sheet was used to fabricate straps to wrap the CFRP pultruded plates at discrete locations and avoid premature debonding of the pultruded plates. These straps were applied using the procedures described for the CFRP wet-layup system in Section C.3. The procedure is illustrated in Figure C.3.

The thickness of the pultruded plates system was approximately 1/8 in. after placement on the concrete surface. Therefore, to place the woven fabric straps and avoid having a sharp bend at the plate boundary, epoxy paste was built up forming a ramp. The woven fabric straps were placed on the reinforced concrete element after the epoxy paste that formed the ramps had hardened.

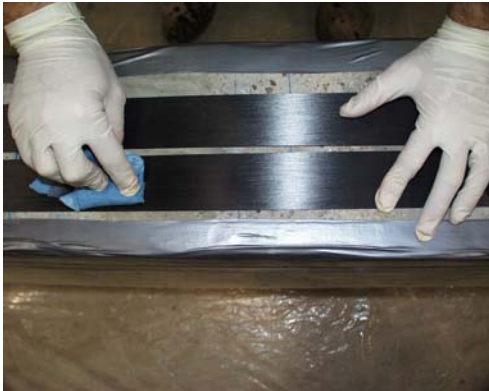
a) Surface grinding



d) Applying epoxy to surface



b) CFRP plate cleaning



e) Positioning CFRP plate on beam



c) Mixing epoxy paste



f) Strengthened beam



Figure C.2 Application of CFRP Pultruded Plates to Reinforced Concrete Beam

a) Cutting Woven CFRP mat



c) Placing woven straps around beam



b) Applying epoxy on concrete surface



d) Final configuration of beam



e) Final configuration of full-scale joist after strengthening



Figure C.3 Application of Woven Straps Around CFRP Pultruded Plates

C.3 WET-LAYUP CFRP SYSTEM

C.3.1 Description of Composite System

The CFRP composite system that was used in this research project consisted of dry unidirectional carbon fiber sheets that were impregnated with an epoxy resin to form the composite in the laboratory. The fabrication process is termed “wet-layup process” because the carbon fiber sheets are impregnated sequentially as they are positioned on the concrete element.

The main disadvantage of this composite system is caused by the large variability introduced by the manufacturing process. Because the epoxy resin that forms the matrix of the composite is applied manually, significant variations in the composite thickness can result. For the composites that were used in this study, the actual composite thickness ranged from 0.04 to 0.06-in. per carbon fiber ply. Recognizing this inherent variability, the manufacturer of this system suggests using the carbon fiber thickness for design calculations because the uniaxial tensile stress behavior is controlled by the carbon fibers.

C.3.2 Application to Reinforced Concrete Element

The procedure that was used in this research project to apply this CFRP composite system is summarized below. These steps were followed according to recommendations from the manufacturer of the system (Figure C.4):

a) Preparation of concrete surface

- Remove loose concrete particles from surface using a grinding tool. Remove dust generated during grinding using compressed air.
- Fill concrete voids with epoxy putty.

b) CFRP system application

- Apply epoxy primer to seal the concrete surface. Wait until primer reaches a tack-free condition before applying epoxy on the concrete surface.
- Mix two-component epoxy resin using the mixing ratio specified by the manufacturer. Mix using a power drill at a low speed (approximately 400 RPM) using an epoxy paddle.
- Apply a coat of mixed epoxy resin on the concrete surface. This layer will partially impregnate the carbon fibers after they are placed on the concrete element.
- Cut carbon fiber sheets to the required width and length.
- Place carbon fiber sheets on concrete surface over area that was previously coated with epoxy resin. Placement should begin on one end of the concrete element and continue toward the other end.
- Remove backing paper and use a ribbed roller to remove air bubbles that are trapped behind the carbon fiber sheet. Let carbon fibers impregnate in the epoxy resin for approximately 30 minutes.
- Apply a coat of epoxy resin on top of the carbon fibers to enhance impregnation and to form the composite matrix.
- Apply subsequent layers (plies) of carbon fiber sheets and epoxy coat, if required by design, following the procedure described above.

a) Unidirectional carbon fiber sheet



d) Placing carbon fiber sheet on joist



b) Cutting carbon fiber sheets



e) Eliminating air bubbles from sheets



c) Applying epoxy to surface



f) Coating placed sheets with epoxy



Figure C.4 Application of CFRP Wet-Layup System to Reinforced Concrete Element

APPENDIX C: APPLICATION OF CFRP COMPOSITE SYSTEMS TO EXISTING REINFORCED CONCRETE ELEMENTS... 368

C.1 Introduction 368

C.2 Pultruded CFRP System 368

C.2.1 Description of Composite System 368

C.2.2 Application to Reinforced Concrete Element 370

C.3 Wet-Layup CFRP System 374

C.3.1 Description of Composite System 374

C.3.2 Application to Reinforced Concrete Element 374

Figure C.1 Schematic Representation of the Fabrication of a Fiber Reinforced Polymer Plate using the Pultrusion Process [Mallick, 1993] 369

Figure C.2 Application of CFRP Pultruded Plates to Reinforced Concrete Beam 372

Figure C.3 Application of Woven Straps Around CFRP Pultruded Plates 373

Figure C.4 Application of CFRP Wet-Layup System to Reinforced Concrete Element 376

Appendix D: Measured Strains

Measured readings from strain gages located at four different sections for the test specimens are presented in this appendix. The instruments were positioned on the reinforcing bars, CFRP composites and concrete surface.

For the pan-joint specimens, each instrumented section contained four strain gages on the reinforcing bars, four strain gages on the CFRP composite, and five concrete gages in Specimen J-1 or three concrete gages in Specimen J-2. For the flat-slab specimens, three strain gages were attached to the reinforcing bars, four to the CFRP composites, and three to the concrete surface at each instrumented section. The location of the instrumented sections for the pan-joint specimens and the flat-slab specimens is shown in **Figures D.1 and D.2**, respectively. Only the concrete gages are indicated in these figures, but the positions of gages on the reinforcement and CFRP composites are indicated in each of the corresponding strain plots. Characteristics of the strain gages are listed in Table D.1.

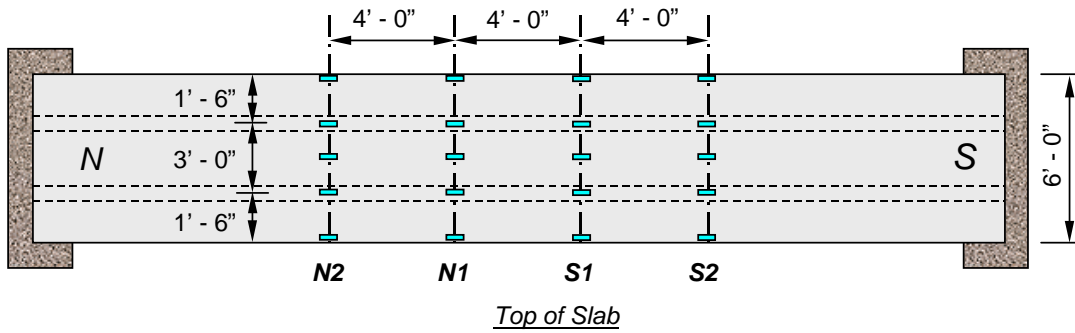


Figure D.1 Position of Instrumented Sections for Pan-Joist Specimens

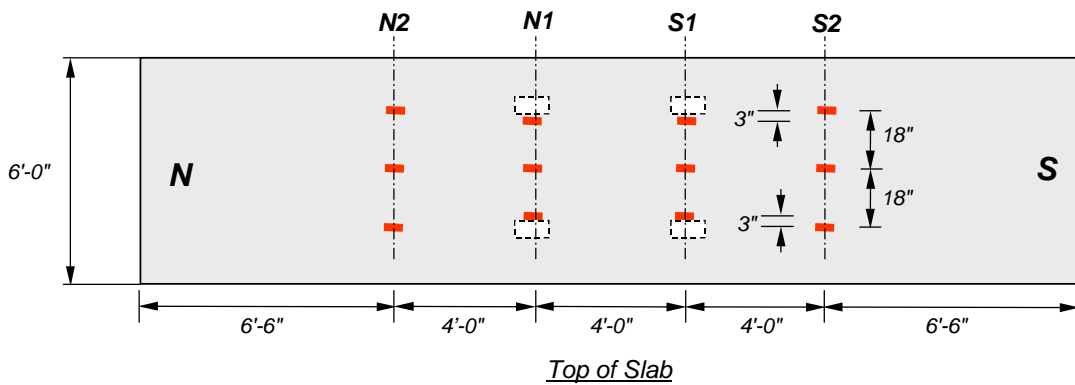


Figure D.2 Position of Instrumented Sections for Flat-Slab Specimens

Table D.1 Characteristics of Strain Gages

| Material | Strain Gage Type | Nominal Resistance, Ohms | Gage Length, mm | Gage Factor |
|----------|------------------|--------------------------|-----------------|-------------|
| Steel | Foil | 119.5±0.5 | 6 | 2.12±1% |
| CFRP | Foil | 119.5±0.5 | 6 | 2.12±1% |
| Concrete | Wire | 120±0.5 | 60 | 2.09±1% |

Strain gage readings were used to compute internal stresses and forces and to determine the location of the neutral axis during the tests. These results are presented in Chapter 6 for the pan-joist specimens and in Chapter 9 for the flat-slab specimens. Only the outputs from the instruments as were recorded during the tests without any modification are presented in this appendix.

Figures D.3 to D.14 show load vs. strain plots for the four-instrumented sections in Specimen J-1. Measured strains on the reinforcement are contained in Figures D.3 to D.6, on the CFRP plates in Figures D.7 to D.10, and on the concrete slab in Figures D.11 to D.14, respectively.

Figures D.15 to D.26 show load vs. strain plots for the four-instrumented sections in Specimen J-2. Measured strains on the reinforcement are contained in Figures D.15 to D.18, on the CFRP sheets in Figures D.19 to D.22, and on the concrete slab in Figures D.23 to D.26, respectively.

Figures D.27 to D.30 show load vs. strain plots for the four-instrumented sections in Specimen FS-1. Measured strains on the reinforcement are contained in Figures D.27 to D.30, on the concrete slab in Figures D.31 to D.34, and on the CFRP plates in Figures D.35 to D.38, respectively.

Finally, Figures D.39 to D.50 show load vs. strain plots for the four-instrumented sections in Specimen FS-2. Measured strains on the reinforcement

are contained in Figures D.39 to D.42, on the concrete slab in Figures D.43 to D.46, and on the CFRP plates in Figures D.47 to D.50, respectively.

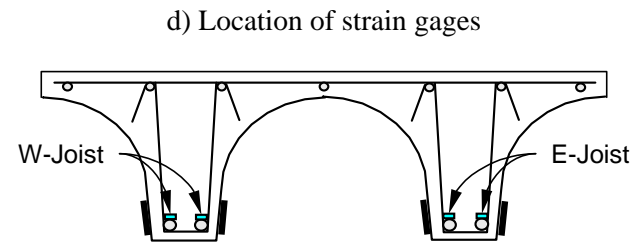
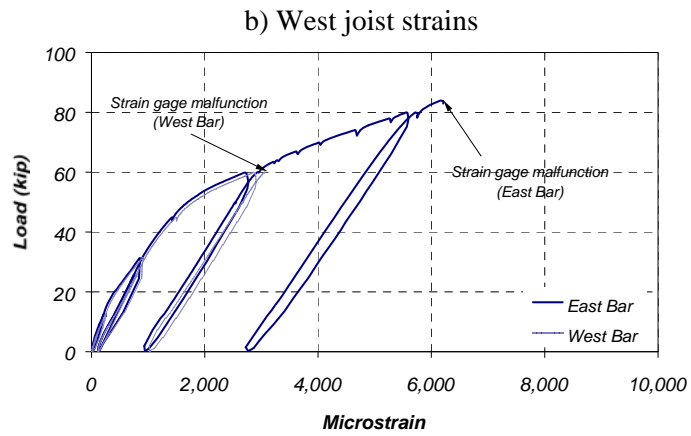
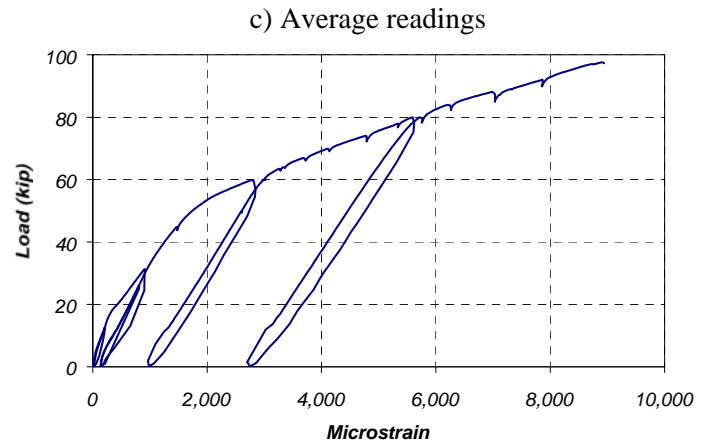
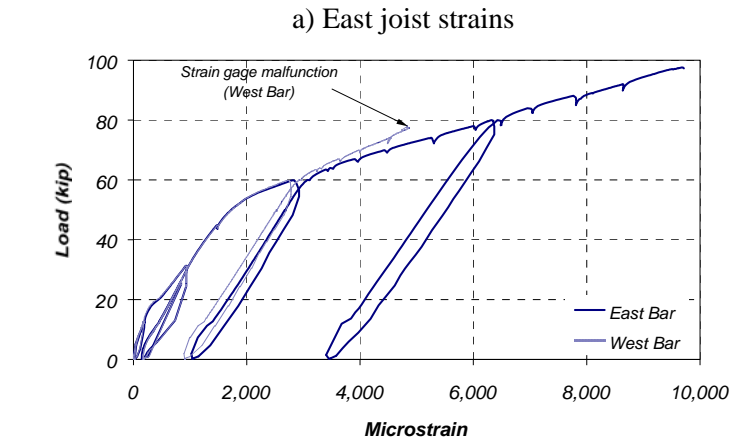


Figure D.3 Measured #8 Reinforcing Bar Strains in Specimen J-1 (Section N1)

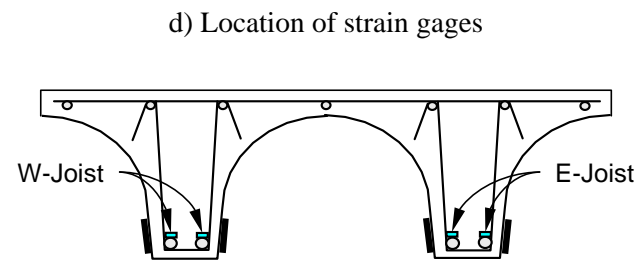
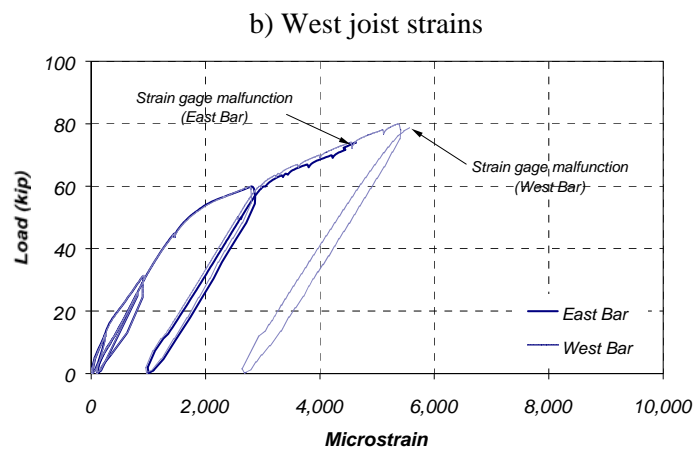
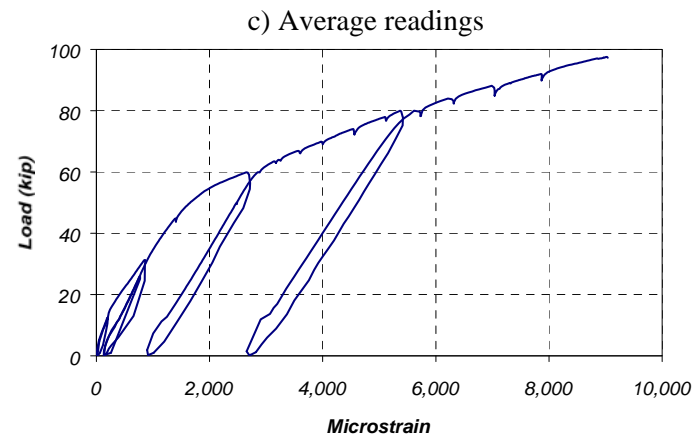
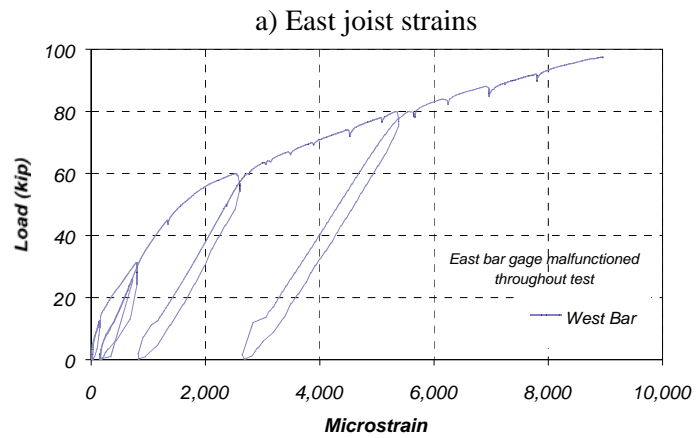


Figure D.4 Measured #8 Reinforcing Bar Strains in Specimen J-1 (Section S1)

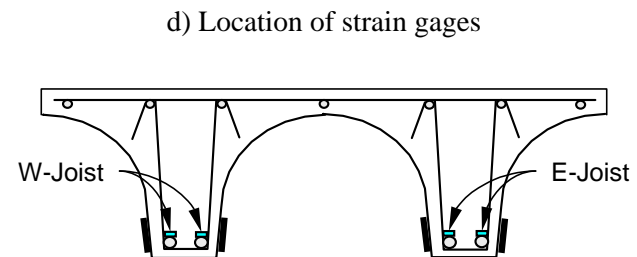
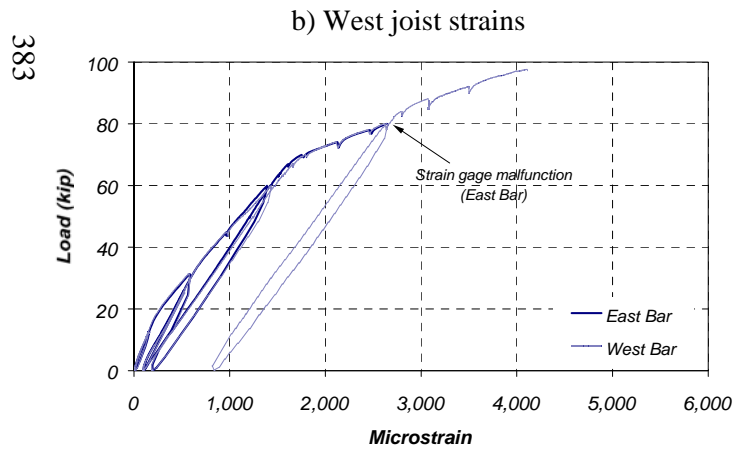
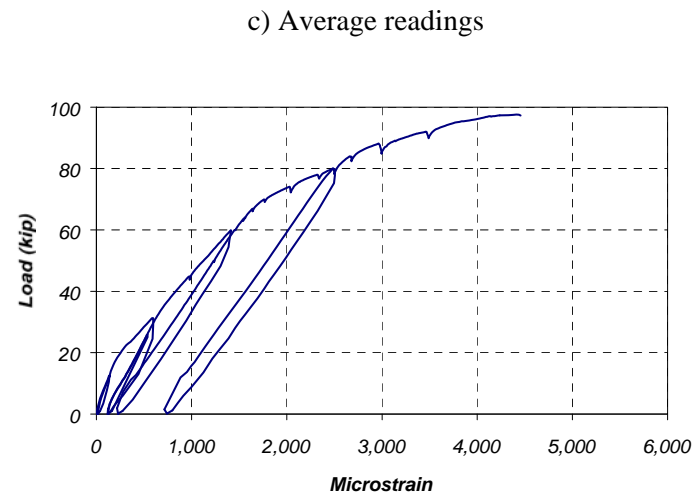
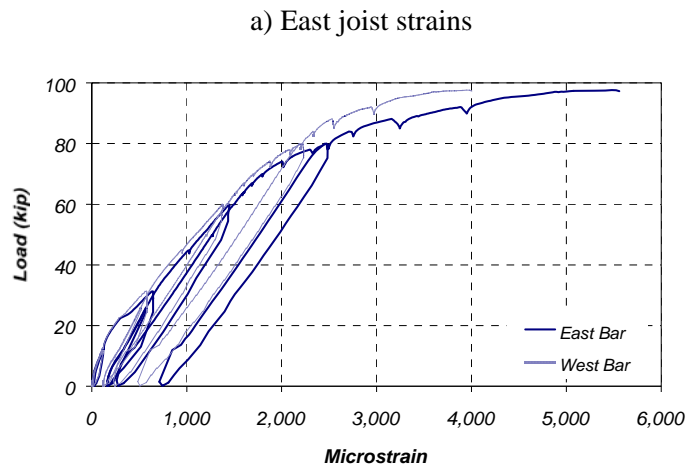


Figure D.5 Measured #8 Reinforcing Bar Strains in Specimen J-1 (Section N2)

383

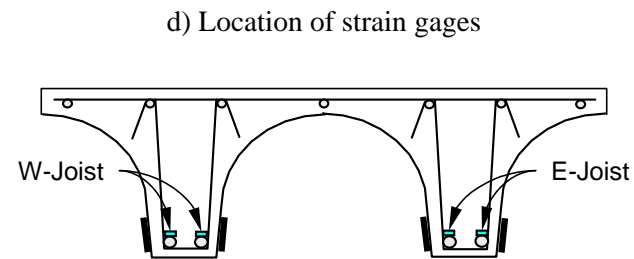
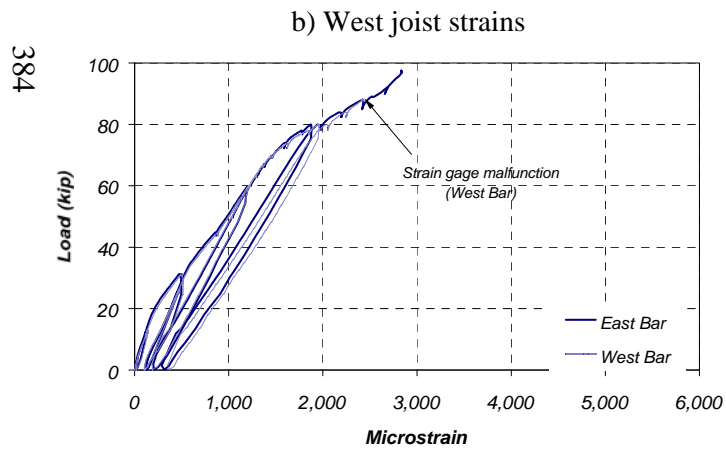
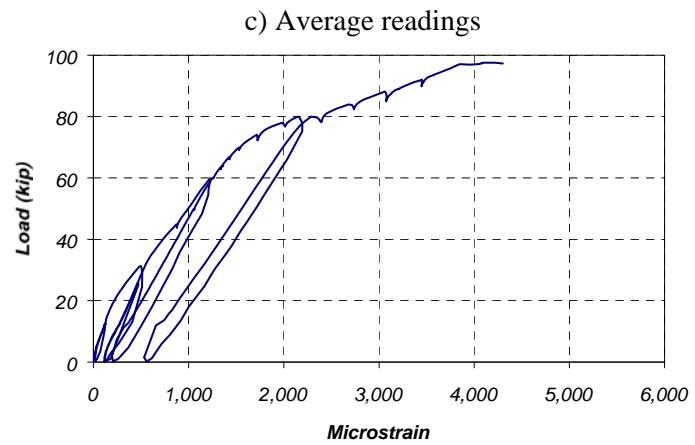
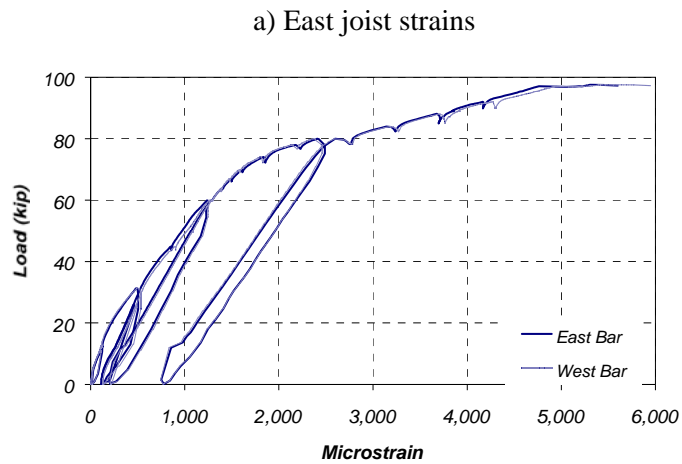


Figure D.6 Measured #8 Reinforcing Bar Strains in Specimen J-1 (Section S2)

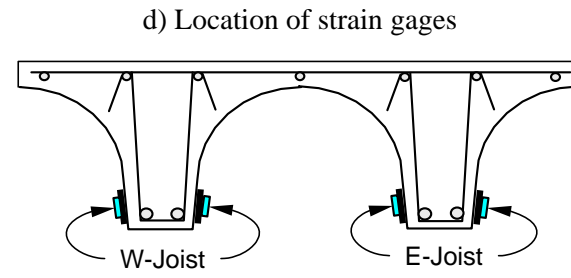
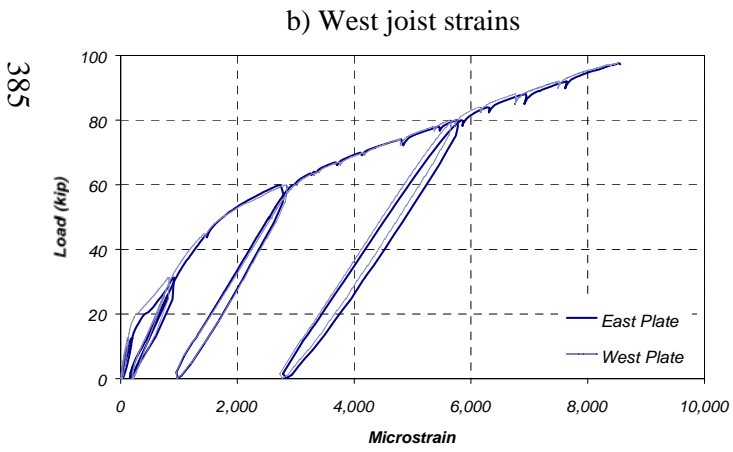
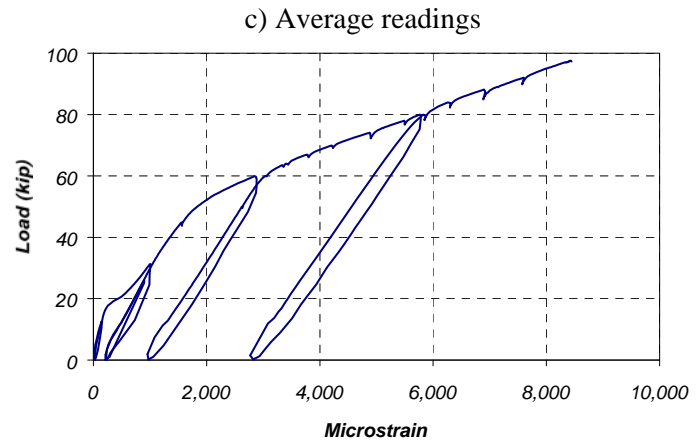
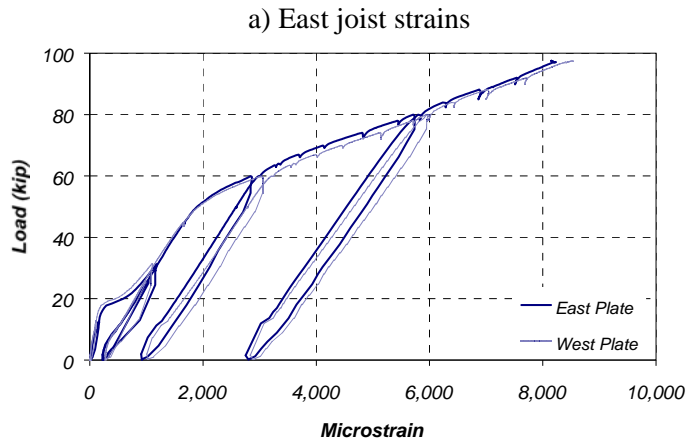


Figure D.7 Measured CFRP Strains in Specimen J-1 (Section N1)

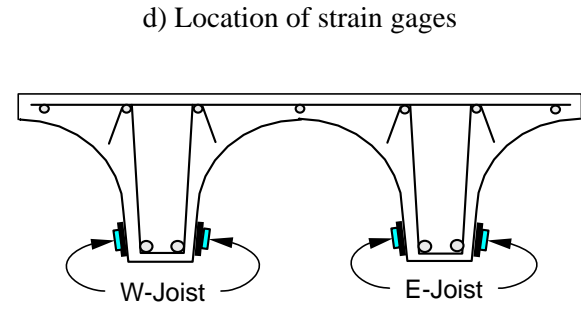
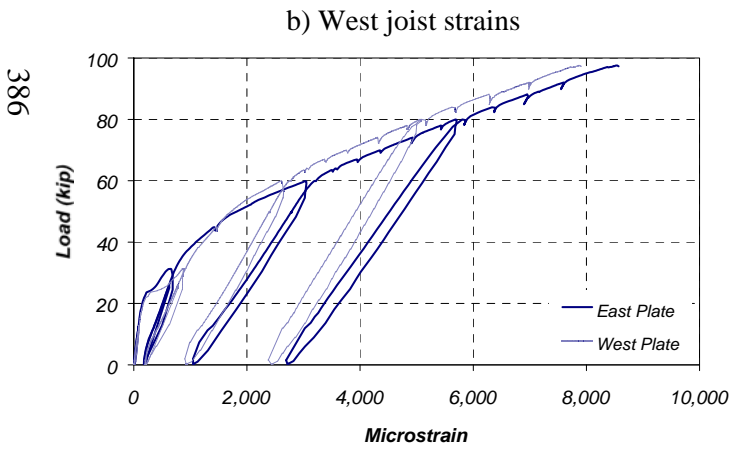
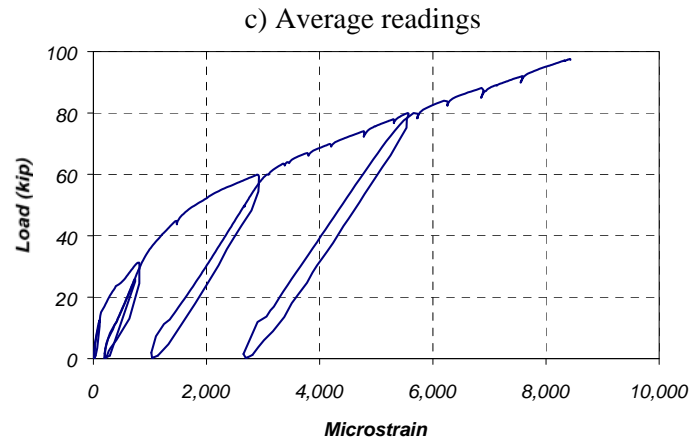
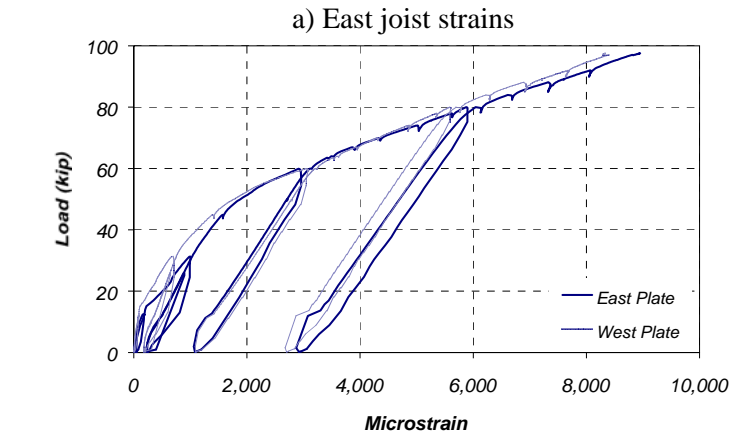


Figure D.8 Measured CFRP Strains in Specimen J-1 (Section S1)

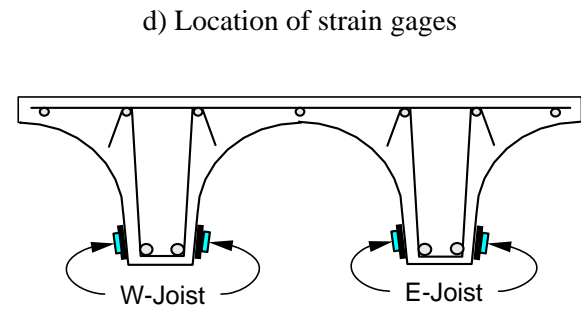
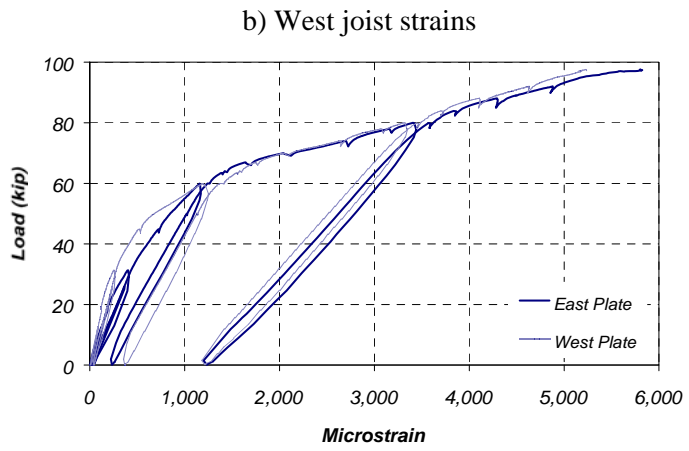
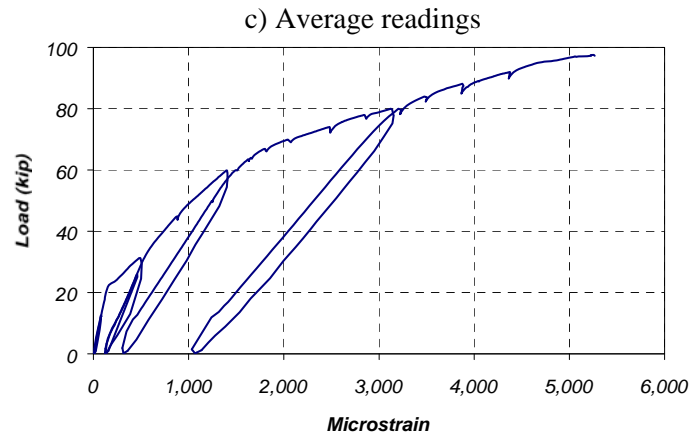
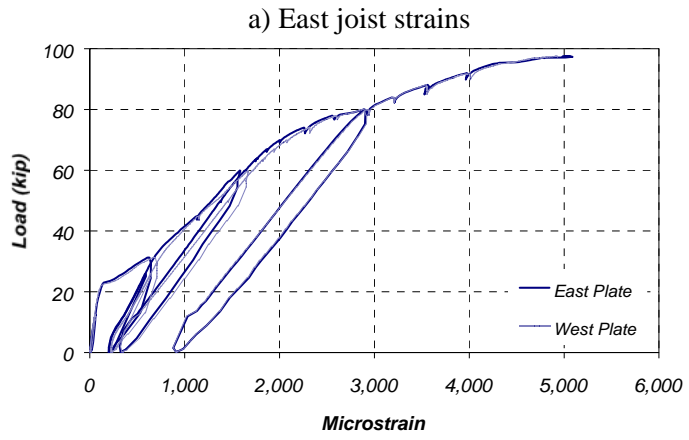


Figure D.9 Measured CFRP Strains in Specimen J-1 (Section N2)

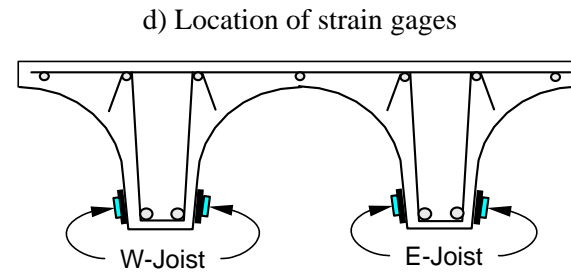
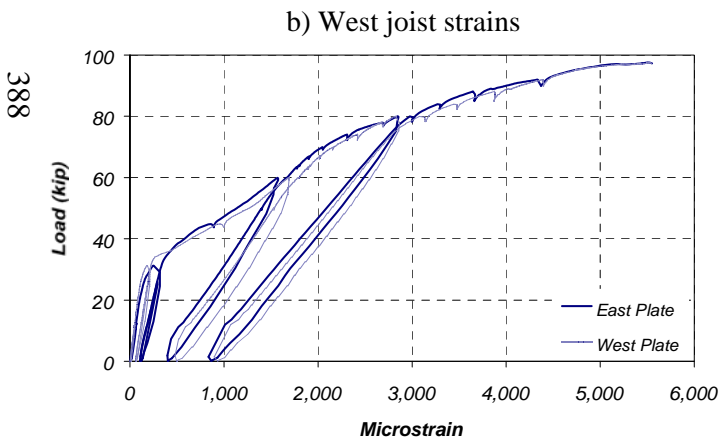
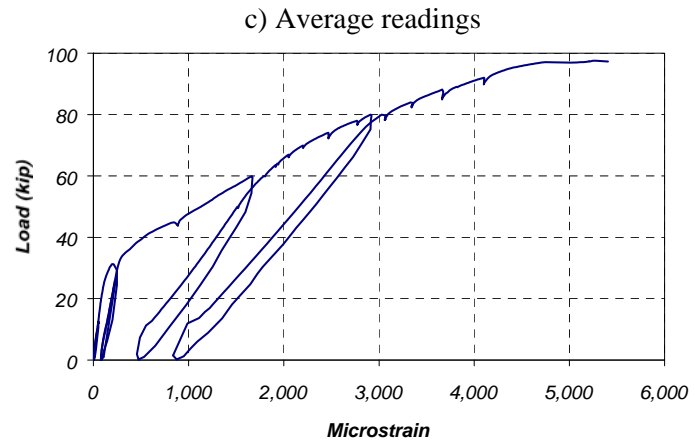
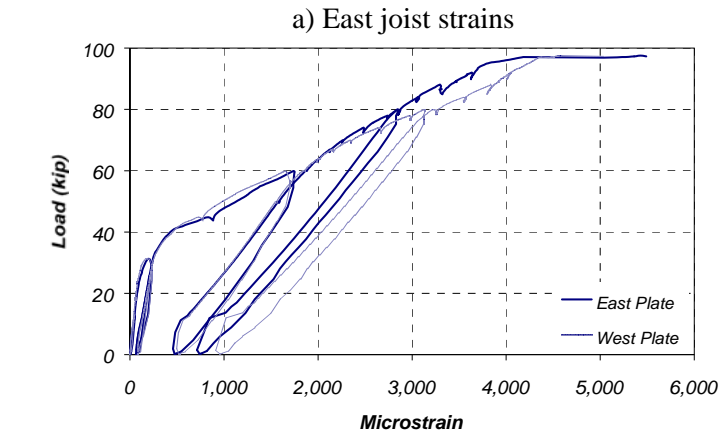


Figure D.10 Measured CFRP Strains in Specimen J-1 (Section S2)

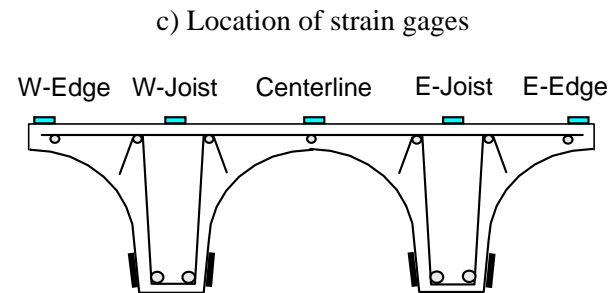
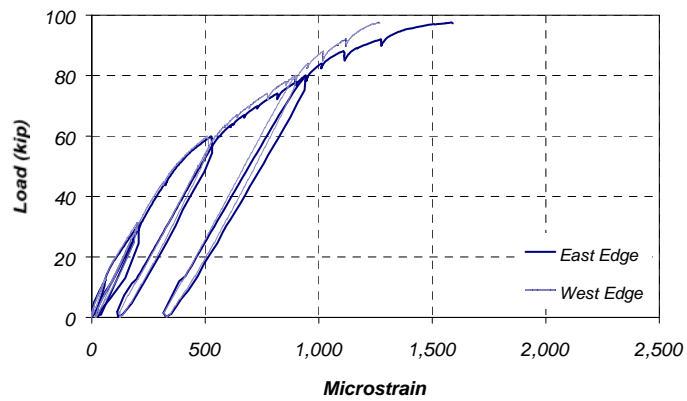
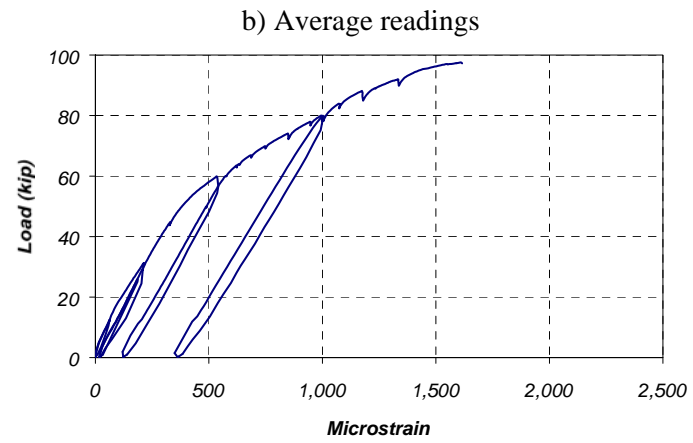
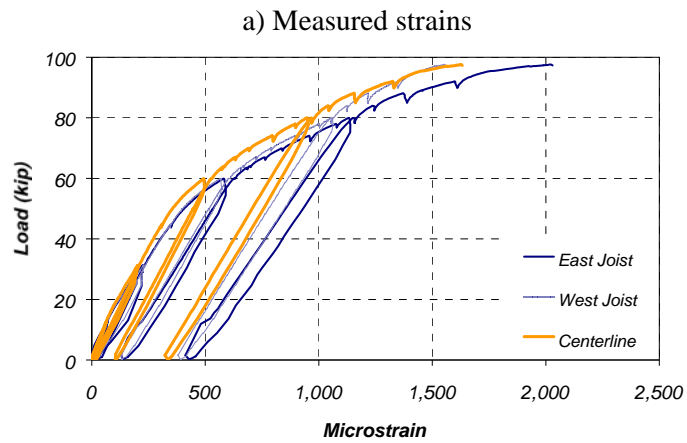


Figure D.11 Measured Strains on Concrete Slab in Specimen J-1 (Section N1)

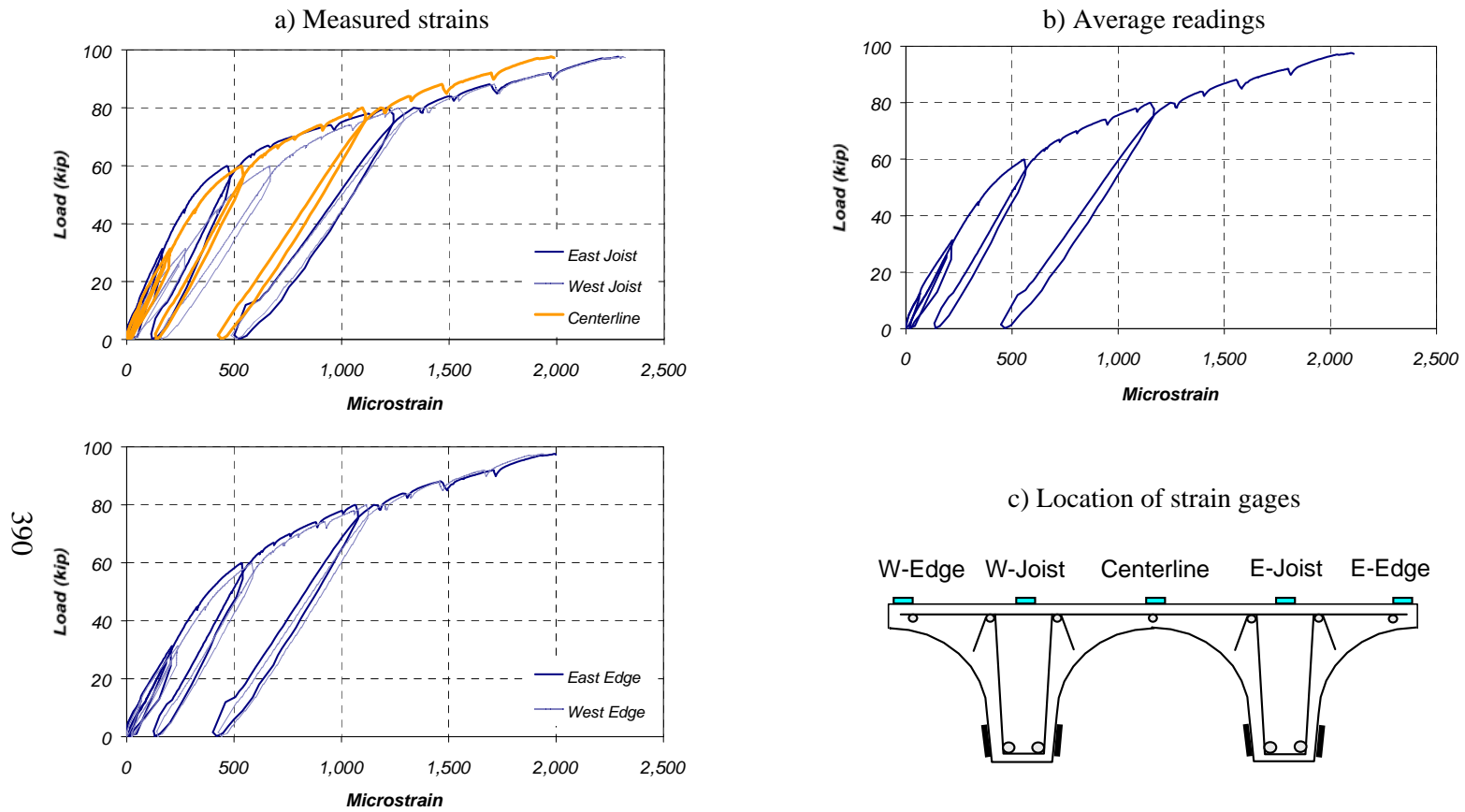


Figure D.12 Measured Strains on Concrete Slab in Specimen J-1 (Section S1)

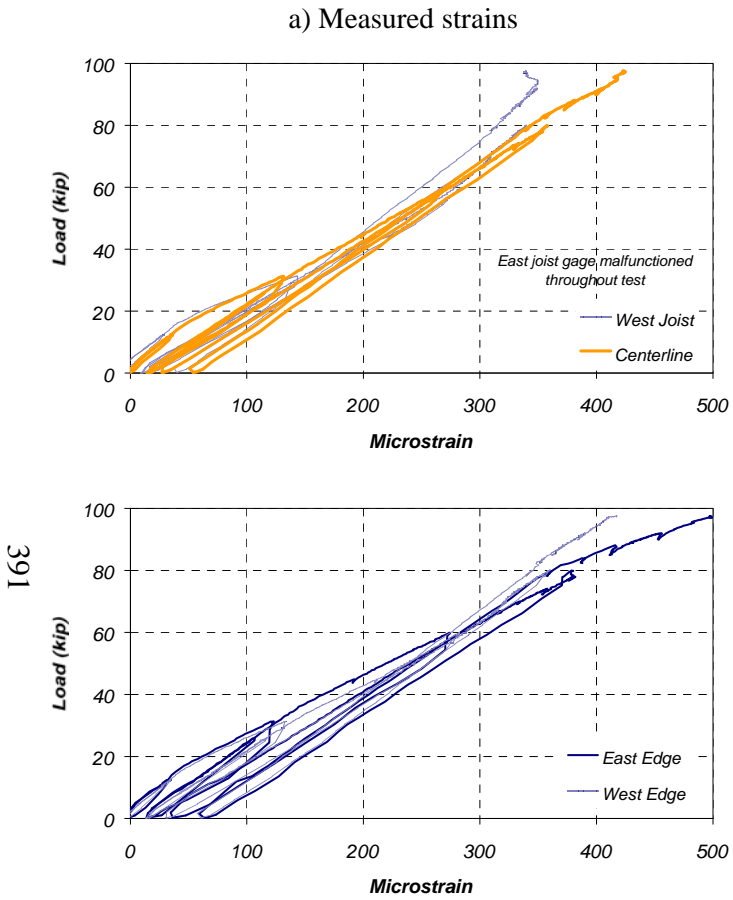


Figure D.13 Measured Strains on Concrete Slab in Specimen J-1 (Section N2)

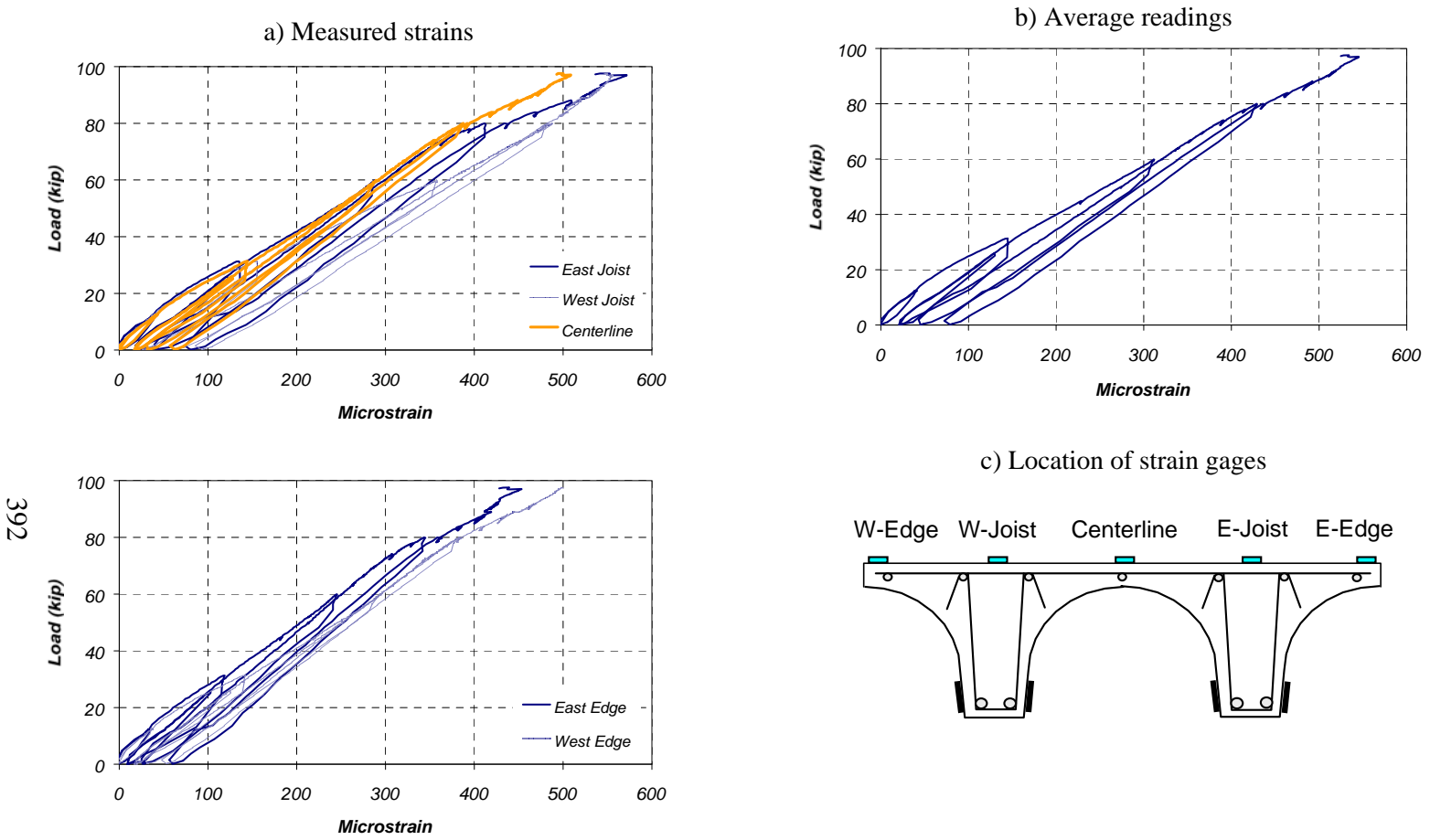


Figure D.14 Measured Strains on Concrete Slab in Specimen J-1 (Section S2)

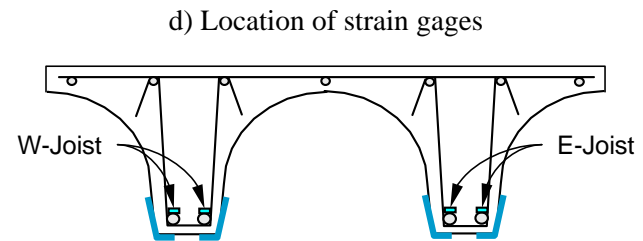
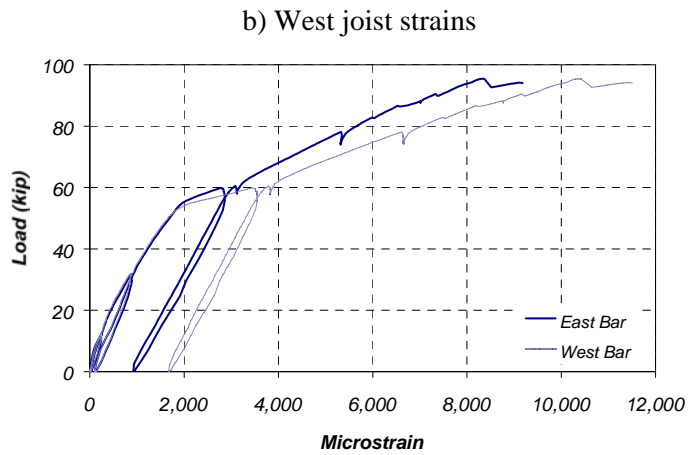
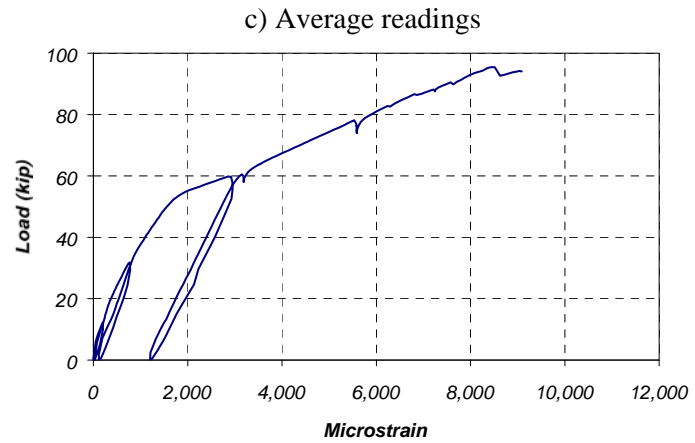
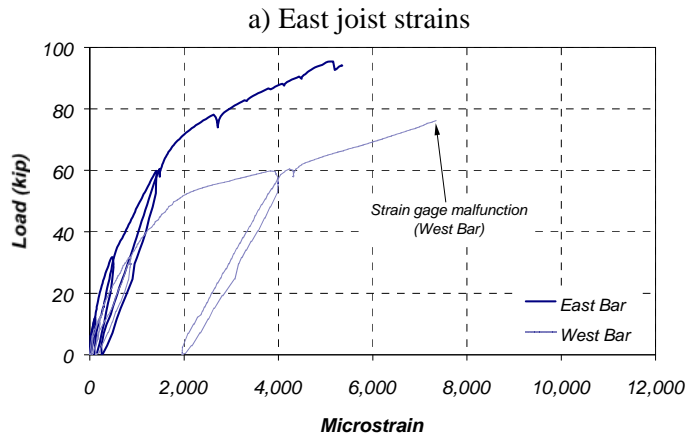


Figure D.15 Measured #8 Reinforcing Bar Strains in Specimen J-2 (Section N1)

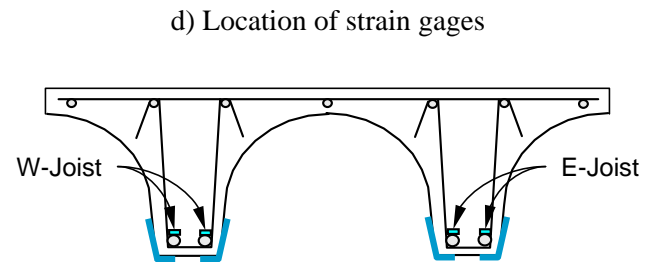
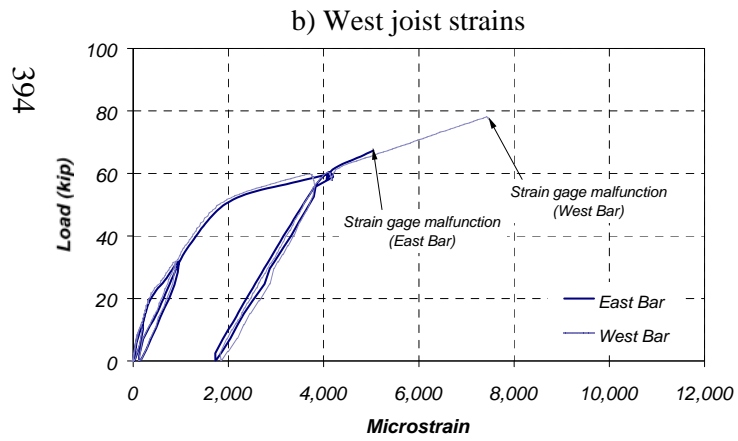
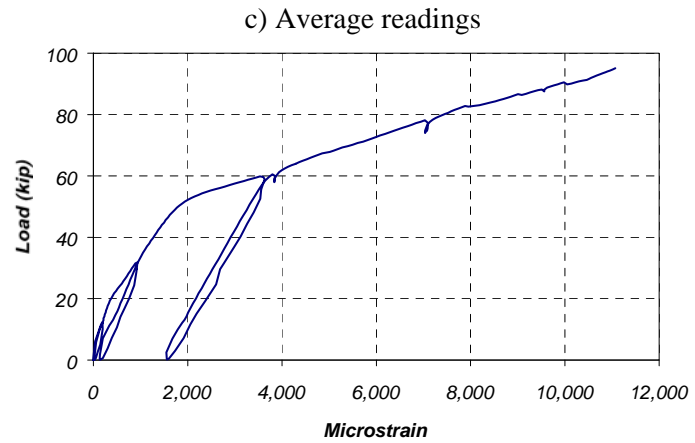
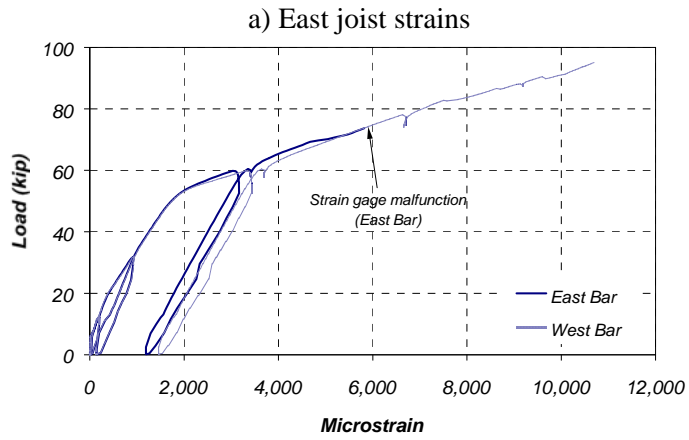


Figure D.16 Measured #8 Reinforcing Bar Strains in Specimen J-2 (Section S1)

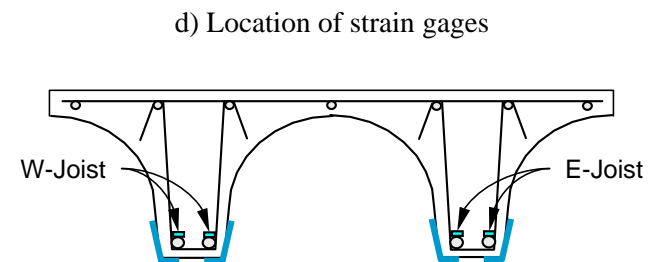
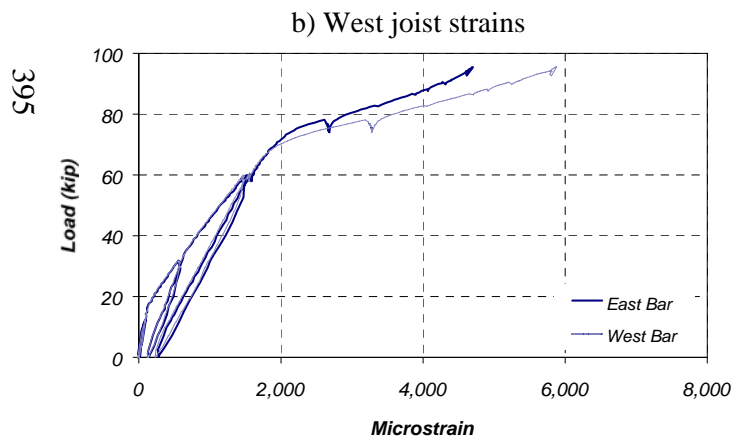
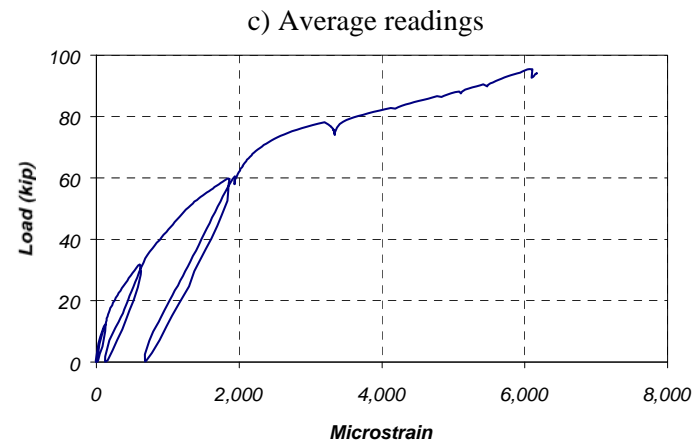
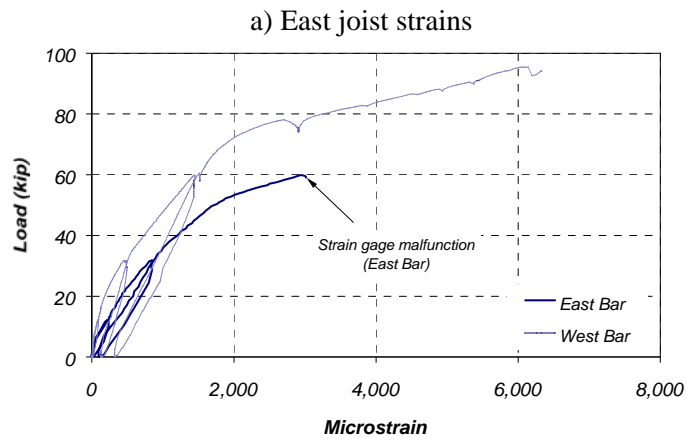


Figure D.17 Measured #8 Reinforcing Bar Strains in Specimen J-2 (Section N2)

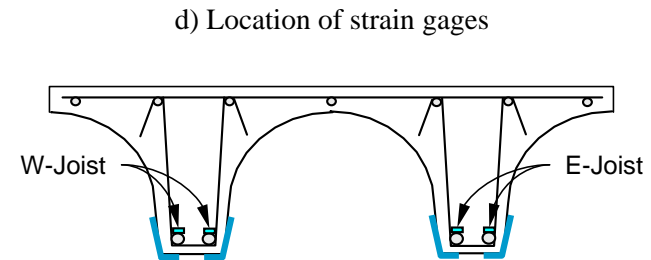
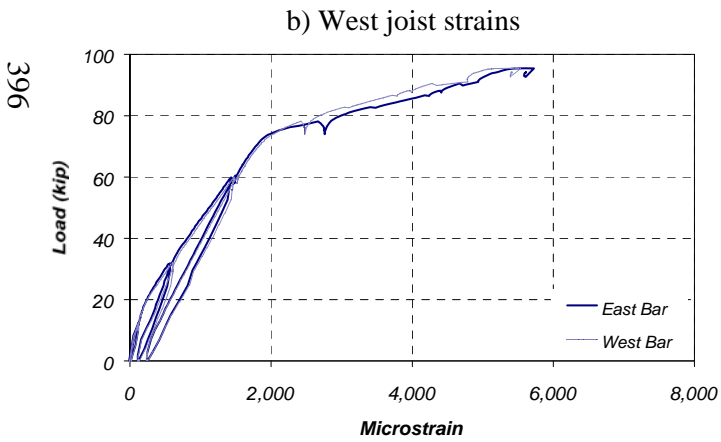
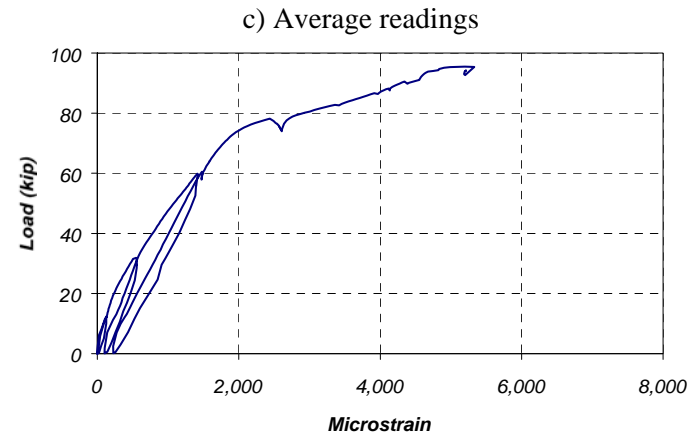
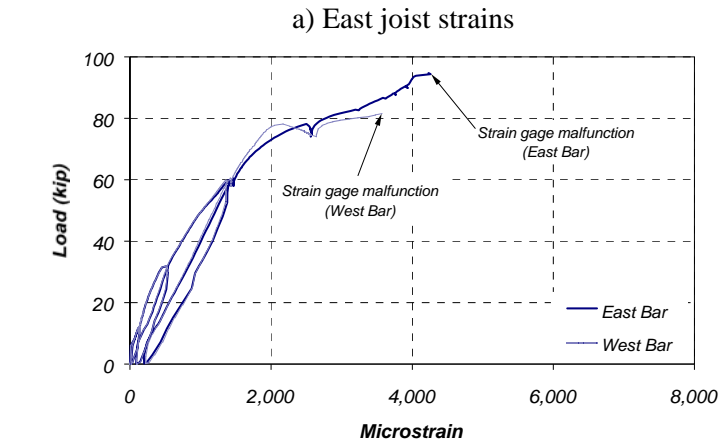


Figure D.18 Measured #8 Reinforcing Bar Strains in Specimen J-2 (Section S2)

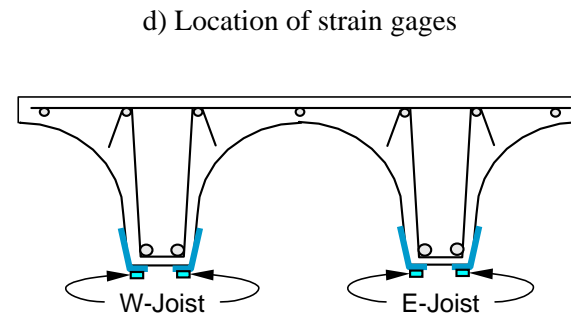
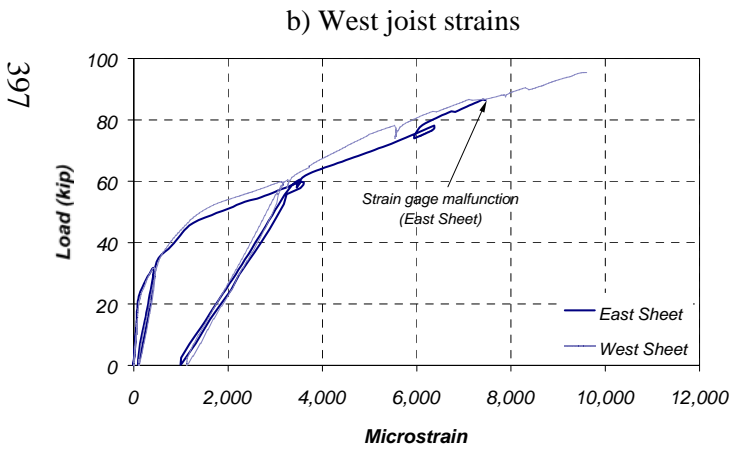
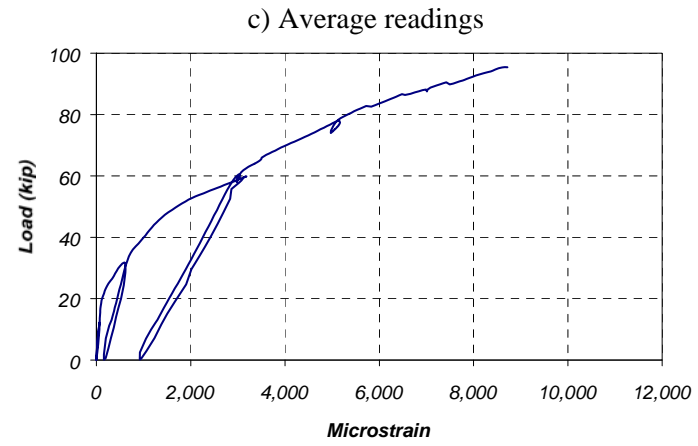
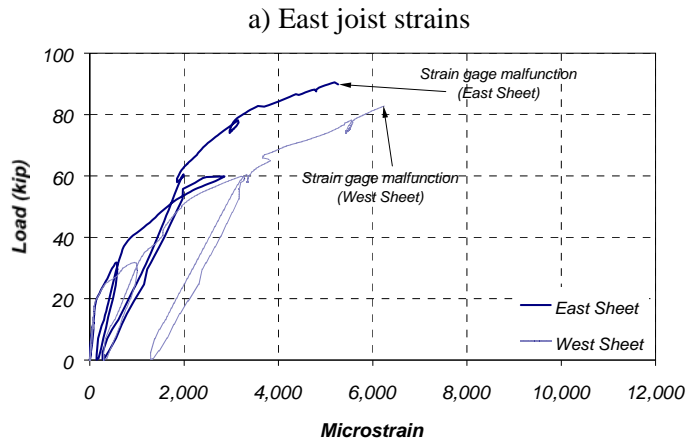


Figure D.19 Measured CFRP Strains in Specimen J-2 (Section N1)

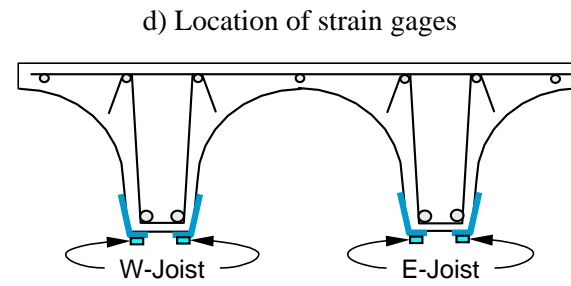
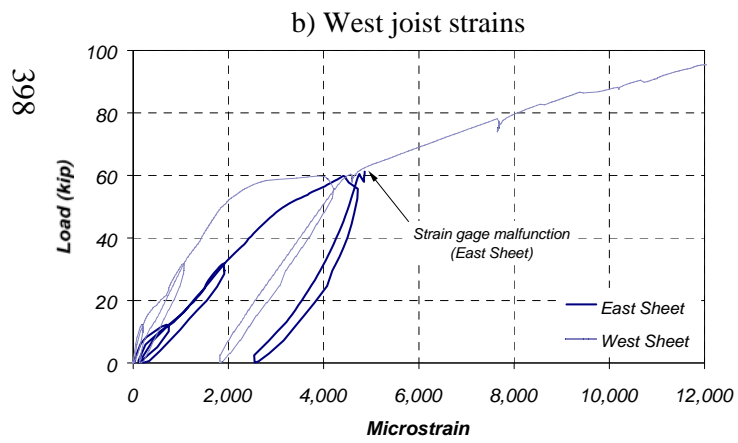
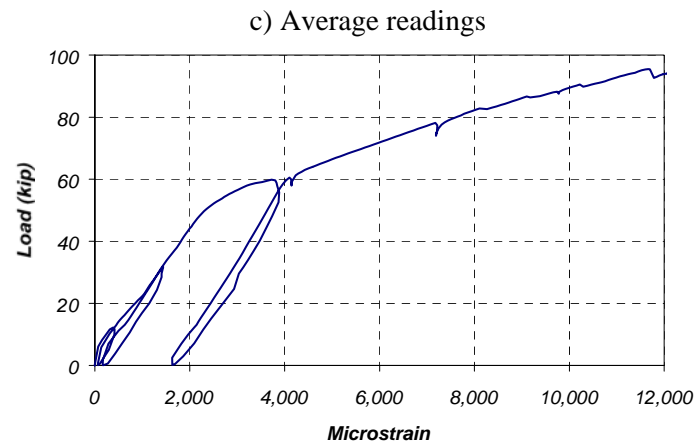
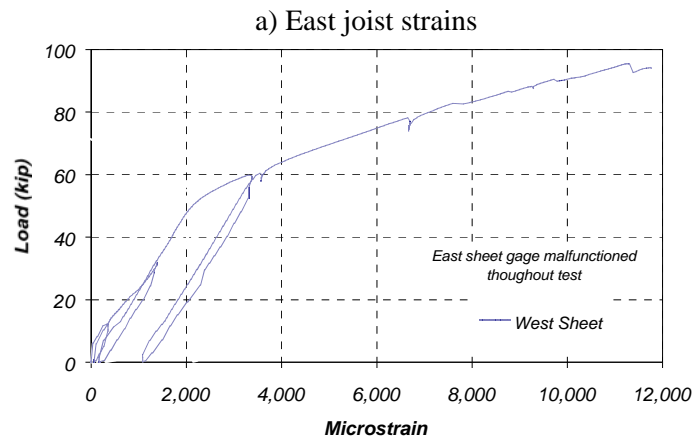


Figure D.20 Measured CFRP Strains in Specimen J-2 (Section S1)

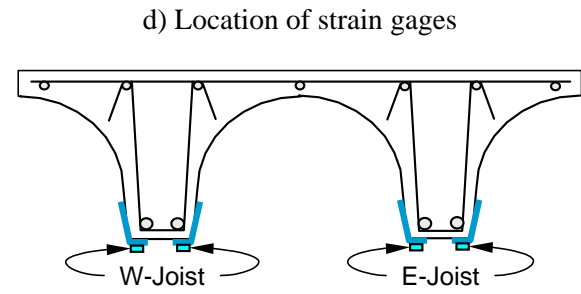
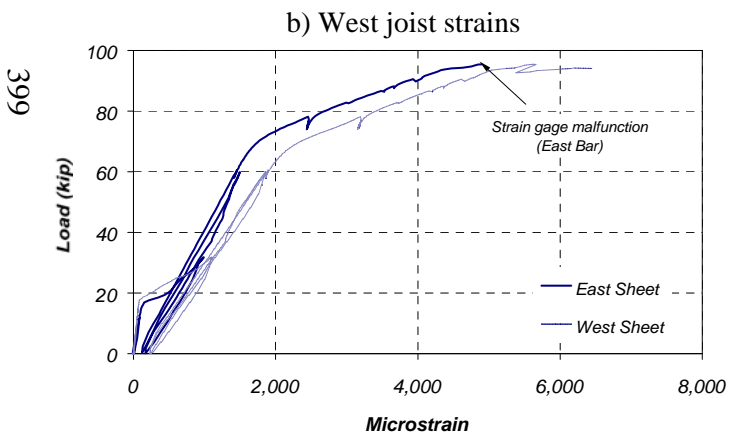
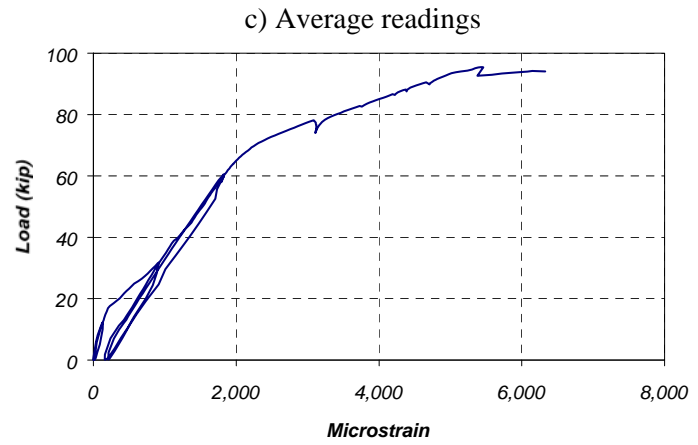
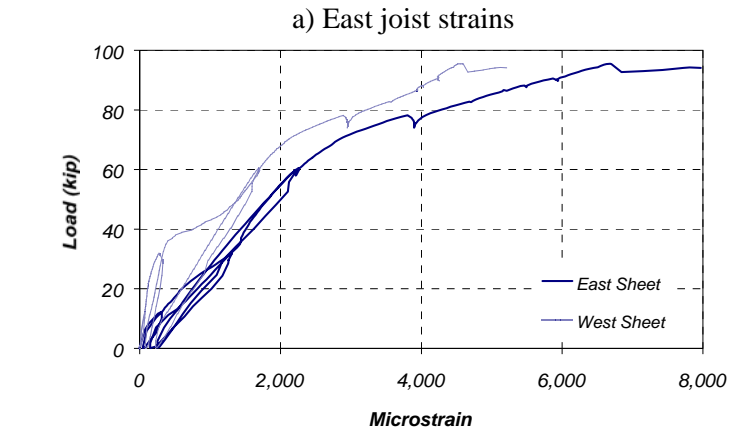


Figure D.21 Measured CFRP Strains in Specimen J-2 (Section N2)

399

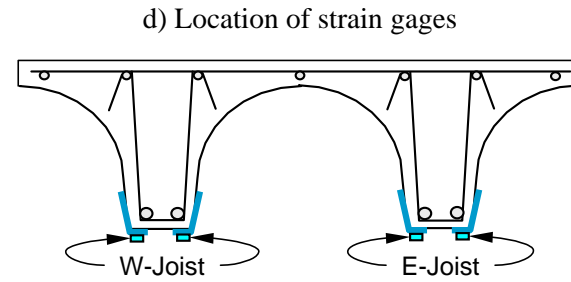
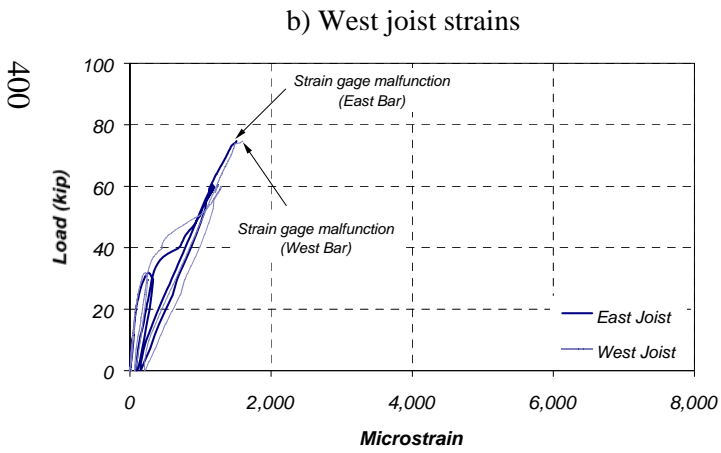
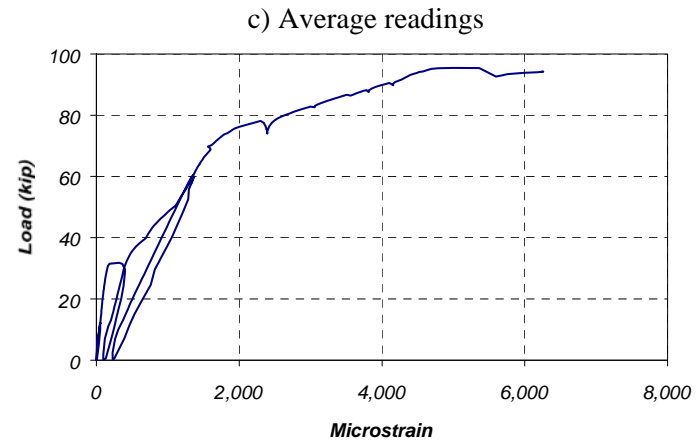
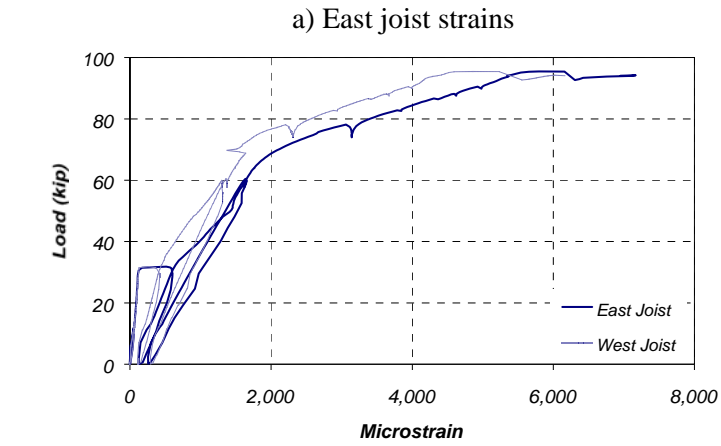


Figure D.22 Measured CFRP Strains in Specimen J-2 (Section S2)

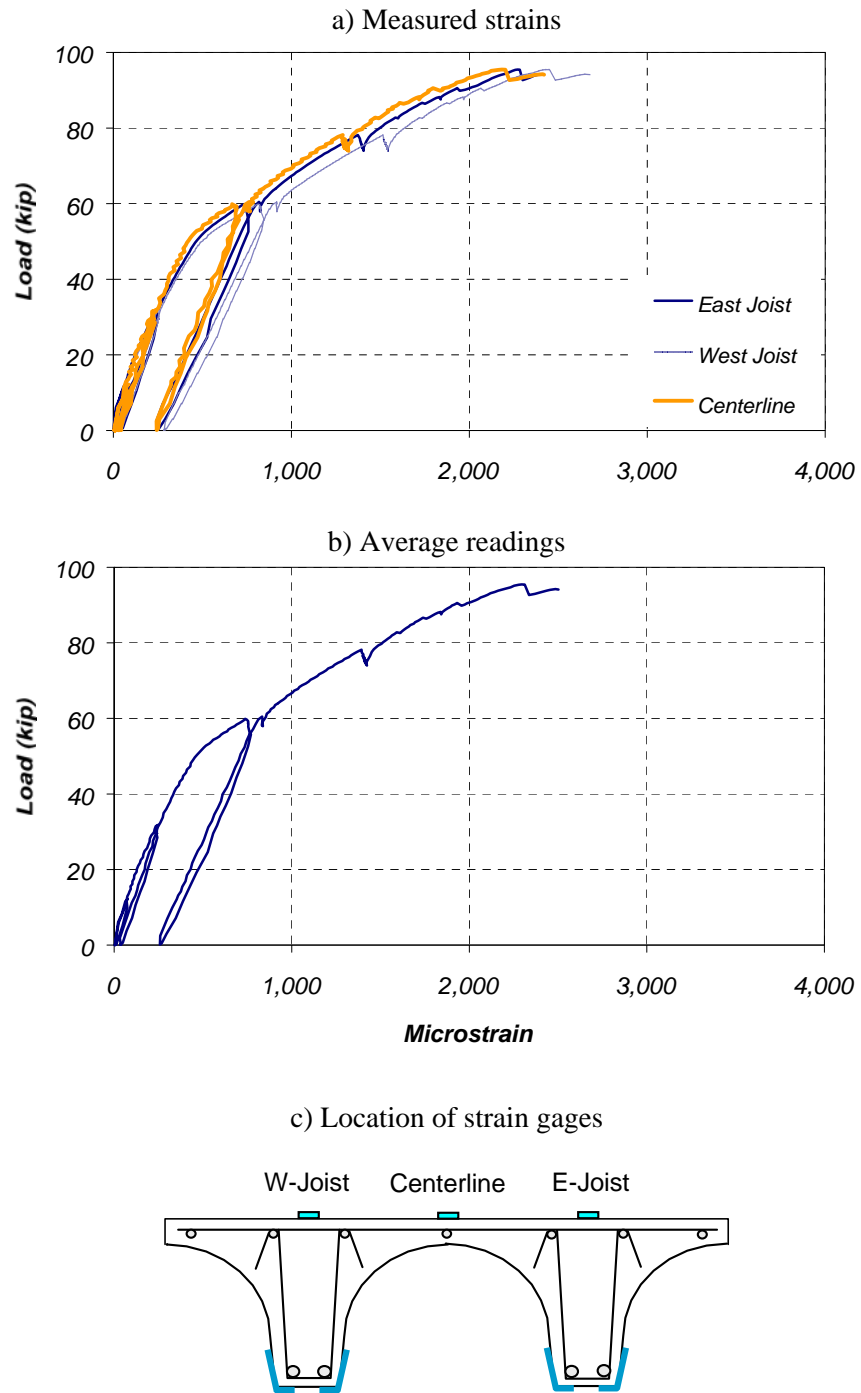


Figure D.23 Measured Strains on Concrete Slab in Specimen J-2 (Section N1)

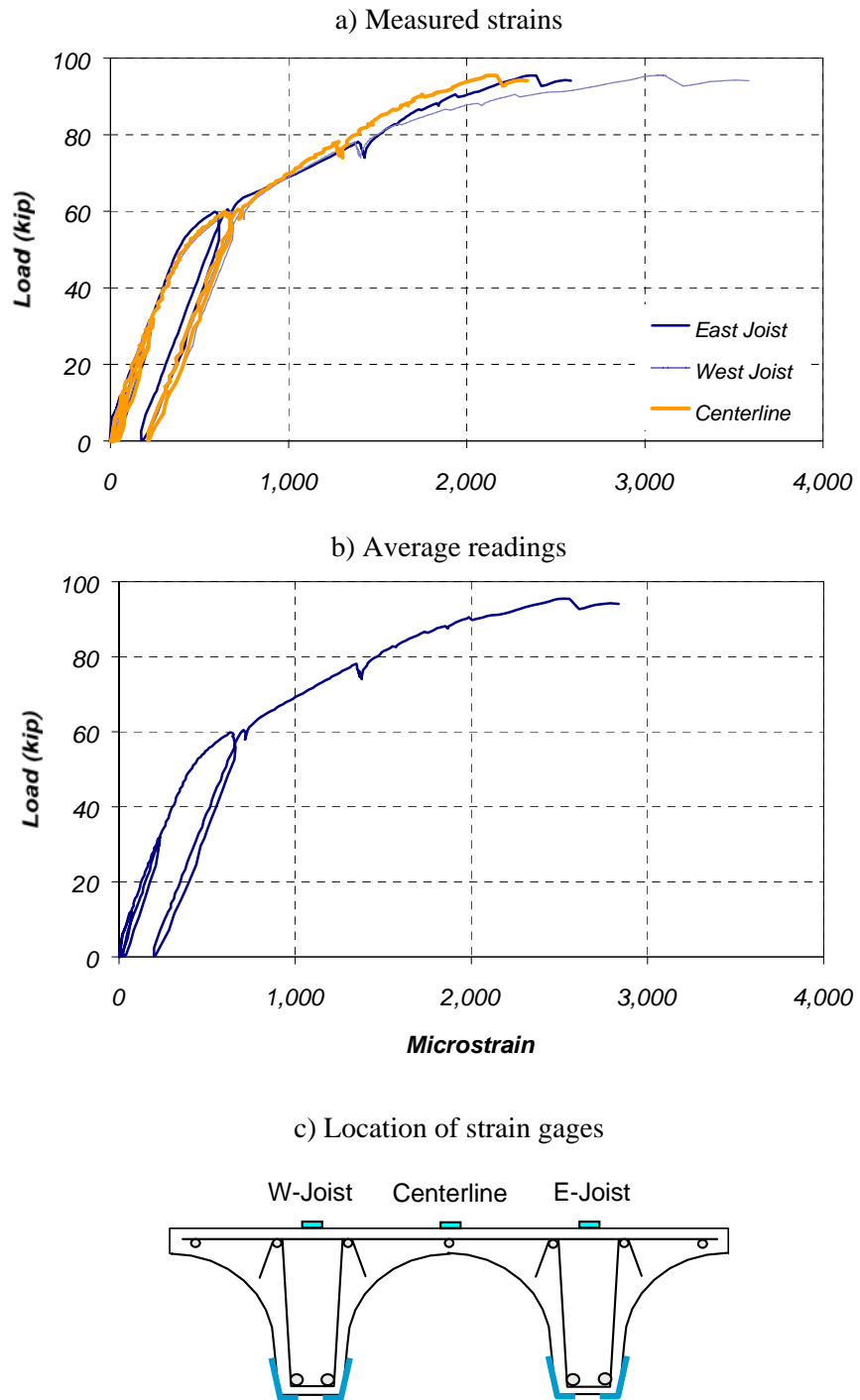


Figure D.24 Measured Strains on Concrete Slab in Specimen J-2 (Section S1)

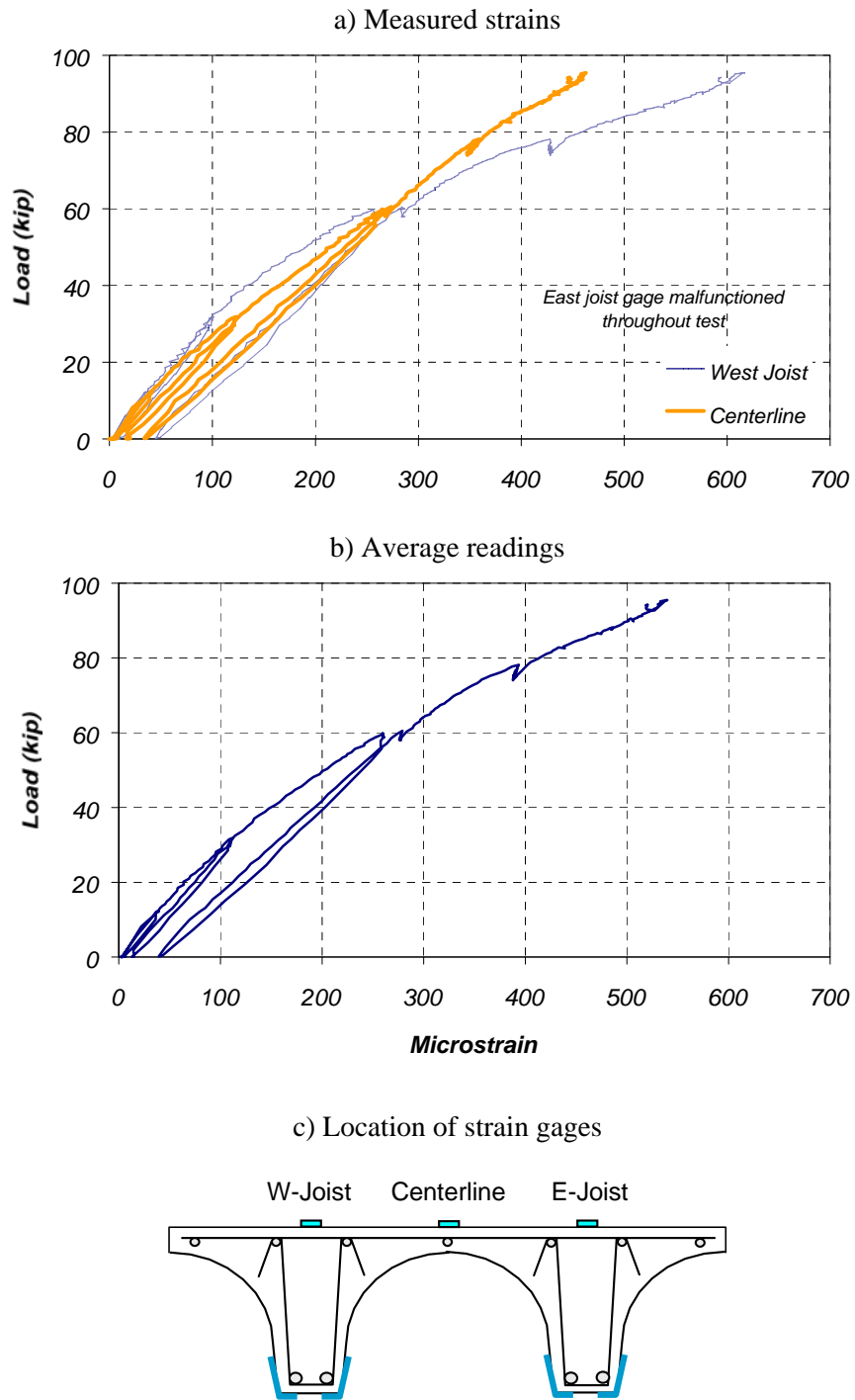


Figure D.25 Measured Strains on Concrete Slab in Specimen J-2 (Section N2)

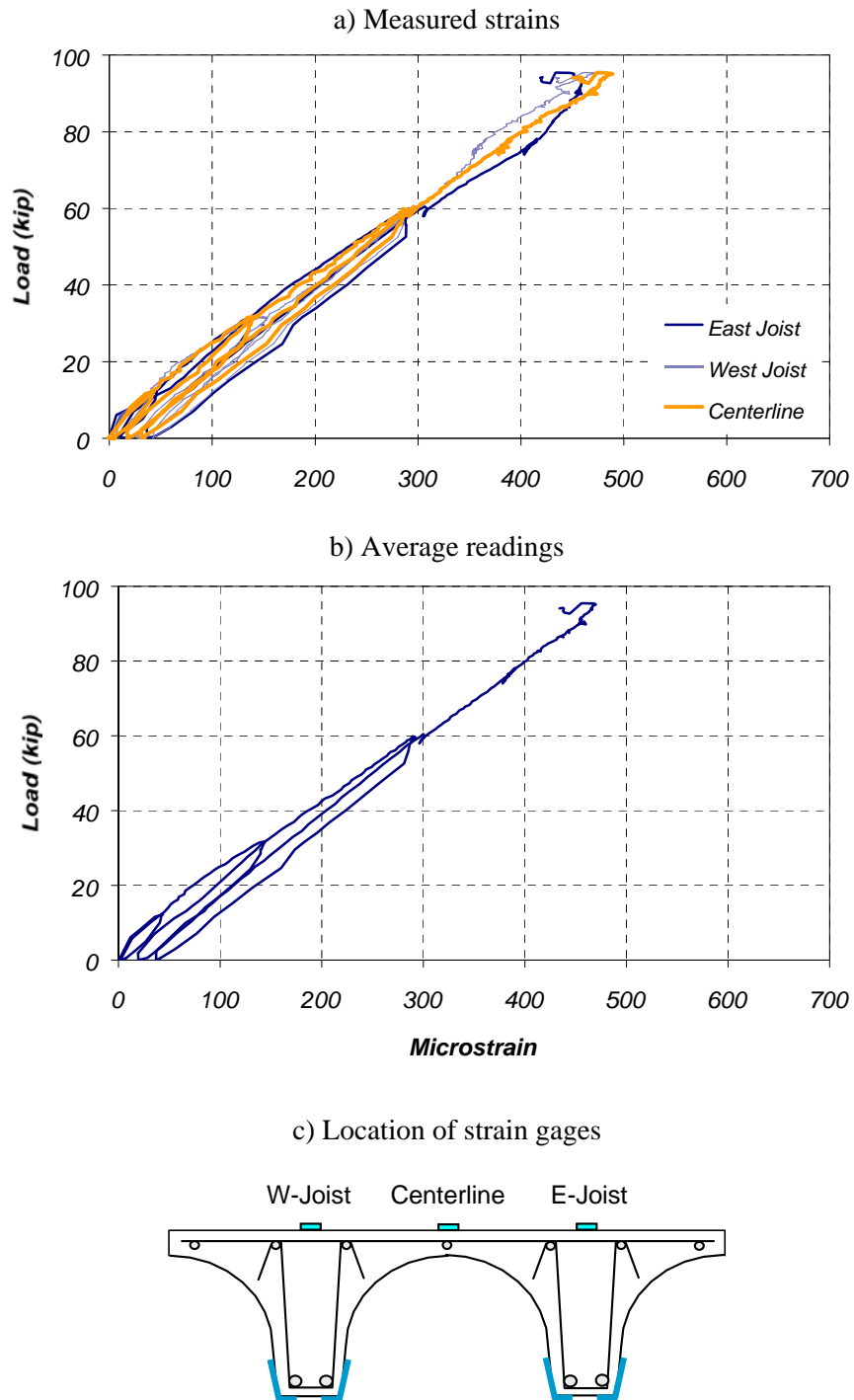


Figure D.26 Measured Strains on Concrete Slab in Specimen J-2 (Section S2)

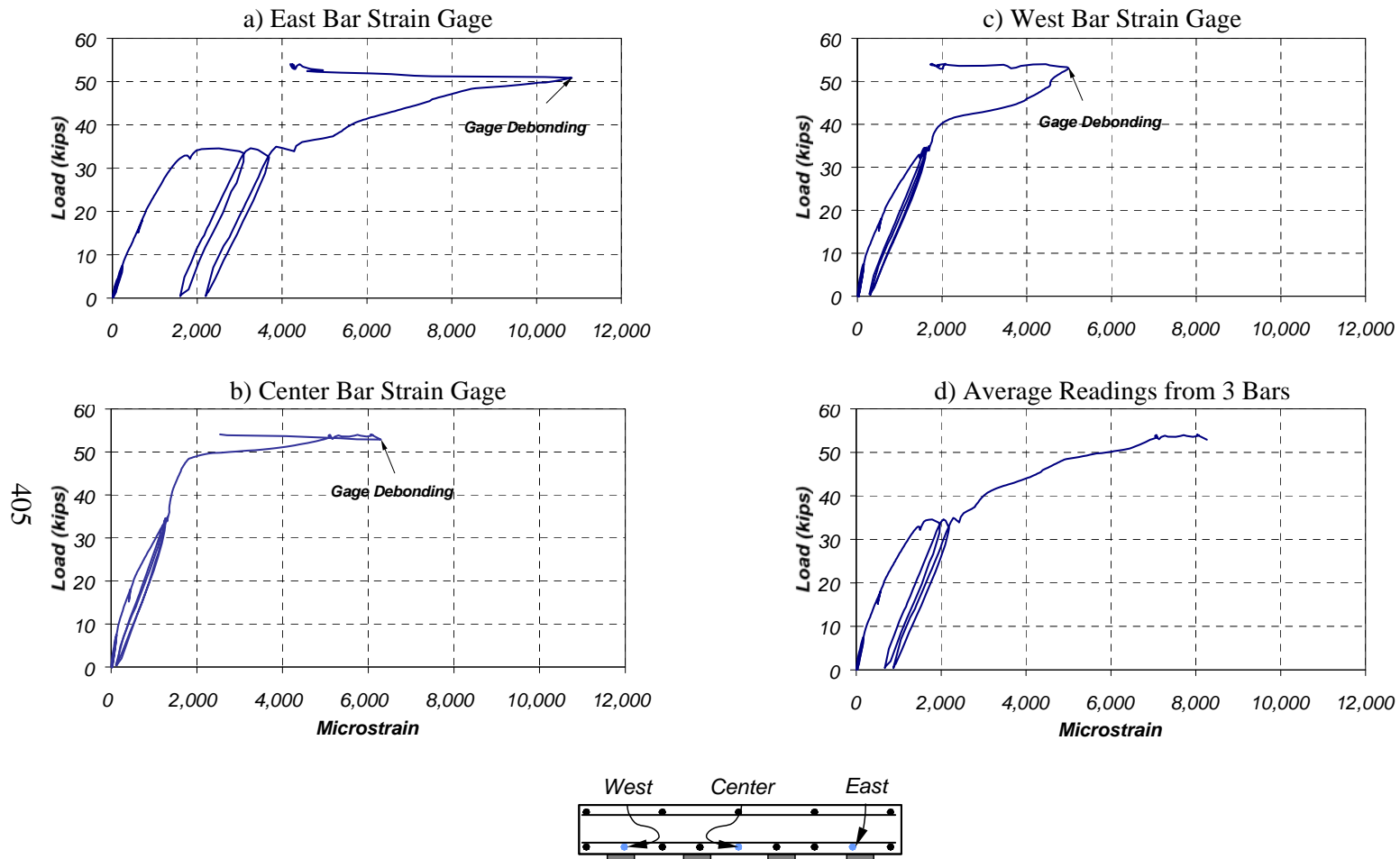
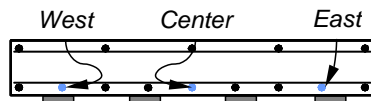
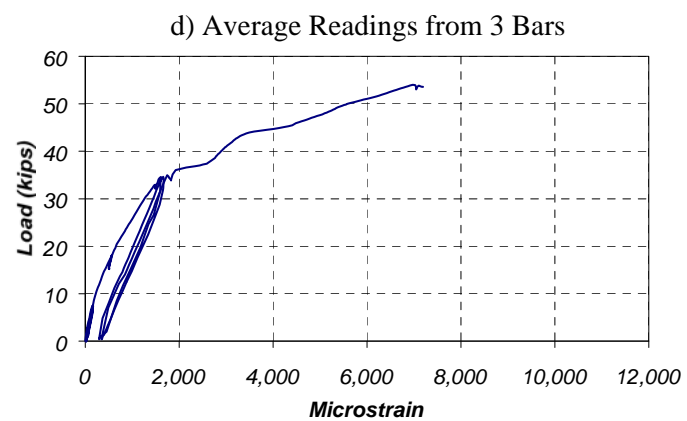
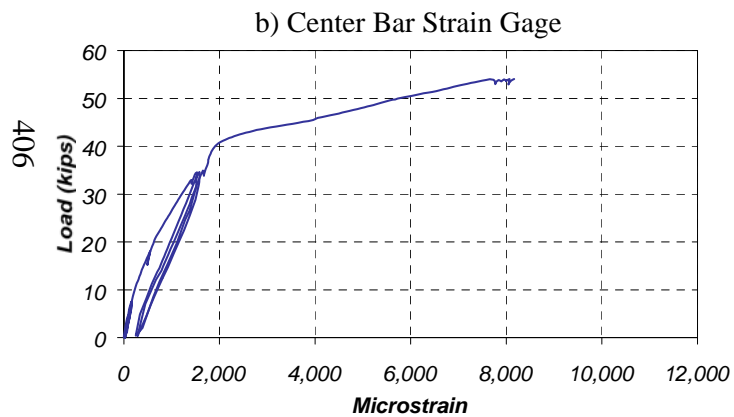
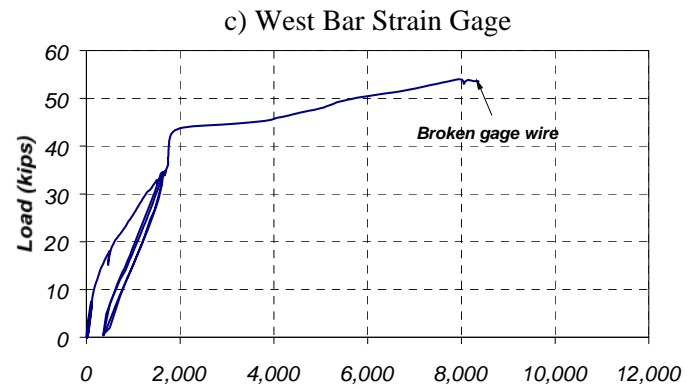
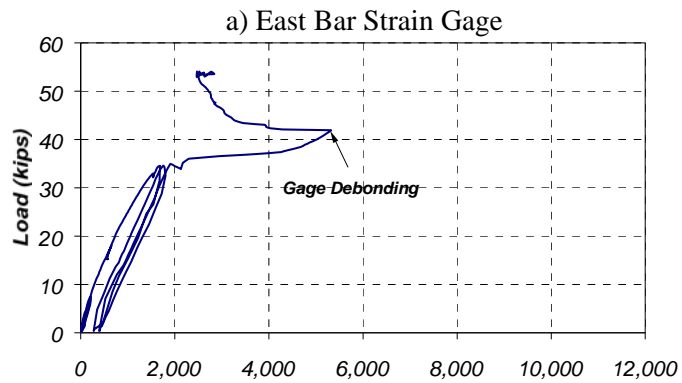
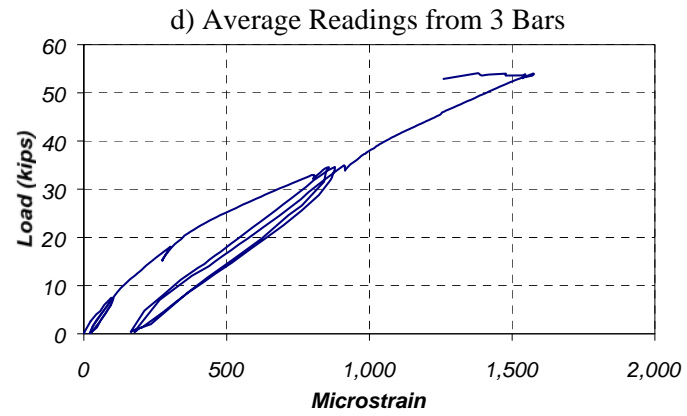
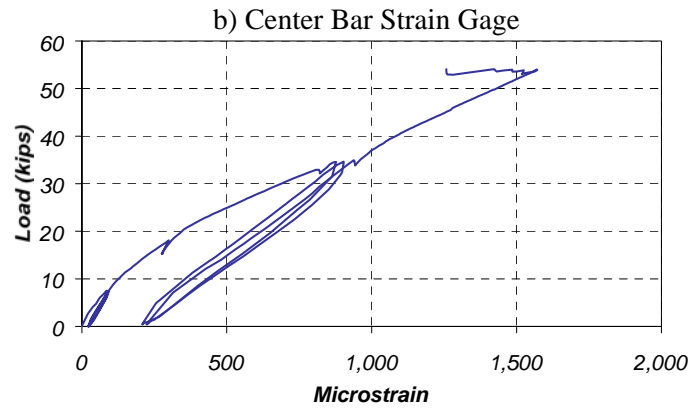
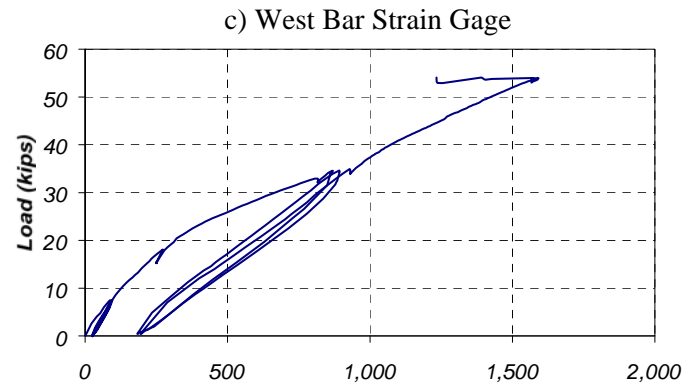
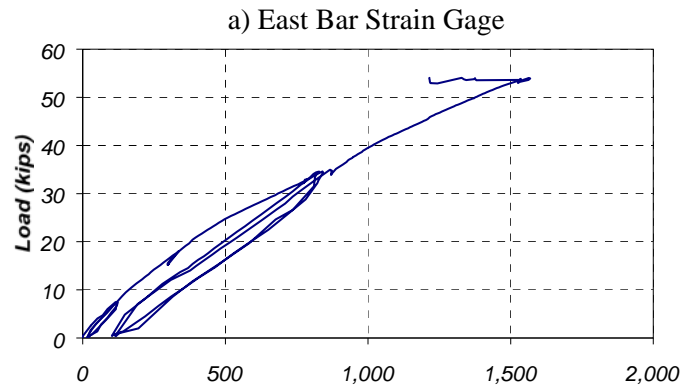


Figure D.27 Measured Reinforcing Bar (#6) Strains on Specimen FS-1 (Section N1)



406

Figure D.28 Measured Reinforcing Bar (#6) Strains on Specimen FS-1 (Section S1)



407

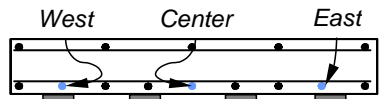
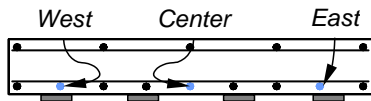
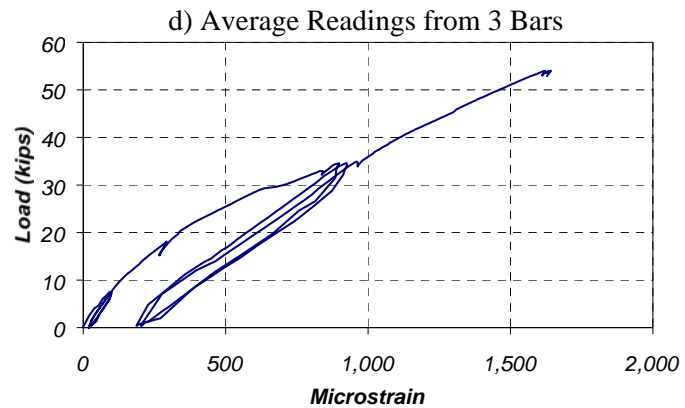
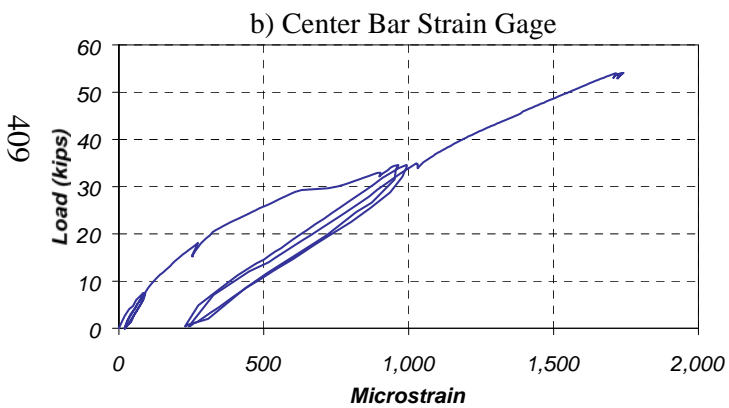
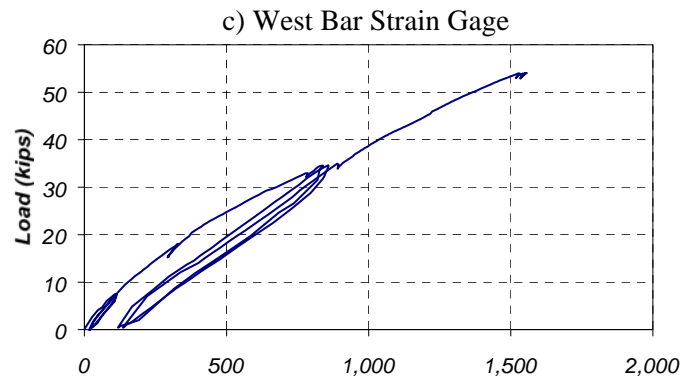
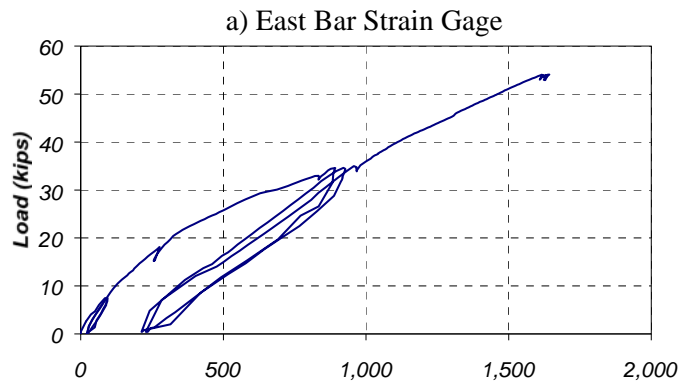


Figure D.29 Measured Reinforcing Bar (#6) Strains on Specimen FS-1 (Section N2)



409

Figure D.30 Measured Reinforcing Bar (#6) Strains in Specimen FS-1 (Section S2)

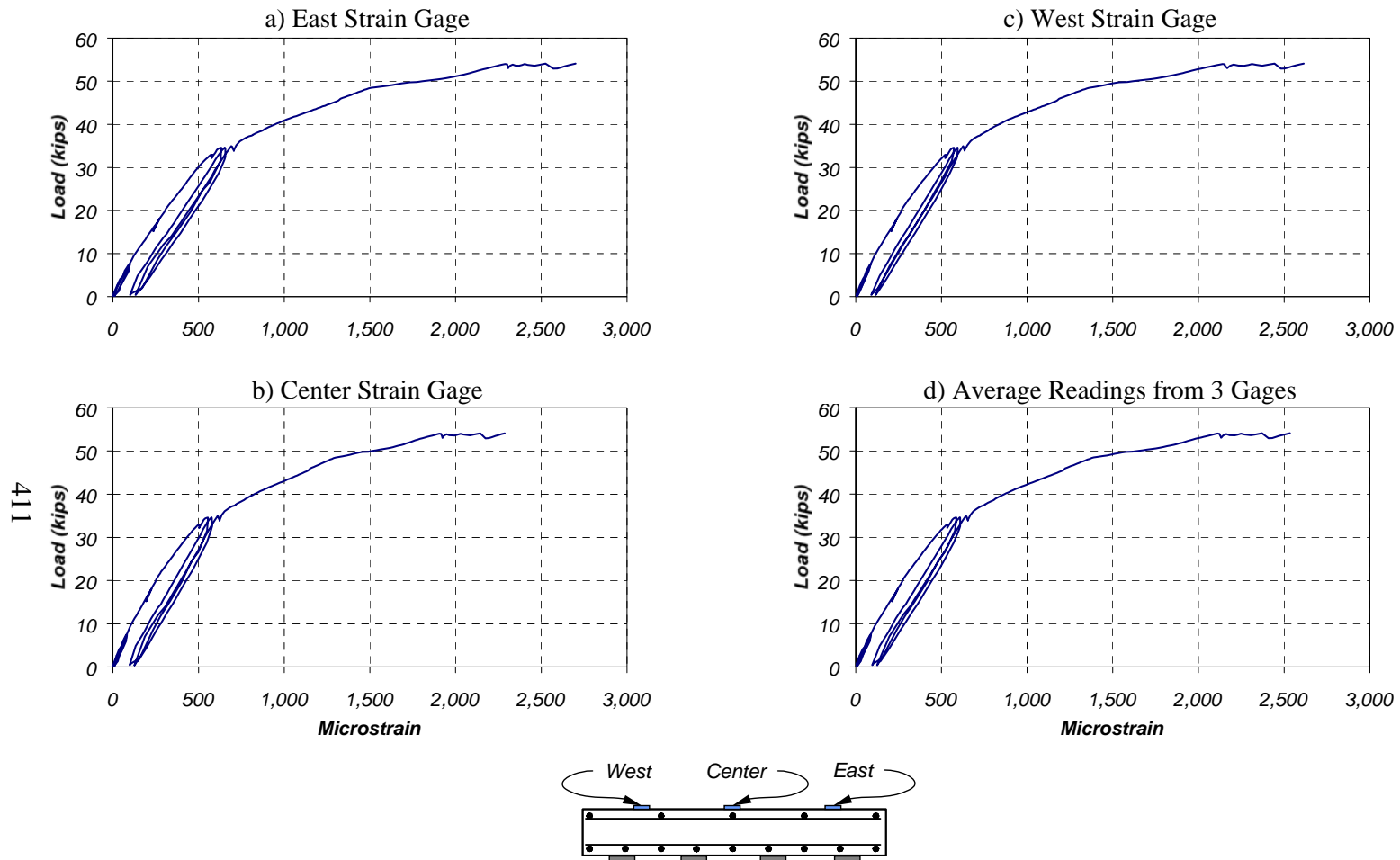


Figure D.31 Measured Strains on Concrete Slab in Specimen FS-1 (Section N1)

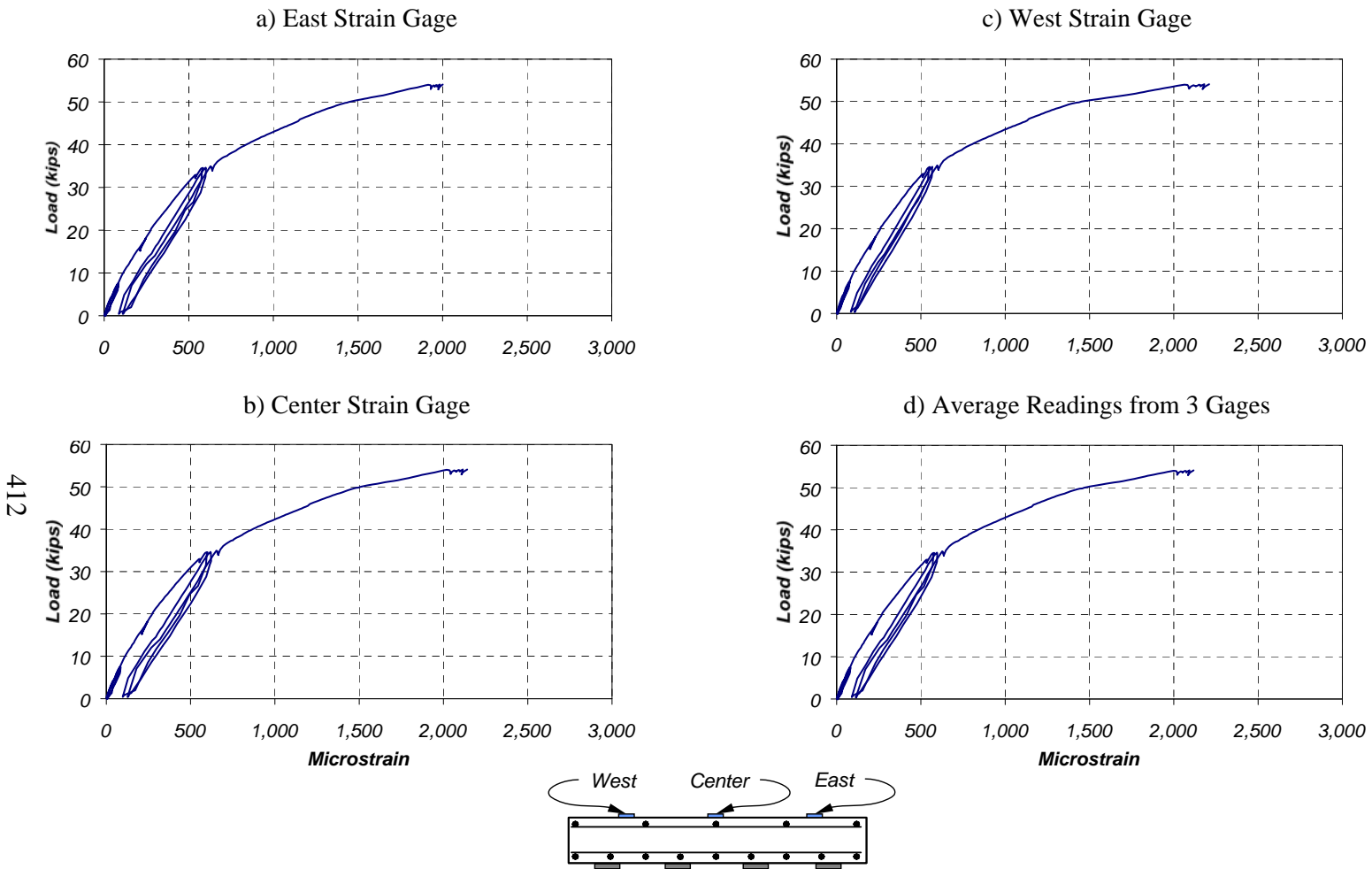


Figure D.32 Measured Strains on Concrete Slab in Specimen FS-1 (Section S1)

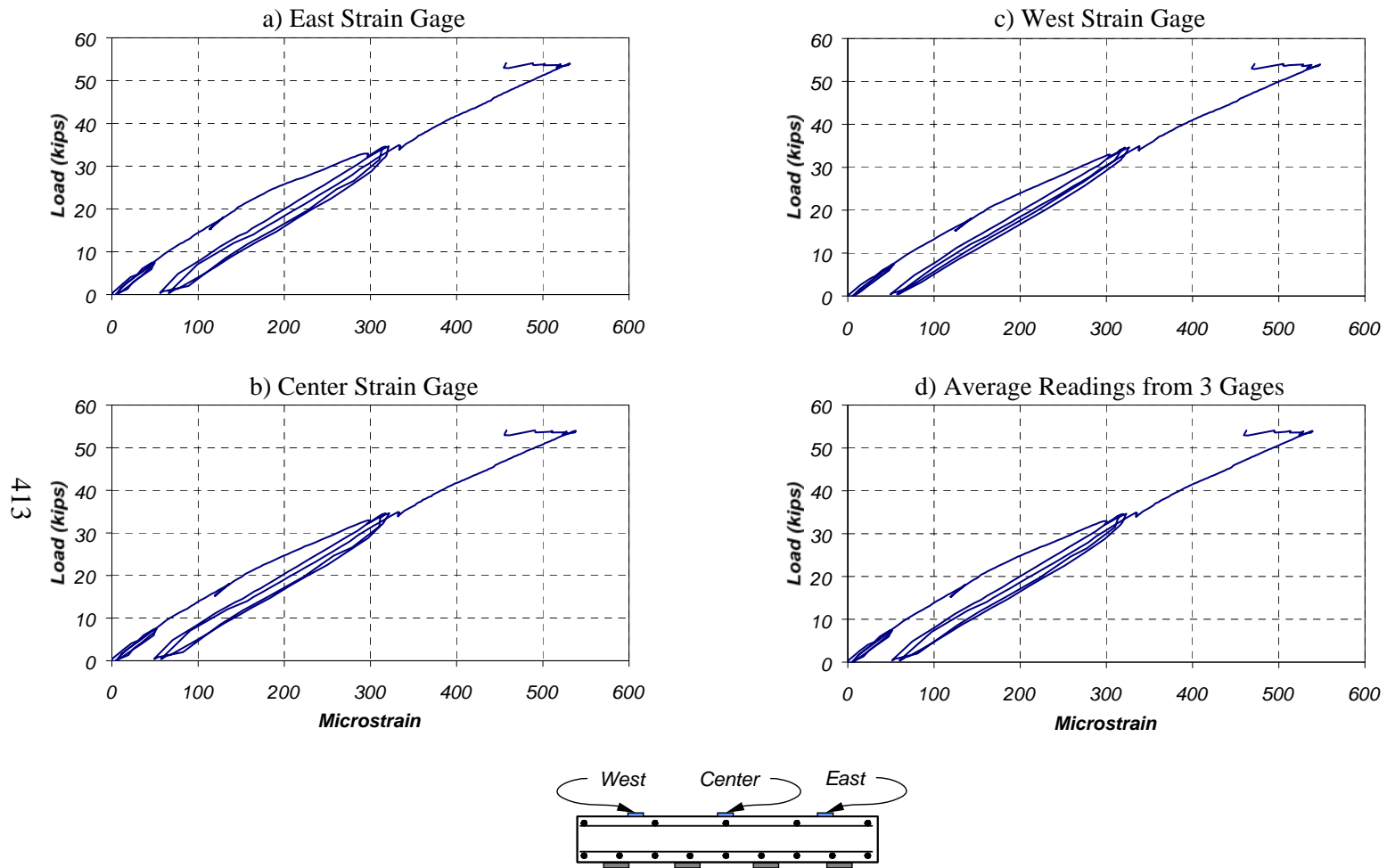


Figure D.33 Measured Strains on Concrete Slab in Specimen FS-1 (Section N2)

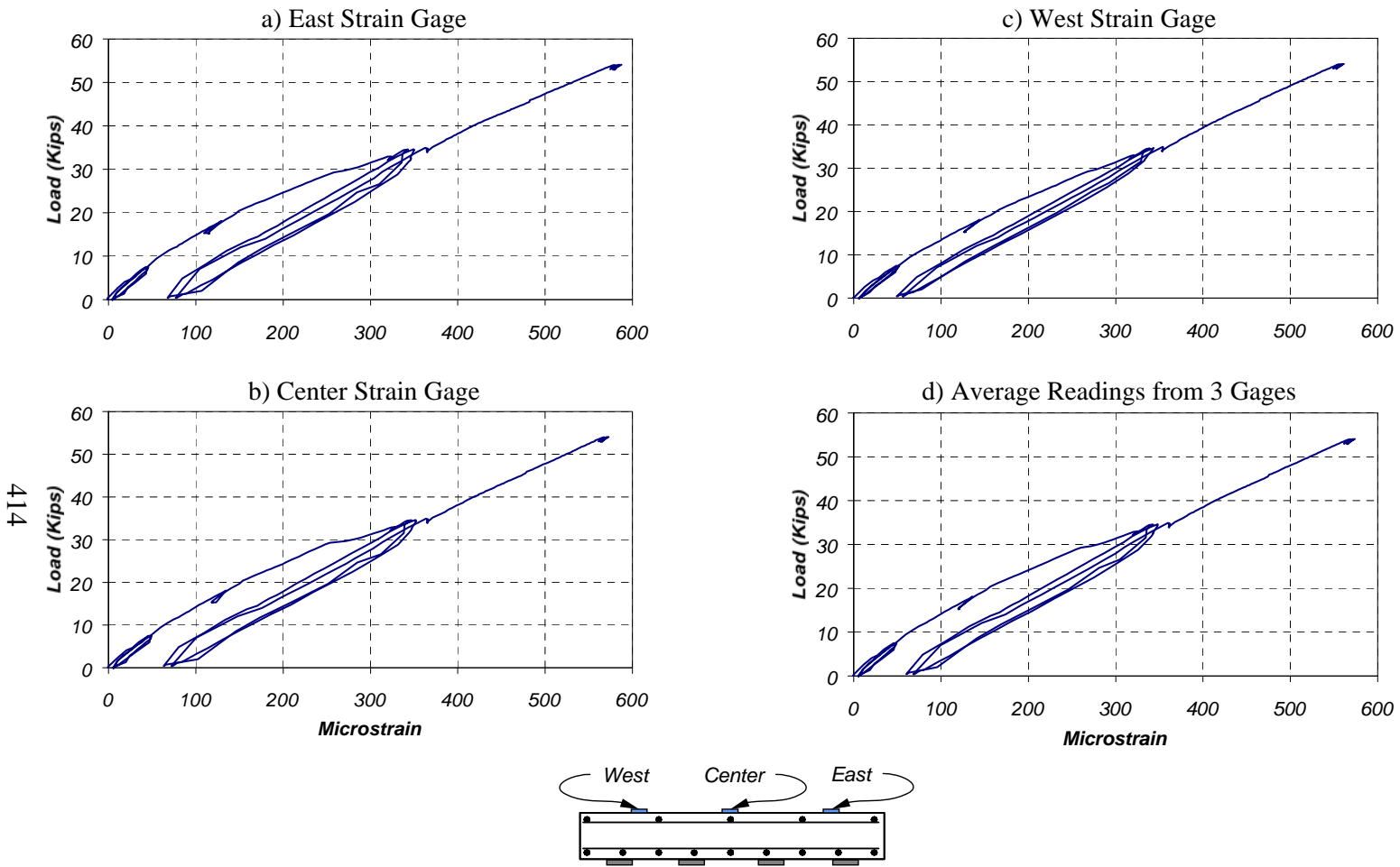


Figure D.34 Measured Strains on Concrete Slab in Specimen FS-1 (Section S2)

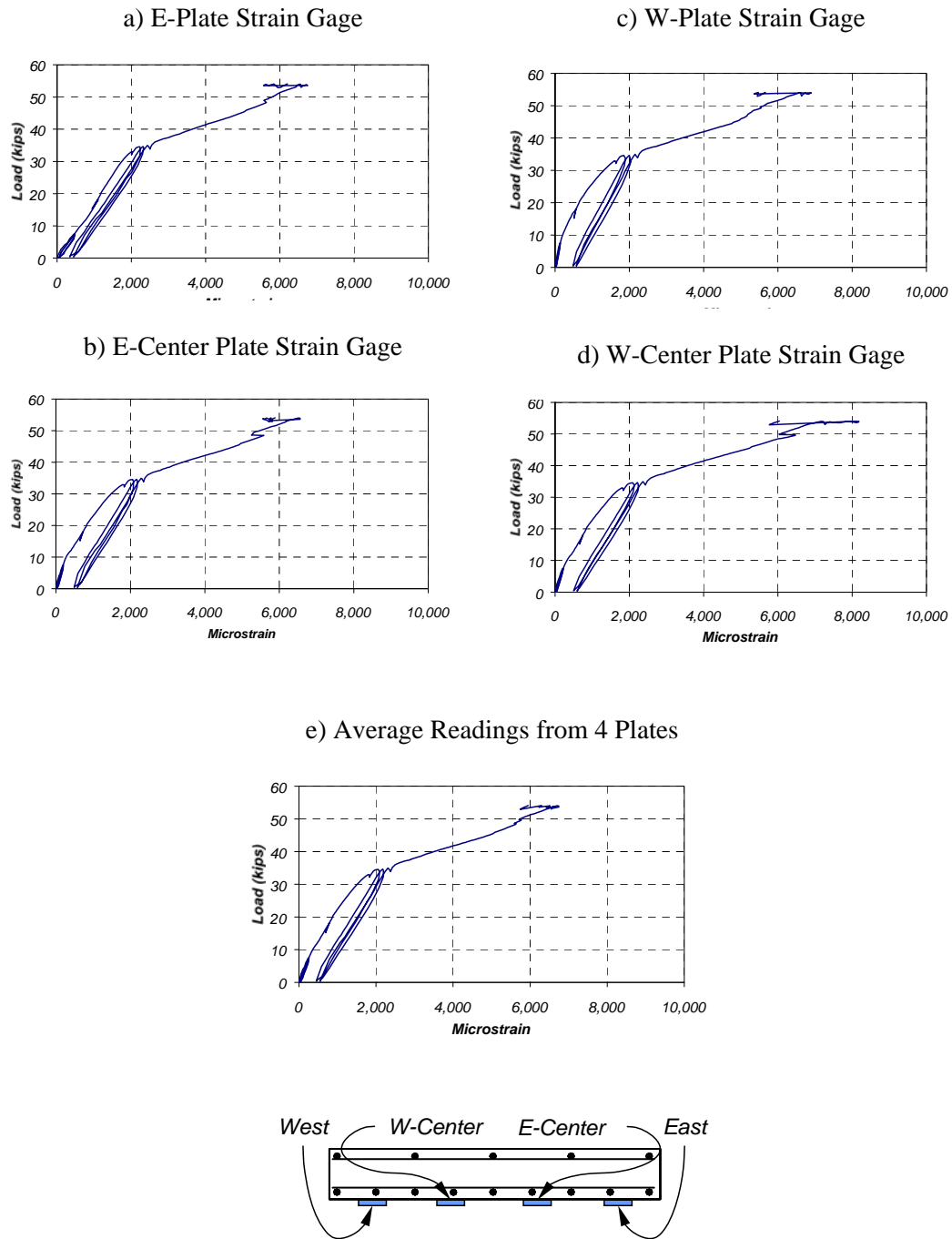


Figure D.35 Measured Strains on CFRP Plates in Specimen FS-1 (Section N1)

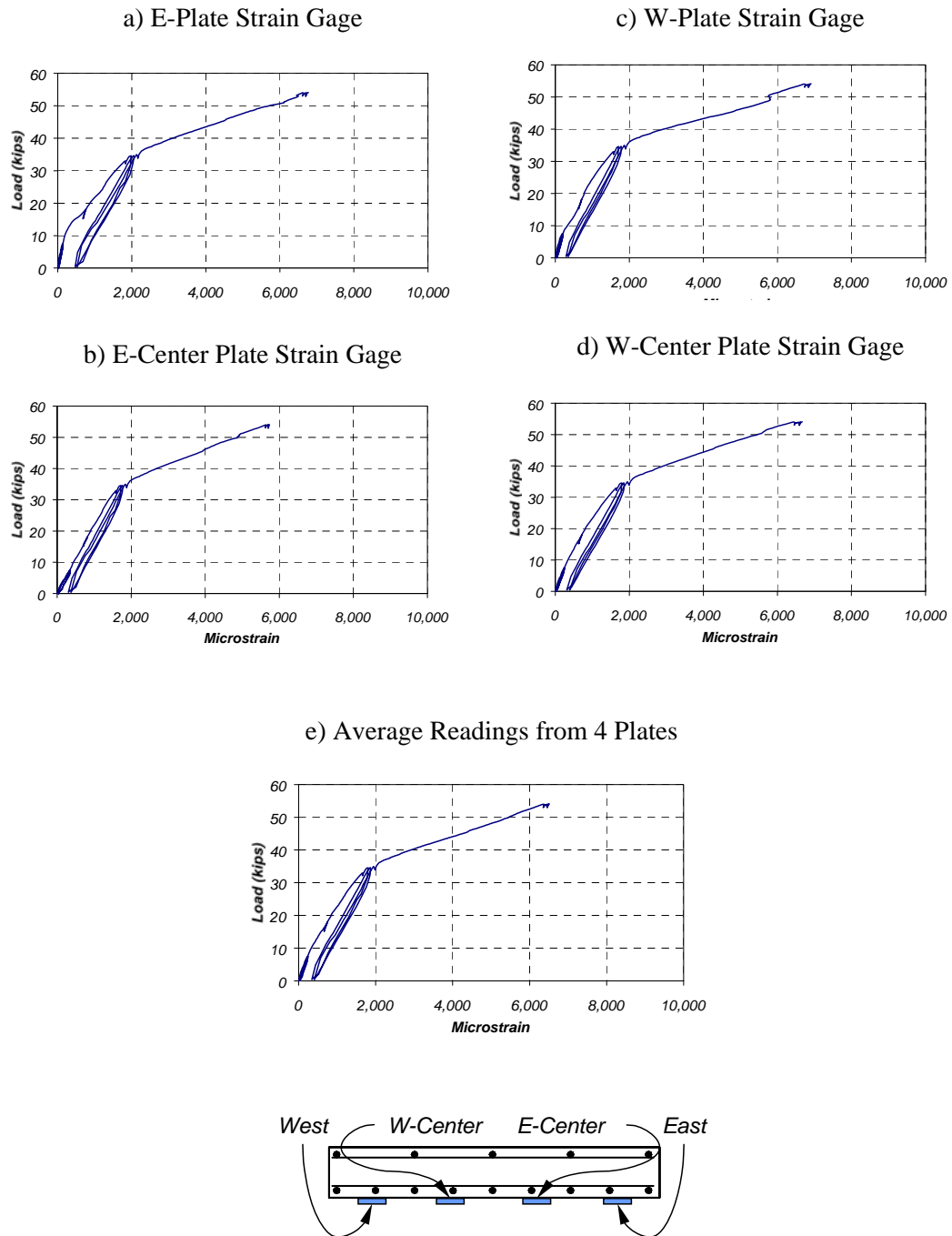


Figure D.36 Measured Strains on CFRP Plates in Specimen FS-1 (Section S1)

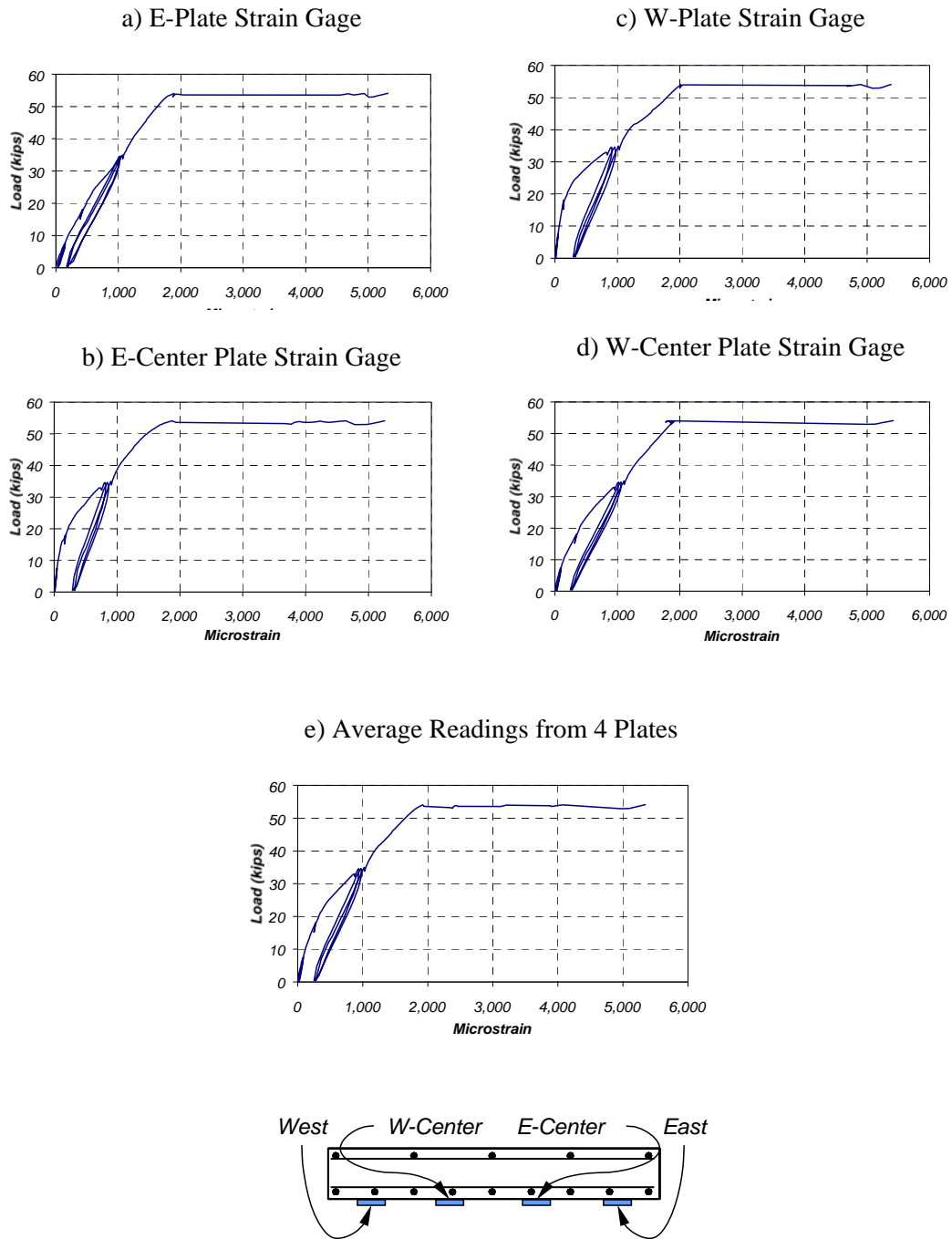


Figure D.37 Measured Strains on CFRP Plates in Specimen FS-1 (Section N2)

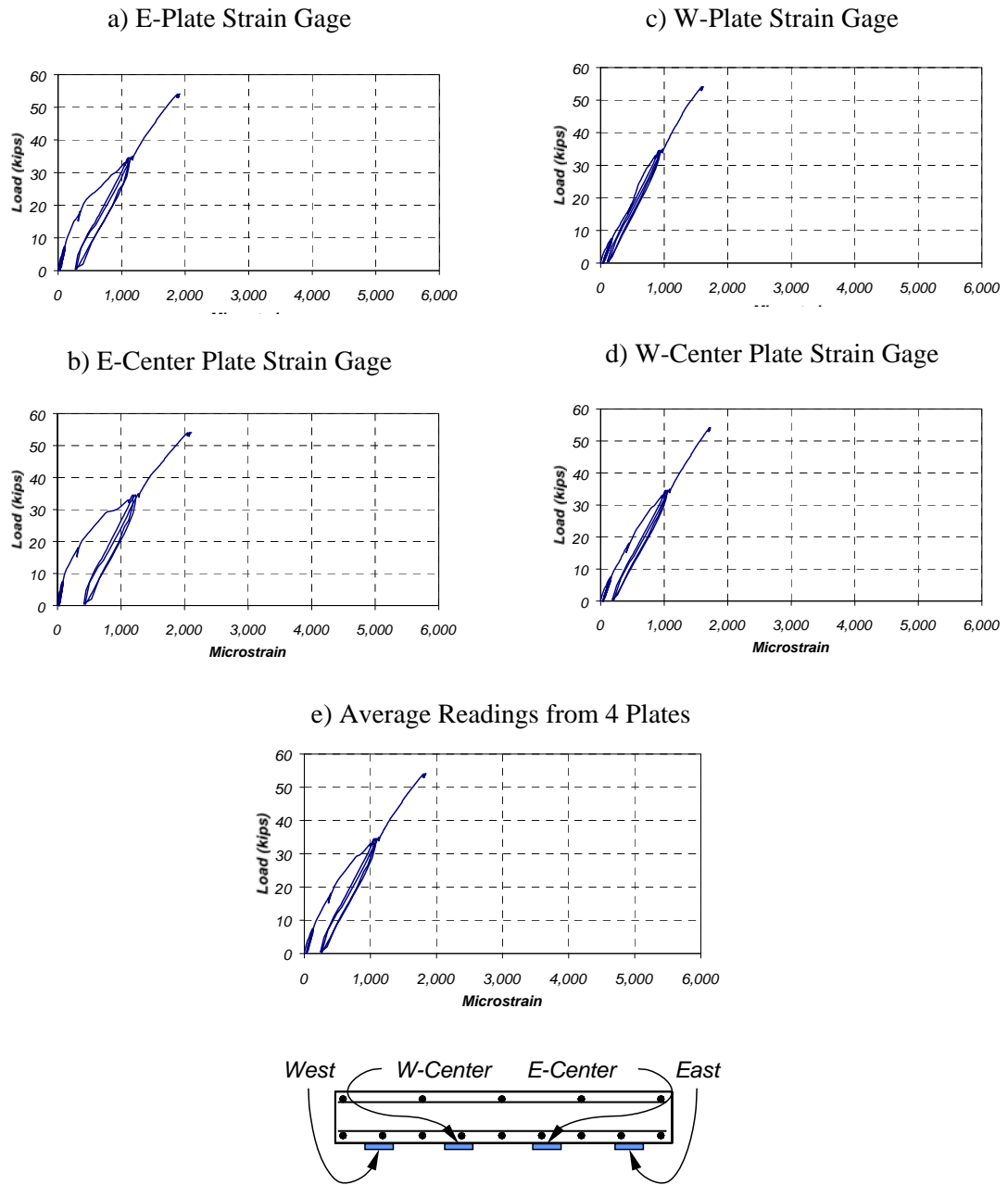


Figure D.38 Measured Strains on CFRP Plates in Specimen FS-1 (Section S2)

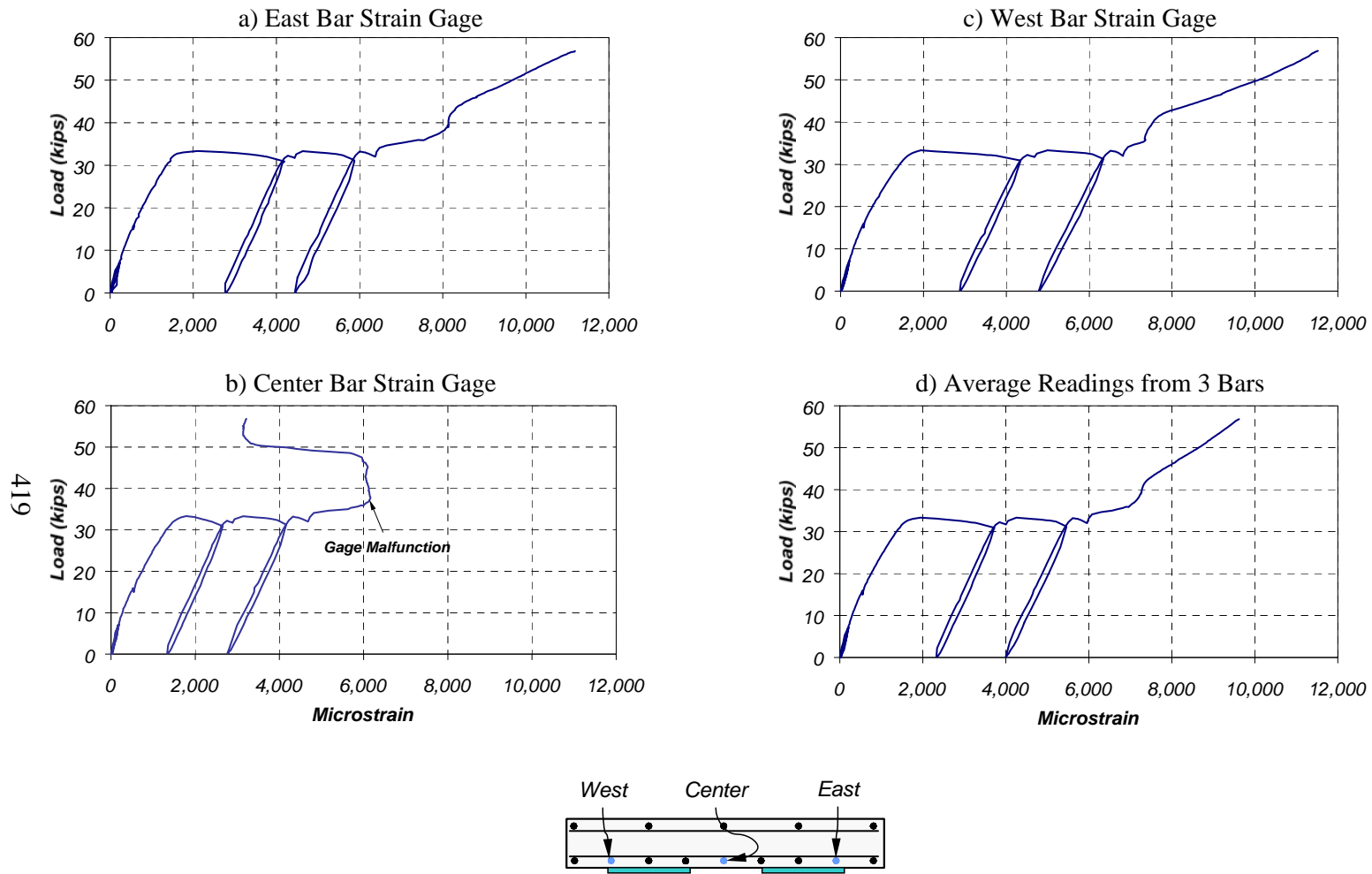
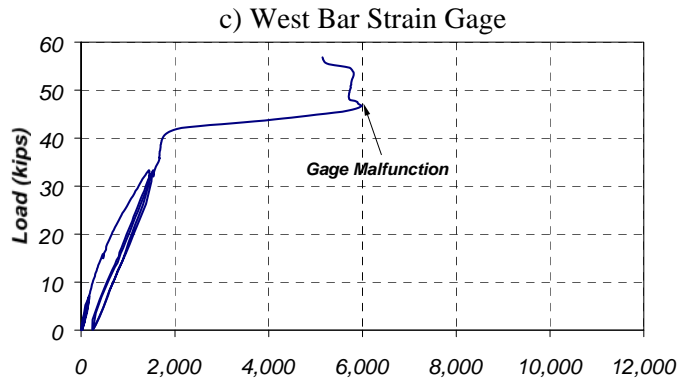
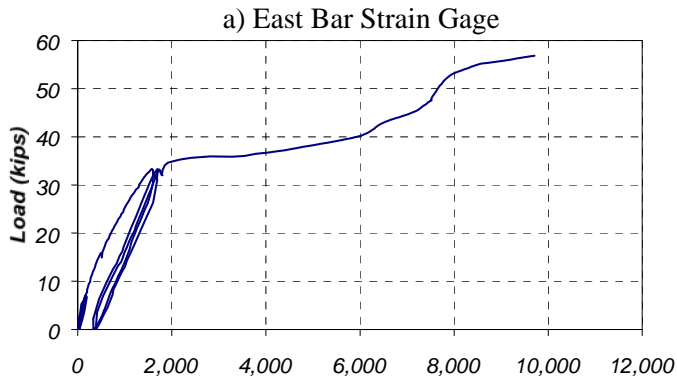


Figure D.39 Measured Reinforcing Bar (#6) Strains in Specimen FS-2 (Section N1)



b) Center Bar Strain Gage
Gage not working

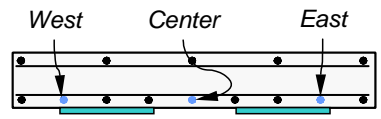
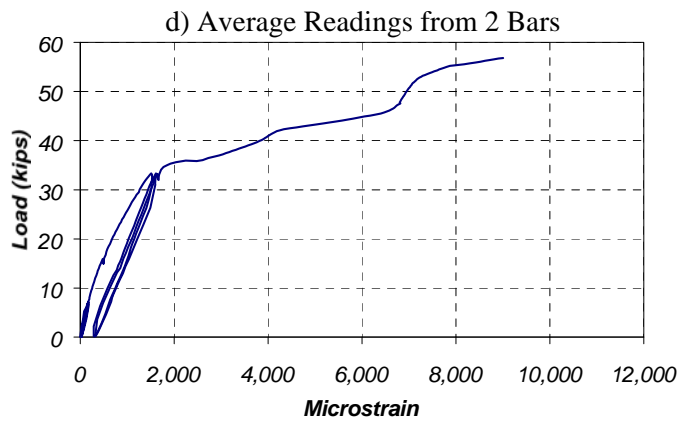


Figure D.40 Measured Reinforcing Bar (#6) Strains in Specimen FS-2 (Section S1)

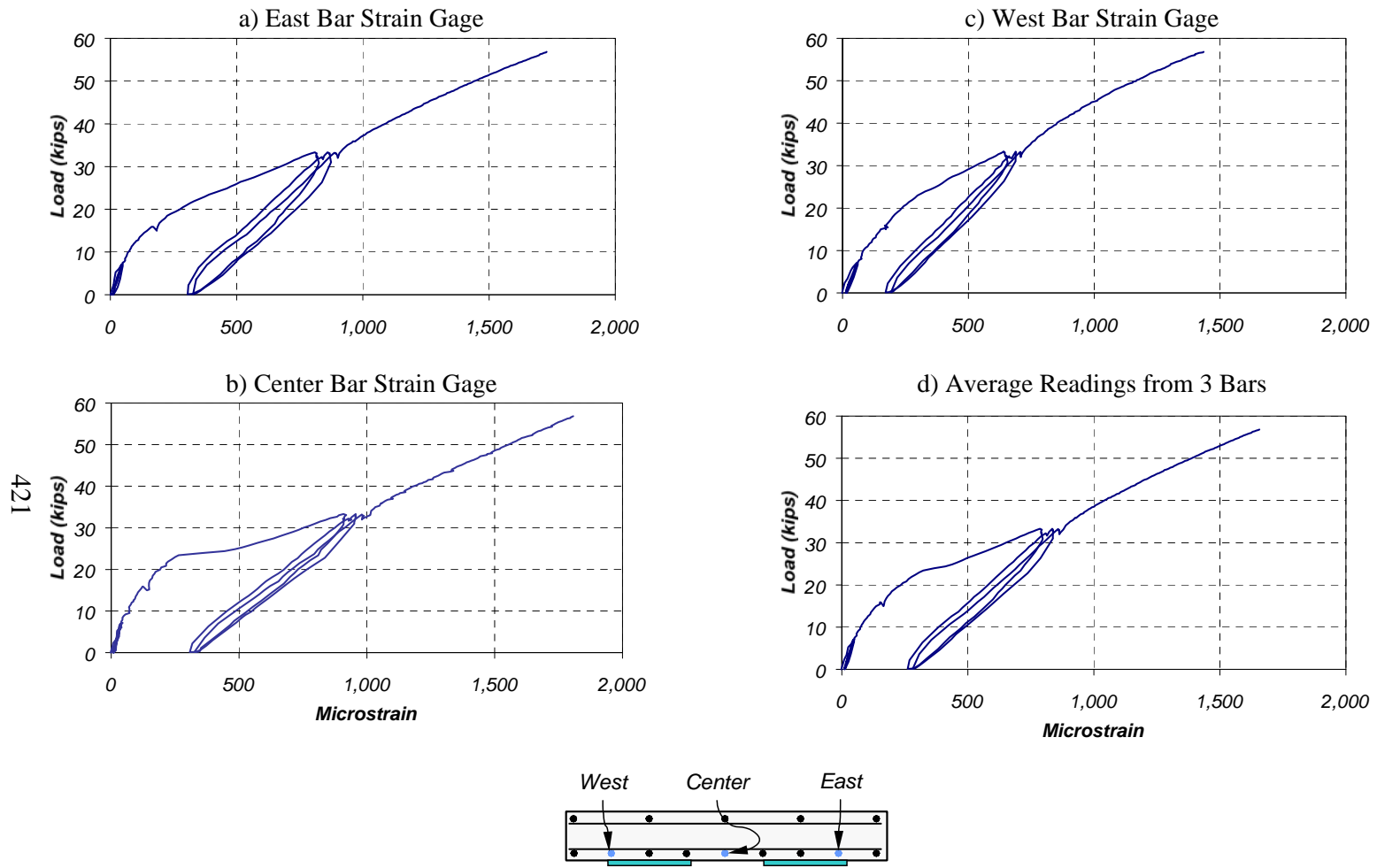


Figure D.41 Measured Reinforcing Bar (#6) Strains in Specimen FS-2 (Section N2)

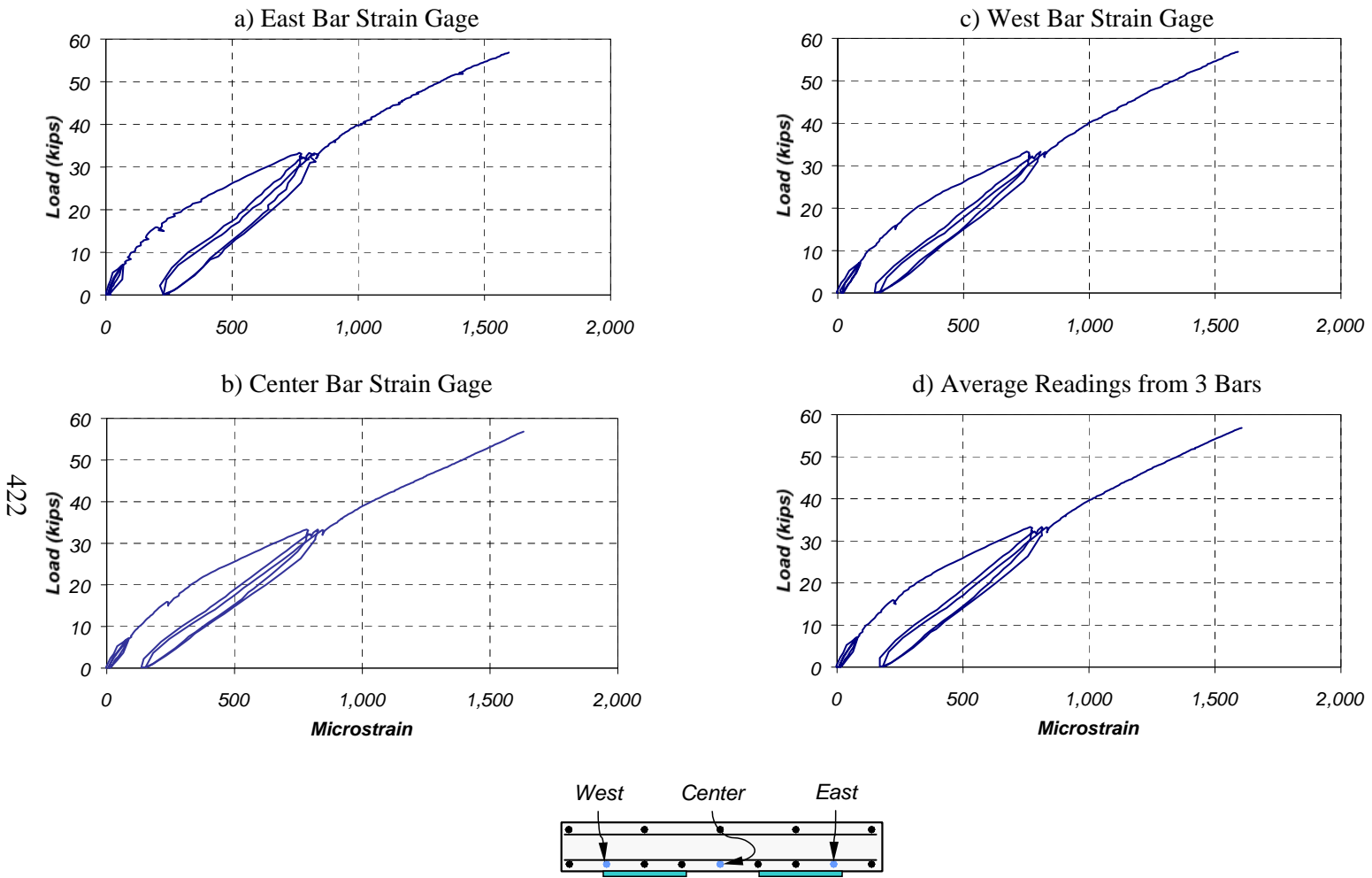


Figure D.42 Measured Reinforcing Bar (#6) Strains in Specimen FS-2 (Section S2)

422

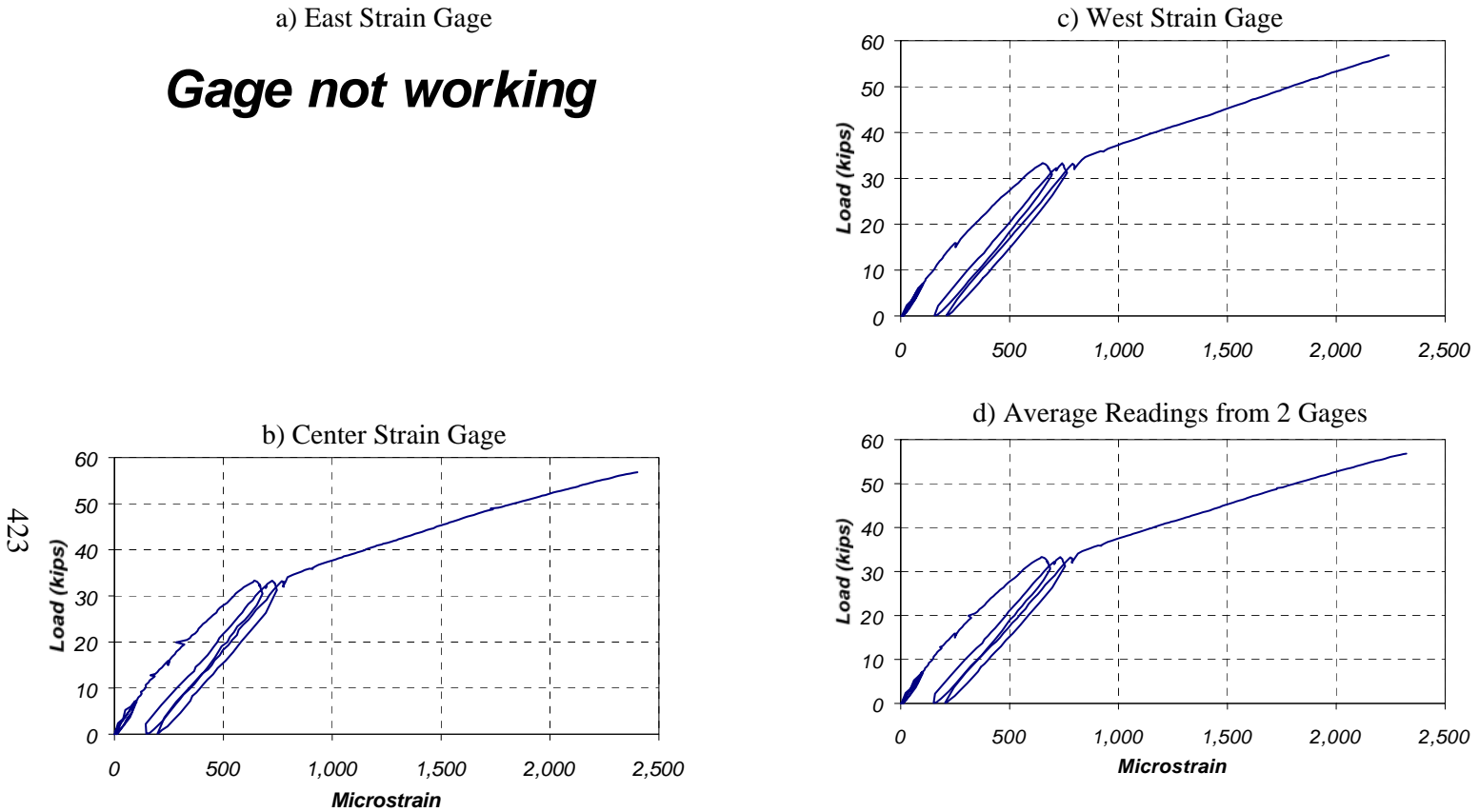


Figure D.43 Measured Strains on Concrete Slab in Specimen FS-2 (Section N1)

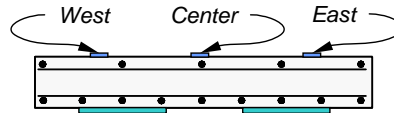
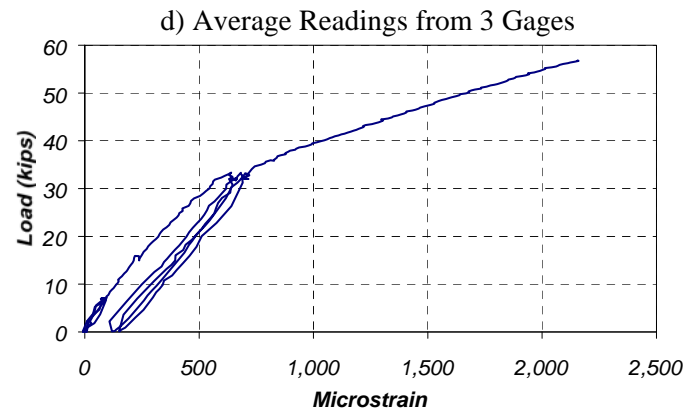
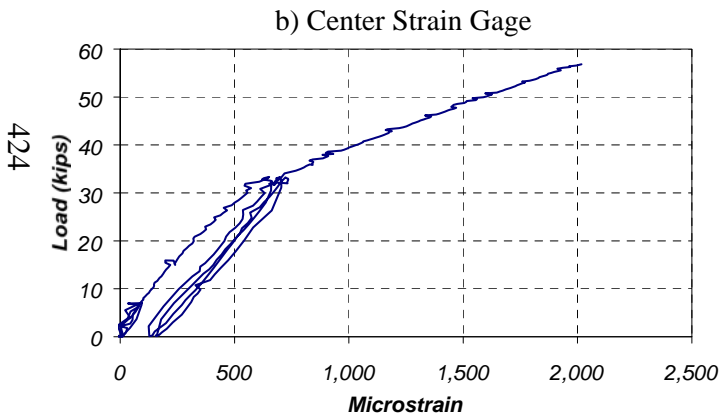
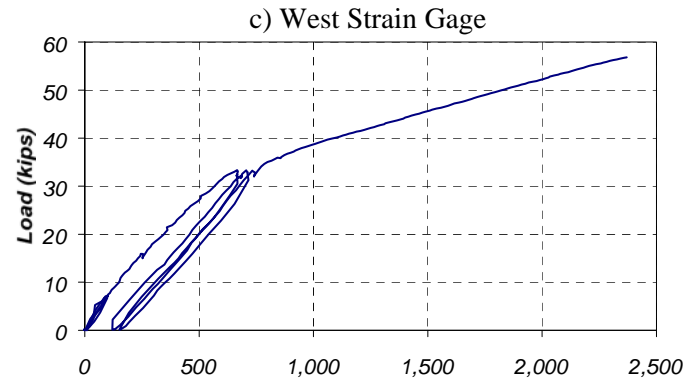
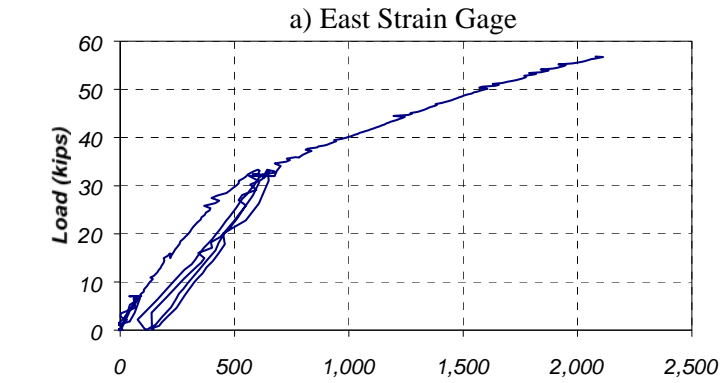


Figure D.44 Measured Strains on Concrete Slab in Specimen FS-2 (Section S1)

424

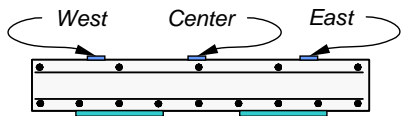
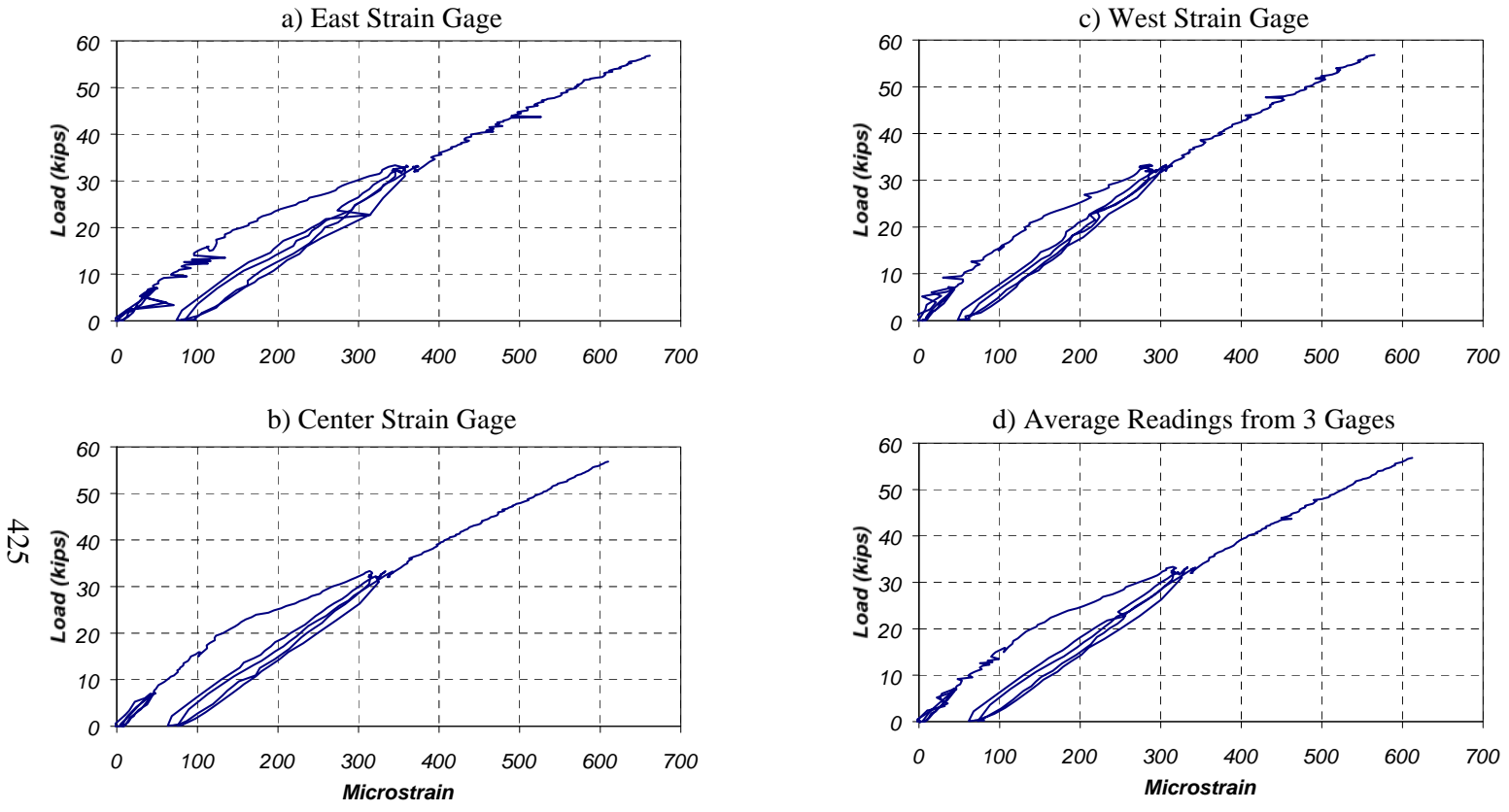


Figure D.45 Measured Strains on Concrete Slab in Specimen FS-2 (Section N2)

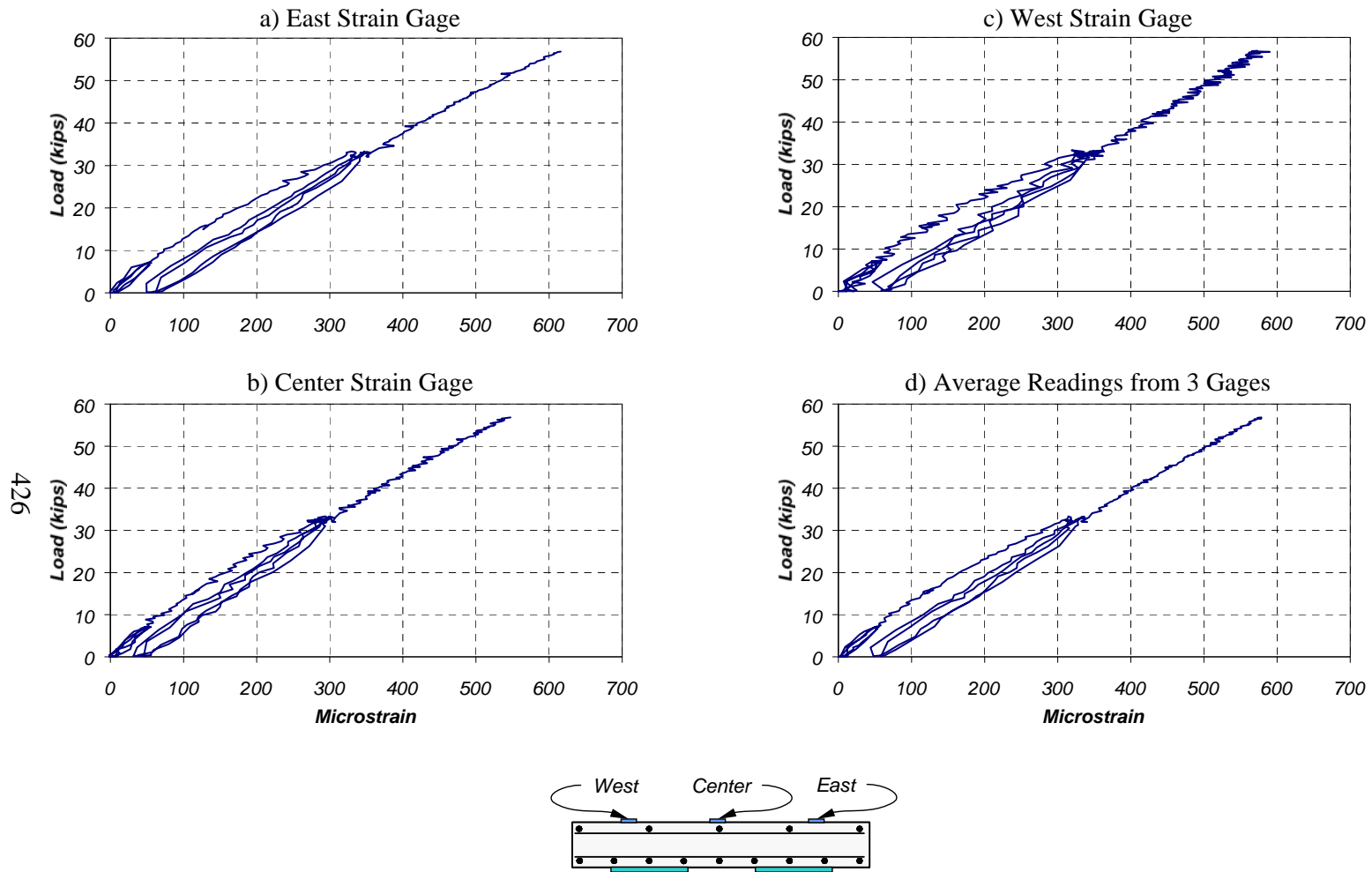
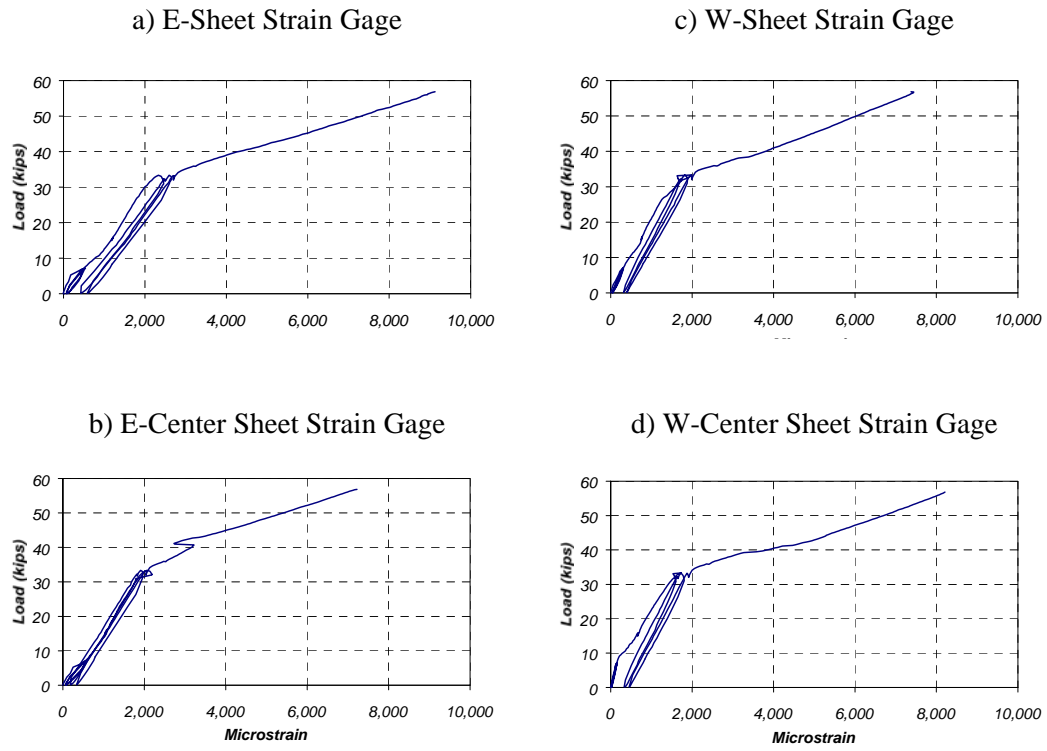


Figure D.46 Measured Strains on Concrete Slab in Specimen FS-2 (Section S2)



e) Average Readings from 4 Strain Gages

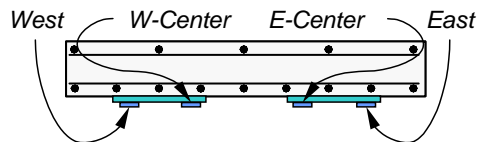
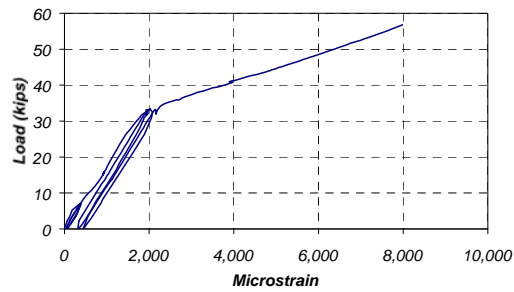


Figure D.47 Measured Strains on CFRP Sheets in Specimen FS-2 (Section N1)

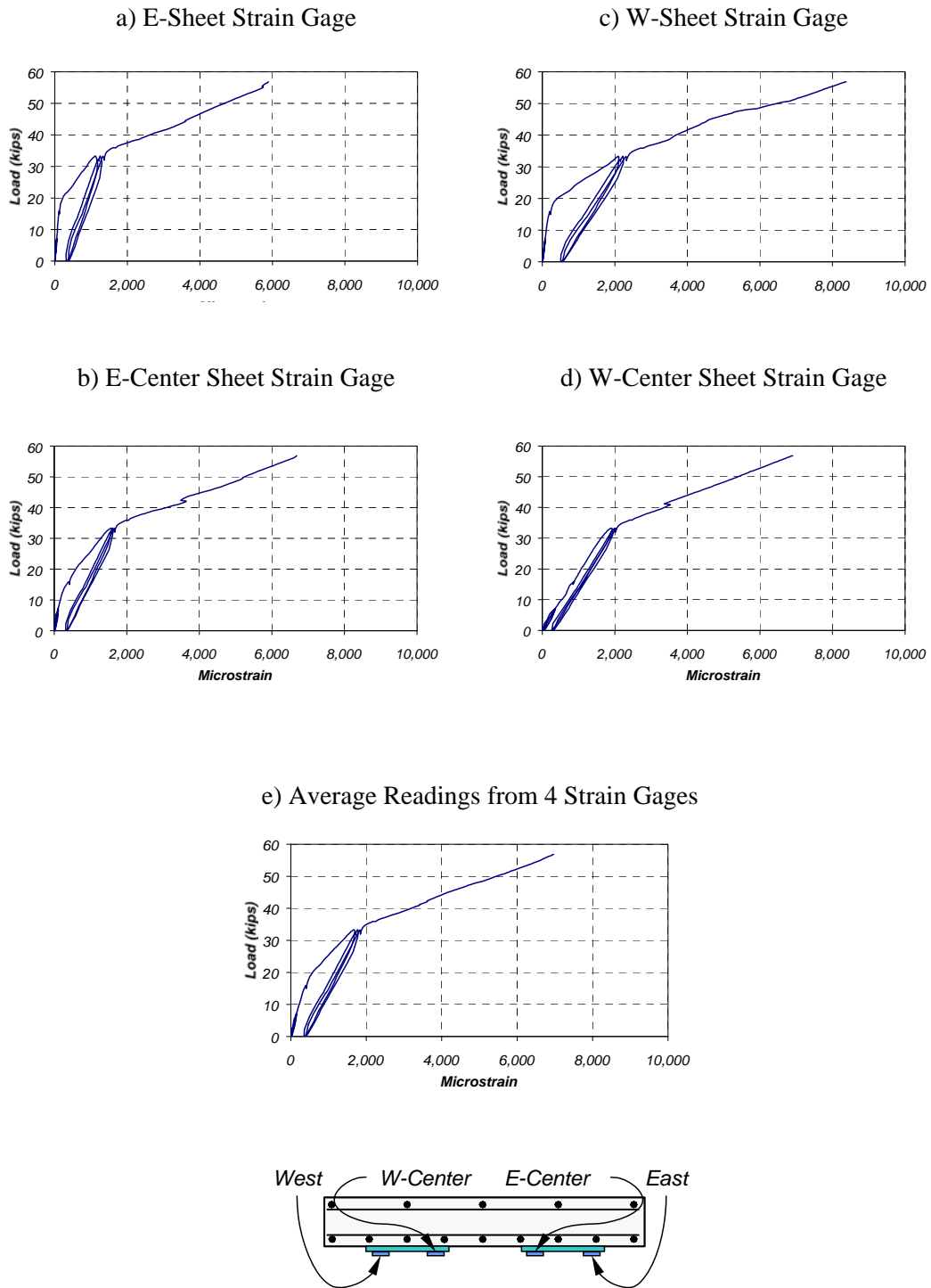


Figure D.48 Measured Strains on CFRP Sheets in Specimen FS-2 (Section S1)

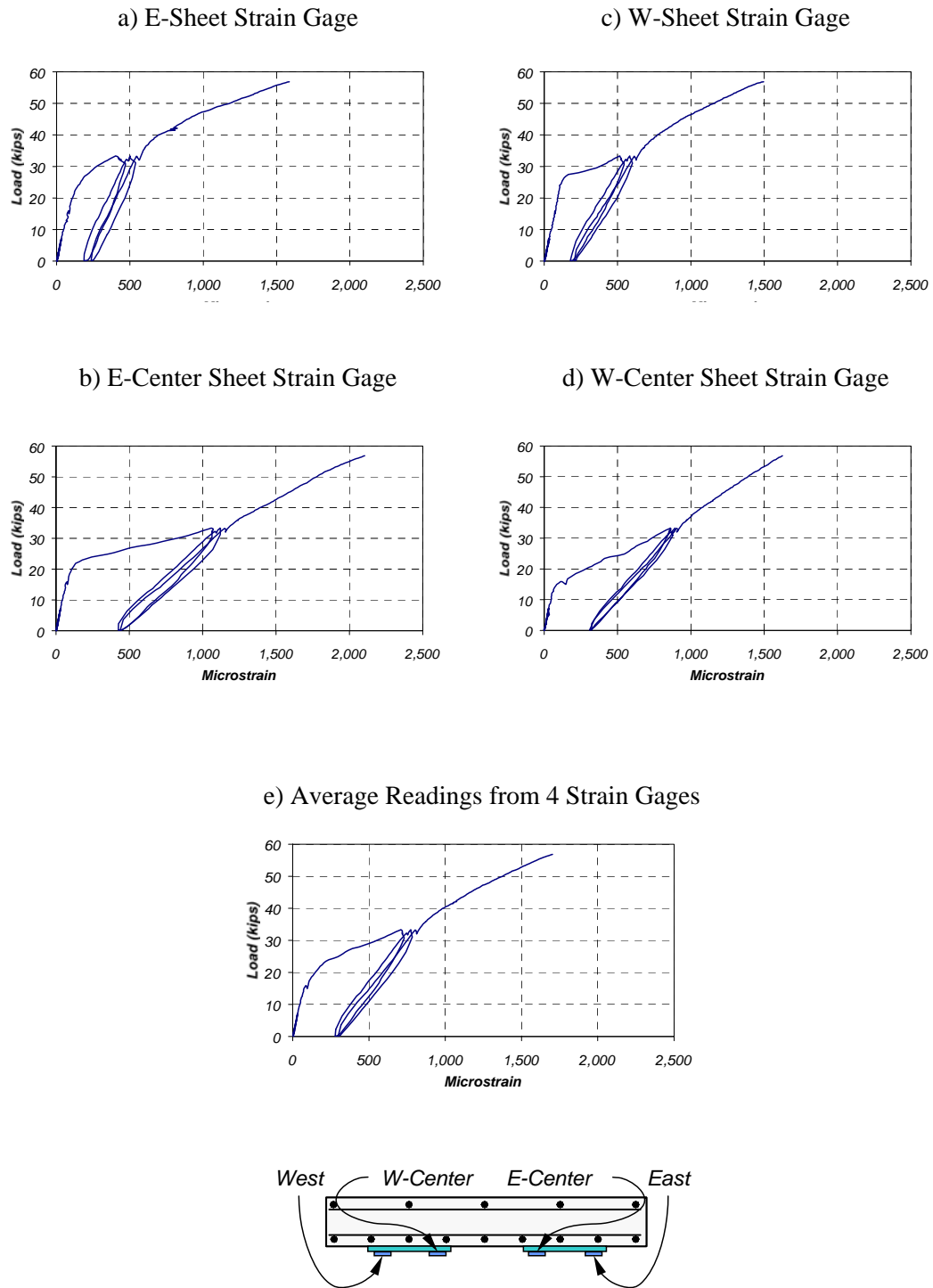


Figure D.49 Measured Strains on CFRP Sheets in Specimen FS-2 (Section N2)

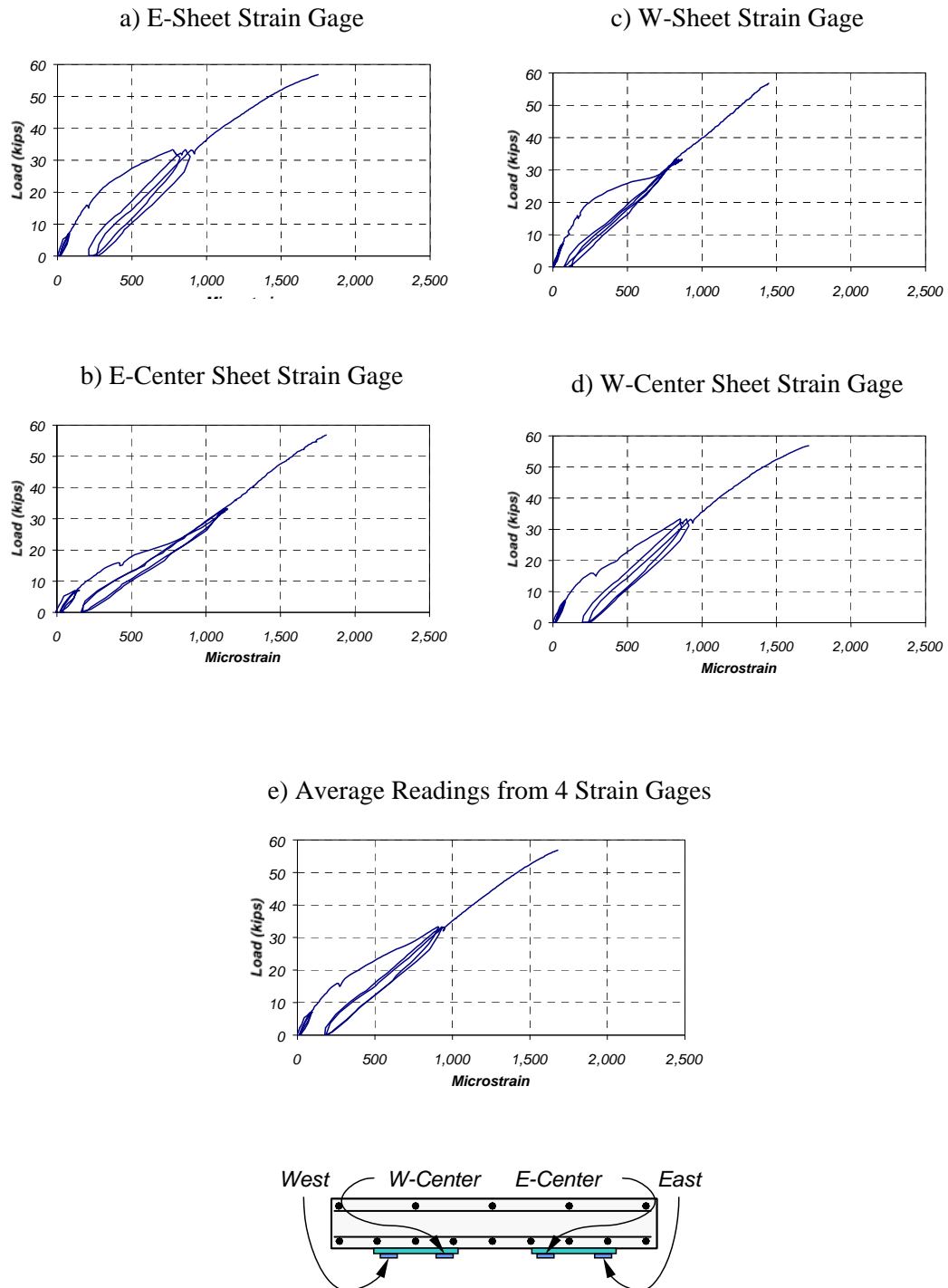


Figure D.50 Measured Strains on CFRP Sheets in Specimen FS-2 (Section S2)

| | |
|--|-----|
| Appendix D: Measured Strains | 377 |
| Figure D.1 Position of Instrumented Sections for Pan-Joist Specimens | 378 |
| Figure D.2 Position of Instrumented Sections for Flat-Slab Specimens | 378 |
| Figure D.3 Measured #8 Reinforcing Bar Strains in Specimen J-1 (Section N1) | 381 |
| Figure D.4 Measured #8 Reinforcing Bar Strains in Specimen J-1 (Section S1) | 382 |
| Figure D.5 Measured #8 Reinforcing Bar Strains in Specimen J-1 (Section N2) | 383 |
| Figure D.6 Measured #8 Reinforcing Bar Strains in Specimen J-1 (Section S2)..... | 384 |
| Figure D.7 Measured CFRP Strains in Specimen J-1 (Section N1)..... | 385 |
| Figure D.8 Measured CFRP Strains in Specimen J-1 (Section S1)..... | 386 |
| Figure D.9 Measured CFRP Strains in Specimen J-1 (Section N2)..... | 387 |
| Figure D.10 Measured CFRP Strains in Specimen J-1 (Section S2)..... | 388 |
| Figure D.11 Measured Strains on Concrete Slab in Specimen J-1 (Section N1)..... | 389 |
| Figure D.12 Measured Strains on Concrete Slab in Specimen J-1 (Section S1) | 390 |
| Figure D.13 Measured Strains on Concrete Slab in Specimen J-1 (Section N2)..... | 391 |
| Figure D.14 Measured Strains on Concrete Slab in Specimen J-1 (Section S2) | 392 |
| Figure D.15 Measured #8 Reinforcing Bar Strains in Specimen J-2 (Section N1) | 393 |
| Figure D.16 Measured #8 Reinforcing Bar Strains in Specimen J-2 (Section S1)..... | 394 |
| Figure D.17 Measured #8 Reinforcing Bar Strains in Specimen J-2 (Section N2) | 395 |
| Figure D.18 Measured #8 Reinforcing Bar Strains in Specimen J-2 (Section S2)..... | 396 |
| Figure D.19 Measured CFRP Strains in Specimen J-2 (Section N1)..... | 397 |
| Figure D.20 Measured CFRP Strains in Specimen J-2 (Section S1) | 398 |
| Figure D.21 Measured CFRP Strains in Specimen J-2 (Section N2)..... | 399 |
| Figure D.22 Measured CFRP Strains in Specimen J-2 (Section S2)..... | 400 |
| Figure D.23 Measured Strains on Concrete Slab in Specimen J-2 (Section N1)..... | 401 |
| Figure D.24 Measured Strains on Concrete Slab in Specimen J-2 (Section S1) | 402 |
| Figure D.25 Measured Strains on Concrete Slab in Specimen J-2 (Section N2)..... | 403 |
| Figure D.26 Measured Strains on Concrete Slab in Specimen J-2 (Section S2) | 404 |
| Figure D.27 Measured Reinforcing Bar (#6) Strains on Specimen FS-1 (Section N1) ... | 405 |
| Figure D.28 Measured Reinforcing Bar (#6) Strains on Specimen FS-1 (Section S1) ... | 407 |
| Figure D.29 Measured Reinforcing Bar (#6) Strains on Specimen FS-1 (Section N2) ... | 408 |
| Figure D.30 Measured Reinforcing Bar (#6) Strains in Specimen FS-1 (Section S2)..... | 410 |
| Figure D.31 Measured Strains on Concrete Slab in Specimen FS-1 (Section N1) | 411 |
| Figure D.32 Measured Strains on Concrete Slab in Specimen FS-1 (Section S1)..... | 412 |
| Figure D.33 Measured Strains on Concrete Slab in Specimen FS-1 (Section N2) | 413 |
| Figure D.34 Measured Strains on Concrete Slab in Specimen FS-1 (Section S2)..... | 414 |
| Figure D.35 Measured Strains on CFRP Plates in Specimen FS-1 (Section N1)..... | 415 |
| Figure D.36 Measured Strains on CFRP Plates in Specimen FS-1 (Section S1)..... | 416 |
| Figure D.37 Measured Strains on CFRP Plates in Specimen FS-1 (Section N2)..... | 417 |
| Figure D.38 Measured Strains on CFRP Plates in Specimen FS-1 (Section S2) | 418 |
| Figure D.39 Measured Reinforcing Bar (#6) Strains in Specimen FS-2 (Section N1) ... | 419 |
| Figure D.40 Measured Reinforcing Bar (#6) Strains in Specimen FS-2 (Section S1)..... | 420 |
| Figure D.41 Measured Reinforcing Bar (#6) Strains in Specimen FS-2 (Section N2) ... | 421 |

| | |
|--|-----|
| Figure D.42 Measured Reinforcing Bar (#6) Strains in Specimen FS-2 (Section S2)..... | 422 |
| Figure D.43 Measured Strains on Concrete Slab in Specimen FS-2 (Section N1)..... | 423 |
| Figure D.44 Measured Strains on Concrete Slab in Specimen FS-2 (Section S1)..... | 424 |
| Figure D.45 Measured Strains on Concrete Slab in Specimen FS-2 (Section N2)..... | 425 |
| Figure D.46 Measured Strains on Concrete Slab in Specimen FS-2 (Section S2)..... | 426 |
| Figure D.47 Measured Strains on CFRP Sheets in Specimen FS-2 (Section N1)..... | 427 |
| Figure D.48 Measured Strains on CFRP Sheets in Specimen FS-2 (Section S1)..... | 428 |
| Figure D.49 Measured Strains on CFRP Sheets in Specimen FS-2 (Section N2)..... | 429 |
| Figure D.50 Measured Strains on CFRP Sheets in Specimen FS-2 (Section S2)..... | 430 |
| Table D.1 Characteristics of Strain Gages | 378 |

References

- American Association of State Highway and Transportation Officials (AASHTO 1994), *Manual for Condition Evaluation of Bridges*, Washington, D.C., 1994.
- American Association of State Highway and Transportation Officials (AASHTO 1996), *Standard Specifications for Highway Bridges*, 16th Edition, Washington, D.C., 1996.
- American Concrete Institute (ACI 318-99), *Building Code Requirements for Structural Concrete (318-99) and Commentary (318R-99)*, Farmington Hills, Michigan, 1999.
- American Society of Civil Engineers (1984), *Structural Plastics Design Manual*, ASCE Manuals and Reports on Engineering Practice No. 63, New York, 1984.
- American Society of Mechanical Engineers (1992), *Reinforced Thermoset Plastic Corrosion Resistant Equipment*, ASME RTP-1, New York, 1992.
- American Society of Mechanical Engineers (1998), *Fiber-Reinforced Plastic Pressure Vessels*, Reported by ASME Boiler and Pressure Vessel Committee, New York, 1998.
- American Society for Testing and Materials (1996), *Standard Test Method for Compressive Properties of Rigid Plastics*, Annual Book of ASTM Standards, Vol. 08.01, Designation: D 695-96, 1996.
- American Society for Testing and Materials (2000a), *Standard Test Method for Tensile Properties of Plastics*, Annual Book of ASTM Standards, Vol. 08.01, Designation: D 638-99, 2000.

- American Society for Testing and Materials (2000b), *Standard Test Methods for Flexural Properties of Unreinforced and Reinforced Plastics and Electrical Insulating Materials*, Annual Book of ASTM Standards, Vol. 08.01, Designation: D 790-99, 2000.
- Arduini, M., Di Tommaso, A., and Nanni, A. (1997), "Brittle Failure in FRP Plate and Sheet Bonded Beams", *ACI Structural Journal*, Vol. 94, No. 4, July-August 1997.
- Arduini, M. and Nanni, A. (1997), "Parametric Study of Beams with Externally Bonded FRP Reinforcement", *ACI Structural Journal*, Vol. 94, No. 5, September-October 1997.
- Benouaich, M.A. (2000), *Fatigue Loading of Reinforced Concrete Members Strengthened Using Carbon Fiber Reinforced Polymer Composites*, Thesis presented to the Department of Civil Engineering in partial fulfillment of the requirements for the Diploma of Civil Engineer, Swiss Federal Institute of Technology at Lausanne, March 2000.
- Bizindavyi, L. and Neale, K.W. (1999), "Transfer Lengths and Bond Strengths for Composites Bonded to Concrete", *Journal of Composites for Construction*, Vol. 3, No. 4, November 1999, pp. 153-160.
- Blaschko, M., Niedermeier, R., and Zilch, K. (1998), "Bond Failure Modes of Flexural Members Strengthened with FRP", *Second International Conference for Composites in Infrastructure*, Vol. 1, Ehsani and Saadatmanesh, Editors, Tucson, AZ, 1998, pp.
- Bramblett, R. M. (2000), *Strengthening of Reinforced Concrete Beams Using Carbon Fiber Reinforced Polymer Composites*, Thesis presented to the Graduate School in partial fulfillment of the requirements for the degree of Master of Science in Engineering, The University of Texas at Austin, August 2000.

- Brosens, K. and VanGemert, D. (1997), "Anchoring Stresses between Concrete and Carbon Fibre Reinforced Laminates", *International Conference: Composite Construction – Conventional and Innovative*, Innsbruck, 1997, pp. 181-186.
- Bussell, L. C. (1997), *Diagnostic Testing for Improved Load Rating of Reinforced Concrete Slab Bridges*, Thesis presented to the Graduate School in partial fulfillment of the requirements for the degree of Master of Science in Engineering, The University of Texas at Austin, May 1997.
- Chajes, M.J., Finch, W.W., Januszka, T.F., and Thomson, T.A., "Bond and Force Transfer of Composite Material Plates Bonded to Concrete", *ACI Structural Journal*, Vol. 93, No. 2, March-April 1996, pp. 208-217.
- David, E., Djelal, C., and Buyle-Bodin, F. (1997), "Repair and Strengthening of Reinforced Concrete Beams using Composite Materials", *Proceedings of the Seventh International Conference on Structural Faults and Repair*, Vol. 2, Engineering Technics Press, University of Edinburgh, Scotland, 1997, pp. 169-173.
- Ferguson, P.M., *Reinforced Concrete Fundamentals*, 3rd Ed., John Wiley & Sons, 1958.
- Federal Highway Administration (1997), *FHWA Study for Advanced Composites in Bridges in Europe and Japan*, United States Department of Transportation, December 1997.
- Federal Highway Administration (1999), *Strategic Goals for Deficient Bridges*, Memorandum Retrieved August 8, 2000 from the World Wide Web: <http://www.fhwa.dot.gov/bridge/defbrid.htm>, July 1999.
- GangaRao, H.V.S. and Vijay, P.V. (1998), "Bending Behavior of Concrete Beams Wrapped with Carbon Fabric", *Journal of Structural Engineering*, Vol. 124, No. 1, January 1998, pp. 3-10.

- Garden, H.N. and Hollaway, L.C. (1998), "An Experimental Study on the Influence of Plate End Anchorage of Carbon Fibre Composite Plates Used to Strengthen Reinforced Concrete Beams", *Composite Structures*, Vol. 42, No. 2, June 1998, pp. 175-188.
- Grace, N.F., Sayed, G.A., Soliman, A.K., and Saleh, K.R. (1999), "Strengthening Reinforced Concrete Beams Using Fiber Reinforced Polymer (FRP) Laminates", *ACI Structural Journal*, Vol. 96, No. 5, September-October 1999, pp. 865-874.
- He, J.H., Pilakoutas, K., and Waldron, P. (1997), "CFRP Plate Strengthening of RC Beams", *Proceedings of the Seventh International Conference on Structural Faults and Repair*, Vol. 2, Engineering Technics Press, University of Edinburgh, Scotland, 1997, pp. 119-127.
- Hognestad, E. (1950), *An Experimental Study of Combined Bending and Axial Load in Reinforced Concrete Members*, University of Illinois, Engineering Experiment Station, October 1950.
- Hognestad, E., Hanson, N.W., and McHenry D. (1955), "Concrete Stress Distribution in Ultimate Strength Design", *Journal of the American Concrete Institute*, Vol. 27, No. 4, December 1955, pp. 455-479.
- Hollaway, L.C. and Leeming, M.B., Editors (1999), *Strengthening of Reinforced Concrete Structures Using Externally-Bonded FRP Composites in Structural and Civil Engineering*, CRC Press LLC, 1999.
- Iketani, J. and Jinno, Y. (1997), "Adhesive Properties of a Carbon Fiber Blanket on to the Concrete Surfaces", *Proceedings of the 42nd International SAMPE Symposium*, May 1997, pp. 109-116.
- Jensen, V.P., Kluge, R.W., and Williams, C.B. (1943), *Highway Slab-Bridges with Curbs: Laboratory Tests and Proposed Design Method*, University of Illinois, Engineering Experiment Station, July 1943.

- Mallick, P.K. (1993), *Fiber-Reinforced Composites: Materials, Manufacturing and Design*, 2nd Ed., Marcel Dekker, Inc., 1993.
- Master Builders, Inc. (1998), *MBraceTM Composite Strengthening System-Engineering Design Guidelines*, Cleveland, OH, 1998.
- Meier, U., Deuring, M., Meier, H., and Schwegler, G. (1992), “Strengthening of Structures with CFRP Laminates: Research and Applications in Switzerland”, *Advanced Composite Materials in Bridges and Structures*, Canadian Society for Civil Engineering, 1992.
- Meier, U. and Winistörfer, A. (1995), “Retrofitting of Structures through External Bonding of CFRP Sheets”, *Non-metallic (FRP) Reinforcement for Concrete Structures*, Ed. L. Taerwe, 1995, pp. 465-472.
- Menegotto, M. and Pinto, P. (1973), “Method of Analysis for Cyclically Loaded Reinforced Concrete Plane Frames Including Changes in Geometry and Nonelastic Behavior of Elements Under Combined Normal Force and Bending”, *IABSE Symposium on the Resistance and Ultimate Deformability of Structures Acted on by Well-Defined Repeated Loads*, Lisbon, 1973.
- Modern Plastics* (1959), “U.S. Pavilion in Moscow”, Vol. 37, No. 4, December 1959.
- Nakamura, M., Sakai, H., Yagi, K., and Tanaka T., (1996), “Experimental Studies on the Flexural Reinforcement Effect of Carbon Fiber Sheet Bonded to Reinforced Concrete Beam”, *1st International Conference on Composites in Infrastructure*, Tucson, Arizona, 1996, pp. 760-773.
- Norris, T., Saadatmanesh, H., and Ehsani, M.R. (1997), “Shear and Flexural Strengthening of R/C Beams with Carbon Fiber Sheets”, *Journal of Structural Engineering*, Vol. 123, No. 7, July 1997, pp. 903-911.

- Ritchie, P.A., Thomas, D.A., Lu, L., and Connelly G.M. (1991), "External Reinforcement of Concrete Beams using Fiber Reinforced Plastics", *ACI Structural Journal*, Vol. 88, No. 4, July-August 1991, pp. 490-500.
- Ross, C.A., Jerome D.M., Tedesco, J.W., and Hughes, M.L. (1999), "Strengthening of Reinforced Concrete Beams with Externally Bonded Composite Laminates", *ACI Structural Journal*, Vol. 96, No. 2, March-April 1999, pp. 212-220.
- Rüsch, H. (1960), "Researches Toward a General Flexural Theory for Structural Concrete", *Journal of the American Concrete Institute*, Vol. 32, No. 1, July 1960, pp. 1-28.
- Saadatmanesh, H. and Ehsani, M.R. (1991), "RC Beams Strengthened with GFRP Plates. I: Experimental Study", *Journal of Structural Engineering*, Vol. 117, No. 4, November 1991, pp. 3417-3433.
- Shahawy, M.A. and Beitelman, T. (1996), "Flexural Behavior of Reinforced Concrete Beams Strengthened with Advanced Composite Materials", *41st International SAMPE Symposium*, 1996, pp. 1015-1025.
- Sika Corporation (1997), *Engineering Guidelines for the Use of CarboDur→ (CFRP) Laminates for Structural Engineering*, Lyndhurst, NJ, 1997.
- Sika Corporation (1999), *Sika Carbodur→ Structural Strengthening Systems*, Lyndhurst, NJ, 1999.
- Spadea, G., Bencardino, F., and Swamy, R.N. (1998), "Structural Behavior of Composite RC Beams with Externally Bonded CFRP", *Journal of Composites for Construction*, Vol. 2, No. 3, August 1998, pp. 132-137.

Stanton, J. F. and McNiven, H. D. (1979), *The Development of a Mathematical Model to Predict the Flexural Response of Reinforced Concrete Beams to Cyclic Loads, Using System Identification*, Earthquake Engineering Research Center, Report No.UCB/EERC-79/02, January 1979.

Texas Department of Transportation (TxDOT 1999), Bridge Inventory, Inspection, and Appraisal Program (BRINSAP) Load Rating Spreadsheet, 1999.

Timoshenko, S.P. and Goodier, J.N. (1970), *Theory of Elasticity*, 3rd Edition, McGraw-Hill, 1970.

Velázquez, B. M. (1998), *Diagnostic Load Tests of a Reinforced Concrete Pan-Girder Bridge*, Thesis presented to the Graduate School in partial fulfillment of the requirements for the degree of Master of Science in Engineering, The University of Texas at Austin, August 1998.

Whittier, R.P. (1957), *Design and Evaluation of Plastics House of Future*, ASME Report 57-A212, December 1957, 13 pp.

REFERENCES429